# Synthèse et caractérisation des oligomères et polymères Ä-conjugués nanostructurés pour applications en photovoltaïque

Wan Zaireen Nisa Yahya

UNIVERSITÉ DE GRENOBLE

# THÈSE

Pour obtenir le grade de

## DOCTEUR DE L'UNIVERSITÉ DE GRENOBLE

Spécialité : **Chimie-Sciences des Polymères**

Arrêté ministériel : 7 août 2006

Présentée par


**Wan Zaireen Nisa YAHYA**


Thèse dirigée par **Jean-Pierre TRAVERS** et

codirigée par **Renaud DEMADRILLE**

préparée au sein du **Laboratoire d'Electronique Moléculaire Organique et Hybride, Service des Structure et Propriétés d'Architectures Moléculaires, CEA Grenoble**
dans **l'École Doctorale Chimie et Sciences du Vivant, de l'Université Joseph Fourier, Grenoble, France**

# Synthèse et caractérisation d'oligomères et polymères nanostructurés $\pi$-conjugués pour les applications photovoltaïques

Thèse soutenue publiquement le **12 Novembre 2012**,
devant le jury composé de :

**Prof. Guy ROYAL**
Professeur, Université de Grenoble (Président)
**Prof. Thomas HEISER**
Professeur, Université de Strasbourg (Rapporteur)
**Dr. Christine DAGRON-LARTIGAU**
Maître de Conférence, IPREM/EPCP, Université de Pau (Rapporteur)
**Dr. Guillaume WANTZ**
Maître de Conférence, IMS (site ENSCBP), Université de Bordeaux (Examinateur)
**Dr. Jean-Pierre TRAVERS**
Directeur de Recherche,SPRAM, Université de Grenoble (Directeur de thèse)
**Dr. Renaud DEMADRILLE**
Ingénieur-Chercheur, CEA Grenoble (Co-directeur de thèse)

*Université Joseph Fourier / Université Pierre Mendès France /*
*Université Stendhal / Université de Savoie / Grenoble INP*

UNIVERSITÉ DE GRENOBLE

## Thesis

submitted to the

## University of Joseph Fourier in Grenoble

to obtain the degree of

## Doctor of Philosophy

Subject: **Chemistry: Polymer Science**


**Wan Zaireen Nisa YAHYA**

PhD Advisors:
**Dr. Jean-Pierre TRAVERS** and **Dr. Renaud DEMADRILLE**


# Synthesis and characterisation of nanostructured $\pi$-conjugated oligomers and polymers for organic photovoltaic


Thesis defended: **12 Novembre 2012**
PhD Thesis committee members:

**Prof. Guy ROYAL**
Professor, University of Grenoble (President)
**Prof. Thomas HEISER**
Professor at University of Strasbourg (Referee)
**Dr. Christine DAGRON-LARTIGAU**
Assistant Professor, Laboratoire IPREM/EPCP, University of Pau (Referee)
**Dr. Guillaume WANTZ**
Assistant Professor, Laboratoire IMS (site ENSCBP), University of Bordeaux (Member)
**Dr. Jean-Pierre TRAVERS**
Research Director, SPRAM, University of Grenoble (Thesis Director)
**Dr. Renaud DEMADRILLE**
Researcher, CEA Grenoble (Supervisor)

*Université Joseph Fourier / Université Pierre Mendès France /*
*Université Stendhal / Université de Savoie / Grenoble INP*


SIGILLUM UNIVERSITATIS GRATIANOPOLITANÆ 1339

# Abstract

Organic photovoltaic (OPV) cells have been a subject of increasing interest during the last decade as they are promising candidates for low cost renewable energy production. In order to obtain reasonably high performance organic solar cells, development of efficient light absorbing materials are of primary focus in the OPV field. In this context, the present work is focused on the design and development of new electron donor materials (oligomers and polymers) as light absorbing materials based on “Donor-Acceptor” approach alternating electron donating group and electron withdrawing group. Three main families of electron donating group are studied: oligothiophenes, fluorene and indacenodithiophene. Fluorenone unit is the principal electron withdrawing group studied and a direct comparison with the system based on benzothiadiazole unit as electron withdrawing unit is also provided. Three main synthetic methods were employed: oxidative polymerization mediated by Iron (III) chloride and Palladium cross-coupling reactions according to Suzuki coupling or Stille coupling conditions. Spectroscopic studies on absorption and photoluminescence have demonstrated the presence of characteristic charge transfer complex in all the studied D-A oligomers and polymers allowing the extension of the absorption spectrum. The D-A oligomers and polymers have shown an overall low optical band gap of 1.6-2 eV with absorption spectra up to 600 to 800 nm. The nature of the charge transfer complex transitions bands were found to be depending on the strength of the electron donating unit and the electron withdrawing unit. Furthermore molecular packing in solution and in solid state has also demonstrated to contribute to extension of absorption spectrum. The HOMO and LUMO energy levels of the oligomers and polymers were determined by electrochemical measurements. Fluorene-based polymers have shown low lying HOMO energy levels, and these polymers demonstrate high open circuit voltage (Voc) in photovoltaic cell when combined with fullerenes derivatives PCBM with Voc values close to 0.9 V. The oligomers and polymers tested in photovoltaic devices have shown promising results with the highest power conversion efficiency obtained of 2.1 % when combined with fullerenes PCBMC70. These results were obtained after only limited numbers of device optimizations such as the active materials ratios and thermal annealing. Therefore further optimization of devices may exhibit higher power conversion efficiencies.



# Résumé

Les cellules photovoltaïques organiques ont fait l'objet d'un intérêt croissant au cours de ces dernières décennies car elles offrent un grand potentiel pour une production d'énergie renouvelable à faible coût. Afin d'obtenir des cellules solaires organiques à haut rendement de conversion d’énergie, beaucoup de recherches se focalisent sur les matériaux ayant des capacités à absorber la lumière efficacement. Dans ce contexte, le présent travail se concentre sur la conception et le développement de nouveaux matériaux donneurs d'électrons (oligomères et polymères) comme matériaux absorbant de la lumière basée sur l’approche « Donneur-Accepteur » alternant des segments riches en électron (donneur d’électron) et des unités pauvres en électron (accepteur d’électron). Trois séries d’unités riches en électron ont été étudiées: oligothiophènes, fluorène et indacenodithiophene. L’unité fluorénone est la principale unité « accepteur d’électron » étudiée. Une comparaison directe avec le système basé sur l'unité benzothiadiazole comme accepteur d'électron est également rapportée. Trois méthodes principales de synthèse ont été utilisées: polymérisation oxydante par le chlorure de fer (III), et les couplages croisés au palladium de type Suzuki ou de Stille. Les études spectroscopique UV-Visible en absorption et en photoluminescence sur ces oligomères et polymères ont démontré la présence de complexes à transfert de charges permettant d’élargir le spectre d'absorption. Les oligomères et les polymères possèdent des faibles largeurs de bande interdite de 1,6 eV à 2 eV. Les systèmes ayant des unités fluorénones présentent des spectres d'absorption étendus allant jusqu’à 600-700 nm, tandis que les systèmes ayant des unités benzothiadiazoles présentent des spectres d'absorption allant jusqu’à 700- 800 nm. La nature des bandes de complexes à transfert de charge se révèle d’être dépendant de la force de respective des unités « donneur d'électrons » et des unités « accepteur d'électrons ». Les niveaux d’énergies HOMO et LUMO des oligomères et les polymères sont déterminés par des mesures électrochimiques. Les polymères à base de fluorène possèdent des niveaux d’énergie HOMO les plus bas. Ces polymères testés en mélange avec les fullerenes PCBM en cellules photovoltaïques ont démontré des valeurs élevées de tension en circuit ouvert (Voc) proche de 0,9 V. Tous les oligomères et les polymères ont été testés dans des dispositifs photovoltaïques et ont montré des résultats encourageants avec des rendements de conversion allant jusqu’à 2,1 %. Ce sont des premièrs résultats obtenus après seulement quelques optimisations (ratios oligomères ou polymères : fullerènes et recuit thermique). Ce travail prometteur permet ainsi d’envisager des résultats plus élevés dans le futur.

# TABLE OF CONTENTS

# REMERCIEMENTS

*Ces travaux de thèse est un fruit de participations et de soutiens de différentes personnes que je tiens à remercier.*

*Je remercie en premier lieu mon directeur de thèse Renaud Demadrille qui depuis plus de trois ans m'a beaucoup épaulé, m'a instruit, m'a donné des conseils tout le long. Merci pour la patience, la pertinence et de me toujours pousser jusqu'au bout. Je remercie également Jean Pierre Travers mon directeur de thèse ainsi que le directeur de laboratoire SPRAM qui m'a accueilli, m'a soutenu et qui était à l'écoute pendant ces trois ans.*

*Je tiens à remercier tous les membres de jury. Prof Guy Royal d'avoir présidé le jour de soutenance, Prof Thomas Heiser et Dr Christine Dagron-Lartigau d'avoir accordé leurs temps pour être rapporteurs de cette thèse. Je remercie également Dr Guillaume Wantz d'avoir complété ce membre de jury même aux dernières minutes. Vos conseils et vos partages de savoir me sont très utiles pour mon futur.*

*Je remercie également les membres de LEMOH notamment avec les personnes lesquelles j'ai beaucoup travaillé : Yann Kervella pour toutes les synthèses organiques ainsi que ses lessons sur les plantes, Patrice Rannou pour les manips en SEC, Benjamin Grévin pour les manips en AFM, ainsi que Brigitte Pepin-Donat et Christian Lombard pour les manips en RPE. Les post-doctorants, les doctorants, et les stagiaires qui sont passés dans les laboratoires avec qui j'ai travaillé ensemble: Angéla, Evan, Léa, Shuichi et Kazuo, Gaëlle, Vincent, Nicolas et Kars. Sans oublier tous les autres membres de l'équipe pour tous les moments de bonheur dans le couloir, à la cafétéria, dans les laboratoires, dans la salle de café pour les goutés, ainsi que pendant nos sorties ensembles.*

*Je remercie également les autres collaborateurs externes : Solenn Berson et Remi de Bettignies de l'Institut National d'Energie Solaire (INES) à Chambery pour les fabrications et les tests des dispositifs photovoltaïques, Caroline Celle et Jean-Pierre Simonato de CEA-LITEN pour les fabrications des transistors, Philippe Leclère de l'Université de Mons pour les manips avancées en AFM et Mathieu Linares pour les modélisations.*

*Je remercie tous les personnels de INAC-CEA-Grenoble avec lesquelles j'ai partagé des agréables et inoubliables moments de ma vie.*

*Finally, my heartiest thanks to my loved ones, my parents, my brothers and sisters, my family and my friends in Malaysia and in France who always support me and believe in me. Thank you again and love each and every one of you so much.*

*Verily! In the creation of the heavens and the earth, and in the alternation of night and day, there are indeed signs for men of understanding. (Ali Imran: 190)*

# RESUME ETENDU DE LA THESE

La demande mondiale en énergie ne cesse de croître de façon exponentielle. Ces dernières décennies, la production d'électricité à partir des combustibles a été complémentée par l'émergence des énergies renouvelables qui exploitent l'énergie du soleil, du vent, de l'hydraulique etc. afin de produire de l'électricité. Parmi ces nouvelles énergies renouvelables, la technologie photovoltaïque se présente comme une source d'énergie potentielle pour subvenir des besoins en énergie[1]. L'énergie photovoltaïque permettant la conversion d'énergie la lumière solaire en énergie électrique[2] offre une promesse d'énergie propre et inépuisable[3]. Cette technologie en pleine expansion se classifie en trois générations : la première les cellules solaires à base de silicium, la deuxième les cellules solaires à base de couche minces des semi-conducteurs inorganiques et la troisième les technologies émergeants tels que les cellules concentrateur (à base de semi-conducteurs inorganiques), les cellules photovoltaïques organiques, les cellules hybrides organique-inorganique, les cellules photovoltaïques à base de colorants et tous les autres technologies qui sont dans la phase de recherche dans les laboratoires et qui ne sont pas encore entrées dans le marché. A présent, le marché des cellules photovoltaïques est principalement dominé par les cellules en silicium avec un part de marché à plus de 80 %[4] avec des rendements de conversion de l'ordre de 12 à 27 %[5]. A ce jour, les technologies photovoltaïques sont plutôt couteuses et leurs capacités sont limitées.

Les matériaux semi-conducteurs organiques sont porteurs d'un potentiel de développement important dans la recherche de modules photovoltaïques à coût relativement bas et le marché visé est la production d'électricité domestique. Ils présentent des facilités de fabrication et des procédés de mise en œuvre par des techniques imprimeries sont envisageables, ce qui permettra de diminuer fortement leur coût. Contrairement aux cellules à base de silicium, ils peuvent être fabriqués facilement sur des substrats souples et flexibles, ce qui leur permettra de s'intégrer facilement dans les objets courants. Les cellules organiques apparaissent comme une voie d'avenir complémentaire et crédible. Les recherches sur ces composés s'intensifient et beaucoup de défis sont encore à relever, notamment pour améliorer l'efficacité des cellules organiques en termes de taux de conversion en énergie, stabilité et durabilité.

L'état de l'art de l'efficacité des cellules photovoltaïques à base de semi-conducteurs organiques a atteint des rendements de conversion de l'ordre de 8,62% publié récemment par l'équipe de recherche de Yang Yang[6] en utilisant un polymère à faible largeur de bande interdite en configuration tandem. Très récemment, le groupe a optimisé leurs cellules en utilisant un autre nouveau polymère capable à absorber la lumière jusqu'au proche infra-rouge et a réalisé des performances de 10,6 % certifié par le Laboratoire Nationale en Energie Renouvelable (NREL)[7].

Ces résultats encourageants nous ont donc incités à développer de nouveaux matériaux semi-conducteurs organiques à base de polymères et de petites molécules pour les applications photovoltaïques.

Dans ce contexte, quatre points principaux sont abordés et discutés en détail dans ces travaux:

Développement de nouveaux matériaux donneurs d'électrons (matériaux absorbant de la lumière)
Etude des propriétés chimiques et opto-électroniques de ces nouveaux matériaux
Évaluation des performances photovoltaïques en cellules photovoltaïques
La relation entre les structures et propriétés des macromolécules et les performances en photovoltaïques

Les cellules photovoltaïques organiques[8,9,10,11,12,13,14] peuvent être définies comme des cellules à base de semi-conducteurs organiques tels que des polymères et des petites molécules π-conjugués. Les oligomères et polymères π-conjugués sont d'excellents candidats pour les applications en photovoltaïques grâce à leurs capacités d'absorber la lumière, de photo-générer les charges et de transporter ces charges. Le plus grand avantage des oligomères et polymères π -conjugués réside dans la possibilité de moduler leurs propriétés optiques et électroniques par ingénierie moléculaire.

Pour la conception des nouveaux oligomères et polymères, la stratégie adoptée est :

- De concevoir les oligomères et des polymères ayant des faibles largeurs de bande interdites afin d'élargir le domaine d'absorption dans le visible de nos matériaux. La largeur de bande interdite idéal pour les matériaux devrait se situer entre 1,5 eV et 2 eV pouvant absorber jusqu'au 800 nm.
- De moduler les positions des niveaux d'énergie des orbitales frontières de nos matériaux et en particulier de diminuer les niveaux d'énergie de HOMO (orbitale moléculaire la plus haute occupée) afin d'augmenter la tension en circuit ouvert Voc. Les niveaux d'énergies de HOMO idéals sera de l'ordre de -5,2 eV et -5,8 eV.
- De contrôler la morphologie des oligomères et polymères en film pour obtenir une bonne auto-organisation et une ségrégation de phases optimale en mélange avec les accepteurs. L'organisation des matériaux est importante pour obtenir un bon transport des charges et éviter les phénomènes de recombinaison.

Pour la conception et le développement de nouveaux matériaux donneurs d'électrons (oligomères et polymères), nous avons développé de nouveaux matériaux donneurs d'électrons basant sur l'approche « Donneur-Accepteur » alternant des segments riches en électrons (donneur d'électrons) et des unités pauvres en électrons (accepteur d'électrons).

Nous présentons d'abord deux exemples des oligomères « Donneur-Accepteur » QTF et TVF2 avec fluorénone comme unité électro-attracteur principale dans ces systèmes conjugués. Dans cette étude, les segments donneurs d'électrons étudiés sont les oligothiophènes de type quaterthiophene linéaire (QTF8) et le thienylène vinylène (TVF2). Les propriétés optiques et électrochimiques de ces oligomères sont étudiées afin d'évaluer l'effet de la modification de la structure sur les propriétés électroniques.

Nous avons trouvé que la combinaison des unités donneurs d'électrons (des blocs oligothiophènes) et de l'unité accepteur d'électron (fluorénone) a fait apparaître une nouvelle bande d'absorption correspondant au complexe de transfert de charge intramoléculaire qui donne lieu à l'élargissement du spectre d'absorption[15]. L'extension du système π-conjugué conduit également à l'élargissement du spectre d'absorption comme le montre le dimère TVF2. Les oligomères QTF présentent des domaines d'absorption inférieure au dimère TVF2 avec une largeur de bande interdite de 1,90 eV à comparer avec celle de TVF2 de 1,71 eV.

Les niveaux d'énergies d'HOMO et de LUMO des deux oligomères sont correctement positionnés par rapports aux niveaux d'énergie des matériaux accepteurs (tels que fullerène PCBM), avec des valeurs de -5,01 eV (HOMO) et -3,20 eV (LUMO) pour QTF et -5,07 eV (HOMO) et -3,27 (eV LUMO) pour TVF2. Par conséquent, ces deux oligomères sont des matériaux donneurs appropriés pour l'application photovoltaïque en combinaison avec des matériaux accepteurs communs tels que le PCBM.

Nos oligomères QTF et TVF2 présentent également une propriété d'auto-organisation supramoléculaire à l'état solide. L'étude par microscopie en champ proche en microscopie à force atomique (AFM) a révélé pour ces deux oligomères des auto-organisations sous formes des nano-fibres[16].

Ces deux oligomères ont été testées comme matériaux donneurs dans des dispositifs photovoltaïques en combinaison avec différents matériaux accepteurs tels que les fullerènes PCBMs. Des cellules photovoltaïques à base des oligomères QTF en mélange avec PCBMC70 donnent des rendements de conversion allant jusqu'à 1,24%. Pour la TVF2 oligomère, les résultats préliminaires ont montré de faibles rendements de conversion d'énergie pour tous nos tests avec des accepteurs différents. Les faibles rendements de conversion d'énergie sont essentiellement dus à la mauvaise ségrégation phase entre l'oligomère TVF2 et les fullerènes dans les couches actives. L'étude en AFM a révélé des formations de larges bandes des domaines riches en TVF2 de taille plusieurs centaines de nanomètres. La taille de domaines dépassant la taille dépassant la longueur de diffusion (de l'ordre de 20 nm) favorise ainsi la recombinaison de charges.

Nous avons ensuite étudié les systèmes conjugués de type polymères. Trois séries de polymères ont été étudiées. Les polymères à base des oligothiophènes, fluorène et indacenodithiophene. L'unité fluorénone est la principale unité « accepteur d'électron » étudiée. Une comparaison directe avec le système basé sur l'unité benzothiadiazole comme accepteur d'électron est également rapportée.

Trois méthodes principales de synthèse ont été utilisées: polymérisation oxydante par le chlorure de fer (III), et les couplages croisés au palladium de type Suzuki ou de Stille. Selon les méthodes de synthèses et de purifications de ces polymères, nous avons obtenu des polymères présentant des paramètres macromoléculaires très différents en termes de poids moléculaire et d'indice de polydispersité. Par ailleurs, l'étape de purification s'avère comme un point crucial afin d'éliminer les traces d'impuretés catalytiques ou autres qui peuvent nuire des performances en photovoltaïques.

Les études spectroscopique UV-Visible en absorption et en photoluminescence sur ces oligomères et polymères ont démontré également la présence de complexes à transfert de charges [17] permettant d'élargir le spectre d'absorption. Les oligomères et les polymères possèdent des faibles largeurs de bande interdite de 1,6 eV à 2 eV. Les systèmes ayant des unités fluorénones présentent des spectres d'absorption étendus allant jusqu'à 600-700 nm, tandis que les systèmes ayant des unités benzothiadiazoles présentent des spectres d'absorption allant jusqu'à 700- 800 nm. La nature des bandes de complexes à transfert de charge se révèle d'être dépendant de la force de respective des unités « donneur d'électrons » et des unités « accepteur d'électrons ».

Les niveaux d'énergies HOMO et LUMO de ces polymères sont déterminés par des mesures électrochimiques. Les polymères à base de fluorène possèdent des niveaux d'énergie HOMO les plus bas par rapport aux autres polymères à base de thiophène et d'indacenodithiophène, comme présenté au Figure 1 ci-dessous. Par conséquent, ces polymères à base de fluorène en mélange avec les fullerènes PCBM testés en cellules photovoltaïques ont démontré des valeurs élevées de tension en circuit ouvert (Voc) proche de 0,9 V.

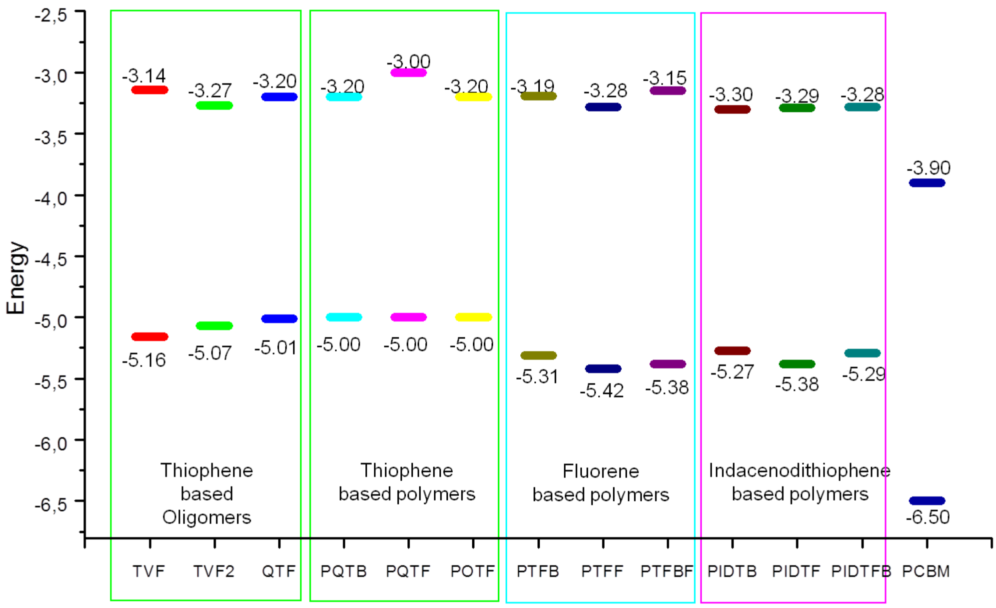


**Figure 1: Diagramme d'énergie des différentes oligomères et polymères étudiés dans nos études**

Tous les polymères ont été testés dans des dispositifs photovoltaïques et ont montré des résultats encourageants avec des rendements de conversion allant jusqu'à 2,1 %. Ce sont des premiers résultats obtenus après seulement quelques optimisations (ratios oligomères ou polymères : fullerènes et recuit thermique). Ce travail prometteur permet ainsi d'envisager des résultats plus élevés dans le futur.

## Référence


1 European Photovoltaic Industry Association, http://www.epia.org/

2 A.E. Becquerel, Compt. Rend. Acad. Sci. 9 (1839) 145.

3 http://www.iea.org/

4 L. El Chaar, L.A. Lamont, N. El Zein, Review of photovoltaic technologies, Renewable and Sustainable Energy Reviews, Volume 15, Issue 5, June 2011, Pages 2165-2175

5 http://www.nrel.gov

6 L. Dou, J. You, J. Yang, C-C. Chen, Y. He, S. Murase, T. Moriarty, K. Emery, G. Li and Y. Yang, Tandem polymer solar cells featuring a spectrally matched low-bandgap polymer, Nature Photonics 6, 180–185 (2012)

7 http://newsroom.ucla.edu/portal/ucla/ucla-engineers-create-tandem-polymer-228468.aspx

8 C. J. Brabec, N. S. Sariciftci, J. C. Hummelen, Plastic Solar Cells, Adv. Funct. Mater. 2001, 11,

9 H. Hoppe and N. S. Sariciftci, Organic solar cells: An overview, J. Mater. Res., Vol. 19, No. 7, Jul 2004

10 J-L. Brédas, J. E. Norton, J. Cornil, and V. Coropceanu, Molecular Understanding of Organic Solar Cells: The Challenges, Acc. Chem. Res. 2009 42 (11), 1691-1699

11 S. Gunes, H. Neugebauer, N. S. Sariciftci, Conjugated polymer-based organic solar cells. Chem. Rev. 2007, 107, 1324–1338.

12 R. Kroon,M. Lenes, J.C. Hummelen,P. W. M. Blom, B. De Boer, Small bandgap polymers for organic solar cells (polymer material development in the last 5 years), Polym. Rev. 2008, 48, 531–582.

13 B. Walker, C. Kim, T.-Q. Nguyen, Small Molecule Solution-Processed Bulk Heterojunction Solar Cells, Chemistry of Materials 2011 23 (3), 470-482

14 J-M. Nunzi, Organic photovoltaic materials and devices, C. R. Physique 3 (2002) 523–542

15 R. Demadrille, M. Firon, J. Leroy, P. Rannou, A. Pron, Plastic Solar Cells Based on Fluorenone-Containing Oligomers and Regioregular Alternate Copolymers, Adv. Funct. Mater. 2005, 15, 1547

[16] E. J. Spadafora, M. Linares, W. Z. Nisa Yahya, F. Lincker, R. Demadrille and B. Grevin, Local contact potential difference of molecular self-assemblies investigated by Kelvin probe force microscopy, Appl. Phys. Lett. 99, 233102-1-3 (2011).

[17] N. Banerji, E. Gagnon, P. Morgantini, S. Valouch, A. R. Mohebbi, J. Seo, M. Leclerc, A. J. Heeger, Breaking Down the Problem: Optical Transitions, Electronic Structure, and Photoconductivity in Conjugated Polymer PCDTBT and in Its Separate Building Blocks, J. Phys. Chem. C 2012, 116, 11456

# INTRODUCTION: MOTIVATION AND OUTLINE

# I. Motivation

With the global economic growth, the world primary energy consumption has also grown exponentially. Over the last decade, photovoltaic technology has shown the potential to become a major source of power generation for the world – with robust and continuous growth even during times of financial and economic crisis[1]. Photovoltaic energy allowing conversion of sunlight energy to electrical energy, offers promises of renewable energy. The photovoltaic effect first published by Alexandre-Edmund Becquerel in 1839[2], involve photophysical phenomenon of conversion of the absorbed photon by the semiconductor to free electron that can be channelled into an electrical current.

**Photovoltaic technologies can be classified into three different generations. First generation technology is based on crystalline silicon. The silicon solar cells have been a major key player in the photovoltaic market representing up to 80 % of the market[3]. These technologies benefited the maturity in this field and the large quantities produced by the semiconductor industry despite its expensive manufacturing process. The National Renewable Energy Laboratory has reported in 2012 the state of the art in terms of performances of the different technologies as shown in**

Figure 2. Silicon solar cells have shown power conversion efficiency from 12 % to 27 % with energy payback time of 2 to 4 years[4].

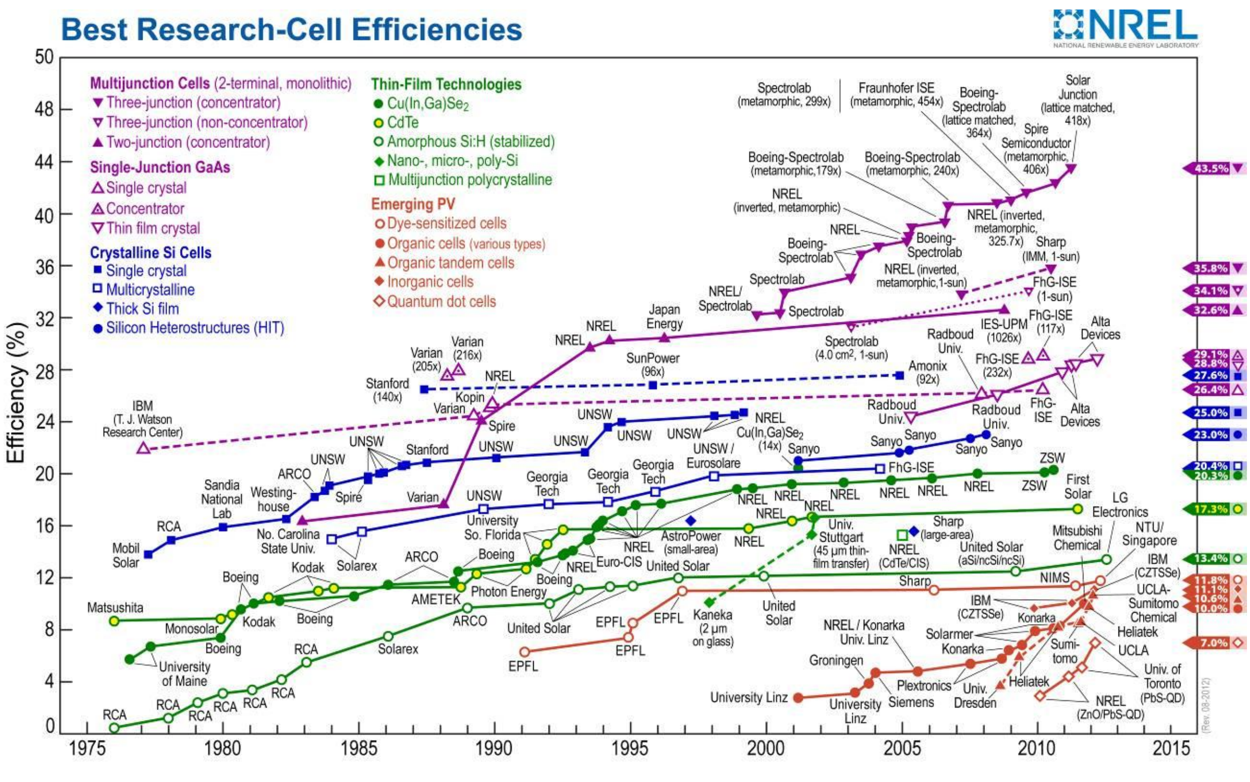


**Figure 2: NREL certified research-cell efficiencies**

The second photovoltaic generation includes thin film technologies, using thin layers of semiconductors materials such as Cadmium Telluride (CdTe), Copper Indium diSelenide(CIS) or Copper, Indium, Gallium, Selenide (CIGS), etc. Researches in this field have started in the middle of the 70's and today, the state of art for this technology is up to 20 % of efficiency using the CIGS technology[5].

The third generation of photovoltaic technologies is emerging new photovoltaic technologies such as concentrator photovoltaic, organics, quantum dot cells, organic-inorganic hybrid and other technologies that have not yet been commercialized at large scale. Up to date, the state-of-art of research-cell efficiencies has achieved a power conversion of 43.5 % using multi-junction concentrators of GaInP/GaAs/GaInNAs (Gallium Indium Phosphide/Gallium Arsenide/Gallium Indium Nitrogen Arsenide)[6]. However a major draw back of highly efficient cells based on inorganic semiconductors is the high cost of fabrication[7,8].

The photovoltaic field is still dominated by silicon technology, however emerging organic photovoltaics and hybrid organic-inorganic photovoltaic cells have been a subject of increasing interest in the field during the last decade[9]. Organic solar cells can be defined as solar cells based on organic semiconductors such as polymers or small molecules. In hybrid solar cells, organic semi-conductors are combined to inorganic materials. Some of the advantages of the organic solar cells can be listed as follows:

- Low cost materials and processes: A recent study suggested the levelised electricity cost for organic photovoltaic to be in between 0.19 €/kWh and 0.50 €/kWh for modules containing photovoltaic cells of 7 % efficiency and assuming a 5 year module lifetime [10]
- Organic solar cells are efficient under dim light or indoor light[11,12]
- Requirement concerning the purity of the materials are lower than the silicon technology
- New applications can be envisioned (flexible, low weight, colorful…)[13]
- Large area panels can be produced by printing technologies on both rigid and flexible substrates[14]
- Shorter energy payback time (less than 1 year)

The state-of-art of photovoltaic cell efficiencies based on organic semiconductors has achieved power conversion efficiencies up to 8.62 % published recently by Yang Yang research group[15] using low band gap polymer in tandem configuration and the group further optimised their devices using a new infra-red absorbing material and achieved higher performance device of power conversion efficiency of 10.6 % certified by NREL.[16]

These encouraging results on organic photovoltaic cell have therefore motivated us to develop new organic semiconductor materials based on polymers and small molecules for photovoltaic application.

## II. Outline of the thesis

We particularly focused these studies on the organic photovoltaic cells more specifically on the elaboration of π-conjugated systems of small molecules and polymers as electron donor materials. These materials could be used with fullerenes electron acceptors or inorganic nanocrystals.

Four main aspects that we will discuss in this thesis are:

- Development of new electron donor materials
- Study of the opto-electronic properties of the materials
- Evaluation of the photovoltaic performances in solar cell configuration
- Establish the relation between molecule structures and photovoltaic properties

For the development of the new p-type materials also called electron donor materials, we will first develop series of oligomers which can be used as model systems for developing polymers and for a better understanding on the structure properties relationship regarding to the photovoltaic phenomenon. An in the later part, we will develop new series of polymers.

We adopt the approach of donor-acceptor concept by employing the fluorenone as electron withdrawing unit (or are also called electron-acceptor, or electron-deficient) and several examples of electron-rich (also called electron-donor) units.

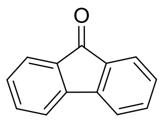

9-Fluorenone

**Figure 3: Structure of the electron withdrawing unit 9-fluorenone**

In this thesis, we want to further develop new donor materials based on fluorenone units in order to increase the cell performance. We will describe first the synthesis of the new materials, the intrinsic properties, photophysical, and electronic characterisation and the photovoltaic performance in devices. As the benzothiadiazole unit is one of the most used building blocks for the preparation of new materials of interest for organic photovoltaics, we will develop analogues of the fluorenone-based materials suitable for an accurate comparison of the performances of the different systems.

The outline of this manuscript is as follow:

In the first chapter we will cover a brief overview of organic photovoltaic. Fundamental principle on organic photovoltaic, different materials used in organic photovoltaic, and the control of device fabrication parameters are discussed.

In the second chapter we will discuss the preparation and the complete characterization of two types of oligomers containing fluorenone units. The first family will be based on linear oligothiophene units as electro donating segments and the second family will be based on thienylene vinylene units as electro donating segments.

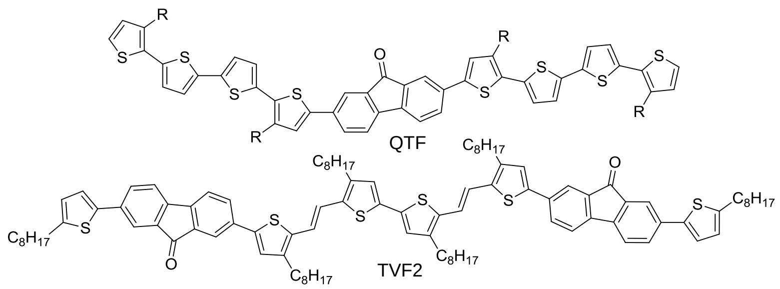


**Figure 4: Molecules structures of two oligomers studied in the thesis: bis-quaterthiophene fluorenone QTF and dimer thienylene-vinylene fluorenone TVF2**

In the third chapter we will present examples of low band gap alternating donor-acceptor D-A polymers based on electron donating oligothiophenes and electron withdrawing fluorenone unit. The choice of using oligothiophenes as the electron-donating subunits in the polymer back bone is rather straight-forward concept to increase the absorption spectrum of the reference studied polymers P3HT. We have also synthesised an analogue polymer based on benzothiadiazole unit. The polymers studied are poly (quaterthiophenes-fluorenone) PQTF, poly(quaterthiophenes-benzothiadiazole) PQTB, and poly (octathiophenes-fluorenone) POTF as shown in Figure 5.

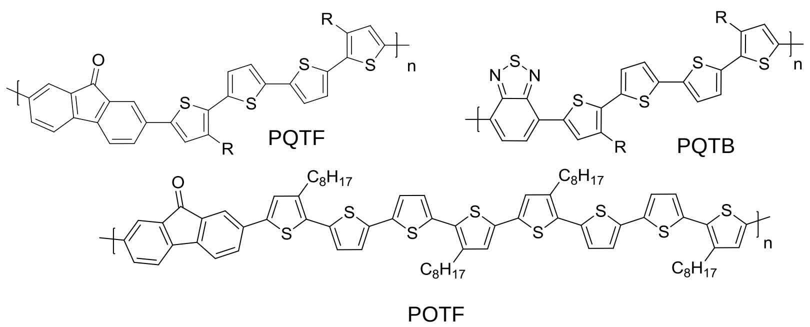


**Figure 5: Low band gap thiophene-based Donor-Acceptor polymers poly (quaterthiophenes-fluorenone) PQTF, poly(quaterthiophenes-benzothiadiazole) PQTB and poly (octathiophenes-fluorenone) POTF**

In the forth chapter, we will investigate new type of D-A polymers incorporating new electron rich building block with an additional fluorene units. Fluorene units are well known in the field of conjugated systems especially in organic light emitting diodes technologies (OLED) as well as potential candidates in organic solar cells. We take advantage of our readily precursor of thiophene based polymers (PQTF and PQTB) to construct the new regioregular D-A polymers poly(bithiophene fluorene- fluorenone) PTFF and poly(bithiophene fluorene-benzothiadiazole) PTFB. We will also present a new single-component copolymer poly( PTFBF consisting of the two repeating units of PTFF and PTFB bithiophene fluorene-fluorenone units and bithiophene fluorene-benzothiadiazole units respectively in the polymer backbone as shown in Figure 6.

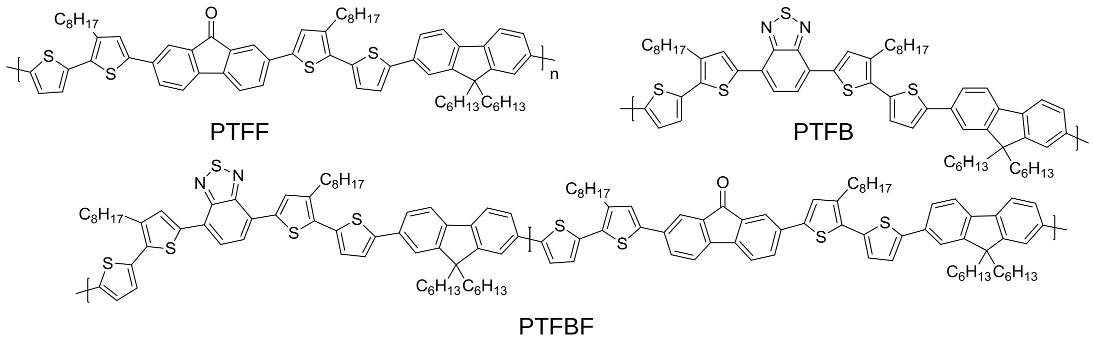


**Figure 6: Low band gap fluorene-based Donor-Acceptor polymers PTFF, PTFB and PTFBF**

In the fifth chapter, a new series of ladder type polymers based on indacenodithiophenes is developed incorporating the fluorenone and the benzothiadiazole core units. The particularity of the indacenodithiophene structures lies at the fusion of benzene ring and the thiophene rings to reinforce the planarity and may improve the charge transport. Three different polymers are synthesised with the chemical structures as follow.

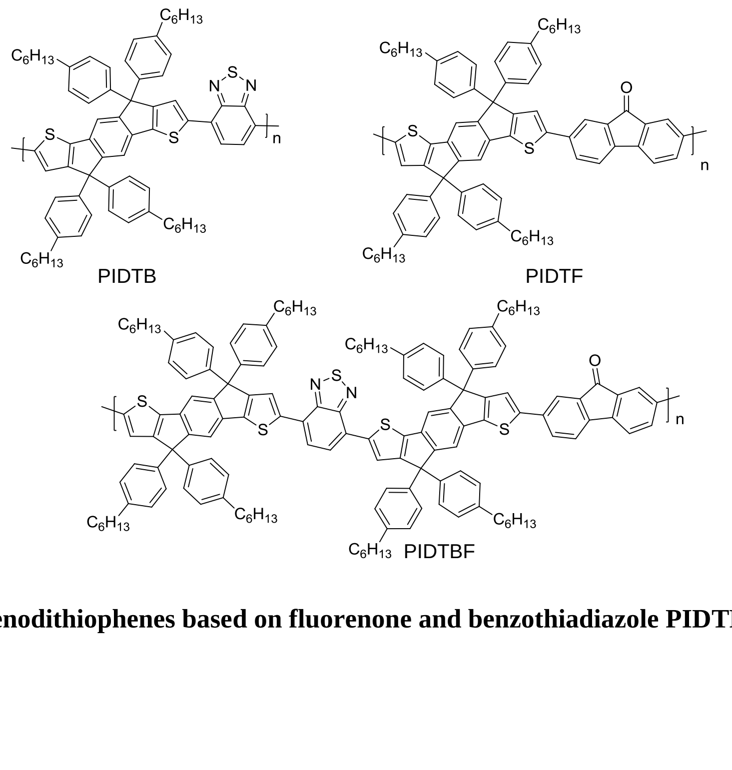


**Figure 7: Polyindacenodithiophenes based on fluorenone and benzothiadiazole PIDTF, PIDTB and PIDTFB**

After presenting all the different results of this thesis, the chapter Conclusion and Perspective will resume the major results obtained and future work. The studies of these oligomers and polymers will provide understanding of the design rules for controlling the intrinsic parameters of the electron donor materials, and show their influence on the device performance in photovoltaic cells. Further device optimisations of the photovoltaic cells are not the subject of this thesis, and can be extensively studied in future work in order to increase the photovoltaic cell performance.

In appendix are included different experimental methods and materials, as well as the synthesis procedures for preparing the different new materials.

# III. Reference


1 European Photovoltaic Industry Association, http://www.epia.org/

2 A.E. Becquerel, Compt. Rend. Acad. Sci. 9 (1839) 145.

3 L. El Chaar, L.A. Lamont, N. El Zein, Review of photovoltaic technologies, Renewable and Sustainable Energy Reviews, Volume 15, Issue 5, June 2011, Pages 2165-2175

4 http://www.nrel.gov/docs/fy04osti/35489.pdf

5 Repins, I., Contreras, M. A., Egaas, B., DeHart, C., Scharf, J., Perkins, C. L., To, B. and Noufi, R. (2008), 19·9%-efficient ZnO/CdS/CuInGaSe2 solar cell with 81·2% fill factor. Prog. Photovolt: Res. Appl., 16, 235–239

6 M.A. Green, K. Emery, Y. Hishikawa, W. Warta, E.D. Dunlop, Solar cell efficiency tables (version 39), Progress in Photovoltaics: Research and Applications 20 (2012) 12–20.

7 K. Branker, M.J.M. Pathak, J.M. Pearce, A review of solar photovoltaic levelized cost of electricity, Renewable and Sustainable Energy Reviews, Volume 15, Issue 9, December 2011, Pages 4470-4482

8 D. M. Powell , M. T. Winkler , H. J. Choi , C. B. Simmons , D. Berney Needleman and T. Buonassisi, Crystalline silicon photovoltaics: a cost analysis framework for determining technology pathways to reach baseload electricity costs, Energy Environ. Sci., 2012,5, 5874-5883

9 B. Parida, S. Iniyan, R. Goic, A review of solar photovoltaic technologies, Renewable and Sustainable Energy Reviews, Volume 15, Issue 3, April 2011, Pages 1625-1636

10 a) B. Azzopardi, C.J.M. Emmott, A. Urbina, F.C. Krebs, J. Mutale, J. Nelson, Economic assessment of solar electricity production from organic-based photovoltaic modules in a domestic environment, Energy & Environmental Science 4 (2011) 3741–3753.

b) S. Lizin, S. Van Passel, E. De Schepper, L. Vranken, The future of organic photovoltaic solar cells as a direct power source for consumer electronics, Solar Energy Materials and Solar Cells, Volume 103, August 2012, Pages 1-10

11 T. Tromholt, E. A. Katz, B. Hirsch, A. Vossier, and F. C. Krebs, Effects of concentrated sunlight on organic photovoltaics, Appl. Phys. Lett. 96, 073501 (2010)

12 F.C. Krebs, T.D. Nielsen, J. Fyenbo, M. Wadstrøm, M.S. Pedersen, Manufacture, integration and demonstration of polymer solar cells in a lamp for the Lighting Africa initiative, Energy & Environmental Science 3 (2010), 512–525.

13 C.J. Brabec, Organic photovoltaics: technology and market, Solar Energy Materials and Solar Cells 83 (2004) 273–292.

14 a) F. C. Krebs, H. Spanggard, T. Kjær, M. Biancardo, J. Alstrup, Large area plastic solar cell modules, Materials Science and Engineering: B, Vol. 138, Issue 2, 2007, 106-111

b) F.C. Krebs, Roll-to-roll fabrication of monolithic large-area polymer solar cells free from indium-tin-oxide, Solar Energy Materials and Solar Cells 93 (2009) 1636–1641

15 L. Dou, J. You, J. Yang, C-C. Chen, Y. He, S. Murase, T. Moriarty, K. Emery, G. Li and Y. Yang, Tandem polymer solar cells featuring a spectrally matched low-bandgap polymer, Nature Photonics 6, 180–185 (2012)

16 http://newsroom.ucla.edu/portal/ucla/ucla-engineers-create-tandem-polymer-228468.aspx

# CHAPTER 1: ORGANIC PHOTOVOLTAIC: SMALL MOLECULES PHOTOVOLTAIC CELLS & POLYMERS PHOTOVOLTAIC CELLS

# I. Introduction on organic photovoltaic

## I.1. Organic and hybrid organic-inorganic photovoltaic cells: Background

Organic photovoltaic cells [1,2,3,4,5,6,7] can be defined as solar cells based on organic semiconductors such as polymers or small molecules. In Hybrid solar cells, organic semi-conductors are combined to inorganic materials[8,9,10.] Organic and hybrid solar cells have been a subject of increasing interest by researchers and industries because of their potential to deliver low cost solar cells. [11,12]

The first organic solar cell based on a single layer also known as Schottky diode was reported in 1958 when Kearns and Calvin worked with magnesium phthalocyanines (MgPh), measuring a photovoltage of 200 mV[13]. In 1977, Shirakawa and coworkers[14] presented the electrically doped polyacetylenes that resulted in increasing electrical conductivity $10^7$ times higher than the undoped polymers. This discovery paved the way for extensive research on π-conjugated organic systems which had been long time considered as insulating materials. In 1986, C.W Tang[15] showed the first bilayer organic solar cell (cf Figure 8) based on small molecules. The active layer was fabricated using copper phthalocyanine (CuPc) and a perylene-disimide derivatives (PDI) both materials where deposited by evaporation using vacuum process. The power conversion efficiency obtained was closed to 1%[15].

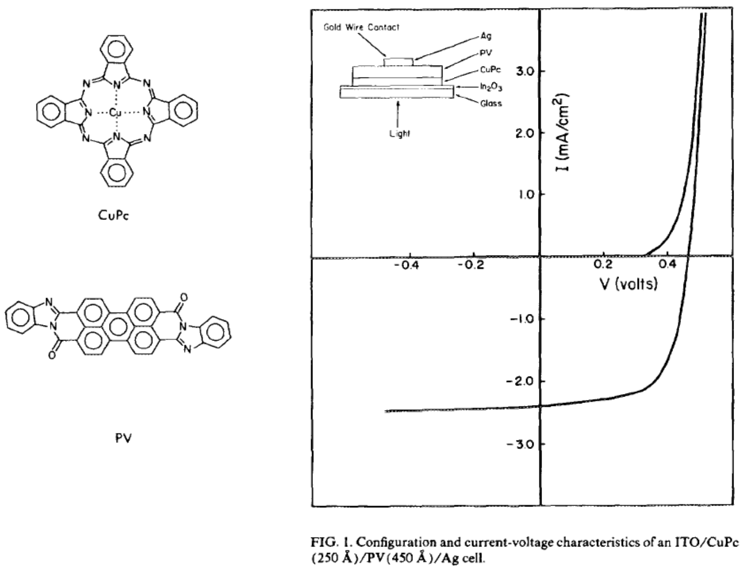


**Figure 8: Tang's bilayer solar cell[15]**

In 1992, Sariciftci, Heeger and coworkers[16] demonstrated the photoinduced electron transfer in composites of semi-conducting π-conjugated polymers based on poly[2-methoxy-5-(2-ethyl-hexyloxy)-1,4-phenylene-vinylene] MEH-PPV as electron donor and Buckminster fullerene C60 as an electron acceptor. The discovery allows fundamental understanding of the photovoltaic phenomenon in organic solar cell. Hence extensive research was developed ever since for new organic materials and on increasing the power conversion efficiency of such solar cells. In 1995, Heeger and coworkers [17] developed an interpenetrating network comprising a semi-conducting pi-conjugated polymer as electron donor and a new soluble fullerene derivative [6,6]-phenyl-C61-butyric acid methyl ester PCBM as an electron acceptor, this gives rise to the development of the so-called bulk heterojunction solar cells. Figure 9 showed the configuration of bulk heterojunction and the materials used in the active layers. The principle of the organic solar cell will be further described below.

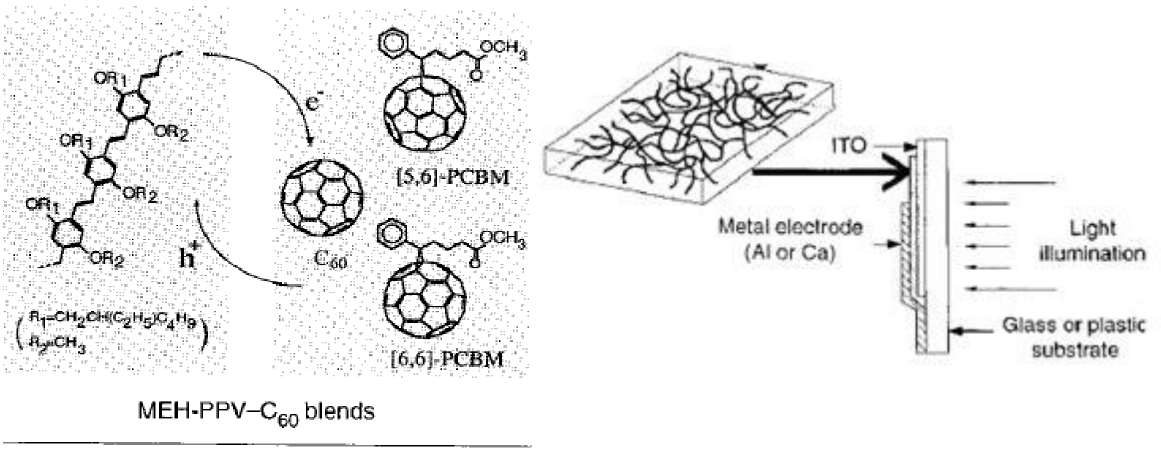


**Figure 9: Bulk heterojunction configuration solar cell proposed by Heeger and coworkers[17]**

Based on this interpenetrating network or bulk heterojunction concept, a close variant to the all organic photovoltaic cells is the organic-inorganic hybrid solar cells which are based on inorganic semiconductors as electron acceptors and π-conjugated polymers or small molecules as electron donors which have been also been largely studied for the last 10 years[18,9,10] Inorganic nanoparticles such as cadmium selenide (CdSe)[19], lead sulfide (PbS)[20,21], titanium dioxide ($TiO_2$)[22], zinc oxide (ZnO) [23] have been blended with conjugated polymers to form organic–inorganic hybrid BHJ solar cells[24]. In our laboratory, P. Reiss and coworkers[25] reported a hybrid solar cell based on P3HT and nanorods of CdSe exhibiting a power conversion efficiency of 1.44% with an active area of 0.28cm².

## I.2. Operating principle of organic photovoltaic cell

In organic photovoltaic cells the active layer is composed of two organic semiconducting materials, a donor material and an acceptor material, in between two electrodes (cathode and anode. Donor materials are molecules which are rich in electrons and can easily release its electron. Acceptor materials are molecules poor in electron and are more readily reduced than more electron rich materials (donor). [2,7]

The operating principle of organic photovoltaic cell can be described in these following key steps[16] depicted as shown in Figure 10 :

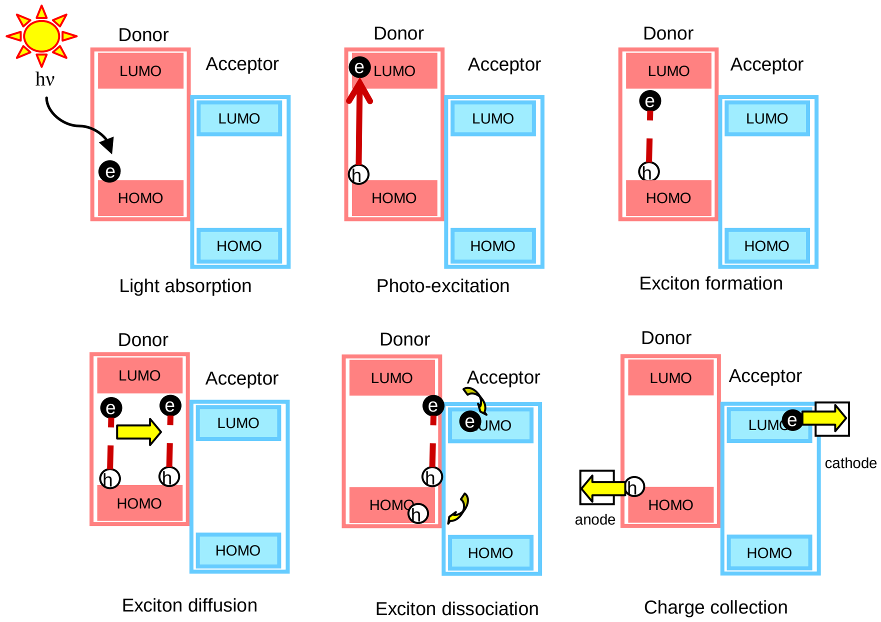


**Figure 10: The operating principle of organic photovoltaic**

1. Light absorption and photo-excitation

Photons can be absorbed both by the donor and acceptor materials but in organic solar cells they are mainly absorbed by the donor materials. For each material, the photons absorption depends on its energy band gap. The energy band gap (Eg) is defined as the difference in energy between the highest occupied molecular orbital (HOMO) and the lowest unoccupied molecular orbital (LUMO) energy levels. It is important for the materials to absorb maximum photons of the solar spectrum. The solar spectrum, the photon flux density and the fraction of photon flux calculated from the integral of the photon density between 300 nm to 2500 nm are presented in Figure 11 with the corresponding correlation between the energy band gaps of materials according to the absorption edge or offset wavelength in the table at the bottom.

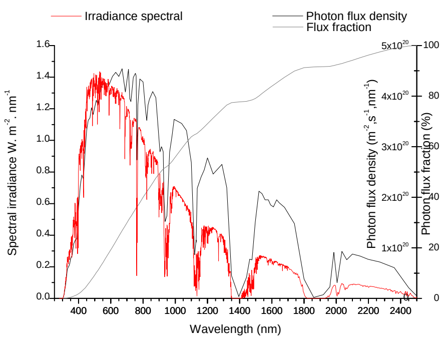


**Figure 11: Optical absorption edge (offset) wavelength with the corresponding energy band gap and solar photon flux. Reproduced from NREL data[26]**

| Absorption offset wavelength (nm) | Energy band gap (eV) | Solar photon flux (%) [from 300 nm to 2500 nm] |
|---|---|---|
| 400 | 3.1 | 2 |
| 500 | 2.5 | 9 |
| 600 | 2.1 | 18 |
| 650 | 1.9 | 23 |
| 700 | 1.8 | 30 |
| 750 | 1.6 | 35 |
| 800 | 1.5 | 40 |
| 900 | 1.4 | 48 |
| 1000 | 1.2 | 55 |

**Table 1:Optical absorption edge (offset) wavelength with the corresponding energy band gap and solar photon flux. Reproduced from NREL data**

In the domain organic semiconductors, donor materials which exhibit energy band gap of less than 2 eV are considered as low band gap materials[5]. The low band gap materials allow photon absorption more than 620 nm. Low band gap materials can therefore absorb more than 20 % photon flux of the sun. The energy absorbed from the photons ($E_{photon}$) then allows excitation of the electron to promote from its ground state to an electronic excited state.

2. Exciton formation

In organic semiconductor upon photon energy absorption, the molecules once promoted to an electronic excited state, a spatially localized electron-hole pair that is bound by coulombic interactions is formed. This hole-electron pair is called exciton. The exciton is electrically neutral with exciton binding energies ranging from 0.1 eV to as high as 1.5 eV as summarised by Knupfer[27].

3. Exciton diffusion

The formed excitons need to delocalize in the donor materials towards the interface of donor-acceptor to allow the dissociation process via an electron-transfer process. These excitons diffuse during their short lifetime (of femtosecond)[28,29] with diffusion lengths generally limited to about 5–20 nm in organic materials[30,31]. This consideration is important to the design of active layer architectures. If the excitons created far away from the donor-acceptor interface, it will relax back to its ground state They eventually recombine by emitting a photon or decaying via thermalization (non radiative recombination)[16].

4. Exciton disscociation

At the donor-acceptor interface, the excitons can dissociate by transferring the electron which is located in the LUMO of the donor to the LUMO of acceptor. The driving force required for this charge transfer is the difference in ionization potential (LUMO) of the excited donor and the electron affinity (HOMO) minus the exciton Coulomb binding energy[16]. Moreover, exciton dissociation can take place only if the energy gained by the electron when being transferred from the LUMO of the donor to the LUMO of the acceptor compensates the binding energy of the intrachain exciton. The difference of these two energy levels which is required to facilitate the electron transfer process and to allow charge separation is estimated by Scharber and coworkers[32] to be at least of 0.3 eV.

5. Charge transport and collection

After exciton dissociation, the free charges need to be transported to the corresponding electrodes and extracted by external circuit to generate current. The hole will be transported in the donor material and the electron will be transported in the acceptor material. Hence, the donor materials are called hole transporting material while acceptor materials are called electron transporting material. Therefore it is necessary to create percolation pathways for each type of charge carrier to the electrodes to avoid recombination via trapping into isolated domains. The charge carrier extraction is driven by internal electric field across the photoactive layer caused by the different work function electrodes for holes and electrons. Moreover, $\pi$–stacking phenomenon in organic semi-conductors can lead to higher mobilities[33]. For example discotic liquid crystals[34,35] can display high carrier mobilities due to their spontaneous organization into one-dimensional columns. Therefore, strong electronic coupling between molecules, which is associated with excellent overlap between the $\pi$-conjugated systems of adjacent molecules, is a necessary criterion for ensuring high mobilities as well as the overlap between the orbitals of each molecule[36].

## I.3. Device architectures

Typical organic photovoltaic cell configuration can be depicted as follow:

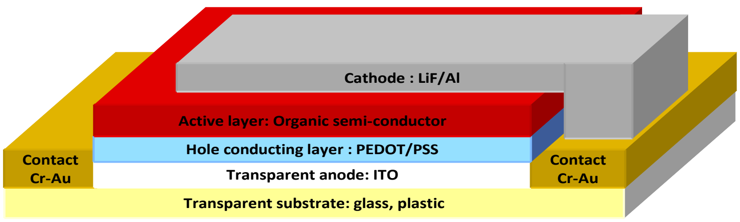


**Figure 12: Device configuration of organic photovoltaic cell**

The active layer of the photovoltaic cell containing organic semi-conductor is sandwiched between two electrodes: a transparent anode layer of indium tin oxide (ITO) and as cathode a layer of metal electrode such as aluminium. To allow better extraction of the charges, the bottom electrode is modified with a hole conducting layer. The hole conducting layer commonly used is a conducting polymer (poly [3,4 (ethylenedioxy)thiophene]:poly(styrene sulfonate)] PEDOT:PSS which also allows to smoothen the rough surface of ITO. On the aluminium electrode a thin layer of lithium fluoride (~1 nm) LiF is deposited between the active layer surface and the cathode electrode.

In order to meet the specific requirement for efficient photon to charge conversion, different device architectures have been developed configurations as depicted in Figure 13.

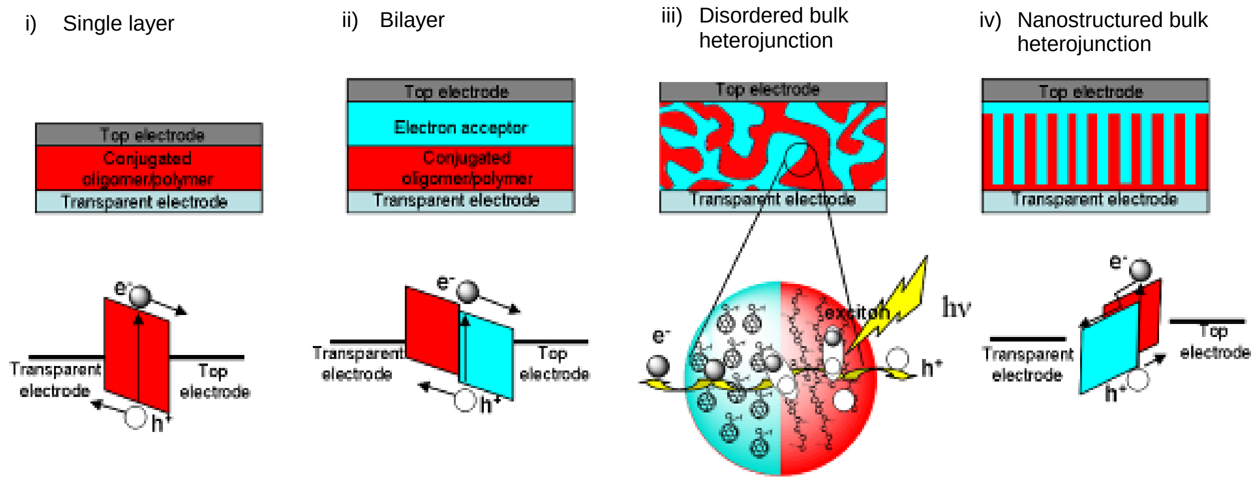


**Figure 13: Device architectures of the active layer of the photovoltaic cells in four different configurations: single layer, bilayer, bulk heterojunction and nanostructured bulk heterojunction**

## Single layer cell

The first organic photovoltaic cell is composed of a single layer of one conjugated semi-conductor sandwiched between two metal electrodes[13]. This cell configuration is also called Schottky junction solar cell. In a Schottky junction solar cell, only a small region of the layer (depletion region) can take place the photo-induced charge transfer by the dissociation of the excitons close to the interface of the metal electrode as showed in Figure 14 below.

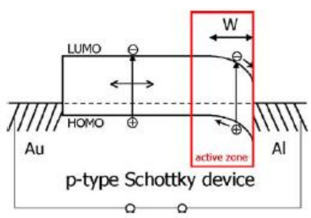


**Figure 14: Dissociation of excitons to form charge carriers in a limited zone in a single layer device[2]**

Therefore the power conversion efficiency is very low due to poor charge carrier and unbalanced charge transport. The structure is simple but an absorption covering the entire visible range is rare using a single molecule. The photoactive region is often very thin and since both positive and negative photo-excited charges may travel through the same material recombination losses are generally high.[7]

### Bilayer cells

A bilayer heterojunction contains a layer of donor material (or hole transporting material) and a layer of an acceptor material (or electron transporting material). Among pioneer work based on this configuration was published by Tang in 1986[15]. The layers are mainly deposited by layer by thin film evaporation. A bilayer heterojunction is the simplest model of operating donor-acceptor photovoltaic cell with the working principle as described previously.

Bilayer cells benefit from separated charge transport layers that ensure connectivity with the correct electrode and give a separated charge carrier only a small chance to recombine with its counterpart. However as described previously, the photogenerated excitons diffusion is limited to the diffusion length of ca. 5-20 nm. Therefore the disadvantage of this bilayer configuration is the limited effective thickness of a bilayer configuration is of a maximum of 20 nm for each donor and acceptor material (see Figure 15).

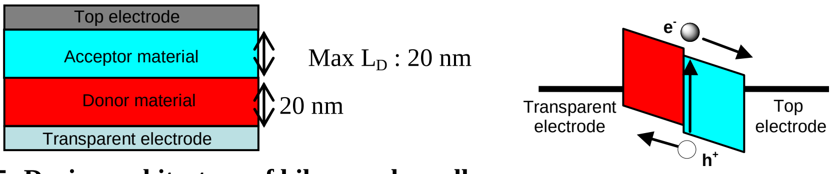


**Figure 15: Device architecture of bilayer solar cell**

### Bulk heterojunction cells

To overcome the problem of limited active zone, a revolutionary concept was proposed by Heeger and coworkers[17] which consists of blending the two semiconductors, the electron donor and the electron acceptor. The two materials are usually processed from solution and deposited by spin coating to form a thin film with typical thicknesses comprised between few tens of nanometers and few hundreds of nanometers. The two materials form a non miscible blend and create a disordered percolating network domain throughout the bulk or volume as represented in Figure 16 below.

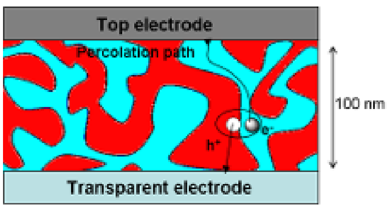


**Figure 16: Percolation pathway in bulk heterojunction**

In order to meet the requirement of effective dissociation site within exciton diffusion length of *ca*. 20 nm, nano-size disordered network of the two materials is therefore necessary. In addition to allow effective charge carriers transport to the corresponding electrode, percolating phase segregation is required to avoid excitons decay or charge recombination in isolated traps. Therefore it is of great importance to control the nanoscale morphology of the thin films to ensure effective power conversion[37,38].

Among the advantages of bulk heterojunction configuration are, an increase of effective thickness for absorption in the active layer for up to 100 nm as compared to the bilayer configuration (max of 40 nm) and the ease of fabrication by solution process and film cast deposition. Typical method is by dissolution of the two materials in a good solvent and spin-coating the blend on substrate. Bulk heterojunction configuration is currently the most used architecture device in the organic photovoltaic field giving good power conversion efficiency up to 9.1%[39].

### Nanostructured bulk heterojunction

Nanostructured bulk heterojunction configuration is an ideal architecture for solar cell as the two active materials donor and acceptors are highly organised and form ordered pathway connected to the corresponding charges extracting electrodes as shown in Figure 17. The scale of each pathway should not exceed 20 nm in width.

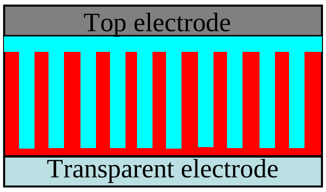


**Figure 17: Device architecture of highly ordered nanostructured bulk heterojunction solar cell**

Few examples of this configuration in the literature are self-assembled inorganic nanostructures[40,41-42], di-block copolymers[43,44, 45,46]and nanoimprint lithography[47], as seen in Figure 18 examples of each case.

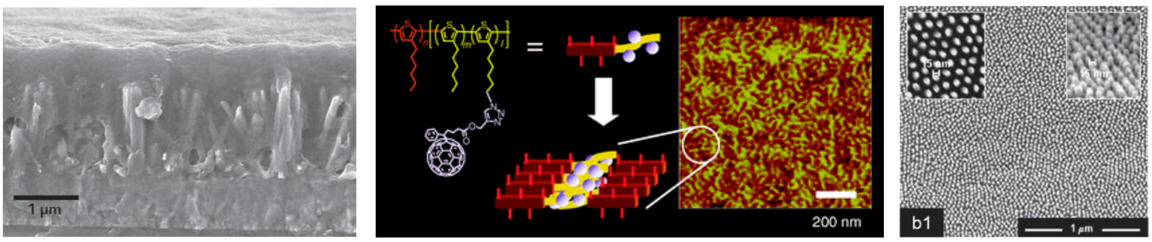


**Figure 18: Example of nanostructured device: SEM cross section view of P3HT inflitrated into TiO2 nanowires prepared by Weickert et al[40], fullerene attached diblock copolymer[48], nanoimprint P3HT polymer[49] .**

Nanostructured devices are quite tricky to manufacture, and the power conversion efficienciesuntill now are still lower compared to the disordered bulk heterojunction.

# II. Materials for organic photovoltaic cells

Organic photovoltaic cells are composed of all organic semiconductors. Some examples of organic semiconductors used in organic photovoltaic cells are polymers, oligomers, dendrimers, dyes, pigments, liquid crystals, organo-mineral hybrid materials and other small molecules which are based on conjugated π electrons[1,6, 50,51,52]. A π-conjugated system is made of an alternation between single and double bonds. Ethene butadiene and benzene are basic representative elements of conjugated systems.

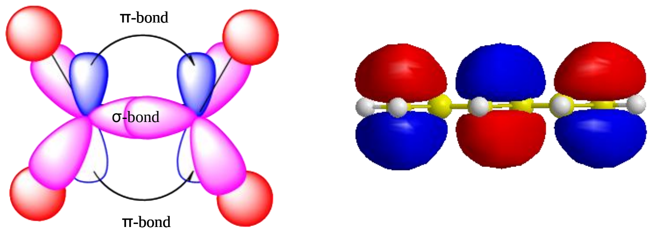


**Figure 19: Pictorial description of pi-orbital of ethylene and the conjugation orbitals in butylenes**

The essential property which comes out from conjugation is that the π electrons are much more mobile than the σ electrons; they can jump from site to site between carbon atoms with a low potential energy barrier as compared to the ionisation potential. The π electron system has all the essential electronic features of organic materials: light absorption and emission, charge generation and transport[7]

## II.1. Organic semiconductors: Acceptor materials

Acceptor materials are electron deficient materials capable of accepting reversibly electrons that are transferred to it[36]. The key parameter for electron acceptor is the position of the lowest unoccupied molecular orbital (LUMO) energy level. The lower the LUMO energy level of the molecule is, the easier for the molecule can be reduced and thus it shows a higher degree of electron accepting capability. Another crucial parameter for the acceptor semiconductor is its electron transporting properties or electron mobility. This is of crucial importance to enable efficient transfer of electron to the corresponding electrode[36].

Below we present several pertinent examples of acceptor materials used in organic solar cells. The commonly known acceptor material is the family of fullerenes derivatives with the classical Phenyl-C61-Butyric-Acid-Methyl Ester, PCBMC60 that was first demonstrated by Yu and coworkers[17]. To date, fullerenes derivatives, with their good electron mobility, excellent electron accepting capability and good miscibility with conjugated polymers, are considered the most successful acceptors[36,53,54]. In Table 2 below is presented the performance in photovoltaic cells of several fullerenes derivatives in combination with polymer P3HT as electron donor.

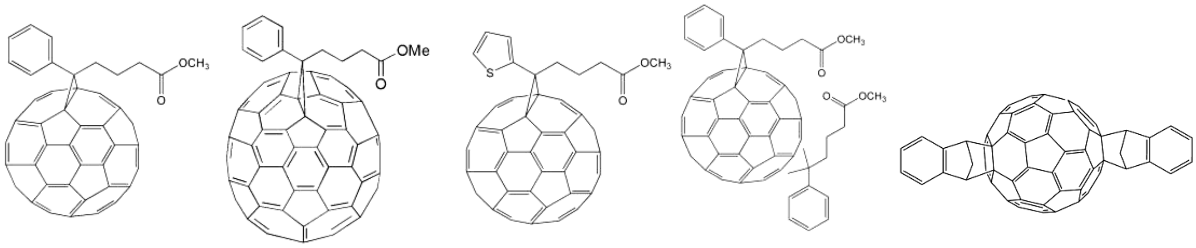


[60]PCBM [70]PCBM [60]ThCBM bis[60]PCBM ICBA

**Figure 20: Examples of fullerenes derivatives used in organic photovoltaic cells**

| Donor | Acceptor | Voc (V) | Jsc (mA/cm²) | FF | PCE (%) | Ref |
|---|---|---|---|---|---|---|
| P3HT | PCBM C60 | 0.58 | 10.8 | 0.62 | 3.9 | [55] |
| P3HT | PCBM C70 | 0.59 | 10.8 | 0.63 | 4.1 | [56] |
| P3HT | BisPCBM C60 | 0.73 | 9.14 | 0.68 | 4.5 | [57] |
| P3HT | ThCBM C60 | 0.62 | 10.33 | 0.62 | 4.0 | [58] |
| P3HT | ICBA | 0.84 | 9.67 | 0.67 | 5.4 | [55] |

**Table 2: Performance of photovoltaic device using different types of PCBM with P3HT as donor materials**

The table shows good power conversion efficiency for all type of fullerenes, and an increase performance for solar cell using fullerenes indene-C60-bisadduct (ICBA) which has a higher LUMO energy of 0.17 eV than PCBMC60. This allows for an immediate increase of open circuit voltage. Other examples of acceptor materials include perylene-disimides (PDI) families. PDI-based small molecules, and polymers have attracted interest as alternative acceptors since they exhibit wide and intense absorption, high electron mobilities, electron affinities similar to those of fullerenes and each of these properties can be readily tailored through either variation of substituents on the imide nitrogen atoms or on the perylene core[13,59]. For example Friend and coworkers[60] have demonstrated bulk heterojunction solar cells based on PDI as acceptor affording good power conversion efficiency PCE of 1.95 % when combined with discotic liquid crystalline molecule.

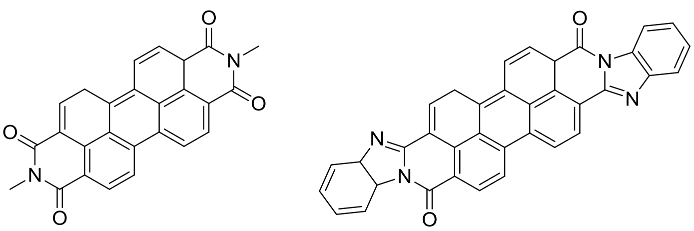

**Figure 21: Example of perylene based acceptor**

Another emerging class of accepting materials are the carbon nanotubes (CNT)[61,62]. A recent review on utilisation of carbon nanotubes in organic solar cell was published by Bernard

Ratier and coworkers[63]. They discuss the potential of utilisation these materials to increase the crystallinity and ordering of the bulk heterojunction active layer. However for the moment, solar cells based on carbon nanotubes exhibit of lower power conversion efficiency as compared to fullerenes PCBM. Higher performance in photovoltaic devices were observed in the case of ternary blend using donor materials, carbon nanotubes and PCBM in the active layers for example previous work in the laboratory by Berson and coworkers[64] on solar cells based on the composite of P3HT:PCBM:CNT (1:1:0.1%) leads to a power conversion efficiency of 2.0%. Ternary blends using molecular donor materials, carbon nanotubes and PCBM in the active layers were also investigated recently in our laboratory.[65]

The development of organic semiconductors to be used as acceptor materials in organic photovoltaic has been far less numerous than the donor materials. However the more and more new acceptors are presented in the literature[66,67,68] and many others can be found in a recent review by Anthony and coworkers[36] on acceptor materials for organic solar cells.

## II.2. Organic semiconductors: Donor materials

Organic semiconductors to be used as donor materials have been extensively developed for applications in photovoltaic cells. The donor type materials can be for example polymers or small solution processable molecules. The donor materials are often combined with fullerene derivatives (commonly PCBMC60 and PCBMC70) as electron acceptor material in bulk heterojunction solar cells. The requirements for the design of new donor materials are good light absorption (the molecules need to match with the solar emission spectrum), appropriate energy levels positioning to allow efficient exciton dissociation and a high open circuit voltage, as well as high molecular weights polymers and high solubility in blend-processing solvent.

As we have discussed previously, the most important characteristics to determine the optical and electronic properties of the π-conjugated systems are the band gap and the positions of HOMO and LUMO energy levels. Therefore much work on the development of new donor materials have been focusing on the band gap engineering to fine tuning the energy band gap and the positions of the HOMO LUMO energy levels of the π-conjugated systems [69,70].

## II.3. Band gap engineering

Band gap engineering of the π-conjugated systems has been a research interest for years to design useful light absorbing materials. One of the most straightforward ways to lower the band gap of molecules is by increasing the conjugation length of the systems[71,72] as shown in Figure 22.

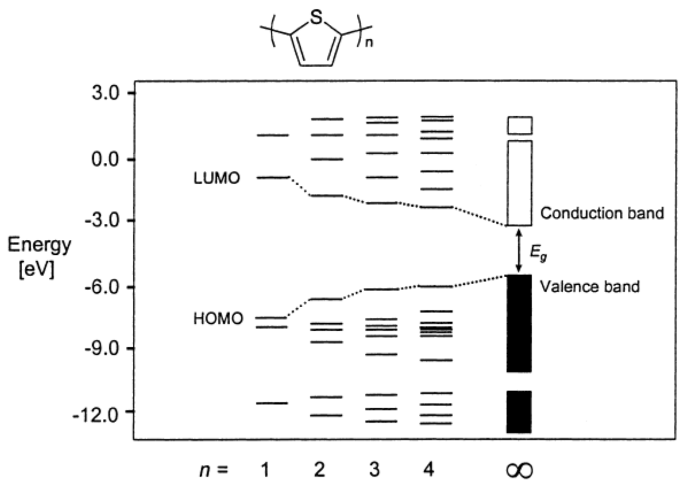


**Figure 22: Theoretical calculation of electronic properties showing the diminution of the band gap by increasing the conjugated system[72]**

An excellent review presenting the different strategies to finely tune the band gap of pi-conjugated systems was pusblished by J. Roncali[73]. The structural factors influencing the band gap of a material derived from a linear π-conjugated system can be briefly described in the Figure 23.

$$Eg = E_{BLA} + E_{Res} + E_{Sub} + E\theta + E_{Int}$$

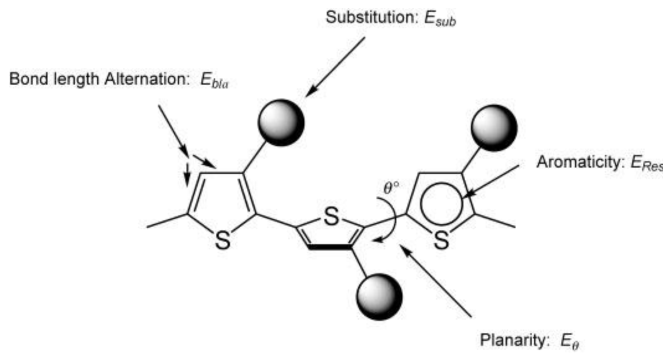


**Figure 23: Structural factors determining the band gap of materials derived from linear π-conjugated systems. Eg = Energy band gap, $E_{BLA}$= Bond length alternation energy, $E_{Res}$= Energy resonance of aromatic rings, Esub= Energy contribution from substitution group, $E_{\theta}$= angle torsion energy, and $E_{int}$= intermolecular interactions**

### Energy bond length alternation

The origin of the finite energy gap in conjugated systems lies in the alternation of single and double bonds. Equal length of single and double bonds may exhibit complete delocalisation of π-electron and reduce the band gap. Therefore a first approach by reducing the bond length alternation ($E_{BLA}$) (thus suppression of Peierls instability) will decrease the HOMO-LUMO energy band gap. Good example is in the case of polyacetylene[14]. Although the bandgap of these polymers depends mainly on $E_{BLA}$, several other specific parameters also influenced the energy band gap as described below.

## Energy resonance

In aromatic systems, like poly (p-phenylene) or polythiophene, the mesomeric forms of the systems are not energetically equivalent. Simple considerations show that the energy needed to switch from the aromatic to the quinoid form directly depends on the aromatic stabilisation resonance energy (Eres) of the aromatic unit. The aromatic form is energetically more stable and the quinoid form has a higher energy. Therefore the band gap decreases as a function of increasing quinoid character of the backbone[74]. A good example is seen for the case of polyphenylene and polythiophene as shown in Figure 24.

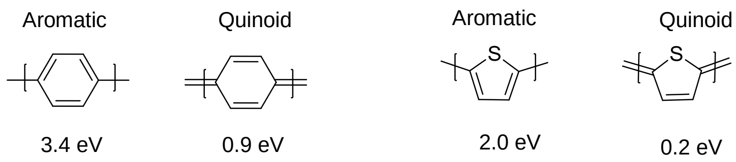


**Figure 24: The band gap for the ground-state aromatic structures of polyphenylene and polythiophene largely reduced in quinoid forms**

Using this strategy, fusion of thiophene ring with a benzenic ring allows stabilizing the quinoid form thus decreasing the band gap. The first poly(benzo[c]thiophene) ou polyisothianaphtene PITN synthesised by Wudl and coworkers showed a band gap of 1.1 eV to be compared with polythiophenes with 2 eV[75]. Example of other quinoid structures are for examples poly(thieno[3,4-b]pyrazine[76] with low band gap Eg of 0.85 eV and poly(thieno[3,4-b]-thiophene)[77] of Eg =0.8-0.9 eV.

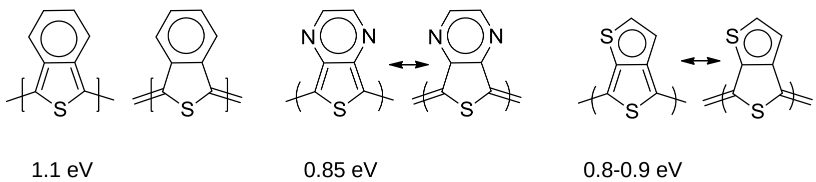


**Figure 25: Examples of polymers with stabilised quinoidal form; polyisothianaphtene, poly(thieno[3,4b]pyrazine), and poly(thieno[3,4-b]thiophene)**

## Angle torsion energy

One way to decrease the angle torsion energy is by reinforcing the planarity of the system. For example the vinylene linkage allows suppression of the rotational freedom of thiophene-thiophene rings thus reducing the band gap of the system. The Figure 26 shows structural modification of linear oligothiophene by addition of double bond vinylene linkage resulting the maximum wavelength to shift to higher wavelength. In the case of the poly thiophenevinylene the band gap of 1.7 eV[78] is therefore lower than polythiophenes of 2 eV.

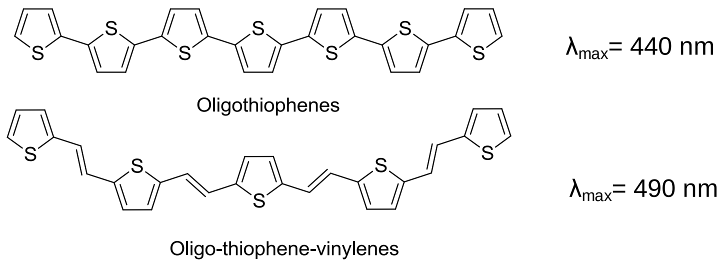


**Figure 26: Example of structural modification showing the effect of adding double bonds between the thiophene units in the molecule.**

Another solution to suppress the rotational freedom involves the rigidification of the conjugated system by covalent bridging of elemental units. Rigidification of the conjugated systems allows suppressing the bond length alternation[79]. Ladder type molecules are good example of structural modification. Ladder type molecules are defined as uninterrupted series of rings connected by sterically restrictive links around which rotation cannot occur without bond rupture[80]. For example in the case of polymer based on fused thiophenes rings as shown in Figure 27, afford and increase of the planarity of the polymer backbone resulting to a reduced band gap of 1.35 eV.


**Figure 27: Examples of fused thiophene ring system**

### Substitution group effect

Introduction of electron-donating or electron-withdrawing groups represents the most immediate way to tune the HOMO and LUMO energy levels positions of a conjugated system. Introduction of electron-donating groups to a conjugated system produces the rise of the HOMO level, generally accompanied by a reduction of band gap. For example, the inductive effect of simple alkyl groups decreases the oxidation potential of the thiophene ring by approximately 0.20 V[81]. To the contrary, by introducing electron withdrawing groups or electron acceptor groups such as cyano, carboxy, or nitro in the backbone can results to an increase in the oxidation potential [82] thus lowering the HOMO level position.

### Alternating Donor Acceptor Approach

To take advantage of the effect of the electron donating group and the electron withdrawing group on the electronic energy levels, one of the most effective ways to decrease the band gap is by alternating electron rich donor subunits and electron deficient acceptor subunits along the π-conjugated backbone. The donor-acceptor approach (D-A) was first proposed by Havinga and coworkers in the early 90's[83]. They designed small band gap polymers based on polysquaraine and poycroconaines down to 0.5 eV (Figure 28).

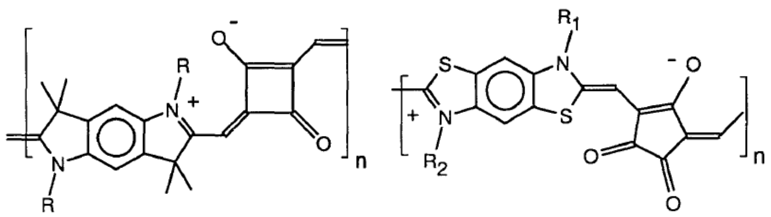


**Figure 28 : First donor-acceptor polymers polysquaraines and polycroconaines with band gaps of 0.5 eV**

In Figure 29 is presented a diagram of molecular orbital theory, for a better understanding of the principle of the band-gap engineering and fine tuning of the energy levels.

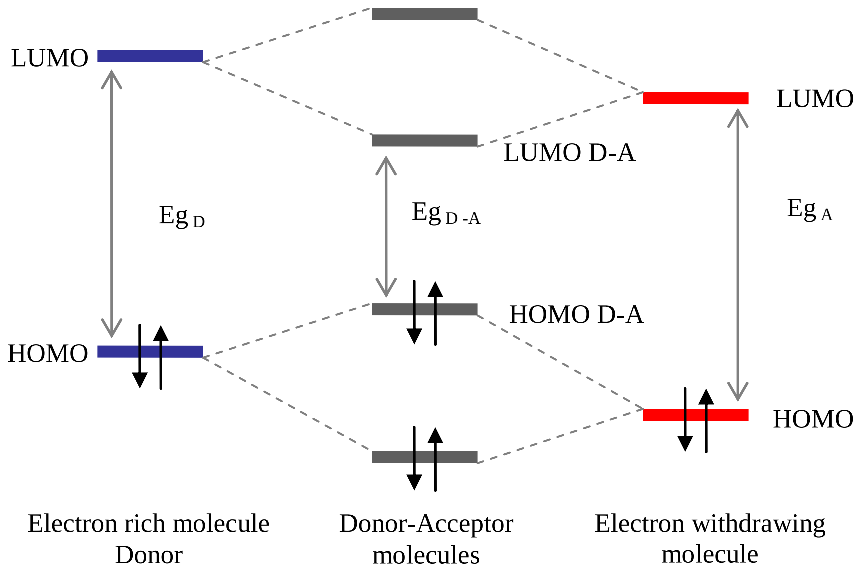


**Figure 29 : Synergistic combination of molecular orbital to form a new molecule with a lower energy band gap**

The electron rich molecule (D) with a higher position of HOMO energy levels than the HOMO of electron deficient molecules will interact and hybridise to form two new HOMOs positions of the donor-acceptor molecules. Similarly, the LUMO of the donor will interact with the LUMO of acceptor to form two new hybridized LUMOs of the donor-acceptor molecules. The newly formed hybridized orbitals for the D-A molecules will have higher HOMO energy levels and lower LUMO energy levels. This leads rather straightforwardly to a narrower energy band-gap thus new materials with a broad absorption across the solar spectrum. These interesting features have therefore attracted many groups to develop new absorbing materials using this D-A approach, for example conjugated oligomers[84,52] and conjugated polymers [69,70,85,86]. The donor-acceptor polymers are also known as push-pull polymers.

# III. Pi-conjugated small molecules as donor materials for organic photovoltaic

Small molecules pi-conjugated systems have gained a lot of interest in the field of organic photovoltaics. Small molecules are particularly interesting as they are monodisperse with well-defined chemical structures. In terms of material preparation fabrication protocols are reproducible and they are also easier to purify compared to the polymers. This allow to a better understanding of molecular structure and property relationships. Small molecules organic solar cells can be either processed by evaporation techniques[87,88] or by solution processed techniques provided that they are functionalised by solubilising chains.[89] The current state-of-art for small molecules solar cells by evaporation-processed techniques are of power conversion efficiency PCE of 10.7 %[90] while for solution processed small molecules, a high performance of PCE of 6.7 %[91] was obtained recently in a bulk heterojunction configuration.

Some of the examples of vacuum evaporation solar cells are presented below in Figure 30. The small molecules used as donor materials are for examples highly ordered and planar molecules such as phtalocyanines[15, 92], squaraines[93], and oligothiophenes[88] with fullerenes as electron acceptor in solar cells.

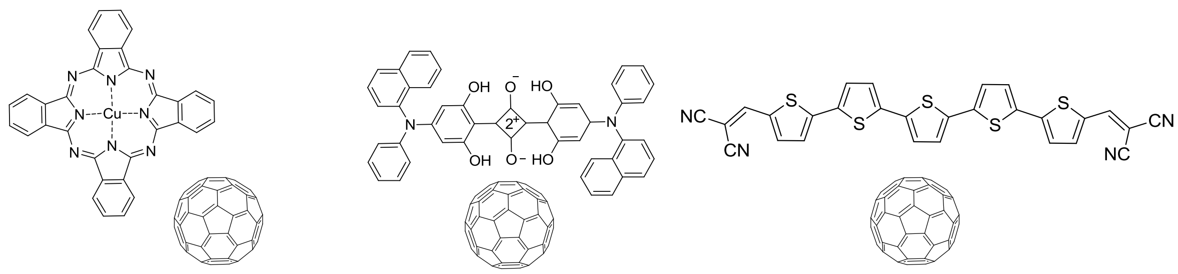


Phtalocyanines/C60
3.5% [92]
Bilayer Planar heterojunction

Squaraines/C60
5.7% [93]
Bilayer Planar heterojunction

DCV-thiophenes/C60
5.2% [88]
Bilayer Planar heterojunction

**Figure 30: Examples of vacuum evaporation process organic solar cells**

Vacuum evaporation processes offer the possibility to prepare multilayer device structures with high structural ordering and can therefore afford high power conversion efficiency. This technique is also efficient for tandem configuration of multiple layers. However the disadvantages of this technique are high processing cost, and limited thickness.

Examples of solution processed photovoltaic cells are presented in Figure 31 below with different types of molecules. The small molecules used are for examples diketopyrolopyroles[94], oligothiophenes[101], low band gap D-A-D oligomers[95], dendrimers[96], liquid crystals[97], triphenylamines derivatives[98] mixed with fullerenes acceptor in bulk heterojunction configuration. A good example of single component solar cells donor-acceptor dyads are presented by L. Bu and coworkers forming highly ordered films comprising well-defined and tunable alternating D-A lamellar[99], etc.

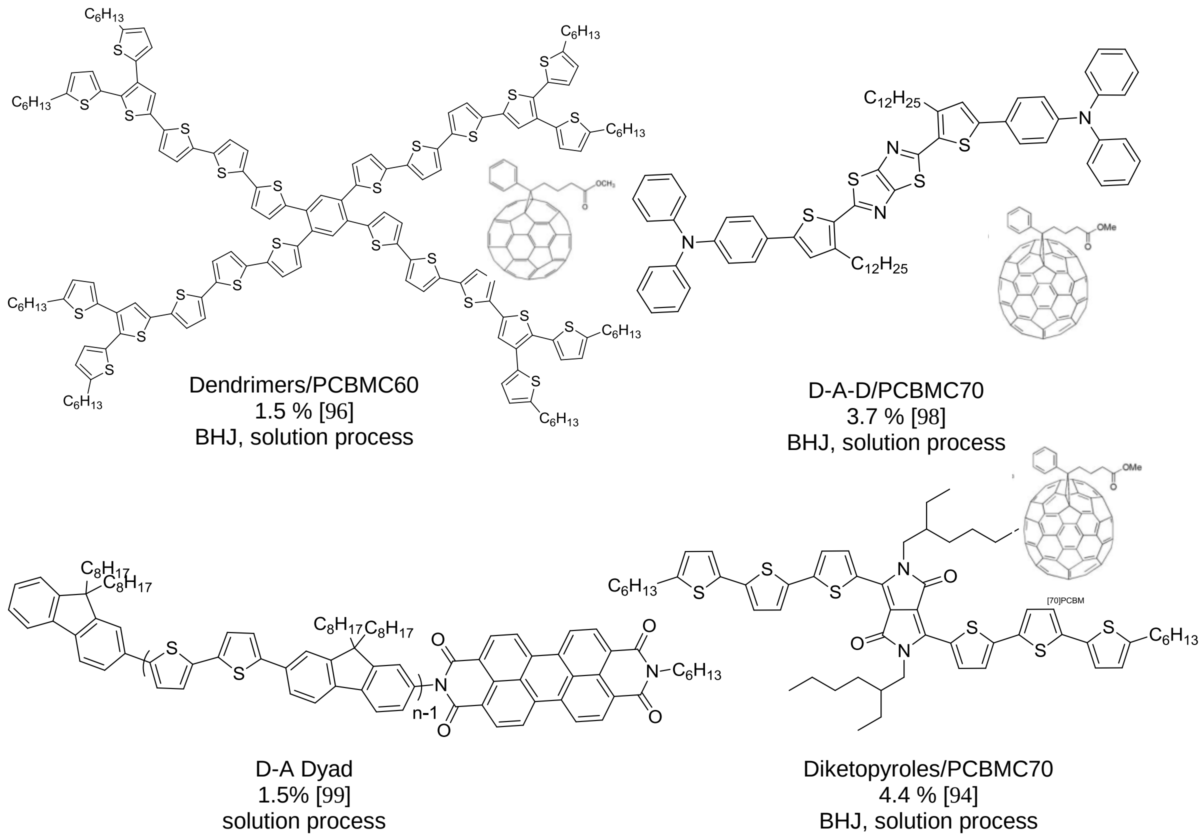


**Figure 31: Solution processed solar cells based on small molecules. BHJ= bulk heterojunction solar cells**

For further discussion, we will focus here only on few examples of solution-processable small molecules showing high efficiencies in organic photovoltaic in bulk heterojunction configuration, which can be useful for the discussion for this work. The presented molecules showed hereafter followed the donor-acceptor concept with a common thiophene-based electron rich moieties which are good transporting molecules coupled with different electron deficient groups.

Chen and coworkers [100] have made two similar small molecules based on linear oligothiophenes as electron rich segment with different electron withdrawing groups as end group noted as oligomers DCN7T[100], DCAO7T[101] as presented below in Figure 32.

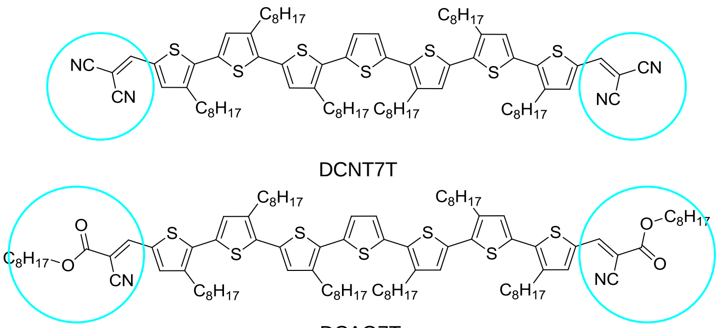


| Oligomer | HOMO (eV) | LUMO (eV) | Eg (eV) |
|---|---|---|---|
| DCN7T | -5.10 | -3.40 | 1.70 |
| DCAO7T | -5.13 | -3.29 | 1.84 |

| Blend | Voc (V) | Jsc (mAcm-2) | FF | PCE (%) |
|---|---|---|---|---|
| DCN7T:PCBMC60 | 0.88 | 12.4 | 0.34 | 3.07 |
| DCAO7T:PCBMC60 | 0.86 | 10.7 | 0.55 | 5.08 |

**Figure 32: Effect of electron withdrawing group and solubilising alkyl chain on the end group of two molecules DCNT7T and DCAO7T**

We can observe that changing the electron-withdrawing end group of DCN7T from nitrile group (-CN) to alkyl cyanoacetate (-$COOC_8H_{17}$) groups, the electronic properties of the showed small changes on the LUMO energy levels, and both showed low energy band gap of 1.7 and 1.8 eV. However the the power conversion efficiency of the oligomer DCAO7T is much higher of 5 % compared to the power conversion efficiency of DCN7T of 3 %. The key parameter that contributes for this increase is the improvement in fill factor from 34 % to 55 %. The authors attributed this improvement to a better film morphology with the addition of solubilising alkyl chains in both ends.

**Following this work on the oligomer DCAO7T, Chen and coworkers[102] further modify the molecules structures by changing the electron donating segment and by using the same electron withdrawing end group. They developed a new oligomer incorporated a dithienosilole group which has strong electron donating capabilities in the molecule backbone as shown in**

Figure 33.

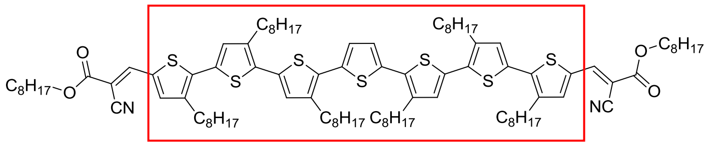

DCAO7T

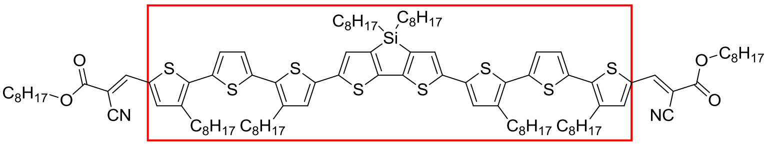

DCAO3TSi

| Oligomer | HOMO (eV) | LUMO (eV) | Eg (eV) |
|---|---|---|---|
| DCAO7T | -5.13 | -3.29 | 1.84 |
| DCAO3TSi | -4.95 | -3.26 | 1.69 |

| Blend | Voc (V) | Jsc ($mAcm^{-2}$) | FF | PCE (%) |
|---|---|---|---|---|
| DCAO7T:PCBMC60 | 0.86 | 10.7 | 0.55 | 5.08 |
| DCAO3TSi: PCBMC60 | 0.80 | 11.5 | 0.64 | 5.84 |

**Figure 33: Solution processed small molecules based on dithienosilole group on the donor segment DCAO3TSi compared to the DCAO7T of thiophene based donor segment**

The strong electron donating group and the coplanar skeleton have been described to contribute to lowering of the band gap to -4.95 eV for the oligomer DCAO3TSi compared to DCAO7T molecules with linear seven thiophenes units (Eg= -5.13 eV ). Furthermore with the coplanar skeleton also contribute to enhance the charge transport (hole mobility of 1.8 $10^{-4}$ $V.cm^2.s^{-1}$). Furthermore both small molecules DCAO7T and DCAO3TSi possess eight solubilising group on the molecules backbones allow to obtain solution processed small molecules with good film forming properties.

The current state of art for small molecules is with power conversion efficiency of 6.7 % with bulk heterojunction configuration published by Bazan's group[91]. They developed a small molecule DTS($PTTh_2$)$_2$ incorporating the strong electron donating dithienosilole group, coupled with a new strong electron withdrawing group [1,2,5]thiadiazolo[3,4-c]pyridine which is a close analogue to the benzothiadiazole group and thiophene-alkyl as end capping group. The molecule structure is shown in Figure 34.

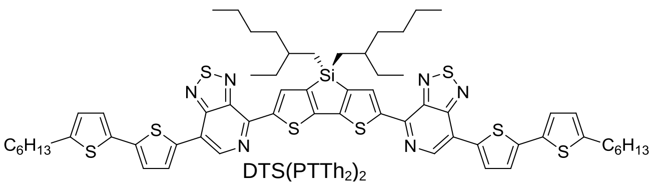

DTS(PTTh2)2

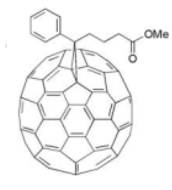

[70]PCBM

**Figure 34: Bulk heterojunction based on small molecules of DTS(PTTh2)2: PCBMC70 exhibit highly efficient bulk heterojunction in presence of diiodooctane as additif**

This particularly high efficiency was obtained with the used of small percentages of solvent additive 1,8-diiodooctane during the film forming process. In absence of the solvent additive during the process they obtained a power conversion efficiency of only 4.52 %. This improvement of efficiency was related to a reduced domain size in the bulk heterojunction active layer[91].

These few examples of small molecules showed the importance of the choice of electron donating group, electron withdrawing group in order to form synergistic combination in the D-A small molecules. Furthermore, solution processed small molecules and good film forming properties have been highlighted to afford efficient bulk heterojuntion solar cells with optimum nano-scale morphology.

As the main advantages of small molecules are they are mono disperse and reproducible, they are particularly interesting for photovoltaic application. The high power conversion efficiencies obtained for small molecules are encouraging and can be as competitive as polymer based solar cells. For further reading, few recent reviews cover plethora of small molecules used for organic photovoltaic applications.[52,103]

# IV. Pi-conjugated polymers as donor materials for organic photovoltaic

Semi-conducting polymers have been a fast-moving subject of research for the past decade. Among pioneer in the field of semi-conducting polymers Heeger has classified the polymers into three generations according to its evolution[104]. The First Generation materials are based on early work on polyacetylene. The Second Generation polymers involve for examples the soluble poly(alkylthiophenes) and the soluble poly(phenylene-vinylene) PPV. And the Third Generation polymers are the new generation of semiconducting polymers with more complex molecular structures and showing improved properties and processability. The Second Generation and Third Generation semiconducting polymers are widely used in photovoltaic applications.

The first conjugated polymers used as donor materials in photovoltaic cells are soluble poly[2-methoxy-5-(2-ethyl-hexyloxy)-1,4-phenylene-vinylene] MEH-PPV reported by Wudl and coworkers[16] in 1992. MEH-PPV polymer solar cells show quite low efficiencies in the range of 1% due to its low solubility[105]. Further research have therefore been made involving more soluble poly paraphenylene vinylenes polymers groups, for example the widely used poly[2-methoxy-5-(3,7-dimethyloctyloxy)-1,4-phenylene-vinylene] MDMO-PPV. Extensive research on the PPVs polymers to optimize their opto-electronic properties has only afforded efficiency up to 3% [106] using regioregular MDMO-PPV. Until 2002-2003 the best performances were obtained with these polymers[107,54]. The major limitation of PPVs polymers are relatively low hole mobility and narrow light absorption with an absorption edge around 500 nm[108]. To overcome these limitations, polythiophenes with higher hole mobility and broader absorption spectra than the PPVs up to 650 nm are suitable materials for photovoltaic applications. In 2002, Brabec and coworkers [109] demonstrate a solar cell with power conversion efficiency of 2.5 % using regioregular poly(3-hexylthiophene) P3HT and PCBMC60. Research on P3HTs and similar polyalkylthiophenes has allowed improved solar cells notably by optimization of the nanoscale morphology with power conversion efficiencies up to 5%[110,111].

The need for new classes of polymers has been developed with different conjugated polymers such as polythienylenevinylenes (PTV)[112,113], polyfluorenes (PF)[114,115], polycarbazoles[116,117], polythienothiophenes (PTT) [118], ladder types polymers [119] such as polybenzodithiophenes(PBDT) [120], poly(indacenothiophenes) [121], and many others[122,123,124,125,126].

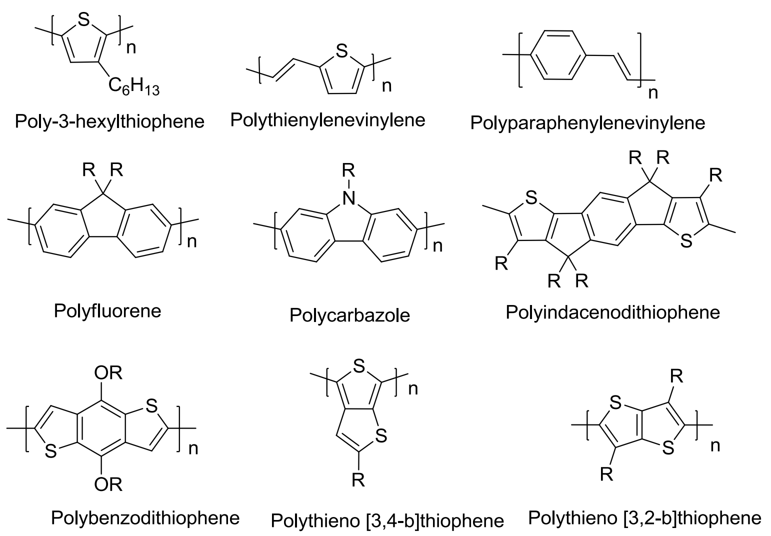


**Figure 35: Structures of common conjugated polymers used in solar cells**

We present here in the Table 3 some of the polymers showing good power conversion efficiency of more than 5 %.

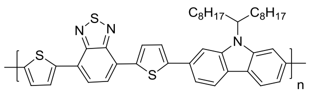
PCDTBT

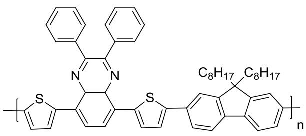
NP-7

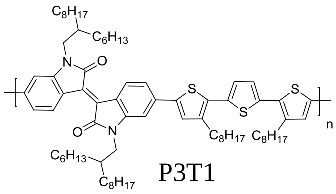
P3T1

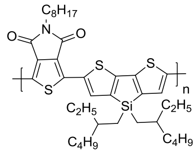
PDTSTPD

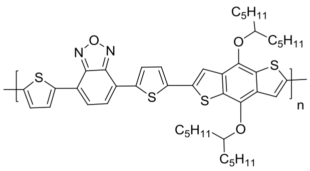
PBDT-BO

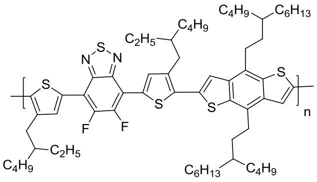
PBnDTD-TffBT

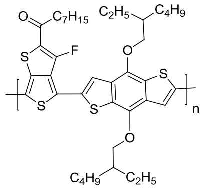
PBDTTT-CF

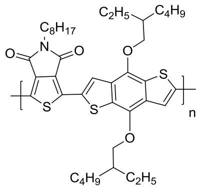
PBDT-TPD

**Figure 36: Few examples of low band gap D-A polymers which show high power conversion efficiency in bulk heterojunction solar cells of more than 5 %.**

| Polymers | Mn (kDa) | HOMO (eV) | LUMO (eV) | Eg (eV) | Voc (V) | $J_{sc}$ ($mAcm^{-2}$) | FF | PCE (%) | Ref. |
|---|---|---|---|---|---|---|---|---|---|
| PCDTBT | 36 | -5.45 | -3.60 | 1.85 | 0.88 | 10.6 | 0.66 | 6.1 | 116 |
| N-P7 | 17 | -5.37 | n.a | 1.95 | 0.99 | 9.7 | 0.57 | 5.5 | 127 |
| P3T1 | 73 | -5.82 | -3.83 | 1.99 | 0.70 | 13.1 | 0.69 | 6.3 | 128 |
| PBDT-BO | 47 | -5.34 | -3.45 | 1.89 | 0.89 | 13.6 | 0.51 | 6.1 | 129 |
| PBDTTT-CF | n.a | -5.22 | -3.45 | 1.77 | 0.76 | 15.2 | 0.67 | 7.4 | 118 |
| PBnDTD-TffBT | 34 | -5.54 | -3.33 | 2.21 | 0.91 | 12.9 | 0.61 | 7.2 | 130 |
| PBDT-TPD | 35 | -5.40 | n.a | 1.73 | 0.85 | 11.5 | 0.68 | 6.6 | 131 |
| PDTSTPD | n.a | -5.57 | -3.88 | 1.69 | 0.88 | 12.2 | 0.68 | 7.3 | 132 |

**Table 3: Few examples of efficient bulk heterojunction solar cells based on polymer/fullerenes PCBMs as acceptor with polymers macromolecular parameters, electronic properties and photovoltaic parameters * n.a (not available)**

We will further discuss the results of the Table 3 in the different requirements to be met to obtain high efficiency solar cells.

# V. Requirements for an enhanced performance in organic solar cells

There are several ways to enhance the performance of organic solar cells. We can look at it in two perspectives:

- Intrinsic properties of materials
- Extrinsic properties : Device parameters

## V.1. Intrinsic properties of the materials

### Broad absorption spectrum: Low band gap donor polymers

The most important key parameter for donor materials is to exhibit an optimized absorption spectrum in order to harvest a maximum energy by absorbing photons over a wide range of wavelengths of the solar emission spectrum. This implies the reduction of the band gap of the materials. We have previously presented several ways to decrease the band gap of the polymers. We present here three examples of highly absorbing polymers of low energy band gap poly(carbazole dithiophene-benzothiadiazole) PCDTBT[116], poly (dithienosilole-thienopyrrolodione) PDTSTPD[132] and poly(benzodithiophene-thienothiophene) PBDTTT-CF[101].

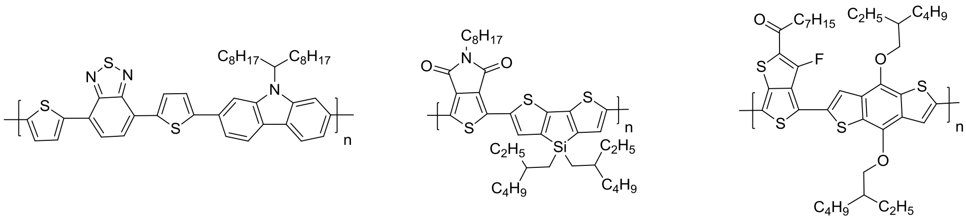

| PCDTBT | PDTSTPD | PBDTTT-CF |
|---|---|---|
| Eg=1.85 eV | Eg=1.69 eV | Eg=1.77 eV |
| PCE= 6.1 % | PCE= 7.3% | PCE= 7.4 % |

**Figure 37: Low band gap polymers exhibiting high power conversion efficiencies in solar cells**

The presented polymers possess band gap between 1.7 eV to 1.9 eV, which cover the spectrum in the UV-Visible up to 730 nm, have afforded high power conversion efficiency up to 7 %. The low band gap properties of these polymers are a result of combination of alternating strong electron rich segment and a strong electron poor segment in the polymer back bone, planar structures in the segment and quinoidal form polymers. Scharber and coworkers[32] proposed a model to estimate the efficiency of solar cells based on band gap and LUMO position of the different components of the heterojunction (see Figure 38). The model was calculated by using PCBM as electron acceptor material and varying the band gap of the donor.

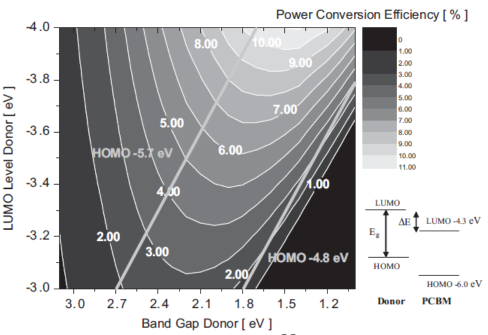


**Figure 38: Proposed model by Scharber and coworkers[32] to predict power conversion efficiency based on band gap of polymers. Contour plot showing the calculated energy-conversion efficiency (contour lines and colors) versus the bandgap and the LUMO level of the donor**

The model proposed that an ideal donor polymer can achieved a power conversion of 10 % with a band gap of 1.2 to 1.8 eV. The current density (Jsc) of the cell can be correlated to the band gap of the materials as more absorption of photons implies more photo-generated charges thus increases the current density.

### Increasing the oxidation potential

A simple correlation can also be made between the oxidation potential of the donor or its HOMO energy levels and the open circuit voltage of the photovoltaic cell[133]. The open circuit voltage as proposed by Scharber and coworkers can be estimated as[32]:

$$Voc = 1/e * ( | E_{Donor}\ HOMO - E_{PCBM} LUMO | ) -0.3\ eV$$

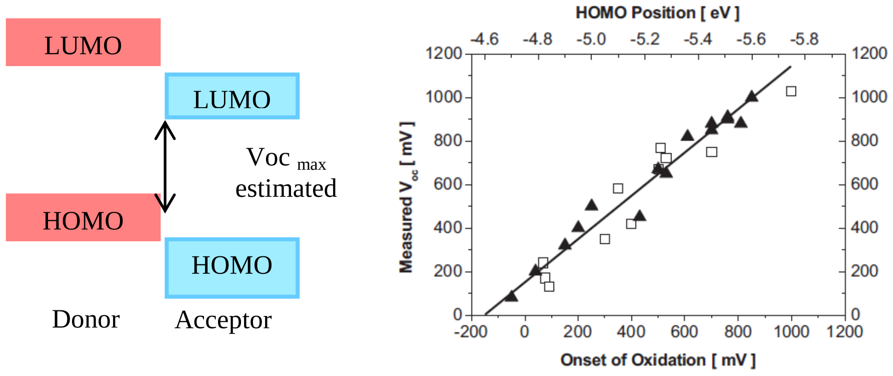


**Figure 39: (Left) Correlation between the difference of HOMO and LUMO energy levels and open circuit voltage in . (Right) Open-circuit voltage (Voc) of different bulk-heterojunction solar cells based on donor polymers/fullerene PCBM plotted versus the oxidation potential or HOMO position of the donor polymer used in each individual device. The straight line represents a linear fit with a slope of 1. (Model proposed by Scharber and coworkers[32]**

Based on this empirical formula we can make first approximation for polymers having oxidation potential of 0.6 V-1 V which correspond to HOMO energy levels of -5.2 eV and -5.8 eV are the best candidates in order to obtain Voc of more than 0.6 V up to 1 V.

The oxidation potential (or HOMO position) of a material depends on its capability of being oxidized or in other words its capability of losing reversibly one electron. The easier for the material to loose one electron, the lower its oxidation potential is. Therefore if we take example of some of conjugated polymers mentioned above, the polyfluorene exhibit a higher degree of oxidation potential than polythiophene as the electron rich thiophenes heteroaromatic rings are easier to oxidize than the fluorene. Svensson and coworkers developed series of polymers solar cells incorporating fluorene group and benzothiadiazole with PCBM as acceptor achieving a Voc of 1.04 V[134].

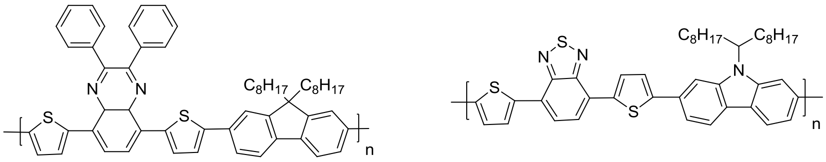


NP-7
HOMO= -5.37 eV  Voc=0.99 V
PCE= 5.5 %

PCDTBT
HOMO=-5.45 eV Voc= 0.88 V
PCE=6.1 %

**Figure 40: Two examples of polymer based on polyfluorene N-P7[127] and polymer carbazole PCDTBT[116] having high Voc with low lying HOMO energy levels**

The polymer NP-7[127] as shown in Figure 40 which integrates the fluorene units to its polymer backbone obtained a high Voc of 0.99 V. The carbazole-containing polymers are also a good example of materials exhibiting a high Voc as mentioned in the table 1, the polymer PCDTBT[116] owing a Voc close to 0.9 V.

Gang Li and coworkers[118] further developed a series of polymers with enhanced open circuit voltage, based on the poly(benzodithiophenes-thienothiophene) PBDTTT (as shown in Figure 41). By replacing the substitution group by a more electron withdrawing group, a lower oxydation potential can be achieved. Using fluorine-substituted polymers, solar cell with the high power conversion efficiencies up to 7.4 % can be achieved with a Voc of 0.76 V.

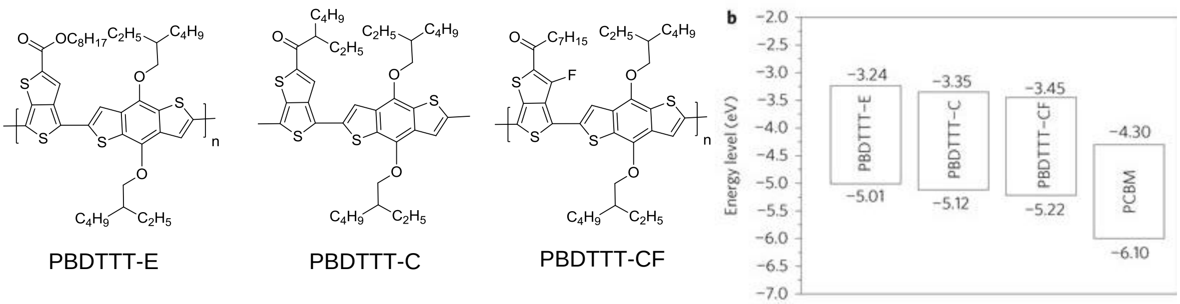


**Figure 41: Effect of electron-withdrawing substitution group on the HOMO energy level of low band gap polymers based on poly(benzodithiophenes-thienothiophene) PBDTTT**

## V.2. Extrinsic properties of materials in blend and device parameters

### Better control of morphology

As the typical exciton diffusion length in conjugated polymers is limited to ca.5-20 nm, the donor and acceptor materials should form nanoscale interpenetrating networks within the whole photoactive layer to ensure an efficient dissociation of excitons.[37,38]. Efficient bulk heterojunction (BHJ) solar cells require good phase segregation between the donor materials and the acceptor materials. An appropriate morphology of the active layer is probably one of the key parameter to achieve a good fill factor[135] of the solar cell and high short circuit current density.

Different parameters influencing the morphology of the blend of polymers (or oligomers) with PCBM as acceptors are presented here and some of these parameters are discussed below.

- Chemical structure of the materials (solubilising chain in the molecules, molecular weight and polydispersity, intermolecular interactions, etc)[136,137]
- Solvent for the solution process deposition[138,139]
- Donor acceptor materials weight ratio
- Overall concentration of the solution (related to the solubility limits of the materials)
- Film thickness
- Temperature of deposition
- Post-treatment of the cast films (thermal annealing[140] or solvent annealing)
- Additives addition[91,141,142]

1. **Chemical structure of the materials:**

One approach to obtain a nanoscale interpenetrating network is to increase the mesoscopic order and crystalline order of each constituent in the bulk. For example regioregular P3HT can self organize into a microcrystalline structure and as a result of efficient interchain transport of charge carriers allow to obtain high short circuit current density in solar cells[136,143]. In the case of poly (3-hexylthiophene) Brinkmann and coworker demonstrate that high molecular weight polythiophenes (> 10 KDa) result to a decrease of crystalline order in films[137] as a result of increasing amorphous polymer chains. The observed differences in morphology and structure of the oriented thin films as a function of Mw reflect different crystallization modes which are attributed to the presence or to the absence of chain folding.

Another study made by Inganas and coworkers[144] showed an increase performance of solar cell made with polymers having a higher degree of polymerisation as shown in Figure 42.

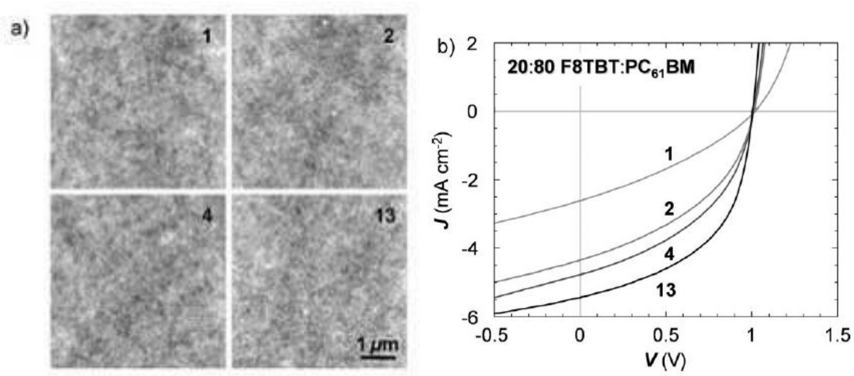


**Figure 42: AFM images of the polymer solar cells with the numbers represent the molecular weight Mn of the polymers in kDa and I-V curves of the corresponding solar cell**

Higher molecular weight polymers showed a good solution processability and optimum domain size between the polymer and PCBM, therefore increase the current density Jsc of the solar cells.

For solution processable conjugated oligomers or polymers, solubilising alkyl side chains are required. The rigid conjugated polymers are usually required to carry flexible side chains to ensure that polymers have certain solubility in organic solvents. A study made by Wang and coworkers[145] gives a good example of the influence of the side chain.

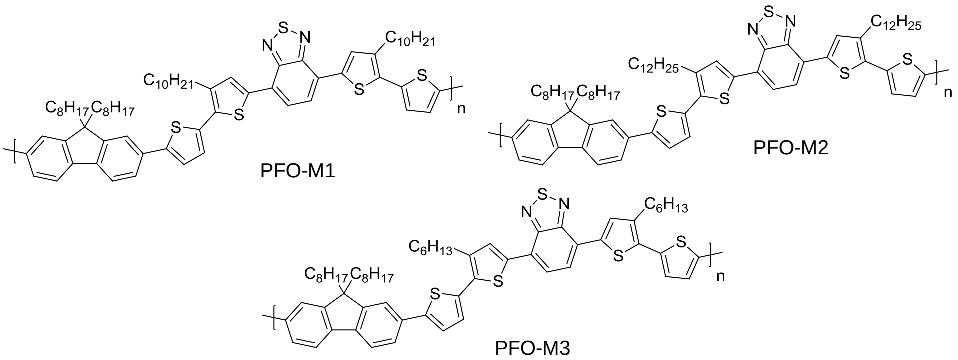


**Figure 43: Chemical structure of polymer fluorene-benzothiadiazole PFOs**

| Polymers | Mn (kg $mol^{-1}$) | HOMO (eV) | LUMO (eV) | Eg (eV) | Voc (V) | $J_{sc}$ (mA$cm^{-2}$) | FF | PCE (%) | Ref. |
|---|---|---|---|---|---|---|---|---|---|
| PFO-M1 | 10.7 | -5.4 | -3.13 | 2.27 | 0.90 | 3.97 | 0.41 | 1.82 | 145 |
| PFO-M2 | 0.9 | -5.37 | -3.17 | 2.37 | 0.70 | 2.80 | 0.38 | 0.74 | |
| PFO-M3 | 6.2 | -5.34 | -3.22 | 2.12 | 0.86 | 5.86 | 0.52 | 2.63 | |

**Table 4: Macromolecular properties, electronic properties and photovoltaic properties of fluorene based polymers PFO-Mx**

This study showed rational counter-balance impact of the side-chain length and the suitable position on the polymer back bone on solar cell performance. Furthermore, the length of the solubilising alkyl chains also play major role on polymer chain packings[146,147].

## 2. Processing conditions: Effect of solvent, annealing and additives

Annealing effect[140] on P3HT/PCBM solar cells have resulted on increase of cristallinity and demixing of donor and acceptor [148]. This effect will likely apply to other material combinations that favor crystallization. Annealing treatment can be performed either by thermal annealing or by solvent annealing.

Solvent of processing play a major key role to ensure high solubility of each active layer component. In bulk hetero-junction solar cells using fullerenes derivatives as acceptors, chlorobenzene and dichlorobenzene have shown high solubility of these materials[149]. The evaporation rate of the solvent will also have influence primarily to tune the cristallinity of the materials after solution deposition on substrates. High boiling point solvent will have slower drying rate therefore enabling the polymers to self organize in the film. Utilisation of solvent mixture can also allow an improve morphology of the active layer[138].

Studies on the effect of additives addition for example alkanedithiol and diiodooctane on the morphology of the blend of polymers/oligomers with PCBM have been developed in the last few years[141,142,91] notably for the new class of low band gap donor materials where thermal annealing do not further improve the crystalline order in the bulk heterojunction. Bazan and coworkers published recently in their papers showed the influence in the blend of small molecules DTS(PTTh2)2 and PCBMC70, by additioning diiodooctane as additives during the solution process increases density by increasing local crystallinity and improving packing at the donor−acceptor interface[150].

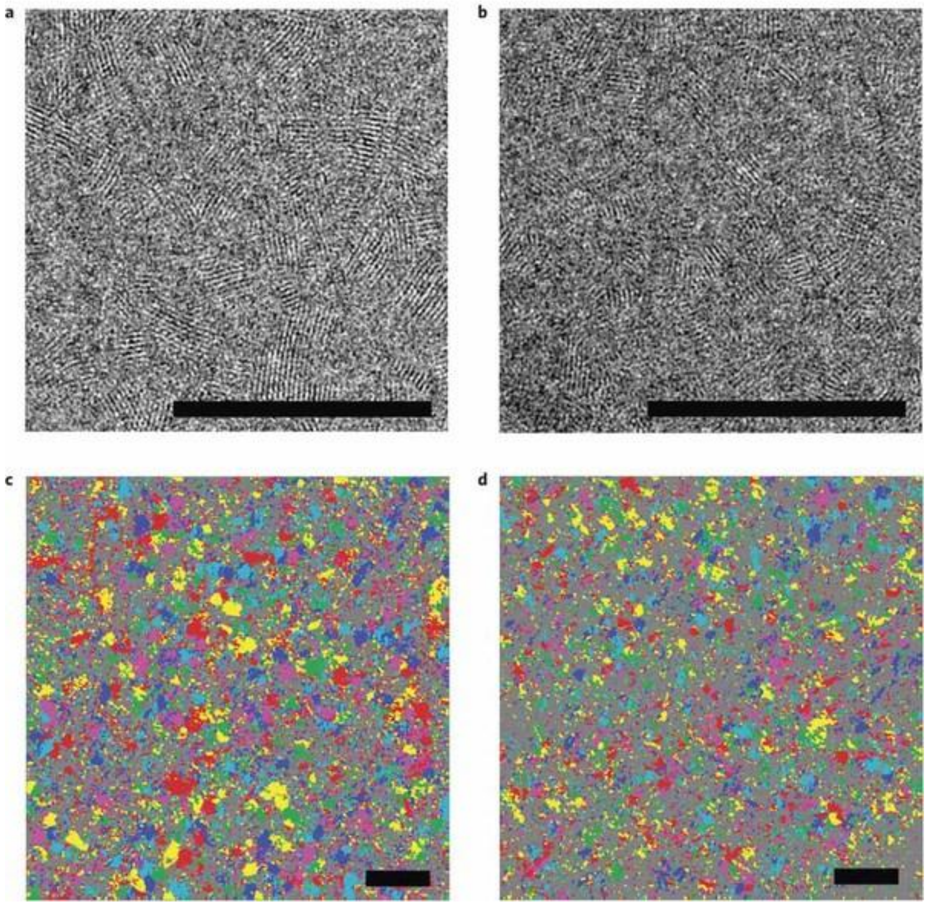


**Figure 44: High-magnification TEM images showing lattice fringes (0.31Å$^{-1}$) from in-plane stacking of the DTS(PTTh2)2 phase: BHJ film cast from a pure solvent (a) and addition of 0.25% v/v DIO solvent additive (b). c,d, Lower magnification, false colour images encoding the direction and size of crystalline regions for BHJ films cast from a pure solvent (c) and addition of 0.25% v/v DIO solvent additive (d). A reduction in the length scale is observed with the 0.25% v/v DIO solvent additive (optimal device) relative to the film cast from a pure solvent. Scale bars, 100 nm.**

# VI. Conclusion

We have overviewed different elements in the photovoltaic domain and more closely on the organic solar cells. We particularly focused these studies on the organic photovoltaic cells more specifically on the elaboration of pi-conjugated systems of small molecules and polymers as donor materials.

Four main aspects that we will discuss in this thesis are:

- Development of new electron donor materials
- Study of the opto-electronic properties of the materials
- Evaluation of the photovoltaic performances in solar cell configuration
- Establish the relation between molecule structures and photovoltaic properties

For the development of the new donor materials, we will first develop series of oligomers which can also be used as model systems for developing polymers and for a better understanding on the structure properties relationship regarding to the photovoltaic phenomenom. An in the later part, we will develop series of polymers.

For developing the new donor materials (oligomers or polymers), we will elaborate a strategy with the following goals:

- Enlarge the absorption spectrum by decreasing the band gap of the materials. The ideal band gap for the materials would be between 1.5 eV and 2 eV
- Controling the position of the energy levels of the frontier orbitals and in particular decrease the HOMO energy levels in order to increase the open circuit voltage Voc. The ideal HOMO energy levels will be in the range of -5.2 eV and -5.8 eV.
- Solution processable molecules with good film forming properties

For the development of new absorbing donor π–conjugated systems, we adopt the approach of D-A concept to afford low band gap molecules by employing fluorenone as electron withdrawing unit (or are also called electron-acceptor, or electron-deficient group) coupled with several of electron-rich (also called electron-donating or electron releasing) units. To avoid confusion when we talked of electron-acceptor unit or electron withdrawing unit this refers to sub-units present in our final donor materials. In the solar cell device, the acceptor is referred to the electron transporting materials such as fullerenes PCBMs.

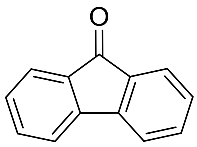
Fluorenone

**Figure 45: 9-Fluorenone molecule as main electron withdrawing unit**

Fluorenone[151 152]is an interesting electron withdrawing unit, with a low lying conduction band (or lowest unoccupied molecular orbital LUMO energy levels) and high electron affinity. Fluorenone unit possesses a good electron injecting properties thanks to its carbonyl group[153]. Another interesting advantage of fluorenone is they induce the pi-pi stacking in film by the low steric hindrance of the carbonyl group, and the polar nature of the fluorenone will induce strong dipole-dipole interchain interactions. [154],[155]

Previous works on D-A macromolecules based on fluorenone have already demonstrated as promising donor materials for photovoltaic cells[156,157,158,159,160,161,162,163]. In this thesis, we want to further develop new donor materials based on fluorenone units in order to increase the cell performance. We will describe first the synthesis of the new materials, the intrinsic properties, photophysical, and electronic characterisation and the photovoltaic performance in devices.

# VII. References


1 C. J. Brabec, N. S. Sariciftci, J. C. Hummelen, Plastic Solar Cells, Adv. Funct. Mater. 2001, 11,

2 H. Hoppe and N. S. Sariciftci, Organic solar cells: An overview, J. Mater. Res., Vol. 19, No. 7, Jul 2004

3 J-L. Brédas, J. E. Norton, J. Cornil, and V. Coropceanu, Molecular Understanding of Organic Solar Cells: The Challenges, Acc. Chem. Res. 2009 42 (11), 1691-1699

4 S. Gunes, H. Neugebauer, N. S. Sariciftci, Conjugated polymer-based organic solar cells. Chem. Rev. 2007, 107, 1324–1338.

5 R. Kroon,M. Lenes, J.C. Hummelen,P. W. M. Blom, B. De Boer, Small bandgap polymers for organic solar cells (polymer material development in the last 5 years), Polym. Rev. 2008, 48, 531–582.

6 B. Walker, C. Kim, T.-Q. Nguyen, Small Molecule Solution-Processed Bulk Heterojunction Solar Cells, Chemistry of Materials 2011 23 (3), 470-482

7 J-M. Nunzi, Organic photovoltaic materials and devices, C. R. Physique 3 (2002) 523–542

8 A. J. Moulé , L. Chang , C. Thambidurai , R. Vidu and P. Stroeve, Hybrid solar cells: basic principles and the role of ligands, J. Mater. Chem., 2012,22, 2351-2368

9 S. Günes, N. S. Sariciftci, Hybrid solar cells, Inorganica Chimica Acta 361 (2008) 581–588

10 P. Reiss , E. Couderc , J. De Girolamo and A.Pron, Conjugated polymers/semiconductor nanocrystals hybrid materials—preparation, electrical transport properties and applications,Nanoscale, 2011,3, 446-489

11 M.A. Green, K. Emery, Y. Hishikawa, W. Warta, E.D. Dunlop, Solar cell efficiency tables (version 39), Progress in Photovoltaics: Research and Applications 20 (2012) 12–20.

12 M. Wright, A. Uddin, Organic—inorganic hybrid solar cells: A comparative review, Solar Energy Materials and Solar Cells, Volume 107, December 2012, Pages 87-111

13 D. Kearns and M. Calvin, Photovoltaic Effect and Photoconductivity in Laminated Organic Systems, J. Chem. Phys. 29, 950 (1958)

14 Shirakawa, H.; Louis, E. J.; MacDiarmid, A. G.; Chiang, C. K.; Heeger, A. J. Journal of the Chemical Society, Chemical Communications 1977, 578-580

15 C.W. Tang, Two layer organic photovoltaic cell, Appl. Phys. Lett. 1986, 48, 183.

16 N.S. Sariciftci, L. Smilowitz, A.J. Heeger, F. Wudl, Semiconducting polymers (as donors) and buckminsterfullerene (as acceptor): photoinduced electron transfer and heterojunction devices, Synth. Met. 59 (1993) 333

17 G. Yu, J. Gao, J. C. Hummelen, F. Wudl, A. J. Heeger, Polymer Photovoltaic Cells: Enhanced Efficiencies via a Network of Internal Donor-Acceptor Heterojunctions, Science 270 (1995) 1789.

18 W. U. Huynh, J. J. Dittmer and A. P. Alivisatos, Hybrid Nanorod-Polymer Solar Cells , Science, 2002, 295,2425–2427.

19 Lek J Y, Xi L, Kardynal B E, Wong L H and Lam Y M , Understanding the effect of surface chemistry on charge generation and transport in poly(3-hexylthiophene)/Cdse hybrid solar cells ACS Appl. Mater. Interfaces, 2011, 3 287–92

20 S. Günes, K. P. Fritz, H. Neugebauer, N. S. Sariciftci, S. Kumar, G. D. Scholes, Hybrid solar cells using PbS nanoparticles, Solar Energy Materials and Solar Cells, 91, 5, 2007, 420-423

21 Seo J, Kim S J, Kim W J, Singh R, Samoc M, Cartwright A N and Prasad P N, Enhancement of the photovoltaic performance in PbS nanocrystals: P3HT hybrid composite devices by post-tratement-driven ligand Exchance, Nanotechnology, 2009, 20, 095202

22 Lin Y-Y, Chu T-H, Chen C-W and Su W-F, Improved performance of polymer/TiO2 nanorod bulk heterojunctionphotovoltaic devices by interface modification, Appl. Phys. Lett., 2008, 92, 053312

23 Beek W J E, Wienk M M and Janssen R A J , Efficient hybrid solar cells from zinc oxide nanoparticles and a conjugated polymer, Adv. Mater. , 2004, 16 1009–13

24 P. Reiss , E. Couderc , J. De Girolamo and A.Pron, Conjugated polymers/semiconductor nanocrystals hybrid materials—preparation, electrical transport properties and applications,Nanoscale, 2011,3, 446-489

25 T. G. Jiu, P. Reiss, S. Guillerez, R. de Bettignies, S. Bailly and F. Chandezon, IEEE J. Sel. Top. Quantum Electron., 2010, 16, 1619–1626

26 http://rredc.nrel.gov/solar/pubs/spectral/model/appendix.html

27 M. Knupfer, Exciton binding energies in organic semiconductors, Appl. Phys. A 77, 623–626 (2003)

28 N. Banerji, S. Cowan, M. Leclerc, E. Vauthey, and A. J. Heeger, Exciton Formation, Relaxation, and Decay in PCDTBT, Journal of the American Chemical Society 2010 132 (49), 17459-17470

29 X.-Y. Zhu, Q. Yang, and M. Muntwiler, Charge-Transfer Excitons at Organic Semiconductor Surfaces and Interfaces,Acc. Chem. Res., 2009, 42 (11), pp 1779–1787

30 J. J. M. Halls, K. Pichler, R. H. Friend, S.C. Moratti, A. B. Holmes, Exciton diffusion and dissociation in a poly(*p*-phenylenevinylene)/$C_{60}$ heterojunction photovoltaic cell Appl. Phys. Lett. 1996, 68, 3120

31 A. Haugeneder, M. Neges, C. Kallinger, W. Spirkl, U. Lemmer, J. Feldmann, U. Scherf, E. Harth, A. Gugel, and K. Mullen, Exciton diffusion and dissociation in conjugated polymer/fullerene blends and heterostructures Phys. Rev. B 1999, 59, 15346.

32 Scharber, M.C., Mühlbacher, D., Koppe, M., Denk, P., Waldauf, C., Heeger, A.J. and Brabec, C.J. ,Design Rules for Donors in Bulk-Heterojunction Solar Cells—Towards 10% Energy-Conversion Efficiency. Adv. Mater., (2006), 18: 789–794

33 J-L. Brédas, D. Beljonne, V. Coropceanu and J. Cornil, Charge-Transfer and Energy-Transfer Processes in π-Conjugated Oligomers and Polymers: A Molecular Picture Chem. Rev. 2004 104 (11), 4971-5004

34 D. Adam, P.Schuhmacher,J. Simmerer, L. Haussling, K. Siemensmeyer, K.H. Etzbach, H. Ringsdorf, D. Haarer, Fast photoconduction in the highly ordered columnar phase of a discotic liquid crystal, Nature, 1994, 371, 141.

35 C. D. Simpson, J.Wu, M. D.Watson, K. Müllen, From graphite molecules to columnar superstructures – an exercise in nanoscience, J. Mater. Chem. 2004, 14, 494.

36 Anthony, J. E., Facchetti, A., Heeney, M., Marder, S. R. and Zhan, X. (2010), n-Type Organic Semiconductors in Organic Electronics. Adv. Mater., 22: 3876–3892

37 H. Hoppe, M. Niggemann, C. Winder, J. Kraut, R. Hiesgen, A. Hinsch, D. Meissner, and N.S. Sariciftci: Nanoscale morphology of conjugated polymer/fullerene based bulk-heterojunction solar cells. Adv. Funct. Mater. (2004).

38 A.J.Moulé , K.Meerholz, Controlling morphology in polymer–fullerene mixtures, Adv.Mater. , 20 (2008) 240–245.

39 http://www.polyera.com/newsflash/polyera-achieves-world-record-organic-solar-cell-performance

40 Weickert, J., Dunbar, R. B., Hesse, H. C., Wiedemann, W. and Schmidt-Mende, L. (2011), Nanostructured Organic and Hybrid Solar Cells. Adv. Mater., 23: 1810–1828

41 Coakley KM, McGehee MD (2003) Photovoltaic cells made from conjugated polymers infiltrated into mesoporous titania. Appl Phys Lett 83:3380

42 I. Gonzalez-Valls and M. Lira-Cantu, Vertically-aligned nanostructures of ZnO for excitonic solar cells: A review, Energy Environ. Sci. 2(1), 19–34 (2008)

43 Topham, P. D., Parnell, A. J. and Hiorns, R. C. (2011) Block copolymer strategies for solar cell technology, J. Polym. Sci. B Polym. Phys., 49: 1131–1156

44 S.-S. Sun , Design of a block copolymer solar cell, Sol. Energy Mater. Sol. Cells 2003, 79 , 257 .

45 M. Sommer , S. Lindner , M. Thelakkat , Microphase-Separated Donor–Acceptor Diblock Copolymers: Influence of HOMO Energy Levels and Morphology on Polymer Solar Cells, Adv. Funct. Mater. 2007 , 17 ,1493

46 Richard, F., Brochon, C., Leclerc, N., Eckhardt, D., Heiser, T. and Hadziioannou, G. (2008), Design of a Linear Poly(3-hexylthiophene)/Fullerene-Based Donor-Acceptor Rod-Coil Block Copolymer. Macromol. Rapid Commun., 29: 885–891.

47 Y Yang, K Mielczarek, M Aryal, A Zakhidov, and W Hu, Nanoimprinted Polymer Solar Cell, ACS Nano 2012 6 (4), 2877-2892

48 S Miyanishi , Y Zhang , K Tajima and K Hashimoto, Fullerene attached all-semiconducting diblock copolymers for stable single-component polymer solar cells ,Chem. Comm., 2010,46, 6723-6725

49 Park, H. J.; Kang, M.-G.; Guo, L. J., Large Area High Density Sub-20 nm SiO2 Nanostructures Fabricated by Block Copolymer Template for Nanoimprint Lithography. ACS Nano 2009, 3, 2601–2608.

50 G. Li, R. Zhu, Y. Yang, Polymer solar cells, Nature Photonics 6, 153–161 (2012)

51 J. Nelson, Organic photovoltaic films, Materials Today, Vol. 5, Issue 5, 2002, 20-27

52 A. Mishra and P. Bäuerle, Small Molecule Organic Semiconductors on the Move: Promises for Future Solar Energy Technology, Angew. Chem. Int. Ed. 2012, 51, 2020 – 2067

53 Y He and Y Li, Fullerene derivative acceptors for high performance polymer solar cells, Phys. Chem. Chem. Phys., 2011,13, 1970-1983

54 Wienk, M. M., Kroon, J. M., Verhees, W. J. H., Knol, J., Hummelen, J. C., van Hal, P. A. and Janssen, R. A. J. (2003), Efficient Methano[70]fullerene/MDMO-PPV Bulk Heterojunction Photovoltaic Cells. Angew. Chem. Int. Ed., 42: 3371–3375.

55 Y He, H-Y Chen, J Hou, and Y Li, Indene−C60 Bisadduct: A New Acceptor for High-Performance Polymer Solar Cells. J. Am. Chem. Soc, 2010 132 (4), 1377-1382

56 S. Yoo, W. J. Potscavage, B. Domercq, J. Kim, J. Holt, and B. Kippelen, Integrated organic photovoltaic modules with a scalable voltage output, Appl. Phys. Lett. 89, 233516 (2006)

57 M. Lenes, G. J. A. H. Wetzelaer, F. B. Kooist, S. J. Veenstra, J. C. Hummelen and P. W. M. Blom, Fullerene Bisadducts for Enhanced Open-Circuit Voltages and Efficiencies in Polymer Solar Cells, Adv. Mater., 2008, 20, 2116

58 H Zhao, X Guo, H Tian, C Li, Z Xie,Y Geng and F Wang, Alkyl substituted [6,6]-thienyl-C61-butyric acid methyl esters: easily accessible acceptor materials for bulk-heterojunction polymer solar cells, J. Mater. Chem., 2010, 20, 3092–3097

59 G. Goretzki, E. S. Davies, S. P. Argent, W. Z. Alsindi, A. J. Blake, J. E. Warren, J. McMaster and N. R. Champness, Bis-morpholine-Substituted Perylene Bisimides: Impact of Isomeric Arrangement on Electrochemical and Spectroelectrochemical Properties, J. Org. Chem., 2008, 73, 8808–8814.

60 L. Schmidt-Mende , A. Fechtenkotter , K. Mullen , E. Moons ,R. H. Friend , J. D. MacKenzie , Self-organized discotic liquid crystals for high-efficiency organic photovoltaics, Science 2001 , 293 , 1119 .

61 M. S. Dresselhaus, G. Dresselhaus and P. Avouris, in Carbon Nanotubes, Synthesis, Structure, Properties and Applications, Springer-Verlag, Berlin and Heidelberg, 2001

62 S Ren, Marco B R R. Lunt, V Bulovic, J C. Grossman, and S Gradečak, Toward Efficient Carbon Nanotube/P3HT Solar Cells: Active Layer Morphology, Electrical, and Optical Properties, Nano Letters 2011 11 (12), 5316-5321

63 B. Ratier, J-M. Nunzi, M. Aldissi, T. M. Kraft, E. Buncel, Organic solar cell materials and active layer designs-improvements with carbon nanotubes:a review, Polym. Int., 2012, 61: 342-354

64 Berson, S., de Bettignies, R., Bailly, S., Guillerez, S. and Jousselme, B. (2007), Elaboration of P3HT/CNT/PCBM Composites for Organic Photovoltaic Cells. Adv. Funct. Mater., 17: 3363–3370.

65 Picard, L.; Lincker, F.; Kervella, Y.; Zagorska, M.; DeBettignes, R.; Peigney, A.; Flahaut, E.; Louarn, G.; Lefrant, S.; Demadrille, R.; Pron, A. Composites of Double-Walled Carbon Nanotubes with bis Quaterthiophene-

Fluorenone Conjugated Oligomer: Spectroelectrochemical and Photovoltaic Properties J. Phys. Chem. C 2009, 113, 17347–17354
66 R. Y. C. Shin, T. Kietzke, S. Sudhakar, A. Dodabalapur, Z. K. Chen and A. Sellinger, Heterojunction topology versus fill factor correlations in novel hybrid small-molecular/polymeric solar cells, Chem. Mater., 2007, 19, 1892–1894
67 F. G. Brunetti, X. Gong, M. Tong, A. J. Heeger, and Fred Wudl, Strain and Hückel Aromaticity: Driving Forces for a Promising New Generation of Electron Acceptors in Organic Electronics, Angew. Chem. Int. Ed. 2010, 49, 532 – 536
68 R. Y. C. Shin, P. Sonar, P. S. Siew, Z. K. Chen and A. Sellinger, Electron-Accepting Conjugated Materials Based on 2-Vinyl-4,5-dicyanoimidazoles for Application in Organic Electronics, J. Org. Chem., 2009, 74, 3293–3298.
69 C Duan , F Huang and Y Cao , Recent development of push–pull conjugated polymers for bulk-heterojunction photovoltaics: rational design and fine tailoring of molecular structures, J. Mater. Chem., 2012,22, 10416-10434
70 Y-J Cheng , S-H Yang , C-S Hsu, Synthesis of Conjugated Polymers for Organic Solar Cell Applications, Chem. Rev. 109 (11): 5868–5923 (2009)
71 U. Salzner, J.B. Lagowski, P.G. Pickup, P.A. Poirier, Comparison of geometries and electronic structures of polyacetylene, polyborole, polycyclopentadiene, polypyrrole, polyfuran, polysilole, polyphosphole, polythiophene, polyselenophene and polytellurophene, Synth. Met. 96 (1998) 177
72 H.A.M. van Mullekom, J.A.J.M. Vekemansb, E.E. Havingab, E.W. Meijer, Developments in the chemistry and band gap engineering of donor acceptor substituted conjugated polymers Materials Science and Engineering 32 (2001)
73 J. Roncali, Molecular Engineering of the Band Gap of p-Conjugated Systems: Facing Technological Applications, Macromol. Rapid Commun. 2007, 28, 1761–1775
74 J. L Brédas, Relationship between band gap and bond length alternation in organic conjugated polymers, J. Chem. Phys. 82, 3808 (1985)
75 F. Wudl, M. Kobayashi, A. J. Heeger, Polyisothianaphtene, J. Org. Chem. 1984, 49, 3382
76 a) Wienk, M. M.; Turbiez, R.; Struijk, M. P.; Fonrodona, M.; Janssen, R. Low-band gap poly(di-2-thienylthienopyrazine):fullerene solar cells,A. J. Appl. Phys. Lett. 2006, 88, 153511
b) M Shahid,R S Ashraf,E Klemm and S Sensfuss, Synthesis and Properties of Novel Low-Band-Gap Thienopyrazine-Based Poly(heteroarylenevinylene)s , Macromolecules**,** 2006 *39* (23), 7844-7853
77 N Kleinhenz, L Yang, H Zhou, S C. Price, and W You, Low-Band-Gap Polymers That Utilize Quinoid Resonance Structure Stabilization by Thienothiophene: Fine-Tuning of HOMO Level ,Macromolecules 2011 44 (4), 872-877
78 F. Banishoeib, A. Henckens, S. Fourier, G. Vanhooyland, M. Breselge, J. Manca,T.J. Cleij, L. Lutsen, D. Vanderzande, Le Huong Nguyen,Helmut Neugebauer, Niyazi Serdar Sariciftci, Synthesis of poly(2,5-Thienylene Vinylene) and its derivatives: Low band gap materials for photovoltaics, Thin Solid Films 516 (2008) 3978–3988
79 Roncali, J. and Thobie-Gautier, C. (1994), An efficient strategy towards small bandgap polymers: The rigidification of the π-conjugated system. Adv. Mater., 6: 846–848.
80 Winslow F H (1955) J Polym Sci 16,101 b) U. Scherf and K. Müllen, The synthesis of ladder polymers, Advances in polymer Science, Vol. 123, 1995
81 J. Roncali , R. Garreau , A. Yassar , P. Marque , F. Garnier , M. Lemaire, Effects of steric factors on the electrosynthesis and properties of conducting poly(3-alkylthiophenes), J. Phys. Chem., 1987, 91 (27), pp 6706–6714
82 R. J. Waltman, J. Bargon, A. F. Diaz, Electrochemical studies of some conducting polythiophene films,J. Phys. Chem. 1983, 87,1459.
83 E. E. Havinga, W. ten Hoeve, H. Wynberg, A new class of small band gap organic polymer conductors, Polym. Bull. 1992, 29, 119
84 S. Steinberger, A. Mishra, E. Reinold, C. M. M_ller, C. Uhrich, M. Pfeiffer, P. Baüerle, A-D-A-D-A-Type Oligothiophenes for Vacuum-Deposited Organic Solar Cells, Org. Lett. 2011, 13, 90
85 L Bian, E Zhu, J Tang, W Tang, F Zhang, Recent progress in the design of narrow bandgap conjugated polymers for high-efficiency organic solar cells, Progress in Polymer Science, Available online 3 April 2012
86 P. M. Beaujuge, C. M. Amb , and J. R. Reynolds,Spectral Engineering in π-Conjugated Polymers with Intramolecular Donor−Acceptor Interactions, Acc. Chem. Res., 2010, 43 (11), pp 1396–1407
87 P Peumans, A Yakimov, and S R. Forrest, Small molecular weight organic thin-film photodetectors and solar cells, J. Appl. Phys., 93 (2003), p. 3693.
88 Fitzner, R., Reinold, E., Mishra, A., Mena-Osteritz, E., Ziehlke, H., Körner, C., Leo, K., Riede, M., Weil, M., Tsaryova, O., Weiß, A., Uhrich, C., Pfeiffer, M. and Bäuerle, P. (2011), Dicyanovinyl–Substituted Oligothiophenes: Structure-Property Relationships and Application in Vacuum-Processed Small Molecule Organic Solar Cells. Adv. Funct. Mater., 21: 897–910.
89 Matthew T. Lloyd, John E. Anthony, George G. Malliaras, Photovoltaics from soluble small molecules, Materialstoday, Volume 10, Issue 11, November 2007, Pages 34–41
90 www.heliatek.com
91 Y. Sun, G. C. Welch, W. L. Leong, C. J. Takacs, G. C. Bazan and A. J. Heeger, Solution-processed small-molecule solar cells with 6.7% efficiency, Nat. Mater., 2012, 11, 44
92 D. Placencia, W. Wang, R. C. Shallcross, K. W. Nebesny,, M. Brumbach and N. R. Armstrong, Organic Photovoltaic Cells Based On Solvent-Annealed, Textured Titanyl Phthalocyanine/C60 Heterojunctions, Adv. Funct. Mater., 2009,19, 1913
93 G. Wei, S. Wang, K. Sun, M. E. Thompson and S. R. Forrest, Adv. Energy Mater., 2011, 1, 184.

94 a) B. Walker, A. B. Tamayo, X.-D. Dang, P. Zalar, J. H. Seo, A.Garcia, M. Tantiwiwat, T.-Q. Nguyen, Nanoscale Phase Separation and High Photovoltaic Efficiency in Solution-Processed, Small-Molecule Bulk Heterojunction Solar Cells, Adv. Funct. Mater. 2009,19, 3063.
b) A. B. Tamayo, B.Walker, T.-Q. Nguyen, A Low Band Gap, Solution Processable Oligothiophene with a Diketopyrrolopyrrole Core for Use in Organic Solar Cells , J. Phys. Chem. C 2008, 112, 11545.
c) A. Tamayo, T. Kent, M. Tantitiwat, M. A. Dante, J. Rogers, T.-Q. Nguyen, Solution-Processed, Small Molecule-based Bulk Heterojunction Solar Cells Using Fullerene Derivatives as Acceptors: Influence of the Alkyl Chain Length and Thermal Annealing Energy Environ. Sci. 2009, 2, 1180.
d) E. Ripaud, D. Demeter, T. Rousseau, E. Boucard-Cétol, M. Allain, R. Po, P. Leriche, J. Roncali, Structure–properties relationships in conjugated molecules based on diketopyrrolopyrrole for organic photovoltaics, Dyes and Pigments, vol. 95 issue 1 October, 2012. p. 126-133

95 Demadrille, R., Firon, M., Leroy, J., Rannou, P. and Pron, A. (2005), Plastic Solar Cells Based on Fluorenone-Containing Oligomers and Regioregular Alternate Copolymers. Adv. Funct. Mater., 15: 1547–1552.

96 N. Kopidakis, W. J. Mitchell, J. Van de Lagemaat, D. S. Ginley, G. Rumbles, S. E. Shaheen,W. L. Rance, Bulk heterojunction organic photovoltaic devices based on phenyl-cored thiophene dendrimers,Appl. Phys. Lett. 2006, 89, 103524

97 a) H. C. Hesse, J.Weickert, M. Al-Hussein, L. Dössel, X. Feng, K.Müllen, L. Schmidt-Mende, Discotic materials for organic solar cells: Effects of chemical structure on assembly and performance, Sol. Energy Mater. Sol. Cells 2010, 94, 560.
b) F. Lincker, B. Heinrich, R. De Bettignies, P. Rannou, J. Pecaut, B. Grevin, A. Pron, B. Donnio and R. Demadrille, Fluorenone core donor–acceptor–donor π-conjugated molecules end-capped with dendritic oligo(thiophene)s: synthesis, liquid crystalline behaviour, and photovoltaic applications, J. Mater. Chem., 2011, 21, 5238

98 Q. Shi, P. Cheng, Y. Li and X. Zhan, A Solution Processable D-A-D Molecule based on Thiazolothiazole for High Performance Organic Solar Cells, Adv. Energy Mater., 2012,2, 63.

99 L. Bu, X. Guo, B. Yu, Y. Qu, Z. Xie, D. Yan, Y. Geng and F. Wang, Monodisperse Co-oligomer Approach toward Nanostructured Films with Alternating Donor−Acceptor Lamellae, J. Am. Chem. Soc., 2009, 131, 13242.

100 B. Yin, L. Yang, Y. Liu, Y. Chen, Q. Qi, F. Zhang, S. Yin, Solution-processed bulk heterojunction organic solar cells based on an oligothiophene derivative, Appl. Phys. Lett. 2010, 97, 023303

101 Y. Liu, X. Wan, F. Wang, J. Zhou, G. Long, J. Tian, J. You, Y.Yang, Y. Chen, Spin-Coated Small Molecules for High Performance Solar Cells, Adv. Energy Mater. 2011, 1, 771

102 J. Zhou, X.Wan, Y. Liu, G. Long, F.Wang, Z. Li, Y. Zuo, C. Li, Y. Chen, A Planar Small Molecule with Dithienosilole Core for High Efficiency Solution-Processed Organic Photovoltaic Cells, Chem. Mater. 2011, 23, 4666

103 Y. Lin , Y. Li and X. Zhan, Small molecule semiconductors for high-efficiency organic photovoltaics Chem. Soc. Rev., 2012,41, 4245-4272

104 A. J. Heeger, Semiconducting polymers: the Third Generation, Chem. Soc. Rev., 2010,39, 2354-2371

105 Shrotriya, V.; Wu, E. H.-E.; Li, G.; Yao, Y.; Yang, Y. Appl. Phys.Lett. 2006, 88, 064104.

106 Tajima, K.; Suzuki, Y.; Hashimoto, K. Polymer Photovoltaic Devices Using Fully Regioregular Poly[(2-methoxy-5-(3′,7′-dimethyloctyloxy))-1,4-phenylenevinylene], J. Phys. Chem. C 2008, 112, 8507.

107 T. Munters, T. Martens, L. Goris, V. Vrindts, J. Manca, L.Lutsen, W. De Ceuninck, D. Vanderzande, L. De Schepper, J. Gelan, N. Sariciftci, C.Brabec, A comparison between state-of-the-art ‘gilch’ and ‘sulphinyl’ synthesised MDMO-PPV/PCBM bulk hetero-junction solar cells, Thin Solid Films 403 – 404 (2002) 247–251

108 Mihailetchi, V.D., Xie, H.X., de Boer, B., Koster, L.J.A. and Blom, P.W.M. (2006), Charge Transport and Photocurrent Generation in Poly(3-hexylthiophene): Methanofullerene Bulk-Heterojunction Solar Cells. Adv. Funct. Mater., 16: 699–708.

109 S. E. Shaheen, C. J. Brabec, N. S. Sariciftci, F. Padinger, T. Fromherz, and J. C. Hummelen, 2.5% efficient organic plastic solar cells, Appl. Phys. Lett. 78, 841 (2001).

110 Ma, W. L., Yang, C. Y., Gong, X., Lee, K. & Heeger, A. J. Thermally stable, efficient polymer solar cells with nanoscale control of the interpenetrating network morphology. Adv. Funct. Mater. 15, 1617–1622 (2005).

111 Dang, M. T., Hirsch, L. and Wantz, G. (2011), P3HT:PCBM, Best Seller in Polymer Photovoltaic Research. Adv. Mater., 23: 3597–3602

112 L. H. Nguyen, S. Günes, H. Neugebauer, N. S. Sariciftci, F. Banishoeib, A. Henckens, T. Cleij, L. Lutsen, D. Vanderzande, Precursor route poly(thienylene vinylene) for organic solar cells: Photophysics and photovoltaic performance, Solar Energy Materials & Solar Cells 90 (2006) 2815–2828

113 A. Henckens, M. Knipper, I. Polec, J. Manca, L. Lutsen, D. Vanderzande, Poly(thienylene vinylene) derivatives as low band gap polymers for photovoltaic applications, Thin Solid Films, Vol. 451–452, 2004, 572-579

114 Svensson, M.; Zhang, F. L.; Veenstra, S. C.; Verhees, W. J. H.; Hummelen, J. C.; Kroon, J. M.; Inganas, O.; Andersson, M. R.High-performance polymer solar cells of an alternating polyfluorene copolymer and a fullerene derivative Adv. Mater.2003, 15, 988– 991

115 O Inganäs, F Zhang, and M R. Andersson, Alternating Polyfluorenes Collect Solar Light in Polymer Photovoltaics, Accounts of Chemical Research 2009 42 (11), 1731-1739

116 S. H. Park, A. Roy, S. Beaupre, S. Cho, N. Coates, J. S. Moon, D. Moses, M. Leclerc, K. Lee and A. J. Heeger, Nat. Photonics, 2009, 3, 297–303.

117 J. Li and A. C. Grimsdale, Carbazole-based polymers for organic photovoltaic device, Chem. Soc. Rev., 2010,39, 2399-2410, DOI: 10.1039/B915995A

118 Chen, H.; Hou, J.; Zhang, S.; Liang, Y.; Yang, G.; Yang, Y.; Yu, L. P.; Wu, Y.; Li, G., Polymer solar cells with enhanced open-circuit voltage and efficiency, Nat. Photonics 2009, 3, 649–653

119 U. Scherf and K. Müllen, The synthesis of ladder polymers, Advances in polymer Science, Vol. 123, 1995

120 W. Nie, C. M. MacNeill, Y. Li, R. E. Noftle, D. L. Carroll and R. C. Coffin, Macromol. Rapid Commun., 2011, 32, 1163–1168.

121 I. McCulloch, R. S. Ashraf, L. Biniek, H. Bronstein, C. Combe, J. E. Donaghey, D. I. James, C. B. Nielsen, B. C. Schroeder, and W. Zhang, Design of Semiconducting Indacenodithiophene Polymers for High Performance Transistors and Solar Cells, Accounts of Chemical Research 2012 45 (5), 714-722

122 Y. Li, Molecular Design of Photovoltaic Materials for Polymer Solar Cells: Toward Suitable Electronic Energy Levels and Broad Absorption, Acc. Chem. Res., 2012, 45 (5), pp 723–733

123 Q Zheng, B J Jung, J Sun, and H E. Katz, Ladder-Type Oligo-p-phenylene-Containing Copolymers with High Open-Circuit Voltages and Ambient Photovoltaic Activity, Journal of the American Chemical Society, 2010 132 (15), 5394-5404

124 R. K. Cheedarala , G.-H. Kim , S. Cho , J. Lee , J. Kim , H.-K. Song , J.Y. Kim and C. Yang, Ladder-type heteroacene polymers bearing carbazole and thiophene ring units and their use in field-effect transistors and photovoltaic cells, J. Mater. Chem., 2011,21, 843-850

125 Y-J Cheng , S-W Cheng , C-Y Chang , W-S Kao , M-H Liao and C-S Hsu, Diindenothieno[2,3-b]thiophene arene for efficient organic photovoltaics with an extra high open-circuit voltage of 1.14 ev, Chemical Communications 48, 3203 (2012)

126 C. Li, M. Liu, N. G. Pschirer, M. Baumgarten, and K Müllen, Polyphenylene-Based Materials for Organic Photovoltaics,Chem. Rev. 2010, 110, 6817–6855

127 D. Kitazawa, N. Watanabe, S. Yamamoto and J. Tsukamoto, Appl. Phys. Lett., 2009, 95, 053701

128 Wang, E.; Ma, Z.; Zhang, Z.; Vandewal, K.; Henriksson, P.; Inganas, O.; Zhang, F.; Andersson, M. R. J. Am. Chem. Soc. 2011, 133, 14244−14247

129 W. Nie, C. M. MacNeill, Y. Li, R. E. Noftle, D. L. Carroll and R. C. Coffin, Macromol. Rapid Commun., 2011, 32, 1163–1168.

130 Zhou, H.; Yang, L.; Stuart, A.; Price, S.; Liu, S.; You, W. Angew.Chem., Int. Ed. 2011, 50, 2995–2998

131 C. Piliego, T. W. Holcombe, J. D. Douglas, C. H. Woo, P. M. Beaujuge, J. M. J. Fréchet, Synthetic Control of Structural Order in N-Alkylthieno[3,4-c]pyrrole-4,6-dione-Based Polymers for Efficient Solar Cells, J. Am. Chem. Soc. 2010, 132, 7595–7597

132 Chu, T.; Lu, J.; Beaupr, S.; Zhang, Y.; Pouliot, J.; Wakim, S.; Zhou, J.; Leclerc, M.; Li, Z.; Ding, J.; Tao, Y. J. Am. Chem. Soc. 2011, 133, 4250–4253

133 A. Cravino, Origin of the open circuit voltage of donor-acceptor solar cells: Do polaronic energy levels play a role, Appl Phys Lett 91, 243502 (2007).

134 Svensson, M.; Zhang, F. L.; Veenstra, S. C.; Verhees, W. J. H.; Hummelen, J. C.; Kroon, J. M.; Inganas, O.; Andersson, M. R.High-performance polymer solar cells of an alternating polyfluorene copolymer and a fullerene derivative Adv. Mater.2003, 15, 988– 991

135 M.-S Kim, B-G Kim, and J Kim, Effective Variables To Control the Fill Factor of Organic Photovoltaic Cells, ACS Applied Materials & Interfaces 2009 1 (6), 1264-1269

136 Y. Kim, S. Cook, S. M. Tuladhar, S. A. Choulis, J. Nelson, J. R. Durrant, D. D. C. Bradley, M. Giles, I. McCulloch, C-S Ha and M. Ree, A strong regioregularity effect in self-organizing conjugated polymer films and high-efficiency polythiophene:fullerene solar cells,Nature Materials 5, 197 - 203 (2006)

137 Brinkmann, M. and Rannou, P. (2007), Effect of Molecular Weight on the Structure and Morphology of Oriented Thin Films of Regioregular Poly(3-hexylthiophene) Grown by Directional Epitaxial Solidification. Adv. Funct. Mater., 17: 101–108.

138 Y Yao, J Hou, Z Xu, G Li, and Y Yang, Effects of Solvent Mixtures on the Nanoscale Phase Separation in Polymer Solar Cells, Adv. Funct. Mater. 2008, 18, 1783–1789

139 M.T. Dang, G. Wantz, H. Bejbouji, M. Urien, O. J. Dautel, L. Vignau, Lionel Hirsch, Polymeric solar cells based on P3HT:PCBM: Role of the casting solvent, Solar Energy Materials and Solar Cells, Volume 95, Issue 12, December 2011, Pages 3408-3418

140 a) Padinger, F., Rittberger, R. S. & Sariciftci, N. S. Effects of postproduction treatment on plastic solar cells. Adv. Funct. Mater. 13, 85–88 (2003).
b) Y. Kim, S. A. Choulis, J. Nelson, D. D. C. Bradley, S. Cook and J. R. Durrant, Appl. Phys. Lett., 2005, 86, 063502.

141 J. Peet, C. Soci, R.C. Coffin, T.Q. Nguyen, A. Mikhailovsky, D. Moses, G.C. Bazan, Method for increasing the photoconductive response in conjugated polymer/fullerene composites, Appl. Phys. Lett. 89 (2006) 252105–252107.

142 J.Peet, J.Y.Kim, N.E.Coates, W.L.Ma, D.Moses, A.J.Heeger, G.C.Bazan, Efficiency enhancement in low-bandgap polymer solar cells by processing with alkanedithiols, Nat.Mater.6(2007)497–500.

143 S. Berson, R. De Bettignies, S. Bailly, and S. Guillerez, (2007), Poly(3-hexylthiophene) Fibers for Photovoltaic Applications. Adv. Funct. Mater., 17: 1377–1384

144 Müller, C., Wang, E., Andersson, L. M., Tvingstedt, K., Zhou, Y., Andersson, M. R. and Inganäs, O. (2010), Influence of Molecular Weight on the Performance of Organic Solar Cells Based on a Fluorene Derivative. Adv. Funct. Mater., 20: 2124–2131.

145 E. Wang, M. Wang, L.Wang, C. Duan, J. Zhang, W. Cai, C. He, H. Wu, and Y. Cao, Donor Polymers Containing Benzothiadiazole and Four Thiophene Rings in Their Repeating Units with Improved Photovoltaic Performance, Macromolecules 2009 42 (13), 4410-4415

146 W. Li, R. Qin, Y. Zhou, M. Andersson, F. Li, C. Zhang, B. Li, Z. Liu, Z. Bao and F. Zhang, Tailoring side chains of low band gap polymers for high efficiency polymer solar cells, Polymer, 2010, 51, 3031.
147 W. D. Oosterbaan,V. Vrindts, S. Berson, S. Guillerez, O. Douhéret, B. Ruttens, J. D'Haen, P. Adriaensens, J. Manca, L. Lutsen and D. Vanderzande, Efficient formation, isolation and characterization of poly(3-alkylthiophene) nanofibres: probing order as a function of side-chain length, J. Mater. Chem., 2009, 19, 5424–5435
148 X. Yang, J. Loos,S. C. Veenstra, W.J. H. Verhees,M. M. Wienk, J. M. Kroon, M. A. J. Michels and R. A. J. Janssen, Nanoscale Morphology of High-Performance Polymer Solar Cells,Nano Lett., Vol. 5, No. 4, 2005
149 P A. Troshin, H Hoppe, J Renz, M Egginger, J Yu. MAndrey E. Goryachev, Alexander S. Peregudov,R. N. Lyubovskaya, G. Gobsch, N. S. Sariciftci, and V. F. Razumov, Material Solubility-Photovoltaic Performance Relationship in the Design of Novel Fullerene Derivatives for Bulk Heterojunction Solar Cells, Adv. Funct. Mater. 2009, 19, 779–788
150 Loren G. Kaake, Gregory C. Welch, Daniel Moses, Guillermo C. Bazan, and Alan J. Heeger, Influence of Processing Additives on Charge-Transfer Time Scales and Sound Velocity in Organic Bulk Heterojunction Films, The Journal of Physical Chemistry Letters 2012 3 (10), 1253-1257
151 P. Song and F. Ma, Tunable Electronic Structures and Optical Properties of Fluorenone-Based Molecular Materials by Heteroatoms, J. Phys. Chem. A 2010, 114, 2230–2234
152 G. L. Eakinsa, J. S. Alfordb, B. J. Tiegsa, B. E. Breyfoglea and C. J. Stearmana,Tuning HOMO–LUMO levels: trends leading to the design of 9-fluorenone scaffolds with predictable electronic and optoelectronic properties, J. Phys. Org. Chem. (2011)
153 X. Gonga, D. Mosesa, A.J. Heeger, S. Xiao, Excitation energy transfer from polyfluorene to fluorenone defects, Synthetic Metals 141 (2004) 17–20
154 F Uckert, S Setayesh, and K Müllen, A Precursor Route to 2,7-Poly(9-fluorenone), Macromolecules, 1999 32 (14), 4519-4524
155 S. Panozzo, J-C. Vial, Y. Kervella, and O. Stéphan, Fluorene–fluorenone copolymer: Stable and efficient yellow-emitting material for electroluminescent devices, J. Appl. Phys. 92, 3495 (2002)
156 R. Demadrille, M. Firon, J. Leroy, P. Rannou, A. Pron, Plastic Solar Cells Based on Fluorenone-Containing Oligomers and Regioregular Alternate Copolymers, Adv. Funct. Mater. 2005, 15, 1547
157 F. Lincker, N. Delbosc, S. Bailly, R. De Bettignies, M. Billon, A. Pron, and R. Demadrille, Fluorenone-Based Molecules for Bulk-Heterojunction Solar Cells: Synthesis, Characterization, and Photovoltaic Properties, Adv. Funct. Mater. 2008, 18, 3444–3453
158 R. Demadrille, M. Zagorska, M. Billon, G. Louarn, S. Lefrant and A. Pron, Solution versus solid-state electropolymerization of regioregular conjugated fluorenone–thienylene vinylene macromonomers—voltammetric and spectroelectrochemical investigations, Journal of Solid State Electrochemistry, August 2007, Volume 11, Issue 8, pp 1051-1058
159 F. Lincker, N. Delbosc, S. Bailly, R. De Bettignies, M. Billon, A. Pron, and R. Demadrille, Fluorenone-Based Molecules for Bulk-Heterojunction Solar Cells:Synthesis, Characterization, and Photovoltaic Properties, Adv. Funct. Mater. 2008, 18, 3444–3453
160 Grévin, B., Demadrille, R., Linares, M., Lazzaroni, R. and Leclère, P. (2009), Probing the Local Conformation within π-Conjugated One-dimensional Supramolecular Stacks using Frequency Modulation Atomic Force Microscopy. Adv. Mater., 21: 4124–4129.
161 R. Demadrille , N. Delbosc , Y. Kervella , M. Firon , R. De Bettignies , M. Billon , P. Rannou and A. Pron, Conjugated alternating copolymer of dialkylquaterthiophene and fluorenone: synthesis, characterisation and photovoltaic properties, J. Mater. Chem., 2007,17, 4661-4669
162 W.Porzio , S. Destri , M. Pasini , U. Giovanella , M. Ragazzi , G. Scavia , D. Kotowski , G. Zotti and B. Vercelli, Synthesis and characterisation of fluorenone–thiophene-based donor–acceptor oligomers: role of moiety sequence upon packing and electronic properties, New J. Chem., 2010,34, 1961-1973
163 C. Qin , A. Islam and L. Han, Incorporating a stable fluorenone unit into D–A–π–A organic dyes for dye-sensitized solar cells, J. Mater. Chem., 2012,22, 19236-19243

# CHAPTER 2: Π-CONJUGATED OLIGOMERS FOR ORGANIC PHOTOVOLTAIC: SYNTHESIS, PHYSICAL CHARACTERISATION AND PHOTOVOLTAIC PROPERTIES

# I. Introduction

The development of new π-conjugated oligomers for photovoltaic applications is our first approach towards developing new donor materials. As discussed in chapter 1, small molecules are particularly interesting materials as they are easier to purify and to process compared to polymers. Their optical electrochemical and self-organization properties can be precisely tuned; they are monodisperse and show higher reproducibility when they are studied in devices. Small molecules allow us to create model systems for our studies and to establish structure properties relationships. The research on the small molecules for photovoltaic applications rooted back in 2005 when our laboratory published the first oligomer thienylene-vinylene-fluorenone TVF. The oligomer TVF alternates thienylene vinylene as electron-donating unit and fluorenone as the electron withdrawing unit at the centre giving rise to a D-A-D chemical structure. TVF blended with PCBMC60 gives a power conversion efficiency of 0.66 %[1] as shown in Figure 46.

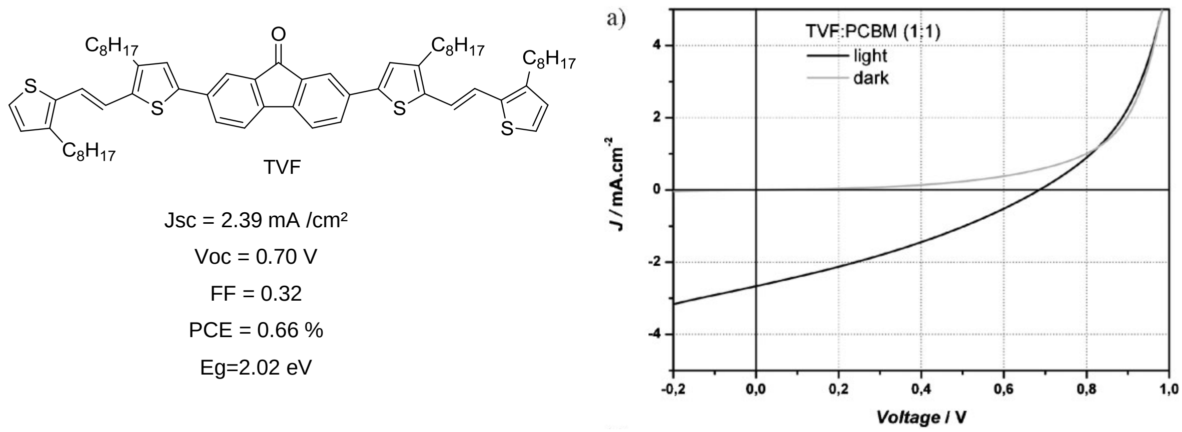


**Figure 46: Photovoltaic properties and current density-voltage curves of the device based on the blend TVF: PCBMC60 in dark and under illumination under AM 1.5 at 100 mW cm$^{-2}$; Jsc= short-circuit current density, Voc= open circuit voltage, FF= fill factor, PCE= power conversion efficiency.**

Based on this promising result, we decided to develop new low band gap oligomers based on the aforementioned aims:

- Enlarge the absorption spectrum by decreasing the band gap of the materials. The ideal band gap for the materials would be between 1.5 eV and 2 eV[2]
- Suitable position of the LUMO and HOMO energy levels of donors for improving charge separation[3]
- Low lying HOMO energy levels in order to increase the open circuit voltage Voc[4].
- High solubility allowing solution processing in the fabrication of the bulk heterojunction solar cells[5]

- Control of the morphology and the nanoscale phase separation of the interpenetrating network of the donor materials/acceptormaterials blend to favor the exciton dissociation in photovoltaic cells[6].

In order to use the oligomer TVF as a reference, which has been previously described by our group, we have reproduced its synthesis. Following the same strategy we replaced the thienylene vinylene groups by four linear thiophene-based oligomers to form symmetrical bis(quaterthiophene)-fluorenone molecules QTF. In addition, it has been demonstrated in polymer solar cells that the nature and the length of the solubilizing groups play a major role on the supramolecular organization and the photovoltaic performances[7]. However to the best of our knowledge it exist no similar studies carried out with small molecules. For this reason, a series of three different bis(dialkyl-quaterthiophene)-fluorenone small molecules were developed differing only by the length of the side alkyl chains. The different alkyl chains incorporated onto the pi-conjugated backbone were hexyl (-$C_6H_{13}$), octyl (-$C_8H_{17}$) and dodecyl (-$C_{12}H_{25}$). The first family prepared using dialkyl-quaterthiophene and fluorenone QTF is shown in Figure 47.

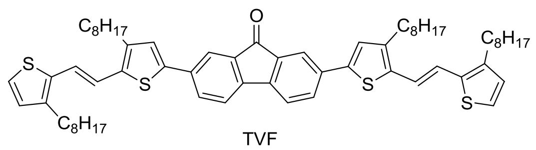


D-A-D

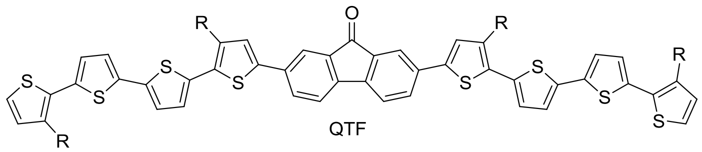

D-A-D

**Figure 47: Molecular structures of oligomers with alternating donor-acceptor D-A units : thienylene-vinylene-fluorenone TVF and quaterthiophene-fluorenone QTFn.**

The second family investigated in this work contains thienylene-vinylene units. In 2005 the first example of thienylene vinylene –fluorenone based oligomer was reported in the laboratory. The combination of this electron donor component with PCBMC60 in the active layer of a photovoltaic device yielded a PCE of 0.68%. After polymerization this molecule gave an alternating copolymer PTVF which shown improved photovoltaic properties in solar cells. The extension of the pi-conjugated systems allowed improving the current densities delivered by the cells and the fill factor[1]. One drawback of the PTVF polymer was the lack of control of the macromolecular parameters which lead to a poor solubility of the polymer and a poor reproducibility of the results (ranging from 1 to 1.3%).

To continue this work we decided to develop new thienylene vinylene based oligomers showing an extended pi-conjugated system, with the aim to control precisely the molecular structure.

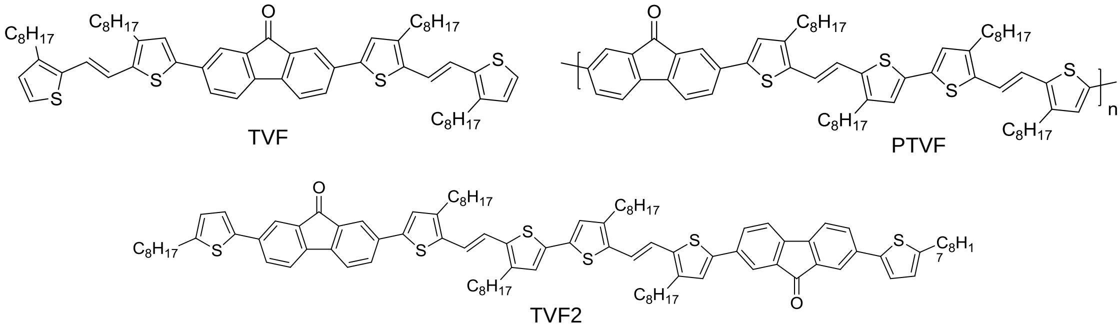


**Figure 48: Molecular structure of the new thienylene-vinylene based oligomers dimer thienylene vinylene fluorenone TVF2 in comparison with TVF and the polymer PTVF**

# II. Synthesis and purification of oligomers QTF and TVF2

## II.1. Synthesis and purification of quaterthiophene fluorenone QTF

The synthetic route towards 2,7-bis-(3,3'''-dialkyl-[2,2'; 5,2'';5'',2'''] quaterthiophen-5-yl)-fluoren-9-one (QTFn) is schematically described in the Scheme 1 below.

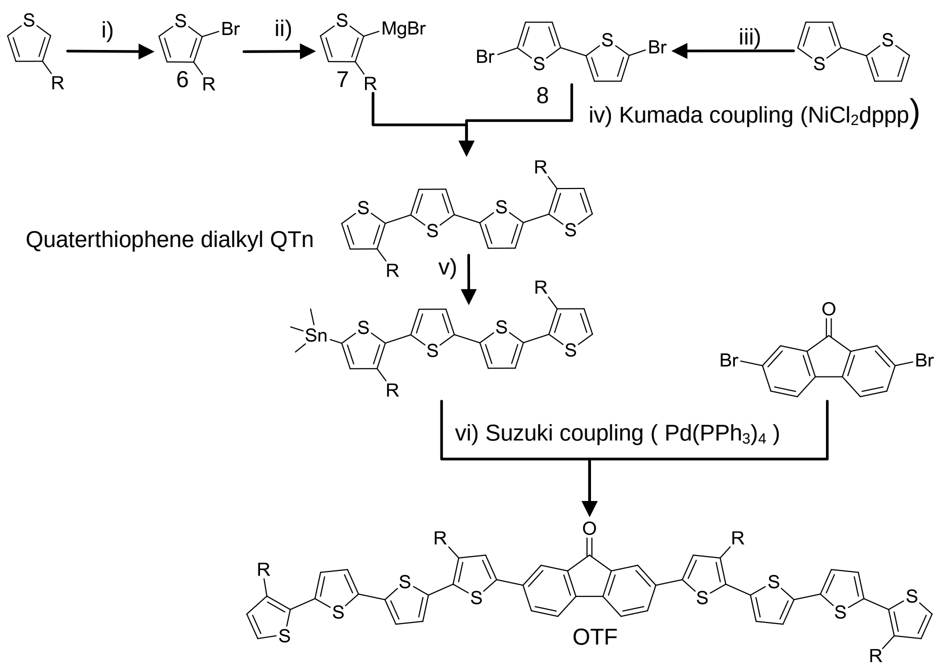


**Scheme 1: Synthetic route towards oligomers QTFn. R=hexyl, octyl and dodecyl. Reagents and condition: i) NBS, DMF, RT; ii) Mg,$Et_2O$, reflux; iii) NBS, DMF, MeOH; iv) $NiCl_2$dppp, $ET_20$/THF, reflux; v) n-BuLi, $Me_3SnCl$, -80°C; vi) $Pd(PPh_3)_4$, DMF, $K_3PO_4$**

The electron donor building block 3,3'''-dialkyl-[2,2'; 5,2'';5'',2'''] quaterthiophen-5-yl (QTn) was reported by Bauerle and coworkers[8] and prepared departing from commercially available 3-alkylthiophene and 2-2'-bithiophene. The preparation of 3,3'''-dialkyl-[2,2'; 5,2'';5'',2'''] quaterthiophen-5-yl involved the α-bromination of 3-alkylthiophene using N-bromosuccinimide at room temperature in a polar solvent dimethylformamide (DMF) in the absence of light. This reaction afford selectively 2-bromo-3-alkylthiophene (6) with a high yields ranging from 75% to 95% depending on the starting material. The Grignard reactant (3-alkylthiophen-2-yl) magnesium bromide (7) was prepared in situ by adding diluted 2-bromo-3-alkylthiophene (6) in dry diethyl ether to freshly activated magnesium covered by diethyl ether. The Grignard reaction is delicate and highly sensitive to water, therefore the whole apparatus were kept dried in oven before usage. The magnesium turnings are highly heated to eliminate residual oxide before the reaction. In order to maintain the reactivity of the magnesium throughout the reaction, the addition of 2-bromo-3-alkylthiophene was controlled in a way we can observe bubbles of gas were continuously forming. After complete addition, the reaction was kept at reflux for 3 h.

On the other hand, 5,5'-dibromo-2,2'-bithiophene (8) was readily prepared by dibromination of bithiophene using 2 equivalent of N-bromosuccinimide. The 3,3'''-dialkyl-[2,2'; 5,2'';5'',2''']quaterthiophen-5-yl (9) was then synthesised following the procedure of Kumada coupling reaction[9]. The freshly prepared (3-alkylthiophen-2-yl) magnesium bromide was added via a cannula into a flask containing dissolved 5,5'-dibromo-2,2'-bithiophene and Nickel (II) catalyst dichloro[1,3-bis(diphenylphosphino)propane]nickel in a mix solvent of 60 ml of diethylether and 10 ml of freshly distilled THF, then kept at reflux overnight. A yellow product obtained after purification by silica gel column chromatography.

Following the synthetic strategy described above, QT6, QT8 and QT12 were prepared starting respectively from 3-hehylthiophene, 3-octylthiophene and 3-dodecylthiophene. Among the three dialkyl-quaterthiophenes synthesized in this work we were able to obtain a crystal of QT6 derivative suitable for X-ray diffraction, by crystallization at -4°C. In the triclinic P-1 structure the quaterthiophene is fully planar with alkyl chains substituents pointing in opposite directions with respect to the axis of the linear pi-conjugated system. (see Figure 49).

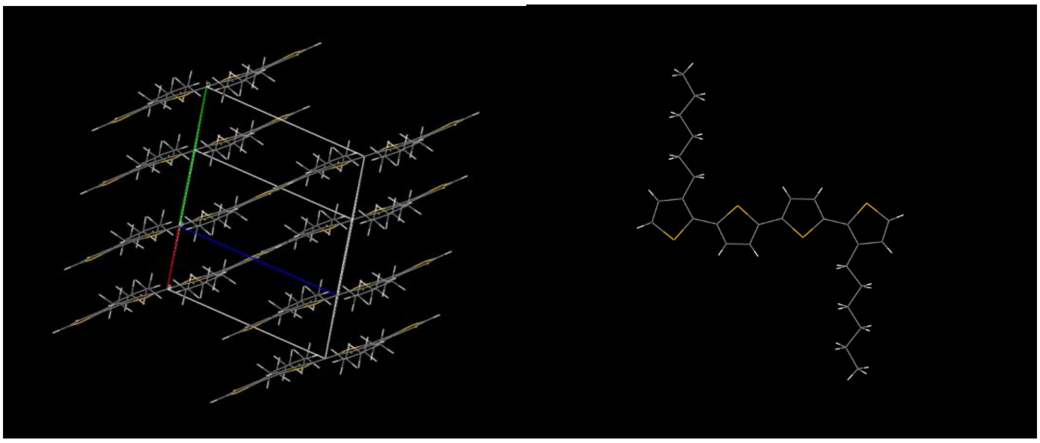

**Figure 49: Cristallographic structure of 3,3'''-dihexyl-[2,2'; 5,2'';5",2'''] quaterthiophen-5-yl QT6 crystal**

Therefore it is expected that the geometry of the final oligomers containing two highly planar oligothiophene segments will favour supramolecular aggregation by means of π-stacking interactions.

Next, for the final step of the preparation of 2,7-bis-(3,3'''-dialkyl-[2,2'; 5,2'';5",2'''] quaterthiophen-5-yl)-fluoren-9-one (QTFn), we carried out a cross coupling Stille reaction[10]. The donor block 3,3'''-dialkyl-[2,2'; 5,2'';5",2'''] quaterthiophen-5-yl (9) was first transformed to organostannane via monolithiation then addition of trimethyltin chloride to form trimethyl (3,3'''-dialkyl-[2,2'; 5,2'';5",2'''] quaterthiophen-5-yl )stannane (10). These stannane intermediates are toxic compound [11] therefore minimal work up were performed. The formation rate of the organostannanes was verified by $^1$H NMR to be 100%. The Stille reaction was then performed by introducing 2 equivalent of trimethyl (3,3'''-dialkyl-[2,2'; 5,2'';5",2'''] quaterthiophen-5-yl )stannane (10), one equivalent of 2,7-dibromo-9H-fluoren-9-one, and 5% of palladium (0) tetrakisphosphine catalyst formed in-situ. This Stille cross-coupling reaction gives two products, a small portion of mono coupling product (5 %) and the desired product 2,7-bis-(3,3'''-dialkyl-[2,2'; 5,2'';5",2'''] quaterthiophen-5-yl)-fluoren-9-one (QTFn).

QTF6, QTF8 and QTF12 were similarly synthesized. However, the reaction yield for QTF12 was quite low since we obtained only 10 % of pure product (50 mg). QTF8 and QTF6 were obtained with a yield of 20 % of pure product. The low yield can be explained by the purification steps which require several runs on column chromatography and several washings to achieve a high purity suitable for the later utilization of these products in the active layer of solar cells.

These products were characterised and identified by NMR spectroscopy and showed a good purity. Their NMR spectra were easily identified and correlate with the symmetrical character of the QTFn molecules. Side products of the reaction which differed with more peaks in the spectra where identified and correspond to the mono coupling products.

## II.2. Synthesis and purification of dimer thienylene-vinylene fluorenone TVF2

For the preparation of TVF and TVF2 it is necessary to synthesis thienylene vinylene units. The synthesis of thienylene vinylene compound is described in the literature using different coupling methods. One example was reported by Toyoshima and coworkers[12] via Kumada[13] cross coupling reaction of thienylene Grignard reagent with 1,2-transdichlomethylene using Nickel (II) as catalyst. In this work, we have conducted our preparation of thienylene vinylene via Titanium-induced dicarbonyl-coupling reactions proposed by John E. McMurry reaction[14] using titanium (IV) chloride with 3-octylthiophene-2-carbaldehyde. This one-pot synthesis reaction is presented in Scheme 2 .

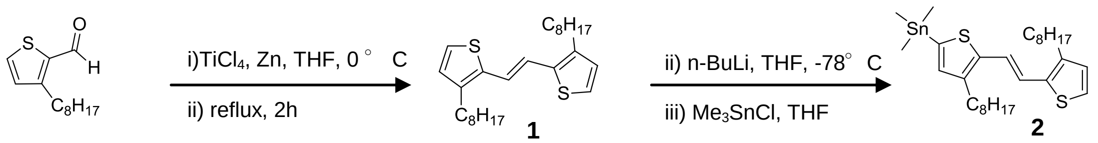


**Scheme 2: Synthesis of thienylene vinylene intermediate**

This reaction involves first the reduction of Titatium (IV) to Titanium (0) by zinc. The coupling reaction takes place in two steps, first an initial carbon-carbon-bond-forming of pinacol reaction of the two carbaldehydes, followed by a deoxygenation step to form the vinylene linkage. This reaction affords the desired thienylene vinylene compound (1) with a good yield of 55% after purification. It is to be noted that this reaction is highly exothermic and extra precautions are to be taken when dealing with $TiCl_4$ which reacts immediately with water in air, forming $TiO_2$ and corrosive fuming hydrochloric acid.

Next, we synthesised the thienylene-vinylene mono-stannane derivative via the classical procedure described previously. The oligomer TVF is prepared according to Stille coupling reaction. Two equivalents of the prepared (E)-trimethyl(4-octyl-5-(2-(3-octylthiophen-2-yl)vinyl)thiophen-2-yl)stannane (2) and 2,7-dibromo-9H-fluoren-9-one were heated at reflux in DMF and with presence of $Pd(PPh_3)_4$ as catalyst and $K_3PO_4$ salt as a base. (cf. Scheme 3)

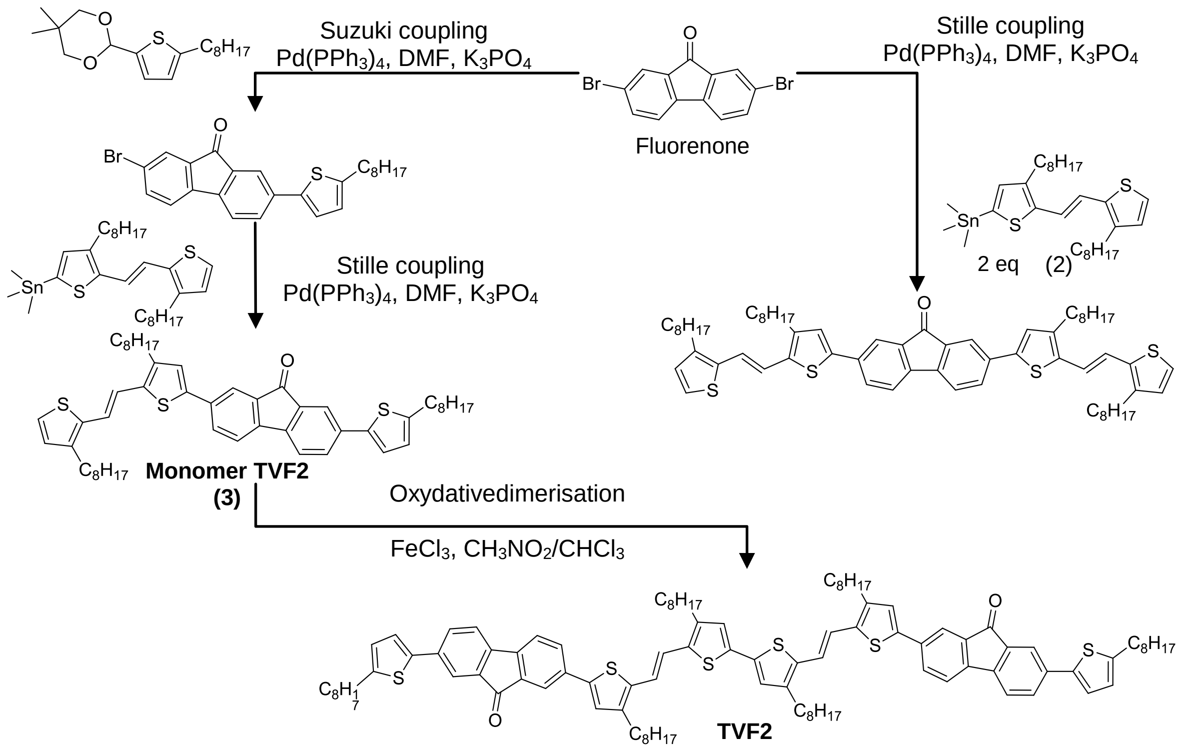


**Scheme 3: Synthetic routes for preparation of oligomers TVF and TVF2 departing from 9-dibromofluorenone and thienylene vinylene segment**

For the synthesis of the TVF2 molecule, we prepared first the dissymmetric monomer 2-bromo-7-(5-octylthiophen-2-yl)-9H-fluoren-9-one (3) via Suzuki coupling[10] between 5,5-dimethyl-2-(5-octylthiophen-2-yl)-1,3,2-dioxaborinane and 2,7-dibromo-9H-fluoren-9-one in DMF and with presence of $Pd(PPh_3)_4$ as catalyst and $K_3PO_4$ salt as a base. The dissymmetric monomer containing on one side a thienylene-vinylene unit and on the other side of the fluorenone moiety a thiophene unit was prepared via Stille cross coupling reaction of (E)-trimethyl(4-octyl-5-(2-(3-octylthiophen-2-yl)vinyl)thiophen-2-yl)stannane (2) and 2-bromo-7-(5-octylthiophen-2-yl)-9H-fluoren-9-one (3). The molecule (E)-2-(4-octyl-5-(2-(3-octylthiophen-2-yl)vinyl)thiophen-2-yl)-7-(5-octylthiophen-2-yl)-9H-fluoren-9-one (monomer TVF2) was obtained with a yield of 34%. The poor yield of this reaction can be related to a problem of solubility of the products in DMF but no optimization of this reaction was carried out in this work.

For the synthesis of TVF2, the obtained monomer (E)-2-(4-octyl-5-(2-(3-octylthiophen-2-yl)vinyl)thiophen-2-yl)-7-(5-octylthiophen-2-yl)-9H-fluoren-9-one (4) was then dimerised by oxidizing reagent iron (III) chloride in nitromethane and dichloromethane at 0 °C then allowed to warm to room temperature and stirred overnight. This dimerisation method was chose for it has proven to effective reaction for homopolymerisation of polyalkylthiophene[15]. As a work up procedure, the dimer TVF2 was then precipitated in methanol and treated with ammoniac solution with hydrazine for dedoping. It was then purified by column chromatography using silica gel to afford a product yield of 52 %. After removal of the solvent under vacuum, we obtained a dark metallic film similarly to a polymer film.

The dimer TVF2 was characterised by $^{1}H$ NMR and $^{13}C$ NMR spectroscopy. From $^{13}C$ NMR spectroscopy we have detected the presence of the CO groups of the molecule at 193.26 ppm. Moreover we have used infra red spectroscopy to confirm the molecular structures showing characteristic stretching vibration band of C=O, and of the vinyl units and the mass spectroscopy analysis showed the molecule dimer TVF2 with high purity showing a perfect accordance between the calculated and the found values. (Mass spectrometry $M^+$ ($C_{102}H_{126}O_2S_6$): z = 1 m/z Calculated: 1574.80767; Found: 1574.8073)

# III. Photo-physical characterisation of oligomers QTF and TVF2

## III.1. UV-Visble absorption spectroscopy study of QTF and TVF2

The optical and electrochemical properties of the molecules were studied using UV-Vis spectroscopy, photoluminescence spectroscopy and electrochemistry in order to understand the effect of chemical and structural modification on electronic properties.

The absorption spectra of QTFn molecules were similar and in this part we will report the results obtained for QTF8. Absorption spectrum of QTF8 in solution and in film is shown in Figure 50.

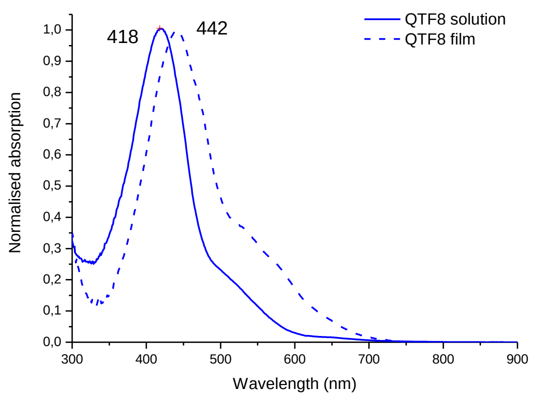


**Figure 50: UV Visible absorption spectra of QTF8 in solution (concentration= $10^{-5}$ mol.$L^{-1}$ ) and in film spin-coated on glass substrate from a 20 mg.$ml^{-1}$ chlorobenzene solution.**

| Compound | Absorption (solution) λmax (nm), ξmax ($M^{-1}$. cm-1) | Absorption (film) λmax (nm), | Eg $^{optic}$film eV |
|---|---|---|---|
| QTF8 | 418 (82700)<br>515 (19200) | 442<br>550 (weak) | 1.8 |

**Table 5: UV-Visible absorption peaks and optical band gap for QTF8**

In solution, QTF8 shows two absorption peaks. One intense peak is located at 418 nm with high molar extinction coefficient of *ca.* 82700 $M^{-1}.cm^{-1}$ that can be attributed to a π-π* transition[16]. The second peak appeared as a weak shoulder at 515 nm has been a subject of discuss by many groups and has been attributed to the n-π* transition of the carbonyl group of the fluorenone unit[1,17,] or to an internal charge transfer between the oligothiophene electron donating block and electron withdrawing fluorenone unit[18,19,20]. Another hypothesis was also made by Jaramillo and Turner, attributing the weak shoulder to a π-π* transition band of the aromatic ring of the fluorenone[21]. In our molecule QTF8, the shoulder showed a molar extinction coefficient of *ca.* 19 200 $M^{-1}.cm^{-1}$. This value is largely superior to the ones expected for a n-π*, indeed this type of transition are known to give a generally low transition molar extinction coefficient of *ca.* $\xi < 1000$ $M^{-1}.cm^{-1}$ [22]. Therefore we can attribute the weak shoulder to an internal charge transfer (ICT) absorption band, however a partial contribution of n-π* transition cannot be totally excluded.

In thin film, the maximum π-π* transition band is shifted by +24 nm at 442 nm. It can be attributed to a better delocalisation of the electrons of the pi-conjugated systems thanks to pi-stacking interaction and maybe a better planarity of the molecule induced by the quaterthiophene units. Indeed it has been shown earlier by determining the crystal structure of the quaterthiophene unit that this building block is highly planar. This feature could help for a better molecular packing in the solid state. This hypothesis is further demonstrated by apparition of vibronic sidebands showing the effect of aggregation. Such features have already been observed in highly organized oligothiophenes[23,24] and polythiophenes[25]. The optical band gap calculated from the offset wavelength of the absorption spectrum in film is found at 1.8 eV for QTF8.

To further confirm the different attribution of the absorption transition bands, we have also recorded absorption spectra of the electron-donating segment quaterthiophene QT8 and another similar molecule to QTF8 but with only two thiophene rings on each end, bithiophene fluorenone BTF8. The molecules structures and the absorption spectra are shown in Figure 51.

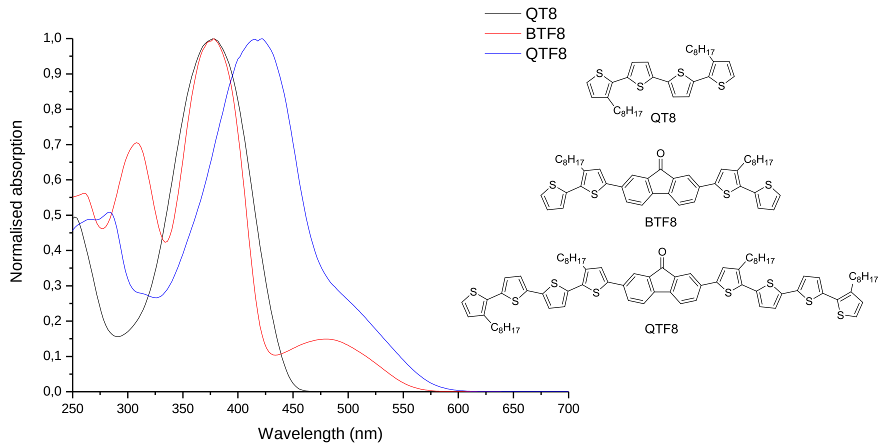


**Figure 51: UV visble absorption spectra of dioctyl quaterthiophene QT8, dioctyl bithiophene fluorenone, and dioctyl quaterthiophene fluorenone**

From the absorption spectra of these three molecules, we can clearly observed a bathochromic shift (+40 nm) of the π-π* transition band of QTF8 as compared to the molecules QT8 and BTF8 as an effect of increasing conjugation lengths. No weak peak or shoulder can be observed at higher wavelengths in the case of QT8. The internal charge transfer bands can clearly be observed in the alternating bithiophenes electron donating segments and fluorenone electron withdrawing unit. Replacing the bithiophene segment by a quaterthiophene segment which is a stronger electron donating unit results in a more intense internal charge transfer absorption band for the molecule QTF8 compared to the molecule BTF8. Besides the position of the ICT band is slightly shifted towards higher wavelengths. This result confirms that our design strategy is appropriate to obtain materials better matching the solar emission spectrum.

**As mentioned at the beginning of this chapter we seek to further increase the absorption spectrum for the new molecules. TVF2 is a symmetrical molecule which is composed of alternating electron-deficient subunit (fluorenone) and electron rich subunits (thienylene vinylene). TVF2 possesses two fluorenones, two thienylene vinylenes subunits at the centre and end-capped with an n-octyl thiophene. (see** Figure 52).

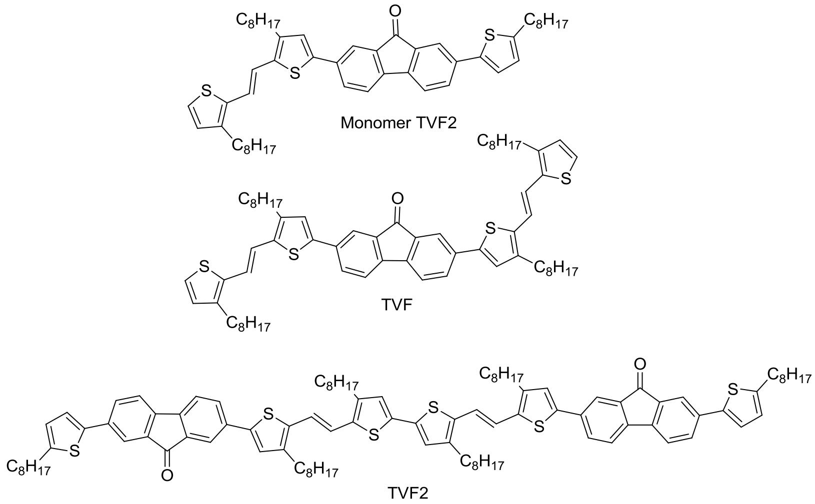


**Figure 52: monomer TVF2, TVF and TVF2 molecules structures**

As we can see, each molecule differs in terms of the number of thienylene vinylene units and/or fluorenone units, as well as its position in the structures. TVF has a symmetrical structure with fluorenone unit at the centre in between the thienylene vinylene group. Therefore it is interesting to investigate the effect of the chromophoric units on the molar coefficients of absorption and the absorption spectra of the molecules.

The absorption spectra for the molecules TVF, monomer of TVF2 and TVF2 are measured in a dilute solution of chloroform under the same concentration to allow effective comparison. The absorption spectra are presented in Figure 53.

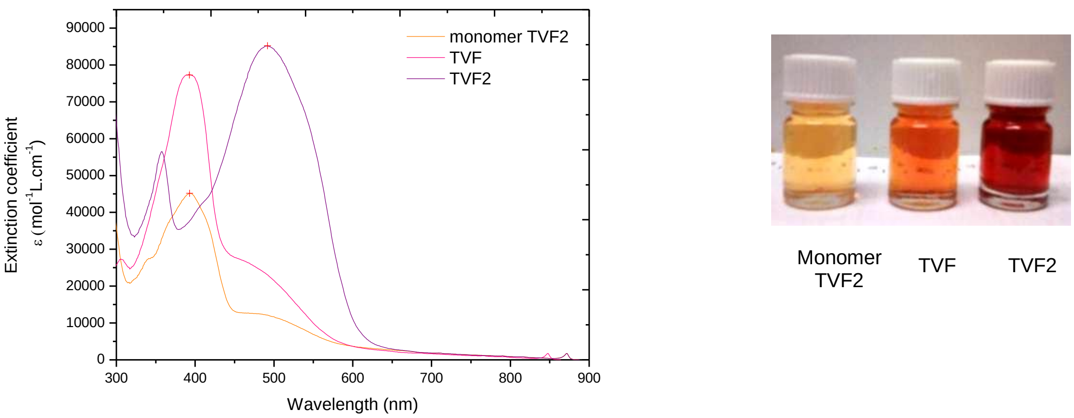


**Figure 53: Absorption spectra of monomer of TVF2, TVF and TVF2 in diluted chloroform solution (12.5 x $10^{-6}$ mol $L^{-1}$)**

| Compound | Absorption ($\lambda max$, nm ($\xi$, $M^{-1}.cm^{-1}$) ) |
|---|---|
| Monomer | 393 (45100); |
| | 491 (12200) |
| TVF | 393 (77300) ; |
| | 484 (24200) |
| TVF2 | 357; (56500); |
| | 492 (85200) |

**Table 6: Absorption peaks and molar extinction coefficients of monomer of TVF2, TVF and TVF2**

First we compare the absorption spectra of the monomer and TVF. We can note that replacing the thiophene unit at one end by a thienylene vinylene unit allows an increase in the absorption band intensity especially on a more pronounced internal charge transfer band. The maximum absorption peaks $\lambda_{max}$ for the monomer and TVF are located at the same wavelength at 393 nm. This suggest that this absorption band corresponds to a π-π* transition[21] originating from the thienylene vinylene unit being in conjugation with the fluorenone core. By adding a thienylene unit in the chemical structure, one can see that the molar coefficient of absorption of the monomer for this transition is strongly increased (almost double). The molecular coefficient of absorption for TVF2 associated with the transition at 484 nm (at 24200 $M^{-1}$. $cm^{-1}$) is consistent with the ICT character of this type of transition. (In the case of n-π* transition epsilon values are lower than 1000 $M^{-1}$. $cm^{-1}$)[26]. The optical spectra of the monomer and TVF showed similar offset values, therefore the optical band gap of both molecules are equivalent.

After dimerisation, the π-conjugated system associated with the thienylene vinylene units is fully extended in the dimer TVF2. The absorption spectrum of the dimer TVF2 exhibits an extra shoulder at the high-energy side of the absorption spectrum at 357 nm and an intense broad dissymmetric peak at low energy side of the spectrum (492 nm). We observe a red shift of *ca*. 100 nm of the maximum absorption peak from 393 nm to 492 nm. This increase is a result of a strong delocalization of the electrons over the thienylene segments as it has already been evidenced by Roncali and co-workers[27] on oligothienylene coumpounds. The intense and broad absorption peak at 492 nm can be distributed to the synergistic contribution of the π-π* transition band of the thienylene bridge that superimpose with the ICT band.

By increasing the conjugation length of the system as well as increasing the number of electron releasing (thienylene vinylene) and electron withdrawing units (fluorenone) we managed to broaden the absorption spectrum and increasing simultaneously the molar extinction coefficient of absorption from ca 45100 $M^{-1}$. $cm^{-1}$ to 77300 $M^{-1}$. $cm^{-1}$ and to 85200 $M^{-1}$. $cm^{-1}$ for the monomer, TVF and TVF2 respectively. The dimerisation has resulted in a strong improvement of the optical properties of the final system. As a general trend we can notice that in this series of molecules the measured values of the molar absorption coefficients of the ICT bands are higher with increasing donor strength.

In order to study the photo-physical properties of the dimer TVF2 in the solid state, the absorption spectrum of TVF2 in film is presented in Figure 54 as well as the absorption spectrum in solution for comparison.

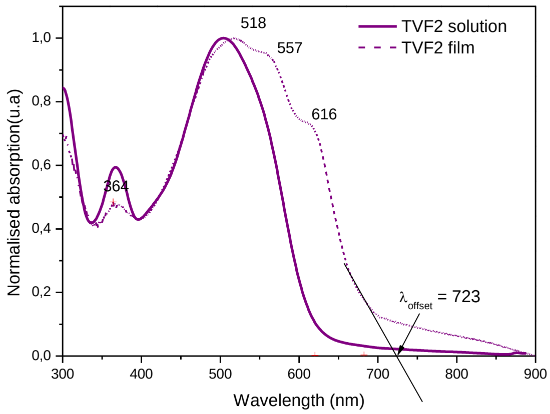


**Figure 54: Normalised absorption spectra of TVF2 in diluted chloroform solution (12.5 x $10^{-6}$ mol $L^{-1}$) and in thin film deposited by spin coating on glass substrate**

In solution, we observed two peaks: one located at 357 nm and an intense peak at 492 nm with a broad absorption close to 700 nm. In solid state, the absorption spectrum is broadened with the first peaks at 364 nm, the second peak at 518 nm which is slightly red-shifted of 26 nm. This confirms a better planarity and more enhanced conjugation in the solid state that result in strong π-stacking interactions[2829]. Moreover, vibronic sidebands can be observed in the solid-state spectrum of TVF2 at 557 nm and 616 nm, attributed to strong molecular aggregation in solid states[30]. Such features have previously been observed for other π-conjugated systems such as oligothiophenes[37] and polythiophenes[25] indicating the formation of densely packed layers involving π-stacking interactions and can eventually form nanofibres.The optical band gap value calculated for TVF2 derived from the absorption edge tangent was found to be 1.71 eV.

Several studies on polymers and oligomers have shown that it is also possible to grow nanoaggregates in solution as for the poly(3-alkylthiophene) which can form nanofibers.[31, 25, 32]. Therefore we have performed preliminary tests of formation of nanoaggregates of the dimer TVF2 in solutions. The study on formation of nanoaggregates in solutions is delicate and we have to choose a good solvent to dissolve completely the molecules and a poor solvent to favour the aggregates formation. After several tests carried out to determine the solubility of the molecule in various solvents, we have chosen chloroform as a good solvent and acetonitrile as poor solvent. The dimer TVF2 is completely dissolved in chloroform and acetonitrile is added to these dilute solutions. The absorption spectra of the solutions according to the solvent mixture ratios are shown in Figure 55.

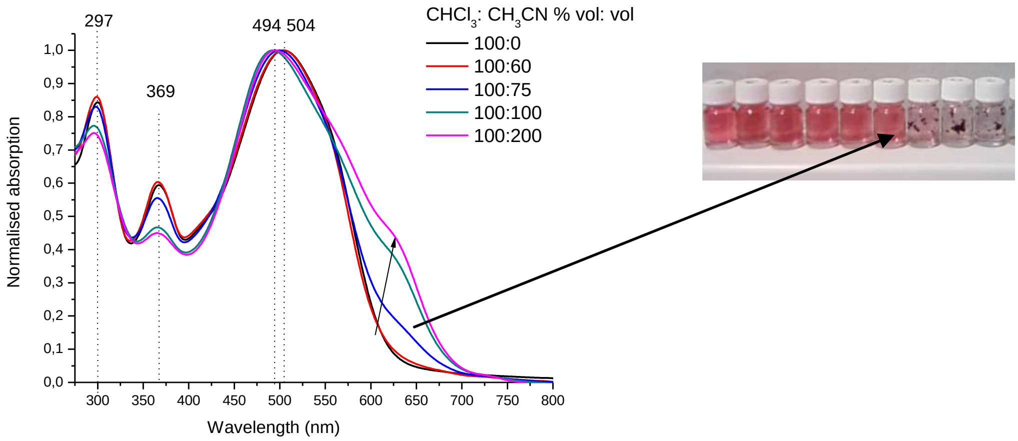


**Figure 55: Absorption spectra of dimer TVF2 in solutions mixture of chloroform (good solvent): acetonitrile (poor solvent).**

The solutions are prepared by making soleuvent mixtures of chloroform and acetonitrile. A solution of 100:60 is equivalent to 10 ml of choloroform and 6 ml of acetonitrile. The solution is then prepared by dissolving TVF2 in order to have a concentration of $10^{-6}$ mol.$L^{-1}$. The molecules TVF2 are completely dissolved and give red solution for the concentration ratios below 60 % of acetonitrile and 100 % chloroform. At concentration ratios of 75 % acetonitrile and 100% of chloroform, we observed change of colour of solution to light purple and formation of large aggregates in the solution. At this point, the absorption spectrum also demonstrated apparition of new vibronic bands at 650 nm which is consistent the wavelength of the vibronic feature observed in this films. Bigger aggregates are then formed when we further increase the volume of acetonitrile in the mixture. Therefore from this preliminary test on aggregates formation in solution, we did not succeed to form nanoaggregates soluble in the solution mixture, and rather form large aggregates. This might be an indication of a strong tendency of this molecule to self-assemble. This will be investigated more into details later by scanning probe microscopy techniques.

We now compare the optical properties of TVF2 compared to QTF8. The absorption spectra of QTF8 and TVF2 are presented in Figure 56 and the values of absorption peaks and optical band gap reported in the Table 7 for comparison.

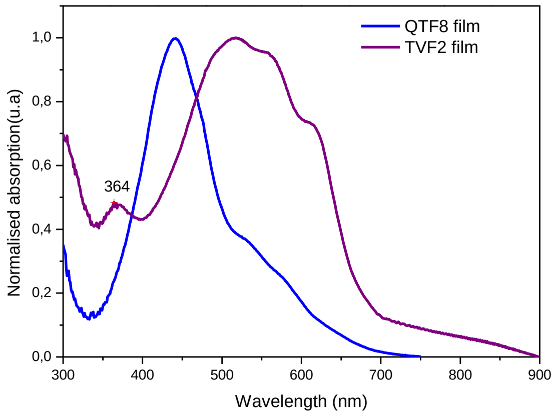


**Figure 56: Absorption spectra of QTF8 and TVF2 films**

| Compound | Absorption (solution) λmax, nm (ξ, M-1.cm-1) | Absorption (film) λmax, nm | Eg optic(film) eV |
|---|---|---|---|
| TVF2 | 357, (56492); 492 (85187) | 364; 518; 557; 616 | 1.71 |
| QTF8 | 415 (82736) 515 (19161) | 425; 515 (weak) | 1.80 |

**Table 7: UV-Visible absorption parameters of TVF2 and QTF8**

TFV2 molecules have a broader absorption thus a smaller band gap of 1.80 eV compared to 1.90 eV for QTF8. The decrease of band gap for the molecule TVF2 is expected with the increasing planarity of the thienylene-vinylene bridge which enhanced the π-electron delocalisation[33]. Similar results have been demonstrated by several research groups with polythienylene-vinylene showing lower band gap values (~1.60 eV-1.80 eV)[1, 34] than polythiophenes[35] (~1.9 eV).

## III.2. Photoluminescence emission spectroscopy study of QTF and TVF2

For further investigation of the photo-excited state of the molecule QTF8, photoluminescence emission spectrum of QTF8 is recorded at different excitation wavelengths of 400 nm and at 550 nm as shown in Figure 57.

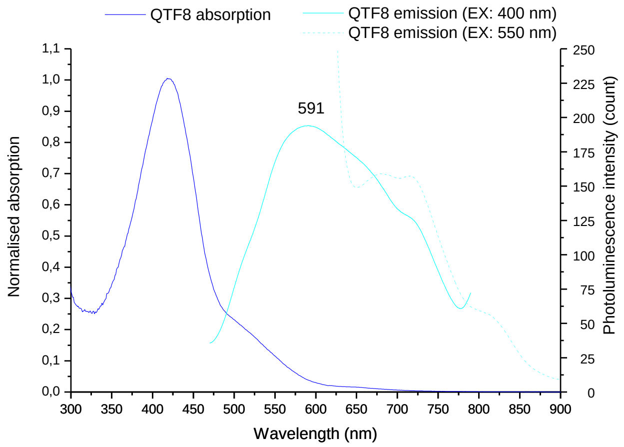


**Figure 57: Normalised absorption spectra of QTF8 (blue line) and photoluminescence spectra of QTF8 in solution with excitation wavelength of 400 nm (light blue line) and at 550 nm (light blue dotted line).**

When we excite the molecule at this band at 400 nm, a broad emission peak is observed with a maximum peak at 591 nm. This gives rise to a large Stokes shift of 173 nm. Large Stokes shifts are expected for ICT transitions[20]. In our case, the large Stokes shift could be considered as a confirmation of our previous hypothesis. Excitation at 550 nm, also exhibit similar intense emission band and more resolved vibronic bands confirming the attribution of the internal charger transfer ICT band. The featureless ICT absorption band and the vibrationally resolved luminescence indicate that the excited-state geometry is more defined and more ordered than the ground-state conformation[36]. The vibronic bands are also well resolved in both emission spectra as previously observed in the absorption band in film, suggesting high interchain interaction of the molecules[37, 38].

Nguyen and coworkers[38] also observed this phenomenon on the polymer MEH-PPV photoexcitation and have attributed the presence of vibronic bands to aggregates formation on solution. More over they suggested that ‘‘memory’’ of the solution-phase conformation is retained through the casting process, and can form readily aggregates in film. This further confirmed our previous hypothesis on aggregation in solid state based on film absorption spectrum. Their study on the on the role of the aggregates also demonstrated that the aggregate band clearly results in a longer photo-induced absorption decay. Therefore from the absorption and fluorescence spectroscopy we can hypothesize that supramolecular organisation of the QTF8 molecules occurs[39] and this might lead to longer photoinduced absorption decay. To further confirm the good self-assembly properties the molecules will be later investigated in solid state using scanning probe microscopy techniques.

In order to study the photo-excitation properties of the molecules TVF2, photoluminescence emission study of the TVF2 molecules in dilute solutions are recorded as shown in Figure 58.

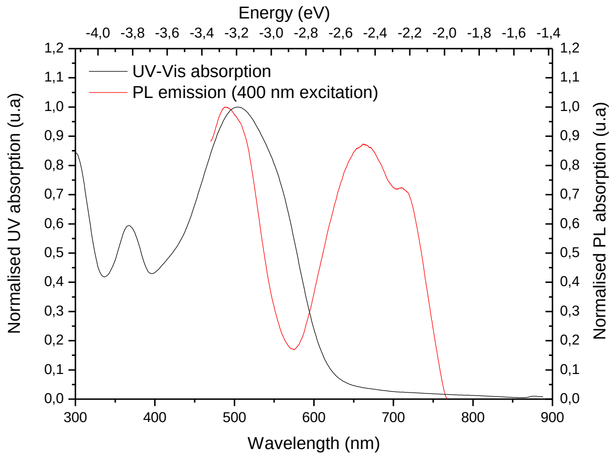


**Figure 58: UV-Visible absorption spectra and photoluminescence emission spectra of dilute solution of TVF2**

TVF2 in solution was excited at a wavelength of 400 nm. We observed a first emission band with a maximum at 500 nm, a second broad emission band at 650 nm, and apparition of a shoulder band at longer wavelength. Interestingly we observed partial quenching of the emission for the region between 550 nm to 600 nm which is overlapped with the internal charge transfer absorption weak shoulder band. The Stokes shift value is large at about 150 nm. These two features confirm the presence of the internal charge transfer band in the oligomer TVF2 in addition to the luminescence originating from a classical radiation emission from a π-π* transition (peak at 500 nm). Furthermore, the inhomogeneously broadened absorption and the vibrationally resolved luminescence indicate that the excited-state geometry is more defined and more ordered than the ground-state conformation.[36] The result obtained is similar to the molecule QTF8 and suggests similarly that supramolecular organisation of the π-conjugated system occurs in solution and in solid state[38,39].

# IV. Electrochemical characterisation of oligomers QTF and TVF2

## IV.1. Electrochemical characterisation of quaterthiophene fluorenone QTF8

Optical band gap measurements can provide estimation of the energy differences of the frontier orbitals, whereas oxidation and reduction potentials provide additional information on the absolute positions of HOMO and LUMO energy levels which are particularly important parameters for a better understanding of solar cells performances.[40] We have performed cyclic voltammetry CV measurements using the oligomer QTF8 for determination of its energy levels. Cyclic voltammogram was recorded from a dilute dichloromethane solution in presence of tetrabutylammonium hexafluorophosphate (0.1M) as supporting electrolyte, presented in Figure 59.

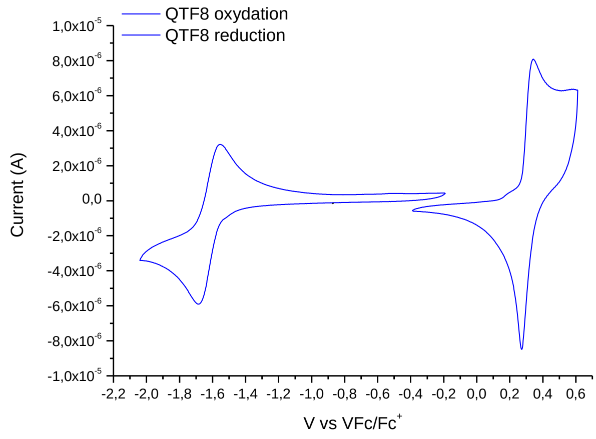


**Figure 59: Cyclic voltammogram of QTF8 recorded in $CHCl_2$ solution in 0.1 M $nBu_4FP_6$ with scan rate of 20 mV/s.**

Electrochemical oxidation of QTF8 gives rise to an anodic peak at E = 0.21 V and upon negative potentials a reduction peak is observed at -1.60 V. Both peaks are reversible and allowing us to calculate the energy levels of the molecules. For the calculation of the energy levels we used the ferrocene/ferrocenium redox couple as calibration reference[41]. From the oxidation and reduction potentials values, calculation of the HOMO and LUMO energy levels showed values at -5.01 eV and -3.20 eV respectively following empirical formula ($E_{HOMO}$ = - ( $E^{oxydation}$ - 4.8 ) eV ; $E_{LUMO}$ = - ( $E^{reduction}$ - 4.8) eV ) as described in the Chapter Experimental Methods and Materials. Estrada and coworkers[18] who studied molecules based on fluorenone with similar donor-acceptor-donor configuration as our molecule QTF8, have demonstrated by DFT calculations that the HOMO orbitals are mainly localised in the electron-donating segment, while LUMO orbitals are localized in the electron accepting fluorenone unit. They recorded reduction potentials in their systems at -1.5 V (V vs $V_{Fc/Fc+}$) close to the value obtained for the molecule QTF8. Turner and coworkers[21] has also recorded a LUMO value of -3.2 eV for fluorenone based molecule with D-A-D configuration. For the HOMO energy levels which localised on the quaterthiophene segment, a value of -5.1 eV was found by E. Lim and coworkers [42] of a oligomer based on benzothiadiazole-quaterthiophene, consistent with our experimental value.

We obtained electrochemical band gap of $Eg^{ec}$ = 1.81 eV for QTF8. The calculated electrochemical band gap is slightly higher by 100 mV than the value obtained by optical band gap calculation of 1.90 eV. All the values are reported in the Table 8 with comparison of calculated values of optical band gap.

| Compound | Eg optic(film) | Eoxydation/V | Ereduction /V | HOMO | LUMO | Eg elec |
|---|---|---|---|---|---|---|
| QTF8 | 1.80 | 0.21 | -1.60 | -5.01 | -3.20 | 1.81 |

**Table 8: Optical and electrochemical properties of QTF8**

## IV.2. Electrochemical characterisation of dimer thienylene-vinylene fluorenone TVF2

Cyclic voltamperometry analyses were performed for the monomer TVF2 and the dimer TVF2, and the cyclic voltammograms are as shown in Figure 60.

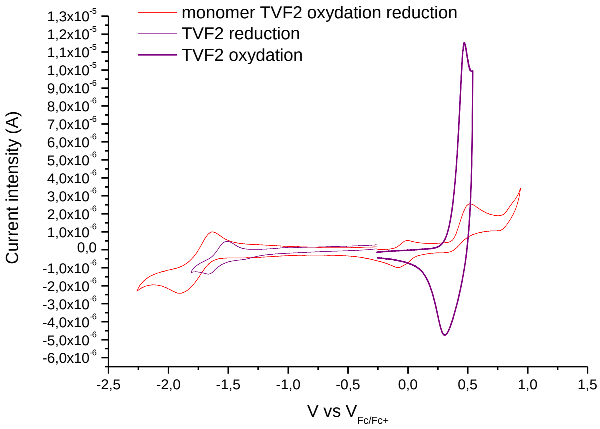


**Figure 60: Cyclic voltammograms of the monomer TVF2 and the dimer TV2 prepared by chemical oxidation**

The electrochemical parameters of the three different molecules monomer TVF2, dimer TVF2 and TVF are reported in Table 9.

| Compound | Eox(V) | Ered (V) | HOMO | LUMO | $Eg^{elec}$ |
|---|---|---|---|---|---|
| Monomer TVF2 | 0.38 | -1.64 | -5.18 | -3.16 | 2.02 |
| TVF2 | 0.27 | -1.53 | -5.07 | -3.27 | 1.80 |
| TVF | 0.36 | -1.66 | -5.16 | -3.14 | 2.02 |

**Table 9: Electrochemical parameters of the monomer TVF2 and dimer TVF2 compared to the previously published TVF molecule[16]**

From the cyclic voltammograms, the monomer TVF2 showed reversible oxidation and reduction peaks upon anodic and cathodic polarization. The first weak oxidation peaks at about 0 V is attributed to ferrocene which was used as a reference for the accurate positioning of the redox potential. The second intense peak corresponds to the oxidation potential of monomer TVF2 at 0.38 V and upon cathodic voltage a reduction potential at -1.64 V is observable. These oxidation and reduction potentials give HOMO and LUMO energy levels of monomer TVF2 at -5.18 eV and -3.16 eV respectively.

The dimer TVF2 showed reduced oxidation potential value of 0.27 V and a higher reduction potential value of -1.53 V, giving HOMO and LUMO energy levels of -5.07 eV and -3.27 eV respectively. The band gap of the dimer TVF2 of 1.8 eV is therefore 0.2 eV lower than the band gap of its monomer (2.02 eV). The lower energy band gap of the dimer TVF2 is fully consistent with the optical properties observed previously. This trend is also observed in polymer PTVF having lower band gap of 1.52 eV[1] as compared to the monomer TVF having a band gap of 2.02 eV[16] as a result of extended π-conjugation length. The HOMO and LUMO energy levels of the monomer TVF2 are closed to the values of the molecule TVF with the same electrochemical band gap, which are expected from the previously studied optical properties.

Furthermore, The dimer TVF2 can also be prepared by electrochemical oxidative polymerization (or electropolymerisation) by departing from monomer TVF2 as demonstrated for the polymer PTVF by departing from the monomer TVF[1,43]. The monomer TVF2 was dissolved in a mixture of dichloromethane: acetonirile 1:1 and by applying anodic potentials between 0-0.75 V (V vs $V_{Ag/Ag+}$) repetitively up to 40 cycles for electropolymerization. We therefore formed thin layer of dimer TVF2 on the surface of the working electrode. Cyclic voltammetry scans accompanying the voltammetric electrodimerisation of the monomer of TVF2 are shown in Figure 61. In addition to the onset of the irreversible oxidation peak at 0,60V, a redox couple increasing in intensity with each consecutive scan can clearly be seen. This couple is associated with the doping and dedoping of the dimer deposited on the electrode[43].

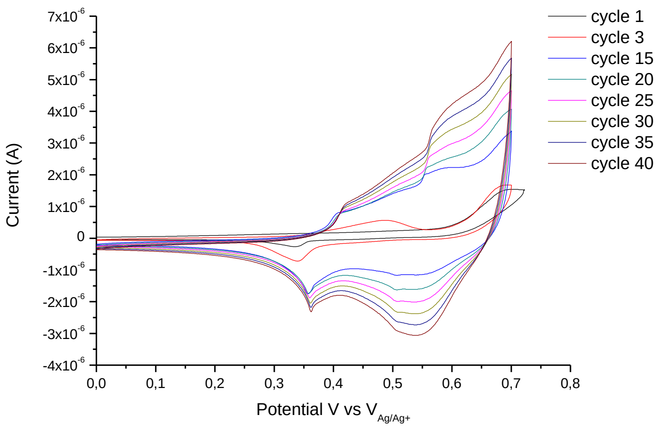


**Figure 61: Oxydative polymeristaion by electrochemistry of monomer TVF2 by repetitive cycles of oxidation in dichloromethane: acetonirtile with a scan rate of 100 mV. $s^{-1}$.**

Similarly we also performed electrodimerisation of monomer TVF2 on ITO/glass substrate to allowed direct characterisation of optical properties. A solution of 0.25 mmol/L of TVF in a micture of solvent dichloromethane: acetonitrile 1:1 with 0.1 M tetrabutylammonium hexfluorophosphate as supporting electrolyte. After applying 40 cycles of anodic voltage, a thin layer of film is deposited on the surface of ITO.

The film was characterized by UV-visible absorption and the spectrum was recorded. Similarly, we also deposited on ITO substrate by spin-coating a thin film of a solution of TVF2 at a concentration of 10 mg/ml in chlorobenzene prepared by chemical dimerization. The UV-visible absorption spectra are presented in Figure 62. We observed very similar absorption spectrum in terms of the peaks for both of the films. However for thin film deposited by electrodimerization, we observed improved vibronic bands intensity. The electro-deposited film allows layer by layer packing of the molecules therefore the vibronic bands are more resolved[36] as compared to the spin-coated TVF2 prepared by chemical oxidative dimerisation. Similar results have also been observed in the polymer PTVF absorption spectra prepared from chemical polymerisation[1] and electropolymerisation[43].

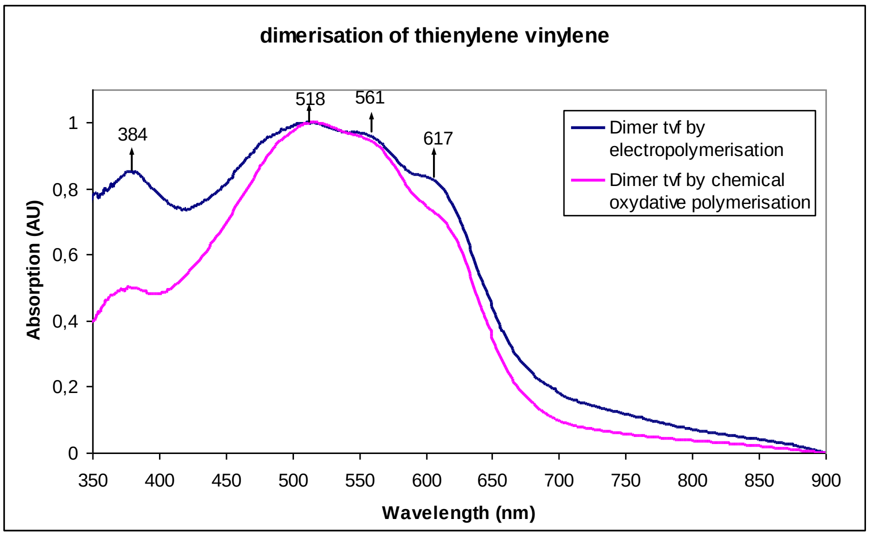


**Figure 62: UV-Visible absorption spectra of TVF2 film deposited on ITO by electrochemical oxidative polymerisation and chemical oxidative polymerisation**

To conclude, the solid state absorption spectra of TVF2 unequivocally indicate that the polymerization reaction of monomer TVF2 either performed using oxidating reagent or via electrochemical process give rise to the formation of the same dimeric species.

# V. Supramolecular assemblies of oligomers QTF and TVF2

Previous photophysical studies of quaterthiophene fluorenone QTF and the dimer thienylene vinylene fluorenone TVF2 have suggested that these molecular systems are suitable for the preparation of ordered layers thanks to supramolecular organisation of the π-conjugated system in the solid state. Atomic force miscroscopy (AFM) study can allow investigation of the self assembly properties of the molecules. The AFM studies on these molecules are performed in collaboration with Dr. Benjamin Grevin, Dr. Evan Spadafora, Dr. Shuichi Nagamatsu and Dr. Philippe Leclerc. Molecular modelling of the assemblies was performed by Dr. Mathieu Linares.

## V.1. Quaterthiophene fluorenone molecules QTF

In order to investigate the self-assembly properties of the different materials prepared in this work we prepared thin films and monolayers on HOPG, Mica, Silicon, and Glass substrates. The following results have been obtained using glass substrates. The oligomers QTF6; QTF8 and QTF12 were deposited by drop-casting onto the substrates from dilute toluene solutions of 0.05mg/ml. The solvents were slowly evaporated under toluene saturated atmosphere for 24 h allowing the molecules to self organise onto the substrates forming one monolayer or few layers Figure 63.

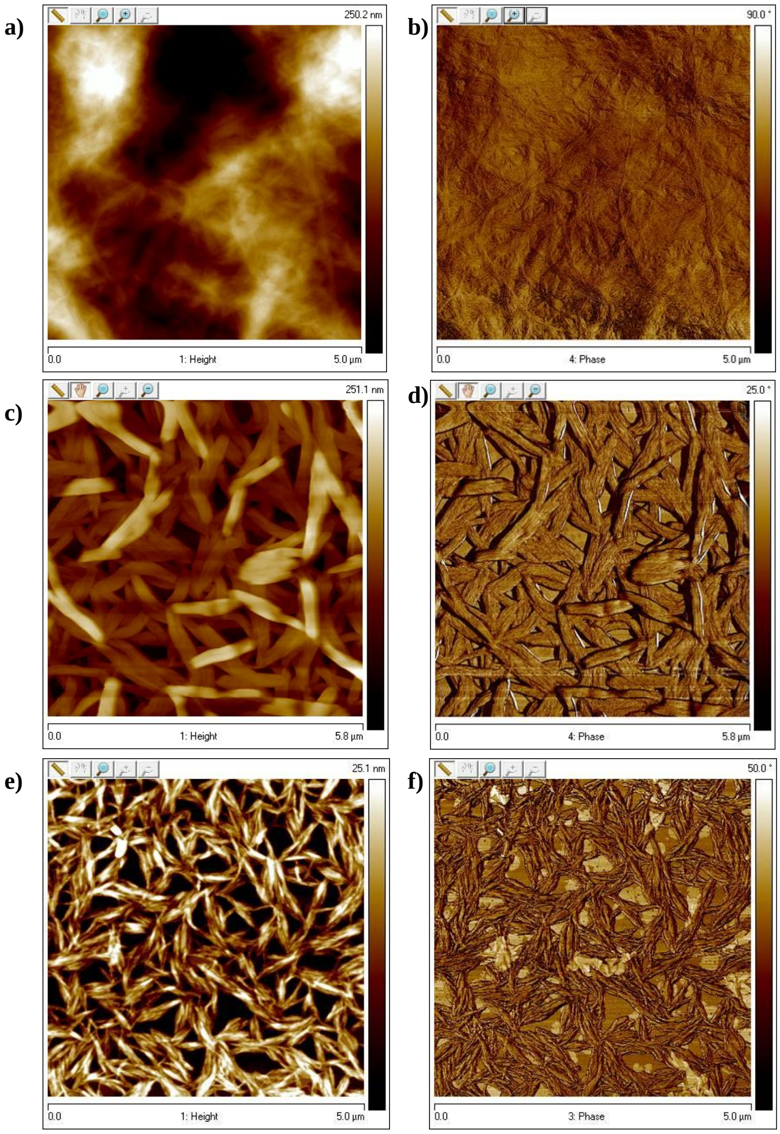


**Figure 63: 5.0 µm x 5.0 µm AFM height (left) and phase (right) images of thin deposits of QTF6 (a and b), QTF8 (c and d) and QTF12 (e and f) from dilute solution of toluene (0.05 mg.ml$^{-1}$) drop-cast on glass substrates.**

The AFM images in Figure 63 revealed all three molecules of QTFn can spontaneously self-organise forming entangled nanofibres. QTF6 with short hexyl side-chain showed long and finer fibres, while QTF8 molecules showed larger nanofibers compared to QTF6 and QTF12. For QTF6 with shorter hexyl chain, the molecules will have smaller packing therefore we observed finer but densely packed fibers. Similar tendency was observed for poly(alkylthiophenes) bearing side alkyl chains of different lengths [44]. In the case of QTF12 bearing dodecyl chains compared to QTF8 bearing octyl chains, we would expect that the molecular packing would give larger fibre, but upon increasing the alkyl chain length we also increase the solubility in the solvent, therefore QTF12 will have longer time to self-organise compared to QTF8.[44] In addition we can observe that the fibres are composed of super fine nanowires stack side by side, notably visible in the QTF8 image.

We decided to investigate more into details the structure of the nanofibers fabricated using QTF8 molecule. Further investigations of the molecules QTF8 were then performed with non-contact AFM[45] and Kelvin probe microscopy[46] allowing investigation of local conformation within 1D stacks and local contact potential difference of the molecules self assembly.

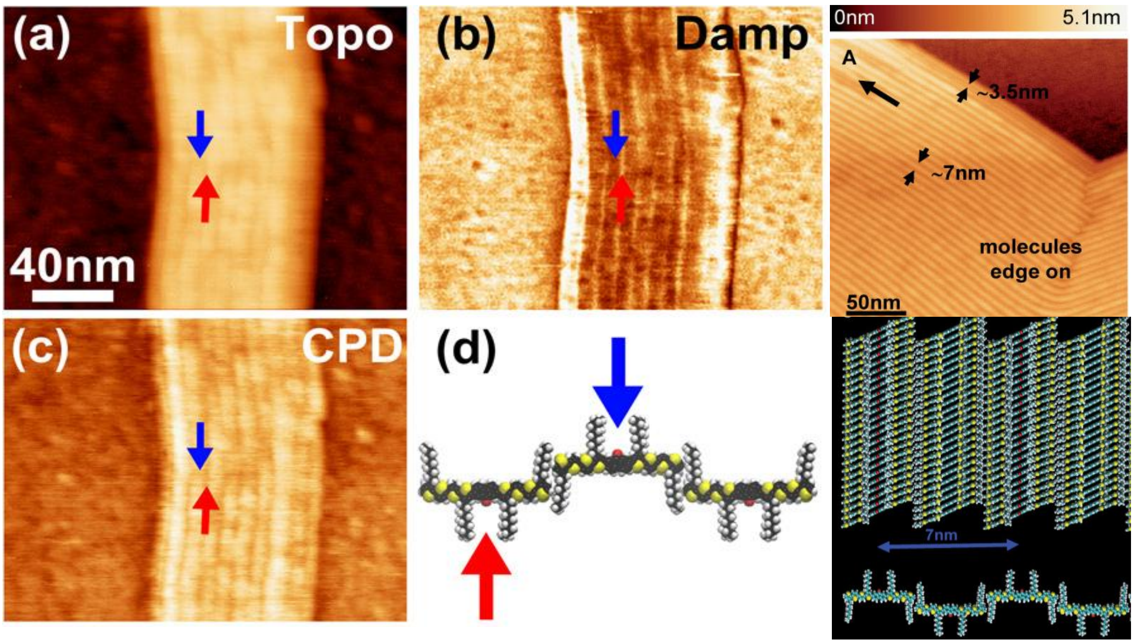


**Figure 64: Frequency modulation atomic force microscopy topographic image (a) and damping image (b). (c) Kelvin Probe microscopy contact difference potential image. (d) and (e) Molecular modeling of 'edge-on' stacks of the molecules QTF8 on HOPG substrates. Arrows pointing up and down highlight the locations corresponding to the two different molecular orientations.**

When deposited from solutions on HOPG, QTF8 molecules self-assemble into edge-on pi-conjugated nanowires stacks[45,46], which structural organization has been established by combining the results of NC-AFM with molecular mechanics (MM) and molecular dynamics

(MD) simulations as shown in Figure 64. After in-situ annealing, QTF8 stacks consist in non-polar layers in which the orientation of the fluorenone unit (carrying the main molecular electric dipole) alternates from one wire (C=O bond pointing upward) to the next (C=O bond pointing downward), leading to a doubling of the lattice periodicity (ca. 7 nm) with respect to the single nanowire width.

This study fully confirms the hypothesis that we made on the basis of the UV-Vis spectroscopy study in solution and in solid state. QTFn oligomers show a strong tendency to spontaneously self organize in solid state and this peculiar behaviour is expected to improve the photovoltaic performances when the molecules will be investigated in real devices.

## V.2. Dimer thienylene-vinylene fluorenone TVF2

Self assembly of the dimer molecules TVF2 was investigated on various substrates. We prepared thin films and monolayers on HOPG, Mica, Silicon, and Glass substrates. The following results have been obtained mica glass substrates. The samples were prepared by drop-casting 10 µL of dilute solution of TVF2 in toluene of 0.4 mg/ml concentration onto the substrates.

**AFM topographic image and phase image of thin deposits of TVF2 are presented in**

Figure 65. The surface morphology images revealed highly ordered packing of TVF2 forming nanofibers similar to the QTFn molecules in the solid state.

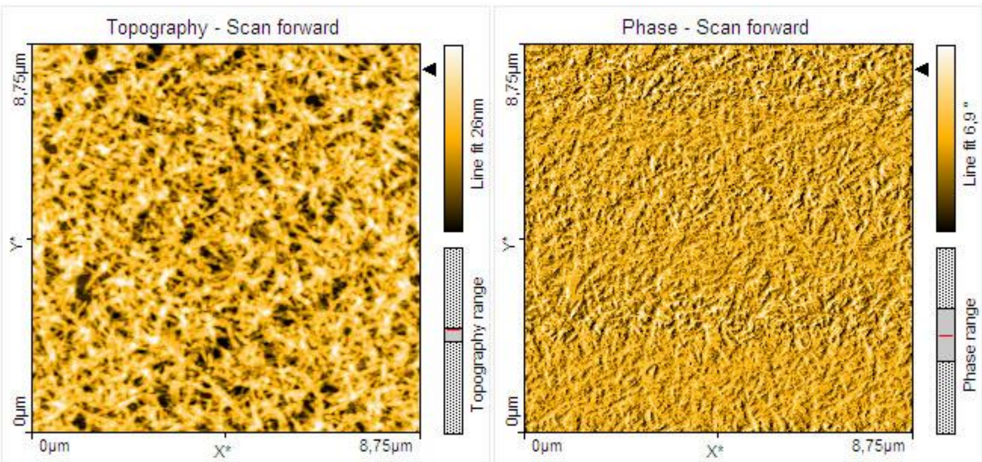


**Figure 65: 8.75µm×8.75µm AFM topographic image (left) and phase image (right) of thin deposit of TVF2 in toluene (0.4mg/ml) drop-cast on mica**

Based on the preliminary results obtained on various substrates, we hypothesized that the nanofibers based of the dimer TVF2 in solid state are formed by π-stacked oligomers organised according to a herring bone configuration. This conclusion is drawn from the histogram height values. In herring bone configuration, the molecules are oriented almost perpendicular to the substrate plane in their crystalline form[47] (see Figure 66). Herring bones packing are commonly obtained in polar substrates such as mica and on polar substrates like mica and oxidized silicon (SiOx)[37].

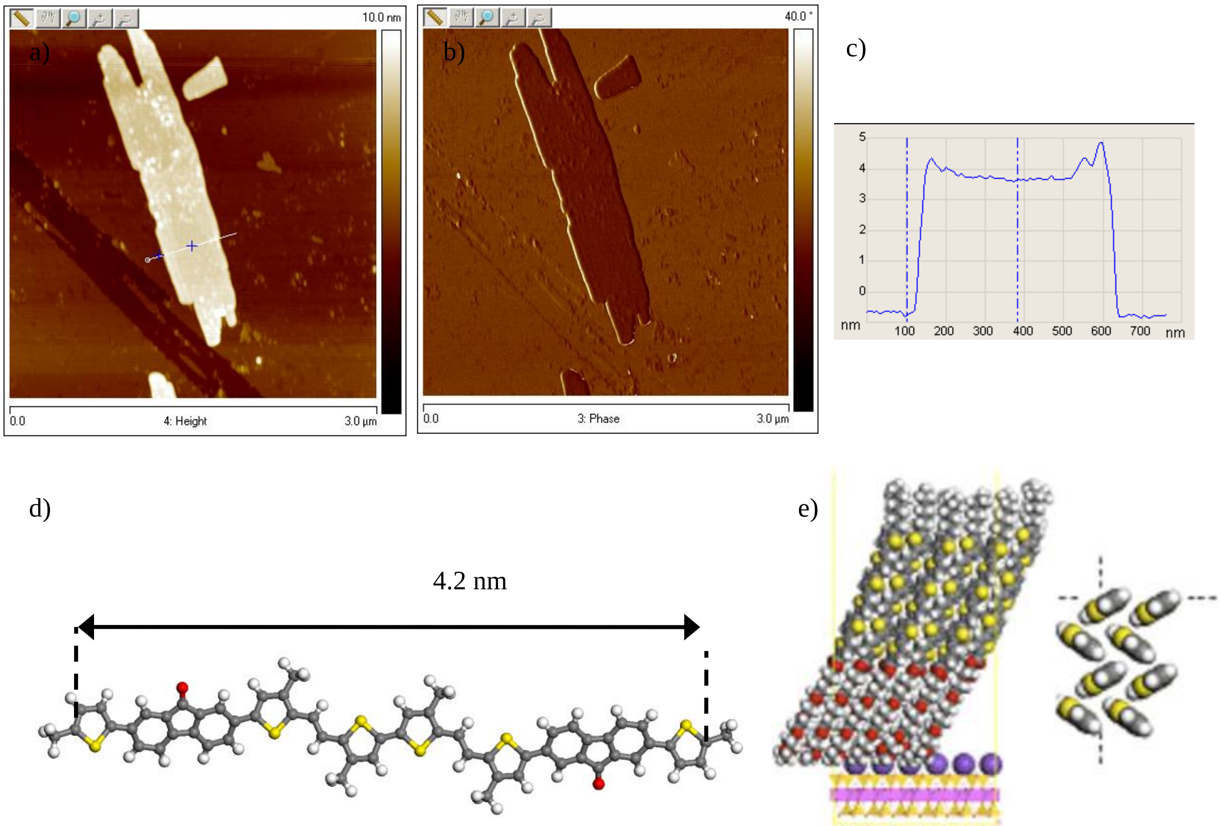


**Figure 66: AFM topographic image (a) and phase image (b) of the dimer TVF2 molecules on mica substrate from dilute toluene solution (0.12 mg. mL$^{-1}$). (c) Histogram of the height values extracted from the cross section area in the image (a). Geometry optimized of the molecule TVF2 shown with groups instead of octyl by molecular modelling. (e) Model molecules adopting herring bone configuration ( image reproduced from Ph. Leclerc and coworkers[37])**

From the atomic force microscopy studies, we can therefore conclude the oligomers QTFs and TVF2 exhibit highly ordered nanofibres in the solid state when deposited in film from dilute solutions. However the oligomers show different preferential orientations with respect to the substate. QTFn molecules are going to give rise to the formation of edge on stracks whereas the TVF2 molecule will form stacks with an hering bone orientation. The results are particularly interesting for application in organic photovoltaic as the transport processes of the electronic excitations and the charge carriers are very strongly affected by the degree of order in the thin films. This has been demonstrated in polymers (poly 3-alkylthiophenes) with nanofibres structures showing enhanced photovoltaic efficiency compared to amorphous structures[25, 48].

# VI. Photovoltaic properties of oligomers QTF and TVF2

## VI.1. Photovoltaic properties of QTF

### Prior results on QTF8: PCBMC60 photovoltaic cells

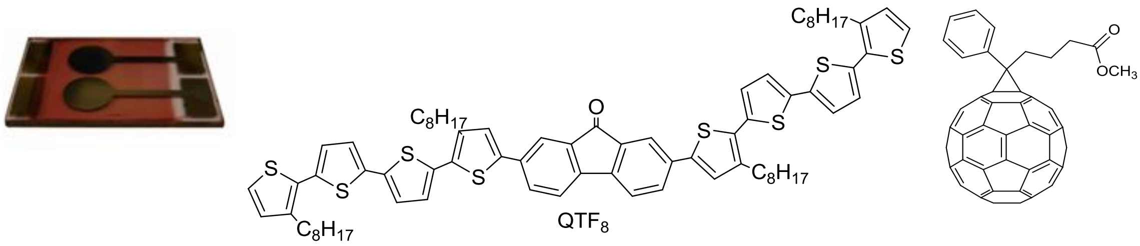


**Figure 67 : Photovoltaic device based on QTF8:PCBMC60**

The photovoltaic properties of the oligomer QTF8 has been studied previously in bulk heterojunction solar cells as donor materials in blend with fullerenes PCBMC60[49] (see Figure 67). The oligomer QTF8 was tested in mixture with PCBMC60 using chlorobenzene as solvent with 1:1 ratio at a weight concentration of 18 mg/ml for each material (36 mg/ml in total), with film thickness of 100 ± 20 nm. Other devices were also fabricated by varying the ratios QTF8:PCBMC60 to 1:2 and 1:3, but these devices showed lower power conversion efficiencies and are not presented here.

As cast blends of QTF8:PCBMC60 (1:1) gave a power conversion efficiency of 0.98 % with open circuit voltage Voc of 0.88 V, short-circuit current density Jsc of 3.48 mA.cm$^{-2}$ and fill factor of 0.32. A short post-thermal treatment of 5 min at 70°C of the device afforded an improve power conversion efficiency to 1.19 % as a result of higher Jsc of 3.61 mA.cm$^{-2}$ and a fill factor of 0.40. Other tests of post thermal treatment at higher temperature of 80°C have shown decrease performance for the device QTF8:PCBMC60. The current density-voltage (J-V) curves of the device after post annealing treatment (5 min at 70°C) are presented in Figure 68.

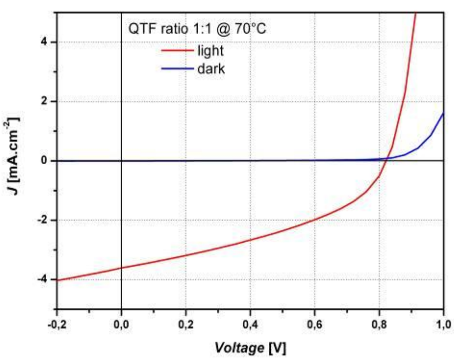


**Figure 68: J-V curves of solar cells based on QTF8:PCBMC60 after thermal annealing 5 min at 70 ° C.**

**The positive effect of post annealing treatment is similar to the one obtained in some polymers solar cells and this can be attributed to an improvement of the morphology of the blends[50,51]. In the case of QTF8 this hypothesis was supported by the morphology characterisation of the device QTF8:PCBMC60 after annealing as shown in**

Figure 69. The AFM image reveals small phase separation between the molecules QTF8 and PCBMC60. Furthermore the QTF8 molecules organised into fibre-like aggregates which allowed contribution to the increase current density, also observed in fibre like poly (3-hexylthiophene)[25].

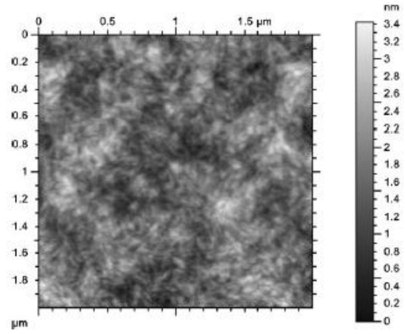


**Figure 69: Topographic AFM image of QTF8:PCBMC60 active layer film of the tested device after thermal annealing at 70°C for 5 min**

Subsequently, the best solar cell is further tested its incident photon to current efficiency (IPCE) in function of wavelengths. For correlation, we presented in the same graph, the measured IPCE along with the results from UV-Visible absorption of QTF8 on film presented in Figure 70. The curve of incident photon current efficiency demonstrates that major contribution of the photon to current conversion of up to 38 % were from the absorption region of π-π* transition band and the internal charge transfer band. Interestingly the molecule is capable to convert photons into electrons up to 800 nm.

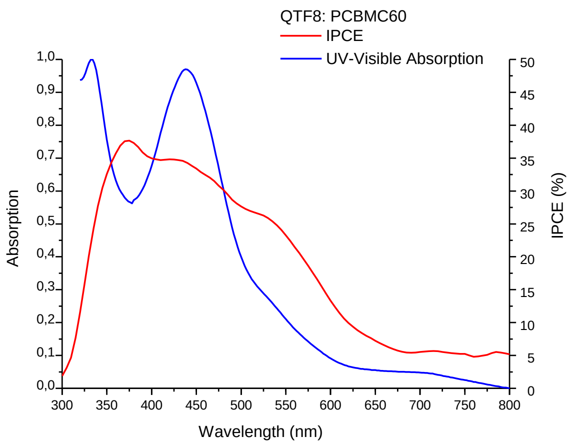


**Figure 70: (Red line) Incident photon to current efficiency curve as a function of wavelength ofthe photovoltaic device QTF8:PCBMC60 after thermal annealing 5 min at 70 °C. (Blue line) Recorded UV visible absorption of the blend QTF8:PCBMC60 1:1 in film**

Based on these results, we can conclude that we have obtained best performance for the blend QTF8:PCBMC60 with a ratio of 1:1 with a total concentration of 36 mg/ml and active layers thickness of 100 ± 20 nm. Moreover post thermal treatment for 5 min at 70°C has shown improved efficiency compared to as cast device. Therefore further work on photovoltaic tests is based on these parameters.

**Study on QTF8 with different fullerenes derivatives as acceptors in bulk heterojunction solar cells**

To further optimise utilisation of QTF8 as donor material in the bulk heterojunction, we decided to test in blend with other acceptor materials. We have tested the oligomer QTF8 with three different fullerenes derivatives which have close similarity to PCBMC60; PCBMC70, ThCBM and bisPCBMC60. The molecules structures are given in Figure 71 and further details on these materials are discussed in Chapter Experimental Methods and Materials.

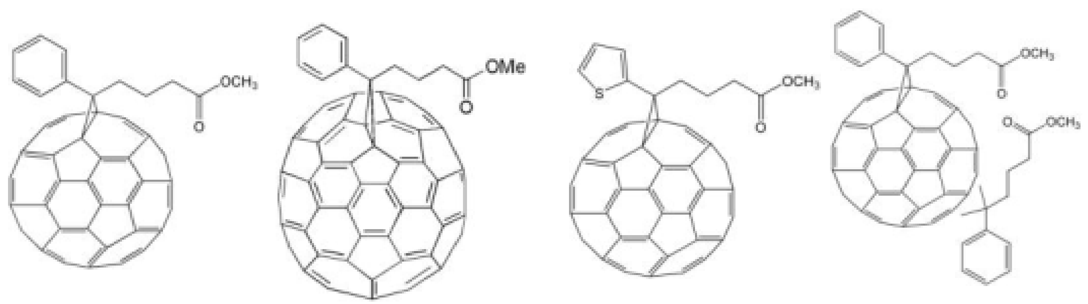


[60]PCBM [70]PCBM [60]ThCBM bis[60]PCBM

**Figure 71: Structures of fullerenes derivatives PCBMC60, PCBMC70, ThCBM and bisPCBMC60**

The fabrication process (i.e.: ratio, solvent, concentration, device configurations, spin-coating parameters) were kept the same as the previous tests with PCBMC60 to enable coherent comparison i.e : ratio QTF8: fullerenes of 1:1, total weight concentration of 36 mg/ml, active layer thickness 100 ± 20 nm, and chlorobenzene as solvent for the preparation of the blends.

**Study on QTF8: PCBMC70 photovoltaic cells**

The motivation of using PCBMC70 as an electron acceptor is to take advantage of the higher capability of photons absorption in UV-Visible as compared to PCBMC60[52]. The oligomer QTF8 in blend with PCBMC70 was tested in photovoltaic and the photovoltaic measurements are recorded as cast in dark and under illumination, and after 5 min post thermal annealing at 70°C. The current density curves as a function of voltage are presented in Figure 72.

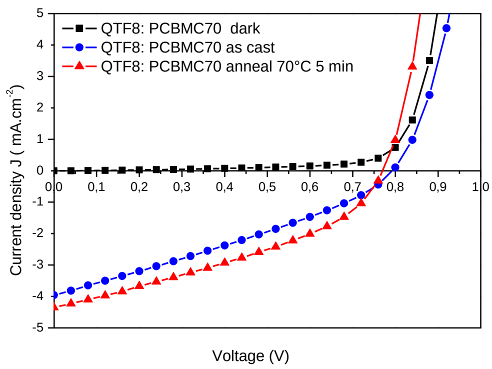


**Figure 72: Current density as function of voltage curves of the device QTF8:PCBMC70 (1:1) in dark, under illumination and after thermal annealing 5 min at 70°C**

As cast, device based on QTF8:PCBMC70 (1:1) blend showed short-circuit current density of 3.97 mA.cm$^{-2}$, open circuit voltage of 0.79 V, a fill factor of 0.31, and an overall power conversion efficiency of 0.98 %. The device cell showed improvement after annealing with increase of power conversion efficiency from 0.98 % to 1.24 %. The increase of efficiency was attributed to an increase of current density from 3.97 mA.cm$^{-2}$ to 4.36 mA.cm$^{-2}$ and improved fill factor up to 0.37. This result may be attributed to a better organisation of the molecules resulting in an improvement of the transport properties of the charges in the film[53,45].

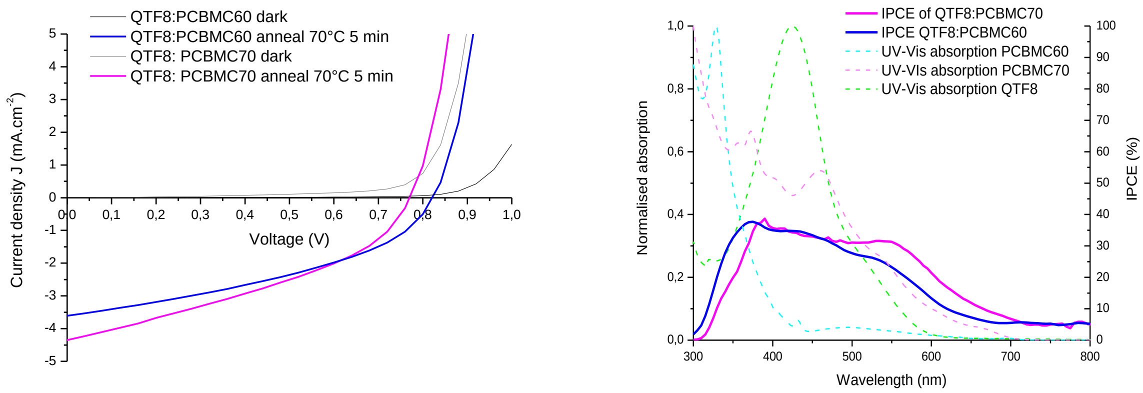


**Figure 73: (Left) Current density-Voltage curves of the annealed device QTF8: PCBMC60 (blue line) and annealed device QTF8: PCBMC70 (pink line). (Right) Incident photon to current efficiency as a function of wavelength curves of the devices QTF8:PCBMC60 (blue line) and QTF8:PCBMC70 (pink line), UV-Visible absorption spectra of PCBMC60 (light blue dotted line), PCBMC70 (pink dotted line) and QTF8 (green dotted line).**

| Active layer (1:1) | Jsc [mA/cm²] | | Voc [V] | | FF | | PCE [%] | |
|---|---|---|---|---|---|---|---|---|
| | 20°C | 70°C | 20°C | 70°C | 20°C | 70°C | 20°C | 70°C |
| QTF8:PCBMC60 | 3.48 | 3.61 | 0.88 | 0.82 | 0.32 | 0.40 | 0.98 | 1.19 |
| QTF8:PCBMC70 | 3.97 | 4.36 | 0.79 | 0.77 | 0.31 | 0.37 | 0.98 | 1.24 |

**Table 10: Photovoltaic properties of the device based on QTF8:PCBMC70 as cast and after annealing compared with the device based on QTF8:PCBMC60**

If we compared the device based on PCBMC70 with the one with PCBMC60, we can notice an improvement in terms of current density as shown in Table 10. The measurement of incident photon to current efficiency (IPCE) of the annealed device QTF8:PCBMC70 at 70 °C showed a conversion of up to 40 %. If we compare the IPCE curves of the two devices, both showed similar curves with slightly higher conversion in the region 500 nm to 700 nm for the annealed device based on QTF8:PCBMC70, which can partly come from the absorption of PCBMC70. However the open circuit voltage of the annealed device QTF8: PCBMC70 is lower by 0.05 V compared to the device QTF8:PCBMC60. This is rather unexpected as the LUMO energy levels of PCBMC70 was found to be higher at -3.8 eV as compared to -3.9 eV for the PCBMC60 and can theoretically increase the Voc based on the presumably linear relation between Voc and the difference of energy levels ($E_{HOMO}^{Donor}$-$E_{LUMO}^{Acceptor}$)[2]. Therefore the device QTF8: PCBMC70 exhibits higher voltage loss but it is difficult to identify the reason to explain this loss. A slightly but noticeable higher efficiency for the annealed device QTF8:PCBMC70 of 1.24% is obtained as compared to 1.19 % for the annealed device QTF8: PCBMC60.

**We also investigated the morphology of active layer film of the best performance device of QTF8:PCBMC70 by AFM microscopy in tapping mode. The AFM image of the tested device is shown in** Figure 74. The active layer showed small segregation domain between the molecules QTF8 and PCBMC70 of nanometric scale. The morphology of the active layer film of the device based on QTF8: PCBMC70 is very similar to morphology of the active layer of QTF8:PCBMC60. The molecules QTF8 also self-organised in the blend forming short fibers, contributing to the good current density[25],[16].

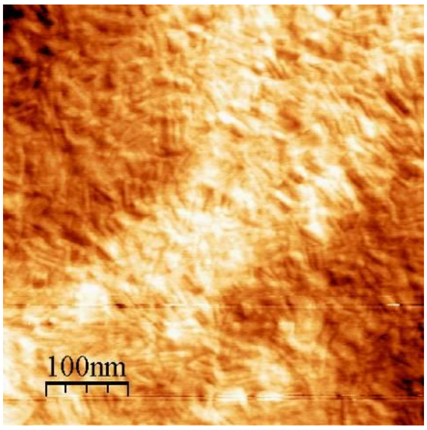


**Figure 74: AFM topographic image of the active layer film of best performance device (annealed QTF8:PCBMC70 1:1) with power conversion efficiency of 1.24 %.**

### Study on QTF8: bisPCBMC60 photovoltaic cells

The bis-adduct analogue of PCBMC60, the bis-PCBMC60 has higher LUMO energy level as compared to PCBMC60 (up to 100 meV), and therefore it could contribute to obtain higher open circuit voltage (Voc) in solar cells[54]. We tested the oligomer QTF8 in blend with bisPCBMC60 in photovoltaic devices and the photovoltaic measurements are recorded in dark, as cast under illumination and after leaving the device under solar simulator illumination for additional 5 minutes before re-measured the device performance. The current density curves as a function of voltage are presented in Figure 75.

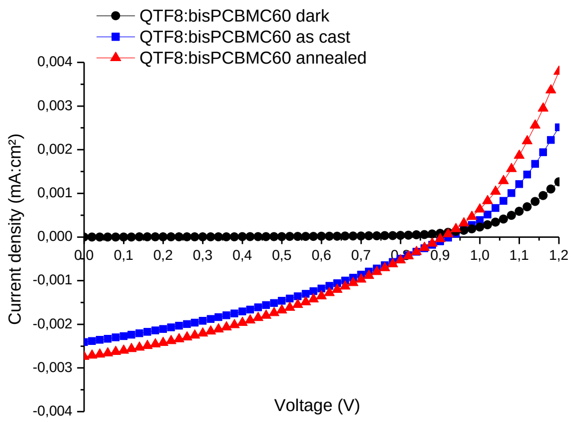


**Figure 75: Current-density as a function of voltage curves of QTF8:bisPCBM in dark, as cast under illumination and after 5 min post-annealing under solar irradiation**

| Active layer (1:1) | Jsc [mA/cm²] | | Voc [V] | | FF | | PCE [%] | |
|---|---|---|---|---|---|---|---|---|
| | As cast | anneal | As cast | anneal | As cast | anneal | As cast | Anneal |
| QTF8:bisPCBMC60 | 2.60 | 2.74 | 0.92 | 0.91 | 0.34 | 0.34 | 0.80 | 0.84 |
| QTF8:PCBMC60 | 3.48 | 3.61 | 0.88 | 0.82 | 0.32 | 0.40 | 0.98 | 1.19 |

**Table 11: Photovoltaic properties of device QTF8:bisPCBMC60 1:1 compared with photovoltaic device QTF8:PCBMC60**

A high open circuit voltage is obtained of 0.92 V. This expected result show a Voc which is higher of 0.1V compared to Voc the devices based on PCBMC60. Hummelen and coworkers have also reported an open-circuit voltage of the P3HT:bisPCBM cell up to 0.73 V, which is higher by 0.15 V compared to that of the P3HT:PCBM cell [54].

As cast, QTF8:bisPCBMC60 device showed a low current density of 2.60 $mA.cm^{-2}$ that was slightly improved to 2.74 $mA.cm^{-1}$ after 5 min continous irradiation under solar simulator. This result is similar to the result obtained after 5 min annealing with PCBMC60[16]. However the overall current density of the device based on bisPCBMC60 is much lower than the device based on PCBMC60. These observations are also observed by J.C Hummelen groups[55], due to the fact of insufficient charge transport and inefficient charge dissociation postulated to be the effect of electron trapping[56]. This can be related to the additional functional group which renders bulkier fullerenes molecules thus increasing the nanophase segregation domain between QTF8 and bisPCBM. However, optimization of the blend to form nanophase segregation morphology can indeed increase the performance. Lenes and coworkers[54] reported enhanced efficiencies of solar cells based on P3HT:bisPCBMC60 up to 4.5 % after optimization in terms of ratios, annealing, thickness etc.

In overall, this preliminary test gives the best device of annealed QTF8:bisPCBMC60 (5 min under solar simulator) a current density of 2.74 mA.cm$^{-2}$, open circuit voltage of 0.91 V, a fill factor of 0.34 and power conversion efficiency of 0.84%.

### Study on QTF8: ThCBMC60 photovoltaic cells

The thienyl analog of PCBM, the thienyl fullerene ThCBMC60 was first developed to allow improvement of the miscibility of fullerene with thiophene-based polymer P3HT. [57] QTF8 having predominantly thiophene rings can afford better compatibility with the fullerene ThCBM. We tested the QTF8 with ThCBMC60 according the same procedure as PCBMC60 and the current density-voltage curves are recorded in dark, as cast and after thermal annealing (5 min at 70°C) as shown in Figure 76.

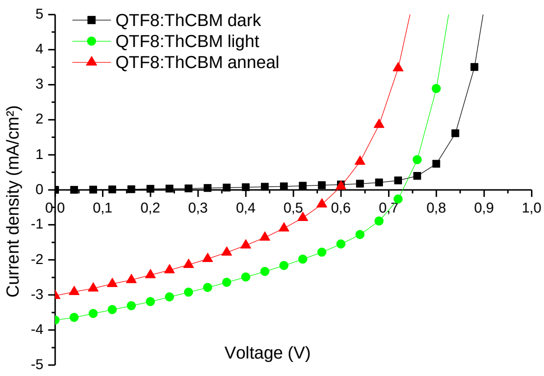


**Figure 76: I-V curves of QTF8:ThCBM in dark, as cast under illuimination and after annealing treatment.**

As cast device give a current density of 3.73 mA.cm$^{-2}$, open circuit voltage of 0.72 V, fill factor of 0.38 and power conversion efficiency of 1.03%. We can noticed the device degraded upon annealing 5 min at 70°C decreasing the current density to 2.91 mA.cm$^{-2}$, lower open circuit voltage of 0.64 V and an overall lower power conversion efficiency of 0.72 %. However we can note that better fill factor is obtained with the as cast cell that showed a value of 0.37. The FF was further improved to 0.40 after annealing. The overall poor results for the device based on QTF8:ThCBMC60 do not match our expectation, however these results open doors for further optimisation of this type of blend.

All the photovoltaic parameters of the device based on QTF8 combined with different fullerenes electron acceptors are presented in Table 12. We can conclude from our study, that the utilisation of PCBMC70 as electron acceptor material offers higher current density probably originating from its contribution to optical absorption in the visible region. Highest open circuit voltage is obtained by using bisPCBMC60, with value of 0.92 V. And for the acceptor ThCBMC60, improved fill factor was obtained but further optimisation of the blends fabrication are necessary in order to increase the performances.

| Active layer (1:1) | Jsc [mA/cm²] | | Voc [V] | | FF | | PCE [%] | |
|---|---|---|---|---|---|---|---|---|
| | 20°C | 70°C | 20°C | 70°C | 20°C | 70°C | 20°C | 70°C |
| QTF8:PCBMC60 | 3.48 | 3.61 | 0.88 | 0.82 | 0.32 | 0.40 | 0.98 | 1.19 |
| QTF8:PCBMC70 | 3.97 | 4.36 | 0.79 | 0.77 | 0.31 | 0.37 | 0.98 | 1.24 |
| QTF8:ThCBM | 3.72 | 2.91 | 0.73 | 0.64 | 0.38 | 0.40 | 1.03 | 0.72 |
| QTF8:bisPCBMC60 | 2.60 | 2.74 | 0.92 | 0.91 | 0.34 | 0.34 | 0.80 | 0.84 |

**Table 12: Characteristic properties of solar cells based on QTF8 with different fullerenes derivatives as acceptor**

**Study on effect of alkyl chain substituents of quaterthiophene fluorenone oligomers on photovoltaic cells**

The oligomers quaterthiophene fluorenone, with hexyl side chains (QTF6), octyl (QTF8) and dodecyl (QTF12) were tested in photovoltaic cells in order to study the effect of alkyl chains on the power conversion. Some preliminary tests were performed by former post-doctorate Frédéric Lincker of the device based on oligomers QTFs: PCBMC60 according to the ratios 1:1, 1:2 and 1:3. In each solution, the weight concentration of the different oligomers was kept constant at 18 mg/ml, and the quantities of PCBMC60 were added according to the ratios.

For the device based on QTF6, highest power conversion efficiency was obtained with the device with QTF6:PCBMC60 with the ratio 1:1. The cell gave a high short-circuit current density of 4.53 $mA.cm^{-2}$ , high open circuit voltage of 0.88 V, a fill factor of 0.32 and power conversion efficiency of 1.30 %. No thermal annealing was further applied. For the device based on QTF12, much lower power conversion efficiency was obtained. The best device was based on annealed QTF12:PCBMC60 (5 min at 80°C) with the ratio of 1:1, with a power conversion efficiency of 0.51 %. The short circuit current density was much lower at 2.12 $mA.cm^{-2}$ as well as the open circuit voltage of 0.64 V, but a good fill factor of 0.43 was obtained. The current density-voltage curves of the three devices based on QTF6, QTF8 and QTF12 are presented in Figure 77.

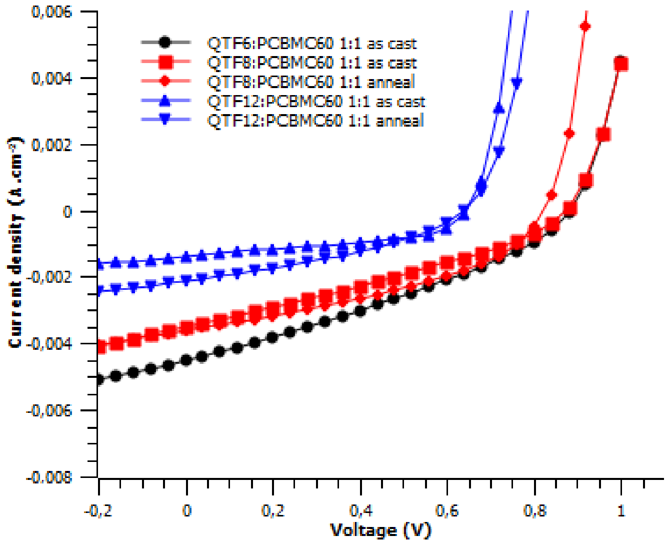


**Figure 77: Current density as a function of voltage curves of the as cast devices QTF6:PCBMC60, QTF8:PCBMC60, and QTF12:PCBMC60**

| Active layer | Jsc [mA/cm²] | | Voc [V] | | FF | | PCE [%] | |
|---|---|---|---|---|---|---|---|---|
| | As cast | Anneal | As cast | Anneal | As cast | Anneal | As cast | anneal |
| QTF6:PCBMC60 1 :1 | 4.53 | - | 0.88 | - | 0.32 | - | 1.30 | - |
| QTF8:PCBMC60 1 :1 | 3.48 | 3.61 | 0.88 | 0.82 | 0.32 | 0.40 | 0.98 | 1.19 |
| QTF12:PCBMC60 1 :1 | 1.39 | 2.12 | 0.65 | 0.64 | 0.46 | 0.37 | 0.42 | 0.51 |

**Table 13: Photovoltaic properties of devices based on QTF6, QTF8 and QTF12 with fullerene PCBMC60**

From these results, we have obtained the best performance for QTF6 with short hexyl side chain, and much lower performance for QTF12 with the long dodecyl side chains. We have also seen that for QTF8 and QTF12 thermal annealing treatment are necessary to allow the molecules QTFn and fullerenes to further organise in the active layers. Similar features have also been found for the case of polythiophenes, where longer alkyl chains showed lower miscibility with the PCBM[58] therefore thermal annealing are of crucial steps to improve the phase separation and diffusion of PCBM in the blend. Our results are in accordance with the results obtained with polyalkylthiophenes were poly (3-hexylthiophene) have so far showed higher power conversion efficiency up to 5%[59], compared to longer poly(octyl)thiophenes[60,61]and poly (dodecyl)thiophenes polymers[62,63].

## VI.2. Photovoltaic properties of dimer thienylene-vinylene fluorenone TVF2

The dimer TVF2 are tested in bulk heterojunction solar cells with different electron acceptor compounds: PCBMC60, PCBMC70, bisPCBMC60 and CdSe nanorods. For the blend containing fullerenes derivatives, the solutions were prepared by dissolving the dimer TVF2 and the fullerenes derivatives in chlorobenzene according to weight ratios. The concentration of TVF2 is fixed at 20 mg/ml. TVF2:PCBMC60 and TVF2:PCBMC70 were tested with two different ratios 1:1 and 1:1.5. While for TVF2: bisPCBM we have only tested with 1:1 concentration.

As for the test for hybrid solar cells, we have mixed in solution TVF2 with CdSe nanorods. The CdSe nanorods were synthesized by Angela Fiore from our laboratory. According to previous studies carried out in the laboratory, the concentration used for the fabrication of the hybrid blends is as follows: the nanorods of CdSe are dispersed in a mixture of orthodichlorobenzene (ODCB) and pyridine (90 %:10% v:v) with a concentration of 60 mg/ml. In each blend the weight concentration of TVF2 is fixed at 15 mg/ml. The solutions were prepared by dissolving the dimer TVF2 following the weight ratios TVF2: CdSe 1:2, 1:3 and 1:4 in the CdSe solution. Preliminary results on photovoltaic cells based on TVF2 are presented in the Table **14**.

| Donor | Acceptor | Ratio | Voc (V) | Jsc (mA/cm²) | FF | PCE (%) |
|---|---|---|---|---|---|---|
| TVF2 | PCBMC60 | 1:1 | Sc | - | - | - |
| TVF2 | PCBMC60 | 1:1.5 | 0.55 | 0.67 | 0.27 | 0.10 |
| TVF2 | PCBMC70 | 1:1 | 0.54 | 0.20 | 0.21 | 0.03 |
| TVF2 | PCBMC70 | 1:1.5 | 0.55 | 0.62 | 0.24 | 0.08 |
| TVF2 | PCBMC70 | 1:1.5[a] | 0.55 | 0.62 | 0.24 | 0.08 |
| TVF2 | bisPCBMC60 | 1:1 | 0.52 | 0.65 | 0.36 | 0.12 |
| TVF2 | bisPCBMC60 | 1:1[a] | 0.58 | 0.66 | 0.36 | 0.14 |

**Table 14: The photovoltaic parameters of solar cells TVF2: acceptors. sc: short circuit; a: post annealing condition: 5 minutes at 70 °C of device after cathode deposition**

All the photovoltaic cells show quite low photovoltaic conversion with the highest conversion from the solar cells of TVF2: bisPCBM (1:1) of power conversion efficiencies of 0.14 % after annealing. The low power conversion efficiencies for all the cells were mainly due to low short circuit current density. The short circuit current densities for all of the solar cells are below 1 $mA.cm^{-2}$. The solar cell based on bisPCBMC60 showed highest efficiency thanks to a better fill factor of 36 % and higher open circuit voltage than others 0.58 V. In general the open circuit voltage of the devices are low between 0.52-0.58 for the devices based on TVF2:Fullerenes. These values are much lower compared to the device based on QTF:Fullerenes where the open circuit voltages were found at about 0.8 V. This is rather expected as the open circuit voltage depends on the difference of energy levels of HOMO donor and LUMO acceptor. The HOMO energy level of TVF2 was found at -5.07 eV where else the HOMO energy level of QTF was found at -5.25 eV. Therefore the open circuit voltage of the device based on TVF2 with the same acceptor could be lower of about 0.20 V compared to the devices using the QTFn molecules.

The current density-voltage curves of the tested cells based on TVF2 with fullerenes acceptors PCBMC60, PCBMC70 and bisPCBMC60 are presented in Figure 78 showing very low current density obtained for all the devices.

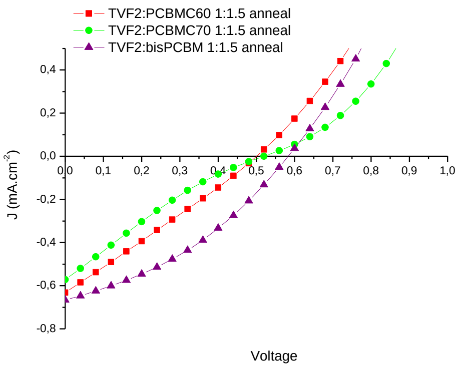


**Figure 78: Current density as a function of voltage curves of photovoltaic devices TVF2: PCBMC60 1:1.5 (red line), TVF2: PCBMC70 1:1.5 (green line) and TVF2: bisPCBMC60 1:1.5 (purple line) with post annealing treatment of 5 min at 70°C.**

If we try to look to the intrinsic properties of TV2, the dimer TVF2 has shown broader absorption spectrum in UV-Visible with a lower band gap of 1.85 eV as compared to QTF8 with a band gap of 2.0 eV. Since the photocurrent is mostly limited by photoinduced charge carrier generation and transport, we postulated that the low current density can be due to poor morphology of the active layer films. We then investigate the morphology of the system by near field AFM microscopy. The Figure 79 below shows AFM image of the annealed TVF2:bisPCBM device which give the highest efficiency.

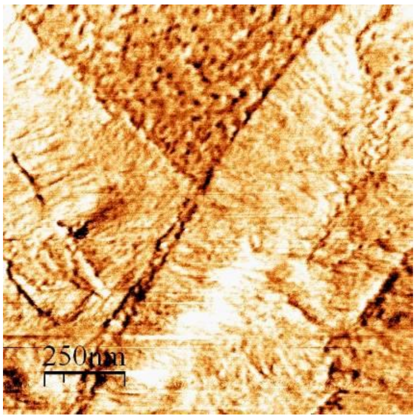


**Figure 79: AFM image of annealed photovoltaic cell TVF2: bisPCBM (left) and images of a film of TVF2 in toluene (0.4mg/ml) drop-cast on mica (right)**

From the image above, we can observe a large strip at about 500 nm large that can be attributed to the TVF2. We can also observed fine fibers finely stacked in the strips. Therefore we can conclude that the segregation domains are too large to achieve an optimum dissociation of excitons and that the recombination of excitons is predominant inside the strips. In order to further optimize the phase segregation between the dimer TVF2 and PCBM, utilization of solvent additive diiodooctane could be a good option [64] and should be investigated in the laboratory in a near future.

Preliminary tests of the dimer TVF2 in blend with CdSe have also shown very poor power conversion efficiencies due a very low short circuit current density of about 0.1 mA.cm$^{-2}$ as shown in Table 15. The results for the devices based on nanorods CdSe have even shown lower efficiency compared to the one using fullerenes with a maximum PCE of 0.02 %.

| Donor | Acceptor | Ratio | Voc (V) | Jsc (mA/cm²) | FF | PCE (%) |
|---|---|---|---|---|---|---|
| TVF2 | CdSe nanorods | 1:2 | 0.41 | 0.14 | 0.30 | 0.02 |
| TVF2 | CdSe nanorods | 1:3 | 0.55 | 0.08 | 0.27 | 0.01 |
| TVF2 | CdSe nanorods | 1:4 | 0.47 | 0.10 | 0.28 | 0.01 |

**Table 15: The photovoltaic parameters of solar cells TVF2: CdSe. The photovoltaic parameters of solar cells TVF2: acceptors.**

It is acknowledged in the field a minimum offset of approximately 0.3‑0.4 eV between the LUMO of the donor and the LUMO of the acceptor is necessary to ensure efficient exciton dissociation at the D/A interface. Therefore as the difference between HOMO of the TVF2 and the LUMO of CdSe is about 0.35 eV[65,2] we can postulate that this leads to inefficient excitons dissociation. Hence the low short circuit current density reported.

# VII. Conclusion

In this chapter we have presented examples of donor-acceptor oligomers with fluorenone as principal electron-withdrawing unit in the conjugated systems, and oligothiophenes as electron releasing units. In this study the oligothiophenes units used are either linear quaterthiophene or thienylene vinylene. Spectral and electrochemical properties of the different oligomers allowed assessing the effect of structural modification on electronic properties.

We have found the combination of electron-donating oligothiophenes building blocks with the electron-accepting fluorenone unit results in the emergence of a new band assigned to an intramolecular charge transfer transition that gives rise to the extension of the absorption spectral range of the resulting molecules. More extended π-conjugation length also allows to extension of the absorption spectral by the bathorochromic shift or the absorption band, as shown for the dimer TVF2. The oligomer based on QTF exhibit lower optical absorption than the dimer TVF2 with a band gap of 1.90 eV as compared to the TVF2 with a band gap of 1.71 eV.

The HOMO and LUMO energy levels of both oligomers are correctly positioned to the energy levels of acceptor materials, with values of -5.01 eV (HOMO) and -3.20 eV (LUMO) for QTF8 and -5.07 eV (HOMO) and -3.27 eV (LUMO) for TVF2. Therefore both oligomers are suitable donor material for photovoltaic application in combination with common acceptor materials such as PCBM. (see Figure 80)

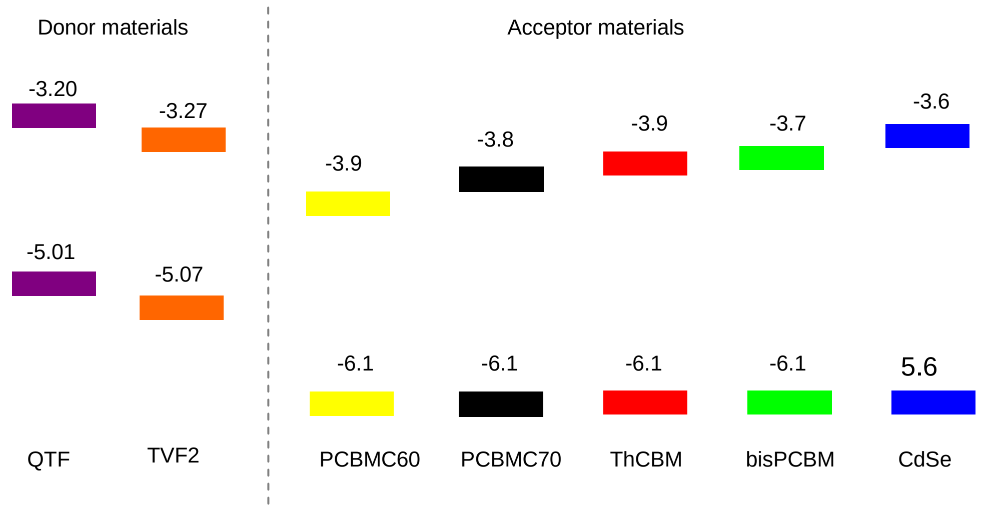


**Figure 80: Energy levels diagram of donor materials (QTFn and TVF2) and acceptor materials used in the study (PCBMC60, PCBMC70, ThCBM, bisPCBMC60 and CdSe)**

Our oligomers QTF and TVF2 also exhibit strong ability to supramolecular organisation of in the solid state. The strong molecular packing is well observed in solid state from photophysical study and from morphological study. The oligomers were demonstrated to self organise forming nanofibers.

The oligomers were tested as donor materials in bulk heterojunction organic photovoltaic devices in combination with differents acceptor materials. Photovoltaic device based on oligomer QTF8 in blend with PCBMC70 give promising power conversion efficiencies of up to 1.24 %. This is attributed to high short current density due to its small phase segregation with PCBMC70 and form fibre-like aggregates.

However for the oligomer TVF2, preliminary results showed low power conversion efficiencies for all our tests with different acceptors. The low power conversion efficiencies are essentially due to poor phase segregation with acceptors in the active layers. AFM study revealed formation of large strips of TVF2 domain of hundrends of nanometer large.

It is also note-worthy that the devices QTF8: fullerenes have shown high open circuit voltages (Voc) of about 0.80 V thanks to its low lying HOMO energy level. In contrary, the high lying HOMO energy levels of oligomer TVF2 give low open circuit voltage for the all the devices with different acceptors, with Voc values of not more than 0.6 V. Therefore it is important to have low-lying HOMO energy levels in order to obtain high open circuit voltages in solar cells devices.

# VIII. Reference


1 R. Demadrille, M. Firon, J. Leroy, P. Rannou, A. Pron, Plastic Solar Cells Based on Fluorenone-Containing Oligomers and Regioregular Alternate Copolymers, Adv. Funct. Mater. 2005, 15, 1547

2 Scharber, M.; Muhlbacher, D.; Koppe, M.; Denk, P.;Waldauf, C.; Heeger, A. J.; Brabec, C.,Design Rules for Donors in Bulk-Heterojunction Solar Cells;Towards 10% Energy-Conversion Efficiency. Adv. Mater. 2006, 18, 789–794.

3 Ohkita, H.; Cook, S.; Astuti, Y.; Duffy, W.; Tierney, S.; Zhang, W.; Heeney, M.; McCulloch, I.; Nelson, J.; Bradley, D. D. C.; Durrant, J. R. Charge carrier formation in polythiophene/fullerene blend films studied by transient absorption spectroscopy, J. Am. Chem. Soc. 2008, 130, 3030–3042.

4 Rand, B. P.; Burk, D. P.; Forrest, S. R. Offset energies at organic semiconductor heterojunctions and their influence on the open-circuit voltage of thin-film solar cells. Phys. Rev. B: Condens. Matter Mater. Phys. 2007, 75, 115327.

5 B. Walker, A. B. Tamayo, X.-D. Dang, P. Zalar, J. H. Seo, A.Garcia, M. Tantiwiwat, T.-Q. Nguyen, Nanoscale Phase Separation and High Photovoltaic Efficiency in Solution-Processed, Small-Molecule Bulk Heterojunction Solar Cells Adv. Funct. Mater. 2009,19, 3063.

6 V.I.Arkhipov,P.Heremans,H.Bassler,Why is exciton dissociation so efficient at the interface between a conjugated polymer and an electron acceptor?, Appl.Phys.Lett 82, (2003), 4605–4607.

7 W. D. Oosterbaan,V. Vrindts, S. Berson, S. Guillerez, O. Douhéret, B. Ruttens, J. D'Haen, P. Adriaensens, J. Manca, L. Lutsen and D. Vanderzande, Efficient formation, isolation and characterization of poly(3-alkylthiophene) nanofibres: probing order as a function of side-chain length, J. Mater. Chem., 2009, 19, 5424–5435.

8 P. Bäuerle, T. Fischer, B. Bidlingmeier, J.P. Rabe, A. Stabel, Oligothiophenes—Yet Longer? Synthesis, Characterization, and Scanning Tunneling Microscopy Images of Homologous, Isomerically Pure Oligo(alkylthiophene)s Angew. Chem., Int. Ed. Engl., 34 (1995), pp. 303–307

9 N. Miyaura and A. Suzuki, Palladium-catalyzed Cross-coupling Reactions of Organoboron Compounds, Chem.Rev, 1995, 95, 2457-2483

10 Miyaura, N; Yamada, K ; Suzuki, A (1979), A new stereospecific cross-coupling by the palladium-catalyzed reaction of 1-alkenylboranes with 1-alkenyl or 1-alkynyl halides.Tetrahedron Letters 20 (36): 3437–3440

11 A.G. Davies, 3.14 - Tin Organometallics, In: Editors-in-Chief: Robert H. Crabtree and D. Michael P. Mingos, Editor(s)-in-Chief, Comprehensive Organometallic Chemistry III, Elsevier, Oxford, 2007, Pages 809-883

12 R. Toyoshima, K. Akagi, and I. Shirakawa, Synthesis and properties of poly(thienylenevinylene) derivatives with hexyl groups, , Synthetic Metals, 84 (1997) 431-432

13 K. Tamao, K. Sumitani, and M. Kumada, Selective carbon-carbon bond formation by cross-coupling of Grignard reagents with organic halides. Catalysis by nickel-phosphine complexes, Journal of the American Chemical Society 1972 94 (12), 4374-4376

14 J.E McMurry, Titanium-Induced Dicarbony1 - Coupling Reactions, Acc. Chem. Res. 1983,16, 405-411

15 P. Coppo, D. C. Cupertino, S. G. Yeates and M. L. Turner, New routes to poly(4,4-dialkylcyclopentadithiophene-2,6-diyls), J. Mater. Chem. 2002, 12, (9), 2597.

16 F. Lincker, N. Delbosc, S. Bailly, R. De Bettignies, M. Billon, A. Pron, and R. Demadrille, Fluorenone-Based Molecules for Bulk-Heterojunction Solar Cells: Synthesis, Characterization, and Photovoltaic Properties, Adv. Funct. Mater. 2008, 18, 3444–3453

17 W. Porzio , S. Destri , M. Pasini , U. Giovanella , M. Ragazzi , G. Scavia , D. Kotowski, G.Zotti and B. Vercelli, Synthesis and characterisation of fluorenone–thiophene-based donor–acceptor oligomers: role of moiety sequence upon packing and electronic properties, New J. Chem., 2010,34, 1961-1973

18 L.A. Estrada, J.E. Yarnell, and D. C. Neckers, Revisiting Fluorenone Photophysics via Dipolar Fluorenone Derivatives, J. Phys. Chem. A 2011, 115, 6366–6375

19 R.-K. Chen, G.-J. Zhao, X.-C. Yang, X. Jiang, J.-F. Liu, H.-N. Tian, Y. Gao, X. Liu, K.-L. Han, M.-T. Sun, L.-C. Sun, Photoinduced intramolecular charge-transfer state in thiophene-p-conjugated donor–acceptor molecules J. Mol. Struct. 2008, 876, 102

20 G-J Zhao, R-KChen, Meng-Tao Sun, Jian-Yong Liu, Guang-Yue Li, Yun-Ling Gao, Ke-Li Han, Xi-Chuan Yang, and Licheng Sun, Photoinduced Intramolecular Charge Transfer and S2 Fluorescence in Thiophene-p-Conjugated Donor–Acceptor Systems: Experimental and TDDFT Studies, Chem. Eur. J. 2008, 14, 6935 – 6947

21 F. Jaramillo-Isaza and M. L. Turner, Synthesis and properties of conjugated oligomers containing fluorene, fluorenone, thiophene and cyclopentadithiophenone units, J. Mater. Chem., 2006, 16, 83–89.

22 P. J. Homnick and P. M. Lahti, Modular electron donor group tuning of frontier energy levels in diarylaminofluorenone push–pull molecules, Phys. Chem. Chem. Phys., 2012,14, 11961-11968

23 D. P. Ostrowski, L.A. Lytwak, M. L. Mejia, K. J. Stevenson, B. J. Holliday, and D. A. Vanden Bout, The Effects of Aggregation on Electronic and Optical Properties of Oligothiophene Particles, ACS Nano 2012 6 (6), 5507-5513

24 A. B. Tamayo, M. Tantiwiwat, B. Walker, and T.-Q. Nguyen, Design, Synthesis, and Self-assembly of Oligothiophene Derivatives with a Diketopyrrolopyrrole Core, J. Phys. Chem. C 2008, 112, 15543–15552

25 S. Berson, R. De Bettignies, S. Bailly, and S. Guillerez, (2007), Poly(3-hexylthiophene) Fibers for Photovoltaic Applications. Adv. Funct. Mater., 17: 1377–1384.

26 L. H. Cross and A. C. Rolfe, Molar extinction coefficients of certain functional groupings with special reference to compounds containing carbonyl, Trans. Faraday Soc., 1951,47, 354-357

27 J. Roncali, Molecular Engineering of the Band Gap of p-Conjugated Systems: Facing Technological Applications, Macromol. Rapid Commun. 2007, 28, 1761–1775

28 B. Lim, K.-J. Baeg, H.-G. Jeong, J. Jo, H. Kim, J.-W. Park, Y.-Y. Noh, D. Vak, J.-H. Park, J.-W. Park and D.-Y. Kim, Synthesis and characterization of low-band-gap poly(thienylenevinylene) derivatives for polymer solar cells, Adv.Mater., 2009, 21, 2808

29 E. H. Elandaloussi, P. Frère, P. Richomme, J. Orduna, J. Garin and J. Roncali, Effect of Chain Extension on the Electrochemical and Electronic Properties of π-Conjugated Soluble Thienylenevinylene Oligomers J. Am. Chem. Soc., 1997, 119, 10774.

30 A. J. Cadby, J. Partee, J. Shinar, S. J. Martin, C. W. Spangler, D. D. C. Bradley, and P. A. Lane, Optical studies of molecular aggregates: The photophysics of a thienylene vinylene oligomer, Phys. Rev. B, Vol. 65, 245202

31 K. J. Ihn, J. Moulton and P. Smith, Whiskers of poly(3-alkylthiophene)s, J. Polym. Sci., Part B: Polym. Phys., 1993, 31, 735–742

32 Gizelle A. Sherwood, Ryan Cheng, Kelly Chacon-Madrid, Timothy M. Smith, and Linda A. Peteanu, Chain Length and Substituent Effects on the Formation of Excimer-Like States in Nanoaggregates of CN-PPV Model Oligomers, J. Phys. Chem. C 2010, 114, 12078–12089

33 F. Banishoeib, A. Henckens, S. Fourier, G. Vanhooyland, M. Breselge, J. Manca, T.J. Cleij, L. Lutsen, D. Vanderzande, Le Huong Nguyen, Helmut Neugebauer, Niyazi Serdar Sariciftci, Synthesis of poly(2,5-Thienylene Vinylene) and its derivatives: Low band gap materials for photovoltaics, Thin Solid Films 516 (2008) 3978–3988

34 J. C. Speros, B. D. Paulsen, S. P. White, Y. Wu, E. A. Jackson, B. S. Slowinski, C. D. Frisbie, and M. A. Hillmyer, An ADMET Route to Low-Band-Gap Poly(3-hexadecylthienylene vinylene): A Systematic Study of Molecular Weight on Photovoltaic Performance, Macromolecules 2012 45 (5), 2190-2199

35 A. Marrocchi , D. Lanari , A. Facchetti and L. Vaccaro, Poly(3-hexylthiophene): synthetic methodologies and properties in bulk heterojunction solar cells, Energy Environ. Sci., 2012,5, 8457-8474

36 M Bellette, L Mazerolle, N Desrosiers, M Leclerc, and G Durocher , Spectroscopy and Photophysics of Some Oligomers and Polymers Derived from Thiophenes , Macromolecules, Vol. 28, No. 25, 1995

37 Ph. Leclère, M. Surin, P. Viville, R. Lazzaroni, A. F. M. Kilbinger, O. Henze, W. J. Feast, M. Cavallini, F. Biscarini, A. P. H. J. Schenning, and E. W. Meijer, About Oligothiophene Self-Assembly: From Aggregation in Solution to Solid-State Nanostructures, Chemistry of Materials 2004 16 (23), 4452-4466

38 T-Q Nguyen, V Doan, and B. J. Schwartz, Conjugated polymer aggregates in solution: Control of interchain interactions, J. Chem. Phys., Vol. 110, No. 8, 22 February 1999

39 Freek J. M. Hoeben, Pascal Jonkheijm, E. W. Meijer, and Albertus P. H. J. Schenning, About Supramolecular Assemblies of Pi-Conjugated Systems, Chem. Rev. 2005, 105, 1491-1546

40 Haubner, K., Jaehne, E., Adler, H.-J. P., Koehler, D., Loppacher, C., Eng, L. M., Grenzer, J., Herasimovich, A. and Scheiner, S. (2009) Assembly, Structure, and Performance of an Ultra-Thin Film Organic Field-Effect Transistor (OFET) Based on Substituted Oligothiophenes, in Organic Electronics: Structural and Electronic Properties of OFETs (ed C. Wöll), Wiley-VCH Verlag GmbH & Co. KGaA, Weinheim, Germany

41 Polec, I., Henckens, A., Goris, L., Nicolas, M., Loi, M. A., Adriaensens, P. J., Lutsen, L., Manca, J. V., Vanderzande, D. and Sariciftci, N. S. (2003), Convenient synthesis and polymerization of 5,6-disubstituted dithiophthalides toward soluble poly(isothianaphthene): An initial spectroscopic characterization of the resulting low-band-gap polymers. J. Polym. Sci. A Polym. Chem., 41: 1034–1045

42 E. Lim, S.Lee and K. K. Lee, Improved photovoltaic performance of P3HT:PCBM cells by addition of a low band-gap oligomer,Chem. Commun., 2011, 47, 914–916

43 R. Demadrille, M. Zagorska, M. Billon, G. Louarn, S. Lefrant and A. Pron, Solution versus solid-state electropolymerization of regioregular conjugated fluorenone–thienylene vinylene macromonomers—voltammetric and spectroelectrochemical investigations, Journal of Solid State Electrochemistry, August 2007, Volume 11, Issue 8, pp 1051-1058

44 Nguyen, L. H., Hoppe, H., Erb, T., Günes, S., Gobsch, G. and Sariciftci, N.S. (2007), Effects of Annealing on the Nanomorphology and Performance of Poly(alkylthiophene): Fullerene Bulk-Heterojunction Solar Cells. Adv. Funct. Mater., 17: 1071–1078.

45 Grévin, B., Demadrille, R., Linares, M., Lazzaroni, R. and Leclère, P. (2009), Probing the Local Conformation within π-Conjugated One-dimensional Supramolecular Stacks using Frequency Modulation Atomic Force Microscopy. Adv. Mater., 21: 4124–4129.

46 E. J. Spadafora, M. Linares, W. Z. N. Yahya, F. Lincker, R. Demadrille, and B. Grevin, Local contact potential difference of molecular self-assemblies investigated by Kelvin probe force microscopy, Appl. Phys. Lett. 99, 233102 (2011)

47 A.J. Lovinger, D.D. Davis, A. Dodabalapur, H.E. Katz, Comparative Structures of Thiophene Oligomers, Chem. Mater. 8 (1996) 2836- 2838

48 H. Xin, F. S. Kim, and S. A. Jenekhe, Highly Efficient Solar Cells Based on Poly(3-butylthiophene) Nanowires, J. Am. Chem. Soc., 2008, 130 (16), pp 5424–5425

49 F. Lincker, N. Delbosc, S. Bailly, R. De Bettignies, M. Billon, A. Pron, and R. Demadrille, Fluorenone-Based Molecules for Bulk-Heterojunction Solar Cells:Synthesis, Characterization, and Photovoltaic Properties, Adv. Funct. Mater. 2008, 18, 3444–3453

50 U. Zhokhavets, T. Erb, H. Hoppe, G. Gobsch, N. S. Sariciftci, Effect of annealing of poly(3-hexylthiophene)/fullerene bulk heterojunctioncomposites on structural and optical properties, Thin Solid Films 2006, 496, 679.

51 X. Yang, J. Loos, S. C. Veenstra,W. J.H. Verhees, M. M. Wienk, J. M. Kroon, M. A. J.Michels, R. A. J. Janssen, Nanoscale Morphology of High-Performance Polymer Solar Cells, Nano Lett. 2005, 5, 579

52 Wienk, M. M.; Kroon, J. M.; Verhees, W. J. H.; Knol, J.; Hummelen, J. C.; van Hal, P. A.; Janssen, Efficient Methano[70]fullerene/MDMO-PPV Bulk Heterojunction Photovoltaic Cells, A. J. Angew. Chem. Int. Ed. 2003, 42, 3371

53 Uckert, F., Tak, Y.-H., Müllen, K. and Bässler, H. (2000), 2,7-Poly(9-fluorenone): A Trap-Free Electron-Injection Material with a High Charge Carrier Mobility for Use in Light-Emitting Diodes. Adv. Mater., 12: 905–908.

54 Lenes, M., Wetzelaer, G.-J. A. H., Kooistra, F. B., Veenstra, S. C., Hummelen, J. C. and Blom, P. W. M. 2008), Fullerene Bisadducts for Enhanced Open-Circuit Voltages and Efficiencies in Polymer Solar Cells. Adv. Mater., 20: 2116–2119.

55 Azimi, H., Senes, A., Scharber, M. C., Hingerl, K. and Brabec, C. J. (2011), Charge Transport and Recombination in Low-Bandgap Bulk Heterojunction Solar Cell using Bis-adduct Fullerene. Adv. Energy Mater., 1: 1162–1168.

56 Lenes, M., Shelton, S. W., Sieval, A. B., Kronholm, D. F., Hummelen, J. C. and Blom, P. W. M. (2009), Electron Trapping in Higher Adduct Fullerene-Based Solar Cells. Adv. Funct. Mater., 19: 3002–3007

57 L M. Popescu, P V Hof, A B. Sieval, H T. Jonkman, and J C. Hummelen, Thienyl analog of 1-(3-methoxycarbonyl)propyl-1-phenyl-[6,6]-methanofullerene for bulk heterojunction photovoltaic devices in combination with polythiophenes, Appl. Phys. Lett. 89, 213507 (2006)

58 Nguyen, L.H., Hoppe, H., Erb, T., Günes, S., Gobsch, G. and Sariciftci, N.S. (2007), Effects of Annealing on the Nanomorphology and Performance of Poly(alkylthiophene):Fullerene Bulk-Heterojunction Solar Cells. Adv. Funct. Mater., 17: 1071–1078.

59 Dang, M. T., Hirsch, L. and Wantz, G. (2011), P3HT:PCBM, Best Seller in Polymer Photovoltaic Research. Adv. Mater., 23: 3597–3602.

60 R. Demadrille , N. Delbosc , Y. Kervella , M. Firon , R. De Bettignies , M. Billon , P. Rannou and A. Pron, Conjugated alternating copolymer of dialkylquaterthiophene and fluorenone: synthesis, characterisation and photovoltaic properties, J. Mater. Chem., 2007,17, 4661-4669

61 E A. Parlak, The blend ratio effect on the photovoltaic performance and stability of poly (3-hexylthiophene):[6,6]-phenyl-C61 butyric acid methyl ester (PCBM) and poly(3-octylthiophene):PCBM solar cells, Solar Energy Materials and Solar Cells, Volume 100, May 2012, Pages 174-184

62 B.C. Thompson, N.J. Kim, D.F. Kavulak, K. Sivula, C. Mauldin, J.M.J. Fréchet, Influence of Alkyl Substitution Pattern in Thiophene Copolymers on Composite Fullerene Solar Cell Performance, Macromolecules 40 (2007) 7425

63 G. Wantz, F. Lefevre, M.T. Dang, D. Laliberté, P.L. Brunner, O.J. Dautel, Photovoltaic solar cells using poly(3,3-didodecylquaterthiophene), Solar Energy Materials and Solar Cells, Volume 92, Issue 5, May 2008, Pages 558-563

64 Y. Sun, G. C. Welch, W. L. Leong, C. J. Takacs, G. C. Bazan and A. J. Heeger, Solution-processed small-molecule solar cells with 6.7% efficiency, Nat. Mater., 2012, 11, 44

65 J. J. M. Halls, J. Cornil, D. A. dos Santos, R. Silbey, D. H. Hwang, A. B. Holmes, J. L. Bredas, R. H. Friend, Charge- and energy-transfer processes at polymer/polymer interfaces: A joint experimental and theoretical study , Phys. Rev. B, 1999, 60, 5721

# CHAPTER 3: THIOPHENE-BASED POLYMER FOR ORGANIC PHOTOVOLTAIC: SYNTHESIS, PHYSICAL CHARACTERISATION AND PHOTOVOLTAIC PROPERTIES

# I. Introduction

Among multitude examples of π-conjugated polymers[1,2] polythiophenes are one of the most promising materials for organic photovoltaic cells because of their good thermal and chemical stability, as well as for their unique electronic and optical properties[3,4,5]. The widely known example of thiophene-based polymers in the photovoltaic field is the polymer poly(3-hexylthiophene) P3HT, which in combination with fullerene derivative [6,6]-phenyl-C61-butyric acid methyl ester (PCBMC60) in photovoltaic devices, has achieved now up to 6.5 % of power conversion efficiency after extensive optimisation ever since 2002[6,7,8, 9]. Polymer P3HT with a band gap of 1.9-2.0 eV can absorbs up to 650 nm, which represent only to 22 % of influx photons of the solar spectrum[10,11]. An alternative to this polymer is the low band gap polymers which offer broader absorption spectra, and could therefore further improve the power conversion efficiency[12, 13]. One effective approach towards low band gap polymers is the combination of alternating electron donating groups and electron withdrawing groups in the polymer back bone, commonly known in the field by so called donor-acceptor (D-A) polymers.[12,13, 14,15]

Following this approach, our group has previously demonstrated D-A low band gap polymers based on oligothiophene as electron donating group and fluorenone as electron withdrawing group. The first attempt of developing D-A polymers alternating dioctyl-bithiophene units with fluorenone units in the D-A polymer, poly(dioctyl-bithiophene-fluorenone) PDOBTF[16] (see the polymer structure in Figure 81) resulted in absorption spectrum edge up to 650 nm in thin film and highly ordered supramolecular organization originating from the presence of stiff fluorenone sub-units which efficiently block the chain folding processes comparable to the poly(3-alkylthiophene)s P3AT[17]. However preliminary photovoltaic devices test of the polymer PDOBTF with fullerenes PCBM only showed a weak power conversion efficiency of 0.09 % related to the weak intensity of absorption band in the region of 500 nm to 650 nm[18].

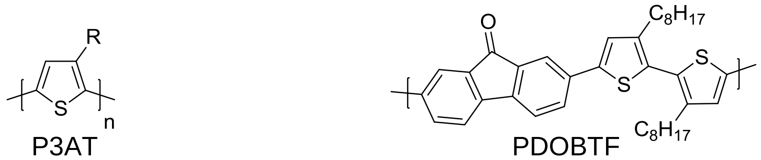


**Figure 81: Molecules structures of poly(3-alkylthiophene) P3AT and poly(dioctyl-bithiophene-fluorenone) PDOBTF**

A more extended thiophenes unit was then introduced as electron donating segment consisting of four thiophene units in order to increase the electron donating strength and the conjugation length[19]. The D-A polymer based on alternating dioctyl-quaterthiophene units and fluorenone unit poly(dioctyl-quaterthiophene-fluorenone) PQTF [20] were developed along with the polymer based on poly(dioctyl-quaterthiophene) PQT for comparison as shown in Figure 82.

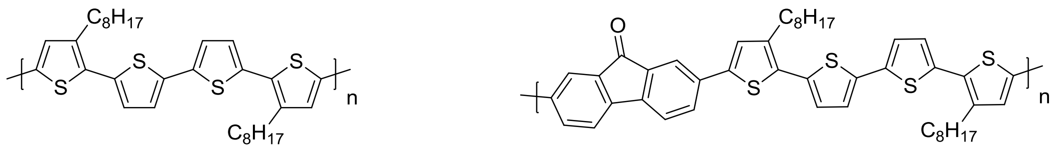


**Figure 82: Molecules structures of polymer poly(dioctyl-quaterthiophene) PQT and poly(dioctyl-quaterthiophene-fluorenone) PQTF**

The polymer PQT composed of all oligothiophene units showed a band gap of 2.3 eV, while for PQTF the incorporation of electron withdrawing fluorenone units alternately positioned in the polymer backbone in between quaterthiophene units showed a lower band gap of about 2.0 eV[20]. Both polymers tested in photovoltaic cells showed highest power conversion efficiencies obtained with these two polymers were 0.45 % for PQT8 and 1.45 % for PQTF8 in combination with PCBMC60 in bulk heterojunction configuration. The comparison of these two similar polymers clearly demonstrated the efficient incorporation of fluorenone in the polymer backbone to increase the power conversion efficiency. Moreover the polymer PQTF8 with longer conjugation lengths thanks to the extended thiophene based units compared to the polymer PDOBTF showed higher intensity of the absorption band in the region of longer wavelength as shown in Figure 83.

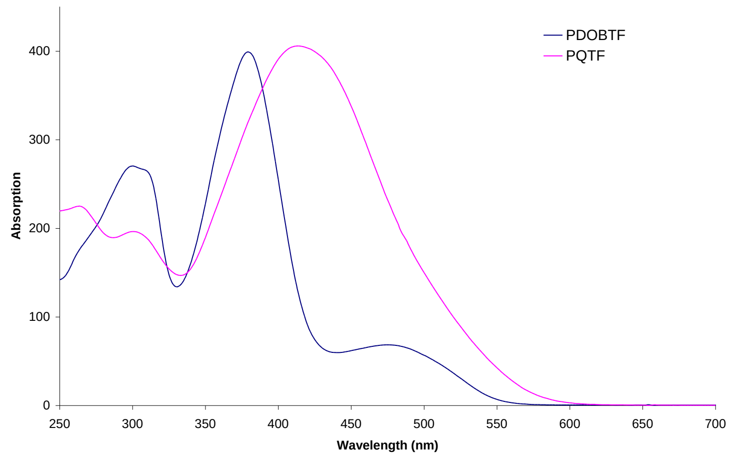


**Figure 83: Absorption spectra of polymer PDOBTF and PQTF in solution**

In the previous chapter we have also demonstrated that the oligomers bis-quaterthiophenes fluorenones QTF8 have demonstrated similar effect of increased intensity of absorption band compared to the bis-bithiophene fluorenone BTF8.

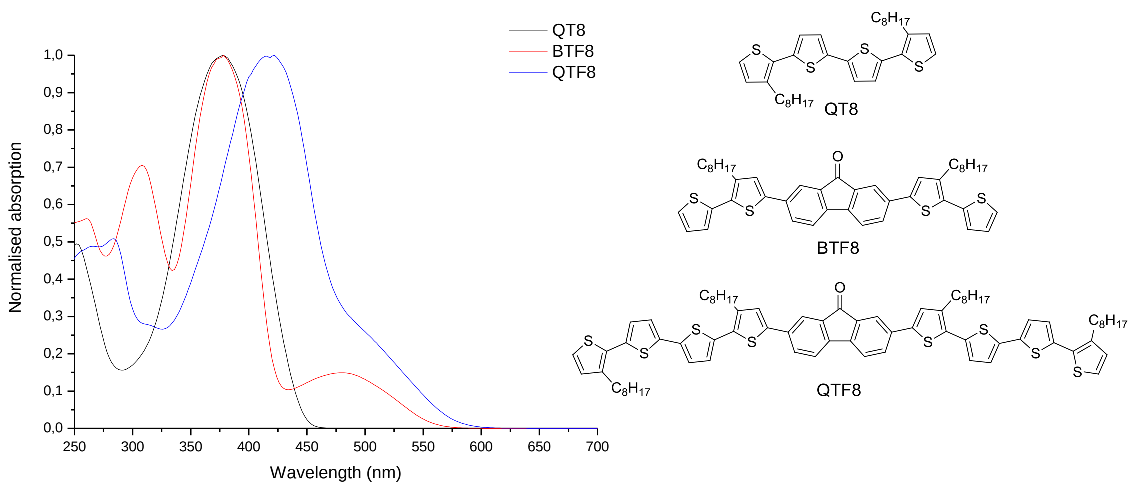


**Figure 84: UV visble absorption spectra of dioctyl quaterthiophene QT8. dioctyl bithiophene fluorenone BTF8 and dioctyl quaterthiophene fluorenone QTF8**

It is to be noted that the polymerisation of BTF8 affords the polymer PQTF, therefore in continuity of this perspective we can further made investigation on this series of D-A polymers of linear oligothiophenes and fluorenone units by direct polymerisation of oligomer QTF to afford the polymer poly(octathiophene-fluorenone) POTF as shown in Figure 85.

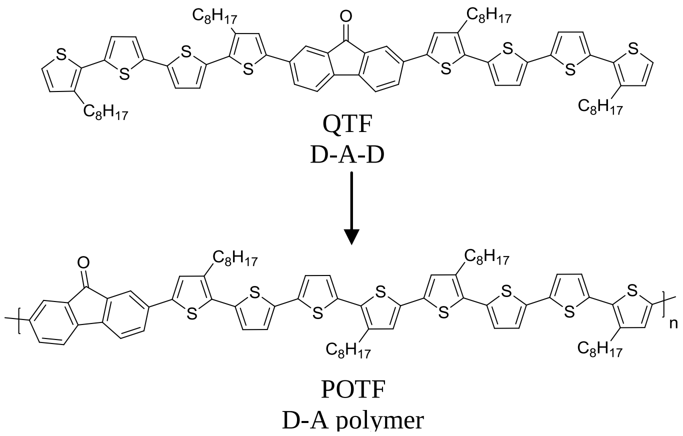


**Figure 85: Molecules structures of octathiophenes with octyl as alkyl side chain as electron donating unit (D) , fluorenone as electron withdrawing unit (A), and the D-A polymer poly (octyl-octathiophenes) units.**

The development of D-A polymer, poly(octathiophene-fluorenone) POTF can allow us to extend the study on the polymers based on linear oligothiophene ( bithiophene, quaterthiophene and octathiophene) as electron donating units in combination with fluorenone as electron withdrawing units in the D-A polymers. We can therefore address the influence of the thiophenes motifs on the electronic, optical and self assembly properties of the materials and eventually draw the relationship between the molecular structures and photovoltaic properties.

In another perspective, it is also interesting to investigate the effect of the nature of the electron withdrawing unit on the thiophene-based polymers properties. We have previously demonstrated fluorenone as potential electron withdrawing group in the donor acceptor D-A polymers with suitable electronic, optical and self assembly properties for photovoltaic applications. Another example of electron withdrawing group is the benzothiadiazole unit which has a strong electron withdrawing properties, and has been extensively used as building block in D-A polymers for photovoltaic applications[21,22,23,24,25,26]. It is therefore judicious to study and to make a direct comparison of the intrinsic properties of donor materials containing either benzothiadiazole units or fluorenone units and to investigate the role of the electron withdrawing unit on the photovoltaic performances.

We decided to develop a D-A polymer based on quaterthiophene-alternate-benzothiadiazole PQTB having the same polymer structure as the polymer quaterthiophene-alternate-fluorenone PQTF, as the latter polymer has shown good performance in solar cells[20]. For the purpose of comparative study with the polymer PQTF, octyl side alkyl chains will be introduced on the polymer backbone at the same position as in the polymer PQTF. The molecular structure of PQTB is presented in Figure 86 below.

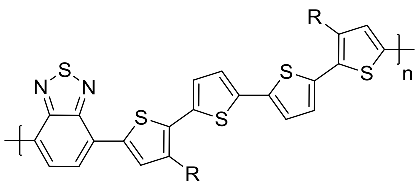

PQTB

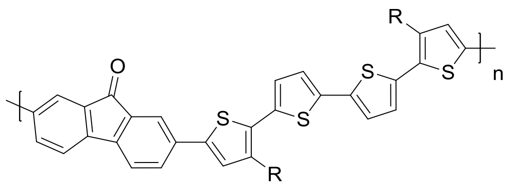

PQTF

**Figure 86: Molecular structure of poly (quaterthiophene-alt-benzothiadiazole) PQTB side by side with the polymer**

Previous works in the field on D-A polymers based on linear oligothiophenes and benzothiadiazole are for example a series of polymers described by Bundgaard and coworkers[27] with different side alkyl chains (3,7,11-trimethyldodecyl and 3-ethylhexyl chain) at different positions on the thiophene rings. Some of their polymers structures which have closest structures to PQTB are presented in Figure 87 below. These series of polymers based on poly(oligothiophenes-benzothiadiazole) were tested in photovoltaic devices and have shown highest power conversion efficiency of 1 % after different optimisations in terms of molecular weights, active layer thickness, blends materials ratios, choice of solvents, etc[28].

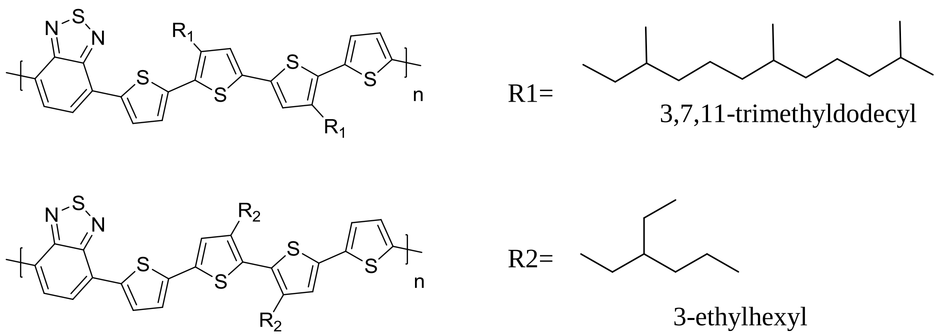


**Figure 87: Low band gap polyquaterhiophene-benzothiadiazole developed by Bundgaard and coworkers[27]**

Other linear oligothiophene-benzothiadiazole long oligomers[29] and polymers[30,31,32,33] have also been published in the literature but we have not yet found polymers showing identical chemical structures to the one of polymer PQTB.

For both polymers PQTB and POTF we will discuss in details the synthesis methods and purifications, the photophysical and electronic properties as well as performances of these polymers in the photovoltaic devices. Some of the results of PQTF8 are also presented for direct comparison and helpful discussion.

# II. Synthesis and purification of thiophene-based polymers PQTF, PQTB and POTF

For preparation of the polymer PQTB there are several possible routes that could be applied for the synthesis as shown in Scheme 4

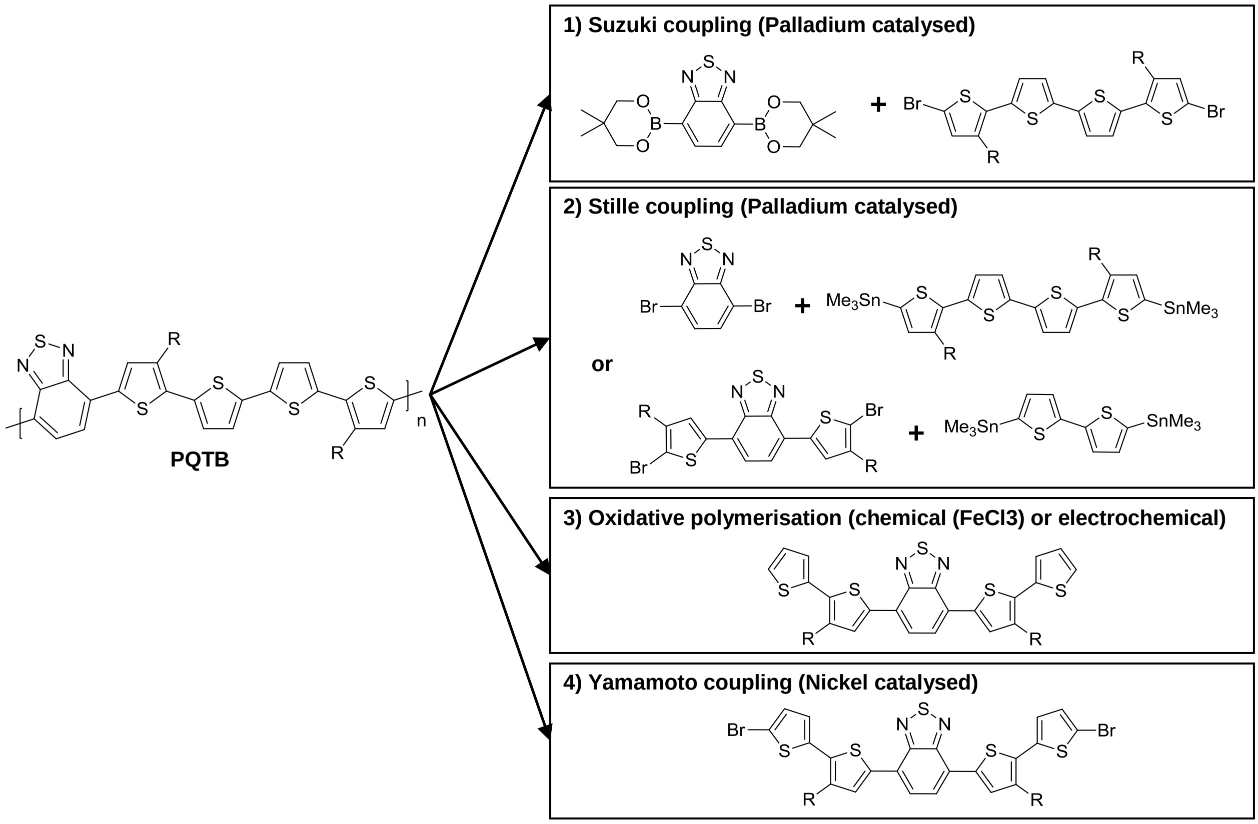


**Scheme 4: Four possible routes for preparation of polymer PQTB**

Lim and coworkers[29] have synthesised similar molecules structures to PQTB but with different side alkyl chains (R=dodecyl (-$C_{12}H_{25}$) and hexyl (-$C_6H_{13}$)) by departing from dibromo(dialkyl-quaterthiophene) and benzothiadiazole diboronic ester via Suzuki coupling polymerisation affording long oligomers (ca. Mn~2.5 kDa). Bundgaard and coworkers[27] have prepared their polymers (quarterthiophene-benzothiadiazole with different side alkyl chains) via Stille coupling polymerisation and oxidative polymerisation. The polymers synthesised by Stille coupling were prepared by departing from distannyl derivates of di(alkyl)dithiophene and dibromo derivatives of benzothiadiazole, while for the oxidative polymerization by ferric chloride salt, di(alkyl)bithiophenebenzothiadiazole monomers were used. Bundgaard and coworkers[27] obtained lower molecular weight (18 kDa) polymers via Stille coupling polymerisation compared to the polymers prepared by oxidative polymerisation (86 kDa).

It is also possible to synthesise PQTB via Yamamoto coupling[34] in presence of zero valent Nickel complex Bis(cyclooctadiene)nickel(0) ($Ni(COD)_2$) as demonstrated by Demadrille and coworkers[16] for the preparation of (polydioctylbithiophene-fluorenone) PDOBTF affording polymers with relatively high molecular weight of ca. 13 kDa. The same polymer prepared by oxidative ferric chloride polymerisation afforded higher molecular weight of ca. 41 kDa[16]. The polymer PDOBTF can also prepared by oxidative electrochemical polymerisation of the corresponding bis-octylthiophene-fluorenone monomer affording high molecular weight polymers but not suitable for large scale production[35]. From these few examples of polymers, oxidative polymerisation has shown to afford polymers with high molecular weight polymers[36].

The polymer PQTF was also prepared by oxidative polymerisation of symmetrical monomer bithiophene-fluorenone BTF as described previously by Demadrille and coworkers[20] as presented in Scheme 5, affording regioregular copolymers. The oxidative polymerisation involves utilisation of ferric (III) chloride salt, an easy and mild reaction conditions (at room temperature) as proposed by Andersson and coworkers[37,38] suitable for large scale production. The oxidative ferric chloride polymerization has been reported to result in higher molecular weight polymers but also high polydispersity indexes and there is also no need for reactive groups such as the halide monomers or stannyl groups. We therefore prepared the polymers PQTB following the same synthetic route as PQTF as shown in Scheme 5.

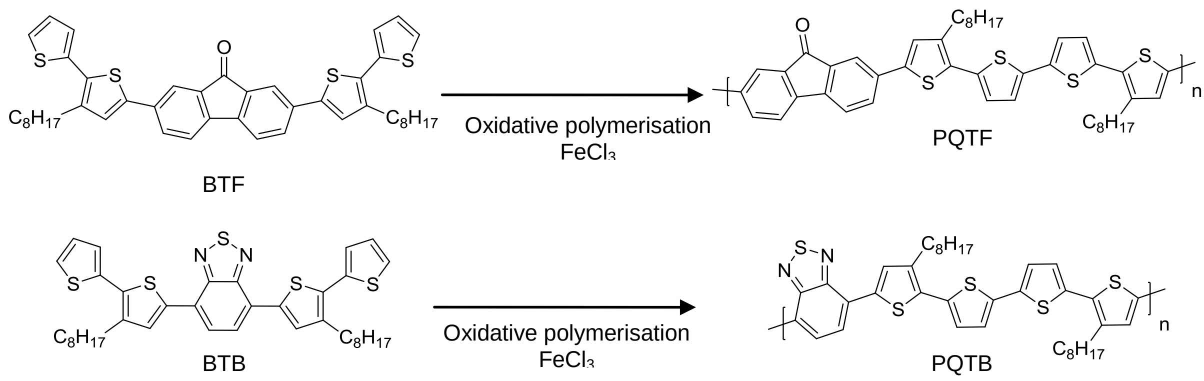


**Scheme 5: Proposed polymerisation for the preparation of polymer PQTB**

Similarly, the polymer POTF will also be prepared via oxidative polymerisation departing from the oligomer QTF.

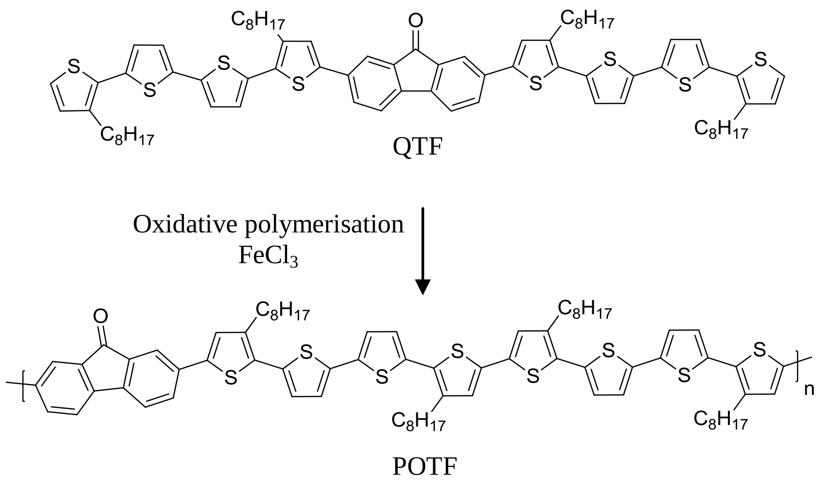


**Scheme 6: Polymerisation method of poly (octathiophene-fluorenone) POTF via oxidative polymerisation of the oligomer QTF**

We described below the details of the synthesis of the monomers BTF and BTB for the preparation of polymers PQTB and PQTF, and the oxidative polymerization of the three polymers PQTF, PQTB and POTF.

## II.1. Synthesis of poly (quaterthiophene-fluorenone) PQTF and poly (quaterthiophene-benzothiadiazole) PQTB

### II.1.1.Synthesis of monomers BTF and BTB

For polymerisation of PQTB and PQTF we have to first prepare the corresponding monomers. Synthesis of the two principal monomers bis-bithiophene-benzothiadiazole BTB for the preparation of polymer PQTB and monomer bis-bithiophene-fluorenone BTF for polymer PQTF are shown in Scheme 7.

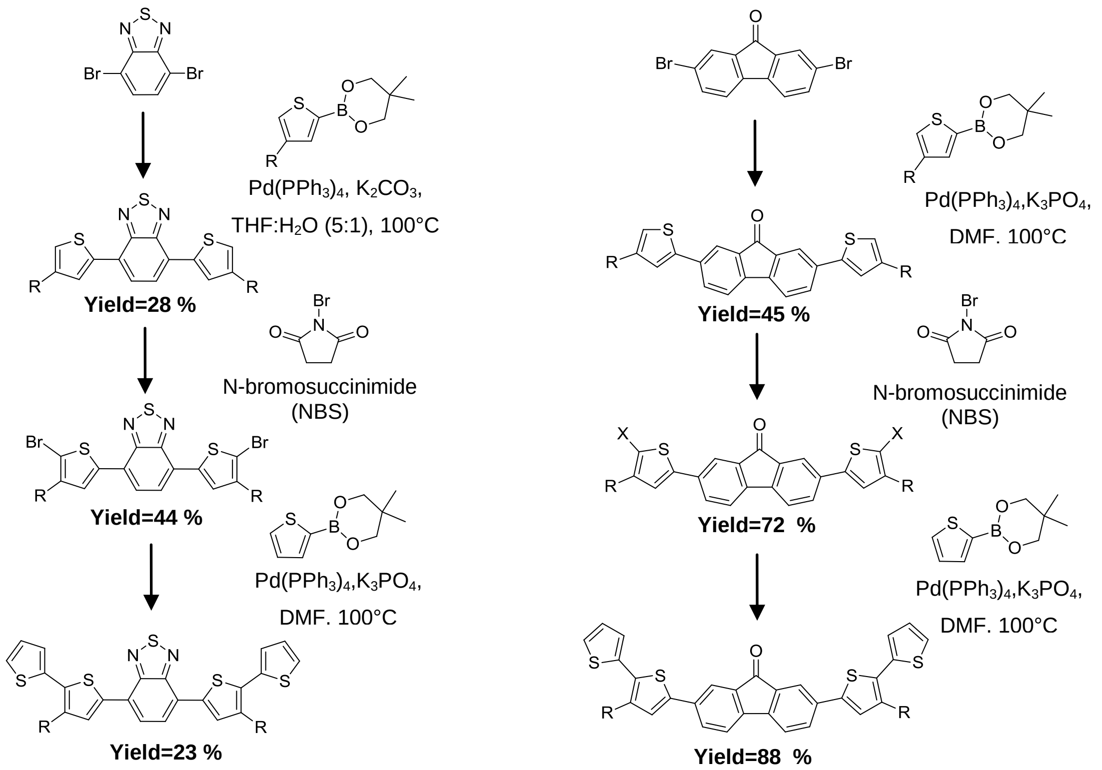


**Scheme 7: Multi step synthesis of monomers bis-bithiophene-benzothiadiazole BTB and monomer bithiophene-fluorenone BTF with R=octyl**

The first step reactions involve Suzuki coupling of commercially available 4,7-dibromobenzo[c][1,2,5]thiadiazole and 2,7 dibromo-9H-fluoren-9-one with (4-octylthiophen-2-yl)boronic ester to form corresponding 4,7-bis(4-octylthiophen-2-yl)benzo[c][1,2,5]thiadiazole (11) and 2,7-bis(4-octylthiophen-2-yl)-9H-fluoren-9-one (13). According to the experimental conditions, we have obtained the products with different yields. The first benzothiadiazole intermediate (11) showed lower yield when prepared in a mixture of solvent THF: $H_2O$ (5:1) in presence of palladium ($Pd(PPh_3)_4$ catalyst and potassium carbonate as base following the procedure in literature by Jannsen and coworkers[32]. The reaction afforded the product in only 28 % yield. On the other hand, the fluorenone intermediate was prepared in DMF as solvent and potassium phosphate as base has shown higher yield of 44 %.

The second step reaction involved the dihalogenation of thiophene-benzothiadiazole derivative (11) and thiophene-fluorenone derivative (13) to form symmetrical 4,7-bis(5-bromo-4-octylthiophen-2-yl)benzo[c][1,2,5]thiadiazole (12) and 2,7-bis(5-bromo-4-octylthiophen-2-yl)-9H-fluoren-9-one (14). The diiodo fluorenone intermediate was also synthesised to allow comparison of Suzuki coupling using either diiodo intermediates or dibromo-intermediates, as iodo-compound are known to afford higher yield in Suzuki coupling compared to bromo-compound[39].The dibromination reactions were performed in chloroform and stirred at room temperature overnight while diiodination reaction was performed in a mixture of chloroform: acetic acid (25:15) as solubility tests have shown N-iodosuccinimide only partly dissolved in chloroform. The dibromination afford a yield of 44% of 4,7-bis(4-octylthiophen-2-yl)benzo[c][1,2,5]thiadiazole (12) product. For fluorenone intermediate, 72 % of the product of 2,7-bis(5-bromo-4-octylthiophen-2-yl)-9H-fluoren-9-one (14) was obtained and a higher yield of 93 % was obtained for 2,7-bis(5-iodo-4-octylthiophen-2-yl)-9H-fluoren-9-one.

In the third step reaction, we coupled on both ends of these two molecules with thiophene boronic ester, dimethyl-2-(thien-2 yl)[1,3,2]dioxoborinane. Suzuki cross-coupling reaction was employed to afford monomer benzothiadiazole BTB and monomer fluorenone BTF. The Suzuki coupling was carried out in DMF, with $Pd(PPh_3)_4$ as catalyst and $K_3PO_4$ was used as a base in all cases. The product yields obtained for monomer benzothiadiazole BTB was only 23 % much lower compared to the product yield of the monomer fluorenone BTF. High yield of monomer BTF was obtained by departing from dibromo intermediate of 88 % of product while departing from diiodo intermediate showed slightly lower yield of 62 %. Therefore for our reactions we found that it is more convenient to use the dibromo-intermediates instead of diiodo-intermediates. The poor coupling reaction for the preparation of benzothiadiazole monomer BTB might be due to a bad choice of solvent for the reaction. In order to improve the reaction, we suggest using toluene as solvent. Recent results obtained in our group have confirmed that better yields can be achieved using toluene. Pure monomers BTB and BTF are used for the preparation of polymer PQTB and PQTF accordingly. Extensive experiments in the laboratory working with different fluorenone intermediates have shown so far utilisation of DMF as solvent of reactions have afforded good yield of product compared to other solvents.

## II.1.2.Synthesis of polymers PQTB and PQTF

The polymerisation of polymers PQTB and PQTF are carried out via oxidative polymerisation with iron chloride (III) salts using the monomers BTB and BTF respectively. For the oxidative polymerisation reactions were conducted according to Andersson's procedure[37] yielding, in many cases, higher molecular weight polymers.

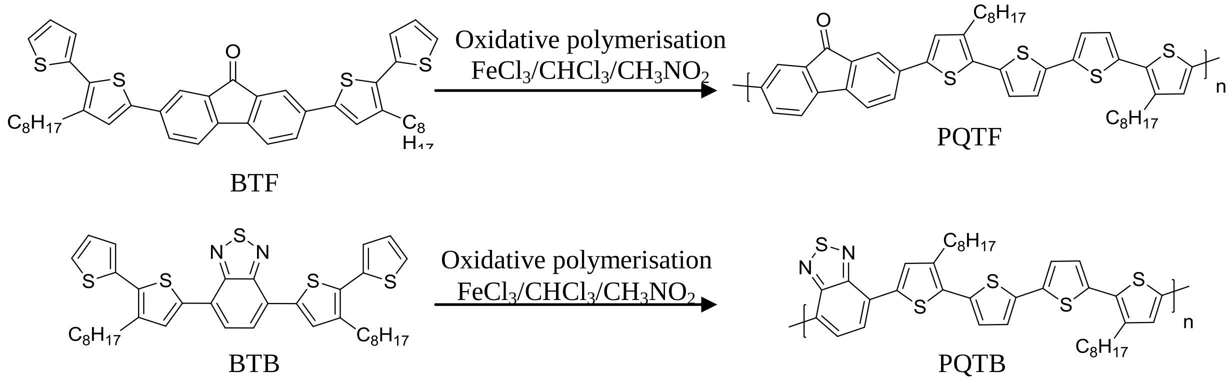


**Scheme 8: Synthetic route to thiophene-benzothiadiazole polymer PQTB and thiophene-fluorenone polymer PQTF**

In this method the potential of the oxidative couple is adjusted by the $Fe^{3+}/Fe^{2+}$ ratio following the Nernst equation. As a result, the polymerization can be carried out at relatively mild conditions without over-oxidation effects[37]. The polymerisations take place at room temperature overnight, in anhydrous conditions in chloroform and in presence of nitromethane to well-dissolved the Iron chloride (III) salts. After polymerisation reaction, the polymers are precipitated from methanol. The polymers are obtained in their doped state and a mixture of methanol/hydrazine is used to reduce the polymers. As-synthesized polymers usually contain minute amounts of dopants of unidentified chemical nature and they require further dedoping. The dedoping was achieved by washing the chloroform solution of the polymer with a solution of 0.1 M ammonium hydroxide solution and 0.02 M of EDTA under stirring for 15 hours. These steps allow eliminating residual iron chloride (III) salts by chelation and to undope the polymers[36,37] .

Oxidative polymerisation affords high dispersity polymers containing a mixture of short oligomers and longer polymer chains of different molecular weights[20]. We have therefore carried out polymer fractionation using the sequential Soxhlet extractions method as described in Chapter Experimental Methods and Materials to obtain polymer fractions of different molecular weights and reduced polydispersity indexes. For polymer PQTB we first extracted with methanol to remove non-reacted monomers. We followed then by extraction with acetone to remove oligomeric and low molecular weight fractions from the polymer. Further extractions were carried out by using dichloromethane, chloroform, toluene and chlorobenzene to obtain higher molecular weights polymer fractions. The different polymer fractions were concentrated, dried and were then analysed by size exclusion chromatography (SEC) with tetrahydrofuran (THF) as solvent. The macromolecular parameters of PQTB are listed in Table 16 along with the data values of polymer PQTF[20] for comparison.

| Polymer | Fraction | Mn [kDa eq. PS] | Mw [kDa eq. PS] | I= Mw/Mn |
|---|---|---|---|---|
| PQTB | F0-Crude | 2.49 | 3.08* | 1.24 |
| | F1-Acetone | 1.99 | 2.08 | 1.05 |
| | F2-Dichloromethane | 2.36 | 2.75 | 1.16 |
| | F3-Chloroform | 4.78 | 5.70 | 1.19 |
| | F4-Toluene | 5.04* | 6.33* | 1.25 |
| | F5-Chlorobenzene | 3.41* | 6.96* | 2.04 |
| PQTF | F0-Crude | 0.81 | 1.15 | 1.43 |
| | F1-Acetone | 0.36 | 0.50 | 1.40 |
| | F2-Dichloromethane | 1.22 | 2.01 | 1.64 |
| | F3-Chloroform | 1.36 | 2.23 | 1.64 |
| | F4-Chlorobenzene | insoluble | Insoluble | insoluble |

**Table 16: Macromolecular parameters of polymer PQTB and PQTF determined by SEC in THF using polystyrene standard. The asterisk * represents partially soluble fraction in THF**

The highest fraction soluble in chloroform shown molecular weight Mn = 4.78 kDa and Mw= 5.70 and a low polydispersity of 1.19. For the polymer fractions obtained from toluene and from chlorobenzene, these two fractions were partially soluble in THF, therefore the recorded values in the Table 16 were underestimated as it represented only the soluble fraction. Soluble toluene polymer fraction gives a molecular weight of 5.04 kDa and polydispersity of 1.25, which can be estimated to have a minimum of seven repeating units in the polymer backbone.

The polymer PQTF afforded lower molecular weight polymers of about 1.4 kDa for the soluble fraction in chloroform which can be estimated to have a minimum of two repeating units as compared to PQTB of a minimum seven repeating units. The molecular weight of PQTB is therefore much higher than the molecular weight of PQTF which can be attributed to higher degree of solubility of the polymer PQTB in the reaction solvent (chloroform) during the polymerisation than the polymer PQTF. Further optimisations of the reaction conditions may afford higher molecular weight polymers with improved solubility by replacing the side alkyl chains with more solubilising side alkyl chains such as 3-ethylhexyl or 3,7,11-trimethyldodecyl as demonstrated by Bundgaard and coworkers[27], or using chlorobenzene as solvent of polymerisation as proposed by Andersson and coworkers for preparation of low band gap polymers[38]. The molecular structure of the polymers synthesised were also confirmed by NMR and elemental analysis.

## II.2. Synthesis of poly (octothiophene-fluorenone) POTF

The POTF was also prepared via oxidative polymerisation departing from the symmetrical oligomer QTF following the same procedure as PQTF[20] and PQTB as shown in Scheme 9.

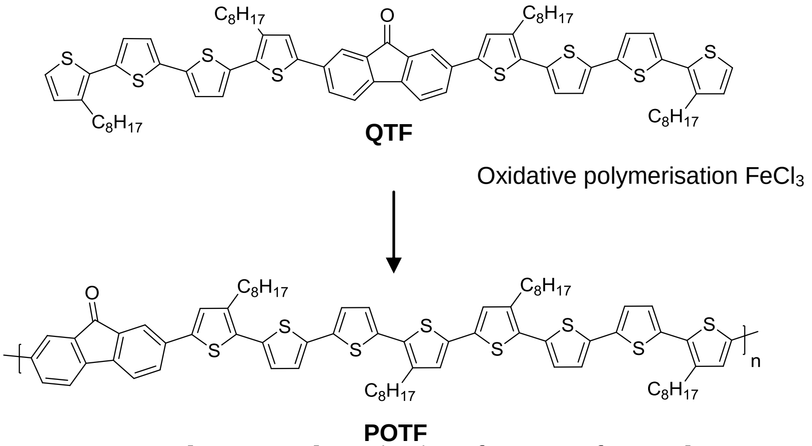


**Scheme 9: Polymerisation of QTF8 to form polymer POTF**

After synthesis and the dedoping process, the polymer POTF was further purified by soxhlet extraction. We decided first to extract the polymer chains with toluene in order to collect most of the soluble chains. The polymer was partially extracted in this first step. Then the obtained soluble fraction was extracted using dichloromethane and finally again with toluene. The molecular weights of the polymers have been determined by analytical SEC in THF using polystyrene standards. The elution diagram of POTF polymer is shown in Figure 88 .

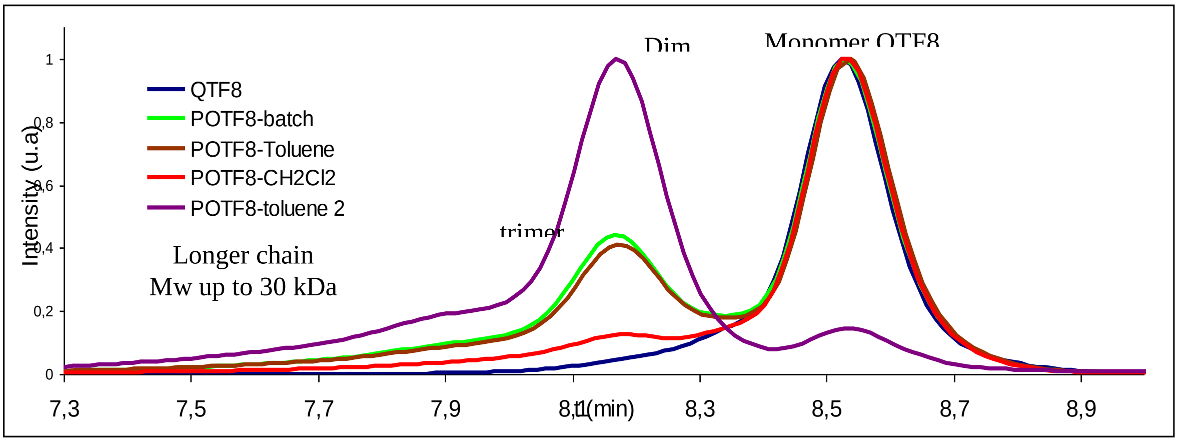


**Figure 88: Elution diagram of SEC analyse measurement in THF as eluent using polystyrene standard**

| Polymer | Fraction | Mn [kDa eq. PS] | Mw [kDa eq. PS] | I= Mw/Mn |
|---|---|---|---|---|
| POTF | F0-Crude | 2.83 | 4.12 | 1.45 |
| | F1-Toluene | 2.76 | 4.03 | 1.46 |
| | F2-Chloroform | 2.40 | 3.11 | 1.29 |
| | F3-Toluene-2 | 4.92 | 6.54 | 1.33 |

**Table 17: Macromolecular parameters of polymer POTF determined by SEC in THF using polystyrene standards**

We can observe that sequential extraction allows decomposition of the polymer according to its chain length. The first fraction of POTF in toluene contains a combination of departing monomer and also longer chains. The third extraction by toluene contains majority of long chains of the polymers. The macromolecular parameters of POTF polymer are listed in Table 17. We obtained a molecular weight average of 4.9 kDa for the highest polymer fraction, which can be estimated having as least two repeating units (or at least 20 aromatic rings). The polymer distribution of POTF is mainly composed of oligomer QTF8, and short polymers. The longer polymer chains have molecular weights up to 30 kDa (~15 repeating units). A direct comparison of the macromolecular parameters obtained for PQTF (~1.4 kDa) and POTF (~5 kDa) shows that longer polymer chains are formed during the polymerisation reaction of POTF. SEC measurements for polymer POTF and PQTF have shown that these polymers are both composed mainly of polymers of two repeating units, therefore higher molecular weight is obtained for polymer POTF as the departing monomer of POTF have longer chain (QTF Mn=2.2 kDa) compared to PQTF (BTF Mn= 0.7 kDa). This demonstrates the advantage of polymerisation of long oligomers to afford high molecular weight polymers.

# III. Photo-physical characterizations of PQTB, PQTF and POTF

UV-Visible absorption spectra of the different fractions (acetone, dichloromethane, chloroform, toluene and chlorobenzene) of PQTB were recorded in chlorobenzene solution and in thin films. UV-Visible absorption spectra of PQTB in solution are presented in **Figure** 89 with the maximum peaks wavelengths presented in the Table 18.

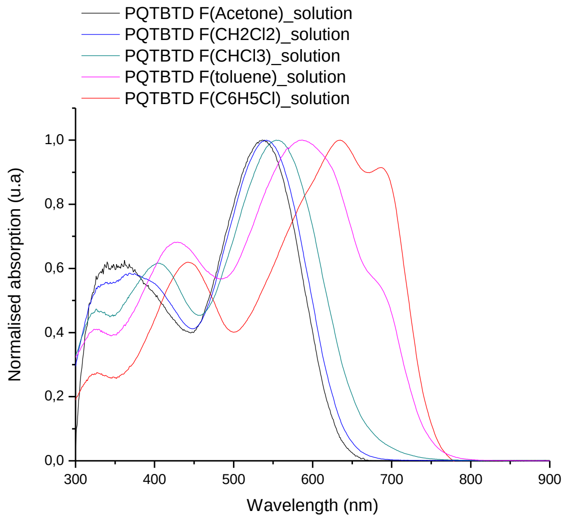


**Figure 89: UV-Visible absorption spectra of polymer PQTB fractions in chlorobenzene solution at 10-5 g/cm3 concentrations.**

| Fraction polymer PQTB | $\lambda_{max}$/nm(Solution) |
|---|---|
| F1-Acetone | 536 |
| F2-Dichloromethane | 542 |
| F3-Chloroform | 405; 554 |
| F4-Toluene | 430; 586; 686 |
| F5-Chlorobenzene | 443; 635; 686 |

**Table 18: Optical properties of polymer PQTB according to polymer fractions**

All polymer fraction showed absorption peaks in short and long wavelength regions which can be attributed to the π–π* transition band of the conjugated polymer backbone and charge transfer transition between electron-rich and electron-poor segments[40,41]. According to the polymer fractions, the absorption spectra are red-shifted with increasing molecular weights fractions as a result of extension of conjugation length[42]. For example the chloroform fraction has a π–π* transition band at 404 nm while the π–π* transition band of chlorobenzene polymer fraction is red shifted up to 39 nm at 443 nm. The intense internal charge transfer band in the long wavelength region[46, 32] for the chlorobenzene fraction at 635 nm is strongly red-shifted of 81 nm compared to the chloroform fraction band at 554 nm. We also observed apparition of vibronic band for the high molecular weights toluene fraction and chlorobenzene fraction. These vibronic bands can be attributed to molecular ordering in the polymer with the extension of conjugation length in the polymer[43] with most probably formation of fine aggregates in solution[44]

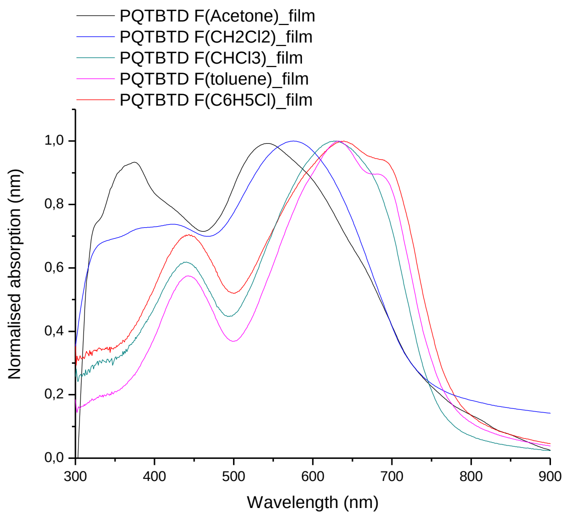


**Figure 90: Normalised UV-Visible absorption spectrum of polymer PQTB fractions in film prepared from chlorobenzene solution at 10 mg/ml. The absorption spectra for acetone and dichloromethane are poorly resolved in the UV region and we present here the smoothed curves.**

| Fraction polymer PQTB | $\lambda_{max}$/nm Solution | $\lambda_{max}$/nm Film | $E_{g\text{-}opt}$/eV ($\lambda_{offset}$/nm) |
|---|---|---|---|
| F1-Acetone | 536 | 546 | 1.61 (770) |
| F2-Dichloromethane | 542 | 572 | 1.61 (770) |
| F3-Chloroform | 405; 554 | 440 ; 626 | 1.61 (770) |
| F4-Toluene | 430; 586; 686 | 443; 632;687 | 1.58 (783) |
| F5-Chlorobenzene | 443; 635;686 | 443; 639; 694 | 1.56 (794) |

**Table 19: UV -Visible absorption optical parameters of PQTB polymer fractions in film**

The absorption spectra of the polymers in film allow to further study the molecular ordering of the polymers (See Figure 90, Table 19). For the chloroform fraction, we observed significant bathochromic shift of 35 nm of the π–π* transition band and 70 nm for the internal charge transfer band. The bathochromic shifts in solid state are commonly observed in conjugated polymer as an effect of increased polymer chain aggregation in the solid state[45, 46]. In the contrary, for the polymers of toluene and chlorobenzene fractions, no significant red-shift is observed as the polymer formed readily aggregates in solution[43]. The polymers PQTB give optical band gap of 1.56 to 1.61 eV.

Normalised UV-visible absorption spectra of polymer POTF in chlorobenzene solution according to the fraction are shown in Figure 91.

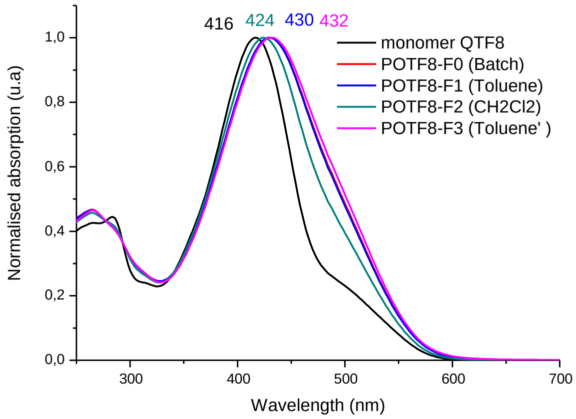


**Figure 91: Normalised UV-Visible absorption spectra of POTF in solution according to polymer fractions.**

| Fraction | λmax/nm Solution | $Eg^{opt}$/eV ($\lambda_{offset}$/nm) |
|---|---|---|
| Monomer QTF8 | 416 | 2.07 |
| POTF batch | 430 | 2.07 |
| POTF F1 toluene | 430 | 2.07 |
| POTF F2 dichloromethane | 424 | 2.07 |
| POTF F3 toluene' | 432 | 2.07 |

**Table 20: UV -Visible absorption optical parameters of PQTB polymer fractions in solution and on film**

We can clearly observed the polymer POTF of different fractions exhibits broader absorption spectrum than its monomer QTF8 We observed one intense peak at 424-432 nm corresponding to the π–π* transition band. These maximum peaks of POTF are also red-shifted from 416 nm for QTF8 to 424 nm for dichloromethane fraction, to 430 nm for the first toluene fraction and 432 nm for the second toluene fraction. This shows that the maximum peak shifted towards longer wavelength for higher molecular weight polymer fractions similar to the results obtained with PQTB. The results are expected as polymers with higher molecular weights possess longer conjugation lengths thus extended absorption band[42]. The increase is however moderate since the conjugation length in QTF8 is already important due to the presence of 10 aromatic rings in this oligomer. A broader absorption band in the region 450 nm to 600 nm can be attributed to synergistic effect of π–π* transition and the internal charge transfer band[47,48] which has been observed in the case of dimer TVF2.

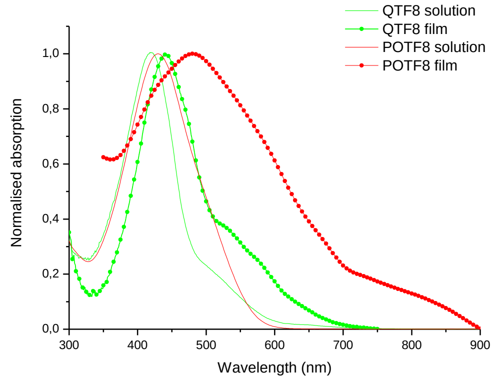


**Figure 92: Comparison of the absorption spectrum of QTF8 and POTF8 in solution and in film**

The absorption spectrum of polymer POTF of toluene fraction in film are presented in Figure 92 in comparison with the absorption spectrum in solution. In film the absorption spectrum of POTF is shifted towards longer wavelength of 480 nm, therefore giving a bathochromic shift of 50 nm, and large band absorption in the region more than 500 nm. The absorption spectrum also showed intense absorption band similar to the one that we have obtained in the case of dimer TVF2. We can therefore postulate an enhanced packing of molecules in film than in solution[43] and that ordered aggregates may be present in thin films[49]. The polymer optical band gap calculated from the absorption edge is at 1.61 eV. POTF also showed broader absorption in film compared to its monomer QTF as shown in Figure 92.

For a better comparison the absorption spectra of the toluene fraction for the polymers PQTB and POTF are traced in the same graph as shown in Figure 93.

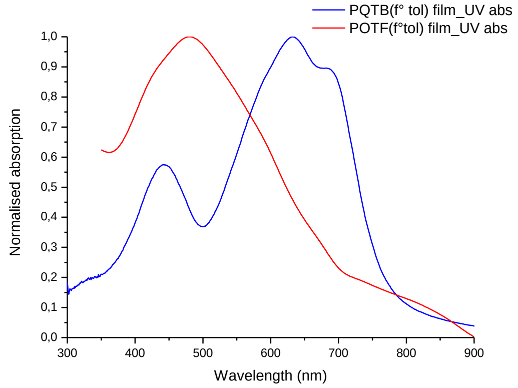


**Figure 93: UV-Visible absorption specta of POTF and PQTB in film.**

| Polymer | $\lambda_{max}$/nm Solution | $\lambda_{max}$/nm Film | $E_{g\text{-}opt}$/eV ($\lambda_{offset}$/nm) |
|---|---|---|---|
| PQTF (f° toluene) | 414 | 463 | 1.77 |
| PQTB(f° toluene) | 430; 587; 686 | 443; 632;687 | 1.58 |
| POTF(f° toluene) | 430 | 480 | 1.61 |

**Table 21: UV -Visible absorption optical parameters of PQTB and POTF in solution and on film compared to PQTF.**

We can first observed for polymer poly (quaterthiophene-benzothiadiazole) PQTB, with stronger electron accepting benzothiadiazole unit, the internal charge transfer absorption band is more pronounced giving additional intense maximum absorption band at 587 nm. PQTB showed an overall broader absorption spectrum than the polymer PQTF and POTF.

The increase of the number of thiophene rings in POTF compared to PQTF8 allows the extension of the conjugation lengths and the maximum absorption band is shifted from 414 nm for PQTF to 430 nm for POTF, and a reduced optical band gap of $Eg^{op}$=1.6 eV compared to $Eg^{op}$=1. 77 eV for PQTF. We can therefore conclude, for polymer POTF having higher molecular weight and extended conjugation length than polymer PQTF allow broadening the absorption spectra notably in film. The polymer POTF having extended thiophene rings (8 units) compared to 4 units in the case of PQTF in between the fluorenone blocks have allowed better packing in film hence reducing the band gap and higher intensity of absorption band.

Moreover, from SEC determination of molecular weight of the polymer POTF of toluene fraction have shown the polymer POTF is composed essentially of dimer with two repeating monomers in the polymer backbone. Therefore we can compare our polymer POTF with the dimer TVF2. The UV visible absorption spectra of polymer POTF and the dimer TVF are presented in Figure 94. We can observe a good correlation of the effect of conjugation and pi-stacking on film to an increase of absorption band intensity where two conjugating segment of thienylene vinylene (or quarterthiophenes units) positioned side by side in between fluorenone units resulted in broadening the absorption spectra. Fluorenone units with strong C=O dipole can also play a role to avoid chain folding in the film[17].

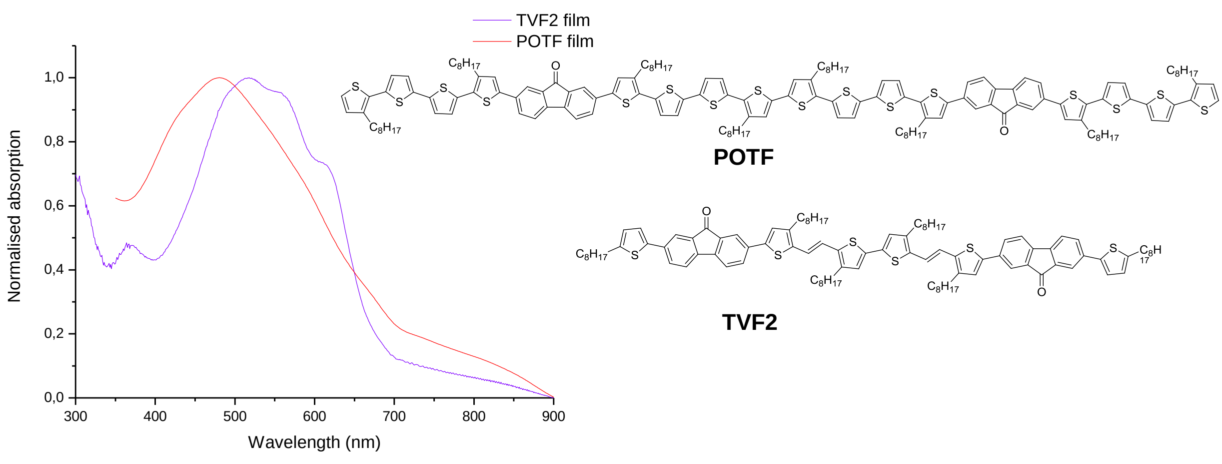


**Figure 94: UV visible absorption spectra of polymer POTF and dimer TVF2 in film**

From these few examples of polymers we can clearly observe the effect of molecular structures on photophysical properties. Higher conjugation results in shifting the absorption spectra towards longer wavelength (bathocromic shift)[50]. Higher molecular weight also results in bathochromic shift of the absorption wavelengths[51] . Extended numbers of linear regioreguliar thiophenes rings in between fluorenone units results in better packing in film and an increase in absorption band intensity[52,53] . Stronger electron withdrawing unit results give rise to a more intense internal charge transfer absorption band[14].

# IV. Electrochemical characterisation of PQTB, PQTF and POTF

We performed electrochemical analysis of the polymer PQTB and POTF by cyclic voltammetry. We performed the analysis by depositing the polymers on platinum electrodes by drop casting and left to dry before measuring the deposited thin film in acetonitrile solution with tetrabutyl ammonium hexafluorophosphate as supporting electrolyte. The cyclic voltammogram of PQTB polymer is presented in Figure 95.

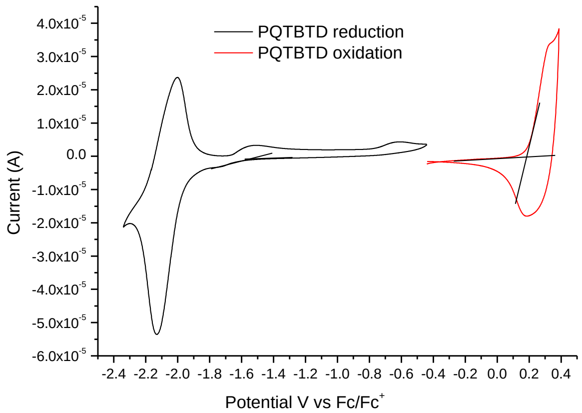


**Figure 95: Cyclic voltammograms of thin film polymer PQTB recorded in 0.1 M $Bu_4NPF_6$ solution in acetonitrile**

The polymer PQTB gives an oxidation potential of 0.18 V upon anodic scan and a reduction potential of -1.51 V upon cathodic scan giving HOMO energy levels of -4.98 eV and LUMO energy levels of -3.29 eV. The HOMO energy level of PQTB is close to the HOMO energy level of PQTF demonstrating that the oxidation potentials values are governed by electron-rich quaterthiophene segments[25]. The LUMO energy level for PQTB is located lower than the LUMO energy level of PQTF (-3.00 eV) which is expected as the benzothiadiazole is a stronger electron withdrawing group than fluorenone[54]. From the HOMO and LUMO energy levels of PQTB, the electrochemical band gap of PQTB is therefore calculated at 1.69 eV which is hence lower than the band gap of PQTF (2.00 eV).

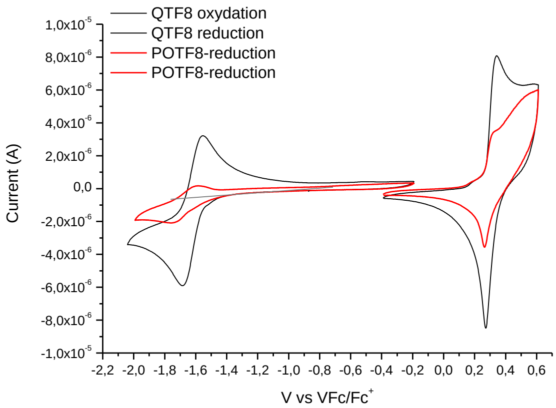


**Figure 96: Cyclic voltammogram of polymer POTF recorded in 0,1 M $Bu_4NPF_6$ solution in dichloromethane. The cyclic voltammogram of QTF8 is also presented for comparison.**

The polymer POTF showed an oxidation potential of 0.19 V upon anodic scan and a reduction potential of -1.48 V upon cathodic scan as shown in Figure 96. This gives HOMO and LUMO energy levels of -5.09 eV and -3.21 eV respectively, and calculated band gap of 1.71 eV. The polymer POTF showed very close value of HOMO level to its monomer QTF8 situated at (QTF $E_{HOMO}$=-5.01 eV) but a lower LUMO energy level compared to QTF (QTF $E_{LUMO}$=-3.20 eV). As we have seen when studying the photophysical properties of POTF8, the polymer showed close similarity to the dimer TVF2. If we compared the HOMO and LUMO energy levels of TVF2, the LUMO energy levels showed closest value to POTF8 (TVF2 $E_{LUMO}$ = -3.27 eV). This is consistent as the LUMO energy levels depend on the electron withdrawing units. As both molecules POTF8 and TVF2 possess 2 units of fluorenone, they have shown similar LUMO energy levels.

| Compound | EonsetOx /V | EonsetRed /V | HOMO /Ev | LUMO /eV | Eg-ec /eV |
|---|---|---|---|---|---|
| PQTB | 0.18 | -1.51 | -4.98 | -3.29 | 1.69 |
| PQTF | 0.20 | -1.80 | -5.00 | -3.00 | 2.00 |
| POTF | 0.19 | -1.52 | -4.99 | -3.28 | 1.71 |
| QTF8 | 0.21 | -1.60 | -5.01 | -3.20 | 1.81 |
| TVF2 | 0.27 | -1.53 | -5.07 | -3.27 | 1.80 |

**Table 22: Electrochemical parameters and energy levels positions of PQTB. PQTF and POTF films**

The band gap of the polymer POTF is therefore reduced by 0.29 eV compared to the polymer PQTF8 at ($E_g$=2.0 eV). The polymer POTF which has a higher degree of polymerisation than PQTF8 exhibit higher $\pi$-conjugation length in its polymer backbone therefore has a lower band gap. The electrochemical properties of the polymer PQTB and POTF are reported in Table 22 as well as the electrochemical values of PQTF8 for comparison.

The polymers PQTB, POTF and PQTF8 are positioned according to their energy levels compared to PCBM (electron acceptor) in Figure 97.

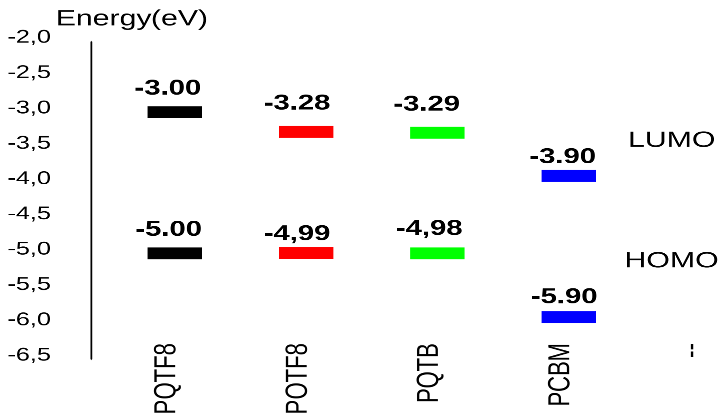


**Figure 97: Energy diagram of HOMO-LUMO energy levels of polymers PQTF8, POTF, PQTB and PCBM**

All three polymers showed higher LUMO energy levels than the LUMO energy levels of PCBM therefore are suitable electron donor materials for photovoltaic applications. The HOMO energy levels of all three polymers are of same values. It is acknowledged in the organic photovoltaic field that the values of open circuit voltage in bulk heterojunction photovoltaic device is directly related to the difference of HOMO energy level of the donor materials and the LUMO energy level of acceptor[55.56]. Therefore, we may expect to obtain close values of open circuit voltages for our polymers based on linear oligothiophenes (PQTB, POTF and PQTF8) in blend with acceptor materials in bulk heterojunction photovoltaic devices.

## V. Charge carrier transport properties

We have demonstrated in the previous topic that our polymers are suitable donor materials for photovoltaic cells and can generate free charges carriers under illumination when they are combined with the suitable acceptor. In such macromolecules, it is also of importance to quantify the transport properties and in particular the mobility of the holes in the materials. Therefore we have conducted charges transport study for our polymers by using field-effect transistor measurement in collaboration with Dr.Jean Pierre Simonato and Dr. Caroline Celle from the group CEA-LITEN-DTNM-LCRE. We have fabricated transistors using polymers PQTB and PQTF as active materials in the channel and the results are shown in (Figure 98). For polymer POTF, we did not have sufficient amount of material for doing these measurements.

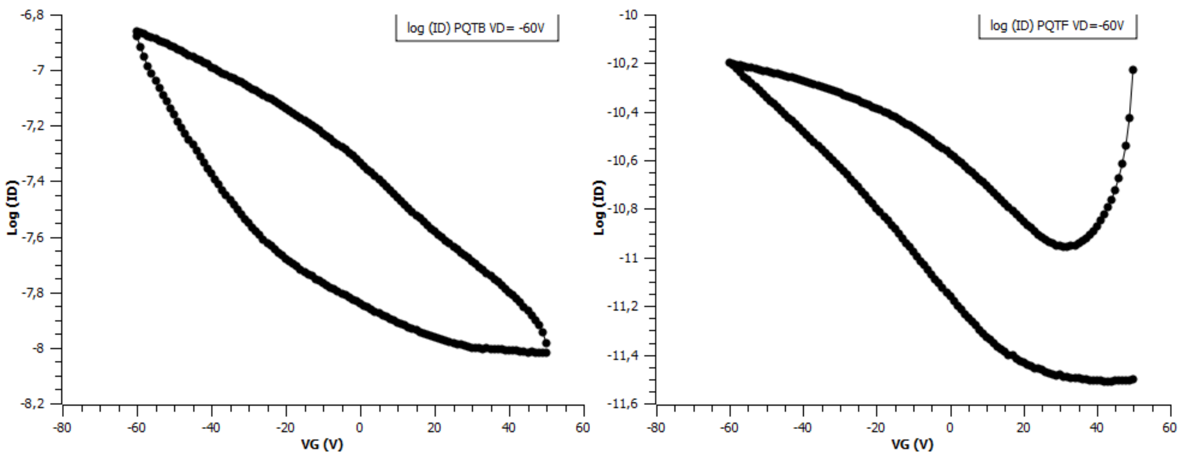


**Figure 98: Transfer characteristic curves of log $I_{DS}$= f($V_G$) for $V_D$=-60V measured for thin films of polymers PQTB and PQTF with channel length of 10 µm, The $V_{DS}$ was kept at −60 V, and the $V_G$ bias was swept from +60V to -60 V and reverse to +60 V again.**

The transfer characteristic curves for polymer PQTB and PQTF are presented in (Figure 98). The drain voltage $V_D$ is held constant at −60 V (voltage found at saturation regime) and the gate voltage $V_G$ is swept from +40 V to −60 V. We then plot the current drain $I_{DS}$ versus gate voltage to determine the transfer characteristic curves log[$I_D$]=f ($V_G$) in the saturation regime. We have plotted the curves log[$I_D$]=f ($V_G$) for the polymer PQTB and polymer PQTF at saturation regime of $V_D$= -60 V with channel length of 10µm. A linear fit to the √Ids-Vg trace permits the extraction of saturation mobility and threshold voltage ($V_T$). It should be underlined that these results should be considered as preliminary since no optimization in the fabrication of the devices and no treatment of the gate oxide were undertaken yet. However all the experiments have been realised under the same conditions and allow a direct comparison of the materials.

Both polymers showed p-type characteristics in negative bias, typical from p-type semiconductors. In this saturation regime, the values for the mobility (µ), short circuit current Ioff (leakage current Ioff = $I_D$($V_D$ =0 V, Vg = 0V)) and the ratio Ion/Ioff can be calculated from the slopes of the of $\sqrt{I_D}$ =f ($V_G$). The transport properties values are presented in Table 23.

| Polymer | µ (cm². $V^{-1}$. $s^{-1}$) | Vthreshold (V) | Ioff (A) | Ion/Ioff |
|---|---|---|---|---|
| PQTB | 1.0 $10^{-5}$ | 74.8 | -1.04 $10^{-8}$ | 13.3 |
| PQTF | 6.1 $10^{-8}$ | 77.3 | -1.11 $10^{-11}$ | 7.4 |

**Table 23: Transport properties at saturation regime of $V_D$= -60 V for the polymer PQTB and PQTF**

We obtained mobility value of the polymer PQTB of 1.0 $10^{-5}$ cm². $V^{-1}$. $s^{-1}$ much higher than the mobility of the polymer PQTF and 6.1 $10^{-8}$ cm². $V^{-1}$. $s^{-1}$. The polymer PQTB also afforded high ratio of Ion/Ioff with a value of 13.3 compared to 7.4 for the polymer PQTF. Based on this results we can conclude that the polymer PQTB affords higher hole mobility than the polymer PQTF. The hole mobility value of our polymer PQTB is found in the range of other reported thiophene-benzothiadiazole polymers (~$10^{-5}cm^2.V^{-1}.s^{-1}$) [57,30,58] and have shown good performance in photovoltaic devices up to more than 2.5 %[30].

# VI. Photovoltaic properties of PQTB and POTF

Photovoltaic properties were investigated in a typical bulk heterojunction configuration ITO/PEDOT:PSS/ Polymer:fullerenes/LiF:Al for the polymers poly (quaterthiophene-benzothiadiazole) PQTB and poly(octathiophene-fluorenone) POTF. The polymers were tested with two fullerenes derivatives PCBMC60 and PCBMC70 which have shown good compatibility and relatively efficient acceptors with most of conjugated polymers[59,60,61]. The photovoltaic cells were first tested as-deposited then the devices were heated for 5 min at temperature of 70 ° C or 80 °C for optimisation.

## VI.1. Polymer solar cells based on PQTB

We described here the photovoltaic tests based on the polymer PQTB of chloroform fraction which have shown high molecular weight of 5 kDa. Other series of photovoltaic tests have already been performed previously by former post doctorate Frédéric Lincker for the polymer PQTB of higher molecular weight fractions (toluene and chlorobenzene). The highest performance was obtained with polymer PQTB of toluene fraction in combination with PCBMC60 at a ratio of 1:1. The cell exhibits a power conversion efficiency of 0.89 %, short current density of 4.53 mA/cm², an open circuit voltage of 0.49 V and a fill factor of 0.40 with film thickness of 100±20 nm. The devices have also shown degradation upon post annealing treatment at 100 °C for 5 min. This series of tests based on chloroform fraction is a further completion of the previous study.

Preliminary solubility tests have shown moderate solubility of polymer in chlorobenzene, and can formed large aggregates in pristine polymer films and in blend with fullerene derivatives. We have therefore prepared the blend solutions with low concentration of PQTB of 6 mg/ml. In order to increase the solubility of the polymer PQTB, we have chosen to use a solvent mixture of chlorobenzene: dichlorobenzene with a ratio of 2:1. This solvent mixture containing dichlorobenzene also allowed improved solubility of fullerenes derivatives in the blend[62,63]. For this set of preliminary tests we have only tested the polymer with the fullerenes derivatives at a ratio of 1:1.

The current density-voltage curve of the device based on PQTB: PCBMC60 is presented in Figure 99 with the photovoltaic properties reported in Table 24.

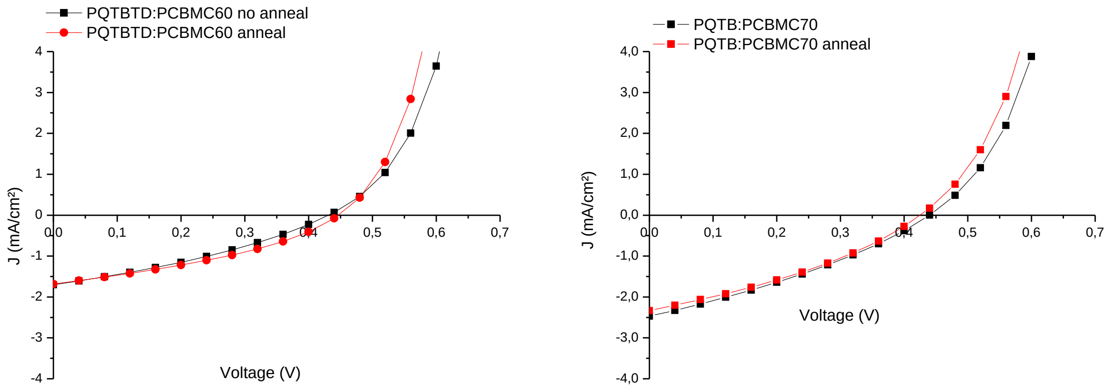


**Figure 99: (left) J-V curves of PQTB:PCBMC60 as cast and after annealing. (right) J-V curves of PQTB:PCBMC70 as cast and after annealing.**

| Active layer (1:1) | Jsc [mA/cm²] | | Voc[V] | | FF[%] | | PCE [%] | |
|---|---|---|---|---|---|---|---|---|
| | 20°C | 70°C | 20°C | 70°C | 20°C | 70°C | 20°C | 70°C |
| PQTB:PCBMC60 | 1.70 | 1.68 | 0.43 | 0.44 | 0.33 | 0.36 | 0.24 | 0.27 |
| PQTB :PCBMC70 | 2.47 | 2.33 | 0.44 | 0.42 | 0.32 | 0.34 | 0.35 | 0.33 |
| PQTBtol:PCBMC60* | 4.53 | - | 0.49 | - | 0.40 | - | 0.89 | - |

**Table 24: Photovoltaic parameters of polymers POTF and PQTB with PCBMC60 and PCBMC70 as acceptors. *previous result with PQTB of fraction toluene**

The device showed low power conversion efficiency of only 0.24 % for as cast device as a result of low values of short-circuit current density of 1.70 mA/cm², open circuit voltage of 0.43 V and a poor fill factor of 0.33. After post thermal-annealing treatment at 70 °C the device showed slight improvement of power conversion efficiency due to a better fill factor of 0.36. The devices heated at 80°C have shown degradation of performance.

In combination with PCBMC70 the polymer PQTB showed slight improvement with power conversion efficiency of 0.35% and 0.33 % for annealed device. Utilisation of PCBMC70 instead of PCBMC60 give rise to a significant improvement in current density from 1.70 mA/cm² for the device PQTB:PCBMC60 to 2.47 mA/cm² for the device PQTB:PCBMC70. The overall current density of the d0evices are compared to the previously obtained with the device PQTB of toluene fraction of Jsc= 4.5 mA/cm². Incident photon to current efficiency (IPCE) measurement was performed to shed light on the photon to current conversion rate.

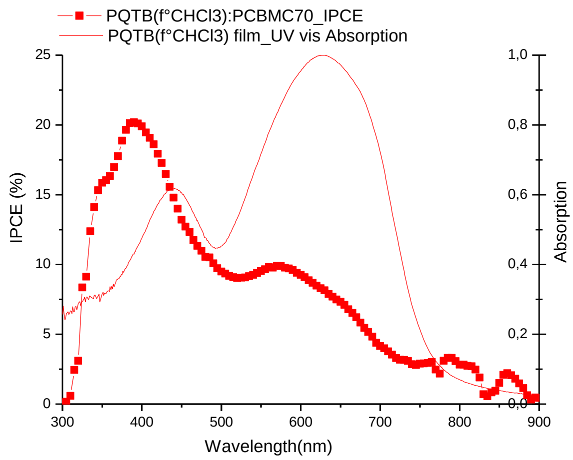


**Figure 100: Incident photon to current efficiency vs wavelength curve of the best device performance PQTB:PCBMC70 overlayered with the absorption spectrum of PQTB in film**

The incident photon to current efficiency (IPCE) vs wavelength curve of the best performance device based on PQTB:PCBMC70 is plotted in Figure 100 superposed with the absorption spectrum of polymer PQTB in film. For the device based on PQTB:PCBMC70, low photon to current conversion rate is observed with only a yield to 20 % of the region corresponding to π–π* transition band. The polymer which have shown high intensity internal charge transfer absorption band in the long wavelength region only converted up to 10 % of its potential. The lost may originated to high recombination of photo-generated excitons in the active layers,[64,65,66] instead of converting to free charge carriers to generate current. This may explain the low performance in photovoltaic devices. Moreover the fabricated cells showed apparition of some large aggregates in the active layer leading to site of charge traps[67,68]. As the polymer have shown strong tendency to form aggregates in solid state from photophysical studies, therefore further work on optimisation of film-forming properties in blends are required.

In overall, the photovoltaic devices based on the polymer PQTB of chloroform fraction exhibit lower performance than the previously studied device based on toluene fraction. As the polymer of toluene fraction has higher molecular weight, therefore may exhibit higher current density (>4 $mA/cm^2$). Inganas and coworkers have also demonstrated similar results for higher molecular weight polymers based on poly(fluorene-benzothiadiazole)[69].

Bundgaard and coworkers[28] who worked with similar poly(quaterthiophene-benzothiadiazole) have also demonstrated apparition of crystalline structure domain in the active layers resulting to a poor performance in photovoltaic device (PCE of 0.33%). Bundgard and coworkers have reported further optimisation of the devices fabrication based on their poly (quaterthiophene-benzothiadiazole) in terms of solvent, spin-coating conditions, thermal annealing, fullerenes ratios, concentration and film thickness, etc have resulted to efficiency up to 1 %[28]. Further optimisation of the devices fabrication may exhibit higher performances for this polymer PQTB based on these parameters. However we did not continue further optimisation based on this polymer during this thesis.

## VI.2. Polymer solar cells based on POTF

For the polymer POTF, we have tested the first toluene fraction of molecular weight consisting of short oligomers and long polymer chains to allow short oligomers to complete interstitial sites. The concentration of each material (POTF and fullerenes) was first tested at 10 mg/ml affording 20 mg/ml of total weight concentration. At this concentration, the films thicknesses are estimated at about 100±20 nm according to our previous results with the same concentration following the same solution deposition procedure. The blends were dissolved using the same solvent as the oligomer QTF which is chlorobenzene. We have only tested here polymer: fullerenes ratios of 1:1. The results in photovoltaic performances are shown in the current density-voltage curves in Figure 101 and reported in the Table 25.

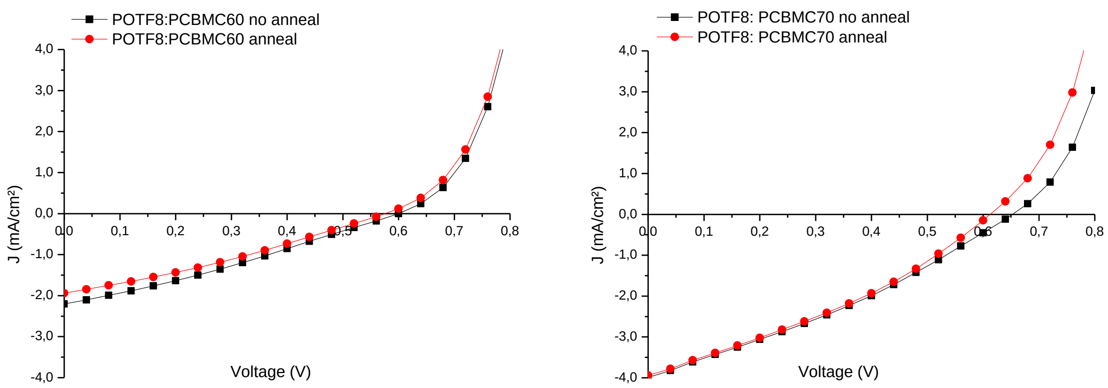


**Figure 101: (left) J-V curves of POTF:PCBMC60 as cast and after annealing. (right) J-V curves of POTF:PCBMC70 as cast and after annealing.**

| Active layer (1:1) | Jsc [mA/cm²] | | Voc[V] | | FF[%] | | PCE [%] | |
|---|---|---|---|---|---|---|---|---|
| | 20°C | 70°C | 20°C | 70°C | 20°C | 70°C | 20°C | 70°C |
| POTF:PCBMC60 | 2.2 | 1.94 | 0.61 | 0.58 | 29 | 30 | 0.38 | 0.34 |
| POTF:PCBMC70 | 3.99 | 3.94 | 0.65 | 0.61 | 30.9 | 32.5 | 0.81 | 0.79 |

**Table 25: Photovoltaic parameters of polymers POTF PCBMC60 and PCBMC70 as acceptors.**

The polymer POTF showed low power conversion efficiency of 0.38 % when combined with fullerene PCBMC60 with current density of 2.2 mA/cm², open circuit voltage Voc of 0.61 V and fill factor of 0.29. Higher efficiency is obtained when using fullerene PCBMC70. A two-fold increase of short-current density in the photovoltaic cells of the blend POTF:PCBMC70 of 3.99 mA/cm² as compared to 2.2 mA/cm² for the solar cell based on POTF:PCBMC60. The photovoltaic cells based on POTF showed higher power conversion efficiency than the solar cells based on PQTB with the highest efficiency of 0.81 % for the device based on POTF: PCBMC70 with no annealing.

To investigate the thermal annealing effect on the device performance, the devices were first treated with by heating 5 min at 70 °C. The results were shown in Table 25. We observed only small variations of performance upon heating especially for the device based on POTF8:PCBMC70. We have therefore performed further thermal treatment on the solar cells based on POTF/PCBMC70 by heating another 5 min at 80 °C. We have plotted graphs for better visualisation of the effect on thermal annealing for this solar cell in Figure 102 below.

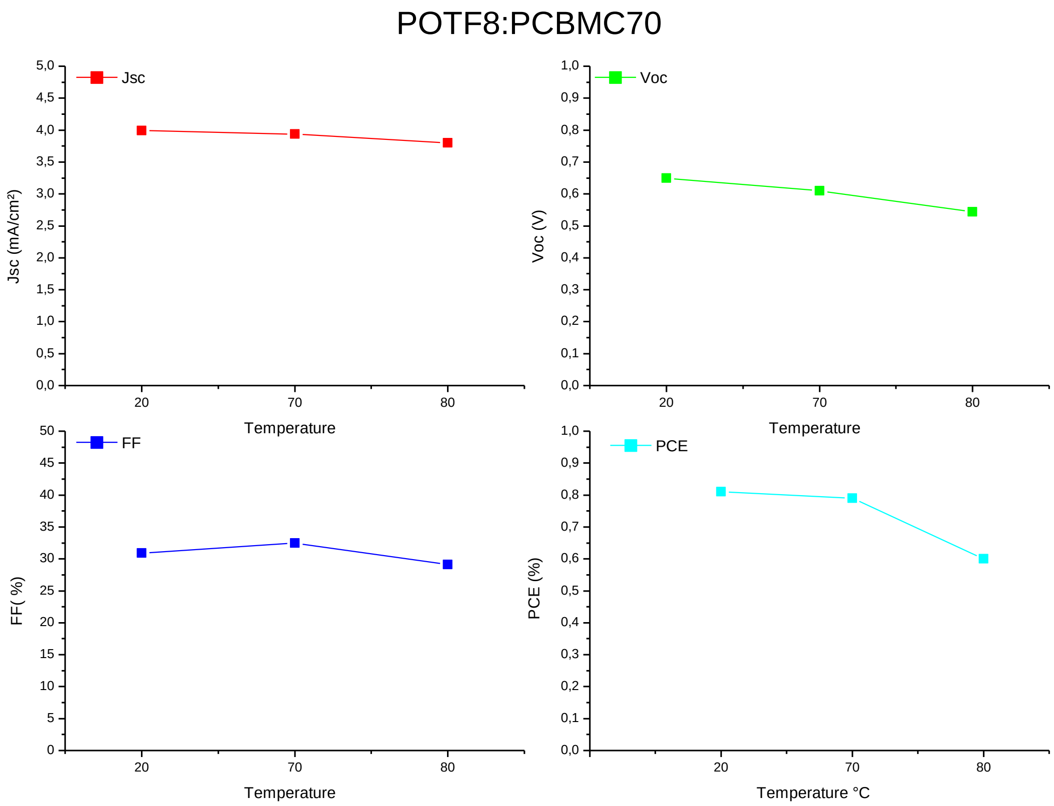


**Figure 102: Relationship between photovoltaic parameters and annealing temperature. Finalized devices were annealed after cathode deposition, on a hot plate for 5 minutes. Cooling to room temperature was performed slowly, Jsc, Voc, FF and PCE, respectively the short circuit current, the open circuit voltage, the fill factor and the power conversion efficiency. The weight ratio for POTF: PVBMC70 is 1:1.**

On the effect of thermal annealing, for the solar cell of POTF:PCBMC70 we observe no increase by thermal heating from 20°C to 70°C to 80 °C. The current density decreased slightly upon heating but more pronounced decrease is visible on the open circuit voltage. In bulk heterojunction organic solar cells, the open circuit voltage have tendency to decrease upon heating[70]. For our device only the fill factor has increased upon heating treatment at 70 °C but degraded at 80 °C. We can conclude that for solar cell based on polymer POTF:PCBMC70 thermal annealing did not further enhanced the power conversion efficiency of the solar cells.

We have also performed investigation on the efficient conversion of photon absorption to current of the photovoltaic device based on POTF. The IPCE-λ curves of the best device performance based on POTF:PCBMC70 is presented in Figure 103 below.

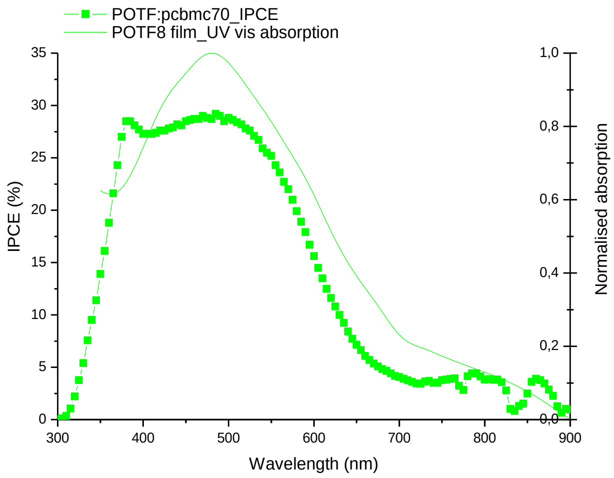


**Figure 103: Incident photon to current efficiency vs wavelength curve of the best device performance POTF:PCBMC70 overlayered with the absorption spectrum of POTF in film**

From the curves, we can clearly observed efficient conversion of photon to current in the region 350 nm to 650 nm up to 30 %, in correlation of strong absorption of POTF in the region. This efficient conversion has contributed to good short current density of *ca.* 4 mA/cm². The polymer POTF has shown consistent high potential photon to current conversion across the visible region compared to the device based on polymer (quaterthiophene benzothiadiazole) PQTB where only the region between 300 nm to 500 nm give IPCE between 10 to 20 %.

## VI.3. Ternary blend solar cells based on PQTB, POTF and fullerenes

We have seen previously polymer PQTB showed poor performance in photovoltaic devices eventhough from the photophysical and electrochemical analysis properties have shown interesting properties, and higher performance in photovoltaic devices is obtained with the polymer POTF. Photophysical properties of polymer PQTB and POTF have shown the polymers showed complementary absorption spectra.

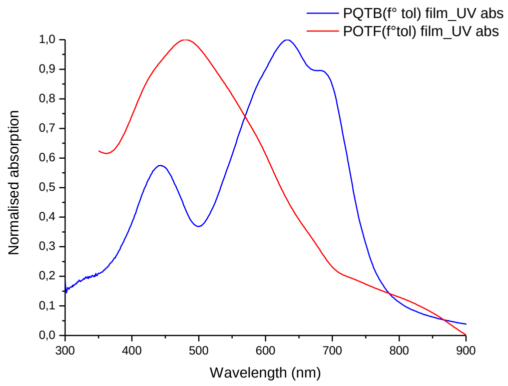


**Figure 104: UV visible absorption spectra of polymer PQTB and POTF in films**

We were tempted to study the effect of combining the two polymers in blend in combination with fullerenes to further push the potential of photon absorption to create more available photo-generated excitons to convert efficiently to free charges generating current.

We have therefore performed solar cells based on ternary blends containing PQTB, POTF and PCBMC60 or PCBMC70. The ternary blends were prepared by using the readily binary blend mixture of Polymer:fullerenes. In order to study coherent effect of each absorbing polymer PQTB and POTF the solutions were prepared in order to have same equivalent amount of polymers in the final blend. Therefore ternary blends were prepared by adding 0.5 ml of the blend of PQTB:PCBMC60 of weight concentration (6 mg/ml : 6 mg/ml) and 0.3 ml of the mixture solution of POTF:PCBMC60 at (10 mg/ml:10mg/ml). The final concentration of each material PQTB: POTF: PCBM is therefore (3.75 mg/ml: 3.75 mg/ml: 7.5 mg/ml). This gives the ternary blend a total weight concentration of 11.25 mg/ml. The same procedure was also used to prepare the blend of PQTB:POTF:PCBMC70.

The results in photovoltaic devices are presented in Table 26 and the current density-voltage (J-V) curves of the photovoltaic devices are showed in Figure 105 below.

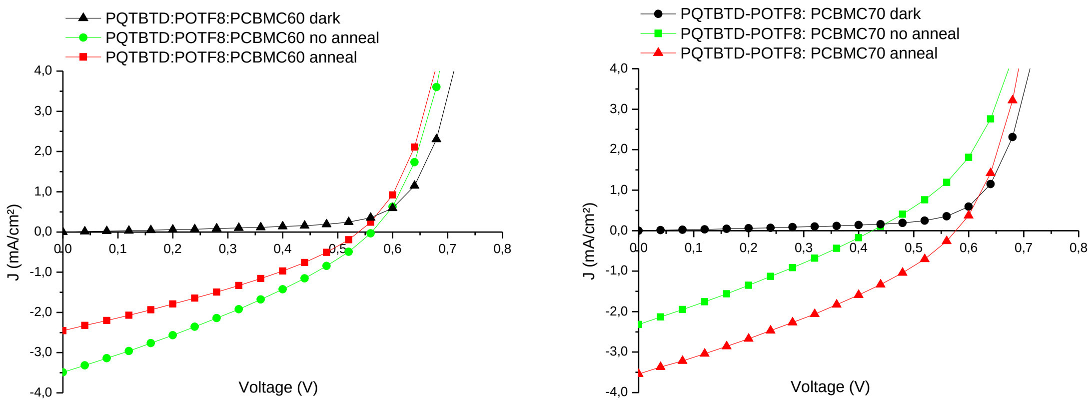


**Figure 105:(left) J-V curves of PQTB:POTF:PCBMC60 as cast and after annealing. (right) J-V curves of PQTB:POTF:PCBMC70 as cast and after annealing.**

| Active layer | Jsc [mA/cm²] | | Voc[V] | | FF[%] | | PCE [%] | |
|---|---|---|---|---|---|---|---|---|
| | 20°C | 70°C | 20°C | 70°C | 20°C | 70°C | 20°C | 70°C |
| PQTB:POTF :PCBMC60 | 3.49 | 2.45 | 0.56 | 0.54 | 0.31 | 0.32 | 0.61 | 0.42 |
| PQTB: PCBMC60 | 1.70 | 1.68 | 0.43 | 0.44 | 0.33 | 0.36 | 0.24 | 0.27 |
| POTF:PCBMC60 | 2.2 | 1.94 | 0.61 | 0.58 | 0.29 | 0.30 | 0.38 | 0.34 |
| PQTB:POTF :PCBMC70 | 2.32 | 3.54 | 0.43 | 0.58 | 0.28 | 0.32 | 0.27 | 0.66 |
| PQTB:PCBMC70 | 2.47 | 2.33 | 0.44 | 0.42 | 0.32 | 0.34 | 0.35 | 0.33 |
| POTF :PCBMC70 | 3.99 | 3.94 | 0.65 | 0.61 | 0.31 | 0.32 | 0.81 | 0.79 |

**Table 26: Photovoltaic parameters of polymers POTF and PQTB with PCBMC60 and PCBMC70 as acceptors. We also included the photovoltaic parameters of PQTF8 as reference.**

For the ternary blends solar cells. the devise based of PQTB:POTF:PCBMC60 showed a good open circuit voltage of 0.56 V. and a short current density of 3.49 mA/cm² with an overall power conversion efficiency of 0.61 %. Upon annealing the device showed degradation especially with a decrease in short current density to 2.45 mA/cm². The thermal annealing only gave an increase in the fill factor. We have therefore improve the device performance of the ternary blend based on PCBMC60 compared to the corresponding polymer binary blend with a significant increase in the short circuit current density to 3.49 mA/cm².

For the solar cells based on PCBMC70, we obtained an overall power conversion efficiency of 0.66 % after thermal annealing with higher short current density of 3.54 mA/cm² and an open circuit voltage of 0.58 V. For a better understanding of the effect of mixing the two polymers PQTB and POTF with fullerene derivative PCBMC70 in the device, we have plotted 4 curves of the device based on POTF: PCBMC70. PQTB: PCBMC70 and PQTB:POTF: PCBMC70 in the same graph. We also included the curve of PQTB:POTF: PCBMC70 after annealing. The J-V curves are presented in Figure 106 below.

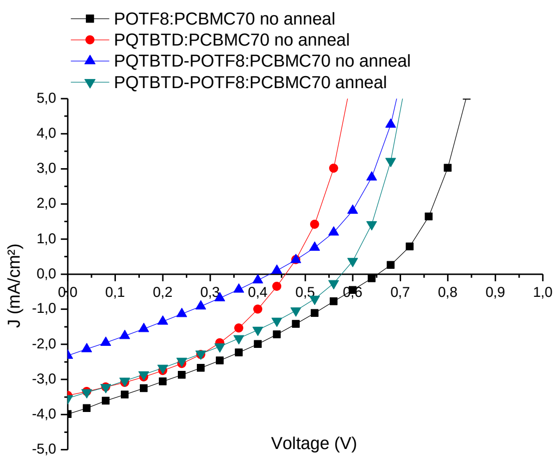


**Figure 106: J-V curves of photovoltaic cells based on POTF:PCBMC70, PQTB:PCBMC70 and PQTB:POTF:PCBMC70 as cast and after annealing.**

As shown in the Figure 106 above the ternary blend devices PQTBDTD:POTF:PCBMC70 showed intermediate photovoltaic parameters values of both of the polymers POTF and PQTB. The maximum short current density of the ternary blend was similar to the short current density of the PQTB:PCBMC70 and the maximum open circuit voltage was situated in between the Voc values of PQTB and POTF devices. We can note that the photovoltaic device showed an important increase upon annealing. Upon annealing the polymer chains of PQTB and POTF become more mobile and self-organisation can occur to form better ordering in the each domain as well as in the PCBM domain of the active layer film therefore we observed an increased in the short current density[71]. However the thermal annealing only gave an overall improvement for the solar cells based on the ternary blends as the solar cells composed by only one polymer donor and one fullerene derivative have shown degradation upon annealing.

Here we observed a different effect on the photovoltaic parameters upon thermal annealing reflecting the complexity to control the parameters in ternary blend and each blend required specific optimisation also demonstrated by Kim and coworkers whom works on ternary blends based on P3HT and polyfluorene-benzothiadiazole F8BT[72].

From these results of the photovoltaic parameters we can observe some encouraging trends in the ternary blend. Firstly the open circuit voltage of the ternary blends based on PQTB: POTF: fullerenes were found at the highest of 0.56-0.58 V. This open circuit voltage is situated in the range of the open circuit voltage of the binary blend based on POTF: fullerenes of 0.61 V compared to 0.45 V for PQTB: fullerenes. Therefore the open circuit voltage of ternary blend is therefore limited to the highest open circuit voltage obtained in binary blend. In literature some groups have worked with ternary blend solar cells have also seen similar trend compared to its binary blends[72, 73, 29].

However to understand the current density produced by ternary blends it is more judicious to investigate the photon to current conversion. The IPCE-λ curves of the ternary blends based on PQTB: POTF: PCBMC70 are presented below as well as the absorption spectra of the pristine films polymers.

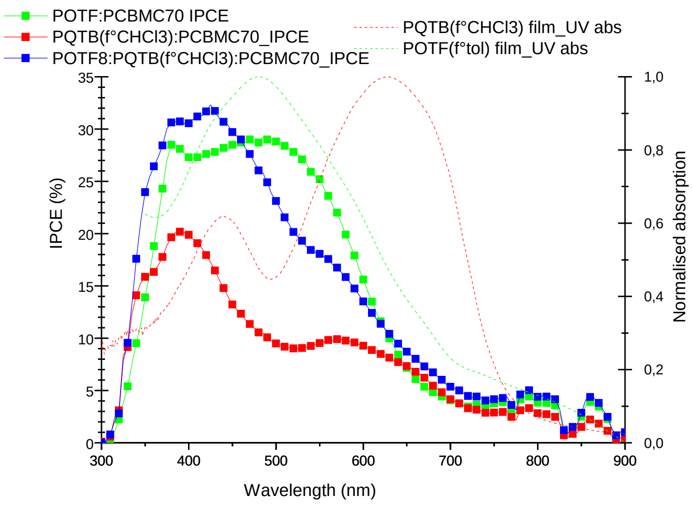


**Figure 107: Incident photon to current efficiency vs wavelength curves of the devices based on POTF:PCBMC70 ; PQTB : PCBMC70 and ternary blend POTF:PQTB:PCBMC70 device. The absorption spectra of the pristine films of POTF and PQTB are presented in dashed lines**

The incident photon to current density curves of the ternary blend showed strong photon conversion up to 32 % in the region 300 nm to 450 nm which can be contributed to the synergistic strong absorption in this region from polymer POTF and PQTB. In the region 450 nm to 600 nm, the POTF have strong absorption band compared to the polymer PQTB, and this have clearly contributed to the photon to current conversion in this region for the ternary blend. The region higher than 600 nm showed similar curves for the ternary blend and the binary blends. From this result we can clearly observe the positive contribution of each polymer notably from the strong absorption of polymer POTF. The results obtained in the ternary blends are very encouraging and we have demonstrated the feasibility and efficient combination of two different donor polymers of complementary absorption spectra with fullerenes as accepting materials. Further optimisation in terms of materials solubility and film forming properties may further increase the power conversion efficiency of the devices.

## VI.4. Comparison of the device based on PQTB. POTF and PQTF

We compared here the results obtained with POTF and PQTB in these series of tests as well as the previously published results on PQTF. The photovoltaic performances are recapitulated in the Table 27. We have also calculated estimated thickness of the blends as reference according to the total weight concentrations based on the thickness reported for polymer PQTF8.

| Active layer (1:1) | Polymer Mn(kDa) | Thickness (nm ±20 nm) | Jsc [mA/cm²] | | Voc [V] | | FF [%] | | PCE [%] | |
|---|---|---|---|---|---|---|---|---|---|---|
| | | | 20°C | 70°C | 20°C | 70°C | 20°C | 70°C | 20°C | 70°C |
| PQTB:PCBMC60 | 4.8 | 60* | 1.70 | 1.68 | 0.43 | 0.44 | 33 | 36 | 0.24 | 0.27 |
| PQTB :PCBMC70 | | 60* | 2.47 | 2.33 | 0.44 | 0.42 | 32 | 34 | 0.35 | 0.33 |
| POTF:PCBMC60 | 2.8 | 100* | 2.2 | 1.94 | 0.61 | 0.58 | 29 | 30 | 0.38 | 0.34 |
| POTF:PCBMC70 | | 100* | 3.99 | 3.94 | 0.65 | 0.61 | 31 | 32 | 0.81 | 0.79 |
| PQTB:POTF:PCBMC60 | | 55* | 3.49 | 2.45 | 0.56 | 0.54 | 31 | 32 | 0.61 | 0.42 |
| PQTB:POTF:PCBMC70 | | 55* | 2.32 | 3.54 | 0.43 | 0.58 | 28 | 32 | 0.27 | 0.66 |
| PQTF8:PCBMC60 | 1.4 | 90 | 4.74 | - | 0.53 | - | 36 | - | 0.91 | - |
| PQTF8:PCBMC60 | | 45 | 5.91 | - | 0.56 | - | 38 | - | 1.25 | - |
| PQTF8:PCBMC60 | | 30 | 5.93 | - | 0.58 | - | 43 | - | 1.45 | - |

**Table 27: Photovoltaic performances of the tested devices PQTB and POTF in comparison with the previous results of PQTF. The films thickness for our tested devices were estimated values according to their total weight concentration**

From the results obtained for the polymer PQTB and POTF we have obtained higher short circuit current density for the device based on polymer POTF. The high current density is attributed to efficient photon to current conversion in the polymer POTF compared to the polymer PQTB. Polymer PQTB exhibit low power conversion efficiency as they have shown poor film forming properties and have formed large aggregates in the active layer.

The device based on POTF:fullerenes have afforded higher open circuit voltages of 0.65 V than the device based on PQTB:fullerenes (~0.45 V) and PQTF:fullerenes (0.56 V). We have postulated earlier that the three polymers have similar HOMO energy levels and may afford similar open circuit voltage in photovoltaic devices according to the linear relation proposed in literature[74,55, 75]

$$Voc\ (exp) = 1/e\ |E_{HOMO}^{Donor} - E_{LUMO}^{Acceptor}|\ - \Delta V \quad \text{with } \Delta V = \text{loss voltage potential}$$

Therefore the polymer POTF showed lower voltage loss than the other three polymers. The polymer PQTB showed high loss of voltage potential most probably due to the polymer aggregation the active layers [76]. The three polymers showed an average of 0.5-0.6 V in photovoltaic devices.

The results in photovoltaic performances presented here for the polymers POTF and PQTB are lower than the results obtained with polymer PQTF[20]. However further optimisation of the devices for examples in terms of thickness for the blend polymer POTF: fullerenes may result in higher power conversion efficiencies as demonstrated for the polymer PQTF. For the polymer PQTB it is crucial to make several tests of solubility and film forming properties to avoid formation of large aggregates by means of changing the solvent of deposition[77] slower rates of deposition[28] by increasing the temperature of the blends solution upon deposition, etc. [28 78]

# VII. Conclusion

In this chapter we have shown two new polymers based on linear oligothiophenes consisting of four units of thiophenes coupled with benzothiadiazole poly (quaterthiophene-benzothiadiazole) PQTB and another linear oligothiophenes consisting of eight units of thiophene coupled with fluorenone poly(octathiophene-fluorenone) POTF. Both polymers are directly compared to the previously studied poly (quaterthiophenes-fluorenone) PQTF[18]. ( see Figure 108 for the polymer structures)

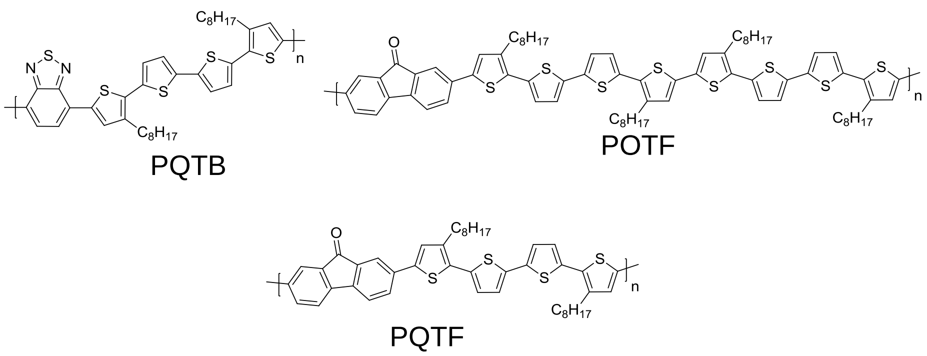


**Figure 108: Poly(quaterthiophene-benzothiadiazole) PQTB and poly (octathiophene-fluorenone) POTF**

These series of linear thiophene-based polymers were prepared by oxidative polymerisation affording high molecular weight polymers of Mn>5 kDa. Further improvement of this method of polymerisation by changing the solvent of polymerisation using for example chlorobenzene may afford higher molecular weight polymers.

Optical and electrochemical analysis measurements have shown that the polymers PQTB and POTF are suitable donor materials for photovoltaic cell applications with broad absorption in UV-visible and correct positioning of HOMO LUMO energy levels as presented in Figure 109 below. We have obtained low band gap polymers of Eg =1.7 eV for both polymer PQTB and POTF which are much lower than the previously published polymer PQTF of Eg =2 eV.

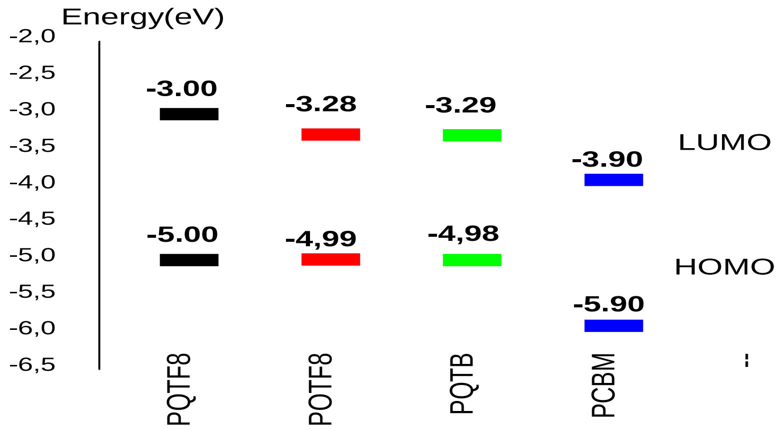


**Figure 109: Energy diagram of HOMO-LUMO energy levels of polymers PQTF8, POTF, PQTB and PCBM**

All three polymers have shown similar HOMO energy levels of about -5.0 eV demonstrating the effect of the oligothiophenes segment as electron donating segment which governs the HOMO energy levels. Our polymers show rather high lying HOMO energy levels. The HOMO energy levels of the donor have been demonstrated to have influence in the open circuit voltage of photovoltaic device[74]. As a result, the polymers tested in photovoltaic devices with fullerenes derivatives PCBMC60 and PCBMC70 give open circuit voltages in the range of 0.45-0.6 V. The open circuit voltages are found similar to the open circuit voltage of the device based on P3HT:PCBM[79].

Preliminary results of photovoltaic devices of the polymer based on PQTB in combination with fullerenes derivatioves have shown low performance in photovoltaic devices most probably due to formation of large aggregates visible in the active layers therefore exhibiting low short circuit current density.

The polymer POTF showed a good performance in photovoltaic devices and incident photon to current efficiency measurements has demonstrated efficient conversion of photogenerated exciton in the region of longer wavelength thanks to the fluorenone as electron withdrawing unit. The polymers based on fluorenone unit as electron withdrawing group in the polymer backbone have shown higher efficiency in photovoltaic device compared to the polymer based on benzothiadiazole based on our results.

We have also demonstrated efficient ternary blends by combining two donor polymers of complementary absorption with fullerenes derivatives allowing absorbing more photons. The test on ternary blends have also demonstrated the limitation of the open circuit voltage depending on the highest open circuit voltage achieved for optimised binary blend.

We can at first approximation postulate our polymers based on linear oligothiophene segments have strong tendency to form aggregates in solid state similar to the properties of poly(alkylthiophene). AFM investigation should be performed in order to prove the exact morphology of the active layers. It is strongly required to control the film morphology in order to obtain high performance solar cells. Further optimisations on photovoltaic device fabrications are necessary in this direction to push the potential of our polymers. Proposed device fabrication optimisations are in terms of processing conditions in terms choice of solvent of deposition[77], spin-coating conditions[80] varying the thickness of the active layer, etc.[81,82,83.]

# VIII. Reference


1 A. J. Heeger, Semiconducting polymers: the Third Generation, Chem. Soc. Rev., 2010,39, 2354-2371
2 A. Facchetti, π-Conjugated Polymers for Organic Electronics and Photovoltaic Cell Applications, Chem. Mater. 2011, 23, 733–758 733
3 C.J. Brabec ,S. Gowrisanker ,J.J. M. Halls,D. Laird ,S. Jia , and S. P. Williams, Polymer–Fullerene Bulk-Heterojunction Solar Cells,Adv. Mater. 2010, 22, 3839–3856
4 B.C Thompson, and J.M.J Fréchet, (2008), Polymer–Fullerene Composite Solar Cells. Angew. Chem. Int. Ed., 47: 58–77
5 N. Camaioni , L. Garlaschelli , A. Geri , M. Maggini , G. Possamai and G. Ridolfi, Solar cells based on poly(3-alkyl)thiophenes and [60]fullerene: a comparative study, J. Mater. Chem., 2002,12, 2065-2070
6 P. Schilinsky, C. Waldauf, C. J. Brabec, Recombination and loss analysis in polythiophene based bulk heterojunction photodetectors, Appl. Phys. Lett., 81, 3885, (2002).
7 M. T. Dang, L. Hirsch, and G. Wantz, P3HT: PCBM, Best Seller in Polymer Photovoltaic Research. Adv. Mater., 23: 3597, (2011).
8 S.-H. Lee , D.-H. Kim, J.-H. Kim, G.-S. Lee, J.-G. Park, Effect of Metal-Reflection and Surface-Roughness Properties on Power-Conversion Efficiency for Polymer Photovoltaic Cells, J. Phys. Chem. C, 113 , 21915, (2009) .
9 A. Marrocchi , D. Lanari , A. Facchetti and L. Vaccaro, Poly(3-hexylthiophene): synthetic methodologies and properties in bulk heterojunction solar cells, Energy Environ. Sci., 2012,5, 8457-8474
10 T-A. Chen, R. D. Rieke, Polyalkylthiophenes with the smallest bandgap and the highest intrinsic conductivity, Synthetic Metals, Vol. 60, Issue 2, 15 September 1993, Pages 175-177
11 R. Kroon, M Lenes, J. C. Hummelen,P. W.M. Blom, B. de Boer, Small Bandgap Polymers for Organic Solar Cells (Polymer Material Development in the Last 5 Years), Polymer Reviews, 48:531–582, 2008
12 J. Chen and Y. Cao, Development of Novel Conjugated Donor Polymers for High-Efficiency Bulk-Heterojunction Photovoltaic Devices, Acc. Chem. Res., 2009, 42 (11), pp 1709–1718
13 Y.Li, Molecular Design of Photovoltaic Materials for Polymer Solar Cells: Toward Suitable Electronic Energy Levels and Broad Absorption, Acc. Chem. Res., 2012, 45 (5), pp 723–733
14 C. Duan , F. Huang and Y. Cao, Recent development of push–pull conjugated polymers for bulk-heterojunction photovoltaics: rational design and fine tailoring of molecular structures, J. Mater. Chem., 2012,22, 10416-10434
15 P-L. T. Boudreault, A. Najari, and M. Leclerc, Processable Low-Bandgap Polymers for Photovoltaic Applications,Chem. Mater. 2011, 23, 456–469
16 R. Demadrille, B. Divisia-Blohorn,M. Zagorska,S. Quillard, P. Rannou,J-P. Travers and A. Pron, Preparation and spectroelectrochemical behaviour of a new alternate copolymer of 3,3'-di-n-octyl-2,2'-bithiophene and fluoren-9-one, New J. Chem., 2003, 27, 1479–1484
17 Brun, M., Demadrille, R., Rannou, P., Pron, A., Travers, J.-P. and Grévin, B. (2004), Multiscale Scanning Tunneling Microscopy Study of Self-Assembly Phenomena in Two-Dimensional Polycrystals of π-Conjugated Polymers: The Case of Regioregular Poly(dioctylbithiophene-alt-fluorenone) . Adv. Mater., 16: 2087–2092.
18 R. Demadrille, M. Firon, J. Leroy, P. Rannou, A. Pron, Plastic Solar Cells Based on Fluorenone-Containing Oligomers and Regioregular Alternate Copolymers, Adv. Funct. Mater. 2005, 15, 1547
19 J. Roncali, Molecular Engineering of the Band Gap of p-Conjugated Systems: Facing Technological Applications, Macromol. Rapid Commun. 2007, 28, 1761–1775
20 R. Demadrille, N. Delbosc, Y. Kervella, M. Firon, R. De Bettignies, M. Billon, P. Rannou, A. Pron, Conjugated alternating copolymer of dialkylquaterthiophene and fluorenone: synthesis, characterisation and photovoltaic properties, J. Mater. Chem., 17, 4661, (2007).
21 S. H. Park, A. Roy, S. Beaupré, S. Cho, N. Coates, J. S. Moon, D. Moses, M. Leclerc, K. Lee, and A. J. Heeger, Bulk heterojunction solar cells with internal quantum efficiency approaching 100%, Nature Photonics 3, 297 - 302 (2009)
22 Y.-C. Chen, C.-Y. Yu, Y.-L. Fan, L.-I. Hung, C.-P. Chen and C. Ting, Low-bandgap conjugated polymer for high efficient photovoltaic applications, Chem. Commun., 2010, 46, 6503–6505.
23 Zhou, H., Yang, L., Stuart, A. C., Price, S. C., Liu, S. and You, W. (2011), Development of Fluorinated Benzothiadiazole as a Structural Unit for a Polymer Solar Cell of 7% Efficiency. Angew. Chem. Int. Ed., 50: 2995–2998
24 S. C. Price, A. C. Stuart, and W. You, Low Band Gap Polymers Based on Benzo[1,2-b:4,5-b']dithiophene: Rational Design of Polymers Leads to High Photovoltaic Performance Macromolecules 2010 43 (10), 4609-4612
25 P. Sonar, E. L. Williams, S. P. Singh and A. Dodabalapur, Thiophene–benzothiadiazole–thiophene (D–A–D) based polymers: effect of donor/acceptor moieties adjacent to D–A–D segment on photophysical and photovoltaic properties, J. Mater. Chem., 2011, 21, 10532
26 L. Biniek, C. L. Chochos, N. Leclerc,G. Hadziioannou,J. K. Kallitsis,R. Bechara,P. Lévêque and T. Heiser, A [3,2-b]thienothiophene-alt-benzothiadiazole copolymer for photovoltaic applications: design, synthesis, material characterization and device performances, J. Mater. Chem., 2009, 19, 4946–4951
27 E. Bundgaard, F.C. Krebs, Low-Band-Gap Conjugated Polymers Based on Thiophene, Benzothiadiazole, and Benzobis(thiadiazole), Macromolecules 39, 2823, (2006).
28 E. Bundgaard, S. E. Shaheen, F. C. Krebs, and D. S. Ginley, Bulk heterojunctions based on a low band gap copolymer of thiophene and benzothiadiazole, Solar Energy Materials and Solar Cells 91, 17, 1631, (2007).
29 E. Lim, S.Lee and K. K. Lee, Improved photovoltaic performance of P3HT:PCBM cells by addition of a low band-gap oligomer,Chem. Commun., 2011, 47, 914–916

30 P. Sonar,E. L. Williams, S. P. Singh and A. Dodabalapur, Thiophene–benzothiadiazole–thiophene (D–A–D) based polymers: effect of donor/acceptor moieties adjacent to D–A–D segment on photophysical and photovoltaic properties, J. Mater. Chem., 2011, 21, 10532

31 F. Liang, J. Lu, J. Ding, R. Movileanu, and Y. Tao, Design and Synthesis of Alternating Regioregular Oligothiophenes/Benzothiadiazole Copolymers for Organic Solar Cells, Macromolecules 2009 42 (16), 6107-6114

32 M. Jayakannan, P.A. Van Hal, R.A.J. Janssen, Synthesis and structure-property relationship of new donor–acceptor-type conjugated monomers and polymers on the basis of thiophene and benzothiadiazole, J. Polym. Sci. Polym. Chem. 40 (2002) 251–261.

33 W. Yue, Y. Zhao, H.K. Tian, D. Song, Z.Y. Xie, D.H. Yan, Y.H. Geng, F.S. Wang, Poly(oligothiophene-alt-benzothiadiazole)s: tuning the structures of oligothlophene units toward high-mobility ’’black’’ conjugated polymers, Macromolecules 42 (2009) 6510–6518.

34 T. Yamamoto, A. Morita, Y. Miyazaki, T. Maruyama, H. Wakayama, Z.-H. Zhou, Y. Nakamura, T. Kanbara, S. Sasaki, and K. Kubota, "Preparation of p-Conjugated Poly (2,5-thienylene), Poly(p-phenylene), and Related Polymers Using Zero-valent Nickel Complexes. Linear Structure and Properties of the p-Conjugated Molecules", Macromolecules, 25, 1214-1223 (1992)

35 R. Demadrille, P. Rannou, J. Bleuse, J.-L. Oddou, A. Pron, and M. Zagorska, Regiochemically Well-Defined Fluorenone−Alkylthiophene Copolymers: Synthesis, Spectroscopic Characterization, and Their Postfunctionalization with Oligoaniline, Macromolecules, 2003, 36, 7045

36 M. R. Andersson, Q. Pei, T. Hjertberg, O. Inganäs, O. Wennerström and J.-E. Österholm, Synthesis of soluble poly(alkylthiophenes) which are thermally stable in the doped state, Synth. Met., 1993, 55, 1227

37 Andersson, M. R.; Selse, D.; Berggren, M.; Jarvinen, H.; Hjertberg, T.; Inganas, O.; Wennerstrom, O.; Osterholm, J. E., Regioselective Polymerization of 3-(4-octylphenyl) thiophene with FeC13 , Macromolecules 1994, 27, 6503-6506

38 T. Cai, Yi Zhou, E. Wang, S. Hellström, F. Zhang, S. Xu, O. Inganäs, M. R. Andersson, Low bandgap polymers synthesized by FeCl3 oxidative polymerization, Solar Energy Materials and Solar Cells, Volume 94, Issue 7, July 2010, Pages 1275-1281

39 N. Miyaura and A. Suzuki, Palladium-Catalyzed Cross-Coupling Reactions of Organoboron Compounds, Chem. Rev. 1995, 95,2457-2483

40 P. M. Beaujuge, C. M. Amb, and J. R. Reynolds, Spectral Engineering in π-Conjugated Polymers with Intramolecular Donor−Acceptor Interactions, Acc. of Chem. Res. 2010 43 (11), 1396-1407

41 F. Liang, J. Lu, J.Ding, R. Movileanu and Y. Tao, Design and Synthesis of Alternating Regioregular Oligothiophenes/Benzothiadiazole Copolymers for Organic Solar Cells,Macromolecules, 2009, 42 (16), pp 6107–6114

42 Rafal Pokrop , Jean-Marie Verilhac , Anna Gasior , Ireneusz Wielgus , Malgorzata Zagorska , Jean-Pierre Travers and Adam Pron, Effect of molecular weight on electronic, electrochemical and spectroelectrochemical properties of Poly(3,3"-dioctyl-2,2':5',2"-terthiophene), J. Mater. Chem., 2006,16, 3099-3106

43 S. Berson, R. De Bettignies, S. Bailly, and S. Guillerez, (2007), Poly(3-hexylthiophene) Fibers for Photovoltaic Applications. Adv. Funct. Mater., 17: 1377–1384

44 T-Q Nguyen, V Doan, and B. J. Schwartz, Conjugated polymer aggregates in solution: Control of interchain interactions, J. Chem. Phys., Vol. 110, No. 8, 22 February 1999

45 Y. Kim, S. Cook, S. M. Tuladhar, S. A. Choulis, J. Nelson, J. R. Durrant, D. D. C. Bradley, M. Giles, I. McCulloch, C-S Ha and M. Ree, A strong regioregularity effect in self-organizing conjugated polymer films and high-efficiency polythiophene:fullerene solar cells,Nature Materials 5, 197 - 203 (2006)

46 M. Wang, X. Hu, P. Liu, W. Li, X. Gong, F. Huang, and Y. Cao, Donor–Acceptor Conjugated Polymer Based on Naphtho[1,2-c:5,6-c]bis[1,2,5]thiadiazole for High-Performance Polymer Solar Cells, Journal of the American Chemical Society 2011, 133 (25), 9638-9641

47 L. A. Estrada, J.E. Yarnell, and D. C. Neckers, Revisiting Fluorenone Photophysics via Dipolar Fluorenone Derivatives, J. Phys. Chem. A 2011, 115, 6366–6375

48 S. A. Jenekhe , L. Lu , and M. M. Alam, ew Conjugated Polymers with Donor−Acceptor Architectures: Synthesis and Photophysics of Carbazole−Quinoline and Phenothiazine−Quinoline Copolymers and Oligomers Exhibiting Large Intramolecular Charge Transfer, Macromolecules, 2001, 34 (21), pp 7315–7324

49 T-Q Nguyen, V Doan, and B. J. Schwartz, Conjugated polymer aggregates in solution: Control of interchain interactions, J. Chem. Phys., Vol. 110, No. 8, 22 February 1999

50 Y. Kim, S. Cook, S. M. Tuladhar, S. A. Choulis, J. Nelson, J. R. Durrant, D. C. Bradley, M. Giles, I. McCulloch, C-S. Ha and M. Ree, A strong regioregularity effect in self-organizing conjugated polymer films and high-efficiency polythiophene:fullerene solar cells, Nature Materials 5, 197 - 203 (2006)

51 Brinkmann, M. and Rannou, P. (2007), Effect of Molecular Weight on the Structure and Morphology of Oriented Thin Films of Regioregular Poly(3-hexylthiophene) Grown by Directional Epitaxial Solidification. Adv. Funct. Mater., 17: 101–108.

52 Ph. Leclère, M. Surin, P. Viville, R. Lazzaroni, A. F. M. Kilbinger, O. Henze, W. J. Feast, M. Cavallini, F. Biscarini, A. P. H. J. Schenning, and E. W. Meijer, About Oligothiophene Self-Assembly: From Aggregation in Solution to Solid-State Nanostructures, Chemistry of Materials 2004 16 (23), 4452-4466

53 E. J. Spadafora, M. Linares, W. Z. N. Yahya, F. Lincker, R. Demadrille, and B. Grevin, Local contact potential difference of molecular self-assemblies investigated by Kelvin probe force microscopy, Appl. Phys. Lett. 99, 233102 (2011)

54 Y-J. Cheng , S-H Yang, C-S Hsu, Synthesis of conjugated polymers for organic solar cell applications, Chem. Rev., 2009, 109 (11), pp 5868–5923

55 A. Cravino, Origin of the open circuit voltage of donor-acceptor solar cells: Do polaronic energy levels play a role, Appl Phys Lett 91, 243502 (2007).

56 C. J Brabec, A. Cravino, D. Meissner, N. S. Sariciftci, T. Fromherz, M. T. Rispens, L. Sanchez, and J. C. Hummelen, Origin of the Open Circuit Voltage of Plastic Solar Cells. Adv. Funct. Mater., 11, 374, (2001).

57 W. Li, R. Qin, Y. Zhou, M. Andersson, F. Li, C. Zhang, B. Li, Z. Liu, Z. Bao and F. Zhang, Tailoring side chains of low band gap polymers for high efficiency polymer solar cells, Polymer, 2010, 51, 3031

58 L. Biniek, C. L. Chochos, N. Leclerc, G. Hadziioannou, J. K. Kallitsis,R. Bechara, P. Lévèque and T. Heiser, A [3,2-b]thienothiophene-alt-benzothiadiazole copolymer for photovoltaic applications: design, synthesis, material characterization and device performances,J. Mater. Chem., 2009, 19, 4946–4951

Anthony, J. E., Facchetti, A., Heeney, M., Marder, S. R. and Zhan, X. n-Type Organic Semiconductors in Organic Electronics, Adv. Mater., (2010), 22, 3876–3892.

a) Y He and Y Li, Fullerene derivative acceptors for high performance polymer solar cells, Phys. Chem. Chem. Phys., 2011,13, 1970-1983

b) Troshin, P. A., Hoppe, H., Peregudov, A. S., Egginger, M., Shokhovets, S., Gobsch, G., Sariciftci, N. S. and Razumov, V. F. (2011), [70]Fullerene-Based Materials for Organic Solar Cells. ChemSusChem, 4: 119–124.

61 J. L. Delgado, P.- A. Bouit, S. Filippone, M. A. Herranz, N. Martin,Organic photovoltaics: a chemical approach, Chem.Commun. 2010, 46, 4853 – 4865

62 P A. Troshin, H Hoppe, J Renz, M Egginger, J Yu. MAndrey E. Goryachev, Alexander S. Peregudov, Rimma N. Lyubovskaya, Gerhard Gobsch, N. Serdar Sariciftci, and Vladimir F. Razumov, Material Solubility-Photovoltaic Performance Relationship in the Design of Novel Fullerene Derivatives for Bulk Heterojunction Solar Cells, Adv. Funct. Mater. 2009, 19, 779–788

63 Y Yao, J Hou, Z Xu, G Li, and Y Yang, Effects of Solvent Mixtures on the Nanoscale Phase Separation in Polymer Solar Cells, Adv. Funct. Mater. 2008, 18, 1783–1789

64 Haskal, E. I.; Shen, Z.; Burrows, P. E.; Forrest, S. R. Excitons and exciton confinement in crystalline organic thin films grown by organic molecular-beam deposition. Phys. Rev. B: Condens. Matter Mater. Phys. 1995, 51, 4449–4462.

65 So, F. F.; Forest, S. R. Evidence for exciton confinement in crystalline organic multiple quantum wells. Phys. Rev. Lett. 1991, 66, 2649–2652.

66 X.-Y. Zhu, Q. Yang,and M. Muntwiler, Charge-Transfer Excitons at Organic Semiconductor Surfaces and Interfaces, Acc. Chem. Res., 2009, 42 (11), pp 1779–1787

67 H. Hoppe, M. Niggemann, C. Winder, J. Kraut, R. Hiesgen, A. Hinsch, D. Meissner, and N.S. Sariciftci: Nanoscale morphology of conjugated polymer/fullerene based bulk-heterojunction solar cells. Adv. Funct. Mater. (2004).

68 C. R. McNeill, I. Hwang and N. C. Greenham, Photocurrent transients in all-polymer solar cells: Trapping and detrapping effects, J. Appl. Phys. 106(2) 024507 (2009)

69 Müller, C., Wang, E., Andersson, L. M., Tvingstedt, K., Zhou, Y., Andersson, M. R. and Inganäs, O. (2010), Influence of Molecular Weight on the Performance of Organic Solar Cells Based on a Fluorene Derivative. Adv. Funct. Mater., 20: 2124–2131

70 C. J.Brabec, S. Gowrisanker, J. J. M. Halls, D. Laird, S. Jia and S. P. Williams, Polymer–Fullerene Bulk-Heterojunction Solar Cells. Adv. Mater., 22: 3839, (2010).

71 G. Li, V. Sharotriya, J. Huang, Y. Yao, T. Moriarty, K. Emery, Y. Yang, High-efficiency solution processable polymer photovoltaic cells by self-organization of polymer blends, Nature Materials 4, 864, (2005).

72 H. Kim, M. Shin, and Y. Kim, Distinct Annealing Temperature in Polymer:Fullerene:Polymer Ternary Blend Solar Cells, J. Phys. Chem. C 2009, 113, 1620–1623

73 Park, S. J., Cho, J. M., Byun, W.-B., Lee, J.-C., Shin, W. S., Kang, I.-N., Moon, S.-J. and Lee, S. K. (2011), Bulk heterojunction polymer solar cells based on binary and ternary blend systems. J. Polym. Sci. A Polym. Chem., 49: 4416–4424.

74 M. C. Scharber, D. Mühlbacher, M. Koppe, P. Denk, C. Waldauf, A. J. Heeger, C. J. Brabec, Design Rules for Donors in Bulk-Heterojunction Solar Cells—Towards 10% Energy-Conversion Efficiency, Adv. Mater., 18, 789, (2006).

75 C. J Brabec, A. Cravino, D. Meissner, N. S. Sariciftci, T. Fromherz, M. T. Rispens, L. Sanchez, and J. C. Hummelen, Origin of the Open Circuit Voltage of Plastic Solar Cells. Adv. Funct. Mater., 11, 374, (2001).

76 B-G Kim, E. J. Jeong, H. J. Park, D. Bilby, L. J. Guo, and J. Kim, Effect of Polymer Aggregation on the Open Circuit Voltage in Organic Photovoltaic Cells: Aggregation-Induced Conjugated Polymer Gel and its Application for Preventing Open Circuit Voltage Drop, ACS Applied Materials & Interfaces 2011 3 (3), 674-680

77 M.T. Dang, G. Wantz, H. Bejbouji, M. Urien, O. J. Dautel, L. Vignau, Lionel Hirsch, Polymeric solar cells based on P3HT:PCBM: Role of the casting solvent, Solar Energy Materials and Solar Cells, Volume 95, Issue 12, December 2011, Pages 3408-3418

78 M.-S Kim, B-G Kim, and J Kim, Effective Variables To Control the Fill Factor of Organic Photovoltaic Cells, ACS Applied Materials & Interfaces 2009 1 (6), 1264-1269

79 Credgington, D., Hamilton, R., Atienzar, P., Nelson, J. and Durrant, J. R. (2011), Non-Geminate Recombination as the Primary Determinant of Open-Circuit Voltage in Polythiophene:Fullerene Blend Solar Cells: an Analysis of the Influence of Device Processing Conditions. Adv. Funct. Mater., 21: 2744–2753.

80 J.-M. Verilhac, G. LeBlevennec, D. Djurado, F. Rieutord, M. Chouiki, J.-P. Travers, A. Pron, Effect of macromolecular parameters and processing conditions on supramolecular organisation, morphology and electrical transport properties in thin layers of regioregular poly(3-hexylthiophene), Synth. Met. 156 (2006) 815–823.

81 A.J.Moulé , K.Meerholz,Controlling morphology in polymer–fullerene mixtures, Adv.Mater. , 20 (2008) 240–245.

82 P. Vanlaeke, A. Swinnen, I. Haeldermans, G. Vanhoyland, T. Aernouts, D. Cheyns, C. Deibel, J. D'Haen, P. Heremans, J. Poortmans, J.V. Manca, P3HT/PCBM bulk heterojunction solar cells: relation between morphology and electro-optical characteristics, Sol. Energy Mater. Sol. Cells 90 (2006) 2150–2158.

83 H. Hoppe, M. Niggemann, C. Winder, J. Kraut, R. Hiesgen, A. Hinsch, D. Meissner, N.S. Sariciftci, Nanoscale morphology of conjugated polymer/ fullerene-based bulk- heterojunction solar cells, Adv. Funct. Mater. 14 (2004) 1005–1011.

# CHAPTER 4: FLUORENE-BASED POLYMERS FOR ORGANIC PHOTOVOLTAIC: SYNTHESIS, PHYSICAL CHARACTERISATION AND PHOTOVOLTAIC PROPERTIES

# I. Introduction

In the previous chapter we have presented low band gap donor-acceptor copolymers based on linear oligo(alkyl)thiophenes coupled with fluorenone and benzothiadiazole units, namely PQTF, POTF and PQTBTD. These polymers exhibit small band gaps in the range of 1.6-1.9 eV. However, by reducing the band gap of the materials we also obtained low open circuit voltage (0.4-0.6 eV) for the solar cells fabricated using these polymers. Open circuit voltage ($V_{oc}$) can be correlated with the energy level difference between the HOMO of the donor polymer and the LUMO of acceptor[1,2]. One interesting strategy to achieve high $V_{oc}$ is to develop new donor polymers with low-lying HOMO energy levels.

The polyfluorenes are commonly known in the field of light emitting diodes as wide band gap polymers[3,4]. Fluorene-containing molecules are highly fluorescent molecules, they are planar and rigid molecules and they exhibit low-lying HOMO levels. The latter property gives to the polymers higher stability towards photo-degradation and thermal oxidation[5,6], and could give high open circuit voltages in presence of fullerenes PCBM[7]. Polyfluorene (PF) copolymers are also well known for their high charge carrier mobility[8,9]. The planarity and the rigidity of fluorene-based materials make them a good hole transporting compounds and they can achieve high short circuit currents in solar cells[10,11]. Fluorene-based polymers are therefore promising materials for photovoltaic cells[12,13,14,15].

Pacios and coworkers[16] tested a blend of red emitting poly(2,7-(9,9-dialkyl)fluorene)/PCBM in photovoltaic devices and have demonstrated low power conversion efficiency of a maximum of 0.75 %. The low efficiency is due to the wide energy band gap of the polymer affording a limited absorption in the ultra-violet - visible region. In order to reduce the energy band gap and extend the absorption domain toward the visible range, Schulz and co-workers[17] have synthesised a more conjugated polyfluorene by introducing bithiophene units in the polymer backbone, namely poly(2,7-(9,9'-dihexyl-fluorene]-co-bithiophene) (F6T2) and tested in photovoltaic device. A power conversion efficiency (PCE) up to 2.7 % with an open-circuit voltage of 1.03 V and a short-circuit current (Jsc) of 4.96 mA $cm^{-2}$, was achieved by blending the F6T2 with [6,6]-phenyl-C61-butyric acid methyl ester(PCBM60).

Another approach in order to reduce the energy band gap of the polyfluorenes is to introduce an electron withdrawing (acceptor unit) in the polymer backbone to form D-A polymers. This strategy allows for the fine tuning of the energy levels and affords smaller band gap polymers. Among earliest works of low band gap polymers based on fluorene for photovoltaic applications were presented by Andersson and coworkers[18] in 2003 by combining fluorene motif as electron donating unit (D), benzothiadiazole as electron-withdrawing unit (A) and thiophene unit as spacer. The polymer poly [2,7-(9-9-dialkyl-9H-fluorene)]-alt-[5,5-(4,7-di-2-thienyl-2,1,3 benzothiadiazole)] known as PFDTBT with 2-ethylhexyl and hexyl as alkyl chain have afforded power conversion efficiencies of 2.2 to 2.4 %. A lot of works were conducted on polymer development based on PFDTBT for example by changing the alkyl chains on the fluorene unit as reported in Figure 110[19,20,21,22]

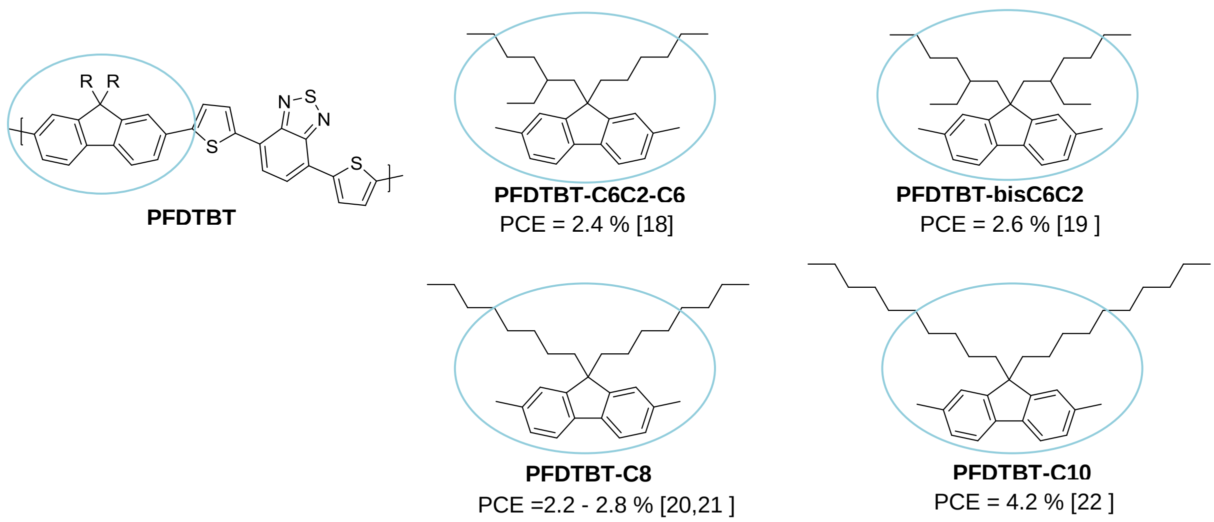


**Figure 110: Poly(fluorene-dithiophene-benzothiadiazole) with different alkyl chains on fluorene ring**

All the PFDTBT polymers showed high power conversion efficiencies from 2 % up to 4 %. The high power conversion efficiencies are contributed to broad optical absorption up to 700 nm (~1.8 eV) affording short-circuit current density of more than 4 mA $cm^{-2}$ and high open circuit voltage of 1.0-1.1 V. For example, Veenstra and coworkers[22] who developed the polymer PFDTBT-C10 by using long decyl (-$C_{10}H_{21}$) chain have obtained high power conversion efficiency of 4.2 %. The latter high efficiency conversion was a result of more solubilising side alkyl chains affording a high molecular weight of 34 kDaand optimization of the film thickness (140 nm) of the active layer. Andersson and coworkers [23] have continued to further develop these polymer series by fine tuning the side alkyl chains, and published in 2010 a series of three new polymers P1, P2, and P3 based on the polymer poly [2,7-(9-9-dioctyl-9H-fluorene)]-alt-[5,5-(4,7-di-2-thienyl-2,1,3 benzothiadiazole)] APFO-3. The polymers structures are presented in Figure 111 and photovoltaic parameters of these different fluorene-based polymers are listed in the Table 28.

.

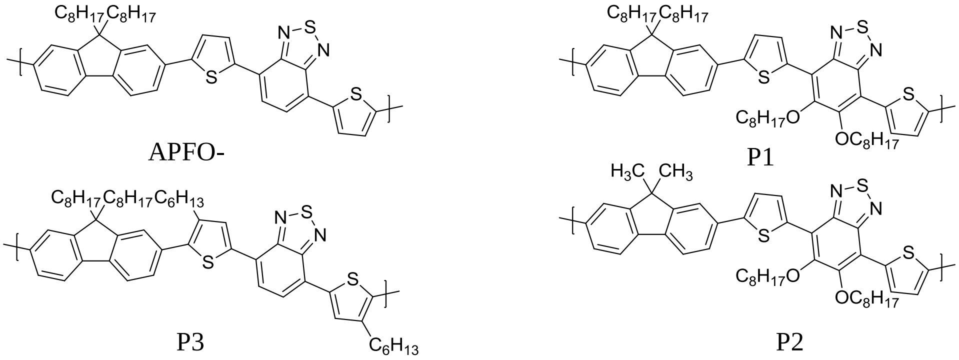


**Figure 111: Fluorene based low band gap polymers APFO series developed by Andersson and coworkers[23]**

| Polymers | Mn (kg mol$^{-1}$) | HOMO (eV) | Eg (eV) | Voc (V) | $J_{sc}$ (mAcm$^{-2}$) | FF | PCE (%) |
|---|---|---|---|---|---|---|---|
| APFO-3 | 6 | -5.5 | 1.86 | 0.94 | 6.2 | 0.46 | 2.7 |
| P1 | 77 | -5.5 | 2.01 | 0.97 | 6.7 | 0.47 | 3.1 |
| P2 | 10 | -5.4 | 1.96 | 0.93 | 6.3 | 0.48 | 2.8 |
| P3 | 175 | -5.6 | 1.97 | 1.06 | 4.9 | 0.41 | 2.2 |

**Table 28: Photovoltaic parameters of the APFO-3 series polymers**

Polymers APFO-3 and P3 vary by the two additional solubilising in plane side alkyl chains attached on the thiophene rings. This modification allows increasing the molecular weight of the polymer P3 up to 175 kg.mol$^{-1}$. However due to steric hindrance of the hexyl chains on the thiophene rings close to the fluorene alkyl chains, the polymer P3 give a moderate power conversion efficiency of 2.2 % as compared to the synthesized APFO-3 with 2.7 % efficiency. On the other hand, the polymer P1 and P2 possess more electron releasing groups, i.e octyloxy chains attached onto the benzothiadiazole rings. Both polymers showed good cell performance with the best power conversion efficiency of 3.1 % for P2. These results demonstrate that by tailoring the side alkyl chain of the polymer backbone attached in appropriate positions, one can further improved the power conversion efficiency. It is also noteworthy that high open circuit voltages were obtained for all photovoltaic devices based on these polyfluorenes of Voc between 0.9 V to 1.1 V.

Other examples of fluorene-based polymers are the series of polymers PFO-Mx by E. Wang and coworkers[24]. Additional thiophene unit was introduced as spacer between the fluorene and benzothiadiazole moities as shown in Figure 112. The effect of side alkyl chains of the polymers is also investigated. The photovoltaic parameters of these polymers are listed in Table 29.

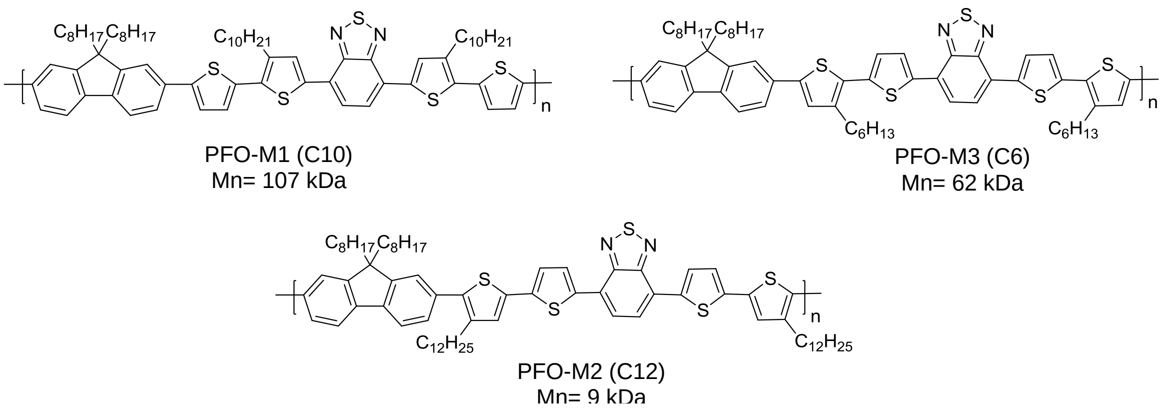


**Figure 112: Polymers PFO-Mx structures alternating fluorene-bithiophene-benzothiadiazole which vary on the side alkyl chains**

| Polymers | Mn (kg mol-1) | HOMO (eV) | LUMO (eV) | Eg (eV) | Voc (V) | Jsc (mAcm$^{-2}$) | FF | PCE (%) |
|---|---|---|---|---|---|---|---|---|
| PFO-M1 | 107 | -5.40 | -3.13 | 2.27 | 0.90 | 3.97 | 0.41 | 1.82 |
| PFO-M2 | 9 | -5.37 | -3.17 | 2.37 | 0.70 | 2.80 | 0.38 | 0.74 |
| PFO-M3 | 62 | -5.34 | -3.22 | 2.12 | 0.86 | 5.86 | 0.52 | 2.63 |

**Table 29: Photovoltaic parameters of polymers PFO-Mx by E. Wang and coworkers [24]**

The polymer PFO-M2 having two dodecyl-thiophene units gave low molecular weight due to steric hindrance that does not favours the coupling reaction of the units during the polymerization reaction. Both PFO-M1 and PFO-M3 with higher molecular weights of more than 60 kg mol$^{-1}$ showed good performance in solar cells. The best performances were obtained for polymer PFO-M3 with hexyl chains on the thiophene rings. Again, these results showed the importance of the side alkyl chain length and their influence on the photovoltaic properties.

Flourishing progress in the fluorene-based polymers have also open doors to develop new type of donor-acceptor polymers with analogous structures to fluorene such as polycarbazoles[25],[26], [27], polysilafluorenes[28], and polygermafluorenes[29]. These new series of polymers showed that by changing the carbon atom on the 9 position of the fluorene ring can afford new interesting materials with unique electronic properties. The polycarbazole have shown higher power conversion efficiency thanks to extensive optimization in photovoltaic devices[25,26,27.]

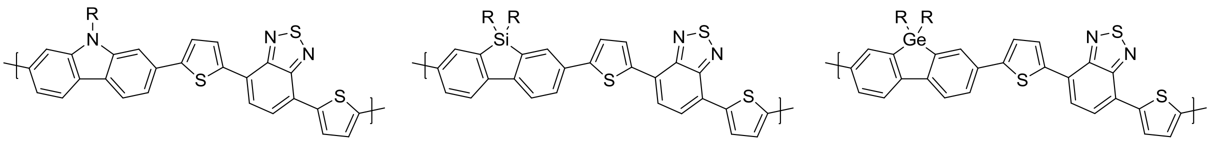

Polycarbazole
PCE=3.6-6.0%
Voc=0.88V
Eg=1.9eV

Polysilafluorene
PCE= 5.4 %
Voc=0.90 V
Eg=1.8 eV

Polygermafluorene
PCE=2.8 %
Voc= 0.79
Eg=1.8eV

**Figure 113: Analogous polymers to polyfluorenes: Polycarbazole, polysilafluorene and polygermafluorene**

Based on these brief literature reviews, our main goals to be achieved for the new polymers are: to obtain high open circuit voltage with polymers showing moderately small band gap energy (close to 2 eV) and to afford broad absorption spectrum. A simple strategy was adopted to develop our new series of D-A polymers by modifying the molecular structure of our previously studied linear oligoalkyl-thiophene based polymer (PQTBTD and PQTF), thus by incorporating fluorene units to its polymer backbone forming the new polymers as shown in Figure 114.

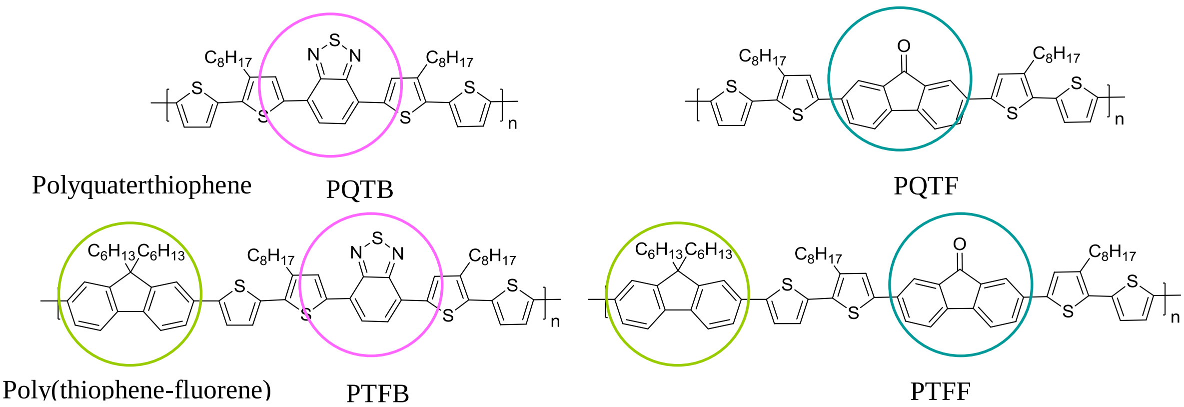


**Figure 114: Structures of new series of polymers incorporating fluorene units, Poly-thiophene-fluorene-benzothiadiazole PTFB and Poly-thiophene-fluorene-fluorenone PTFF**

To form the desired new fluorene-containing polymers, the synthetic method commonly adopted for the preparation of copolymers alternating two different monomers is based on Suzuki coupling[30, 31, 32].

In previous chapter we have formed ternary blend of POTF and PQTB in order to take advantage of the complementary absorption spectra of both polymers. However it is acknowledged that the well-optimized binary blend solar cells performed better than the ternary blend solar cells[33,34]. To solve this problem of ternary blend a smart strategy is to synthesize a block copolymer alternating both the repeating units of each polymer in the polymer backbone. This concept was also adopted by the group S.J Park and coworkers and this group published quite recently a paper[35] on this topic. In their work the polymer solar cells (PSCs) were fabricated using a ternary blend film consisting two conjugated polymers poly(carbazole-benzothiadiazole) PCDTBT and poly(fluorene-benzothiadiazole) PFDTBT and a soluble fullerene derivative (PCBM) as the donor and acceptor materials, respectively. And, to compare with the ternary blend system, the single-component copolymers consisting of the repeating units of each of the copolymers (fluorene-benzothiadiazole and carbazole-benzothiadiazole) , used in ternary blend solar cells were designed and synthesized for use as the electron donor materials in binary blend solar cells.

They have demonstrated that the binary blend solar cell containing a single-component copolymer as the electron donor material performed better than the ternary blend solar cell[35].

We have also developed similar approach by designing a block copolymer incorporating the thiophene-fluorene-benzothiadiazole segment and thiophene-fluorene-fluorenone segment, the polymer PTFBF as shown in Figure 115.

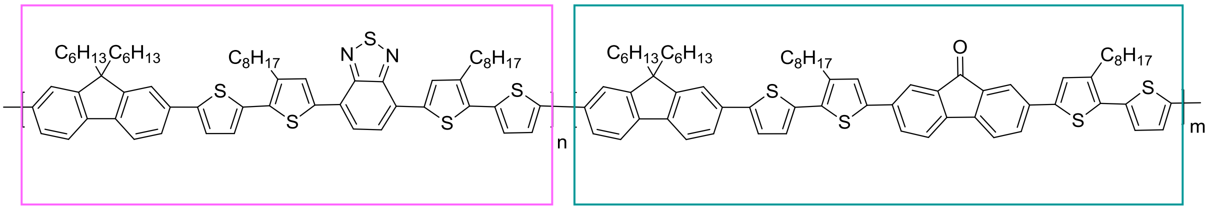

**Figure 115 : Block copolymers poly [(thiophene-fluorene-benzothiadizole)-co-(thiophene-fluorene-fluorenone]] PTFBF**

On a different note, it has been thoroughly described earlier the key role of the solubilising chains on the polymer backbone on the macromolecular properties and in the device performance. Therefore, the choice of the solubilising alkyl chains and adequate positions of the alkyl chains are of crucial parameters. The solubilizing chains connected at the 9 position of the fluorene extend above and below the plane of the monomer because of the sp3 carbon, as shown in Figure 116; these out of plane chains sterically hinder the π-π stacking between polymers depending on the chain length. On the other hand the alkyl solubilising chains on the thiophene ring will be in plane induced by the sp2 carbon of the thiophene ring as shown in Figure 116.

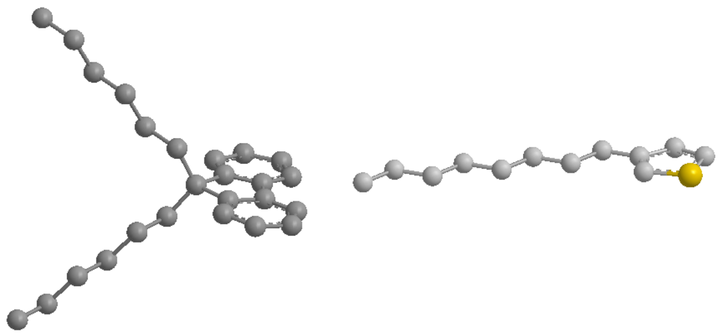

**Figure 116: Conformation of 9,9-dihexyl-9H-fluorene by molecular modelling MM2 calculation (ChemBio3D)**

Therefore, for our polymers we have chosen hexyl chains as the spacer between the polymer stacks in order to have short spacer in between each polymer planes. On the other hand we have selected octyl chains as alkyl substituents for the thiophene rings at the 3-position and an additional thiophene spacer connected to the fluorene unit to minimize steric hindrance between the alkyl chains and to afford a good solubility of the polymer backbone.

# II. Synthesis and purification of fluorene-based polymers PTFB, PTFF and PTFBF

In order to form alternating copolymers combining thiophene, fluorene, and electron deficient units, the possible methods of polymerisation are Stille cross-coupling polymerisation or Suzuki cross-coupling polymerisation. The two types of polymerisation involve an aryl halide with either aryl-stannane (for Stille coupling) or aryl boronic (for Suzuki coupling) precursors. For the preparation of the fluorene-based D-A polymers, Suzuki coupling reactions have been broadly used for preparing benzene-containing polymers with boronic groups on the benzene ring of the monomer [36] giving well defined alternating copolymers with high degree of polymerisation[12,18,37,38.] Hence, the Suzuki coupling reaction was preferred to prepare the desired polymers. Classical Suzuki [39] coupling involved boronic esters and halogenated reagents in presence of palladium catalysts in alkaline condition.

## II.1. Synthesis of monomers PTFB, PTFF and PTFBF

To prepare for the polymers, we used an effective way by departing from previously synthesizes monomers BTB and BTF to form dihalogenated monomers, while fluorene dialkyl-boronic esters are commercially available reagents.

In Suzuki coupling reaction, the halogenated compounds intervene during the oxidative addition to the palladium (0) complex to afford stable trans-palladium complex. In general the relative reactivity of the halogenated compounds decreases in order of I > OTf > Br >> Cl[39] . Therefore, we seek to study the effect of utilization of diiodide monomers in this Suzuki coupling polymerization compared to dibromide monomers.

The synthesis of the monomers of PTFB (BTB-Br2 and BTB-I2) and the monomer of PTFF (BTF-Br2) are shown in Scheme 10.

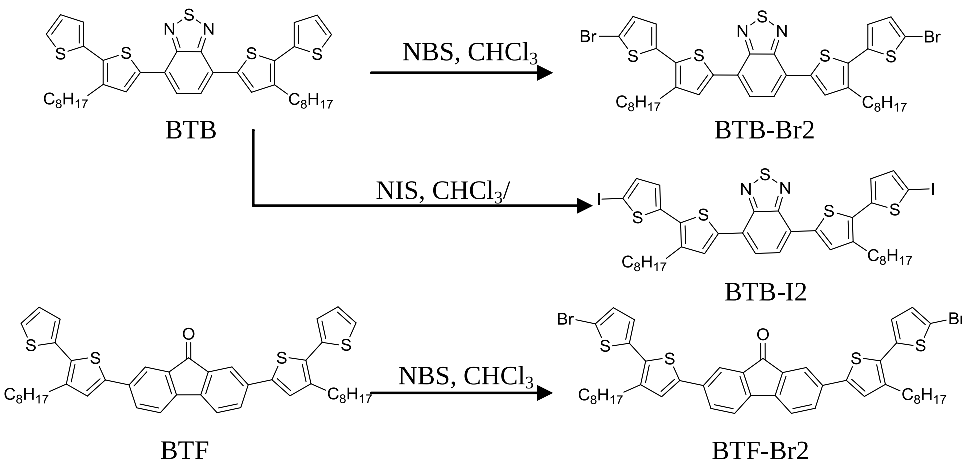


**Scheme 10: Synthesis of monomers PTFB and PTFF: BTB-Br2, BTB-I2 and BTF-Br2**

After dibromination using N-bromosuccinimide in chloroform, we obtained pure symmetrical dibrominated monomers BTB-Br2 with a good yield of 63 % and BTF-Br2 of 64 % respectively. Similarly we also synthesized diiodo substituted monomers 4,7-bis(5'-iodo-3-octyl-2,2'-bithiophen-5-yl)benzo[c][1,2,5]thiadiazole which is an analogue of BTB-Br2.

## II.2. Synthesis and purification of polymers PTFB , PTFF and PTFBF

As shown in Scheme 11 the poly(thiophene-fluorene-benzothiadiazole) abbreviated as PTFB and poly(thiophene-fluorene-fluorenone) abbreviated as PTFF are synthesized by Suzuki-Miyaura cross-coupling polymerization[24] with the monomer BTB-Br2 (or BTB-I2) and monomer BTF-Br2 respectively with dihexyl-fluorene diboronic ester. Both polymerization reactions are carried out under the same conditions in a biphasic mixture of toluene/aqueous (3:1), in presence of the base $Na_2CO_3$ (2.0 M), with palladium catalyst [40] tris(dibenzylideneacetone)dipalladium(0) $Pd_2dba_3$ of 2 % molar equivalent of and 11 % molar equivalent of o-tolylphosphine as ligand.

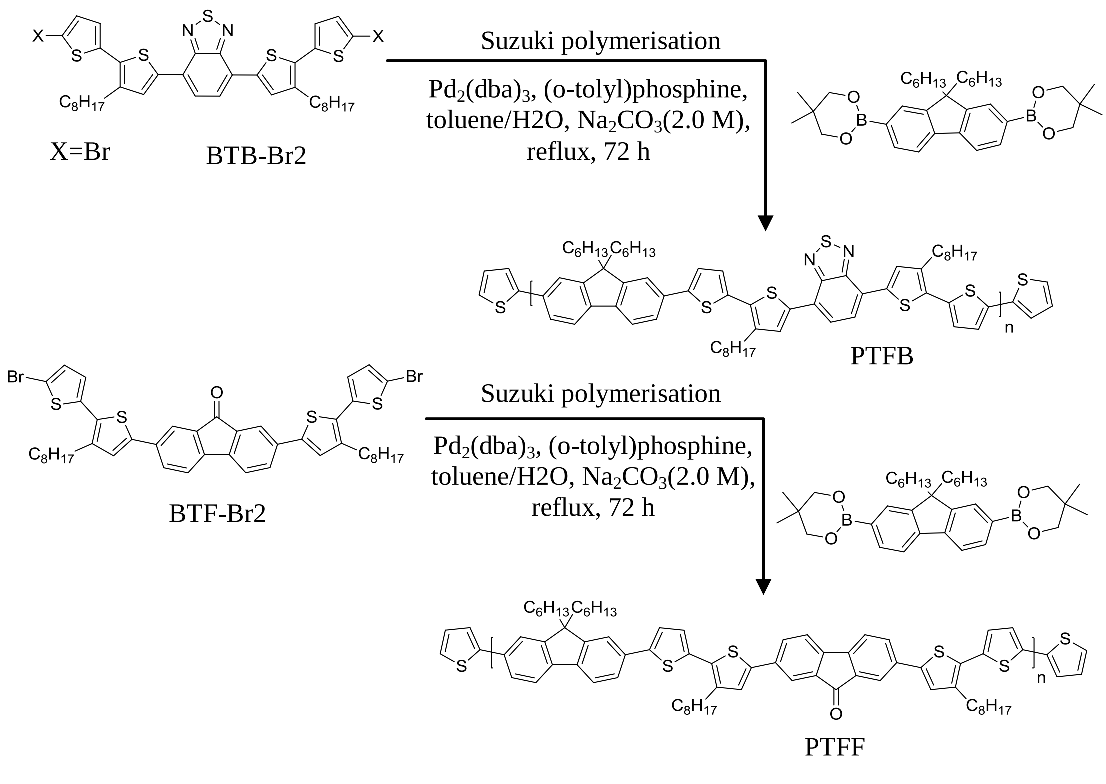


**Scheme 11: Synthesis of poly(thiophene-fluorene-benzothiadiazole) PTFB and poly(thiophene-fluorene-fluorenone) PTFF**

For the polymerization all the reactions are run in a single neck round bottom flask in argon condition. The dihalide monomers and the dihexyl-fluorene diboronic ester are weighed out to be at stoechiometric balance. The alkaline solution of $Na_2CO_3$ was prepared at a concentration of 2.0 M. The solvents are degassed in argon before the addition of catalyst to avoid desactivation by the presence of oxygen in the medium. The polymerisations are performed under reflux for 72 h, then end-capped with 2-thiophene boronic ester and 2-bromothiophene in order to avoid halide or boronic esters as end chain groups.

For the preparation of block copolymer of PTFBF, the monomers BTB-Br2 and BTF-Br2 have similar structures, therefore may have the same reactivity upon Suzuki coupling. Therefore polymerization of 1 equivalent of monomer BTB-Br2 and one equivalent of monomer BTF-Br2 with two equivalents of dihexyl-fluorene diboronic ester units, may conduct to statistically same amount of benzothiadiazole unit and fluorenone unit in the final polymer structure. The polymerization is shown in Scheme 12.

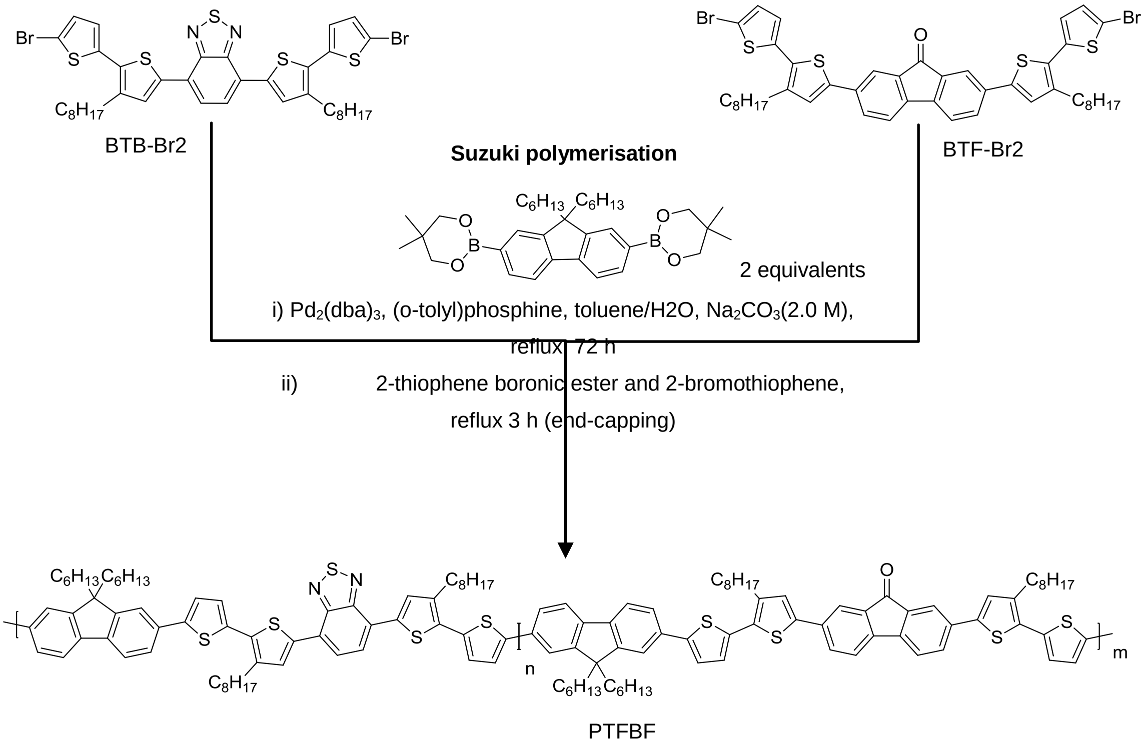


**Scheme 12: Synthetic route to thiophene-fluorene-benzothiadiazole-fluorenone block copolymer PTFBF**

After complete polymerization, the polymers were first concentrated then precipitated in methanol solutions. We obtained dark metallic films for all the three polymers. The crude polymers were then stirred in acetone at room temperature overnight, to remove the catalysts then further purification by soxhlet extraction in acetone and in chloroform.

We performed size exclusion chromatography (SEC) of the three polymers using chloroform as eluent. The molecular weight and molecular weight distribution of the polymers were determined from the size exclusion chromatography (SEC) data. The values were calibrated with polystyrene standards. The yields for each fraction represent the obtained polymer fraction mass after soxhlet extraction over the total weight of the batch polymer. We have also calculated the molecular weight of the polymer with estimated chains (Mabs) to be compared with the molecular weight obtained of the highest peak Mpeak for each fraction. Icorr represent the percentage of error between these two values to evaluate the accordance between calculated values and experimental values. The calculated chain length represents the mostly present chains in each fraction. Mpeak calculation allows first attribution of each peak in the SEC chromatogram.

SEC chromatogram of the polymers PTFB prepared from diiodo-monomers is presented in Figure 117 with the macromolecular parameters of all fractions obtained by sequential extraction are listed in Table 30.

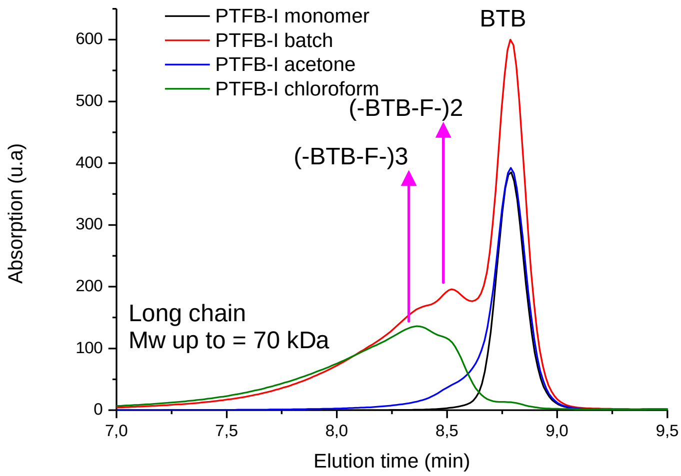


**Figure 117: SEC chromatogram of different fractions of polymers PTFB prepared via Suzuki coupling using diiodinated monomers, with attribution of maximum peaks according to molecular weight. The pink arrows indicate Mpeak with attribution of polymer chain.**

| Polymer | Fraction | Mn [kDa] | Mw [kDa] | I= Mw/Mn | $M_{peak}$ [kDa] | $M_{abs}$ [kDa] | $I_{corr}$= $M_{peak}/M_{abs}$ | Yield (%) |
|---|---|---|---|---|---|---|---|---|
| BTB-I2 | - | 0.97 | 1.02 | 1.06 | 1.01 | 0.94 | 1.07 | - |
| PTFB-I | batch | 1.55 | 3.20 | 2.06 | 1.03 | $1.02_{(n=1)}$ | 1.00 | 100 |
| | acetone | 1.67 | 4.43 | 2.66 | 1.00 | $1.02_{(n=1)}$ | 0.98 | 45 |
| | chloroform | 3.96 | 7.37 | 1.86 | 3.31 | $3.06_{(n=3)}$ | 1.08 | 50 |

**Table 30: Macromolecules parameters of different fractions of polymers PTFB prepared via Suzuki coupling from diiodinated monomers**

From SEC chromatogram and the SEC macromolecules parameters the crude polymer (batch fraction) is composed of non-reacted monomer, oligomeric and polymeric species. Extraction by acetone allows eliminating the non-reacted monomer and oligomeric species. The chloroform fraction showed no longer short oligomer chains and gives a molecular weight of 3.96 kDa. From Mpeak value, this fraction is estimated to be mainly composed of polymers of three repeating units.

The same work has been carried out starting from dibrominated compound. SEC chromatogram for the polymer PTFB prepared from dibromo-monomer (namely PTFB-Br) is presented in Figure 118, with the macromolecular parameters of all fractions obtained by sequential extraction are listed in Table 31 .

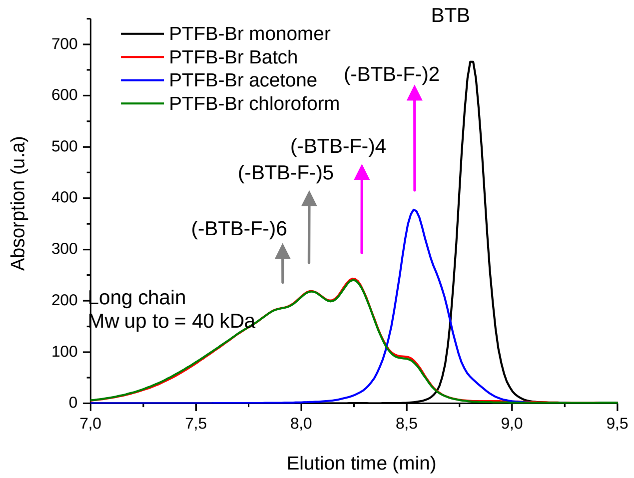


**Figure 118: SEC chromatogram of different fractions of polymers PTFB prepared via Suzuki coupling using dibrominated monomers, with attribution of maximum peaks according to molecular weight. The pink arrows indicate Mpeak with attribution of polymer chain. Grey arrows are approximative attribution of chain lengths**

| Polymer | Fraction | Mn [kDa] | Mw [kDa] | I= Mw/Mn | $M_{peak}$ [kDa] | $M_{abs}$ [kDa] | $I_{corr}$= $M_{peak}/M_{abs}$ | Yield (%) |
|---|---|---|---|---|---|---|---|---|
| BTB-Br2 | | 0.90 | 0.96 | 1.06 | 0.98 | 0.85 | 1.15 | - |
| PTFB-Br | batch | 5.58 | 8.48 | 1.52 | 4.36 | $4.08_{(n=4)}$ | 1.07 | 100 |
| | Acetone | 1.82 | 2.06 | 1.13 | 2.17 | $2.04_{(n=2)}$ | 1.06 | 6.3 |
| | Chloroform | 5.64 | 8.61 | 1.56 | 4.33 | $4.08_{(n=4)}$ | 1.06 | 93.7 |

**Table 31: Macromolecules parameters of different fractions of polymers PTFB prepared via Suzuki coupling from diiodinated monomers**

Better weight distribution is observed in PTFB-Br, with a yield of 93 % of the polymer was collected in the chloroform fraction. The crude fraction is composed mainly of longer polymeric chain and small amount of oligomeric species and traces of non-reacted monomer. Extraction by acetone allowed to separate the oligomeric species and the chloroform fraction is composed of polymeric species with higher molecular weight of 5.6 kDa. Molecular weight of the maximum peak (Mpeak) of the chloroform fraction is estimated to have at least four repeating units and longer polymer chains with molecular weight up to 40 kDa.

The result showed that for the preparation of this copolymer, the dibromide monomer is a better precursor under our conditions. Even though in Suzuki coupling it is reported to give better yield[41] when using iodide compound than bromide compound, our result has showed the opposite result. For the polymer PTFB-I we have obtained almost the same ratio between the acetone fraction and the chloroform fraction. This result demonstrates that we obtained shorter polymer chains (or oligomers) when using the diiodide monomers. Possible interpretation of the result could come from the higher reactivity of diiodide monomers that favors the first addition, however the limiting step in the coupling reaction could be related to the steric hindrance originating from the bulky ligands of the tris(dibenzylideneacetone)dipalladium(0). It should be mentioned that similar results have been obtained in the lab during the preparation of oligomers using the same catalytic system with iodinated precursors. However, as we have performed only once the polymerization with diiodide monomers, it is difficult to drawn conclusion and to generalize the result to other polymers. Hence further investigations are needed to confirm this result.

For the polymer PTFF, SEC chromatogram is presented in Figure 119, with the macromolecular parameters of all fractions obtained by sequential extraction are listed in Table 32.

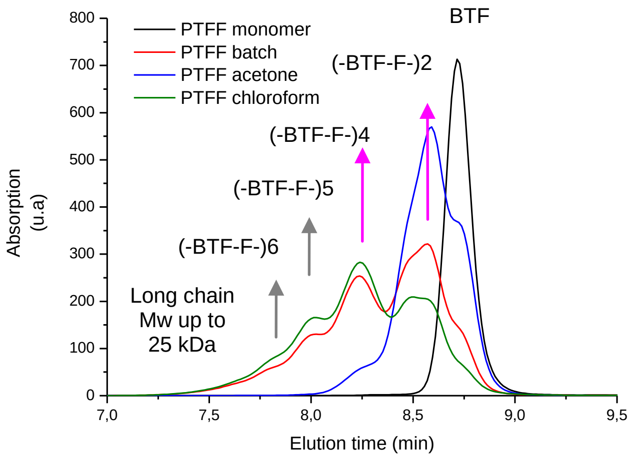


**Figure 119: SEC chromatogram of different fractions of polymers PTFF with proposed attribution of maximum peaks according to molecular weight. The pink arrows indicate Mpeak with attribution of polymer chain. Grey arrows are proposed attribution of chain lengths.**

| Polymer | Fraction | Mn [kDa] | Mw [kDa] | I= Mw/Mn | $M_{peak}$ | $M_{abs}$ | $I_{corr}$= $M_{peak}/M_{abs}$ | Yield (%) |
|---|---|---|---|---|---|---|---|---|
| BTF-Br2 | | 0.66 | 1.26 | 1.05 | 1.30 | 0.89 | 1.45 | |
| PTFF | batch | 2.71 | 4.22 | 1.56 | 1.96 | $2.13_{(n=2)}$ | 0.92 | 100 |
| | acetone | 1.70 | 2.01 | 1.18 | 1.86 | $2.13_{(n=2)}$ | 0.87 | 46.4 |
| | chloroform | 3.24 | 4.96 | 1.53 | 4.38 | $4.26_{(n=4)}$ | 1.03 | 53.6 |

**Table 32: Macromolecules parameters of different fractions of polymer PTFF**

For the polymer thiophene-fluorene-fluorenone PTFF, the crude polymer is composed of non-reacted monomer, and a mixture of oligomeric and polymeric species. Extraction by acetone allows partial separation of oligomeric species, as we observed in the weight distribution of the chloroform fraction to still contain oligomeric species. The polymer gives overall much lower molecular weight of 3.24 kDa for the chloroform fraction, as compared to PTFB with molecular weight of 5.24 kDa. These relatively low molecular weights for both polymers are probably due to a lower degree of solubility in the reaction mixture solvent toluene/water. A higher degree of polymerisation is to be expected with further optimisation in terms of a better choice of solvent for the monomer fluorenone for example polar solvent DMF. However if we looked at the values of Mpeak, both of the polymers showed similar results with the estimated chain lengths to be of four repeating units.

For the terpolymers combining fluorene units with benzothiadiazole monomers and fluorenone monomers PTFBF, the SEC chromatogram is presented in Figure 120, with the macromolecular parameters of all fractions obtained by sequential extraction are listed in Table 33 .

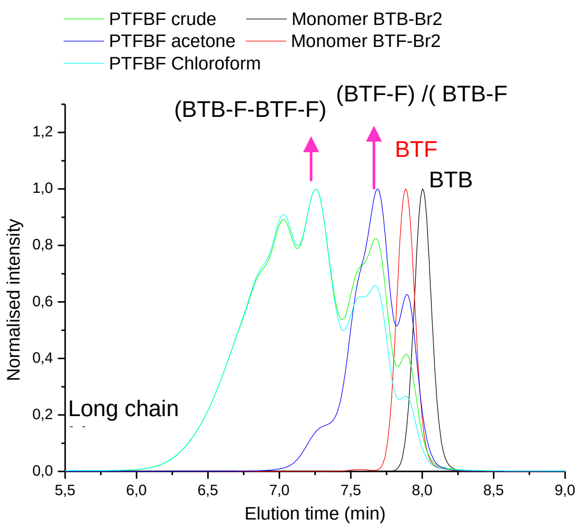


**Figure 120: SEC chromatogram of different fractions of terpolymers PTFBF with proposed attribution of maximum peaks according to molecular weight**

| Polymer | Fraction | Mn [kDa eq. PS] | Mw [kDa eq. PS] | I= Mw/Mn | $M_{peak}$ | $M_{abs}$ | $I_{corr}$= $M_{peak}/M_{abs}$ | Yield (%) |
|---|---|---|---|---|---|---|---|---|
| BTBBr2 | | 0.90 | 0.96 | 1.06 | 0.98 | 0.85 | 1.15 | |
| BTFBr2 | | 0.69 | 0.72 | 1.04 | 0.72 | 0.89 | 0.81 | |
| PTFBF | batch | 2.22 | 4.54 | 2.07 | 0.72 | 0.85 | 0.86 | 100 |
| | acetone | 1.08 | 1.34 | 1.24 | 1.24 | $1.02^{BTBF}$/ $1.14^{BTFF}$ | 1.22/ 1.09 | 16 |
| | chloroform | 2.48 | 4.88 | 1.96 | 2.99 | 2.99 $_{BTBF-BTFF-BTB}$ 2.99 $_{BTFF-BTBF-BTF}$ | 0.99/ 0.99 | 68 |

**Table 33: Macromolecules parameters of different fractions of polymer PTFBF**

For the terpolymers combining fluorene units with benzothiadiazole monomers and fluorenone monomers PTFBF, the reaction gives moderate degree of polymerisation with the highest molecular weight of 2.48 kDafor PTFBF in comparison with 5.6 kDa for PTFB and 3.6 kDafor PTFF. Based on the value of Mpeak of the chloroform fraction, the polymer chain can be estimated to be consisting of BTF-Fluorene-BTB-Fluorene-BTF or BTB-Fluorene-BTF-Fluorene-BTB. From elemental analysis the ratios of elemental compound N/S was found to be N, 1.25; S, 12.46. As the monomer benzothiadiazole-bithiophene has a ratio of N:S = 1:2.5, we suggested only one repeating unit of benzothiadiazole in the polymer backbone. Therefore a more possible composition for the polymer at Mpeak is bithiophene fluorenone-fluorene-bithiophene benzothiadiazole-fluorene- bithiophene fluorenone (BTF-F-BTB-F-BTF).

Polymerisation of the monomers BTB and BTF to form the polymer PTFBF has resulted to short chain formation. One possible reason for the low molecular weight of the polymer PTBFTF can be due to deboronation of the diboronic fluorene esters. The deboronation of the monomers could then lead to limiting amount of fluorene species during the polymerization, causing the termination of polymerization. However as we have only performed this polymerization once, further optimization of synthesis is necessary in order to control the polymerization growth.

**Discussion on the Suzuki coupling polymerisation**

Suzuki coupling polymerization is an effective way for copolymerization of two monomers, and in our study we have performed polymerization of three monomers in one pot reaction. However, the molecular weights obtained for all the polymers were relatively moderate of Mn less than 6 kDa, as compared to the similar polymer PFO-M1 reported by Wang and coworkers[42] with the highest molecular weight obtained at 107 kDa (with decyl alkyl chain on the thiophene and octyl chain on fluorene). Here, we have followed the same procedure described by the paper. One plausible reason to explain such difference would be the higher solubility of PFO-M1 originating from the longer solubilising chains compared to our polymers. However, the determination of the molecular weight of the polymers reported in literature is also subject to debate. It is almost impossible to find elugrams and detailed procedures used for the calibration of the SEC equipments and the determination of the macromolecular parameters.

Other hypothesis can be proposed to explain the lower molecular weight obtained in our case. We suspected that one limiting factor for our polymerizations could be the presence of oxygen in the solvent which deactivate the palladium catalysts. For our polymerization, we have degassed the solvent of reaction by simple bubbling of argon in the solvent about half an hour before the addition of the catalyst. In order to completely eliminate oxygen from the reacting mixture, we suggested performing a freeze-pump-thaw method[43] on the solvent as well as additional time of bubbling argon in the water solvent. The freeze-pump-thaw method consist of freezing the solvent with liquid nitrogen, then pumping off the atmosphere by applying vacuum on the system and finally cutting off the vacuum and leave the solvent to thaw. This procedure should be repeated until no more gas bubbles observed in the solution. Recently, optimization of the polymerization by using the freeze-pump thaw method to eliminate the oxygen in the mixture and by using the mixture of toluene/DMF for the polymerization of PTFF starting from a monomer with branched solubilising groups have resulted polymers of high molecular weight up to more than 50 kDa.

## III. Photo-physical characterisation of PTFB, PTFF and PTFBF

We performed UV-Visible spectroscopy to determine the absorption spectra of the three polymers PTFB, PTFF and PTFBF in chloroform solutions and in thin films. The concentration for each polymer was at 0.02 mg/ml and the thin films were prepared from polymers solutions with a concentration of 20 mg/ml in chlorobenzene and deposited onto glass substrates by spin-coating. The absorption spectra of the polymers in solution are presented in Figure 121.

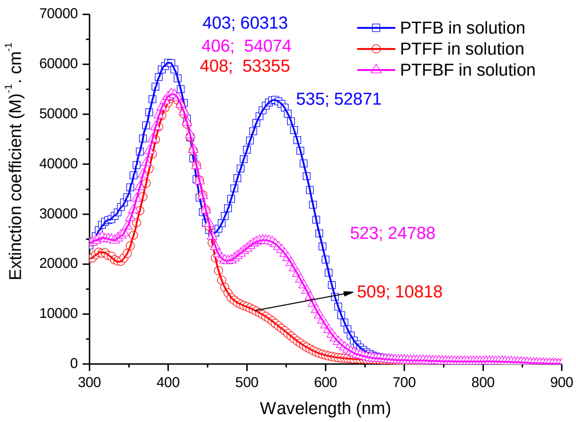


**Figure 121: UV-Visible absorption spectrum of PTFB, PTFF and PTFBF in chloroform solution at 0.02 mg/ml**

| Polymer | Absorption Solution λmax1/nm(ξ/M-1.cm-1) | λmax2/nm (ξ) | Egopt solution /eV |
|---|---|---|---|
| PTFB | 403 (60313) | 535 (52871) | 1.88 |
| PTFF | 408 (53355) | 509 (10818) | 2.03 |
| PTFBF | 406 (54074) | 523(24788) | 1.92 |

**Table 34: Optical parameters of UV-Visible absorption properties of PTFB, PTFF and PTFBF.**

The polymer thiophene-fluorene-benzothiadiazole PTFB showed two intense absorption peaks at 403 nm and 535 nm. For the polymer thiophene-fluorene-fluorenone PTFF we observed a strong absorption peak at 408 nm and weak shoulder at about 509 nm. Interestingly for the terpolymer PTFBF we observed two maximum peaks at 406 nm and 523 nm. The first intense peaks observed for all the polymers in the UV region between 400 to 408 nm can be attributed to the π–π* transition absorption band of the donor thiophene-fluorene segment.[44] In a recent paper Banerji and coworkers stipulated the first peak in the high energy band region can be attributed to partial charge transfer complex[45]. In our case all three polymers showed close values of transition band of π–π* only slight variations of 3-5 nm between each polymers. This confirmed the attribution of this absorption band to a π–π* transition originating from the donor thiophene-fluorene segments which are the same for all the three polymers. In the case of a partial charge transfer complex one would expect that this band would be strongly shifted going from a fluorenone to a benzothiadiazole based polymer.

The second absorption peaks are attributed to the internal charge transfer (ICT) band between the electron rich unit and the electron withdrawing group in the polymer backbone. The polymer PTFB having stronger electron withdrawing group benzothiadiazole compared to fluorenone showed intense ICT band. The polymer PTFBF showed an interesting characteristic with an intermediate absorption intensity of the ICT band. The position of the ICT bands was found close to the wavelength of the ICT band of the polymer fluorenone PTFF. The internal charge transfer intensity which increase with stronger interaction between electron-rich and electron withdrawing segment, indicate that for polymer PTFBF, we have both the presence both strong electron withdrawing group (benzothiadiazole) and weaker electron withdrawing group (fluorenone). These results are interesting and demonstrate that we can alternate two different electron withdrawing groups in the same macromolecule giving an additional internal charge transfer.

To better highlight the effect of polymerization from small molecules of monomers, the UV-Visible absorption of the two monomers BTB and BTF with the corresponding polymers are shown in Figure 122.

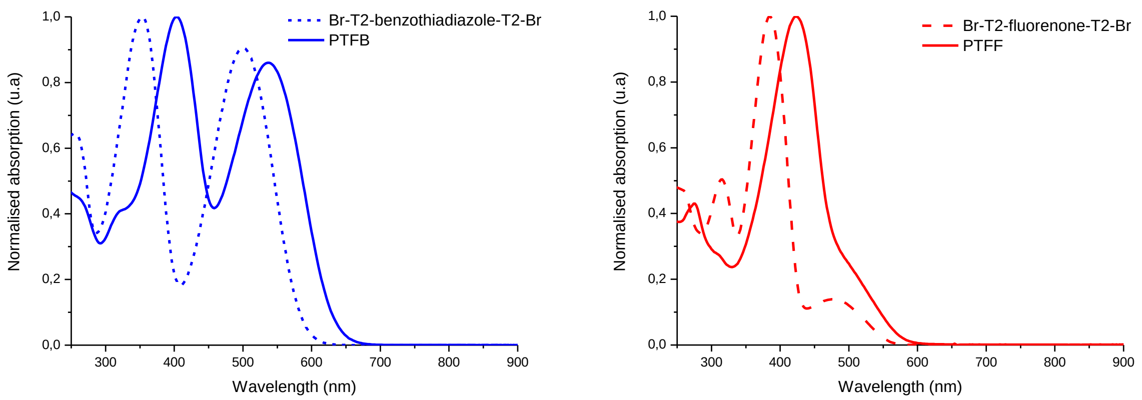


**Figure 122: UV-Visible absorption spectrA of PTFB and PTFF in chloroform solution with its monomer**

For both of the polymers PTFB and PTFF, bathochromic shifts are observed for the absorption peaks towards higher wavelengths and we also observed a broadening of the absorption spectra. This confirms the benefits of polymerization leading to an extended pi-conjugated systems and a better delocalisation of electrons. Combining the two monomers bithiophene-benzothiadiazole (BTB) and bithiophene-fluorenone (BTF) with fluorene units covalently to form block copolymer poly (thiophene-fluorene-benzothiadiazole)-alt-(thiophene-fluorene-fluorenone) PTFBF we obtained a synergistic effect on the absorption spectra (see Figure 123).

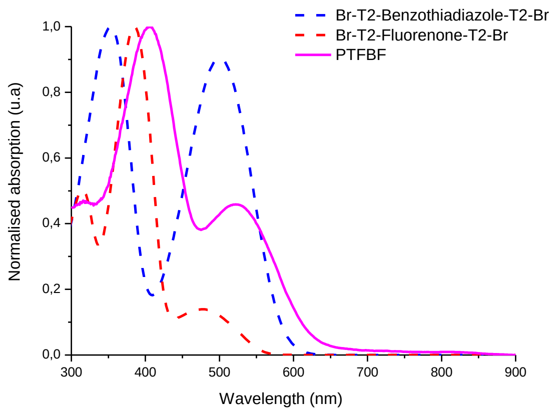


**Figure 123: UV-Visible absorption spectrum of PTFBF in chloroform solution with its monomers**

The UV-Visible absorption spectra of PTFB, PTFF and PTFBF in thin films are showed in Figure 124 with the optical parameters of UV-visible absorption properties of the polymers listed in Table 35.

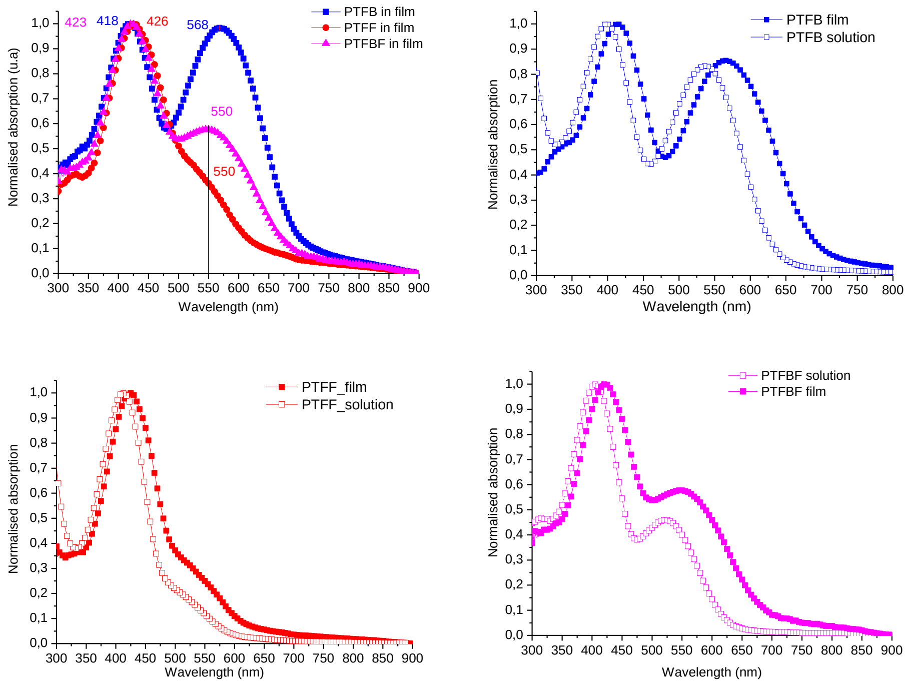


**Figure 124 : UV-Visible absorption spectrum of PTFB, PTFF and PTFBF in thin films**

| Polymer | Absorption Solution | | Absorption Film | | $Eg^{opt}$ film |
|---|---|---|---|---|---|
| | λmax1/nm (ξ) | λmax2/nm (ξ) | λmax1/nm | λmax2/nm | eV |
| PTFB | 403 (60315) | 535 (52870) | 418 | 568 | 1.75 |
| PTFF | 408 (53355) | 509 (10820) | 426 | 550 | 1.91 |
| PTFBF | 406 (54075) | 523(24790) | 406 | 522 | 1.79 |

**Table 35: Optical parameters of UV-Visbile absorption properties of PTFB, PTFF and PTFBF**

For the three polymers the same trends of broadening and bathochromic shifts of the absorption spectra in solid state are observed. For the polymer PTFB the two maximum peaks in the solution were red shifted (bathochromic effect) in film to 418 nm (10 nm shift) and 568 nm (33 nm shift). For the polymer PTFF we also observed bathochromic effect with the peaks shifted to 426 nm (18 nm shift) and 550 nm (35 nm shift) for the weak shoulder. As for the terpolymer PTFBF the peaks are found at 423 nm (17 nm shift) and 550 nm (28 nm shift) in films. These shifts are related the organization and the molecular packing in the solid state as observed in many other conjugated polymers[46,47].

# IV. Electrochemical characterisation of PTFB, PTFF and PTFBF

The electrochemical analyses of the thin films of the three polymers were measured by cyclic voltamperometry. The oxidation-reduction curves are presented in Figure 125 below with the electrochemical parameters in the Table 36.

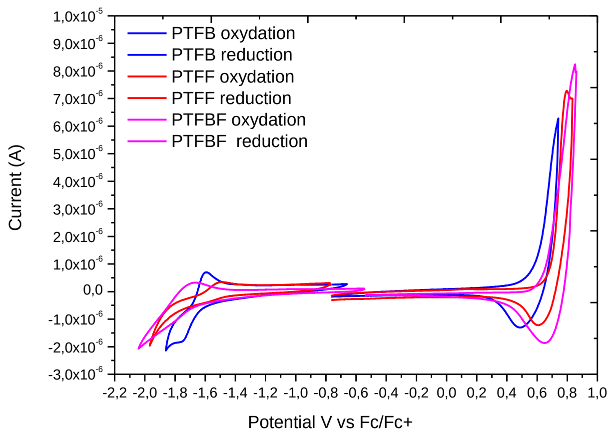


**Figure 125: Cyclic voltamperometry of polymers PTFB, PTFF and PTFBF in thin films**

| Compound | Eg-opt /eV | Eonset/V Oxidation | Eonset/V Reduction | HOMO /eV | LUMO /eV | $Eg^{ec}$ /Ev | $Eg^{opt}$ /eV |
|---|---|---|---|---|---|---|---|
| PTFB | 1.75 | 0.51 | -1.62 | -5.31 | -3.19 | 2.12 | 1.75 |
| PTFF | 1.91 | 0.62 | -1.52 | -5.42 | -3.28 | 2.14 | 1.91 |
| PTFBF | 1.79 | 0.58 | -1.65 | -5.38 | -3.15 | 2.23 | 1.79 |

**Table 36:Cyclic voltammograms of PTFB, PTFF and PTFBF with the electrochemical values**

The oxidation potential for PTFB was measured at 0.51 V and gives a reduction potential of -1.62 V after calibrated with ferrocene/ferrocenium reference potential. This gives a value of highest occupied molecular orbital (HOMO) energy level at -5.31 eV and lowest unoccupied molecular orbital (LUMO) energy level of -3.19 eV. The polymer PTFF showed higher oxidation potential with a potential of 0.62 V, and a lower reduction potential of -1.52 V as compared to PTFB. The HOMO and LUMO energy levels were calculated to be -5.42 eV and -3.28 eV accordingly. The lower oxidation potential observe for PTFB can be related to a more pronounced quinoidal character of the pi-conjugated system induced by the BTD unit[48].

For the polymer PTFBF, the oxidation potential is located in between the oxidation potential of PTFB and PTFF at 0.58 V. However the reduction potential of PTFBF is less reversible at -1.65 V. The HOMO and LUMO energy levels for the polymer PTFBF are calculated to be -5.38 eV and -3.15 eV respectively. We can note here that for all the polymers we obtained relatively high band gaps comprised between 2.12 and 2.23 eV. The values obtained by electrochemical measurements are found to be higher than the values determined by optical measurements. The difference between the optical band gap and electrochemical band gap can be explained by the difference of the method of film preparation of the two methods. In the case of films prepared for optical measurement, the films are prepared by spin-coating the solutions on glass substrates. While for electrochemical measurement, we have deposited the film by drop casting therefore the polymers have probably different interchain packing in the film. The different procedures for the preparation of the film may be responsible for the discrepancy of the values obtained. In addition, another plausible explanation as described by Jenekhe and coworkers[49] , the difference between optical and electrochemical band gap energies is related to the exciton binding energy of conjugated polymers which is believed to be in the range of ~0.4-1.0 eV[49].

In order to act as an efficient donor material for photovoltaic cells the frontiers orbitals of the polymers should be properly positioned to allow the photo induced charge transfer to take place with fullerenes. Furthermore the offset between the LUMOs of the donor and acceptor should be large enough ($\Delta$ $E_{CT}$ > 0.3 eV) to overcome the coulombic attraction and to allow charge separation. In the diagram Figure 126, the positioning of the HOMO LUMO energy levels of the polymers with respect to the one of PCBMC60 is showed.

All the three polymers showed lowest unoccupied molecular orbital LUMO energy levels correctly positioned with respect to the one of the PCBM. They are lying higher than the one of PCBM. Therefore the charge transfer between the donor polymers and the fullerene acceptor can occur. The energy required for the D-A transfer noted $\Delta$ $E_{CT}$ and the theoretical maximum values of the open circuit voltage are calculated and the values are recorded in Table 37.

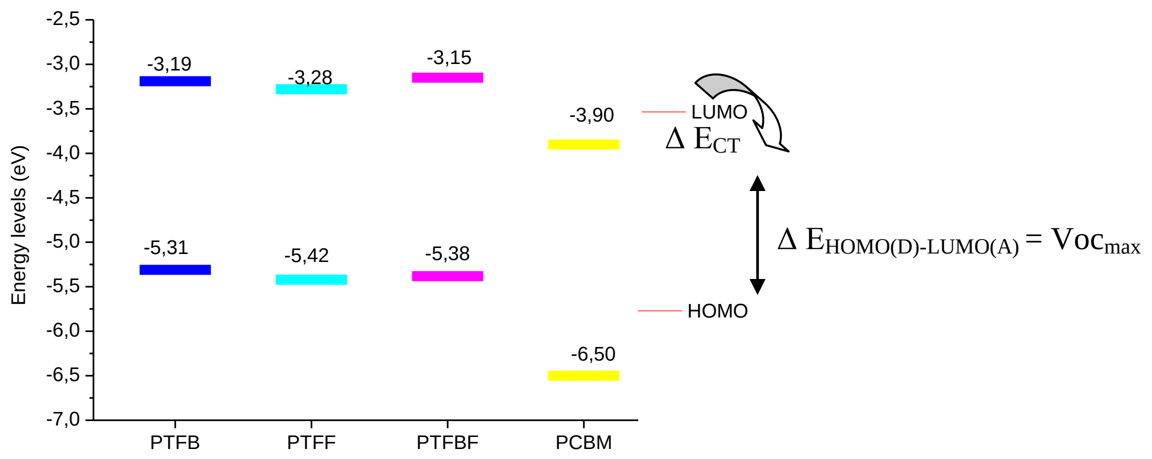


**Figure 126: Energy levels diagram of donor materials polymer PTFB, PTFF and PTFBF with electron acceptor PCBM**

| Compound | HOMO (eV) | LUMO (eV) | $\Delta E_{CT}$ (eV) | $Voc_{max}$(V) |
|---|---|---|---|---|
| PTFB | -5.31 | -3.19 | 0.71 | 1.41 |
| PTFF | -5.42 | -3.28 | 0.62 | 1.52 |
| PTFBF | -5.38 | -3.15 | 0.75 | 1.48 |

**Table 37: Calculated value of charge transfer energy $\Delta E_{CT}$ and theoretical maximum open circuit voltage of PTFB, PTFF and PTFBF**

The charge transfer energy between the polymer PTFF and the acceptor PCBM is the smallest therefore it is easier to form separated charges compared to the two other polymer PTFB and PTFBF. In terms of values of maximum open circuit voltage, all the three polymers showed high values of more than 1.4 V, with the highest for PTFF with 1.52. If we follow the relation propose by Scharber and coworkers[50] for the estimation of Voc, ($Voc = \Delta E_{HOMO(D)-LUMO(A)} - 0.3$) , we can hope to achieve high open circuit voltage for polymer PTFB, PTFF and PTFBF of 1.11 V, 1.22 V and 1.18 V.

# V. Charge and energy transfer properties

## V.1. Introduction

Our donor polymers presenting photoactive properties as demonstrated in the absorption spectra can undergo photoinduced charge and energy transfer process in presence of electron accepting molecule. A brief description of the charge and energy transfer processes is described below.

### V.1.1. Energy transfer mechanism

The energy transfer mechanism of electronic excitation of photoactive molecules has been described by Theodor Förster[51] , known as Förster energy transfer. The Förster energy transfer involved the interaction between a donor molecule in the excited state energetically in resonance with a nearby acceptor molecule via an efficient energy transfer. The transfer mechanism can be simply described by the diagram below (Figure 127).

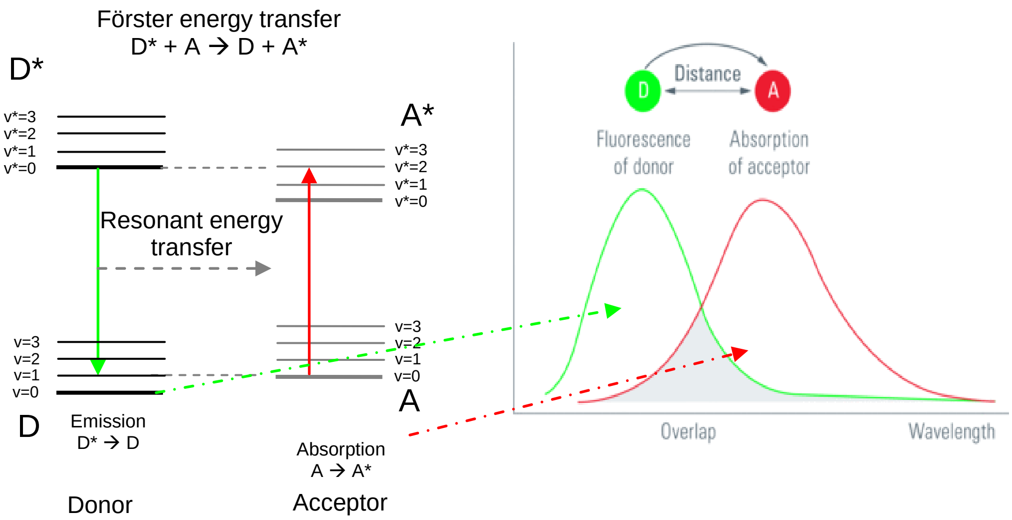


**Figure 127: Energy level diagram illustrating the resonance condition of energy transfer**

Upon illumination, the excited donor molecule can transferred its excitation energy to the acceptor molecule. As shown in (Figure 127), if the energy levels of the donor and the acceptor are in resonant, this would leads to a complete quenching of the donor emission and an increase in the acceptor luminescence. After the transfer, internal relaxation in the acceptor molecules will take place and the excitations are not in resonance anymore. The Förster resonant energy highly depends on the distance between donor and acceptor (3-10 nm)[52], the strength of the donor emission and acceptor absorption and their overlap spectra. In the Förster energy transfer no free charges are created[53]. Forster energy transfer can be well-investigated in photoluminescence spectroscopy. [51,54].

## V.2. Charge transfer mechanism

Photo-induced charge transfer between the donor D and acceptor A upon illumination mechanism is described by Sariciftci and coworkers[55, 53] as follow:

Step 1 : D + A → D* + A (photoexcitation of Donor)
Step 2 : D* + A → (D + A)* (excitation delocalized on the donor-acceptor complex)

Step 3 : $(D + A)^* \rightarrow (D^{\delta+} + A^{\delta-})^*$ (polarization of excitation: charge transfer initiated)
Step 4 : $(D^{\delta+} + A^{\delta-})^* \rightarrow (D^{\bullet+}\text{-}A^{\bullet-})$ (ion radical pair formed)
Step 5 : $(D^{\bullet+}\text{-}A^{\bullet-}) \rightarrow D^{\bullet+} + A^{\bullet-}$ (complete charge separation = free charge formation)

Upon illumination of photon energy higher than the energy gap of the donor, this may leads to the formation of singlet or triplet excitons D*. Such an exciton can interact with the neighboring acceptor, forming a more extended exciton, $D^* + A \rightarrow (D{-}A)^*$.The excitation is therefore delocalized between donor and acceptor. During the next stage, the partial charge transfer $(D{-}A)^* \rightarrow (D^{\delta+}{+}A^{\delta-})^*$ is initiated, and these excitons are reorganized into the donor−acceptor complexes which can then collapse into radical pairs $(D^{\delta+}{-}A^{\delta-})^* \rightarrow (D^{\bullet+}\text{-}A^{\bullet-})$ due to structural relaxation. The formed radical pairs are finally separated into two independent spin charge carriers, $(D^{\bullet+}\text{-}A^{\bullet-}) \rightarrow D^{\bullet+} + A^{\bullet-}$ .

Contrary to energy transfer, in a charge transfer process, complete charge separation occurred forming two separated radical pair ions $D^{\bullet+}$ and $A^{\bullet-}$ . This charge transfer process need to overcome binding energy [56] before complete separation to form free charges [57, 58, 59]. For intramolecular photo-induced electron transfer, the requirements on the spacer between the donor and acceptor units are important (and demanding); for metastability, the molecular orbitals of the D and A components must be decoupled so as to retard the back electron transfer process[55]

In our study two types of photo-induced mechanism transfer can occur, one in the covalently bound alternating electron donating-electron withdrawing D-A polymers [60] (intramolecular transfer) and another in the blends of our polymers (as donor materials) in combination with the fullerene PCBM as acceptor materials[58,61] ( intermolecular charge transfer) as depicted in Figure 128 below.

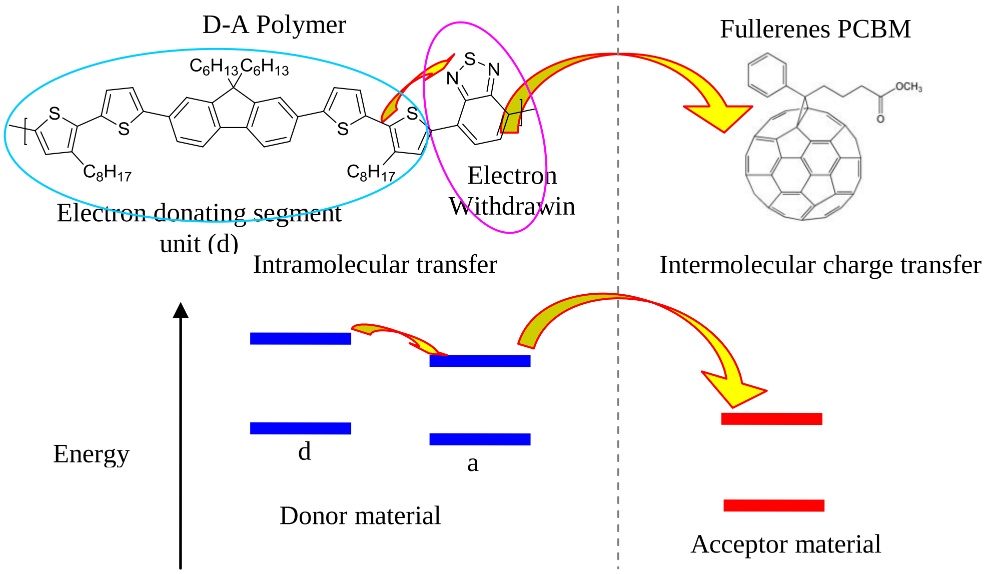


**Figure 128: Representation of intramolecular transfer in the d-a polymer and intermolecular charge transfer between Donor material (d-a Polymer) and Acceptor material (fullerenes) in blend**

Charge transfer processes in the donor–acceptor systems can be investigated by e.g. photoluminescence measurement via quenching luminescence [62] and electron paramagnetic resonance (EPR)[63]. Therefore we performed these two studies to investigate these processes.

## V.3. Photoluminescence spectroscopy

### V.3.1. Energy and charge transfer in D-A polymers

In first hand, we will investigate the energy and charge transfer processes which may occur in the polymers between the electron-donating segment and the electron-withdrawing segment. Photoluminescence spectroscopy measurements were conducted to illustrate this photo-physical phenomenon. Photoluminescence processes are observed when the absorbed energy is dissipated by emission of photons by the molecules.

Previously, the UV-Visible absorption spectra of polymer PTFB in solution have shown two intense band at 398 nm and 537 nm corresponding to the $\pi$–$\pi$* transition band at low wavelength region and to internal charge transfer complex at high wavelength region. In photoluminescence emission measurement, the polymer PTFB in solution is excited at 400 nm and the normalized photoluminescence spectra is recorded in Figure 129 as well as the UV-Visible absorption spectra of the polymer PTFB as comparison. The optical properties of polymer PTFB are listed in Table 38.

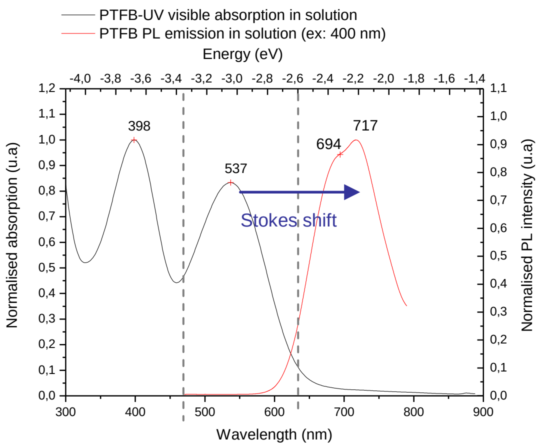


**Figure 129: UV-Visible absorption and photoluminescence spectra in chloroform of PTFB at 400 nm excitation.**

| Polymer | Absorption | | Photoluminescence |
|---|---|---|---|
| | Solution | | Solution |
| | λmax1/nm | λmax2/nm | λmax1/nm |
| PTFB | 398 | 537 | 694, 717 (vibronic) |

**Table 38: Optical properties of the polymers PTFB in UV-Visible absorption and photoluminescence emission.**

For the polymer PTFB, excitation at the wavelength of 400 nm, gives rise to only one intense emission band with first shoulder at about 694 nm and a vibronic peak at 717 nm. Excitation at wavelength of 500 nm has given similar photoluminescence spectrum (not presented here), showing that the photoluminescence spectra do not depend on the excitation wavelength, which may imply some initial relaxation process prior to radiative relaxation to the ground state as suggested by Gieseking and coworkers[64]. They have also suggested that such internal relaxation mechanism should exist in all investigated molecules containing benzothiadiazole units[64].

For the first absorption band corresponding to the π–π* transition band of the electron-donating segment (bithiophene-fluorene), it has been reported in the literature by Jian Pei and coworkers[65] for conjugated polymer based on thiophene-fluorene to be give an emission band in photoluminescence covering the region of 450 nm to 600 nm. We can then observe quenching of luminescence of the π–π* transition band of the electron-donating segment (bithiophene-fluorene) in the region between 450 to 600 nm. This region also corresponds to the region of strong absorption band of the intramolecular charge transfer ICT complex. Therefore, the emission spectrum of π–π* transition band of the electron-donating segment may then overlapped with the intense internal charge transfer complex absorption band between the electron-donating segment and the electron withdrawing segment, thus the observed quenching effect. Therefore the Forster-type energy transfer between the two energy states is a plausible scenario.

In a paper by Buckley and coworkers[66] dedicated to the study of the energy transfer dynamics in alternating polyfluorene-benzothiadiazole based polymer, the same photoluminescence quenching is also observed. This phenomenon was explained as a manifestation of a Förster type energy transfer. The argument is consolidated with the spectral overlap of the donor emission band of π–π* transition of the fluorene, and the absorption band of the acceptor benzothiadiazole units.

On the other hand, recent study of the photoluminescence properties of donor-acceptor polymer based on carbazole-thiophene and benzothiadiazole PCDTBT[67,68] have also showed similar results. However, in these two papers, they explained that the quenching of photoluminescence emission observed for the π–π* transition band can be related to an intramolecular charge transfer ICT between carbazole-dithiophene unit and the benzothiadiazole unit[67,68] in the polymer backbone. Furthermore, the intense emission band at 700 nm region shows a large Stokes shift of 157 nm. This result and has been observed in other D-A polymers based on benzothiadiazole[69,70,71] and has been mostly attributed to internal charge transfer complex emission band.

The poly( thiophene-fluorene-fluorenone) PTFF, the analog of poly (thiophene-fluorene-benzothiadiazole) PTFB, was studied in photoluminescence emission under the same condition.

The normalized photoluminescence spectra of the D-A copolymer PTFF in chloroform is shown in Figure 130 and the optical properties listed in Table 39.

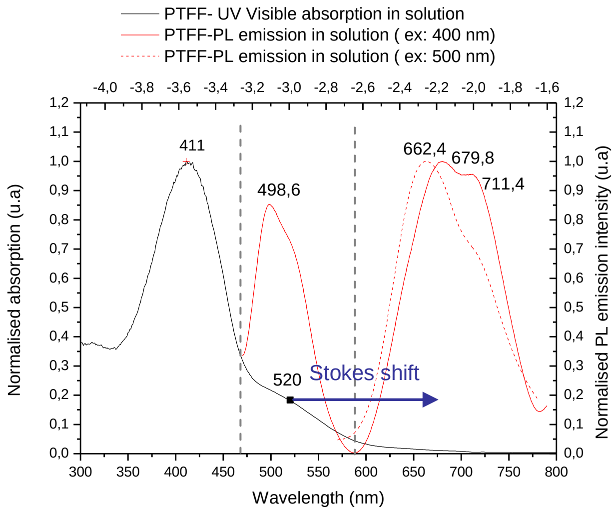


**Figure 130: UV-Visible absorption and photoluminescence spectra in chloroform of PTFF at excitation wavelength of 400 nm (straight lines) and at excitation wavelength 500 nm (dashed lines).**

| | Absorption λmax1/nm | Emission λ ex = 400 nm | Stokes shift/nm | Emission λ ex = 500 nm | Stokes shift/nm |
|---|---|---|---|---|---|
| PTFF | 411 | 499 | 88 | - | - |
| | 520 (weak) | 680 ;711 (vib) | 160 | 662; 711 (vib) | 142 |

**Table 39:Optical properties of the polymers PTFF in UV-Visible absorption and photoluminescence emission at two excitation wavelength (λex) of 400 nm and 500 nm. Vib=vibronic**

For the polymer PTFF when we fixed the excitation wavelength at 400 nm corresponding to the π–π* transition (fluorene-bithiophene), we observed apparition of two peaks at 499 nm and another emission peak at 680 nm. When the polymer is then excited at 500 nm, we observed only one emission band at 662 nm. The photoluminescence spectra is therefore dependent on the excitation wavelength contrary to the case observed in benzothiadiazole based polymers.

For the polymer PTFF, at excitation wavelength of 400 nm, the observed first emission band at 499 nm which correspond to a Stokes shift of 88 nm can be attributed to weak emission band of the π–π* transition (fluorene-bithiophene segment) as it is partially overlapped with the internal charge transfer complex absorption band. The second intense emission band at 680 nm which corresponds to large Stokes shift of 171 nm, can be attributed to the emission of intramolecular charge transfer ICT band. Furthermore, when we excited the polymer at the wavelength of 500 nm, corresponding to the weak shoulder of internal charge transfer complex of the PTFF, the energy was reemitted giving similar broad peak as polymer PTFB with its maximum wavelength at 662 nm with a Stokes shift of 153 nm.

In a paper by X. Gong and coworkers[72] who studied polyfluorene systems with fluorenone defects in the polymer backbone, they have observed similar results with apparition of two emission bands. They have attributed the first emission band at small wavelength region to the π–π* of fluorene and the second intense band at high wavelength region is attributed to the Forster energy resonance band with a charge transfer process. The results for the polymer PTFF have also shown similar spectra reported by Jaramillo and coworkers[73] for oligomers based on thiophene-fluorene-fluorenone. However, Jaramillo attributed the second emission band at high wavelength region to be the emission band of the n-π* of fluorenone. These results demonstrate that in copolymers containing fluorenone units, when the fluorene unit is excited only a partial transfer of excitation to the fluorenone emitter can be observed and both chromophoric units emit. When the fluorenone unit is excited through the ICT band, no emission from fluorene unit can be detected.

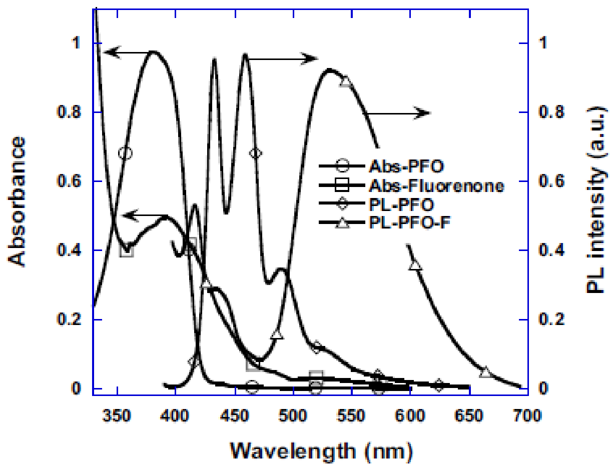


**Figure 131: Normalised thin film absorption spectra of polydioctylfluorene PFO, fluorenone and photoluminescence spectra of PFO and PFO-F (1% of fluorenone in the chain) (published by X. Gong and coworkers[72])**

From these photoluminescence studies, we have demonstrated the presence of intramolecular charge transfer state in both D-A polymers poly(thiophene-fluorene-benzothiadiazole) PTFB and poly(thiophene-fluorene-fluorenone) PTFF. However the two copolymers behave in a different manner. Upon irradiation in PTFB it seems that the fluorene unit transfers totally its excitation to the BTD emitter whereas in PTFF the transfer of excitation is only partial leading to two emission peaks in the visible region. Further investigations using time resolved spectroscopy could help us to determine precisely the transfer energy pathways in those macromolecular systems.

### V.3.2. Energy and charge transfer in blends of D-A polymers and fullerenes PCBM

In perspective for application in photovoltaic cells, we further investigate the efficiency of the photo-induced intermolecular charge transfer between the D-A polymers as donor materials and the fullerene PCBMC60 as acceptor, via photoluminescence measurements[55].

Thin films of the blends of PTFB: PCBM (1:1) and PTFF: PCBM (1:1) were prepared by spin-coating blend solutions in chlorobenzene with a concentration of 10mg/ml for each material Polymer: fullerene (10 mg/ml: 10 mg/ml) on glass substrates. The photoluminescence spectra of the blends are shown in Figure 132 as well as the photoluminescence spectra of the corresponding pristine donor polymers.

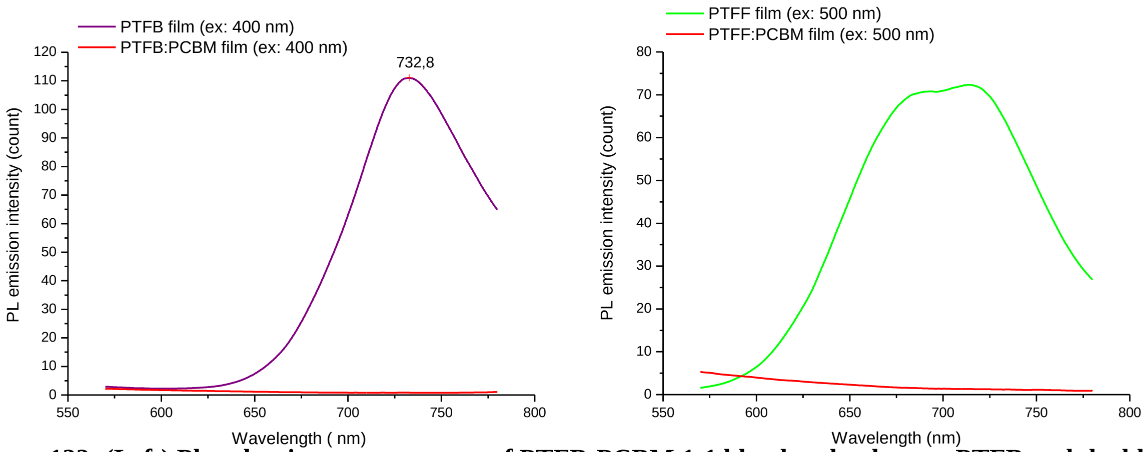


**Figure 132: (Left) Photoluminescence spectra of PTFB:PCBM 1:1 blend and polymers PTFB and the blend PTFB: PCBM (left) and polymer PTFF and PTFB**

For both of the polymers PTFB and PTFF, we observed complete quenching of the emissions when combined with the strong acceptor material PCBMC60 with a ratio of 1:1 for each blend. The quenching effect can be attributed to the photo-induced charge transfer process between the donor polymers to the fullerene acceptor[55]. This could be considered as evidence that the PCBM molecule is well dissolved in the polymer matrix.

From this latter photoluminescence study, we can observe the quenching of luminescence attributed to an intermolecular charge transfer process between donor D-A polymers and the acceptor PCBM. However we can not further conclude on the presence of free charges in the systems. To further demonstrate that photo-induced charge transfer occurs, we decided to use electronic paramagnetic resonance (EPR) spectroscopy.

## V.4. Electronic paramagnetic resonance spectroscopy

Evidence of the photo-induced charge transfer process can be well elucidated by electronic paramagnetic resonance (EPR) spectroscopy performed under light irradiation[55,74]. Actually, if charge transfer process occurs between the conducting donor polymer and the acceptor PCBM (A), this leads to the formation of the two free radicals $D^{+\bullet}$ and $A^{-\bullet}$ , which are easily observable by EPR therefore their main magnetic, relaxation and dynamic properties can be determined.

For the EPR study we have used the polymer PTFB as our model system as we have observed intense internal charge transfer band as compared to the polymer PTFF. We hope therefore that the signals will be more intense in this case. The polymer PTFB is investigated in pristine thin film and in blend with PCBM at a ratio of PTFB: PCBM 1:1.

### V.4.1. EPR analysis of pristine polymer PTFB

The EPR spectrum of pristine polymer PTFB is first recorded at room temperature without illumination, then under illumination. The experimental EPR spectra are shown in Figure 133.

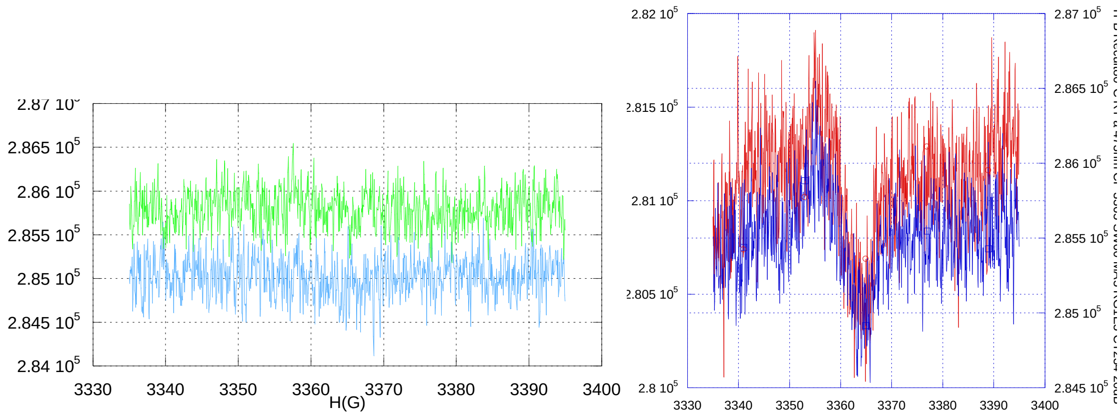

**Figure 133: (Left) EPR spectra of pristine polymer PTFB in dark at room temperature at 10 dB (light blue line) and at 20 dB (light green line). (Right) EPR spectra of pristine polymer PTFB under illumination at room temperature at 10 dB (red line) and at 20 dB (blue line) .The signals are all saturated at 10 dB.**

From the EPR spectra in dark of the polymer PTFB, no visible paramagnetic signal can be observed. The sample PTFB is then observed at room temperature under illumination at 473 nm, we observed apparition of a signal marking a presence of paramagnetic species. Simulation of the observed EPR spectrum reveals the presence of a single line (as shown in Figure 134) of g-landé factor equal to 2.00611 and a linewidth of Hpp= 6.556 G .

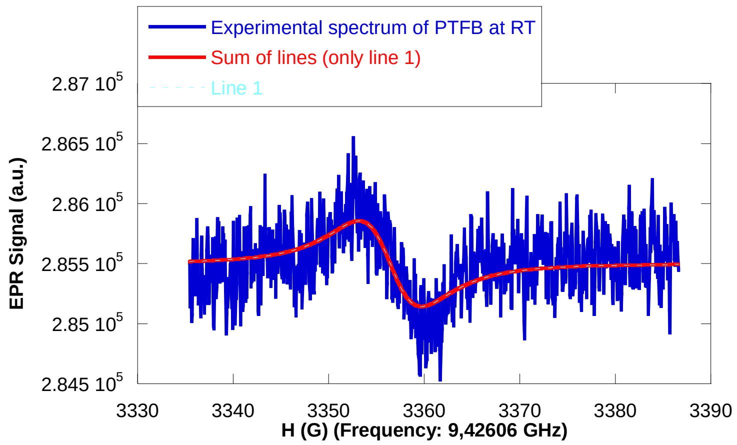


**Figure 134: EPR signal of polymer PTFB at room temperature under illumination at 473 nm (blue). The light blue line represents the simulated curve of the EPR signal. The red line represent the sum of simulated line.**

This line is noted as Line 1 corresponding to the EPR signal of pristine polymer at room temperature under illumination.

| Sample | EPR Signal | Linewidth Hpp (G) | g-factor | Intensity (%) | Intensity (%) |
|---|---|---|---|---|---|
| PTFB at RT under illumination at 473 nm | Line 1 | 6.556 | 2.00611 | 100 % | 100 % |

**Table 40: EPR parameters acquired from data simulation of pristine polymer film at room temperature under illumination at a wavelength of 473 nm**

By comparing the EPR spectra of the pristine polymer in dark and under illumination, we can clearly observe the presence of paramagnetic species. This paramagnetic species can be at first assumption coming from the intramolecular charge transfer occurred in the polymer. However further EPR experiments need to be conducted before we can really support this hypothesis.

### V.4.2. EPR analysis of polymer PTFB:PCBM blend

We then performed the EPR analysis of the polymer PTFB: PCBM blend at room temperature first in dark, then under illumination at 473 nm. The EPR spectra are recorded as shown in Figure 135.

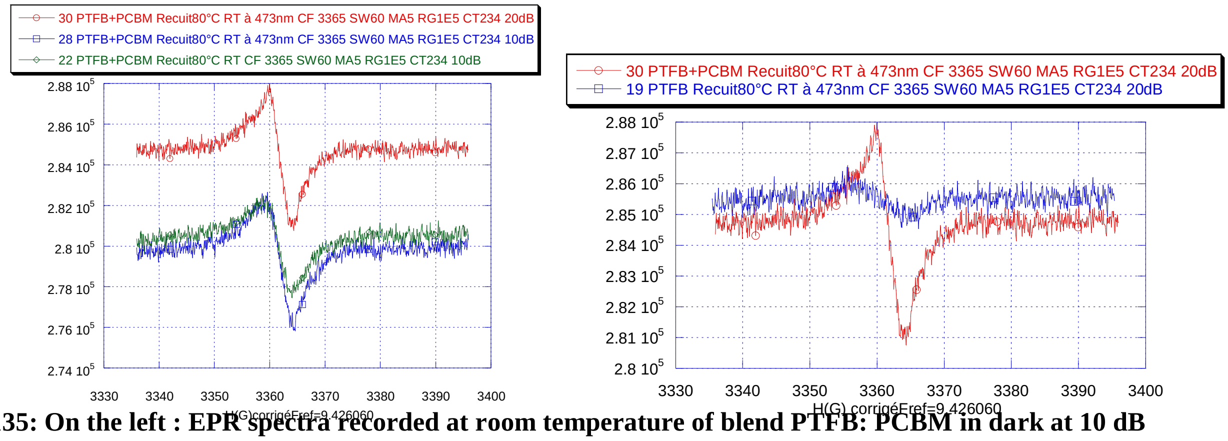


**Figure 135: On the left : EPR spectra recorded at room temperature of blend PTFB: PCBM in dark at 10 dB (green line) and of PTFB: PCBM blend under illumination (473 nm) at 10 dB (blue line) and at 20 dB (red line). On the right : EPR spectra recorded at room temperature and 20 dB of the polymer film under illumination at 473 nm and of the blend PTFB: PCBM film under illumination at 473 nm**

Contrary to what was observed for PTFB alone, the blend PTFB: PCBM at room temperature exhibits a signal in dark. Under illumination at room temperature, a signal is observed for the blend, as it was the case for the PTFB alone. The signal of the blend under illumination is higher than that in the dark of higher intensity than that observed in the dark. If we compare the EPR spectra of the pure polymer PTFB and of the blend PTFB:PCBM under illumination (we stress that intensities cannot be compared because the amount of PTFB is not the same in the sample of pure polymer and in that of the blend) as shown in Figure 135, it seems that a new line is present in the blend. This observation is confirmed by the simulation of the spectrum of the blend, which reveals the presence of two lines the line 1,observed in the pure polymer, and the line 2 ( see Figure 136). EPR parameters of the two lines are presented in Table 41.

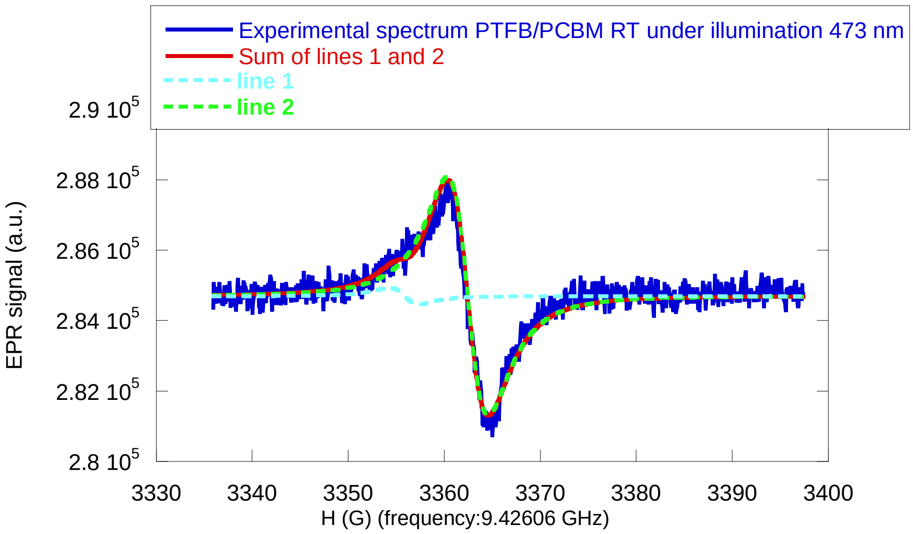


**Figure 136: EPR experimental spectrum of the blend PTFB:PCBM at room temperature under illumination at 473 nm ( blue line). Line 1 (light blue line) and line 2 (green) are simulated lines, and the red line are a combination of the two lines**

| Sample | EPR Signal | Linewidth Hpp (G) | g-factor | Intensity (%) |
|---|---|---|---|---|
| PTFB:PCBM at room temperature under 473 nm illumination | Line 1 | 6.546 | 2.00611 | 2 % |
| | Line 2 | 4.01 | 2.00253 | 98 % |

**Table 41: EPR parameters acquired from data simulation of PTFB:PCBM at room temperature under illumination at 473 nm**

The EPR spectrum of the blend PTFB: PCBM under illumination at room temperature is composed of a strong signal ( of 97% intensity, Line 2) with a g-factor value of 2.00253 and a linewidth Hpp of 4.264 G. and of a  weak signal of 2 % similar to the signal found in the pristine polymer with a g-factor of 2.00611 and a linewidth of 6.56 G At this point, we can already assume that the strong signal can be ascribed to the PTFB$^{+°}$ radical (at RT the radical of the PCBM cannot be observed because of its relaxation time) while the line with a very different g factor can be ascribed to photo induced paramagnetic impurities present in the polymer.

In order to confirm these assumptions, we have observed the blend at 20K: actually at this temperature, if our assumption is correct, the PCBM$^{-°}$ radical should appear. The experimental EPR spectra of the blend at 20 K in dark and under illumination are presented in Figure 137. This figure also presents the simulation of the EPR spectrum of the blend recorded at 20K under illumination at 473 nm.

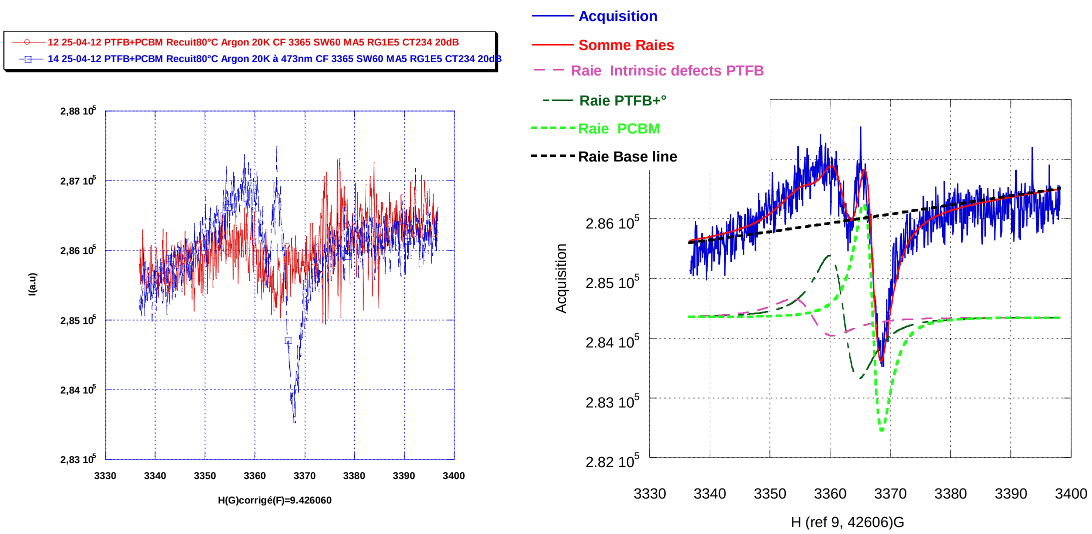


**Figure 137: (Left) EPR experimental spectra of the blend PTFB:PCBM observed at 20 K in dark ( red line) and under illumination at 473 nm (blue line). (Right) EPR spectrum of the blend PTFB: PCBM in blue line presented with  4 different simulated signal lines.  The sum of the 4 lines ( in red) showed perfect adequation with the EPR spectrum**

The recorded EPR spectrum of the sample PTFB: PCBM at 20 K under illumination shows apparition of new signals with a lower g-factor. The EPR spectrum of the sample PTFB: PCBM under illumination at 20 K is simulated as the sum of 3 different lines with a fourth line corresponding to the baseline as presented in Table  42.

| Sample | EPR Signal | Linewidth Hpp (G) | g-factor | Intensity (%) |
|---|---|---|---|---|
| PTFB:PCBM at 20 K under illumination ( 473 nm) | Line 1 | 6.546 | 2.00572 | 24 % |
| | Line 2 | 4.925 | 2.00253 | 45 % |
| | Line 3 | 3.003 | 1.99979 | 31 % |
| | Line 4 ( Baseline) | - | - | 0 |

**Table 42: EPR parameters acquired from data simulation of the blend PTFB:PCBM at 20 K under illumination at 473 nm**

The first line, similar to the line 1 found in all samples in pure polymer under illumination at room temperature and in the blend PTFB: PCBM in dark and under illumination at 20 K is attributed to photo induced paramagnetic species. Taking into account its spin signature of g-factor value of 2.00572-2.00646, this signal is likely due to metallic impurities probably due to traces of catalysts and (or) metal salts[75,76].

The second line with an intensity of 45 %, showed a g-factor value of 2.00253 and a linewidth of 4.925. This line 2 has already been observed in the blend PTFB: PCBM under illumination both at room temperature and at low temperature at 20 K. This signal can therefore be ascribed either to the polymer PTFB or to the fullerene PCBM. Since the relaxation time of the PCBM anion radical does not allow to observe it at RT, this line 2 is ascribed to the cation radical of PTFB. In addition, the value of its g factor is very close to the values obtained for the positive polaron $P^{+\bullet}$ of the poly(3-hexyl-thiophene) which is found at 2.00237[76,77]. Moreover, in a review dedicated to the electron paramagnetic values for conjugated polymers published in 2000 by Krinichny[78], the isotropic g-factors of stable conjugated polymers with structures similar to PTFB were reported to be close to $g_e$ –factor of the free electron= 2.00232. Therefore we can ascribe this signal to the positive polaron of the polymer $PTFB^{+\bullet}$. The third line, with a g-factor value of 1.99979 and a linewidth of Hpp= 3.003, can therefore be ascribed to the negative polaron of $PCBM^{-\bullet}$. The g-factor found is in full agreement with that reported in the literature[79,74, 63]

From these signals attribution we can therefore attribute correctly each signal to the corresponding paramagnetic species.

| Sample | EPR Signal | LinewidthHpp (G) | g-factor | Intensity (%) | Attribution of paramagnetic species |
|---|---|---|---|---|---|
| PTFB at RT illumination | Line 1 | 6.556 | 2.00611 | 100 % | Intrinsic polymer defect |
| PTFB:PCBM at room temperature under illumination ( 473 nm) | Line 1 | 6.546 | 2.00611 | 2 % | Intrinsic polymer defect |
| | Line 2 | 4.01 | 2.00253 | 98 % | Polymer $PTFB^{+\bullet}$ |
| PTFB:PCBM at 20 K under illumination ( 473 nm) | Line 1 | 6.546 | 2.00572 | 24 % | Intrinsic polymer defect |
| | Line 2 | 4.925 | 2.00253 | 45 % | Polymer $PTFB^{+\bullet}$ |
| | Line 3 | 3.003 | 1.99979 | 31 % | $PCBM^{-\bullet}$ |
| | Line 4 | - | - | 0 | Baseline |

**Table 43: EPR parameters and proposed attribution of each signal of the polymer PTFB at room temperature under illumination at the wavelength of 473 nm and the blend PTFB: PCBM (1:1) under illumination at room temperature and at 20 K.**

The pristine polymer PTFB under illumination at room temperature showed the presence of only one signal Line 1 which has been ascribed to the intrinsic polymer defect of metallic nature. We have therefore not observed any signal of free charge formation in the pristine polymer.

The blend polymer PTFB: PCBM (1:1) at room temperature under illumination showed the presence of two signals ascribed to the positive polaron of the polymer $PTFB^{+\bullet}$ and a weak signal coming from the intrinsic polymer defect. The paramagnetic signal of PCBM was not be detected at this temperature.

The blend polymer PTFB: PCBM (1:1) at low temperature 20 K showed the presence of 3 signals marking the presence of the signal of the negative polaron of the fullerene $PCBM^{-\bullet}$. A higher intensity signal of the positive polaron of the polymer $PTFB^{+\bullet}$ is observed as well as the signal of the intrinsic defect.

### V.4.3. Conclusion

The EPR study has allowed us to demonstrate the photo-induced charge transfer processes between the polymer PTFB and the acceptor fullerene PCBM. Therefore in the blend of our polymer donor with the acceptor materials PCBM, we can conclude that, at the molecular scale, charge transfert can occur between PTFB and PCBM, which is the first required step for their application in photovoltaic cells.

The EPR study on the pure D-A polymer PTFB has not provided a clear evidence of intramolecular charge transfer processes. This transient charge transfer occurred in ultra-fast dynamics of femto-second scale[60,62,80] then relaxed to its ground state and can be observed by other method for example transient absorption spectroscopy[61] It is to stress that the EPR analysis allow characterizing the final state of an electronic transfer mechanism, of long lived radical species with lifetimes exceeding 10 ms and with a greater sensitivity for species having lifetimes exceeding milliseconds[81]. However a recent study in the laboratory on other examples of D-A polymers have shown evidence of this transient charge transfer. The trace transient transfers were observed when free radicals are trapped during the process.

The EPR study has also provided us additional information on the presence of traces of metallic impurities in the 'pure' polymer, most probably of the palladium catalysts, or metallic salts not detected by routine polymer characterization method. It is noteworthy that the presence of these defects is detrimental for the generation of current because the defects can act as traps for the charges in the bulk hetero-junction devices[82,83]. Therefore, future work in synthesis of polymers or oligomers should take into account tedious purification of the final material in order to increase cell performance.

# VI. Charge carrier transport properties

We have demonstrated in the previous topic that our polymers are suitable donor materials for photovoltaic cells and can generate free charges carriers under illumination when they are combined with the suitable acceptor. In such macromolecules, it is also of importance to quantify the transport properties and in particular the mobility of the holes in the materials. Therefore we have conducted transport study for our polymers by using field-effect transistor measurement using polymer PTFB and PTFF as active materials in the channel and the results are shown in Figure 98.

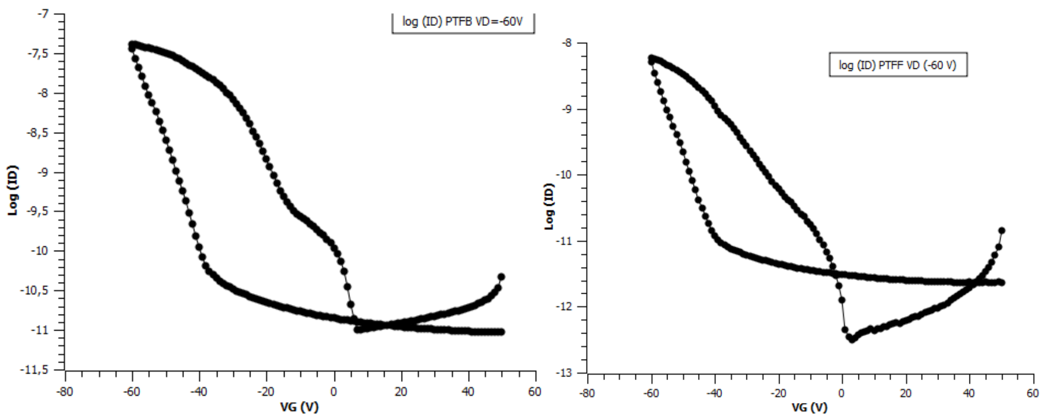


**Figure 138: Transfer characteristic curves of log $I_{DS}$= f($V_G$) for $V_D$=-60V measured for thin films of polymers PTFB and PTFF with channel length of 10 µm, The $V_{DS}$ was kept at −60 V, and the $V_G$ bias was swept from +60V to -60 V and reverse to +60 V again.**

Both polymers showed p-type characteristics in negative bias, typical from p-type semiconductors. In this saturation regime, the values for the mobility (μ), short circuit current Ioff (leakage current Ioff = $I_D(V_D = 0$ V, Vg = 0V)) and the ratio Ion/Ioff can be calculated from the slopes of the of $\sqrt{I_{DS}} = f(V_G)$ (in pink line). For polymer PTFB two slopes were observed in the forward bias and we have chosen to take in account the first linear slopes for the calculation of transport properties. The values are presented in Table 44.

| Polymer | μ (cm². $V^{-1}$. $s^{-1}$) | $V_{Threshold}$ (V) | Ioff | Ion/Ioff |
|---|---|---|---|---|
| PTFB | 4.36 $10^{-5}$ | -12.7 | -2.89 $10^{-12}$ | 14100 |
| PTFF | 5.76 $10^{-6}$ | -13.6 | -4.98 $10^{-13}$ | 1760 |

**Table 44: Transport properties at saturation regime of VDS= -60 V for the polymer PTFB and PTFF**

We obtained mobility value of the polymer PTFB almost 10-fold higher than the mobility of the polymer PTFF i.e 4.36 $10^{-5}$ and 5.76 $10^{-6}$ cm². $V^{-1}$. $s^{-1}$ respectively. The polymer PTFB also afford high ratio of Ion/Ioff is observed for the polymer PTFB with a value of 14100 compared to 1760 for the polymer PTFB. Based on this results we can conclude that the polymer PTFB affords higher hole mobility than the polymer PTFF.

Our fluorene-based polymers exhibit rather low hole mobilities values compared to other reported high mobilites low band gap polymers in the literature which have achieved high performance in photovoltaics. ($\mu > 10^{-4}$ cm².$V^{-1}$. $s^{-1}$)[84,85]. However they are much higher compared to the hole mobilities of previous thiophene based polymer PQTB (1.00 $10^{-5}$ cm².$V^{-1}$. $s^{-1}$) and PQTF (6.10 $10^{-8}$ cm². $V^{-1}$. $s^{-1}$). It should be underlined that these results should be considered as preliminary since no optimization in the fabrication of the devices and no treatment of the gate oxide were undertaken yet. However all the experiments have been realised under the same conditions and allow a direct comparison of the materials.

## VII. Photovoltaic properties of PTFB, PTFF and PTFBF

The photovoltaic devices were prepared using the polymers PTFB, PTFF and PTFBF. For all the polymers, we decided to use the chloroform fractions for the preparation of the active layers, in combination with PCBM C60 or PCBMC70. The solvent used for the dissolution of the active materials was mostly chlorobenzene unless stated otherwise. The blend solutions were stirred at 70 °C overnight before device fabrication for complete dissolution. For all these series of polymers, the active layers were spin-coated from solutions at a speed rate of 1200 rpm/s for 40 s with acceleration at 350 rpm/s.

## VII.1. Photovoltaic devices based on polymer poly(thiophene-fluorene-benzothiadiazole) PTFB

In order to obtain good performances for the solar cells using PTFB, the choice of acceptors is of a crucial importance. We have performed preliminary investigations of spectroscopy UV-visible absorption of fullerenes derivatives in combination with the polymer PTFB to highlight the contribution of the acceptors in absorbing photons. Three fullerene acceptors were investigated; PCBMC60, PCBMC70 and bisPCBMC60. The weight concentrations for the blends PTFB:PCBMx are fixed at 10 mg/ml: 10 mg/ml. The absorption spectra of each blend film are presented without normalization for better comparison as shown in Figure 139.

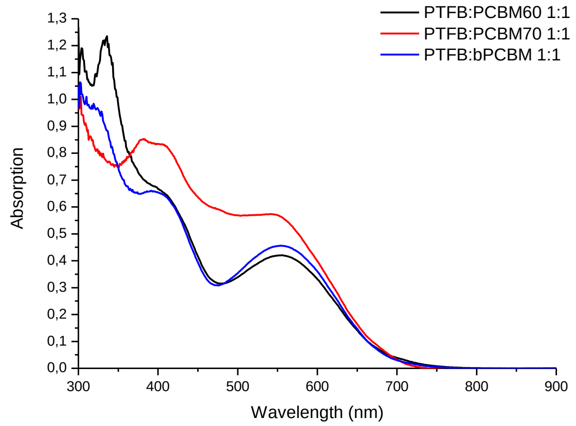


**Figure 139: UV-Visible absorption spectrum of the thin films of the blend PTFB: PCBMs**

The absorption spectra of PTFB: PCBMC70 showed broader and higher degree of absorptions than the other fullerenes. PCBMC60 and bisPCBMC60 showed similar absorption spectra with slightly lower absorption for PTFB:bisPCBMC60. For our photovoltaic devices, we are going to limit our investigations only to PCBMC60 and PCBMC70 as they showed good photon absorption properties. Besides the use of bis adduct fullerenes is known to impact negatively the current density of the solar cells[86].

### Study on cell performance of PTFB: PCBMC60

We have tested our polymer with the fullerene PCBMC60. The performances of the photovoltaic devices are summarized in Table 45.

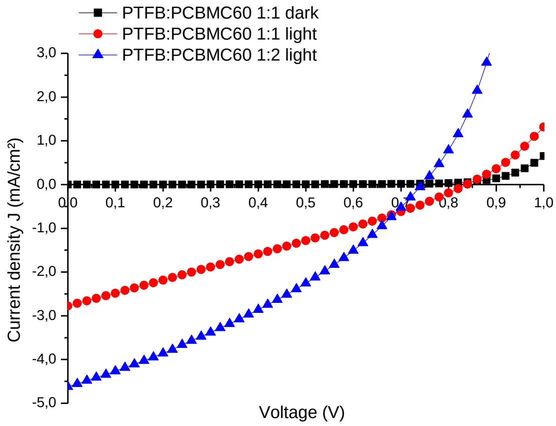


**Figure 140: I-V curves of PTFB: PCBMC60 UV-visible absorption of the blend PTFB:PCBMC60 in thin films with the ratios 1:1 and 1:2**

| Donor | Acceptor | Blend ratio (D:A) | Voc (V) | Jsc (mAcm-²) | FF | PCE (%) |
|---|---|---|---|---|---|---|
| PTFB | PCBM60 | 1 :1 | 0.84 | 2.78 | 0.28 | 0.65 |
| PTFB | PCBM60 | 1 :2 | 0.74 | 4.62 | 0.34 | 1.16 |

**Table 45: Photovoltaic cells parameters of PTFB: PCBMC60**

The polymer PTFB when combined with PCBMC60 at the same weight ratio showed a high open circuit voltage of 0.84 V but a low current density of 2.78 $mA.cm^{-2}$. However, by adding two equivalent of PCBM to 1 equivalent of polymer PTFB (67% content of PCBM), the short current density almost doubled with a value of 4.62 mA $cm^{-2}$. The increasing current density can be attributed to the increasing absorption as shown in Figure 141 and a better phase segregation of the two materials can also be hypothesized.

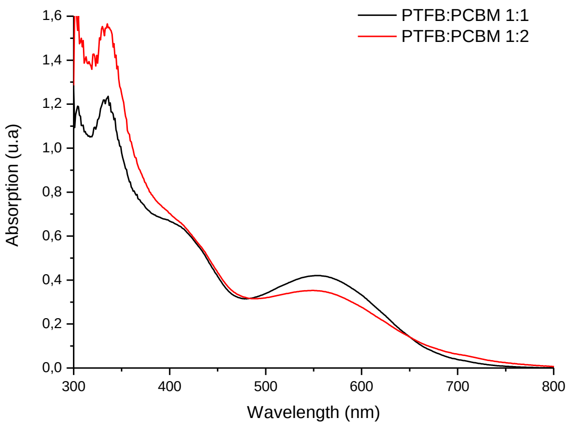


**Figure 141: UV-visible absorption of the blend PTFB:PCBMC60 in thin films with the ratios 1:1 and 1:2**

However the open circuit voltage was found to be decreasing with the amount of PCBMC60, although the difference of $HOMO_{Donor\ (PTFB)}$ and $LUMO_{Acceptor\ (PCBM)}$ is the same here. Other factors such as electronic coupling between fullerene/fullerene and polymer/fullerene are known to influence the open circuit voltage[87]. We have not fully optimized the ratios of polymer PTFB:

PCBM, but have continued the study by changing to another fullerene derivative PCBMC70 hoping better results thanks to its wider absorption domain. The results will be described further.

### Impact of molecular weight on photovoltaic performance

To allow comparison of the polymers PTFB-I and the polymer PTFB-Br which differ in their molecular weights (Mn 3.96 kDa and 5.94 kDa respectively), photovoltaic devices based on these polymers were fabricated under the same conditions and their performances were evaluated. The polymers were mixed with PCBMC60 at ratio of 1:2. The photovoltaic parameters of the devices are reported in Table 46.

| Donor | Molecular weight (kDa) | Acceptor | Blend ratio (D:A) | Voc (V) | Jsc (mAcm-²) | FF | PCE (%) |
|---|---|---|---|---|---|---|---|
| PTFB-Br | 5.64 | PCBM60 | 1 :2 | 0.74 | 4.62 | 0.34 | 1.16 |
| PTFB-I | 3.96 | PCBM60 | 1 :2 | 0.62 | 3.12 | 0.28 | 0.54 |

**Table 46: Photovoltaic parameters of the polymer PTFB at different molecular weight**

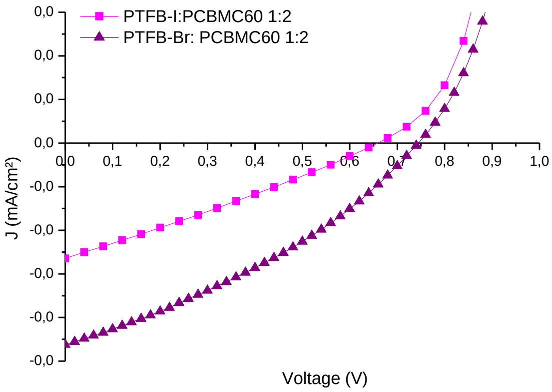


**Figure 142: I-V curves of photovoltaic device based on low molecular weight PTFB-I: PCBM and higher molecular weight PTFB-Br: PCBM**

The photovoltaic device based on the blend PTFB-I:PCBMC60 at a ratio of 1:2, gives an open circuit voltage of 0.62 V, a moderate short current density of 3.12 mA $cm^{-2}$ and fill factor of 28 %, giving an overall low power efficiency of 0.54 % (Figure 142). The polymer PTFB-Br showed improved performance in terms of Jsc, Voc and FF with the best power conversion efficiency of 1.16 % for solar cells with the same ratio of PTFB: PCBMC60 1:2. The results obtained for these two polymers showed that improved power conversion efficiency can be obtained with higher molecular weight polymers. The use of higher molecular weight fractions results in an increase of the short current density and an improvement of the fill factor of the device. The results are consistent with the ones already reported in literature for other low band gap polymers. Indeed longer polymer chains can help to improve the charge transport properties of the materials, resulting in an augmentation of the current densities delivered by the cells[88].

**Study of cell performances of PTFB: PCBMC70**

In order to improve the power conversion efficiency we decided to fabricate photovoltaic devices employing the acceptor PCBMC70 which is the analog of PCBMC60 showing improved absorption properties in the visible rang as demonstrated from a preliminary UV-visible absorption measurement for the blends PTFB: PCBMC60 and PTFB:PCBMC70 presented in Figure 143.

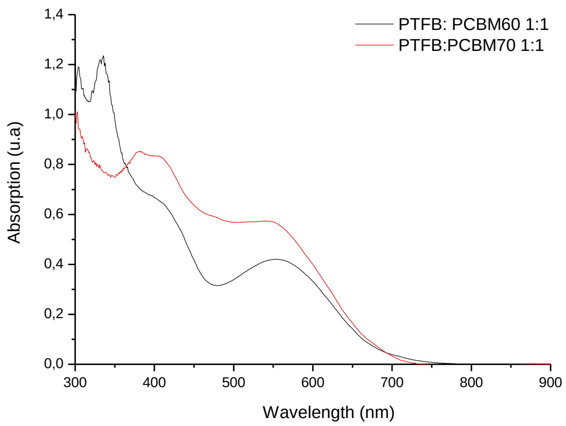


**Figure 143 : UV-Visible absorption spectra of the blend polymer PTFB: PCBMC60 (1:1) and the blend polymer PTFB: PCBMC70 (1:1) in thin films prepared from a solution in chlorobenzene of 20 mg/ml for each material**

The ratios of PTFB: PCBMC70 are varied from 1:1 to 1:4. The photovoltaic cells results are presented in the Table 47.

| Donor (Polymer) | Acceptor | Blend ratio (D:A) | Voc (V) | Jsc (mAcm-²) | FF | PCE (%) |
|---|---|---|---|---|---|---|
| PTFB-Br | PCBMC70 | 1 :1 | 0.85 | 3.44 | 0.28 | 0.81 |
| PTFB-Br | PCBMC70 | 1 :2 | 0.79 | 6.60 | 0.33 | 1.73 |
| PTFB-Br | PCBMC70 | 1 :3 | 0.78 | 7.52 | 0.35 | 2.08 |
| PTFB-Br | PCBMC70 | 1 :3.5 | 0.79 | 6.74 | 0.34 | 1.82 |
| PTFB-Br | PCBMC70 | 1 :4 | 0.78 | 6.18 | 0.34 | 1.66 |

**Table 47: Photovoltaic parameters of PTFB:PCBMC70 with the ratios of 1:1 to 1:4**

The polymer PTFB in combination with the PCBMC70 showed very encouraging results. The best solar cell is obtained with the ratio of PTFB:PCBMC70 1:3 giving a high open circuit voltage of 0.78 V, short current density of 7.52 mA cm-² , a fill factor of 35 % with overall power conversion efficiency of 2.08 %. Higher ratios were found detrimental to the performances. In order to understand the evolution of the photovoltaic parameters in relation with the ratios of PCBMC70, curves trends are traced as follow in Figure 144:

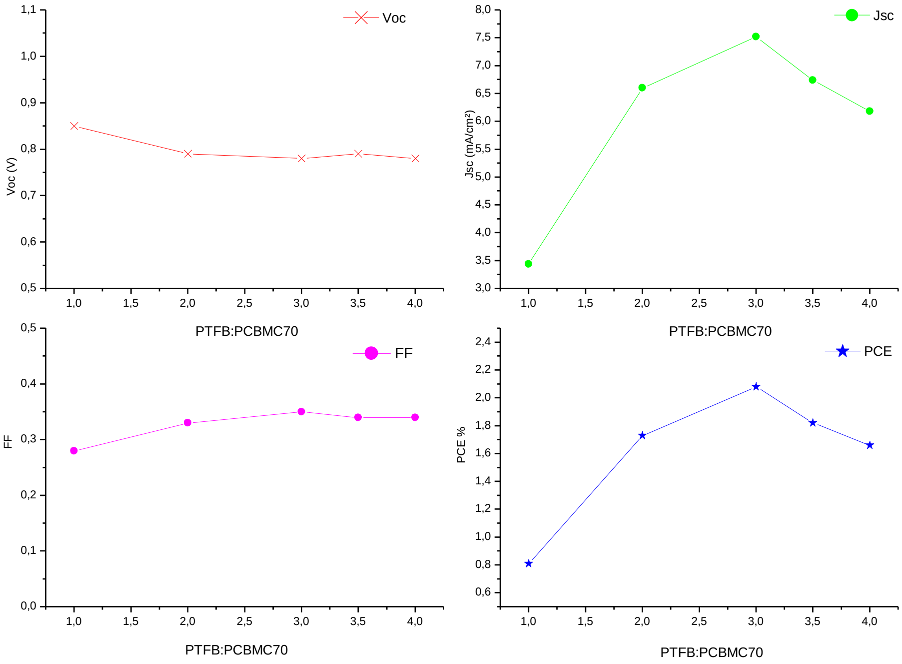


**Figure 144: Evolution of photovoltaic cells characteristics of polymer PTFB in function of the ratio of PCBMC70**

From the curves in Figure 144, we can clearly observe the effect of the amount of PCBMC70 on the current density of the cells. When increasing the PCBMC70 ratios from equivalent mass up to 3 times the weight of the polymer PTFB, the current densities delivered by the solar cells significantly increase from 3.5 mA $cm^{-2}$ up to 7.5 mA $cm^{-2}$. However the current density subsequently drop as the amount of the absorbing polymers are decreasing down to 20 % of polymer compared to 80 % of PCBM (PTFB:PCBMC70 1:4). The optimum ratio for the polymer PTFB was found to be 1:3 and this result was very reproducible. Indeed similar PCE values *i.e* 2.05% and 2.08 % were obtained for two different batches of PTFB showing quite similar molecular weights tested in devices at different time. This indicates the high reproducibility of our fabrication procedures. For all the devices we have obtained quite high open circuit voltage between 0.78 V-0.88 V. This parameter is less influenced by the PCBM ratio.

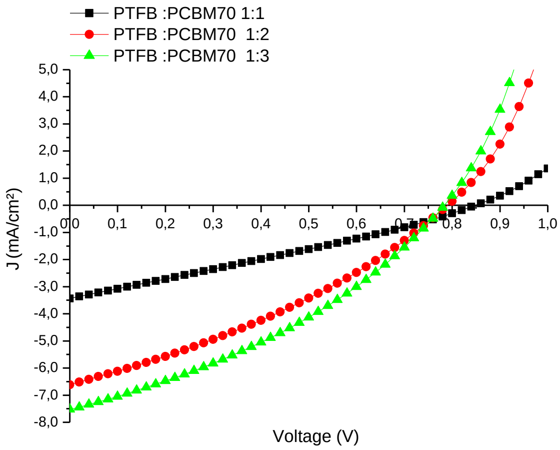


**Figure 145: Evolution of I-V curves of the photovoltaic cells of PTFB: PCBMC70 from 1:1 to 1:3**

As seen in Figure 145 we can observe significant improvement of current densities when we increase the ratio of PCBMC70 in the matrix hence increasing the power conversion efficiency. To give an explanation for the improved efficiencies in the solar cells, we tried to look at the absorption spectra of the PTFB: PCBMC70 blends (Figure 146 ) in order to see if a correlation exists between photon absorption spectra and the photo-generated currents.

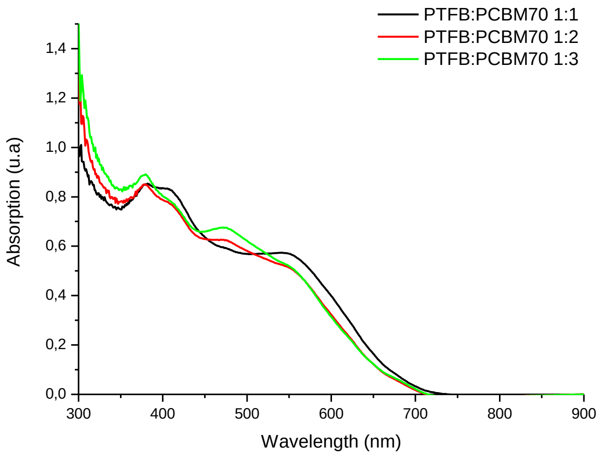


**Figure 146: Absorption spectra of the blends PTFB: PCBMC70 with the ratios of 1:1 to 1:3 in thin films with a total concentration of 40 mg/ml**

The absorption spectra of the blends films PTFB: PCBMC70 with the different ratios showed similar absorption spectra with a slightly higher absorption in the films at the ratio of 1:3. The results were further correlated with the measurements of incident photon to current efficiency IPCE spectra of the device PTFB: PCBMC70 with the ratios 1:2 and 1:3, as shown in Figure 147. The device based on the ratios of 1:3 showed improved conversion of photon to current (increase of 5%) in the region of 320 nm to 550 nm and confirmed the participation of the C70 in the photo generation of the current.

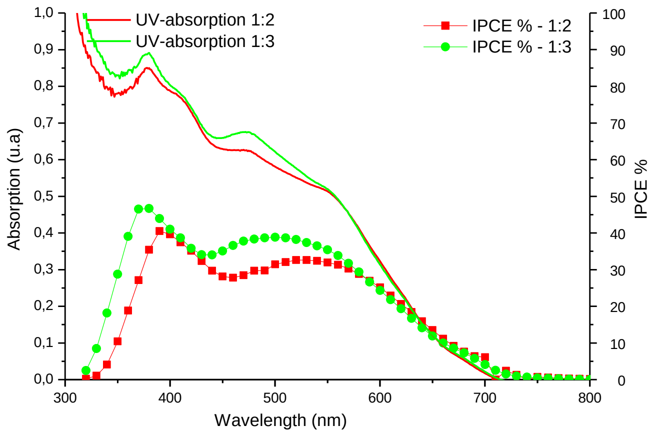


**Figure 147: Incident photon to current efficiency IPCE spectra of PTFB: PCBMC70 according to ratios superposed with the UV absorption spectra of its thin films**

It is however difficult to conclude that the improvement of the current density only originates from the better light harvesting efficiency of the active layer. The improvement of the current densities could also be related to a more favorable morphology of the blend that would lead to a better dissociation of the exciton and an improve transport of the charge carriers.

To verify this hypothesis, we further investigate the morphology of the active layers. Investigations using Atomic Force Microscopy (AFM) of the surface topology of the active layer of the tested photovoltaic cells were performed.

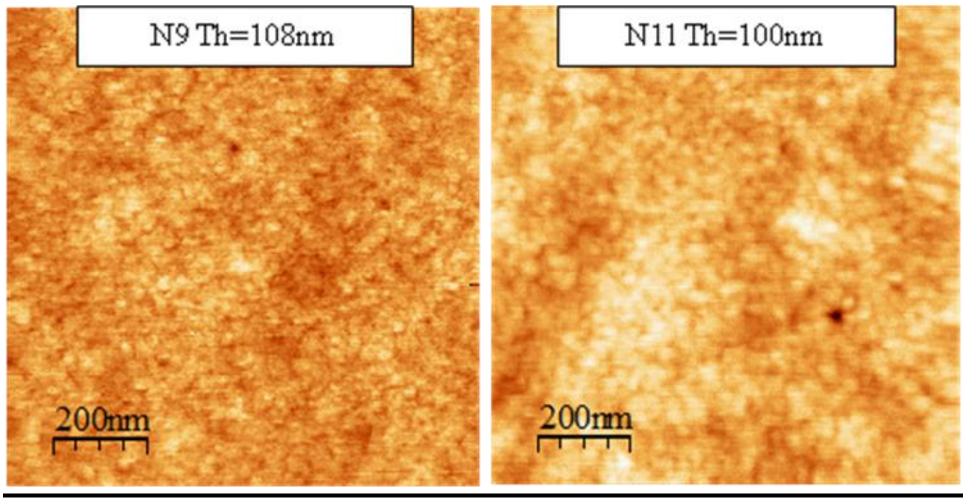


**Figure 148: AFM topographic images of the solar cells PTFB: PCBMC70 1:2 (left) and PTFB: PCBMC70 1:3 (right) with the thickness on top**

As mentioned in chapter 1, two main factors govern the ideal morphology of bulk heterojunction; firstly interpenetrating nanoscale network between donor and acceptor which enables a large interface area for exciton dissociation (10-20 nm scale)[89] and secondly the creation of continuous percolating paths for hole and electron transport to the corresponding electrodes. Both images showed homogeneous nanophase segregated network. The domains are approximately in the range of 10 to 20 nm scale for both devices. This results in a large interfacial area for efficient charge separation in both cases, hence a high short-circuit current density obtained of more than 6.6 mA $cm^{-2}$ for the two devices PTFB:PCBMC70 of the ratio 1:2 and 1:3.

## VII.2. Photovoltaic devices based on polymer Poly(thiophene-fluorene-fluorenone) PTFF

Similarly the photovoltaic devices were fabricated with polymer PTFF in combination with PCBMC60 and PCBMC70 as electron acceptor compounds. We first present the devices based on the polymer PTFF and fullerene PCBMC60 with two different ratios of 1:1 and 1:2. The current density-voltage J-V curves of the two solar cells with the photovoltaic parameters are presented in Figure 149 and in Table 48.

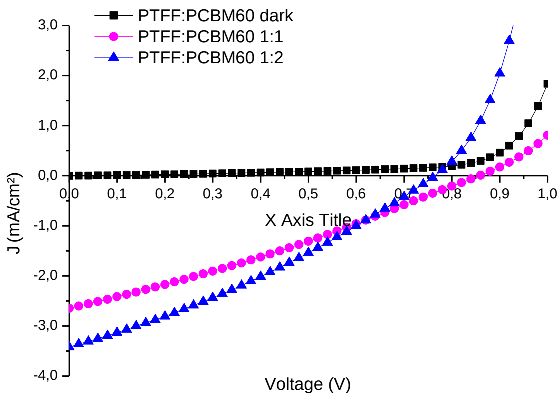


**Figure 149: I-V curves of photovoltaic cells PTFF:PCBMC60 with the ratios 1:1 and 1:2**

| Donor (Polymer) | Acceptor | Blend ratio (D:A) | Voc (V) | Jsc ($mAcm^{-2}$) | FF | PCE (%) |
|---|---|---|---|---|---|---|
| PTFF | PCBM60 | 1 :1 | 0.86 | 2.65 | 0.29 | 0.66 |
| PTFF | PCBM60 | 1 :2 | 0.76 | 3.42 | 0.31 | 0.81 |

**Table 48: Photovoltaic parameters of PTFF:PCBMC60 with increasing ratios of 1:1 to 1:2**

The photovoltaic cells based on PTFF: PCBMC60 showed high open circuit voltages Voc of 0.86 V for the ratio PTFF: PCBMC60 1:1 but the Voc decreases with two equivalents of PCBM from 0.86 V to 0.76 V. The decreasing open circuit voltage of the cells upon addition of PCBM have been also been observed with the polymer PTFB. The current density of both solar cells are relatively low, at 2.65 mA.$cm^{-2}$ at the ratio 1:1 and slightly increasing with the additional amount of two equivalents of PCBM to PTFF, at 3.42 mA.$cm^{-2}$. The best power conversion efficiency for the polymer PTFF with PCBMC60 is quite moderate with 0.81 %.

To further optimize the photovoltaic devices, we performed tests for polymer PTFF with PCBMC70 varying the amount of this molecule from 1:1 to 1:3. The J-V curves and photovoltaic parameters are presented in Figure 150 and Table 49.

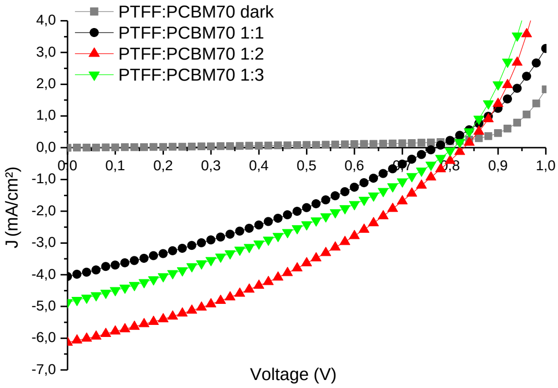


**Figure 150: J-V curves of photovoltaic devices PTFF:PCBMC70 with the ratios 1:1, 1:2, an 1:3**

| Donor (Polymer) | Acceptor | Blend ratio (D:A) | Voc (V) | Jsc (mAcm-²) | FF | PCE (%) |
|---|---|---|---|---|---|---|
| PTFF | PCBMC70 | 1 :1 | 0.76 | 3.93 | 0.30 | 0.90 |
| PTFF | PCBMC70 | 1 :1.75 | 0.85 | 5.23 | 0.37 | 1.62 |
| PTFF | PCBMC70 | 1 :2 | 0.83 | 6.13 | 0.36 | 1.82 |
| PTFF | PCBMC70 | 1 :2.25 | 0.82 | 5.28 | 0.33 | 1.42 |
| PTFF | PCBMC70 | 1 :3 | 0.77 | 5.21 | 0.30 | 1.22 |

**Table 49: Photovoltaic parameters of PTFF:PCBMC70 according to ratios**

In combination with the electron acceptor PCBMC70, PTFF based photovoltaic devices showed improved performances compared to the solar cells using PCBMC60. The highest performance is obtained with the cell with the ratio of 2 equivalent of PCBMC70, with power conversion efficiency of 1.82 %. This cell showed highest values of short-circuits current density at 6.13 $mA.cm^{-2}$, a fill factor of 36 % and open circuit voltage of 0.83 V. In order to find the optimum ratios of the blends, we further made solar cells with ratios 1:1.75 and 1: 2.25. However, we did not obtained improvement of power conversion efficiency but device performances are superior to the cells with the ratios of 1:1 and 1:3. The results obtained for the devices based on the PTFF: PCBMC70 series showed higher performances than the device based on PTFF:PCBMC60, which may originated from a higher absorption spectra of PTFF:PCBMC70 than the device based on PTFF:PCBMC60. Incident photons to current efficiency measurements are therefore performed to confirm this hypothesis.

### Comparison of photovoltaic cells PTFF:PCBMC60 and PTFF:PCBMC70

To correlate the results obtained in the photovoltaic devices with the efficiency of photon absorption to current generation we measured the incident photon to current efficiency versus wavelength of the best solar cell PTFF: PCBMC70 together with the solar cell based on PTFF: PCBMC60. The absorption spectra are also plotted on the background to allow better correlation (Figure 151).

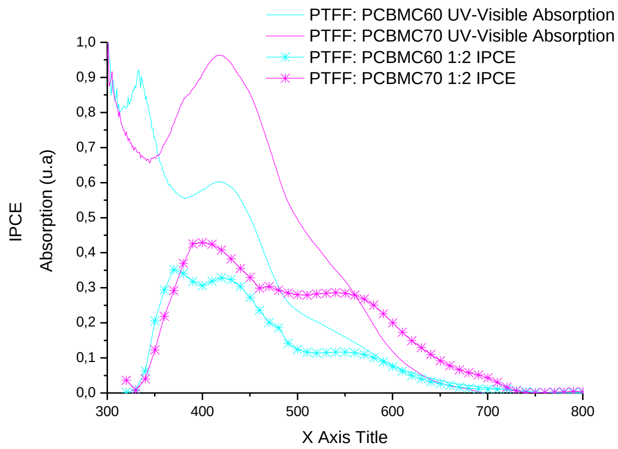


**Figure 151: Incident photon to current efficiency curves of photovoltaic cells PTFF:PCBMC60 (1:2) and PTFF:PCBMC70 (1:2) and UV-Visible absorption of thin films PTFF:PCBMC60 and PTFF:PCBMC70**

The photon to current incident efficiencies curves correspond well to its respective absorption spectra. From the IPCE experiments, it is clear that the blends with the acceptor PCBMC70 absorbed more intensely in the region 350 nm to 500 nm and showed maximum conversion to current in this region up to 45%. The blend PCBMC60 showed lower conversion in this region with highest conversion of 35%. We can also note that in the region 480 nm to 700 nm corresponding to the region of the charge transfer complex between the bithiophene-fluorene segment and the fluorenone, the photon absorbed are efficiently converted to current. These results are rather striking as the maximum absorption was found originating from the $\pi$–$\pi$* transition band. We can therefore conclude that the photon absorption originating from the presence of the fluorenone carbonyl group (located in the region 500 nm to 700 nm leads to high current conversion efficiency.

### Thermal annealing effect on device performance

Investigation on the thermal annealing effect on the device performance is conducted. We have performed thermal annealing treatment following the same procedure as the test made with the device based on our thiophene-based polymers series. We performed 5 minutes thermal annealing at 70°C on our cells but the devices showed slight decrease performance, as shown in

Figure 152. The result demonstrate that the polymer PTFF and the fullerene PCBMC70 may form spontaneously well phase segregation domain and no further annealing is required.

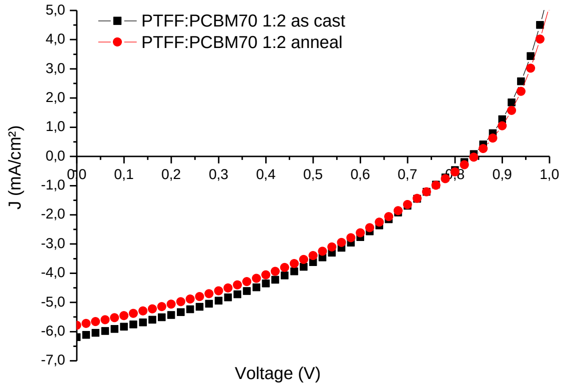


**Figure 152: I-V curves of photovoltaic cells PTFB:PCBMC70 1:2 as cast and after annealing**

To confirm this hypothesis we have conducted morphological studies are also for the three photovoltaic devices PTFF:PCBMC70 with increasing ratios from 1:1 to 1:3. AFM images of the three devices are presented in Figure 153.

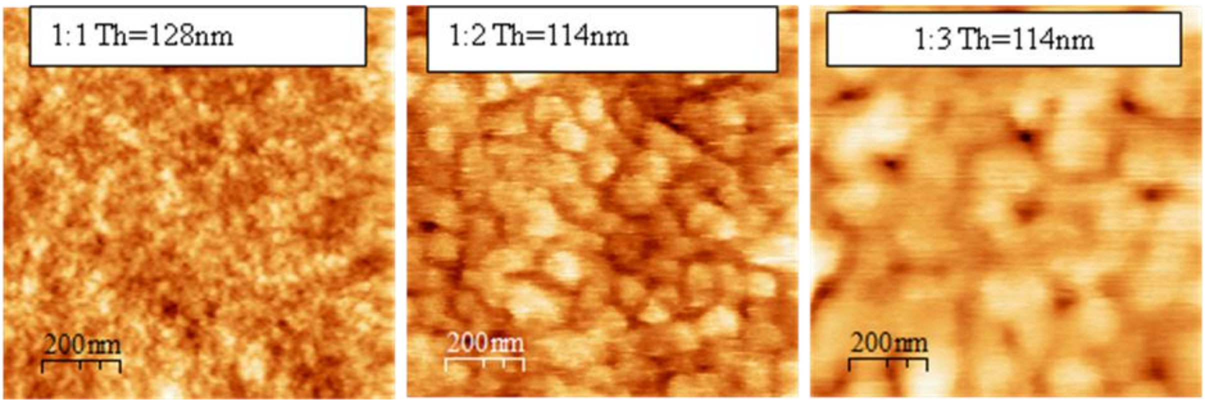


**Figure 153: Topographic AFM images of photovoltaic cells PTFF:PCBMC70 with increasing ratios of PCBM from left to right 1:1, 1:2 and 1:3 . The thicknesses of the active layers are also presented.**

The images of devices PTFF: PCBMC70 of different ratios of PCBM 1:1, 1:2 and 1:3 are presented with the same image scales for comparison. At first observation we can notice the domains size increases with the increasing the amount of PCBMC70. However the three devices showed homogenous nanophase segregated network for charge separation resulting short-circuit current density of more than 4 $mA.cm^{-2}$. At this point it is difficult to conclude the efficient network based on the surface morphology.

### VII.3. Photovoltaic devices based on polymer Poly (thiophene-fluorene-benzothiadiazole-fluorenone) PTFBF

It is interesting to know if the polymer combining the two repeating unit of the two previous polymers PTFB and PTFF will show better performance in solar cells. We fabricated photovoltaic devices using this new terpolymer in combination with PCBMC70 as we have seen previously that both polymers PTFB and PTFF showed highest performances with this electron accepting molecule. The device performances and the photovoltaic parameters are reported in Table 50.

| Donor (Polymer) | Acceptor | Blend ratio (D:A) | Voc (V) | Jsc ($mAcm^{-2}$) | FF | PCE (%) |
|---|---|---|---|---|---|---|
| PTFBF | PCBMC70 | 1:1 | 0.688 | 1.72 | 25.9 | 0.31 |
| PTFBF | PCBMC70 | 1:2 | 0.719 | 3.91 | 28.6 | 0.80 |
| PTFBF | PCBMC70 | 1:3 | 0.654 | 4.53 | 28.8 | 0.95 |
| PTFBF | PCBMC70 | 1:4 | 0.557 | 4.03 | 29.8 | 0.67 |

**Table 50: Photovoltaic devices properties for PTFBF:PCBM with increasing ratios of 1:1 to 1:4**

This new terpolymer PTFBF consisting of both repeating units of the two individual polymers PTFB and PTFF (bithiophene-fluorene-benzothiadiazole and bithiophene-fluorene-fluorenone on the same polymer backbone) has shown encouraging results in photovoltaic devices. We obtained the best photovoltaic performance of 0.95 % with the device based on PTFBF:PCBMC70 with a ratio of 1:3, with open circuit voltage of 0.65 V, short-circuit current density of 4.53 $mA.cm^{-2}$ and a fill factor of 29 %.

To better illustrate the results, we have plotted on the same graph the photovoltaic parameters (Voc, Jsc, FF, and PCE) of the devices based on individual polymers PTFB: PCBMC70, PTFF:PCBMC70 and the terpolymer PTFBF:PCBMC70 on the same graph as shown in Figure 154.

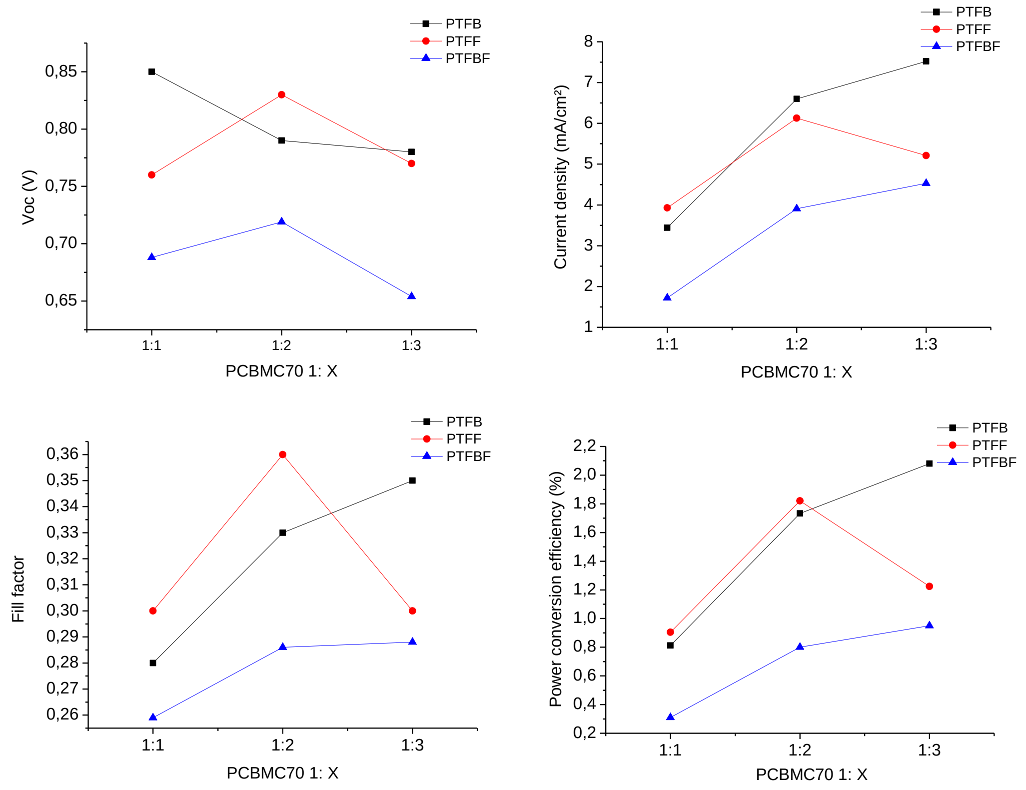


**Figure 154: Evolution of photovoltaic parameters (Voc, Jsc,FF, and PCE) of PTFB, PTFF and PTFBF according to PCBM ratios**

From the curves (Figure 154) we can clearly observe the evolution of the performances with respect to the amount of electron accepting molecule combined to the terpolymer PTFBF in solar cells. The terpolymer PTFBF showed lower photovoltaic properties in terms of open circuit voltage with the highest value of 0.71 V compared to PTFB and PTFF. The devices based on PTFBF also showed current densities lower than the ones obtained using the polymer PTFF in the active layer.

The low current density of polymer PTFBF may due to a lower molecular weight compared to other polymers with a value of Mn of 2.48 kDa, compared to 3.24 kDa for PTFF and 5.36 kDa for PTFB. The lower molecular weight indicates that the polymer has shorter chain lengths and this may be detrimental to the charge transport properties compared to the two other polymers.

These results are preliminary and further optimization of the synthetic procedures is under progress to achieve the synthesis of fractions of PTFBF showing higher molecular weights. With a power conversion efficiency of ca 1% obtained with a sample containing mostly oligomers, this polymer can however be considered as a promising material for further developments. These results are encouraging as not many studies are performed with this type of polymers containing two electron withdrawing units in the same polymer backbone[35]. One similar studied based on this concept has recently been published at the course of this thesis made by S.J Park and coworkers[35] have also shown promising results by combining the repeating unit of the known polymer polycarbazole-benzothiadiazole PCDTBT and the polymer fluorene-benzothiadiazole PFDTBT with power conversion efficiency up to 4.16 % for the polymer P(CDTBT-FDTBT) compared to the individual polymer PCDTBT of PCE= 3.3 % and a PCE of 2.8 % for the polymer PFDTBT in photovoltaic devices using PCBMC70 as acceptor after a complete optimization of the device fabication.

Contrary to the copolymers, our terpolymer combining the two repeating unit of two different electron withdrawing units fluorene-benzothiadiazole and fluorene-fluorenone may offer complementary absorption in UV-Visible. We can therefore expect on a single polymer allowing efficient photon absorption across the UV-Visible spectra.

## VIII. Conclusion

We have synthesized a series of polyfluorene based polymers poly-(thiophene-fluorene-benzothiadiazole) PTFB, poly(thiophene-fluorene-fluorenone) PTFF and the block copolymer poly(thiophene-fluorene-benzothiadiazole)-(thiophene-fluorene-fluorenone) PTFBF. One objective using these polymers was to obtain solar cells with higher open circuit voltages that the ones using the polymers developed in the first part of our work and presented in the previous chapter.

These three polymers prepared by Suzuki coupling polymerization showed average molecular weights of 5.64 kDa, 3.24 kDa and 2.48 kDa probably due to the experimental conditions i.e. deactivation of catalyst by the presence of oxygen during the polymerization reaction. It is crucial to further optimize the condition of polymerization in order to obtain higher molecular weights for these polymers.

We investigated photophysical, electronic and transport properties of these series of polymers.
The polymers PTFB and PTFF can be considered as analog and only vary from the electron deficient (acceptor) unit in the polymer backbone (benzothiadiazole or fluorenone). This modification gives different optical and electronic properties, notably in photon absorption spectra. PTFB gives broader absorption up in the UV-Visible region compared to other polymers. The band gaps of the polymers were found to be higher than the previous oligoalkylthiophenes based copolymers (see chapter 4) at 2.12 eV, 2.14 eV and 2.23 eV for PTFB, PTFF and PTFBF respectively.

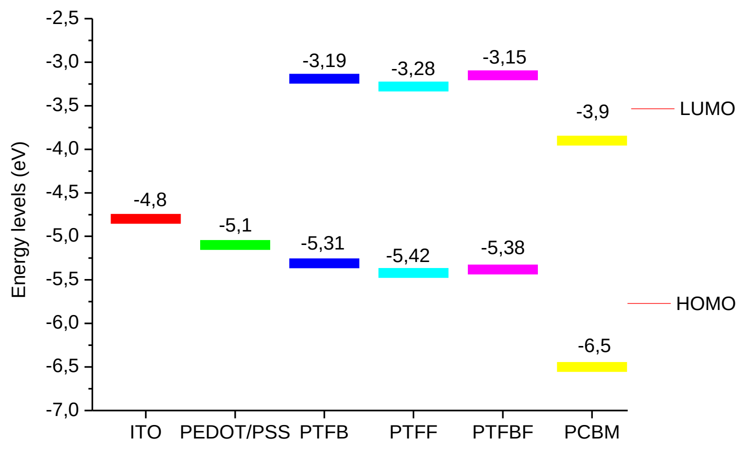


**Figure 155: Energy levels diagram of ITO, PEDOT/PSS, polymers PTFB, PTFF and PTFBF, as well as PCBM**

The three polymers PTFB, PTFF and PTFBF show energy levels correctly positioned (Figure 155) with respect to the ones of fullerenes and they are therefore suitable for photovoltaic applications. We note that by incorporating the fluorene unit, we managed to lower the HOMO energy levels down to -5.31 eV, -5.42 eV and -5.38 eV for these polymers. These result in the improvement of the open circuit voltage ranging from 0.71 to 0.86 V for all the solar cells containing these polymers.

We obtained good photovoltaic performance for this series of polymers. The highest performance is obtained with the device based on polymer PTFB: PCBMC70 with a ratio of 1:3 with overall power conversion efficiency of 2.1 %. The best performance obtained for the device based on polymer PTFF is 1.8 % when combined with 2 equivalents of PCBMC70. The block copolymer PTFBF showed lower performance with power conversion efficiency of 0.95 %.

Thermal annealing study on the device performance was also conducted but the results after annealing treatment did not show any improvement. We postulated that the polymers readily formed good phase segregation in the systems after deposition. AFM images of the morphology of the surface of the tested device confirmed this hypothesis.
We suggested that the power conversion efficiencies can be improved by developing polymers showing higher molecular weight. Therefore the development of polymerization procedures is needed and purification procedures should also be meticulously studied.

In conclusion, we have succeeded in developing new series of polymers based on fluorene units, benzothiadiazole, and fluorenone. We increased the open circuit voltage of the photovoltaic devices by 25% up to 0.8 V compared to the polymers based on linear thiophene that showed highest Voc of 0.6 V. Even if the band gaps of these fluorene based polymers are slightly higher, the photovoltaic performances were improved.

# IX. Reference


1 Scharber, M.C., Mühlbacher, D., Koppe, M., Denk, P., Waldauf, C., Heeger, A.J. and Brabec, C.J. (2006), Design Rules for Donors in Bulk-Heterojunction Solar Cells—Towards 10 % Energy-Conversion Efficiency. Adv. Mater., 18: 789–794.

2 A. Cravino, Origin of the open circuit voltage of donor-acceptor solar cells: Do polaronic energy levels play a role, Appl Phys Lett 91, 243502 (2007).

3 M. Kreyenschmidt, G. Klaerner, T. Fuhrer, J.Ashenhurst, S. Karg, W. D. Chen, V. Y. Lee, J. C.Scott, and R. D. Miller, Thermally Stable Blue-Light-Emitting Copolymers of Poly(alkylfluorene), Macromolecules, 1998, 31 (4), pp 1099–1103

4 P Lu, H Zhang, F Shen, B Yang, D Li, Y Ma, X Chen, J Li, N Tamai , A Wide-Bandgap Semiconducting Polymer for Ultraviolet and Blue Light Emitting Diodes, Macromol. Chem. Phys. 2003, 204, 2274–2280

5 J-H. Huang, C-Y. Yang, Z-Y Ho, D. Kekuda, M-C. Wu, F-C. Chien, P. Chen, C-W. Chu, K-C. Ho, Annealing effect of polymer bulk heterojunction solar cells based on polyfluorene and fullerene blend, Organic Electronics, Vol. 10, 1, 2009, 27-33

6 D. Kekuda, J. H. Huang, K. C. Ho, and C. W. Chu,Modulation of Donor−Acceptor Interface through Thermal Treatment for Efficient Bilayer Organic Solar Cells, J. Phys. Chem. C 114, 2764 (2010).

7 H. Cha, H. Kong, D. S. Chung, W. M. Yun, T. K. An, J. Hwang, Y.-H. Kim, H.-K. Shim, C. E. Park, Thermally stable amorphous polymeric semiconductors containing fluorene and thiophene for use in organic photovoltaic cells, Organic Electronics, Volume 11, Issue 9, 2010, 1534-1542

8 H. Sirringhaus, T. Kawase, R.H. Friend, T. Shimoda, M. Inbasekaran,W.Wu, E.P. Woo, High-resolution inkjet printing of all-polymer transistor circuits, Science 290 (2000) 2123–2126.

9 S.P. Li, C.J. Newsome, D.M. Russell, T. Kugler, M. Ishida, T. Shimoda, Friction transfer deposition of ordered conjugated polymer nanowires and transistor fabrication, Appl. Phys. Lett. 87 (2005) 062101-1–062101-3.

10 M. Redecker, D. D. C. Bradley, M. Inbasekaran, and E. P. Woo, Nondispersive hole transport in an electroluminescent polyfluorene, Appl. Phys. Lett. 73, 1565 (1998)

11 M. Redecker, D. D.C. Bradley, M. Inbasekaran, W. W. Wu, and E. P. Woo, High Mobility Hole Transport Fluorene-Triarylamine Copolymers. Adv. Mater., 11: 241–246, (1999)

12 O Inganäs, F Zhang, and M R. Andersson, Alternating Polyfluorenes Collect Solar Light in Polymer Photovoltaics, *Accounts of Chemical Research* 2009 *42* (11), 1731-1739

13 J Chen and Y Cao, Development of Novel Conjugated Donor Polymers for High-Efficiency Bulk-Heterojunction Photovoltaic Devices, Acc. of Chem. Res. 2009 42 (11), 1709-1718

14 J Zhang, W Cai, F Huang, E Wang, C Zhong, S Liu, M Wang, C Duan, T Yang, and Y Cao, Synthesis of Quinoxaline-Based Donor−Acceptor Narrow-Band-Gap Polymers and Their Cyclized Derivatives for Bulk-Heterojunction Polymer Solar Cell Applications, Macromolecules 2011 44 (4), 894-901

15 Inganäs, O., Zhang, F., Tvingstedt, K., Andersson, L. M., Hellström, S. and Andersson, M. R. (2010), Polymer Photovoltaics with Alternating Copolymer/Fullerene Blends and Novel Device Architectures. Adv. Mater., 22: E100–E116

16 R. Pacios, D.D.C. Bradley, J. Nelson, C.J. Brabec, Efficient polyfluorene based solar cells, Synthetic Metals, Volume 137, Issues 1–3, 4 April 2003, Pages 1469-1470

17 G. L. Schulz, X. Chen, and S. Holdcroft, High band gap poly(9,9-dihexylfluorene-alt-bithiophene) blended with [6,6]-phenyl C61 butyric acid methyl ester for use in efficient photovoltaic devices, Appl. Phys. Lett. 94, 023302 (2009)

18 M. Svensson, F. L. Zhang, , S. C. Veenstra, W. J. H. Verhees, , J. C. Hummelen, J.M. Kroon, O. Inganas, M.R Andersson, High-performance polymer solar cells of an alternating polyfluorene copolymer and a fullerene derivative Adv. Mater.2003, 15, 988– 991

19 A. Calabrese, G. Schimperna, R. Po,T. Yohannes, S. E. Debebe, F. Tinti,and N. Camaioni, Bis-EH-PFDTBT:PCBM solar cells: A compositional, thickness, and light-dependent study, J. Appl. Phys. 110, 113106 (2011)

20 Q Zhou, Q Hou, L Zheng, X Deng, G Yu, and Y Cao, Fluorene-based low band-gap copolymers for high performance photovoltaic devices, Appl. Phys. Lett. 84, 1653 (2004)

21 Zhang, F., Jespersen, K.G., Björström, C., Svensson, M., Andersson, M.R., Sundström, V., Magnusson, K., Moons, E., Yartsev, A. and Inganäs, O. (2006), Influence of Solvent Mixing on the Morphology and Performance of Solar Cells Based on Polyfluorene Copolymer/Fullerene Blends. Adv. Funct. Mater., 16: 667–674

22 L. H. Slooff, S. C. Veenstra, J. M. Kroon, D. J. D. Moet, J. Sweelssen, and M. M. Koetse, Determining the internal quantum efficiency of highly efficient polymer solar cells through optical modeling, Appl. Phys. Lett. 90, 143506 (2007)

23 Li, W.; Qin, R.; Zhou, Y.; Andersson, M.; Li, F.; Zhang, C.; Li, B.; Liu, Z.; Bo, Z.; Zhang, F. Tailoring side chains of low band gap polymers for high efficiency polymer solar cells, Polymer 2010, 51, 3031

24 E. Wang, M. Wang, L.Wang, C. Duan, J. Zhang, W. Cai, C. He, H. Wu, and Y. Cao, Donor Polymers Containing Benzothiadiazole and Four Thiophene Rings in Their Repeating Units with Improved Photovoltaic Performance, Macromolecules 2009 42 (13), 4410-4415

25 N Blouin, A Michaud, D Gendron, S Wakim, E Blair, R Neagu-Plesu, M Belletête,G Durocher,Y Tao, and M Leclerc, Toward a Rational Design of Poly(2,7-Carbazole) Derivatives for Solar Cells, J. Am. Chem. Soc. 2008, 130, 732-742

26 J. Li and A. C. Grimsdale, Carbazole-based polymers for organic photovoltaic devices**,**Chem. Soc. Rev**.**, 2010,39, 2399-2410

27 S. H. Park, A. Roy, S. Beaupré, S. Cho, N. Coates, J. S. Moon, D. Moses, M. Leclerc, K. Lee, and A. J. Heeger, Bulk heterojunction solar cells with internal quantum efficiency approaching 100%, Nat. Photonics 2009, 3, 297– 302

28 Wang, E.; Wang, L.; Lan, L.; Luo, C.; Zhuang, W.; Peng, J.; Cao, Y. High-Performance Polymer Heterojunction Solar Cells of a Polysilafluorene Derivative.Appl. Phys. Lett. 2008, 92, 033307

29 N Allard, R BAíćh, D Gendron, P T. Boudreault, C Tessier, S Alem, S-C Tse, Y Tao, and M Leclerc, Germafluorenes: New Heterocycles for Plastic Electronics, Macromolecules 2010 43 (5), 2328-2333

30 M. Jayakannan, Joost L. J. van Dongen, and René A. J. Janssen, Mechanistic Aspects of the Suzuki Polycondensation of Thiophenebisboronic Derivatives and Diiodobenzenes Analyzed by MALDI−TOF Mass Spectrometry, Macromolecules 2001 34 (16), 5386-5393

31 A Yokoyama, H Suzuki, Y Kubota, K Ohuchi, H Higashimura, and T Yokozawa, Chain-Growth Polymerization for the Synthesis of Polyfluorene via Suzuki−Miyaura Coupling Reaction from an Externally Added Initiator Unit, Journal of the American Chemical Society 2007 129 (23), 7236-7237

32 Sakamoto, J., Rehahn, M., Wegner, G. and Schlüter, A. D. (2009), Suzuki Polycondensation: Polyarylenes à la Carte. Macromol. Rapid Commun., 30: 653–687.

33 K B. Burke, W J. Belcher, L Thomsen, B Watts, C R. McNeill, H Ade, and P C. Dastoor, Role of Solvent Trapping Effects in Determining the Structure and Morphology of Ternary Blend Organic Devices, Macromolecules 2009, 42, 3098–3103

34 H Kim, M Shin, Y Kim, Distinct Annealing Temperature in Polymer:Fullerene:Polymer Ternary Blend Solar Cells, J Phys Chem C 2009, 113, 1620–1623

35 Park, S. J., Cho, J. M., Byun, W.-B., Lee, J.-C., Shin, W. S., Kang, I.-N., Moon, S.-J. and Lee, S. K. (2011), Bulk heterojunction polymer solar cells based on binary and ternary blend systems. J. Polym. Sci. A Polym. Chem., 49: 4416–4424.

36 Y-J. Cheng, S-H. Yang, and C.-S. Hsu, Synthesis of Conjugated Polymers for Organic Solar Cell Applications, Chem. Rev. 2009 109 (11), 5868-5923

37 Pei-Tzu Wu, Felix S. Kim, Richard D. Champion, and Samson A. Jenekhe, Conjugated Donor-Acceptor Copolymer Semiconductors. Synthesis,Optical Properties, Electrochemistry, and Field-Effect Carrier Mobility of Pyridopyrazine-Based Copolymers, Macromolecules 2008, 41, 7021-7028

38 J. Kettle, M. Horie, L.A. Majewski, B.R. Saunders, S. Tuladhar, J. Nelson, M.L. Turner, Optimisation of PCPDTBT solar cells using polymer synthesis with Suzuki coupling, Solar Energy Materials and Solar Cells, Volume 95, Issue 8, August 2011, Pages 2186-2193

39 N. Miyaura and A. Suzuki, Palladium-Catalyzed Cross-Coupling Reactions of Organoboron Compounds, Chem. Rev. 1995, 95,2457-2483

40 Murage, J.; Eddy, J. W.; Zimbalist, J. R.; McIntyre, T. B.; Wagner, Z. R.; Goodson, F. E., Effect of Reaction Parameters on the Molecular Weights of Polymers Formed in a Suzuki Polycondensation, Macromolecules, 2008, 41,7330

41 Schlüter, S., Frahn, J., Karakaya, B. and Schlüter, A. D. (2000), Improved Suzuki polycondensation: A diiodo versus a dibromo monomer. Macromol. Chem. Phys., 201: 139–142.

42 E. Wang, M. Wang, L.Wang, C. Duan, J. Zhang, W. Cai, C. He, H. Wu, and Y. Cao, Donor Polymers Containing Benzothiadiazole and Four Thiophene Rings in Their Repeating Units with Improved Photovoltaic Performance, Macromolecules 2009 42 (13), 4410-4415

43 http://depts.washington.edu/eooptic/linkfiles/Freeze_Pump_Thaw.pdf

44 F Jaramillo-Isaza and M L. Turner, Synthesis and properties of conjugated oligomers containing fluorene, fluorenone, thiophene and cyclopentadithiophenone units, J. Mater. Chem., 2006,16, 83-89

45 N. Banerji, E. Gagnon, P. Morgantini, S. Valouch, A. R. Mohebbi, J. Seo, M. Leclerc, A. J. Heeger, Breaking Down the Problem: Optical Transitions, Electronic Structure, and Photoconductivity in Conjugated Polymer PCDTBT and in Its Separate Building Blocks, J. Phys. Chem. C 2012, 116, 11456

46 Y. Kim, S. Cook, S. M. Tuladhar, S. A. Choulis, J. Nelson, J. R. Durrant, D. D. C. Bradley, M. Giles, I. McCulloch, C-S Ha and M. Ree, A strong regioregularity effect in self-organizing conjugated polymer films and high-efficiency polythiophene:fullerene solar cells,Nature Materials 5, 197 - 203 (2006)

47 M. Wang, X. Hu, P. Liu, W. Li, X. Gong, F. Huang, and Y. Cao, Donor–Acceptor Conjugated Polymer Based on Naphtho[1,2-c:5,6-c]bis[1,2,5]thiadiazole for High-Performance Polymer Solar Cells, Journal of the American Chemical Society 2011, 133 (25), 9638-9641

48 J. Roncali, Molecular Engineering of the Band Gap of p-Conjugated Systems: Facing Technological Applications, Macromol. Rapid Commun. 2007, 28, 1761–1775

49 P Wu, F S. Kim, R D. Champion, and S A. Jenekhe, Conjugated Donor-Acceptor Copolymer Semiconductors. Synthesis, Optical Properties, Electrochemistry, and Field-Effect Carrier Mobility of Pyridopyrazine-Based Copolymers, Macromolecules 2008, 41, 7021-7028

50 Scharber, M.C., Mühlbacher, D., Koppe, M., Denk, P., Waldauf, C., Heeger, A.J. and Brabec, C.J. , Design Rules for Donors in Bulk-Heterojunction Solar Cells—Towards 10% Energy-Conversion Efficiency. Adv. Mater., (2006), 18: 789–794

51 T. Förster, Transfer mechanisms of electronic excitation, Discuss.Faraday Soc., 1959, 7–17

52 A. Moliton, Electronique et optoélectronique organiques, Collection Télécom, Springer

53 R. Koeppe and N. S. Sariciftci, Photoinduced charge and energy transfer involving fullerene derivatives, Photochem. Photobiol. Sci., 2006, 5, 1122–1131

54 Beljonne, D., Poutois, G., Silva, C., Hennebicq, E., Herz, L., Friend, R., et al. (2002). Interchain vs. Intrachain Energy Transfer in Acceptor Capped Conjugated Polymers,Interchain vs. Intrachain Energy Transfer in Acceptor Capped Conjugated Polymers,Journal of Luminescence, 98, 23-33.

55 N. S. Sariciftci, L. Smilowitz, A. J. Heeger, and F. Wudl, Photoinduced Electron Transfer from a Conducting Polymer to Buckminsterfullerene, Science 27 November 1992: Vol. 258 no. 5087 pp. 1474-1476

56 M. Knupfer, Exciton binding energies in organic semiconductors, Appl. Phys. A 77, 623–626 (2003)

57 M. Hallermann, S. Haneder, and E. Da Como, Charge-transfer states in conjugated polymer/fullerene blends: Below-gap weakly bound excitons for polymer photovoltaics, Appl. Phys. Lett. 93, 053307 (2008)

58 Zhou, Y., Tvingstedt, K., Zhang, F., Du, C., Ni, W.-X., Andersson, M. R. and Inganäs, O. (2009), Observation of a Charge Transfer State in Low-Bandgap Polymer/Fullerene Blend Systems by Photoluminescence and Electroluminescence Studies. Adv. Funct. Mater., 19: 3293–3299

59 Y. W. Soon , T. M. Clarke , W. Zhang , T. Agostinelli , J. Kirkpatrick , C. Dyer-Smith , I. McCulloch , J. Nelson and J. R. Durrant, Energy versus electron transfer in organic solar cells: a comparison of the photophysics of two indenofluorene: fullerene blend films,Chem. Sci., 2011,2, 1111-1120

60 V. I. Arkhipov and H. Bässler, "Exciton dissociation and charge photogeneration in pristine and doped conjugated polymers," Physica Status Solidi A, vol. 201, no. 6, pp. 1152–1187, 2004

61 Y. Astuti, W. Duffy, S. Tierney, W. Zhang, M. Heeney, I. McCulloch, J. Nelson, D. D. C. Bradley, and J. R. Durrant, "Charge carrier formation in polythiophene/fullerene blend films studied by transient absorption spectroscopy," *Journal of the American Chemical Society*, vol. 130, no. 10, pp. 3030–3042, 2008

62 N. Banerji, S. Cowan, M. Leclerc, E. Vauthey, and A. J. Heeger, Exciton Formation, Relaxation, and Decay in PCDTBT, Journal of the American Chemical Society 2010 132 (49), 17459-17470

63 V. I. Krinichnyi, LEPR spectroscopy of charge carriers photoinduced in polymer/fullerene composites, 2009th ed. Hauppauge, New York,: In Encyclopedia of Polymer Composites, pp. 417–446

64 B. Gieseking, B. Jaeck, E. Preis, S. Jung, M. Forster, U. Scherf, C. Deibel, and V. Dyakonov, Excitation Dynamics in Low Band Gap Donor–Acceptor Copolymers and Blends, Adv. Energy Mater, Early view

65 J. Pei, W-L. Yu, J. Ni, Y-H. Lai, W. Huang and A. J. Heeger, Thiophene-Based Conjugated Polymers for Light-Emitting Diodes: Effect of Aryl Groups on Photoluminescence Efficiency and Redox Behavior, Macromolecules, 2001, 34 (21), 7241-7248

66 A.R. Buckley, M.D. Rahn, J. Hill, J. Cabanillas-Gonzalez, A.M. Fox, D.D.C. Bradley, Energy transfer dynamics in polyfluorene-based polymer blends, Chemical Physics Letters, Volume 339, Issues 5–6, 18 May 2001, Pages 331-336

67 B. Gieseking, B. Jaeck, E. Preis, S. Jung, M. Forster, U. Scherf, C. Deibel, and V. Dyakonov, Excitation Dynamics in Low Band Gap Donor–Acceptor Copolymers and Blends, Adv. Energy Mater, Early view

68 N. Banerji, E. Gagnon, P. Morgantini, S. Valouch, A. R. Mohebbi, J. Seo, M. Leclerc, A. J. Heeger, Breaking Down the Problem: Optical Transitions, Electronic Structure, and Photoconductivity in Conjugated Polymer PCDTBT and in Its Separate Building Blocks, J. Phys. Chem. C 2012, 116, 11456

69 P. Sonar, E. L. Williams, S. P. Singh and A. Dodabalapur, Thiophene–benzothiadiazole–thiophene (D–A–D) based polymers: effect of donor/acceptor moieties adjacent to D–A–D segment on photophysical and photovoltaic properties, J. Mater. Chem., 2011, 21, 10532

70 Zhou, Y., Tvingstedt, K., Zhang, F., Du, C., Ni, W.-X., Andersson, M. R. and Inganäs, O. (2009), Observation of a Charge Transfer State in Low-Bandgap Polymer/Fullerene Blend Systems by Photoluminescence and Electroluminescence Studies. Adv. Funct. Mater., 19: 3293–3299.

71 L. E. Polander, L. Pandey, S. Barlow,S. P. Tiwari, C. Risko, B. Kippelen, J-L. Bredas, and S. R. Marder, Benzothiadiazole-Dithienopyrrole Donor–Acceptor–Donor and Acceptor–Donor–Acceptor Triads: Synthesis and Optical, Electrochemical, and Charge-Transport Properties,J. Phys. Chem. C, 115(46):23149–23163, 2011.

72 X Gong, D Moses, AJ. Heeger, S Xiao, Excitation energy transfer from polyfluorene to fluorenone defects, Synthetic Metals 141 (2004) 17–20

73 F Jaramillo-Isaza and M L. Turner, Synthesis and properties of conjugated oligomers containing fluorene, fluorenone, thiophene and cyclopentadithiophenone units, J. Mater. Chem., 2006,16, 83-89

74 V I. Krinichnyi, E I. Yudanova, and N G. Spitsina, Light-Induced Electron Paramagnetic Resonance Study of Poly(3-alkylthiophene)/Fullerene Composites, J. Phys. Chem. C 2010, 114, 16756–16766

75 K. Murata, Y. Shimoi, S. Abe, S. Kuroda, T. Noguchi, and T. Ohnishi, Chem. Phys. 227, 191 (1998).

76 Alexander I. Shames, Celine Bounioux, Eugene A. Katz, Rachel Yerushalmi-Rozen, and Eyal Zussman, Light-induced electron paramagnetic resonance evidence of charge transfer in electrospun fibers containing conjugated polymer/fullerene and conjugated polymer/fullerene/carbon nanotube blends, Appl. Phys. Lett. 100, 113303 (2012)

77 V. I. Krinichnyi and E. I. Yudanova, Light-Induced EPR Study of Charge Transfer in P3HT/PC71BM Bulk Heterojunctions, J. Phys. Chem. C 2012, 116, 9189−9195

78 V.I. Krinichnyi, 2-mm Waveband electron paramagnetic resonance spectroscopy of conducting polymers, Synthetic Metals, Volume 108, Issue 3, 1 February 2000, Pages 173-222

79 Poluektov, O. G.; Filippone, S.; Martín, N.; Sperlich, A.; Deibel, C.; Dyakonov, V. J. Phys. Chem. B 2010, 114, 14426

80 I. Hwang , S. Beaupré , M. Leclerc and G. D. Scholes, Ultrafast relaxation of charge-transfer excitons in low-bandgap conjugated copolymers, Chem. Sci., 2012,3, 2270-2277

81 M.D. Heinemann, K. Von Maydell, F. Zutz, J. Kolny-Olesiak, H. Borchert, I. Riedel, J. Parisi, Photo-induced charge transfer and relaxation of persistent charge carriers in polymer/nanocrystal composites for applications in hybrid solar cells, Advanced Functional Materials, 19 (2009), pp. 3788–3795

82 W. L. Leong , Gr. C. Welch , L. G. Kaake , C. J. Takacs , Y. Sun , G. C. Bazan and A.J. Heeger, Role of trace impurities in the photovoltaic performance of solution processed small-molecule bulk heterojunction solar cells, Chem. Sci., 2012,3, 2103-2109

83 N. Camaioni, F. Tinti, L. Franco, M. Fabris, A. Toffoletti, M. Ruzzi, L. Montanari, L. Bonoldi, A. Pellegrino, A. Calabrese, R. Po, Effect of residual catalyst on solar cells made of a fluorene-thiophene-benzothiadiazole copolymer as

electron-donor: A combined electrical and photophysical study, Organic Electronics, Volume 13, Issue 4, April 2012, Pages 550-559

84 Mühlbacher, D., Scharber, M., Morana, M., Zhu, Z., Waller, D., Gaudiana, R. and Brabec, C. (2006), High Photovoltaic Performance of a Low-Bandgap Polymer. Adv. Mater., 18: 2884–2889.

85 Hou, J.; Chen, H. Y.; Zhang, S.; Li, G.; Yang, Y. J. Am. Chem. Soc.,2008, 130, 16144.

86 Azimi, H., Senes, A., Scharber, M. C., Hingerl, K. and Brabec, C. J. (2011), Charge Transport and Recombination in Low-Bandgap Bulk Heterojunction Solar Cell using Bis-adduct Fullerene. Adv. Energy Mater., 1: 1162–1168.

87 Yamamoto, S., Orimo, A., Ohkita, H., Benten, H. and Ito, S. Molecular Understanding of the Open-Circuit Voltage of Polymer:Fullerene Solar Cells. Adv. Energy Mater., (2012), 2: 229–237.

88 Müller, C., Wang, E., Andersson, L. M., Tvingstedt, K., Zhou, Y., Andersson, M. R. and Inganäs, O. (2010), Influence of Molecular Weight on the Performance of Organic Solar Cells Based on a Fluorene Derivative. Adv. Funct. Mater., 20: 2124–2131

89 Hoppe, H., Niggemann, M., Winder, C., Kraut, J., Hiesgen, R., Hinsch, A., Meissner, D. and Sariciftci, N.S. (2004), Nanoscale Morphology of Conjugated Polymer/Fullerene-Based Bulk- Heterojunction Solar Cells. Adv. Funct. Mater., 14: 1005–1011

# CHAPTER 5: INDACENODITHIOPHENE-BASED POLYMERS FOR ORGANIC PHOTOVOLTAIC: SYNTHESIS, PHYSICAL CHARACTERISATION AND PHOTOVOLTAIC PROPERTIES

# I. Introduction

In the two previous chapters, two different series of π–conjugated donor–acceptor polymers (D-A polymers) have been described. The first polymer series are based on linear oligothiophenes alternating with electron-withdrawing units (benzothiadiazole or fluorenone) and the second polymer series are based on fluorene, a fused phenylene-pentacene-phenylene ring alternating with electron-withdrawing units (benzothiadiazole or/and fluorenone). We have demonstrated that the linear oligothiophenes based D-A polymers showed small band gaps but they exhibit high lying HOMO energy levels, giving rise to a low open circuit voltage when they are studied in real devices with fullerenes derivatives as acceptor. On the other hand, the fluorene-based D-A polymers showed low lying HOMO energy levels affording polymers with a much larger energy band gap that give rise to higher open circuit voltage in solar cells. In order to take advantage of the low lying HOMO energy levels and at the same time to achieve a good collection of photons, polymers with a smaller band gap such as ladder type polymers show interesting features and could allow improvements in solar cells.

Ladder type polymers[1] or fused aromatic rings polymers afford extended conjugation by the increase of planarity, which may reduce significantly the band gap of the polymers [2,3]. Utilisation of ladder type polymers is recently a flourishing concept adopted to achieve efficient applications in organic photovoltaic cells. Ladder type polymers have been recently a flourishing concept in the field of organic photovoltaic with utilization of different type of polymers structures for examples based on oligo p-phenylene[4], alternating thiophene-benzene rings[5,6], di-indenothienothiophene arene[7], indenofluorene[8] and indacenodithiophene[9] etc and have shown promising power conversion efficiencies in devices up to 6 % [10].

We have seen previously that employing thiophene oligomers as electron rich donor segments allows for the preparation of small band gap polymers. And for the fluorene-based polymers, fused phenylene rings give low-lying HOMO energy levels [11,12,13]. Therefore it seemed judicious to combine these two building blocks in order to obtain interesting new donor segments. In Figure 156 we illustrate some examples of D-A polymers with different combination of aromatic rings as donor segment allowing fine-tuning the energy levels to best match with desired HOMO-LUMO energy levels and band gap.

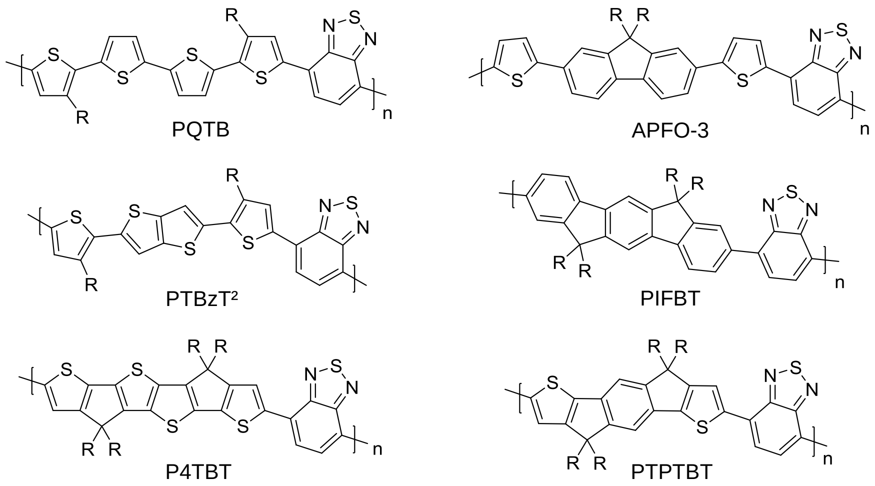


| Polymer | HOMO (eV) | LUMO (eV) | Eg (eV) | Ref |
|---|---|---|---|---|
| PQTB | -5.0 | -3.2 | 1.8 | |
| PTBzT2 | -5.0 | -3.2 | 1.8 | [14] |
| P4TBT | -5.2 | -3.7 | 1.5 | [15] |
| APFO-3 | -5.5 | -3.6 | 1.9 | [16] |
| PIFBT | -5.9 | -3.6 | 2.3 | [17] |
| PTPTBT | -5.3 | -3.6 | 1.7 | [10] |

**Figure 156: Energy levels of polymer PQTB, and other polymers obtained from literature PTBzT2, P4TBT, APFO-3, PIFBT and PTPTBT**

Our polymer poly(quaterthiophenes-benzothiadiazoles) PQTB with four electron rich thiophenes rings showed similar electronic properties with the polymer based on fused bithiophene ring PTBzT[14] showing a small energy band gap of 1.8 eV and the same HOMO and LUMO energy levels positions. By fusing completely all the thiophene rings, the polymer P4TBT showed further reduction of band gap to 1.5 eV. However the HOMO energy levels for all the thiophene based polymers are still high comprised between -5.0 to -5.2 eV. On the other hand, a less electron rich phenylene ring when fused together give high band gap copolymers than thiophene based polymers but afford low-lying HOMO energy levels around -5.5 eV (APFO-3) and -5.9 eV (PIFBT). Consequently, the fusion of alternating thiophene-phenylene-thiophene rings (Figure 157) in the case of polymer indacenodithiophene PTPTBT results in a low lying HOMO energy levels of -5.3 eV and at the same time a narrow band gap of 1.7 eV.

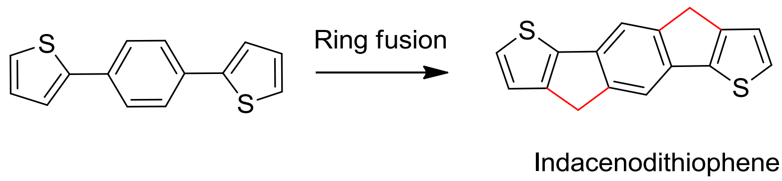


**Figure 157: Ring fusion of thiophene- phenylene-thiophene rings to form indacenodithiophene motif**

Therefore indacenodithiophene-based copolymers have recently attracted many researches for applications in photovoltaic cells[10, 9, 18, 19] for their promising features. Indeed, they demonstrate low lying HOMO energy levels to achieve high open circuit voltage in photovoltaic device[10], a broad absorption spectra and good charges transport properties[18] due to the planarity of the indacenodithiophene unit.

In this chapter we will investigate the indacenodithiophene based polymers by preparing a series of alternating D-A copolymers using benzothiadiazole and fluorenone as electron withdrawing units. The indacenodithiophene-benzothiadiazole copolymer PTBTBT has been published by Chen and coworkers in 2010.[10] This copolymer was synthesized to be compared to its analog containing fluorenone units. To be coherent with our previous study on polymer fluorene series, we also synthesized the random copolymers with two electron acceptors (indacenodithiophene-benzothiadiazole)-(indacenodithiophene-fluorenone) to complete the study. The synthesized polymers are presented in Figure 158.

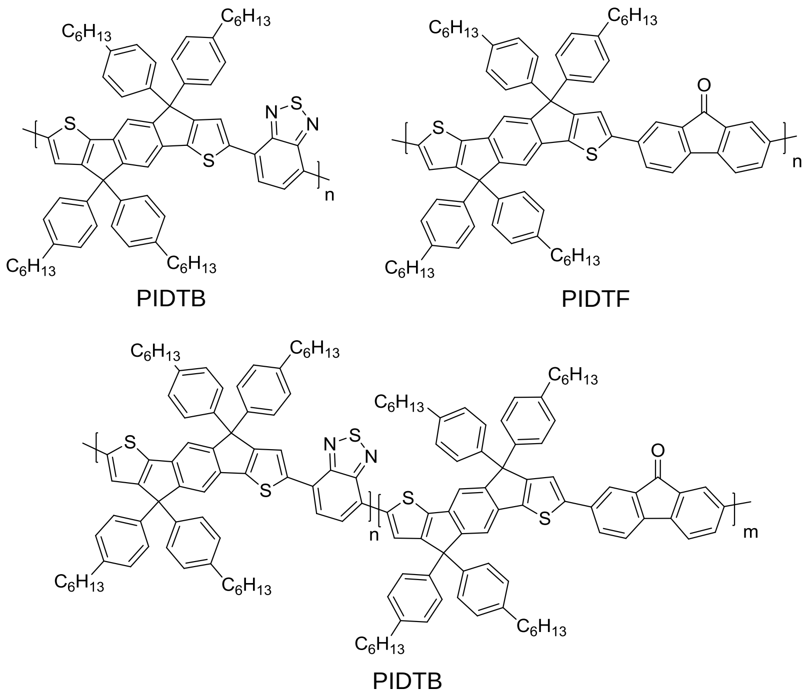


**Figure 158: Molecular structures of the series of polymer indacenoditiophene-benzothiadiazole PIDTB, polymer indacenodithiophene-fluorenone PIDTF, and random copolymer (indacenodithiophene-benzothiadiazole)-(indacenodithiophene-fluorenone) PIDTBF**

# II. Synthesis and purification of indacenodithiophene based polymers PIDTF, PIDTB and PIDTBF

Indacenodithiophene monomers are rigid and planar molecules alternating dithiophene-phenylene-dithiophene moieties. In order to perform alternating copolymerisation of electron rich indacenodithiophenes units with electron-withdrawing units’ benzothiadiazole and fluorenone, the more effective way is to perform Stille coupling polymerisations[10,19]. As a general rule of thumb, coupling reaction of thiophene ring with aryl halide is favored by Stille coupling instead of other condensation methods, for example Suzuki coupling[20,21,22]. We will describe first the preparation of monomer indacenodithiophene followed by the copolymerization with electron withdrawing units' benzothiadiazole and fluorenone.

## II.1. Synthesis of monomer indacenodithiophene IDT

For the preparation of monomer indacenodithiophenes, we have followed the procedure described in reference[19], as shown in Scheme 13.

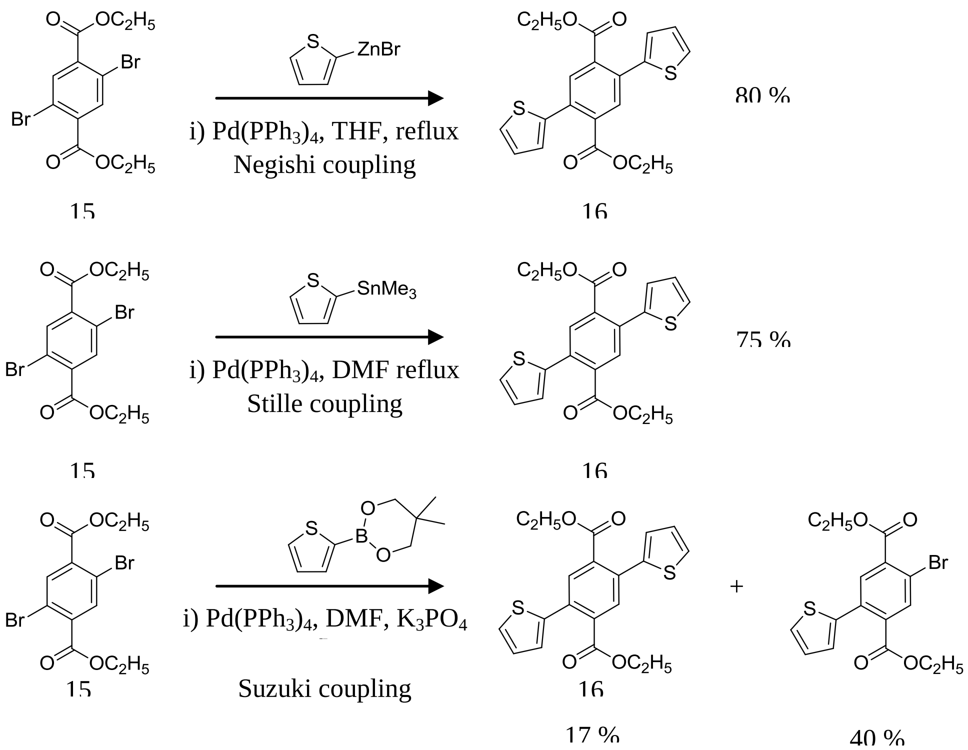


**Scheme 13: Synthesis of primary building block 2,5-di(thiophen-2-yl)terephthalate via Negishi Coupling, and another possible route by Stille coupling**

Our first attempt to prepare diethyl 2,5-di(thiophen-2-yl)terephthalate (16) was carried out under Suzuki coupling conditions, however the expected product was obtained in low yield (17%) and a large amount of the mono-coupling product was isolated (40%). The presence of two carboxylate groups may deactivate the adjacent bromine atoms, and as a consequence be detrimental to the palladium insertion. We then decided to prepare diethyl 2,5-di(thiophen-2-yl)terephthalate (16) via palladium-catalyzed Negishi cross-coupling reaction using organozinc halide. Departing from diethyl 2,5-dibromoterephtalate (15) and a solution of 2-thienylzinc bromide in THF with $Pd(PPh_3)_4$ as catalyst, the reaction are performed under reflux for 3 h. The Negishi coupling affords the pure product with a good yield of 80 %. This building block diethyl 2,5-di(thiophen-2-yl)terephthalate (16) can also be prepared via Stille cross-coupling reaction using organostannic precursor 2-thienyl(trimethyl)stannane. We have conducted this reaction and obtained a slightly lower yield of 75 % pure product. Hence the interest of using Negishi reaction compared to Stille coupling reaction for the preparation of this intermediate which afford higher yield and a lower degree of toxicity than the stannane compound.

In the next step as shown in Scheme 2, we first prepared a organolithiated reagent by adding n-BuLi to 1-bromo-4-hexylbenzene at low temperature in order to form 4-hexylbenzenelithium. Then this reagent is used to react with the synthesised diethyl-2,5-di(thiophen-2-yl)terephthalate (16). The organolithium reagent which is used in excess attacks the carbonyl site of the ester and forms a hydoxyl intermediate with a $sp^3$ carbon after a second nucleophilic addition.

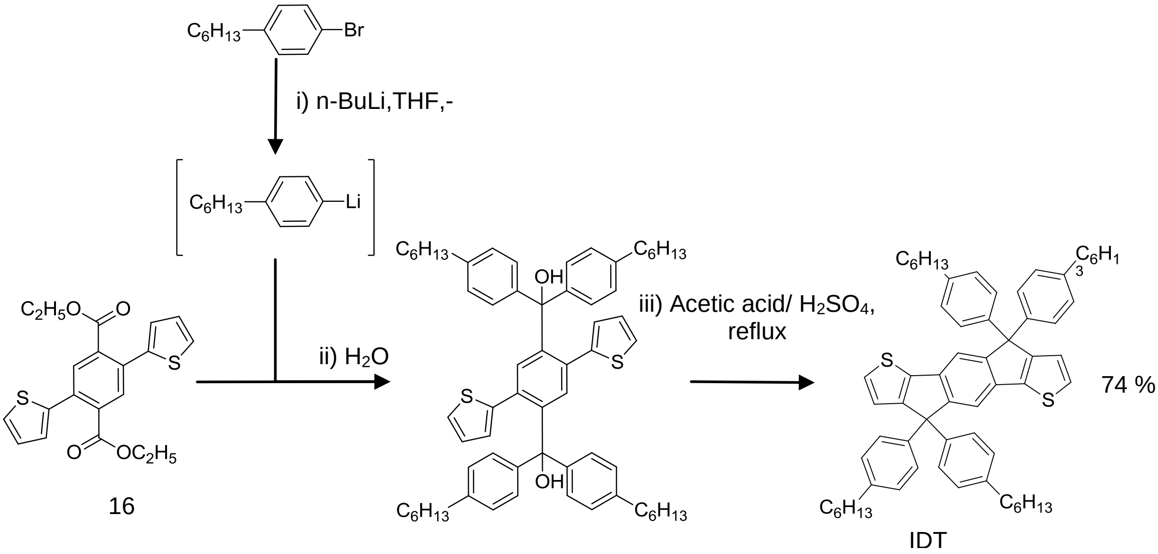


**Scheme 14: Formation of monomer indacenodithiophene via reduction of ester terephtalate to tertiary alcohols, followed by dehydration alcohols in acidic condition and intramolecular cyclization**

The formed hydroxy-diphenyl compound is then quenched with water and extracted with ethyl acetate and concentrated .The crude product was used directly for the next step. The crude product was dissolved in acetic acid, followed by addition of few drops of concentrated sulfuric acid allowing the dehydration of the two tertiary alcohols, to form two carbocations intermediates. The formation of the carbocation intermediates can be observed by an abrupt change of colour from yellow to violet after addition of concentrated sulfuric acid. The highly reactive carbocations undergo intramolecular cyclisation to form the monomer indacenodithiophenes (IDT) with a good yield of 74 %. The structure is verified by $^1H$ NMR characterisation which corresponds to the values described in the reference[19] and further characterized by micro analysis.

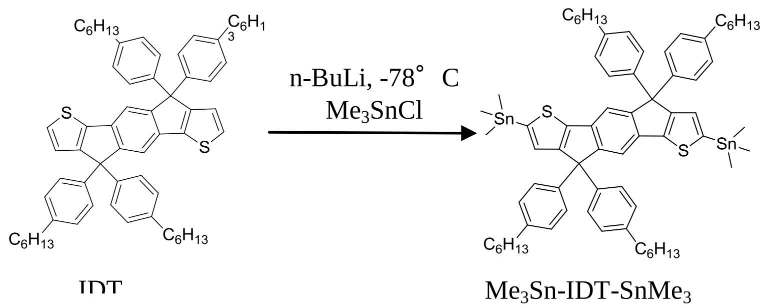


**Scheme 15 : Reaction of distannylation of indacenodithiophenes monomer IDT**

Indacenodithiophene units were then transformed to distannanes monomer $Me_3Sn$-IDT-$SnMe_3$ via stannylation reaction. The obtained precursor was then directly used for the polymerisation reaction using Stille cross-coupling conditions. The distannane monomer was dosed by $^1$H-NMR, and was found to be at 60 %. From the NMR spectrum, we can detect the presence of monostannane and a small amount of unreacted indacenodithiophene in the monomer crude. Stannylated product known for its toxicity[21,22] is difficult to purify as they are not adequate for purification by classical column chromatography due to the interaction of stannanes compound with the silica gel. Therefore the obtained product is used directly for polymerization without any further purification.

## II.2. Synthesis and purification of polymer PIDTB and PIDTF

We performed Stille cross-coupling polymerisation using 2 % equivalent of catalyst $Pd_2(dba)_3$ with corresponding ligand (o-tolyl)$_3$P and toluene as solvent as described in the reference[10], [19] A small amount of DMF (10 %) was also added to increase the polarity of the solvent and to act as coordinating ligand with the palladium catalyst[21]. The polymerization reactions were performed for 48 h in solvent refluxing. 1 equivalent of monomer indacenodithiophene distannanes was added to 1 equivalent of benzothiadiazole for preparation of PIDTB and similarly with 1 equivalent of fluorenone is mixed with 1 equivalent of indacenodithiophene monomer for preparation of PIDTF.

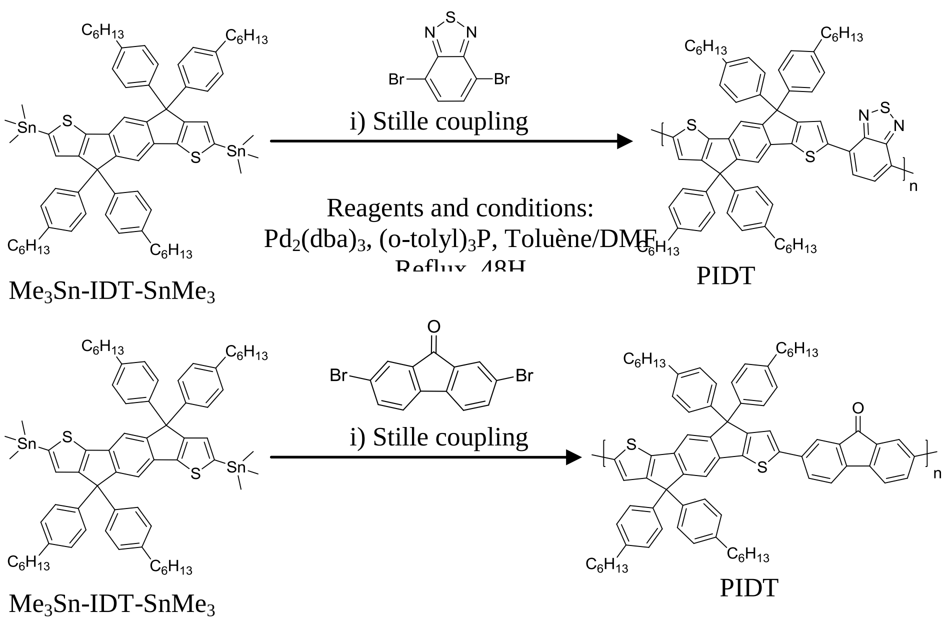


**Scheme 16: Synthesis of polymers PIDTB and PIDTF**

Employing the same experimental conditions, we have conducted the polymerisation reaction to obtain random copolymer PIDTBF as shown in Scheme 17. Synthetic route to random copolymer indacenodithiophene-benzothiadiazole-fluorenone terpolymer PIDTBF combining two equivalents of indacenodithiophene distannanes with 1 equivalent of fluorenone and and 1 equivalent of benzothiadiazole units, was performed using the Stille coupling conditions. It is also to be noted that following the described procedures in the references[10,19], no end-capping was performed as in the case of previous Suzuki polymerisation. Therefore the polymers are likely to have functional groups at the end chains.

It is also to be noted that in the introduced distannyls monomer indacenodithiophene fractions, there is also the presence of monostannyl indacenodithiophene and traces of unreacted indacenodithiophene as we have introduced this intermediate after work up as purification step, directly for polymerization. Therefore the monomer indacenodithiophene distannane could be the limiting reactant and may effect the chain growth during the polymerisation.

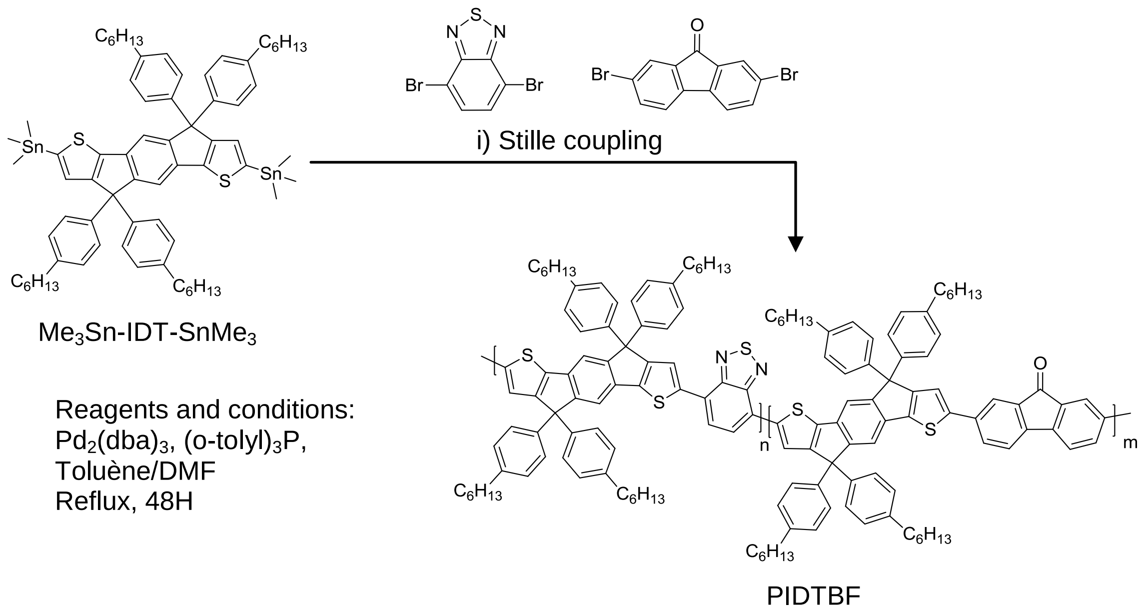


**Scheme 17: Synthetic route to random copolymer indacenodithiophene-benzothiadiazole-fluorenone terpolymer PIDTBF**

After polymerisations, the crude polymers were precipitated in methanol, and were stirred in methanol at room temperature overnight followed by acetone. The polymers PIDTB, PIDTF and PIDTBF were then filtered and purified by soxhlet extraction first with acetone followed by chloroform.

We reported below the $^{1}$H-NMR spectra of the three polymers indacenodithiophenes PIDTB, PIDTF and PIDTBF (of chloroform fractions for all three) including the departing monomers IDT-distannanes to make direct comparison of the chain structure of these polymers. In the Figure 159 only the aromatics spectra regions are showed for more visible comparison.

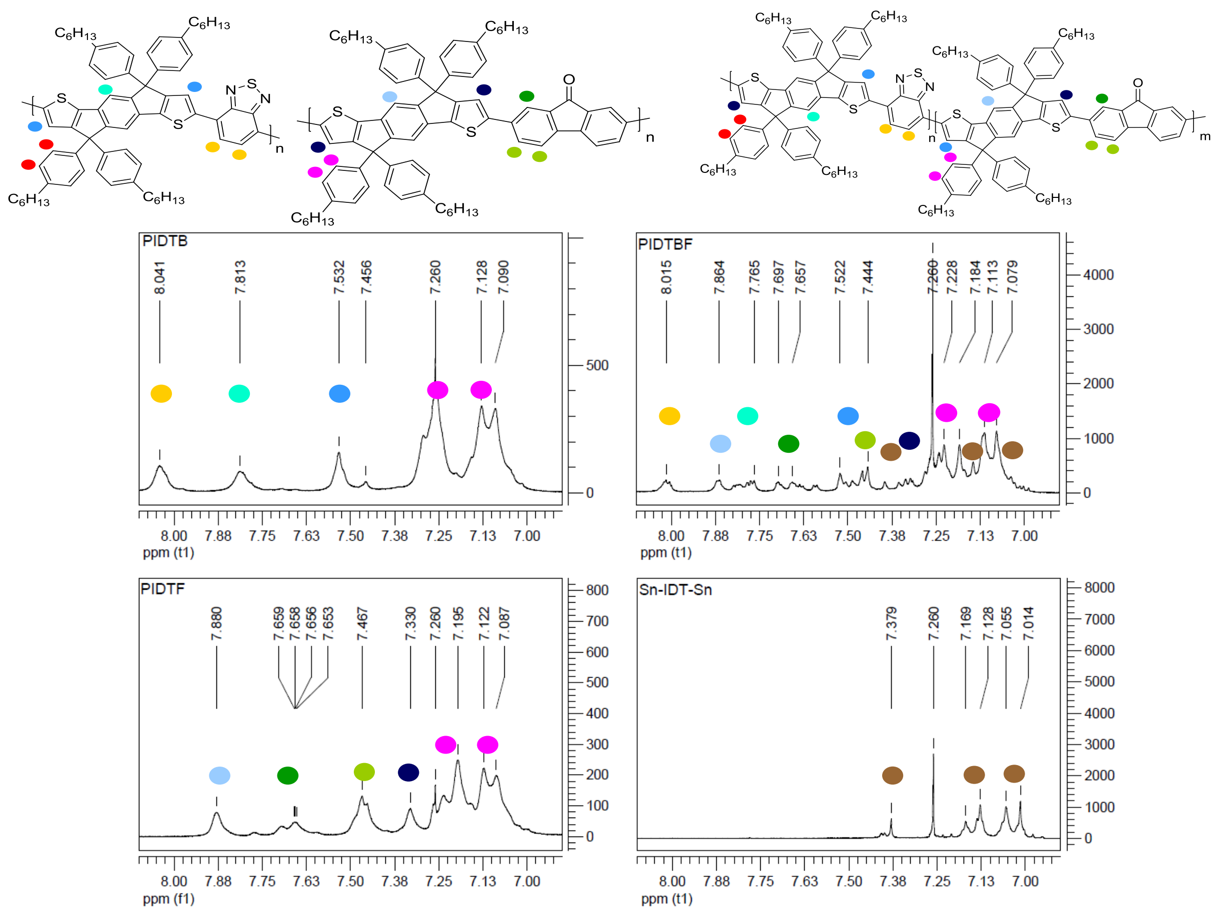


**Figure 159: NMR spectra of PIDTB, PIDTF, PIDTBF and monomer IDT distannyls**

The polymers PIDTB and PIDTF showed broad featureless peaks, typical of polymers. In the case of the polymer PIDTBF, we can observe that the peaks are less broadened peaks. We have first attributed each peak in the polymer PIDTB and PIDTF. The protons on the indacenodithiophene rings are represented by blue dots, the protons on the benzothiadiazole rings are represented by yellow dots and protons on the fluorenone rings are represented by green dots. The protons present in the monomer indacenodithiophene distannane are represented by brown dots. From these first attibutions, we can therefore attribute the peaks observed in the NMR spectrum of PIDTBF. We have consequently found the protons peaks present in the spectrum correspond to a combination of the peaks present in PIDTB and PIDTF. Therefore, we can conclude the presence of both benzothiadiazole-indacenodithiophene and fluorenone-indacenodithiophene segments in the polymer backbone with indacenodithiophene subunits. The monomer indacenodithiophene might also presence in the polymer PIDTBF.

In order to verify the presence or non presence of the stannyl functions at the end chains, NMR measurements can allow detection of the stannyl functions in the region near 0-1 ppm.

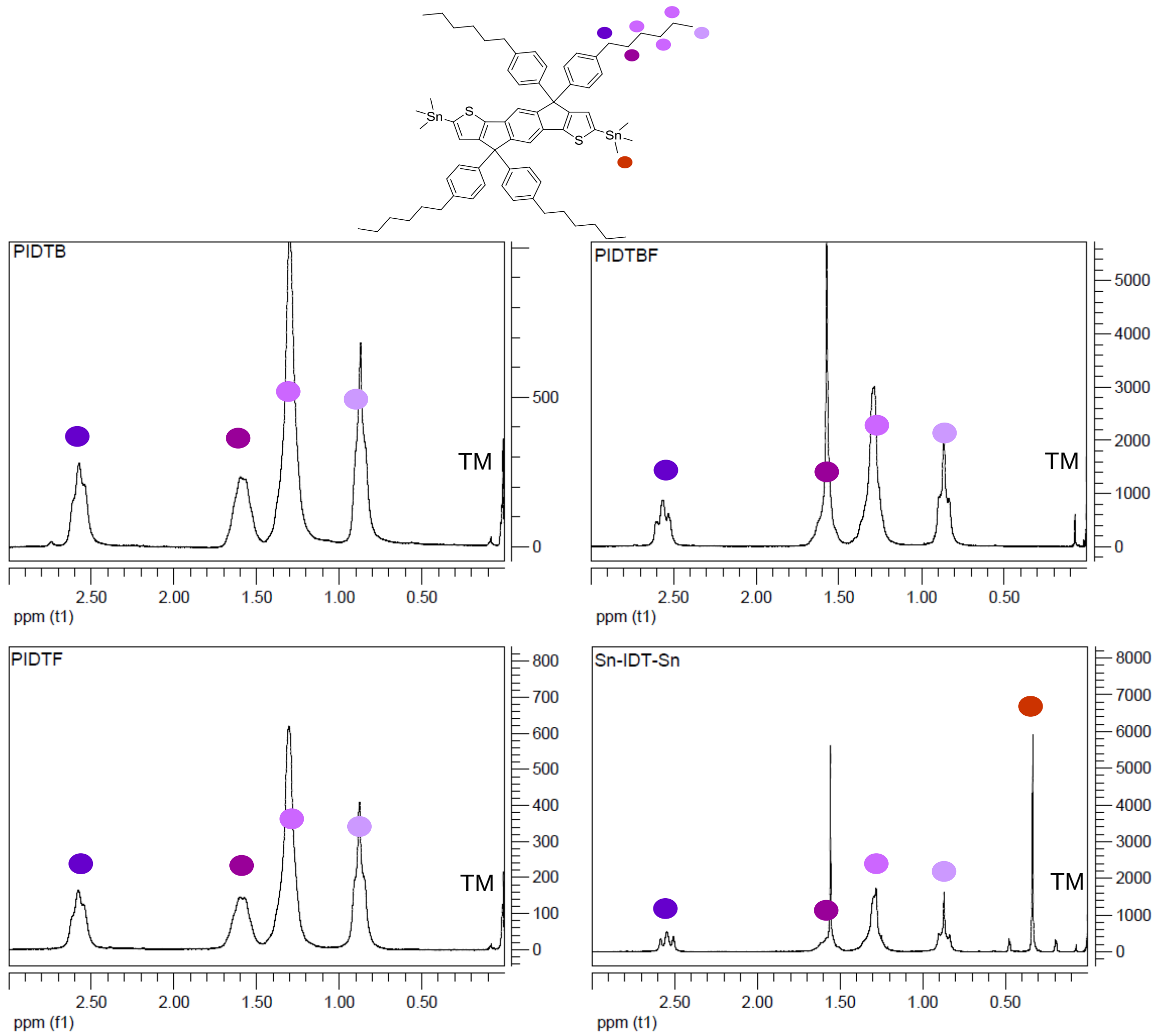


**Figure 160: Zoom of NMR spectra in the region 0 to 3 ppm for the polymers PIDTB, PIDTF and PIDTBF as well as distanyl indacenodithiophene monomers**

In the Figure 160, the spectrum of monomer distannanes indacenodithiophene Sn-IDT-Sn showed the satellite peak of stannyl function at 0.3 ppm. However in all the three polymers, there are no presences of stannyls functions in the chains. Therefore our polymers are most-likely not containing any non-reacted stannyl functions which can be harmful for environment for its toxicity [23] and which could act as recombination sites for the free charges in photovoltaic devices.

Elemental analyses of the determination of the mass fraction ratios of carbon, hydrogen, nitrogen and sulfur were performed for the polymers PIDTB, PIDTF and PIDTFB in order to verify the polymers structures. Based on the ratios obtained from elemental analyses, the proposed polymer structures of PIDTB, PIDTF and PIDTBF that best match with the experimental ratios are; PIDTB ($C_{280}H_{297}BrN_8S_{12}$ ) PIDTF ($C_{398}H_{396}Br_2O_6S_{10}$) and PIDTBF ($C_{83}H_{80}Br_2N_2OS_3$). From these results we can conclude that the chains terminations are most likely with Br- functions from the benzothiadiazole or fluorenone. For all the three polymers PIDTB, PIDTF and PIDTBF, calculated values taking into account the chain termination with bromine atoms showed closest values to the experimentally measured values. (cf. Experimental part). The fact that the polymers are not end-capped and are terminated by bromide function may have a little effect on charge mobility as demonstrated by McGehee and coworkers [24] and not harmful as the stannyl-end group.

The polymers indacenodithiophenes are further characterized by size exclusion chromatography to determine the molecular weight and the polydispersity of each polymer fractions. We performed size exclusion chromatography (SEC) of the three polymers using chloroform as eluent. The molecular weight and molecular weight distribution of the polymers were determined from the size exclusion chromatography (SEC) data. The values were calibrated with polystyrene standards. The yields for each fraction represent the obtained polymer fraction mass after soxhlet extraction over the total weight of the batch polymer. We have also calculated the molecular weight of the polymer with estimated chains (Mabs) to be compared with the molecular weight obtained of the highest peak Mpeak for each fraction. Icorr represent the percentage of error between these two values to evaluate the accordance between calculated values and experimental values. The calculated chain length represents the mostly present chains in each fraction. Mpeak calculation allows first attribution of each peak in the SEC chromatogram. SEC chromatogram of the polymers PIDTB, PIDTF and PIDTBF are presented in Figure 161.

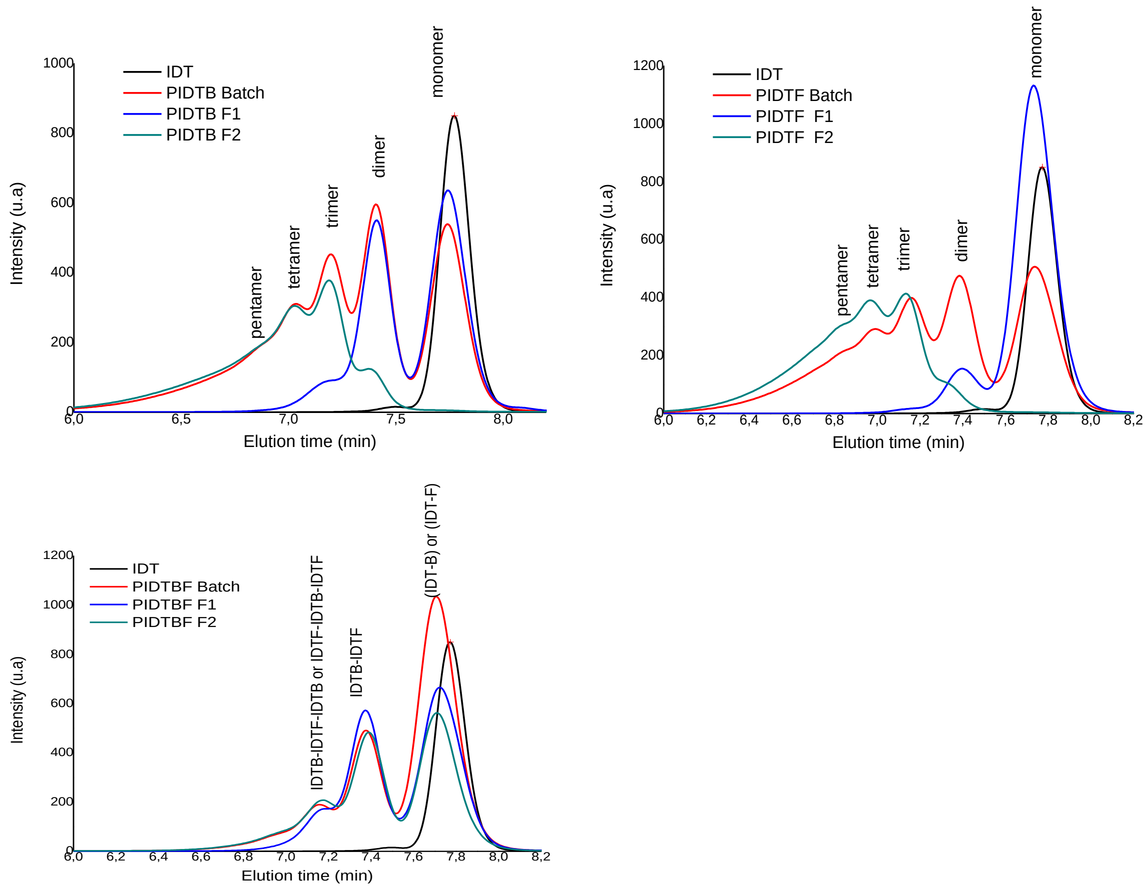


**Figure 161: SEC chromatogram of polymers PIDTB, PIDTF and PIDTBF and comparison of the batch elution diagrams for all three polymers with peak attribution based on chain calculation of Mpeak**

| Polymer | Fraction | Mn [kDa] | Mw [kDa] | I= Mw/Mn | Mpeak | Mabs | Icorr | Mw up to [kDa] | Yield (%) |
|---|---|---|---|---|---|---|---|---|---|
| IDT | | 0.94 | 0.97 | 1.03 | 0.98 | 0.91 | 1.08 | - | - |
| PIDTB | Crude | 2.07 | 4.35 | 1.13 | 2.18 | 2.16 | 1.01 | 67 | 100 |
| | Acetone | 1.36 | 1.71 | 1.26 | 1.05 | 1.12 | 0.93 | 8 | 40 |
| | Chloroform | 4.71 | 7.55 | 1.50 | 3.47 | 3.41 | 1.02 | 72 | 42 |
| PIDTF | Crude | 2.01 | 4.24 | 2.10 | 1.07 | 1.164 | 0.92 | 44 | 100 |
| | Acetone | 1.08 | 1.22 | 1.13 | 1.08 | 1.164 | 0.93 | 6 | 40 |
| | Chloroform | 5.43 | 7.56 | 1.14 | 3.89 | 3.558 | 1.09 | 47 | 60 |
| PIDTBF | Crude | 1.40 | 1.93 | 1.38 | 1.15 | 1.12 $_{IDTB}$ /1.16 $_{IDTF}$ | 1.03 0.99 | 18 | 100 |
| | Acetone | 1.42 | 1.86 | 1.31 | 1.09 | 1.12 $_{IDTB}$ /1.16 $_{IDTF}$ | 0.98 /0.94 | 10 | 20 |
| | Chloroform | 1.58 | 2.29 | 1.45 | 1.13 | 1.12 $_{IDTB}$ /1.16 $_{IDTF}$ | 1.01 /0.97 | 18 | 60 |

**Table 51: Molecular parameters of indacenodithiophene polymers PIDTB, PIDTF and PIDTBF determined by SEC in chloroform using polystyrene standards**

IDT corresponds to the indacenodithiophene monomer without the distannanes function, as it is not recommended to introduce highly reactive distannyls compounds that could be retained irreversibly in the SEC column. From the SEC chromatograms of the three polymers, the batch polymers are a mixture of monomers, short oligomers and longer polymers chains. We can observe the presence of short polymer chains that are highly abundant in the acetone fractions for all the three polymers. However, for the polymers PIDTB and PIDTF, the chloroform fractions are composed of longer polymer chains without the presence of short oligomeric chains. The first peak at the highest elution time for all the polymers are shifted towards shorter elution time as compared to the IDT peak, with different time for all the three polymers. From Mpeak values, the peaks correspond to the first coupling product of indacenodithiophene with either benzothiadiazole IDTB or fluorenone IDTF. We suggested that the indacenodithiophene distannyls compounds react readily with the dibrominated benzothiadiazole or fluorenone precursors.

The polymer PIDTB and PIDTF showed similar polymer chains lengths in the chloroform fraction composed mainly of trimer, tetramer, pentamer and longer chains. The polymer PIDTF showed a slightly higher degree of polymerization and a larger polydispersity index compared to the polymer PIDTB. If we compare these results to the previous results on fluorene-based copolymer obtained by Suzuki polymerizations, it appears that they are completely of the opposite. The better results obtained for the polymer based on fluorenone can be attributed to the utilization of small amount of DMF as co-solvent which was demonstrated as a good solvent in the Stille reaction of oligomer QTF8 (cf. Chapter 2). The chloroform fractions represent the highest molecular weight for the polymers. The polymers PIDTB and PIDTF showed average molecular weights of 4.71 kDaand 5.43 kDa respectively, whereas PIDTBF showed a low molecular weight of 1.58 kDafor the chloroform fractions. The chloroform fractions will be therefore used for further studies and preliminary tests in photovoltaic cells.

In the case of the random alternating copolymer PIDTBF, the acetone and chloroform fractions showed similar elugrams. The chloroform fraction showed slightly higher molecular weight of Mn= 1.58 (chloroform fraction) compared to Mn = 1.42 kDa (acetone fraction. We can postulate that the polymerization only conduct to oligomeric species or short polymer chain compared to polymers PIDTB and PIDTF. We have also obtained similar result of low degree of polymerization in the case of copolymer PTFBF with alternating fluorene-benzothiadiazole-fluorene-fluorenone in the repeating unit. This reflects the difficulty of polymerization of this type of random block polymers as we have three differents departing monomers. Therefore further optimization of this type of polymerization is necessary. One possible reason for the rapid termination of the polymerization of PIDTBF is partly due to the limiting indacenodithiophene units in the reaction as mentioned previously. Stoichiometry composition of the departing monomers is of crucial point in polycondensation reaction.

In overall, the polymerization of polymers indacenodithiophenes PIDTB, PIDTF and PIDTBF afford rather low molecular weight polymers compared to the values obtained in the literature of similar polymer based on benzothiadiazole. As mentioned in the previous chapter, palladium catalysed reactions are highly sensitive to oxygen and impurities. Rather short chains polymers are obtained (of about 5 repeating units) partially due to the deactivation of palladium catalyst in the reaction in presence of oxygen as discussed previously. Besides the presence of mono-stannylated precursors is probably the limiting factor to achieve the preparation of high molecular weight copolymers.

## III. Photo-physical characterisation of PIDTB, PIDTF , PIDTFB

We performed UV-Visible spectroscopy to determine the absorption spectra of the three polymers PIDTB, PIDTF and PIDTBF in chloroform solutions and in thin films. The concentration for each polymer was at 0.02 mg/ml and the thin films were prepared from polymers solutions with a concentration of 20 mg/ml in chlorobenzene and deposited onto glass substrates by spin-coating. The absorption spectra of the polymers PIDTB, PIDTF and PIDTBF in solution and in film are presented in Figure 162.

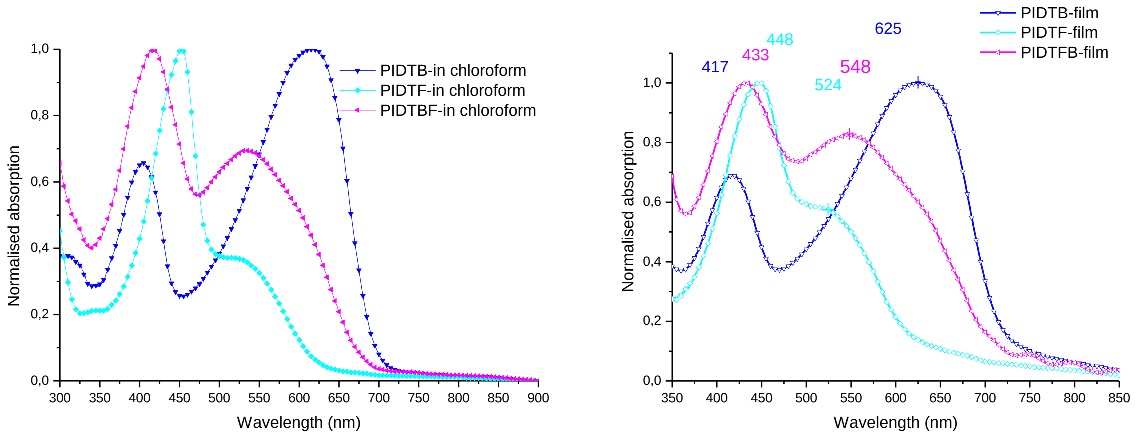


**Figure 162: UV-Visible spectra of polymers PIDTB, PIDTF and PIDTBF in chloroform solutions at 0.02 mg/ml and in film prepared from solutions of 20 mg/ml in chlorobenzene**

The polymer indacenodithiophene benzothiadiazole PIDTB showed broad absorption spectrum up to 710 nm with two maximum peaks at 404 nm and 618 nm. The first maximum peak at 404 attributed to the π–π* transition band of the indacenodithiophene unit and the second intense peak can be assigned to an internal charge transfer complex between the donor indacenodithiophene unit and the electron withdrawing benzothiadiazole. The molar extinction coefficient of absorption for the π–π* transition band of polymer PIDTB is rather low compared to the polymer PIDTF with the values of ξ =15752 M-1.cm-1 (λmax1=404 nm) and 23895 M-1.cm-1 (λmax1=451 nm). In solid state, the polymer further organized by molecular packing25 which is manifested by a bathochromic shift of ca 14nm for the first absorption band (417 nm) and 7 nm for the second one (625 nm). If we compare our absorption spectrum with the reference polymer reported by Chen and coworkers10, both spectra showed similar shape and intensity. All the photophysical properties of the three polymers are reported in Table 52.

| Polymer | Absorption Solution | | $Eg^{-opt}$ eV / (λoffset) | Absorption Film | | $Eg^{-opt}$ eV / (λoffset) |
|---|---|---|---|---|---|---|
| | λmax1/nm (ξ) | λmax2/nm (ξ) | | λmax1/nm | λmax2/nm | |
| PIDTB | 404 (15752) | 618 (23895) | 1.77 ( 700) | 417 | 625 | 1.69 ( 735) |
| PIDTF | 451 (42352) | 528 (15869) | 1.97 (630) | 448 | 524 | 1.91 (650) |
| PIDTBF | 418 (24331) | 536(16662) | 1.82 (680) | 433 | 548 | 1.71 (725) |

**Table 52: UV-visible absorption parameters of polymers PIDTB, PIDTF, and PIDTBF**

For the polymer PIDTF, the first absorption peak corresponding to the π–π* transition band is red-shifted to 451 nm compared to the one from PIDTB. The reason for the red-shifted value can be attributed to longer conjugation length for the polymer PIDTF affording higher molecular weight compared to the polymer PIDTB. A second shoulder is also observed for the polymer PIDTF with enhanced molar extinction coefficient of 15869 $cm^{-1}$ attributed to the internal charge transfer. This value is higher compared to the molar extinction coefficient of the polymer fluorene-fluorenone PTFF at 10818 $cm^{-1}$. The indacenodithiophene unit showed stronger internal charge transfer intensity with fluorenone compared to the fluorene-thiophene unit thanks to the stronger electron donating segment of the indacenodithiophenes. A recent paper by Lahti and coworkers who worked with oligomers based on fluorenone unit [26] also demonstrates the relationship between the intensity of the internal charge transfer band and the electron donor strength, the more the electron rich is the donating segment, the more the intensity of the ICT band is increased. This statement is in perfect accord with our result.

The random copolymer PIDTBF showed a first maximum peak at 418 nm corresponding to the π–π* transition band, at higher wavelength than the peak of polymer indacenodithiophene-benzothiadiazole PIDTB (14 nm red-shifted), but far less than the one from polymer indacenodithiophene-fluorenone PIDTF. Furthermore we observe broad band with maximum peak at 536 nm which can be attributed to combination of the internal charge transfer complex between both indacenodithiophene-benzothiadiazole and indacenodithiophene-fluorenone. This additional phenomenon is also observed in the random polymer fluorene-benzothiadiazole-fluorene-fluorenone, which confirms the synergistic effect of internal charge transfer with the presence of two electron withdrawing units combined into the same polymer chain.

## IV. Electrochemical characterisation of PIDTB, PIDTF and PIDTBF

Electrochemical measurements were performed for the three polymers PIDTB, PIDTF and PIDTBF to allow determination of HOMO and LUMO energy levels. Thin polymers were deposited by drop-casting on the platinum working electrode and analyzed in acetonitrile solution in presence of tetrabutyl ammonium hexafluorophosphate salt as supporting electrolyte at the concentration of 0.1 M. Cyclic voltammograms of the three polymers are presented in Figure 163.

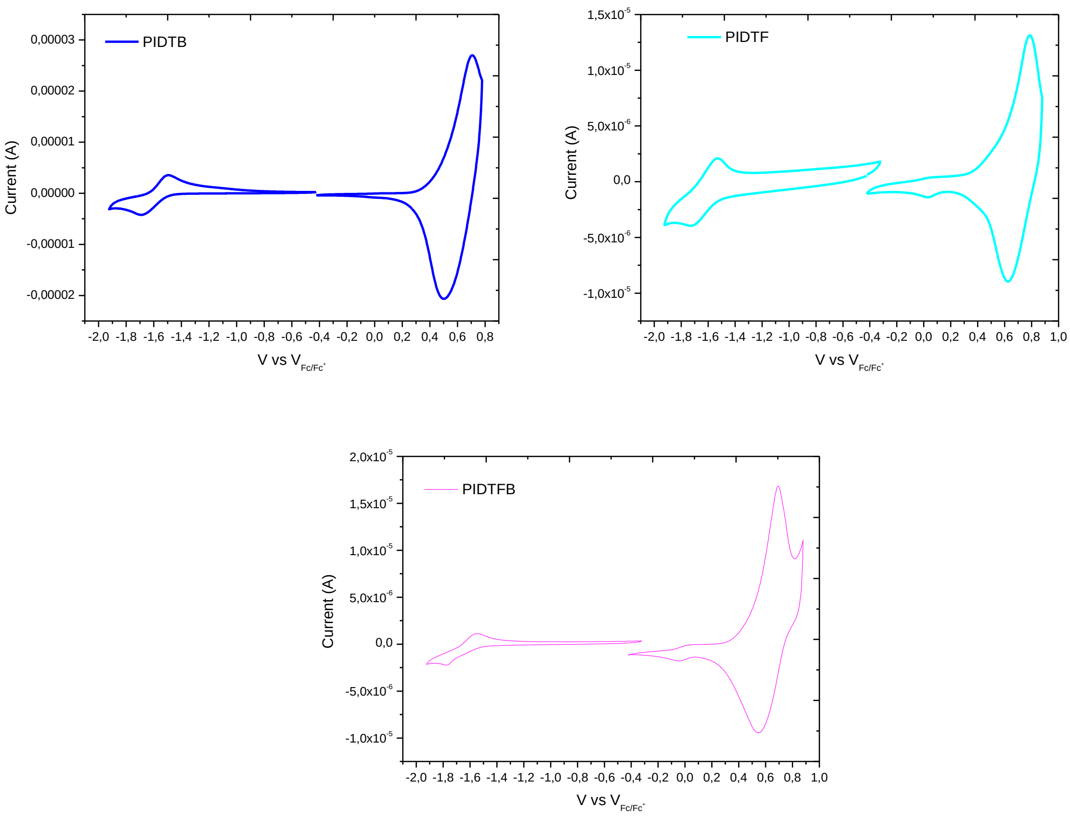


**Figure 163: Cyclic voltammograms of polymers PIDTB, PIDTF and PIDTBF**

The polymer PIDTB showed reversible oxidation and reduction processes with oxidation onset potential at 0.47 V and reduction potential at -1.50 V. These give the HOMO LUMO energy levels at -5.27 eV and -3.30 eV with a band gap of 1.97 eV. In their paper Chen and coworkers[10] have reported values of HOMO and LUMO energy levels at -5. 36 eV and -3.52 eV giving a band gap of 1.84. As our polymer PIDTB has much lower molecular weight Mw=

7.55 kDacompared to their polymer with Mw= 60.9 kg/mol, it is expected for our shorter polymer chains to have higher band gap[27].

| Compound | Eonset/V Oxidation | Eonset/V Reduction | HOMO /eV | LUMO /eV | Eg-opt /eV | Eg-ec /eV |
|---|---|---|---|---|---|---|
| PIDTB | 0.47 | -1.50 | -5.27 | -3.30 | 1.69 | 1.97 |
| PIDTF | 0.58 | -1.51 | -5.38 | -3.29 | 1.91 | 2.09 |
| PIDTBF | 0.49 | -1.52 | -5.29 | -3.28 | 1.71 | 2.01 |

**Table 53: Electrochemical values and calculated HOMO and LUMO energy levels of PIDTB, PIDTF and PIDTFB**

The polymer PIDTF showed higher oxidation potential at 0.58 V, consistent with the results observed with the polymer fluorene-fluorenone PTFF giving a low lying HOMO energy levels of -5.38 eV. While for polymer PIDTBF, the oxidation potential was found to be in between the two polymers PIDTB and PIDTF with a value of 0.49 V giving HOMO value at -5.29 eV. The reduction potentials for all the polymers PIDTB, PIDTF and PIDTFB showed close values of -1.50 V, -1.51 V and -1.52 V giving LUMO energy levels of -3.30 eV, 3.29 eV and -3.28 eV.

The electrochemical band gap results obtained are in agreement with the results obtained from optical band gap calculation for each polymer. The values from electrochemical band gap showed higher values of about 0.2 to 0.3 eV compared to the corresponding optical band gap which has also been reported for the our previously studied polymer fluorenes. It is worth to mention that from these results, we have succeeded to obtain for all the polymers based on indacenodithiophene, lower band gaps than the ones of the polymers based on fluorene PTFB, PTFF and PTFBF ( 2.12 eV, 2.14 eV and 2.23 eV), which is what we have expected. The energy levels of these series of polymers are plotted in the diagram Figure 164 below.

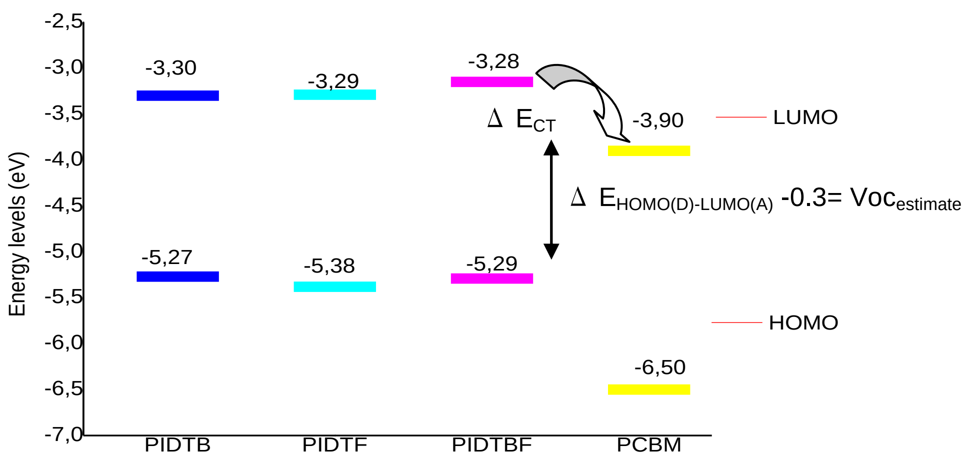


**Figure 164: Energy diagram of HOMO-LUMO levels for the polymers PIDTB, PIDTF, PIDTFB and PCBMC60**

We have made calculation of the offset between the LUMOs of the donor and acceptor corresponding to the energy required for the Donor-Acceptor to allow charge separation noted $\Delta E_{CT}$ and the theoretical maximum values of the open circuit voltage ($E_{HOMO}^{D}$-$E_{LUMO}^{A}$ -0.3 ) are calculated and the values are recorded in Table 54.

| Compound | HOMO /eV | LUMO /eV | Δ ECT /eV | Vocexpected /V |
|---|---|---|---|---|
| PIDTB | -5.27 | -3.30 | 0.60 | 1.07 |
| PIDTF | -5.38 | -3.29 | 0.61 | 1.18 |
| PIDTBF | -5.29 | -3.28 | 0.62 | 1.09 |

**Table 54: Calculated value of charge transfer energy Δ ECT and theoretical maximum open circuit voltage of PTFB , PTFF and PTFBF**

All the three polymers showed lowest unoccupied molecular orbital LUMO energy levels correctly positioned with respect to the one of the PCBM ($\Delta E_{CT}$> 0.3 eV)[28]. They are lying higher than the one of PCBM. Therefore the charge transfer between the donor polymers and the fullerene acceptor can occur. In terms of values of open circuit voltage, if we follow the relation propose by Scharber and coworkers[29] for the estimation of Voc, (Voc = $\Delta E_{HOMO(D)-LUMO(A)}$ -0.3) , we can hope to achieve high open circuit voltage of more than 1 V for polymers PIDTB, PIDTF and PIDTBF of 1.07 V, 1.18 V and 1.09 V respectively.

## V. Charge transfer properties

As we have discussed in previous chapter 5, we can investigate the charge transfer properties via photoluminescence measurements. We have conducted first the investigation of the photoluminescent properties for the pristine polymers PIDTB, PIDTF and PIDTFB in order to investigate the nature of the intramolecular charge transfer complex present in the polymers. We then conducted the second investigation of the photoluminescent properties of the blends containing the polymer as donor with the fullerene as acceptor in order to investigate the nature of the intermolecular charge transfer between the polymers and fullerene.

The measurements were recorded on pristine film polymers at concentration of 10 mg/ml for each polymer, and in blend with PCBM with concentration of 10 mg/ml for each material therefore a ratio of Polymer: PCBM 1:1.

## V.1. Photoluminescent study on pristine film PIDTB, PIDTF and PIDTFB

The photoluminescence emission spectra of the pristine film polymers PIDTB, PIDTF and PIDTFB as well as the corresponding UV-visible absorption spectra of the polymers in film are presented in Figure 165 .

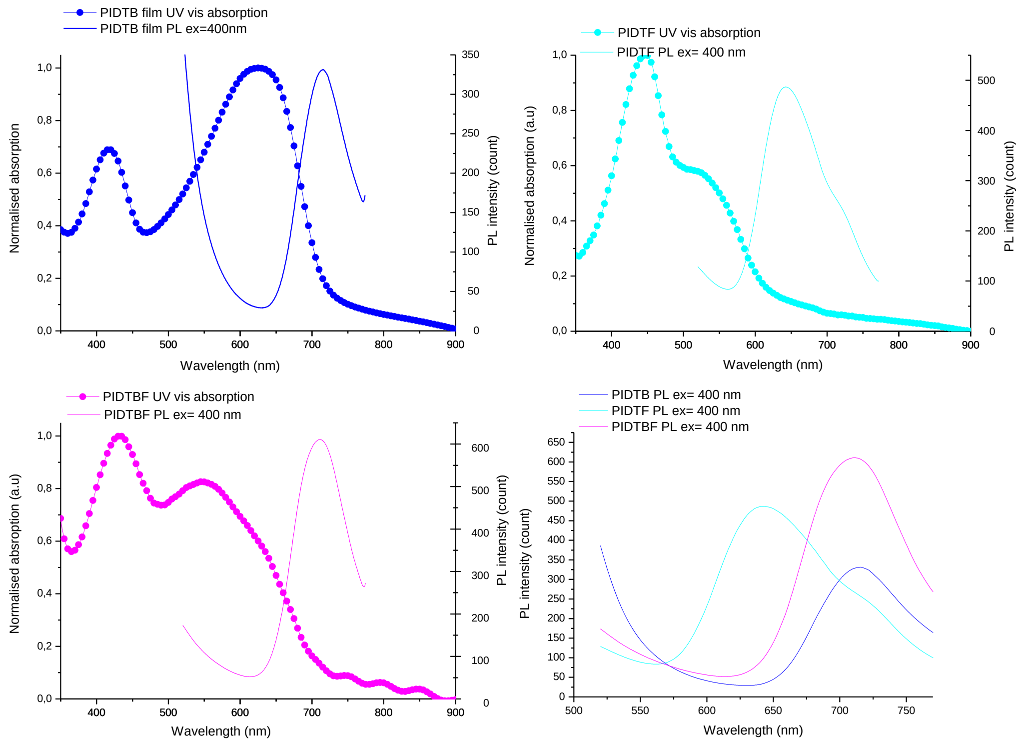


**Figure 165: Photoluminescence emission and UV visible absorption spectra of PIDTB, PIDTF and PIDTFB in film. Excitation wavelength for the photoluminescence measurement is at 400 nm. The three PL emission spectra is also presented in one graph for comparison.**

| Polymer | Absorption Film | | Photoluminescence Film λex=400 nm | Stokes shift |
|---|---|---|---|---|
| | λmax1/nm | λmax2/nm | λmax1/nm | nm |
| PIDTB | 417 | 625 | 715 | 90 |
| PIDTF | 448 | 524 | 642 | 118 |
| PIDTBF | 433 | 548; 634 (weak) | 711 | 77 |

**Table 55: UV Visible absorption and photoluminescence emission of the polymers PIDTB, PIDTF and PIDTBF in films . The excitation wavekength for all the PL measurements is at 400 nm.**

The photoluminescence spectrum of polymer PIDTB afford one band with a maximum peak at 715 nm. This gives a large Stokes shift of 90 nm. The emission band can be assigned to the internal charge transfer complex. No emission at lower wavelengths can be detected.

Interestingly, the polymer PIDTF also afforded only one emission band with a maximum peak at 642 nm giving rise to a large Stokes shift of 118 nm. No luminescence is also observed in the region of 500 nm to 600 nm corresponding to the region of absorption band of the internal charge transfer complex. As a result, we can therefore note that in the case of PIDTF, the polymer exhibits strong internal charge transfer between the fluorenone unit and the indacenodithiophene unit. This is particularly remarkable as we have observed in the case of poly-thiophene fluorene-fluorenone PTFF, we observed two emission bands indicating a partial charge transfer between thiophene fluorene unit and fluorenone. Therefore the results based on photoluminescence study on the PIDTF demonstrate that the indacenodithiophene and the fluorenone unit exhibit stronger internal charge transfer resulting to total transfert of excitation and the occurrence of only one emission band.

For the polymer PIDTBF consisting of the combination of the two repeating unit of PIDTB and PIDTF indacenodithiophene-benzothiadiazole-co-indacenodithiophene fluorenone unit in the polymer backbone, affords a photoluminescence emission spectrum close to the polymer PIDTB with a peak at 711 nm (see Figure 165 at bottom right) with a Stokes shift of 77 nm. This is of no surprising as we observed the presence of the weak absorption shoulder seen in the absorption spectrum corresponding to the weak internal charge transfer complex between indacenodithiophene segment and benzothiadiazole segment. The results fully supported that combination of two electron withdrawing units in the same polymer backbone can exhibit apparition of two internal charge transfer complex in the absorption band. The emission band will therefore correspond to the emission band of the internal charge transfer complex at highest wavelength. We can therefore postulate a multi level internal charge transfer occurred in the polymer PIDTBF as depicted in Figure 166.

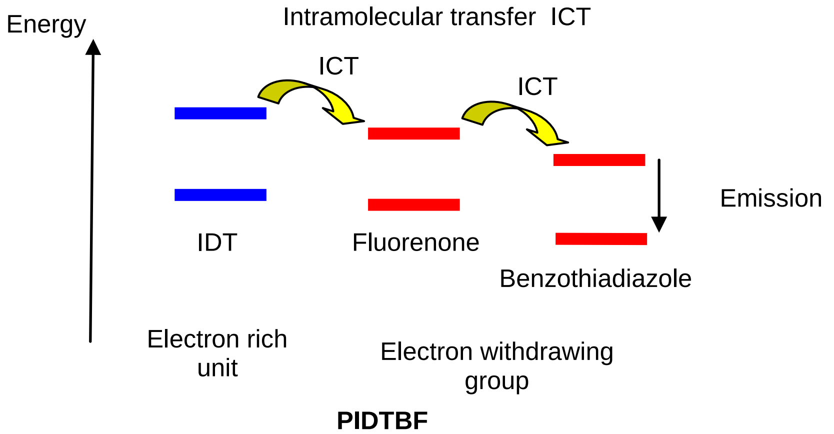


**Figure 166: Hypothesis of multi-step internal charge transfer in the polymer PIDTBF**

However, further investigations using time resolved spectroscopy are necessary to determine precisely the transfer energy pathways in those macromolecular systems.

## V.2. Photoluminescent study on blends of PIDTB, PIDTF and PIDTFB with fullerene PCBM

The photoluminescence emission spectra of the blends of Polymers indacenodithiophenes: PCBM (1:1) are presented in Figure 167.

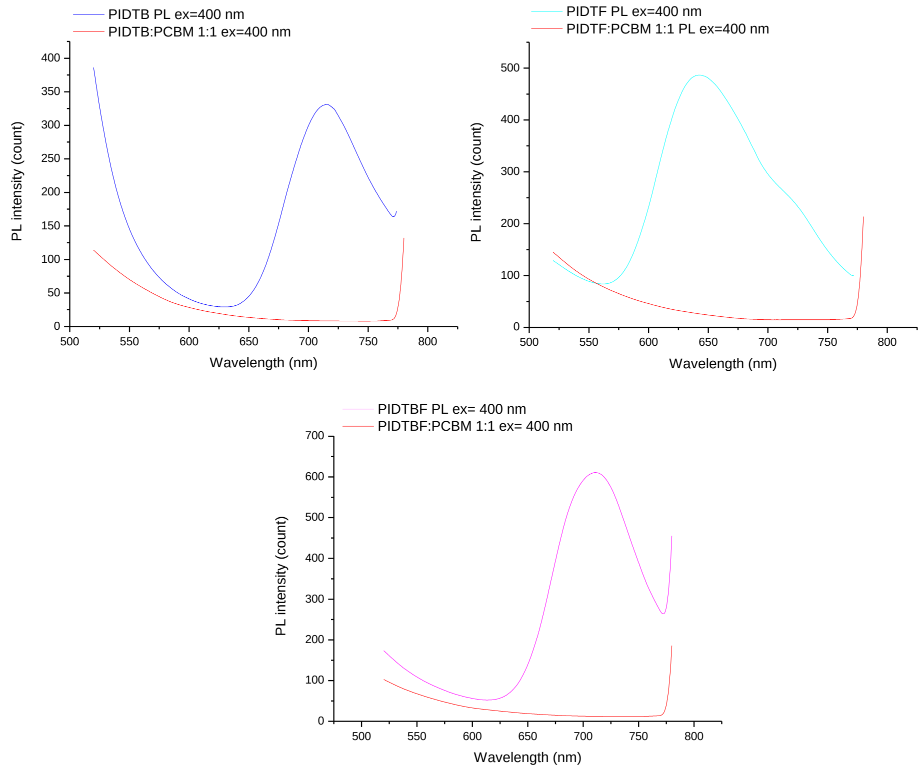


**Figure 167: Photoluminescence emission of the blends of PIDTB:PCBM 1:1 , PIDTF:PCBM 1:1, PIDTBF:PCBM 1:1 at excitation wavelength of 400 nm. The PL emission spectra of the pristine polymers films are also presented for comparison.**

Firstly, when the pristine polymers are excited at 400 nm, the donor polymers showed apparition of emission bands in the region of 600 nm to 770 nm for the different polymers. When the polymers indacenodithiophenes PIDTB, PIDTF and PIDTBF are mixed with acceptor material fullerene PCBM, the photoluminescence emission spectra give in all the three blends complete quenching of luminescence. As we have discussed in the last chapter, the quenching luminescent of the blends marked an efficient charge transfer between the donor polymer and the acceptor fulerene. Therefore the blends films of the polymers and the fullerenes formed suitable interpenetrating network for charge transfer between the donor and acceptor materials. Therefore in the blend of our polymer donor with the acceptor materials PCBM, we can conclude that, at the molecular scale, charge transfer can occur between PTFB and PCBM, which is the first required step for their application in photovoltaic cells.

# VI. Charge carrier transport properties

To investigate the charge carrier mobilities in the polymers indacenodithiophenes, we have preformed thin film field effect transistor measurement of the polymers PIDTB and PIDTF. Transfer characteristic curves of the thin film transistors are presented in Figure 168. The transport properties of the polymers PIDTB and PIDTF at saturation regime ($V_D$= -60 V) are presented in Table 56 as well as the values for polymers PQTB, PQTF, PTFB and PTFF.

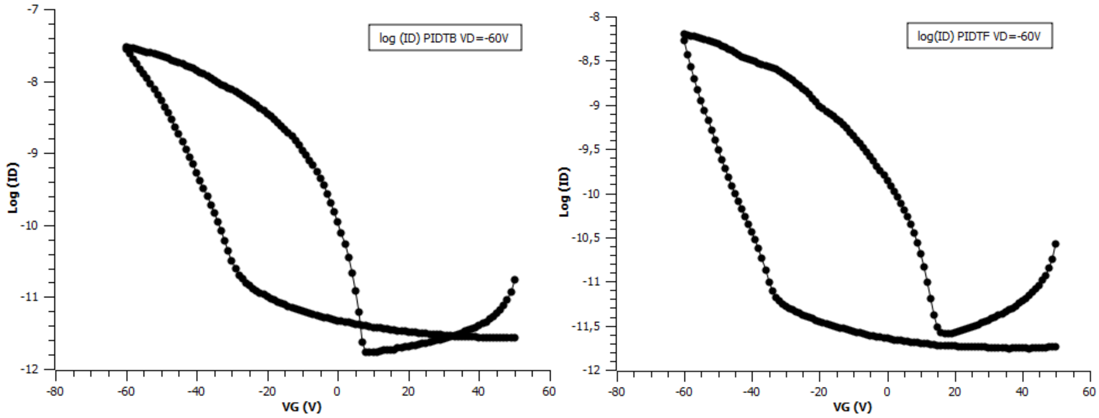


**Figure 168: Transfer characteristic curves of log $I_{DS}$= f($V_G$) for $V_D$=-60V measured for thin films of polymers PIDTB and PIDTF with channel length of 10 µm, The $V_{DS}$ was kept at −60 V, and the $V_G$ bias was swept from +60V to -60 V and reverse to +60 V again.**

| Polymer | µ ($cm^2.V^{-1}.s^{-1}$) | Vthreshold (V) | Ioff (A) | Ion/Ioff |
|---|---|---|---|---|
| PIDTB | $2.47.10^{-5}$ | 1.6 | $-1.99\ 10^{-12}$ | 31900 |
| PIDTF | $2.27\ 10^{-6}$ | 2.7 | $-1.76\ 10^{-12}$ | 4130 |
| PTFB | $4.36\ 10^{-5}$ | -12.7 | $-2.89\ 10^{-12}$ | 14100 |
| PTFF | $5.76\ 10^{-6}$ | -13.6 | $-4.98\ 10^{-13}$ | 1760 |
| PQTB | $1.00\ 10^{-5}$ | 74.8 | $-1.04\ 10^{-8}$ | 13.3 |
| PQTF | $6.10\ 10^{-8}$ | 77.3 | $-1.11\ 10^{-11}$ | 7.4 |

**Table 56: Transport properties at saturation regime of VDS= -60 V for all the studied polymers.**

The polymer indacenodithiophene benzothiadiazole showed a mobility of $2.47.10^{-5}$ $cm^2.V^{-1}.s^{-1}$, voltage threshold (VT) at 1.56 V and the ratios between the maximum and minimum current Ion/Ioff of the drain (at VD=-60V) of 31900. For polymer indacenodithiophene-fluorenone PIDTF, the device showed a mobility $2.27.10^{-6}$ $cm^2.\ V^{-1}.\ s^{-1}$, voltage threshold ($V_T$) at 2.72 V and the current ratios Ion/Ioff of the drain of 4130.

The polymer indacenodithiophene-benzothiadiazole PIDTB showed a ten-fold higher hole mobility than the polymer indacenodithiophene-fluorenone PIDTF. The polymer PIDTB also affords higher Ion/Ioff ratio. Previously the polymer fluorene-benzothiadiazole PTFB has shown higher mobility than the analog polymer thiophene-fluorene-fluorenone PTFF. The three polymers with benzothiadiazole electron-withdrawing groups have shown higher hole mobility than the corresponding polymers with fluorenone unit. The mobility is the highest for fluorene-based polymers, followed by the indacenodithiophenes polymers and at the lowest mobility for the polymers based on quaterthiophenes.

# VII. Preliminary tests of PIDTB, PIDTF and PIDTBF in photovoltaic devices

During the last months of this thesis, we have performed preliminary tests for our polymers in photovoltaic devices. The processing conditions are totally different from the previously tested photovoltaic cells. The photovoltaic device configuration is presented in Figure 169 below and differed from the previous configuration is utilization of calcium/aluminum electrode instead of lithium fluoride/Aluminum cathode.Ca/Al electrode has been demonstrate to afford higher performance photovoltaic devices than the LiF/Al electrode[30].

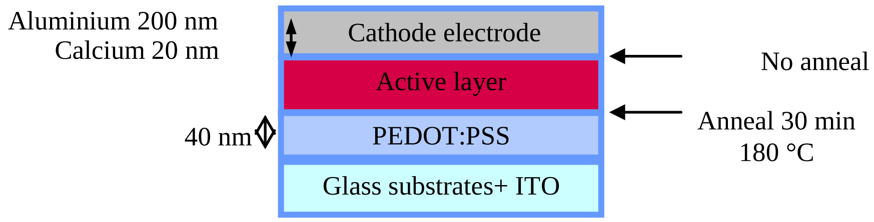


**Figure 169: Photovoltaic device configuration used for the device based on indacenodithiophene polymers**

For these first series of tests, we have chosen the reference fullerenes PCBMC60 as our acceptor materials [31]. For the preparation of the blends we have kept constant the concentration of the donor polymer at 20 mg/ml in order to maximize the photon absorption from the absorbing material, and varied the amount of fullerene acceptor PCBMC60 according to the ratios Polymer: PCBMC60 from 1:1 to 1:3 in order to investigate the optimum ratios for the blends. Ortho-dichlorobenzene was used as solvent for the dissolution of active materials as orthodichlorobenzene allows higher dissolution of fullerene at high concentration than chlorobenzene. In a pure material solution fullerene PCBMC60 showed limiting solubility at 50 mg/ml[32] and 100 mg/ml in o-dichlorobenzene[33].

We present here preliminary results of photovoltaic devices based on the series of polymers indacenodithiophenes.

## VII.1. Photovoltaic devices based on of PIDTB

We have traced the curves of current density-potential characteristics of PIDTB: PCBMC60 devices according to the ratios 1:1, 1:2 and 1:3 as shown in Figure 170, and the photovoltaic parameters in Table 57.

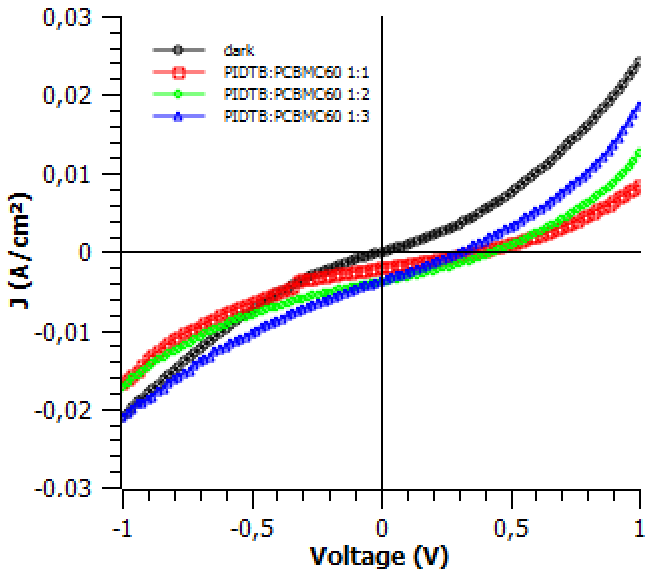


**Figure 170: Current density-potential characteristics of PIDTB: PCBMC60 devices according to the ratios 1:1, 1:2 and 1:3**

| Donor | Acceptor | Ratio D:A | Voc | Jsc (mA.cm-²) | FF | PCE (%) |
|---|---|---|---|---|---|---|
| PIDTB | PCBMC60 | 1:1 | 0.37 | 2.03 | 0.28 | 0.21 |
| PIDTB | PCBMC60 | 1:2 | 0.43 | 3.80 | 0.30 | 0.49 |
| PIDTB | PCBMC60 | 1:3 | 0.34 | 3.71 | 0.28 | 0.36 |

**Table 57: Photovoltaic parameters of polymer PIDTB: PCBM according to ratios 1:1, 1:2 and 1:3**

The photovoltaic devices based on PIDTB:PCBMC60 of different ratios showed an overall low power conversion efficiencies less than 1 %. The short circuit current densities for the devices were obtained of 2 $mA.cm^{-2}$ to 3.80 $mA.cm^{-2}$ for the device of a ratios PIDTB:PCBMC60 1:2. The open circuit voltage for all the devices were quite low with values of 0.34 V to 0.43 V. The fill factors of the devices were found to be comprised between 28 and 30 %. In overall, our polymer PIDTB has shown low performance in photovoltaic device. The polymer indacenodithiophene benzothiadiazole PIDTB gives highest power conversion efficiency for the device PIDTB: PCBMC60 of 1:2 ratio with 0.50 % of power conversion efficiency. The results can be partly due to low molecular weight obtained for our polymer of Mw=7.5 kDa compared to the polymer reference PTPTBT of Mw= 60.9 kDa. The reference device from Chen and coworkers group [10] based on polymer PTPTBT: PCBMC60 1:1 gives a power conversion efficiency of 4.3% with high open circuit voltage of 0.87 V, A short-circuit current density of 8.7 mA.cm-2 and a fill factor of 65%

.

## VII.2. Photovoltaic devices based on of PIDTF

The current density-voltage curves of the photovoltaic devices based on PIDTF and photovoltaic parameters are presented in Figure 171 and in Table 58.

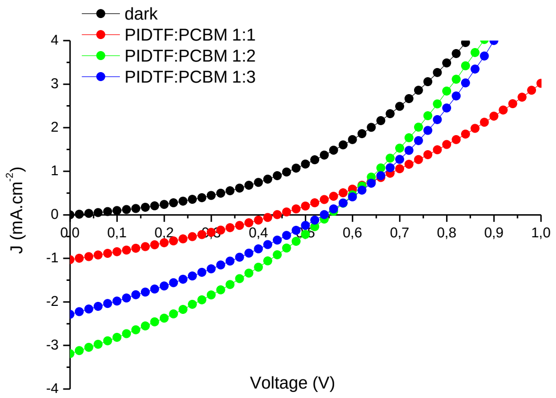


**Figure 171: Current density-potential characteristics of PIDTF: PCBMC60 devices according to the ratios 1:1, 1:2 and 1:3**

| Donor | Acceptor | Ratio D:A | Voc | Jsc (mA.cm-²) | FF | PCE (%) |
|---|---|---|---|---|---|---|
| PIDTF | PCBMC60 | 1:1 | 0.43 | 1.12 | 0.29 | 0.14 |
| PIDTF | PCBMC60 | 1:2 | 0.55 | 3.19 | 0.31 | 0.55 |
| PIDTF | PCBMC60 | 1:3 | 0.54 | 2.29 | 0.30 | 0.37 |

**Table 58: Photovoltaic parameters of polymer PIDTF:PCBM according to ratios 1:1, 1:2 and 1:3**

The devices based on polymer PIDTF:PCBM of ratios 1:1 , 1:2 and 1:3 give a short circuit current density of 1.12 mA.cm$^{-2}$ to 3.12 mA.cm$^{-2}$. Similar to the polymer PIDTB, increase short circuit current density is observed when we doubled the amount of PCBM from 1 equivalent to 2 equivalents of polymer PIDTF, from 1.12 mA/cm² to 3.19 mA/cm². For the polymer PIDTF we obtained in general higher open circuit voltage compared to PIDTB with the highest open circuit voltage at 0.55 V. This result in a better performance with power conversion efficiency of 0.55 % for the device PIDTF: PCBM of ratio 1:2. This is in accordance with the low lying HOMO energy level of PIDTF compared to the polymer PIDTB ( EHOMO PIDTF= -5.38 eV and EHOMO PIDTB =-5.27 eV ) as predicted previously from electrochemical studies.

## VII.3. Photovoltaic devices based on of PIDTBF

The current density-voltage curves of the photovoltaic devices based on PIDTBF and the photovoltaic parameters are presented in Figure 172 and in Table 59.

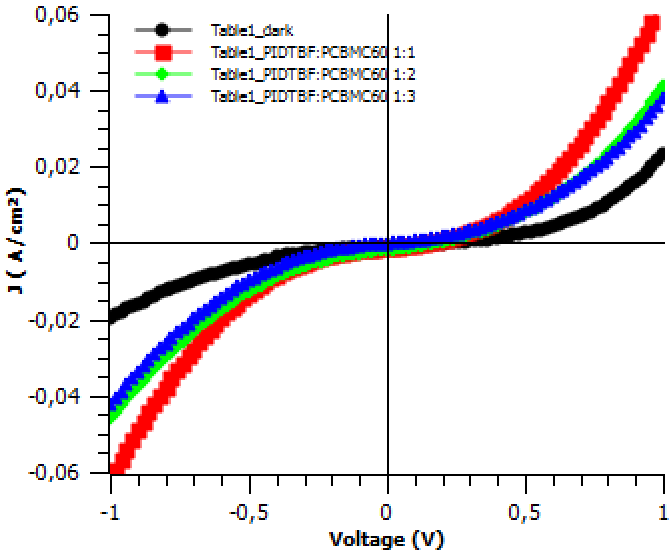


**Figure 172:Current density-potential characteristics of PIDTBF: PCBMC60 devices according to the ratios 1:1, 1:2 and 1:3**

| Donor | Acceptor | Ratio D:A | Voc | Jsc (mA.cm-²) | FF | PCE (%) |
|---|---|---|---|---|---|---|
| PIDTBF | PCBMC60 | 1:1 | 0.16 | 1.35 | 0.30 | 0.06 |
| PIDTBF | PCBMC60 | 1:2 | 0.17 | 1.75 | 0.30 | 0.09 |
| PIDTBF | PCBMC60 | 1:3 | 0.22 | 0.94 | 0.29 | 0.06 |

**Table 59: Photovoltaic parameters of polymer PIDTBF: PCBM according to ratios 1:1, 1:2 and 1:3**

For the copolymer PIDTBF, we obtained very low performance in photovoltaic cells for different ratios of less than 0.1 % of power conversion efficiencies. Low open circuit voltages at about 0.2 V are observed for the tested devices. The low values of the open circuit voltages can be due to reduced effective band gap between the fullerene and the polymer PIDTBF and inefficient charge separation due to presence of traps. The poor film forming ability which can be related to the low molecular weight of the polymer fraction used for the fabrication of the devices can explain these results.

PIDTBF:PCBMC60

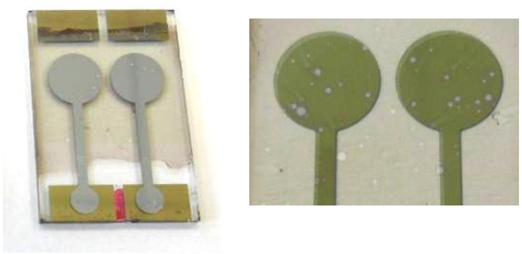

**Figure 173: Image of the tested photovoltaic device PIDTBF:PCBM revealing some visible 'holes' in the active layer surface . (Left) Front view with aluminium on top of the active layer. (Right) View from glass side with active layer on top of the aluminium**

As seen in the image of the device in Figure 173, we can observe some visible holes (right image) on the surface of the active layer which can cause short circuit for the photovoltaic device. This gives overall low performance in solar cells of only 0.09 % of power conversion efficiency. Based on the results obtained for all the polymers based on indacenodithiophenes PIDTB, PIDTF and PIDTBF on photovoltaic devices, we have obtained in general very low performance in power conversion efficiencies.

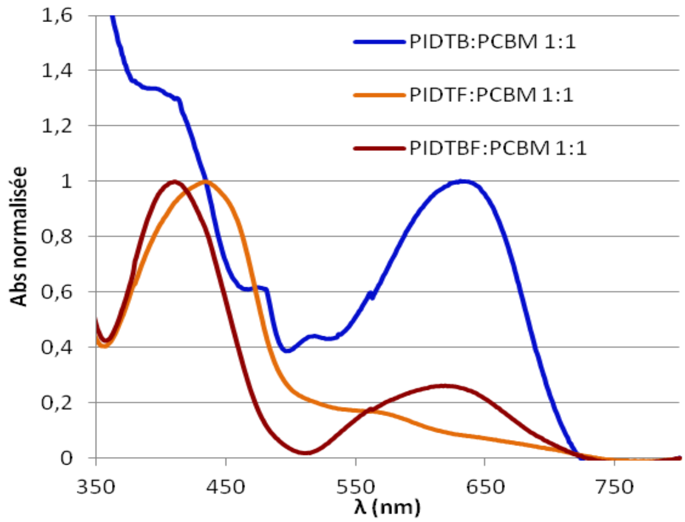


**Figure 174: UV-Visible absorption spectra of the tested device PIDTB:PCBM 1:1 , PIDTF: PCBM 1:1 and PIDTBF: PCBM 1:l**

Even though the polymers in combination with PCBM showed broad absorption spectra across the UV-Visible solar spectrum (see Figure 174), very low short circuit current densities were obtained and low open circuit voltages. We have therefore to further optimize our device fabrication in terms of material solubility and film forming properties to avoid formation of holes in the active layers. The preliminary results are however encouraging since the polymers used in this study were capped by bromine atoms which may act as recombination sites and show low molecular weights. Improvement of the devices performances can also be expected using PCBMC70 as an electron acceptor compound for the fabrication of the blends.

# VIII. Conclusion

We have presented in this chapter the synthetic strategy for the preparation of new series of polymer based on indacenodithiophene electron rich units. This unit is a fully planar segment which has been coupled with two different electron deficient group benzothiadiazole and fluorenone. The indacenodithiophene-based copolymers showed increased planarity that can afford low band gap molecules and good charge carrier properties polymers compared to the all thiophenes based polymers.

We have synthesized three polymers poly-indacenodithiophene-benzothiadiazole PIDTB, poly-indacenodithiophene-fluorenone PIDTF and copolymer poly-indacenodithiophene-benzothiadiazole-fluorenone PIDTBF. After preparation of monomer indacenodithiophene, the polymerization method adopted for the preparation of polymers is via Stille coupling, an efficient method for thiophene-based monomers and aromatic halide. The polymerization of the copolymer combining the two electron withdrawing units in the polymer backbone poly-indacenodithiophene-benzothiadiazole-fluorenone PIDTBF has also afforded short oligomeric chains similar to the copolymer thiophenefluorene-benzothiadiazole-co- thiophenefluorene-fluorenone PTFBF. We have not yet succeeded in optimizing this type of coupling reaction involving three different monomers as departing reactifs.

In terms of photophysical properties, we have further broadened the absorption spectra compared to the polymer polyfluorenes as shown in Figure 175 thanks to the enhanced planarity between the indacenodithiophenes units and benzothiadiazole or fluorenone.

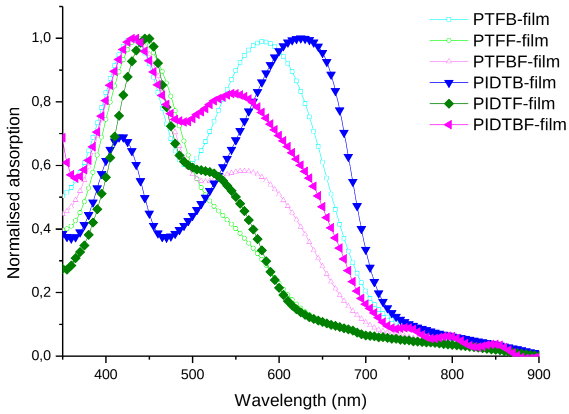


**Figure 175: Comparison of photophysical properties of polymer indacenodithiophenes ( in close symbol) PIDTB, PIDTF and PIDTBF with polymers fluorenes PTFB, PTFF and PTFBF**

By electrochemical analysis the polymers exhibit low lying HOMO between -5.27 eV for PIDTB and -5.38 eV for PIDTF with the band gap of the polymers at about 2 eV. The polymers indacenodithiophenes are correctly positioned to the HOMO LUMO levels of fullerene acceptor PCBM as shown in Figure 176. The polymers PIDT exhibit low LUMO levels closer to the LUMO level of the acceptor PCBM which will favor the excitons dissociations. The moderately low lying HOMO energy levels can offer higher open circuit voltages in photovoltaic cells. Therefore polymers indacenodithiophenes are interesting donor materials for photovoltaic applications.

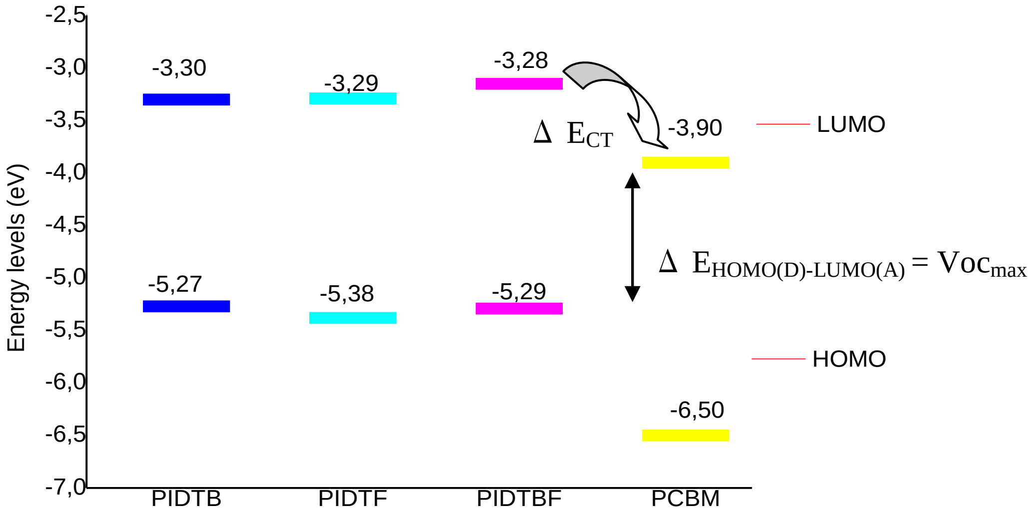


**Figure 176: Energy levels diagram of different polymers with PCBMC60**

We have performed preliminary tests for the polymers indacenodithiophenes in photovoltaic devices. Despite our high expectation on these series polymers, we have obtained rather low photovoltaic performance with the highest photovoltaic cell device giving 0.5 %, with low current density of 3.2 mA/cm², open circuit voltage of 0.5 V and a fill factor or 32 % for the polymer indacenodithiophene-fluorenone:PCBMC60 1:2 .

Further optimization of these series of polymers principally on the polymerization procedures is of high priority in order to achieve high molecular weight polymers with high purities. The polymer indacenodithiophenes showed particularly interesting donor materials for its beneficial properties for solar cells applications. Even though our first tests in photovoltaic devices showed low performance, the essential point of these polymers do generate photocurrents in blend with fullerenes acceptors open doors for improvements for future works.

# IX. References


1 U. Scherf and K. Müllen, The synthesis of ladder polymers, Advances in polymer Science, Vol. 123, 1995

2 J. Roncali, Molecular Engineering of the Band Gap of p-Conjugated Systems: Facing Technological Applications, Macromol. Rapid Commun. 2007, 28, 1761–1775

3 Y. Li, Molecular Design of Photovoltaic Materials for Polymer Solar Cells: Toward Suitable Electronic Energy Levels and Broad Absorption, Acc. Chem. Res., 2012, 45 (5), pp 723–733

4 Q Zheng, B J Jung, J Sun, and H E. Katz, Ladder-Type Oligo-p-phenylene-Containing Copolymers with High Open-Circuit Voltages and Ambient Photovoltaic Activity, Journal of the American Chemical Society, 2010 132 (15), 5394-5404

5 Y-J Cheng, C-H Chen, Y-S Lin, C-Y Chang, and C-S Hsu, Ladder-Type Nonacyclic Structure Consisting of Alternate Thiophene and Benzene Units for Efficient Conventional and Inverted Organic Photovoltaics, Chemistry of Materials 2011 23 (22), 5068-5075

6 R. K. Cheedarala , G.-H. Kim , S. Cho , J. Lee , J. Kim , H.-K. Song , J.Y. Kim and C. Yang, Ladder-type heteroacene polymers bearing carbazole and thiophene ring units and their use in field-effect transistors and photovoltaic cells, J. Mater. Chem., 2011,21, 843-850

7 Y-J Cheng , S-W Cheng , C-Y Chang , W-S Kao , M-H Liao and C-S Hsu, Diindenothieno[2,3-b]thiophene arene for efficient organic photovoltaics with an extra high open-circuit voltage of 1.14 ev, Chemical Communications 48, 3203 (2012)

8 Duan, C., Cai, W., Zhong, C., Li, Y., Wang, X., Huang, F. and Cao, Y. (2011), Bandgap engineering of indenofluorene-based conjugated copolymers with pendant donor-π-acceptor chromophores for photovoltaic applications. J. Polym. Sci. A Polym. Chem., 49: 4406–4415.

9 I. McCulloch, R. S. Ashraf, L. Biniek, H. Bronstein, C. Combe, J. E. Donaghey, D. I. James, C. B. Nielsen, B. C. Schroeder, and W. Zhang, Design of Semiconducting Indacenodithiophene Polymers for High Performance Transistors and Solar Cells, Accounts of Chemical Research 2012 45 (5), 714-722

10 Y. Chen, C. Yu, Y. Fan, L. Hung, C. Chen, C. Ting, Low-Bandgap Conjugated Polymer for High Efficient Photovoltaic Applications. Chem. Commun. 2010, 46, 6503–6505

11 O InganÄs, F Zhang, and M R. Andersson, Alternating Polyfluorenes Collect Solar Light in Polymer Photovoltaics, Accounts of Chemical Research 2009 42 (11), 1731-1739

12 J Chen and Y Cao, Development of Novel Conjugated Donor Polymers for High-Efficiency Bulk-Heterojunction Photovoltaic Devices, Acc. of Chem. Res. 2009 42 (11), 1709-1718

13 J Zhang, W Cai, F Huang, E Wang, C Zhong, S Liu, M Wang, C Duan, T Yang, and Y Cao, Synthesis of Quinoxaline-Based Donor−Acceptor Narrow-Band-Gap Polymers and Their Cyclized Derivatives for Bulk-Heterojunction Polymer Solar Cell Applications, Macromolecules 2011 44 (4), 894-901

14 L Biniek, S Fall, C L. Chochos, D V. Anokhin, D A. Ivanov, N Leclerc, P Lévêque, and T Heiser, Impact of the Alkyl Side Chains on the Optoelectronic Properties of a Series of Photovoltaic Low-Band-Gap Copolymers, Macromolecules 2010 43 (23), 9779-9786

15 H. Bronstein, R.S. Ashraf, Y. Kim, A.J. P. White, T. Anthopoulos, K. Song, D. James, W. Zhang, and I. McCulloch, Synthesis of a Novel Fused Thiophene-thieno[3,2-b]thiophene-thiophene Donor Monomer and Co-polymer for Use in OPV and OFETs. Macromol. Rapid Commun., 2011, 32, 1664–1668.

16 Li, W.; Qin, R.; Zhou, Y.; Andersson, M.; Li, F.; Zhang, C.; Li, B.; Liu, Z.; Bo, Z.; Zhang, F. Tailoring side chains of low band gap polymers for high efficiency polymer solar cells, Polymer, 2010, 51, 3031

17 Y W. Soon , T M. Clarke , W Zhang , T Agostinelli , J Kirkpatrick , C. Smith , I McCulloch , J Nelson and J R. Durrant, Energy versus electron transfer in organic solar cells: a comparison of the photophysics of two indenofluorene : fullerene blend films, Chem. Sci., 2011,2, 1111-1120

18 Bronstein, H.; Leem, D. S.; Hamilton, R.; Woebkenberg, P.; King, S.; Zhang, W.; Ashraf, R. S.; Heeney, M.; Anthopoulos, T. D.; Mello, J. d.; McCulloch, I., Indacenodithiopheneco-Benzothiadiazole copolymers for high performance solar cells or transistors via alkyl chain optimization. Macromolecules 2011, 44 (17), 6649–6652

19 Y. Zhang, J. Zou, H. L. Yip, K.-S. Chen, D. F. Zeigler, Y. Sun, A. K.-Y. Jen, Indacenodithiophene and Quinoxaline-Based Conjugated Polymers for Highly Efficient Polymer Solar Cells, Chem. Mater., 2011, 23 (9), pp 2289–2291

20 M. Forster, K. O. Annan, and U. Scherf, Conjugated Ladder Polymers Containing Thienylene Units, Macromolecules 1999, 32, 3159-3162

21 Z Bao, W K Chan, and LYu, Exploration of the Stille Coupling Reaction for the Syntheses of Functional Polymers, J. Am. Chem. Soc., Vol. 117, No. 50, I995 1243

22 B Carsten, F He, H J Son, T Xu, and L Yu, Stille Polycondensation for Synthesis of Functional Materials, Chem. Rev. 2011, 111, 1493–1528

23 Hamasaki, T., T. Sato, H. Nagase, and H. Kito. The mutagenicity of organotin compounds as environmental pollutants. Mutat. Res. 300, 265-271 (1993).

24 Kline, R.J., McGehee, M.D., Kadnikova, E.N., Liu, J. and Fréchet, J.M.J. (2003), Controlling the Field-Effect Mobility of Regioregular Polythiophene by Changing the Molecular Weight. Adv. Mater., 15: 1519–1522.

25 S. A. Jenekhe and J. A. Osaheni, Excimers and Exciplexes of Conjugated Polymers, Science 265, 765–768 (1994)

26 P J. Homnick and P M. Lahti, Modular electron donor group tuning of frontier energy levels in diarylaminofluorenone push–pull molecules, Phys. Chem. Chem. Phys., 2012, Advance Article

27 C. Müller, E. Wang, L. M Andersson, K Tvingstedt, Y Zhou, M R. Andersson, and O Inganäs, Influence of Molecular Weight on the Performance of Organic Solar Cells Based on a Fluorene Derivative, Adv. Funct. Mater. 2010, 20, 2124–2131

28 J. J. M. Halls, J. Cornil, D. A. dos Santos, R. Silbey, D. H. Hwang, A. B. Holmes, J. L. Bredas, R. H. Friend, Phys. Rev. B, 1999, 60, 5721

29 Scharber, M.C., Mühlbacher, D., Koppe, M., Denk, P., Waldauf, C., Heeger, A.J. and Brabec, C.J. , Design Rules for Donors in Bulk-Heterojunction Solar Cells—Towards 10% Energy-Conversion Efficiency. Adv. Mater., (2006), 18: 789–794

30 H. Jin, M. Tuomikoski, J. Hiltunen, P. Kopola, A. Maaninen, and F. Pino, Polymer-Electrode Interfacial Effect on Photovoltaic Performances in Poly(3-hexylthiophene):Phenyl-C61-butyric Acid Methyl Ester Based Solar Cells,J. Phys. Chem. C, 2009, 113 (38), pp 16807–16810

31 Y He and Y Li, Fullerene derivative acceptors for high performance polymer solar cells, Phys. Chem. Chem. Phys., 2011,13, 1970-1983

32 P A. Troshin, H Hoppe, J Renz, M Egginger, J Yu. MAndrey E. Goryachev, Alexander S. Peregudov, Rimma N. Lyubovskaya, Gerhard Gobsch, N. Serdar Sariciftci, and Vladimir F. Razumov, Material Solubility-Photovoltaic Performance Relationship in the Design of Novel Fullerene Derivatives for Bulk Heterojunction Solar Cells, Adv. Funct. Mater. 2009, 19, 779–788

33 Y Yao, J Hou, Z Xu, G Li, and Y Yang, Effects of Solvent Mixtures on the Nanoscale Phase Separation in Polymer Solar Cells, Adv. Funct. Mater. 2008, 18, 1783–1789

# CONCLUSION AND PERSPECTIVES

# Conclusion and Perspective

Throughout this thesis, four main aspects have been presented and discussed in detail:

- Development of new electron donor materials
- Study of the opto-electronic properties of the materials
- Evaluation of the photovoltaic performances in solar cell configuration
- Establish the relation between molecule structures and photovoltaic properties

In order to meet with the requirements of broad absorption spectra and suitable position of the energy levels of the frontier orbitals (HOMO and LUMO), we have developed new electron donor materials based on the “Donor-Acceptor” approach alternating different electron donating segments with electron withdrawing groups. Three main families of electron donating units have been studied: thiophene unit, fluorene unit and indacenodithiophene unit. For electron withdrawing group, fluorenone unit and benzothiadiazole unit have been chosen.

For the preparation of the different macromolecules, three main synthetic methods were employed: oxidative polymerization or oxidative dimerisation mediated by Iron (III) chloride, and palladium cross-coupling reactions according to Suzuki coupling or Stille coupling conditions. We can conclude that for the preparation of oligomers, the synthesis and purifications have allowed to isolate well-defined molecules showing perfectly controlled chemical structures with satisfactory purity. Contrarily for the polymers, depending on the conditions of polymerisation, we have obtained polymers showing significantly different macromolecular parameters in terms of molecular weights and polydispersity index. We can resumed that for polymerisation, in order to obtain polymers of high molecular weight, the choice of solvent of polymerisation, inert working condition and no presence of oxygen in the solvents mixture (in the case of Suzuki coupling and Stille polymerisation) are the most crucial parameters. In addition, thorough purifications of polymers are necessary to eliminate traces of catalysts impurities in the final polymers. We suggested that the power conversion efficiencies can be improved by developing polymers showing high molecular weight and of high purity with absence of metallic catalysts which are potential sites of traps.

In terms of optical and electronic properties, depending on the family of the electron donating groups, and the electron-withdrawing groups, the macromolecules exhibit different intrinsic properties. From photo-physical study of absorption and photoluminescence spectroscopy, we have demonstrated that all the studied D-A oligomers and polymers presented characteristic charge transfer complex transition bands which allow extension of the absorption spectrum. The D-A oligomers and polymers with fluorenone units exhibit absorption spectra up to 600 nm to 700 nm, while the D-A polymers with benzothiadiazole units exhibit absorption spectra up to 700 to 800 nm. The charge transfer complex transitions bands were found to be depending on the respective strength of the electron donating unit and of the electron withdrawing unit. The benzothiadiazole unit with stronger electron withdrawing properties than the fluorenone exhibit stronger internal charge transfer complex transition bands. We suggested that in the case of fluorene-fluorenone based polymer, a partial internal charge transfer occurred upon photoexcitation while in the case of indacenodithiophene-fluorenone based polymer a stronger internal charge transfer complex was formed. Moreover, these two systems based on fluorenone units and benzothiadiazole units possess complementary absorption spectra, therefore they are suitable candidates for tandem solar cells applications[1].

In terms of electronic properties, the HOMO and LUMO energy levels of these macromolecules have been estimated from electrochemical measurements and are presented in the energy diagram in Figure 177 below:

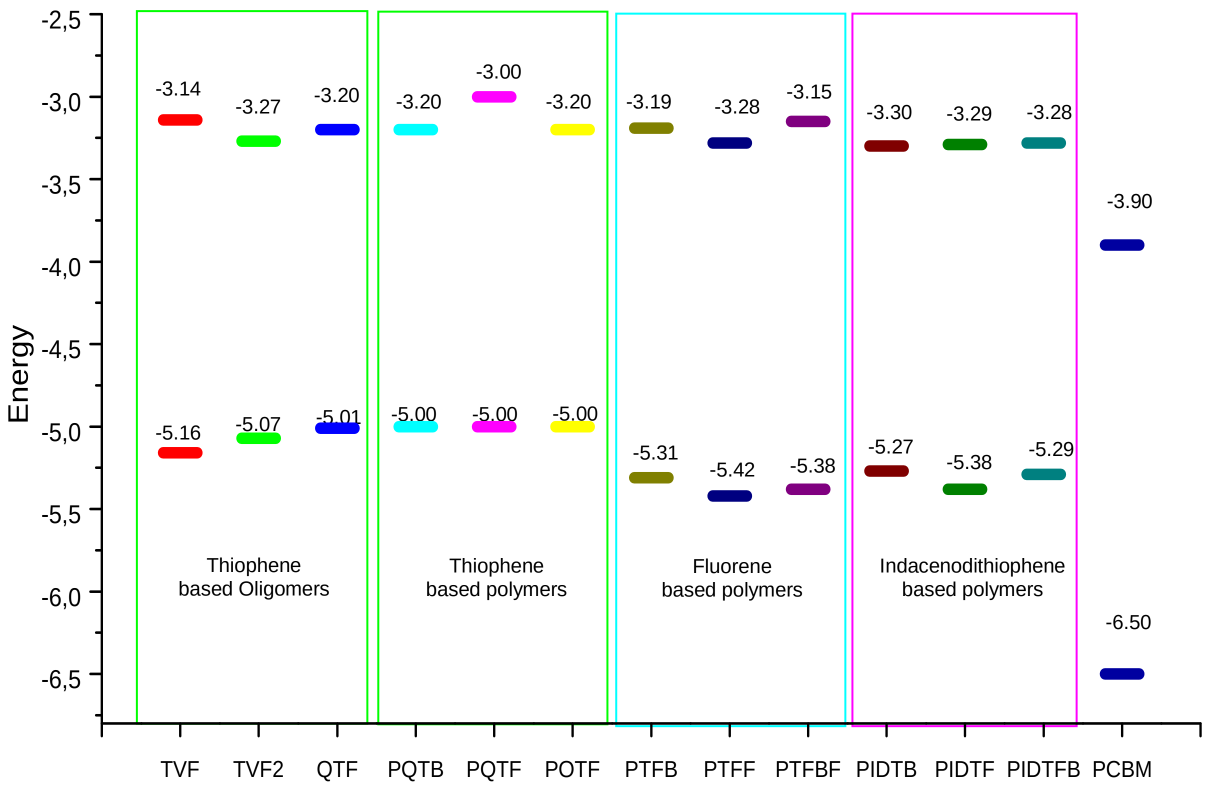


**Figure 177: Energy level diagram of different macromolecules studied during the thesis**

For the first family based on thiophenes as electron donating unit and fluorenone as electron withdrawing unit, two systems are studied; one based on linear thiophenes groups and the other based on thienylene vinylene group. Linear thiophene oligomers and polymers (quaterthiophene and octathiophenes) have shown similar HOMO energy levels of -5 eV while thienylene vinylene based oligomers exhibit lower lying HOMO energy levels than the linear thiophene. The second macromolecules family based on fluorene as electron donating unit exhibit lowest-lying HOMO energy levels compared to other macromolecules with wider band gap than other polymers. These result in the improvement of the open circuit voltage ranging from 0.71 V up to 0.86 V for all the solar cells containing fluorene polymers. The third macromolecules family based on indacenodithiophene segments as electron donating groups has shown moderately low lying energy level with low energy band gap. In general, all the energy levels of the macromolecules are correctly positioned with respect to the ones of fullerenes and they are therefore suitable for photovoltaic applications.

It is also to be highlighted that the investigation on charge transfer properties of the D-A polymers in 'pure polymer' and in blend with fullerene as acceptor via light induced electron paramagnetic resonance EPR has allowed us to get a better understanding of the charge transfer mechanisms. In the case of the blend of donor and acceptor materials, charge transfer with formation of free radical pairs occurs upon light irradiation while for the pure D-A polymers, the transient charge transfer do not form stable free charge radical pairs.

All the oligomers and polymers were tested in photovoltaic devices. The oligomers and polymers used as donor materials when blended with fullerenes as acceptor materials have shown promising results in photovoltaic devices with power conversion efficiencies up to 2.1 %. Photovoltaic results coupled with morphology investigation by atomic force microscopy have indeed highlighted on the importance of nanoscale phase-segregation between the donor materials and acceptor materials for efficient charge generation.

Another worth mentioning work in this thesis is we have provided example of efficient ways to harvest a broader spectrum of solar radiation by combining two polymers with different absorption bands in the active layers with fullerenes derivatives. Two different ways have been tested. The first way is by making ternary blend of two different polymers of different electron withdrawing groups in the polymer backbone (one with fluorenone unit and another with benzothiadiazole unit) mixed with fullerenes PCBM as electron acceptor. The second way is by developing new single-component polymers exhibiting the two electron withdrawing groups (fluorenone and benzothiadiazole) in the same polymer backbone. The results based on these two systems have shown encouraging results in photovoltaic cells and more importantly we have demonstrated that each absorbing component have contributed in the photon conversion to current in devices.

Further work on the optimization of the synthesis method of the polymers is currently undergoing in the laboratory. This thesis has brought fruitful insight on the potential of fluorenone-based polymers for photovoltaic applications. Further optimization of photovoltaic devices based on these new polymers, notably fluorene-based polymers and indacenodithiophene-based polymers, may offer most promising results in power conversion efficiencies based on their optical and electronic properties of PCE which could reach up to 4 % according to the efficiency prediction model proposed by Scharber and coworkers[2] as seen in Figure 178 .

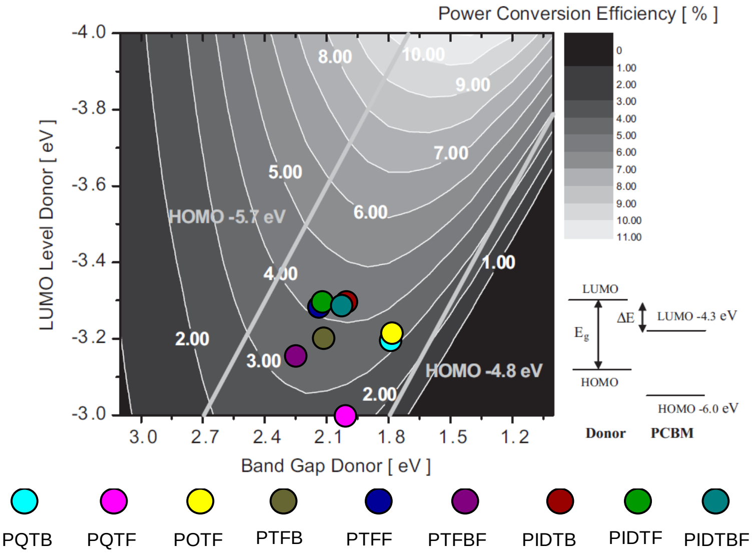


**Figure 178: Model proposed by Scharber and coworkers[2] to predict potential power conversion efficiency in bulk heterojunction solar cell based on LUMO energy levels of donor materials and energy band gap.**

Higher performance in photovoltaic devices can also be expected with utilization of more efficient acceptors such as PCBMC70 and indent fullerene bisadduct C60 ICBA[3].

1 L. Dou, J. You, J. Yang, C-C. Chen, Y. He, S. Murase, T. Moriarty, K. Emery, G. Li and Y. Yang, Tandem polymer solar cells featuring a spectrally matched low-bandgap polymer, Nature Photonics 6, 180–185 (2012)

2 Scharber, M.C., Mühlbacher, D., Koppe, M., Denk, P., Waldauf, C., Heeger, A.J. and Brabec, C.J. ,Design Rules for Donors in Bulk-Heterojunction Solar Cells—Towards 10% Energy-Conversion Efficiency. Adv. Mater., (2006), 18: 789–794

3 Zhao, G., He, Y. and Li, Y. (2010), 6.5% Efficiency of Polymer Solar Cells Based on poly(3-hexylthiophene) and Indene-C60 Bisadduct by Device Optimization. Adv. Mater., 22: 4355–4358.

# EXPERIMENTAL METHODS AND MATERIALS

# I. Experimental Methods

## I.1. Molecules structures analyses

### I.1.1. Nuclear magnetic resonance spectroscopy (NMR)

Nuclear magnetic resonance NMR spectroscopy is routinely used by chemists to elucidate chemical structures using simple one-dimensional techniques. The techniques allow detection of the nuclei spin in intense magnetic field. Interpretation of a simple first order NMR spectrum usually involves evaluation of five principal features; a) the number of signals, b) the chemical shift δ value in ppm (part per million), c) the signal multiplicity quantifying the number of neighboring non-equivalent magnetically active nuclei, d) the coupling constant J correspond to the spacing in Hz between two coupling and e) the signal integral.

The NMR spectra were recorded on a Bruker AC 200 MHz spectrometer. For all the molecules, chloroform-d ($CDCl_3$) containing tetramethylsilane (TMS) as an internal standard (0 ppm) was used as solvent. All synthesized monomers and polymers were characterized by $^{1}H$ NMR and $^{13}C$ NMR. The chemical shifts values are calibrated to the solvent values: $CDCl_3$ = 7.26 ppm for proton and 77.00 ppm for carbon. The following abbreviations have been used for the NMR assignment of signal multiplicity: s for singlet, d for doublet, t for triplet, m for multiplet and br for broad.

All synthesized monomers and polymers were characterized by $^{1}H$ and $^{13}C$ NMR to confirm their structures. For sample preparation, the compound is dissolved in deuterated chloroform. The weight concentration of the samples is at 10-20 mg/ml for $^{1}H$ NMR and at 30-40 mg/ml for $^{13}C$ NMR measurements. For the polymers characterizations, higher concentration and longer scanning time are needed compared to the small molecules. For example 48 hours of scanning time are needed for $^{13}C$ NMR measurement.

### I.1.2. Elemental analysis and mass spectrometer

Elemental analyses and high resolution mass spectra analyses were performed by the Centre Régional de Mesures Physiques de l'Ouest (Rennes). The elemental analyses were performed using Thermo Electron Flash EA1112 CHNS/O micro-analyzer allowing determination of the mass fractions of 4 elements: carbon, hydrogen, nitrogen and sulfur.

The Mass spectra were recorded using Bruker MicrO–Tof-Q II spectrometer, allowing determination of the elemental composition of the sample by ionizing chemical compound by ionizing chemical compounds to generate charged molecules or molecule fragments and measuring their mass-to-charge ratios.

### I.1.3. Infrared spectroscopy

Infrared spectra were recorded by Pelkin Elmer FTIR-ATR Paragon 500. The infrared spectroscopy allows detection of characteristic vibration frequencies of molecules according to respective vibrations modes. Infrared spectroscopy measurement allows detection of different functional groups and can be useful as complementary information to confirm proposed molecules structures.

### I.1.4. Size exclusion chromatography (SEC)

In size exclusion chromatography, the polymers are separated on the basis of hydrodynamic volume. The schematic presentation of SEC is shown Figure 179.

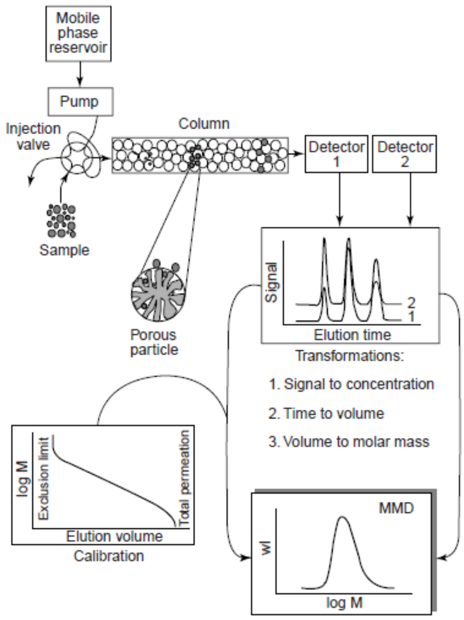


**Figure 179: Schematic representation of SEC[1]**

The sample is injected into the column containing a porous packing. The different molecules are separated in the column where small molecules are trapped in the pores and larger molecules passed through the column more rapidly. The larger molecules are then eluted and exit the column first followed by the smaller molecules. The polymer fractions are detected by UV-Vis detection and the concentration in each fraction can then be determined. The raw data obtained from SEC is a molecular size distribution which is converted to molecular weight distribution using a calibration curve obtained from polystyrene.

The molar mass of polymer can be defined as:

$M_n$: $\frac{\Sigma\, n_i M_i}{\Sigma\, n_i}$ Average number molecular weight

$M_w$: $\frac{\Sigma\, n_i M_i^2}{\Sigma\, n_i M_i}$ Average weight molecular weight

I= Mw/Mn : Polydispersity for I= 1 represents homogenous mass distribution. The higher the value of polydispersity indicates higher heterogeneity of the molecules size in the polymer fraction.

**Experimental description**

Molecular weights of the polymer fractions (obtained by Soxhlet extraction) were measured using SEC on a 1100HP Chemstation equipped with a 300–7.5 mm PLgel Mixed-D 5 mm/104 A° column. Detection was performed by a diode array UV-vis detector and a refractive index detector. The column temperature and the flow rate were fixed to 313 K and 1 $mLmin^{-1}$, respectively. The calibration curve was built using 10 polystyrene (PS) narrow standards (S-M-10* kit from Polymer Labs) and all molecular weights are therefore given in equivalents of PS (eq. PS). Two runs of 20 µL injection of dilute polymer concentration ( in HPLC grade THF solutions (for polymers PQTBTD, POTF8 and polymers in the fluorene series) were typically analyzed for each sample with UV-vis detection located at 375 nm. For polymer in the indacenodithiophene series, the macromolecular parameters were measured using chloroform as solvent. For sample preparation, the concentration of monomers is at *ca*. 0.2 mg/g of solvent, the polymer batch at 1.2 mg/g and the polymer fractions at 0.7 mg/g.

## I.2. Photophysical and electronic characterization techniques

### I.2.1. UV-visible absorption spectroscopy

Ultraviolet and visible radiation interacts with matter which causes electronic transitions (promotion of electrons from the ground state to a high energy state). The ultraviolet region falls in the range between 100-400 nm, the visible region fall between 380-780 nm.

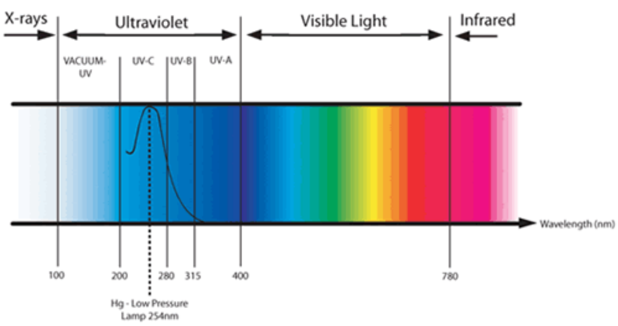


**Figure 180: Ultra-violet region, visible light and infrared region of electromagnetic spectrum[2]**

The following electronic transitions of one molecule are possible as shown Figure 181:

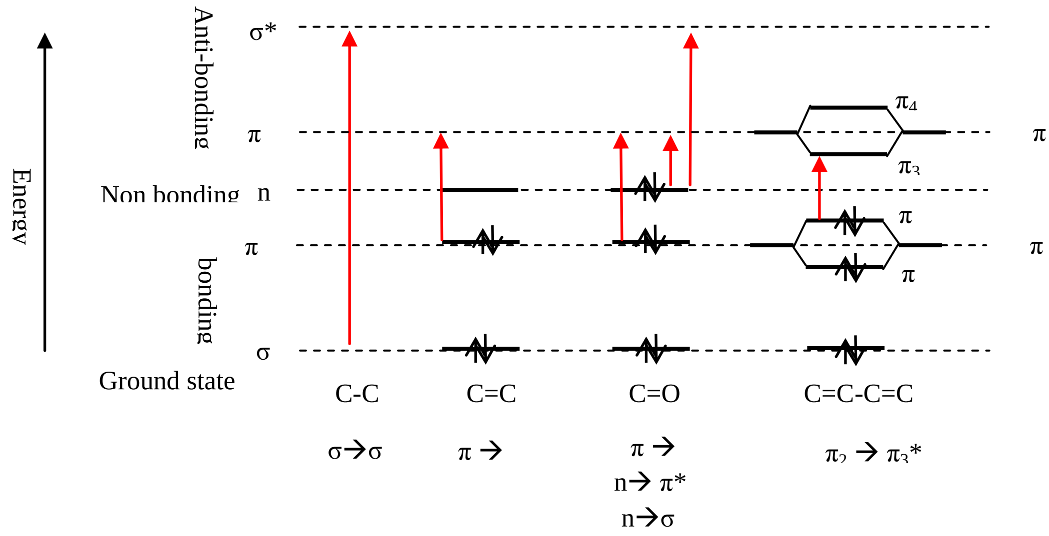


**Figure 181: Molecular orbital energy levels; Examples of allowed electronic transitions of organic compound[3]**

The σ to σ* and n to σ* transitions in organic molecules generally require absorption of photon with wavelengths lower than the UV-vis range (<200 nm). Thus, only π to π* and n to π* transitions occur in the UV-vis region. Other possible electronic transition can also occur for example the internal charge transfer between electron donor and electron acceptor molecule[4].

In photochemistry (for example absorption spectrum or emission spectrum) two terms are often introduced to express changes of spectral band position, either bathochromic shift or hypsochromic shift. Bathochromic shift is a change of spectral band position in the absorption of a molecule to a longer wavelength (lower energy), also referred as red-shifted. Hypsochromic shift is a change of spectral band position in the absorption, of a molecule to a shorter wavelength (higher energy), also referred as blue-shifted.

**Experimental description**

UV-Visible absorption spectroscopy measurements were performed on a Perkin Elmer Lambda 900 spectrophotometer. For the polymers, the absorption spectroscopy measurements were recorded in solutions according to the mentioned solvent and on films. Dilute solutions are prepared with concentration of ca. $10^{-5}$ mol.$L^{-1}$ to avoid saturation. The films were prepared by spin-coating polymers solution in chlorobenzene at concentrations of 20 mg/ml or 10 mg/ml (1200 rpm for 40 s with a speed of 350 rpm/s).

The absorption spectra were plotted following A= f(λ) with A correspond to absorbance intensity and λ, the wavelength in nm. The absorbance corresponds to the variation of intensity as described below. According to Beer-Lambert linear equation we can calculate the molar extinction coefficient (ξ):

A= ξ * $\mathcal{L}$ * *c*

A: absorbance or optical density (without unit)

C: mol.$L^{-1}$ or M

$\mathcal{L}$:width of the cuvette in cm (here the quartz cuvette: 1 cm)

Ξ: (mol.$L^{-1})^{-1}$.$cm^{-1}$ or $M^{-1}$.$cm^{-1}$

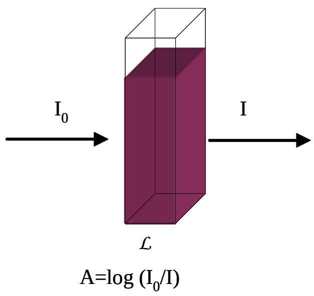


We can calculate the optical band gap of all the molecules, using the formula below. The offset of the curve is presented in Figure 182.

$Eg^{optic}$ = hc/λ = 1240 / $\lambda_{offset}$

h : $4.135667516\times10^{-15}$ eV.s

c: 299 792 458 m·s-1

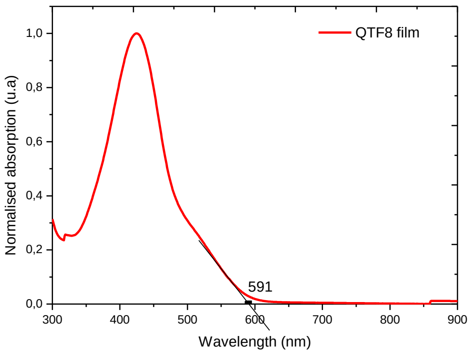


**Figure 182: Determination of optical band gap from the $\lambda_{offset}$ of the absorption spectrum**

### I.2.2. Photoluminescence spectroscopy

Photoluminescence spectroscopy is a useful technique for studying the optical and electronic properties of the excited state of materials providing information about recombination and relaxation processes. Two modes of photoluminescence can be studied by this measurement, excitation mode and emission mode. Photoluminescence excitation is studied by fixing one emission wavelength and varying the excitation wavelength to give excitation spectrum. For our study we will focus on the photoluminescence emission. This mode allows studying the emission spectrum at fixed excitation wavelength. The picture Figure 183 can allow better understanding the photoluminescence emission.

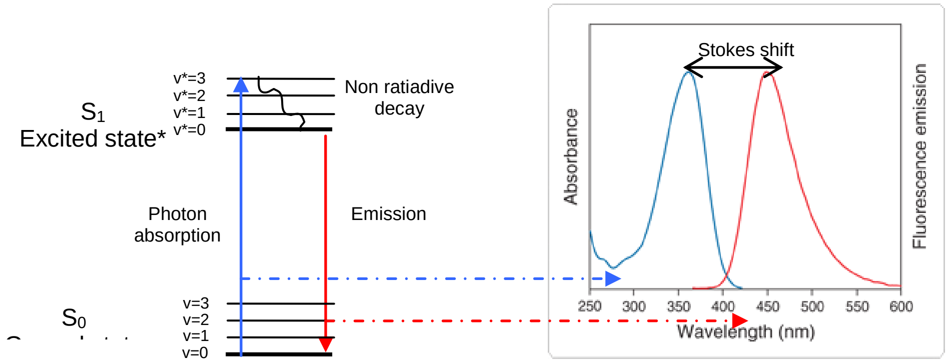


**Figure 183: Jablonski diagram of electronic transitions, absorption spectrum and emission spectrum**

When the photons are absorbed by the molecule, the electrons are excited and moved to the excited electronic singlet state, giving a maximum peak in the absorption spectrum. The excitation energy will first undergo internal conformational conversion, dissipating its energy as a non radiative decay. At the lowest vibrational level ν=0, the electrons will subsequently return to the ground state releasing the remaining energy (emission energy) as fluorescence, giving a peak in the emission spectrum. The difference between the excitation energy and the emission energy is called Stokes shift.

Photoluminescence spectroscopy measurement also allows the study of the charge transfer complex (in our oligomers and polymers) and the photo-induced charge transfer in the blend oligomer/polymer with fullerenes (PCBM)[5]. Charge transfer and energy transfer are non-radiative processes therefore the quenching or absence of emission can be detected by photoluminescence measurement.

Photoluminescence spectra were recorded on F-4500 spectrofluorometer (Hitachi). For measurements, we used the same samples prepared for the UV-Visible absorption either in solutions or in films.

## I.3. Electrochemical measurements

The electrochemical analysis can allow determination of HOMO and LUMO energy levels from cyclic voltammetry or differential pulse voltammetry[6]. In voltammetry current-potential curves showed the measured current against the applied potential difference between working electrode and the counter electrode. We can observe and measure the oxidations and the reductions potentials of the molecules.

In the cyclic voltammetry the potential is continuously changed until a previously defined potential is reached. Then the potential is changed in the other direction, until the starting potential is reached again. However in differential pulse-voltammetry a rectangular pulse potential is applied instead of continuous potential and the current is measured only shortly before the pulse and at the end of the pulse. These two methods give two different current-potential curves as shown in Figure 184.

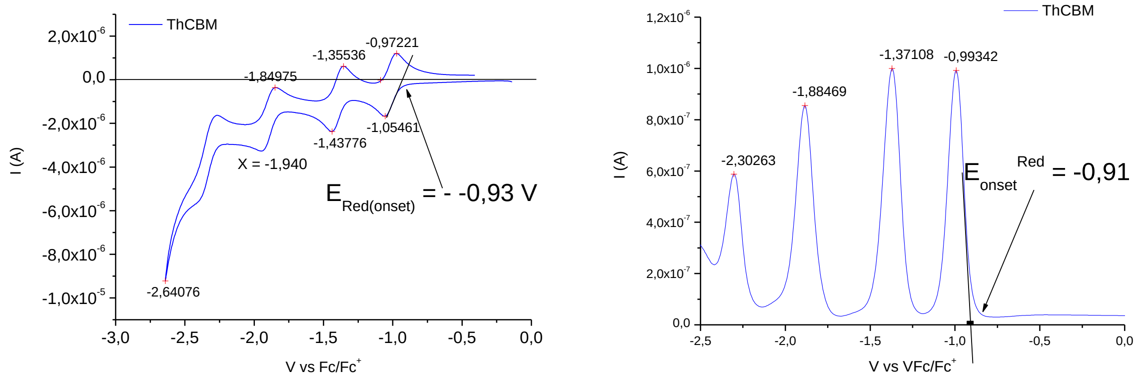


**Figure 184: Example of reduction potentials curves determined by voltammogram(left) and differential pulse voltammogram (right)**

In this study, all electrochemical analyses were performed using a cell composed of one working electrode (flat platinum disk), one counter electrode (a platinum wire) and a pseudo reference electrode (silver wire). To ensure accuracy of the values, the working electrode is cleaned and polished before each measurement. For measurements, dried and distilled solvents are used to avoid the presence of water, and degassed from oxygen by argon bubbling in the cell. For the analysis of oligomers, the molecules are dissolved in dichloromethane in the presence of supporting electrolyte. For the study of polymers, we prepared thin films of polymers drop-casted from a chlorobenzene or chloroform solution. The thin polymer films were then analyzed in acetonitrile in presence of supporting electrolyte. Tetrabutylammonium hexafluorophospate salt is used as supporting electrolyte with a concentration of 0.1M in the solvent of measurement. All the measurements are calibrated to ferrocene/ferrocenium redox couple. The oxidation and reduction potentials are determined at the onset potentials (See Figure 185).

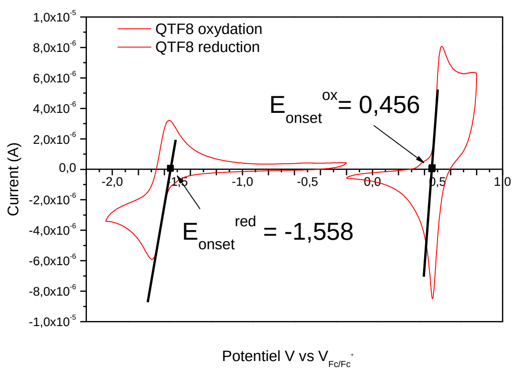


**Figure 185: Example of determination of onset oxidation and reduction potentials values**

Using ferrocene/ferrocenium (Fc) reference, the LUMO and HOMO energy levels can be calculated from the values of oxidation and reduction potentials with the assumption that the energy level of Fc is 4.8 eV below vacuum level as shown in the formula below.[7,8]

$$\text{HOMO} : - ( E^{oxydation} - 4.8)\ \text{eV}$$
$$\text{LUMO} : - ( E^{reduction} - 4.8)\ \text{eV}$$

## I.4. Electron Paramagnetic Resonance spectroscopy (EPR)

Light-induced EPR studies were performed to investigate the charge photo-formation and charge transfer either intramolecular, in the pristine D-A polymers or intermolecular, between the blends of D-A polymers and the fullerenes PCBM[9].

**Basic theory**

Electron paramagnetic resonance (EPR) spectroscopy[10,11,12,13,14] also known as electronic spin resonance (ESR) spectroscopy allows studying materials with paramagnetic properties or unpaired electrons. The basic principle of EPR spectroscopy is similar to NMR technique except that EPR focuses on the interaction of an external magnetic field with electron spins instead of nucleus spins.The interactrion of a magnetic field with a single unpaired electron will create two spin states ms = +½, and ms = -½, The energy difference between the two spin states is given by the equation:

$$\Delta E = h\nu = g^* \beta^* H$$

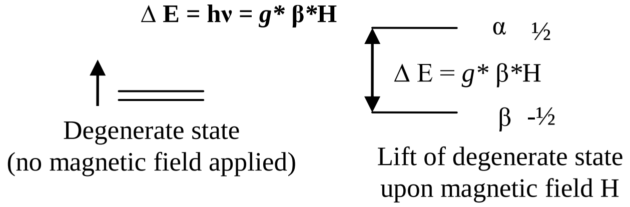


h: Planck’s constant (6.626 x 10-34 J s-1)
ν:the frequency of radiation
β:the Bohr magneton (9.274 x 10-24 J T-1)
H: the strength of the magnetic field in Tesla
g: known as the g-factor (Landé g-factor). The g-factor is a unitless measurement of the intrinsic magnetic moment of the electron.

**Methodology**

We apply the concept of EPR tracing recently developed in our laboratory[15]. It consists of ascribing an EPR fingerprint to each sample. This fingerprint is simply formed by the set of ‘pure’ lines, the sum of which allows simulation of the experimental EPR spectrum. Each ‘pure’ line signs a substructure present in the sample. These EPR fingerprints are used to follow the fate of free radicals trapped on substructures of the whole sample, as a function of various parameters without relaying to their absolute structures. In our case since the studied structures are relatively simple, most of the lines are easily attributed to specific structures.

**Experimental description**

The EPR experiments were made using an X-band (3cm, 9.7 GHz) ER 200D SRC Bruker spectrometer with 100 kHz field ac modulation for phase-lock detection. The sample is located in a Bruker ER 41040R Optical transmission Resonator (unloaded quality factor Q=7000) and illuminated at 473,3 nm with a CW output power of 22,1 mW by a laser module Oxxius 473L-20-COL-PP-LAS-01186 .

For sample preparation, the polymers are deposited on polyethylene substrates covered by indium tin oxide ITO from chlorobenzene solution at a concentration of 10 mg/ml. For the blends of polymers:fullerene PCBMC60 of ratio 1:1 , the concentration of each materials is at 10 mg/ml: 10mg/ml . The films were heated at 70 °C overnight in vacuum to evaporate all the solvents. The thin films are placed in EPR sample tubes and purged in vacuum to avoid any trapped oxygen.

The EPR spectra are simulated as a sum of ‘pure’ lines by a simulation software developed in our laboratory by Christian Lombard and Brigitte Pépin-Donat. Each ‘pure’ line (‘either Lorentzian or Gaussian or both *g*-centered) is characterized by its *g*-factor, its peak-to-peak linewidth $H_{pp}$ and its lineshape (in the present study, the lineshapes are all 100 % Lorentzian)

## I.5. Thin film transistor

**Basic theory**

Organic transistors [16, 17] are metal-insulator-semiconductor (MIS) field-effect transistors (FETs) in which the semiconductor is a conjugated organic material. In all MISFETs, regardless whether organic or inorganic, the semiconductor is separated from the metal gate electrode by a thin insulating layer, the gate dielectric. When a voltage is applied between the gate and the semiconductor, a thin sheet of mobile electronic charges is created in the semiconductor in close vicinity of the semiconductor/dielectric interface. This charge layer balances the charge (of opposite polarity) located on the gate electrode. By tuning the gate voltage, the charge density in the semiconductor channel can be modulated over a wide range, and as a result the electric conductivity of the charge-carrier channel changes dramatically. With two metal contacts attached to the semiconductor (the source contact and the drain contact), the electric current flowing through the transistor can therefore be efficiently controlled over a wide range, simply by adjusting the gate voltage.

In transistor, the charges move from source to drain with the gate allowing the regulation of the charges flow between these two electrodes by applying a voltage ($V_G$).
Different operating modes of transistor[18]:

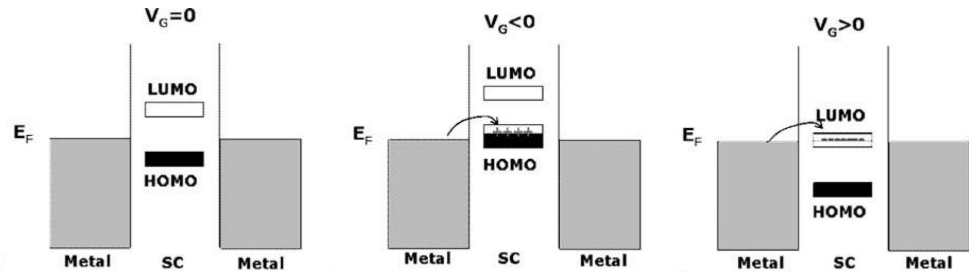


**Figure 186: Three different operating mode of organic thin field effect transistor**

$V_G$=0:
No voltage is applied on the gate. Residual charges present in the transistor channel give short circuit current $I_{off}$.

$V_G$<0; $V_{DS}$=0V:
Negative voltage is applied on the gate while no potential is applied between the source and the drain ($V_{DS}$). Positive charges are accumulated in the channel at the interface between the insulator and the semiconductor. When the Fermi level of source/drain metal is close to the HOMO level, holes can be injected from/to the metal to/from the HOMO of the semiconductor, and a p-type OFET is realized.

$V_G$>0; $V_{DS}$=0V:
When a positive voltage is applied to the gate, negative charges are induced at the organic semiconductor/organic insulator interface and for source/drain metals with Fermi levels close to the LUMO level of the organic semiconductor, electrons can be injected from the source/drain metal to the LUMO of the semiconductor, and an *n*-type OFET is realized.

Linear regime: $V_G<V_D<0$
$V_G$ and $V_D$ are kept negatives. At low potential between the source and the drain $V_{DS}$, the current $I_{DS}$ increases linearly with the potential $V_{DS}$. It is called the linear regime. The current between the source and the drain $I_{DS}$ can then be determined as follow:

$I_{DS} = W/L * C_i * \mu(V_G - V_T)\, V_{DS}$
Ci: capacitance of the insulator W, L: Width and Length of the channel
M: mobility

$V_T$: Threshold voltage corresponding to the gate voltage at the inversion point

Saturation regime: $V_D<V_G<0$ and $V_G-V_D>0$

$V_G$ and $V_D$ are kept negatives, but the difference between gate potential and drain voltage are always positives. When $V_D$ is more negative than $V_G$, $I_{DS}$ tends to saturate (saturation regime) owing to the pinch-off of the accumulation layer, and this regime is modeled by the following equation: $I_{DS}= W/2L* \mu*C_i*(V_G - V_T)^2$

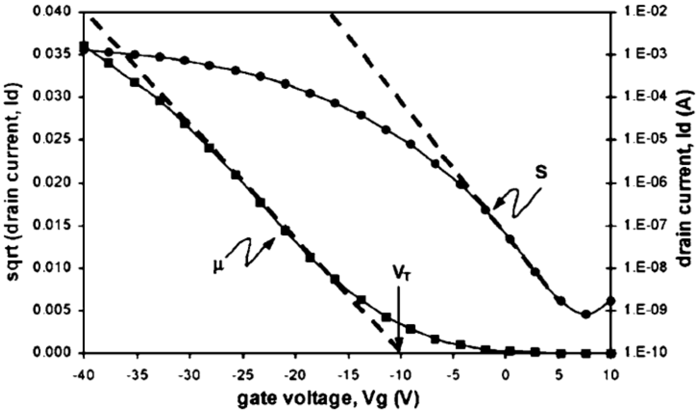


**Figure 187: Representative OFET trace for pentacene deposited on an alumina sample treated with 1 phosphonohexadecane. $V_{DS}$ is held constant at −40 V, and Vg is swept from +10 to −40 V. A linear fit to the $\sqrt{}$ Ids-Vg trace permits the extraction of saturation mobility and threshold voltage ($V_T$)**

We can then trace a linear fit $\sqrt{I_{DS}}=f(V_G-V_T)$ and calculate the mobility from the tangent (a) of the curve:

$\mu= 2*a^2*L / (W*Ci)$ (unit : $cm^2. V. s^{-1}$)

**Experimental description**

Determination of charges mobility of the polymers was performed using thin film field effect transistor. The polymers were deposited on the patterned transistor substrates by spin coating from chlorobenzene solutions at concentration of 10 mg/ml.

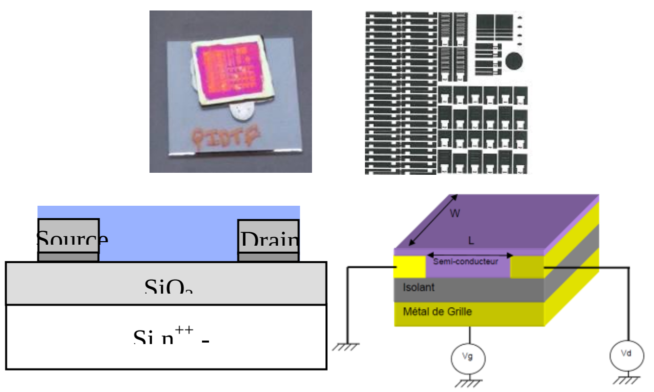


**Figure 188: (Up) Picture of the real device thin film transistor with the patterned circuit on right. (below) Schematic of bottom gate organic field effect transistor with bottom contact structures**

The device geometry is a bottom gate with bottom contact configuration as shown in Figure 188. The gate metal substrate is a highly doped (1,0,0) silicon at $10^{19}$ at/cm$^3$ with 525 µm thickness. The highly doped silicon gate Si $n^{++}$ is covered by thermally grown $SiO_2$ oxide as dielectric layer (insulating layer) of 200 nm thickness. The source and drain electrodes of the device were patterned by optical photolithograph. A thin layer of titanium (Ti) is first evaporated on the silicon oxide of 10 nm thickness followed by evaporation of gold (Au) of 50 nm thickness followed by lift-off.

## I.6. Photovoltaic device fabrication and measurements

### Photovoltaic device fabrication

Photovoltaic devices fabrication and measurement are made in Institute National d'Energie Solaire (INES-RDI) Chambery in collaboration with Remi de Bettignies and Solenn Berson. The device configuration is shown in Figure 189.

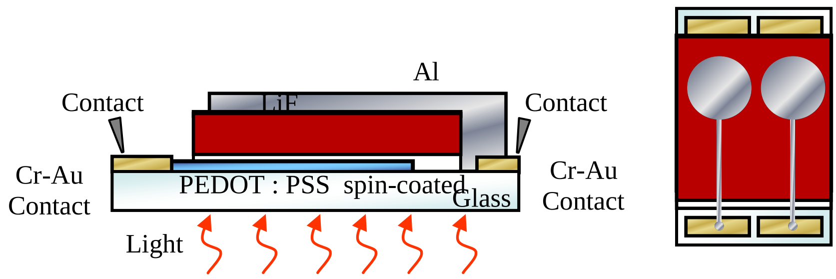


**Figure 189 : The tested photovoltaic cell configuration**

Bulk heterojunction solar cells were fabricated on a glass substrate covered by a transparent conductive oxide ITO (indium-tin oxide). The ITO layer was covered with an 40 nm thick interfacial PEDOT/PSS layer (Baytron) allowing to smooth the rough ITO layer and to facilitate holes injection and transport [19, 20]. The active layer containing the mixture of oligomer/polymer donor and acceptor materials (for example PCBM) according to weight ratios were spin-coated onto the PEDOT layer from chlorobenzene or dichlorobenzene solutions. Finally, a 1.3 nm thick layer of lithium fluoride (LiF) was evaporated on top of the active layer and covered by the aluminium electrode (100 nm) as cathodic electrode. The active surface of the device was 28 mm.

This device configuration, i.e Glass substrate/ITO/PEDOT-PSS/ (oligomer or polymer + acceptor )/LiF/Al, was used for all our tests except for the tests using the indacenodithiophene based polymers. In the latter, LiF layer is replaced by calcium giving a configuration of Glass substrate/ITO/PEDOT-PSS/polymer + acceptor/Ca/Al.

Current-voltage characteristics and power conversion efficiencies of the solar cells were fabricated and measured in inert atmosphere (in glove box). The measurements are recorded via a computer controlled Keithley SMU 2400 unit using simulated white light. In order to allow comparable results between different laboratories, a standard measurement condition is applied. The standard condition of the power incidence of light is at 1000 W. m$^{-2}$ under air mass radiation A.M 1.5, which corresponds to the simulated solar irradiation of the terrestrial atmosphere at the angle of 48.2° (Figure 190). A monocrystalline silicon solar cell, calibrated at the Fraunhofer Institut Solare Energiesysteme (Freiburg, Germany), was used as a reference cell to confirm stabilisation of the 1000 W. m$^{-2}$ illumination.

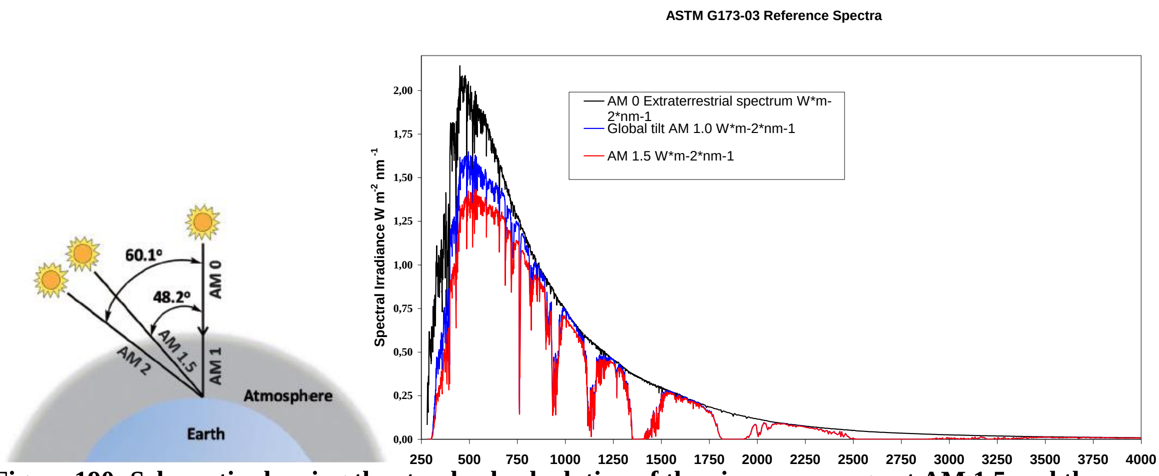


**Figure 190: Schematic showing the standard calculation of the air mass energy at AM 1.5 and the corresponding solar spectrums[21]**

## I.7. Photovoltaic device characterisation and measurement

The photovoltaic cell device is characterised by registration of the current-voltage (J-V) curve of in dark and under illumination as shown in Figure 191. The black curve corresponds to the J-V curve in the dark showing no current and voltage produced. And when the cell is under illumination, the cell produces current at 0 bias and generates a voltage.

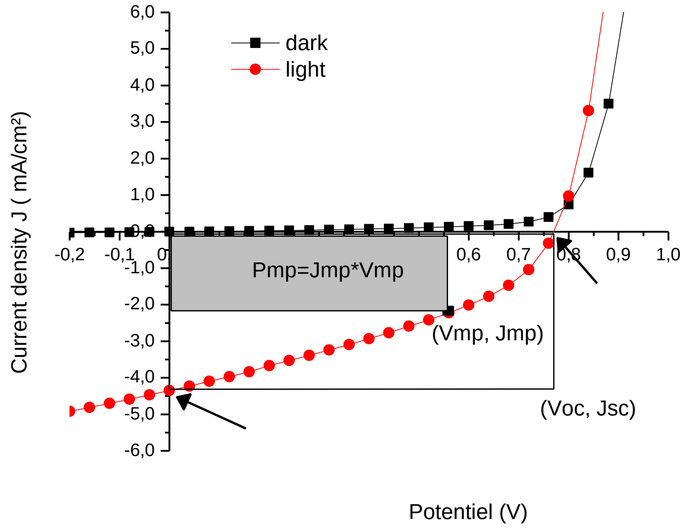


**Figure 191: Current-voltage (J-V) characteristics for a photovoltaic cell**

Relevant parameters allowing the characterization of the photovoltaic cells are:

**$V_{oc}$**: The open circuit voltage is the maximum voltage generated under open circuit conditions where no current can flow.

**$J_{sc}$**: Short circuit current density is the maximum current generated when the cell is short-circuited where the voltage is equal to zero.

**$P_{mp}$**: One point on the I-V curve yielding maximum product of current and voltage is called the maximum power point. (Vmp, Jmp) It is equal to the maximum area under the J-V curve.

**FF**: The ratio of the maximum power point to the product of open circuit voltage and short circuit current is called the fill factor. The power conversion efficiency is defined as the percentage of the output power of the cell to the power incidence to illuminated area.

$$FF = \frac{V_{mp}*J_{mp}}{V_{oc}*J_{sc}} \qquad PCE = \frac{P_{out}}{P_{in}} = \frac{V_{mp}*J_{mp}}{P_{in}} = \frac{FF*J_{sc}*V_{oc}}{P_{in}}$$

## I.8. Morphology characterisation

### I.8.1. Atomic force microscopy

**Basic theory**

Atomic force microscopy (AFM)[22] is a high resolution scanning probe technique, allowing investigations of surfaces at the nanometer scale. In AFM, a sharp tip is scanned over the sample's surface, and the tip-surface interaction forces are used to control the vertical distance through a dedicated feedback mechanism. Nowadays, the most widely used force detection scheme is still the beam deflection method, where a laser beam is reflected from a cantilever and detected with a position-sensitive quadrant detector. In beam-deflection setups, the probe consist in a micro-machined silicon-based (or silicon nitride) cantilever integrating a tip with a typical radius of a few nanometers.

In the static mode (commonly called contact mode), the feedback mechanism is employed to adjust the tip-sample distance in order to maintain a constant cantilever deflection (*i.e.* a constant force between the tip and the surface). In turn, a vibrating cantilever can be used to perform dynamic AFM[23], which has been widely developed for non-destructive investigations of "soft" materials, such as polymers, supra-molecular assemblies[24] and biological molecules. Two major dynamic modes have been so far developed, the amplitude-modulation (AM-AFM) and the frequency modulation (FM-AFM). A brief description of both modes will be given in the following (for a detailed review, see ref. 23).

In AM-AFM (which is sometimes referred as "tapping mode" or "intermittent contact"), the cantilever is excited at or near its free resonance frequency, and the oscillation amplitude is used as the input of the tip-surface distance feedback loop. The material properties variation can be simultaneously mapped[25] (in the so-called "phase imaging" mode) by recording the phase shift between the excitation signal (kept at a constant frequency) and the cantilever oscillation. In turn, the cantilever's amplitude is kept constant in FM-AFM, and the excitation frequency is adjusted to keep the cantilever at its resonance, giving rise the frequency shift signal which is used as the input of the topography feedback loop (the topography is mapped at constant frequency shift). The cantilever vibration amplitude is kept constant by a second feedback loop (which adjusts the excitation amplitude), giving rise to the so-called "damping" signal. The damping reflects the energy dissipated in the tip-surface interaction, and can be used (similarly to the phase contrast in AM-AFM) to map the local properties of the surface. Most experiments in ambient conditions are performed in the amplitude modulation mode, while FM-AFM (also called non-contact AFM, nc-AFM) has been extensively developed in ultra-high vacuum (UHV), because the high quality factor of the vibrating cantilever implies extremely slow feedback responses in amplitude modulation.

In some cases, a resolution matching the one of scanning tunneling microscopy can be achieved in nc-AFM. In turn, FM-AFM requires two feedback loops, which makes its electronic complex, besides the limitations imposed by the operation under UHV. For systematic investigations of the surface morphology with a sub 10 nm resolution, AM-AFM can be advantageously used, while FM-AFM will be preferred for advanced investigations on well-selected samples.

Last, electrostatic and potentiometric modes of the AFM have been developed to map simultaneously the topography and the local charges and/or surface potential. These techniques can be operated either in ambient conditions or under UHV, with several variants. In our laboratory, self-assembled oligomers and bulk-heterojunction solar cells have especially been investigated by Kelvin Probe Force Microscopy (KPFM) in combination with nc-AFM. We refer the reader to our former reports[26, 27] for more details about this topic which is beyond the scope of this manuscript.

**Experimental description**

In this work, the oligomers and bulk hetero-junction thin films have been investigated in ambient conditions in AM-AFM by using a MobileS setup from Nanosurf[28] . It features a dynamic frequency range between 15 kHz and 300 kHz, an automatic adjustment of the laser beam on the cantilever, an integrated dual view video camera, and can be used on samples without limitations regarding their size. Two scan heads can be used (an easily interchanged), with maximum scan ranges respectively of 110µm and 10µm. The last setup is preferentially used for high resolution imaging. For AM-AFM, silicon NCLR cantilevers from Nanoworld [Nanoworld AG, Rue Jaquet-Droz 1, CH-2002 Neuchâtel, Switzerland] have been used, with a typical resonance frequency $f_0$=190kHz, a spring constant of k=48N/m and a tip radius around 10nm.

Some complementary experiments have been carried out by E. Spadafora and B. Grévin in FM-AFM under UHV with a commercial VT-beam AFM from Omicron[29]. The VT-AFM is an UHV variable temperature (30K-300K) AFM with beam deflection and a scanned tip design, with a maximum scan range (xyz) of 10µm×10µm×1.5 µm. The sample size is limited to 10×10mm. SSS-NCH (supersharp silicon) cantilevers from Nanoworld (silicon, $f_0$=320kHz, k=42N/m, tip radius around 1-2nm.) or EFM cantilevers from Nanoworld (PtIr coated silicon, $f_0$=75kHz, k=2.8N/m, tip radius around 10-15nm) have been used for these experiments. All nc-AFM data have been acquired with negative frequency shift setpoints. For more technical details about the setup and nc-AFM experiments, see ref [26, 27].

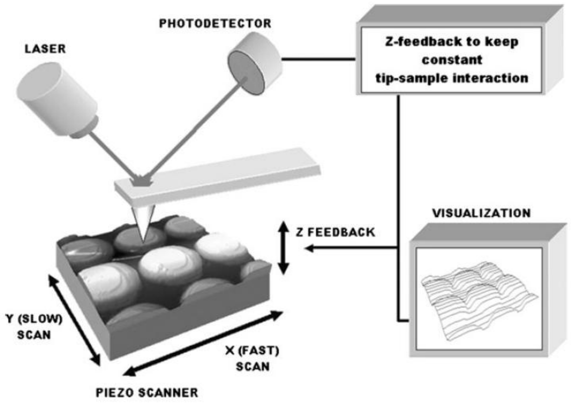


**Figure 192: AFM beam deflection setup. In this example the sample is moved along X and Y direction by the scanner and the tip is fixed. The situation is reversed in the setups used in this work (i.e. the sample is fixed and the tip is moved by the scanner). Adapted and reproduced from P. Samori et al., Phys. Chem. Chem. Phys. 8, 3927-3938, 2006)**

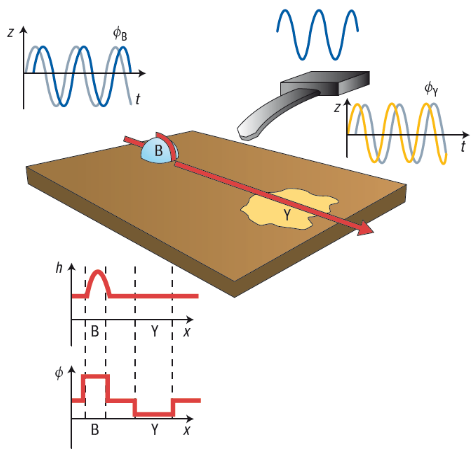

**Figure 193: Phase imaging mode. Ideally, in AM-AFM, the phase shift changes only with variation in the energy dissipated by the cantilever over the surface. In this example, the blue region is made of a different material than the surface, and the yellow one represents a variation of the local properties of the surface. Both give rise to a phase contrast, while only the blue region will be detected in the height image. Adapted and reproduced from R. Garcia et al., Nature Materials 6, 405-411, 2007.**

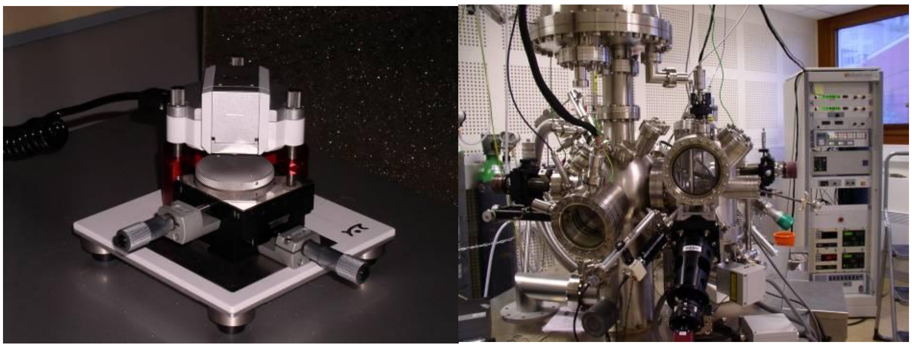

**Figure 194: AFM setups used in this work. Left: ambient conditions Mobile S (from Nanosurf) setup used for AM-AFM experiments. Right: UHV VT-AFM (from Omicron) used for FM-AFM experiments.**

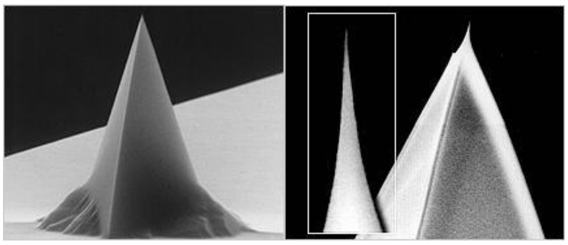

**Figure 195: AFM tips used in this work. Left: Non-Contact / Tapping mode Long Cantilever with Reflex coating (NCLR) cantilever. Right: SuperSharp Silicon Non-Contact High frequency (SSS-NCH) cantilever. Images reproduced from Nanoworld AFM probes broschure, www.nanoworld.com.**

**Sample preparation**

For morphology characterisation of single materials (oligomers QTF and TVF2), thin deposits of oligomers were prepared by drop casting 10µL of dilute toluene solution (concentration 0.05-0.4 mg/ml) on clean substrates (glass substrates, freshly cleaved highly oriented pyrolytic graphite HOPG, or mica substrates). The solvent was slowly evaporated under a toluene saturated atmosphere for 24 h. For the bulk heterojunction solar cells morphology characterisation, AFM images were recorded from the tested photovoltaic device samples.

# II. Active layer materials

The active layer of organic photovoltaic cell is composed of donor materials and acceptor materials.

## II.1. Donor materials

All the final donor materials (oligomer/polymer) are synthesized in our laboratories as described in the experimental sections. All reagents and chemicals were purchased from Aldrich or Acros and used as received, except for THF which was distilled over sodium–benzophenone prior to use. Thin layer chromatography was performed on silica gel-coated aluminium plates with a particle size of 2–25 mm and a pore size of 60 A°. Merck 60 (70–230 mesh) silica was used for flash chromatography.

The oligomers and polymers molecules structured are presented below. The molecules characterisations are further described to the according chapters.

## II.1.1.Donor oligomers:

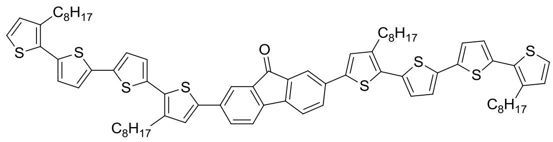

QTF8

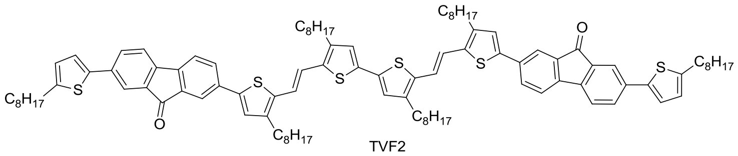

TVF2

**Figure 196: Quaterthiophene fluorenone QTF8 and dimer thienylene vinylene TVF2**

## II.1.2.Donor polymers:

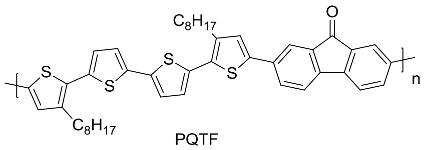

PQTF

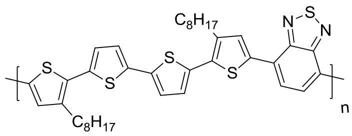

PQTBTD

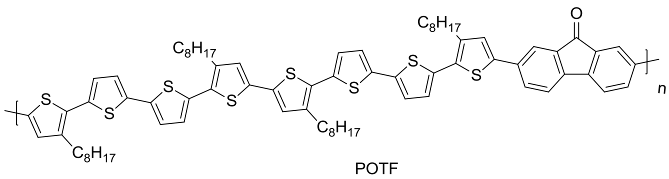

POTF

**Figure 197: Thiophene-based polymers poly(quaterthiophene-fluorenone) PQTF, poly(quaterthiophene benzothiadiazole) PQTBTD, and poly(octathiophene-fluorenone) POTF**

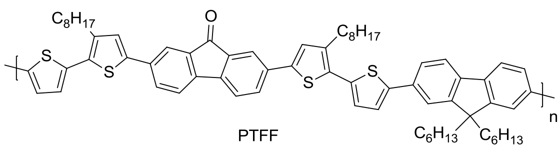

PTFF

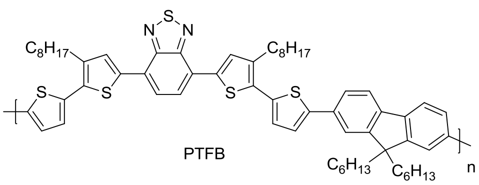

PTFB

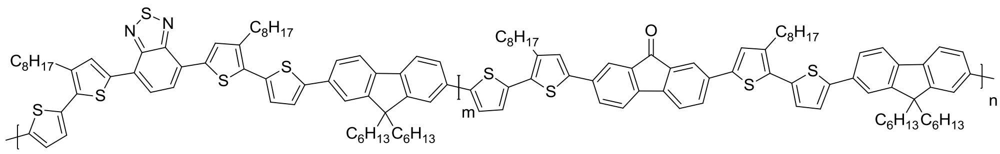

PTFBF

**Figure 198: Fluorene-based polymers poly(thiophene-fluorene fluorenone) PTFF, poly(thiophene-fluorene benzothiadiazole) PTFB, poly (thiophene-fluorene-benzothiadiazole-fluorenone)**

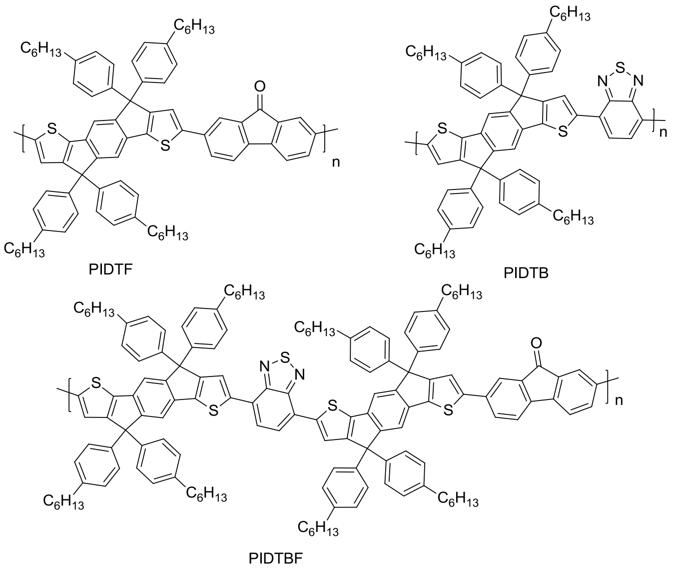


**Figure 199:Indacenodithiophene-based polymers , poly (indacenodithiophene-fluorenone) PIDTF, poly (indacenodithiophene-benzothiadiazole) PIDTB, and poly (indacenodithiophene-benzothiadiazole-fluorenone) PIDTFB**

## II.2. Acceptor materials

For our photovoltaic application studies, we have used two types of acceptor materials. The first type of acceptor is fullerenes derivatives namely PCBMC60, PCBMC70, ThCBMC60 and bisPCBMC60. All the fullerenes derivatives are purchased from Solenn BV. The second type of acceptor used in this work is CdSe nanoparticles. The CdSe nanorods are synthesized in our laboratory by Angela Fiore.

### II.2.1.Fullerenes derivatives

Fullerenes derivatives have been widely chosen as acceptor materials in the organic photovoltaic field [30], [31]. Four different fullerenes derivatives have been chosen for our investigation as potential acceptor materials for photovoltaic applications; [6,6]-phenyl-C61-butyric acid methyl ester PCBMC60 [32], [6,6]-phenyl-C71-butyric acid methyl ester PCBMC70[33], [6,6]-thienyl-C61-butyric acid methyl ester ThCBMC60[34] and [6,6]-phenyl-C61-butyric acid methyl ester PCBMC60[35] as shown in Figure 200 below.

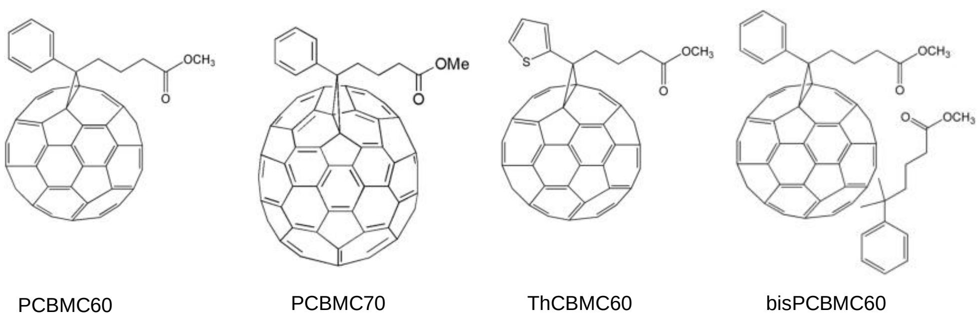


**Figure 200: Structures of fullerenes derivatives PCBMC60, PCBMC70, ThCBM and bisPCBMC60**

PCBMC60 introduced by Hummelen et al. [36] is a reference electron acceptor materials for the fabrication of bulk heterojunction organic photovoltaic cells because of its capability to be used efficiently with versatile electron donor materials[37],[38]. PCBMC70[39] its bigger analogue which possesses stronger visible absorption than PCBMC60 offers almost systematically higher power conversion efficiency than PCBMC60 when combined with low band-gap polymers[40],[41]. Another analog of PCBMC60, ThCBM was introduced by Hummelen et al. [42]. In this coupound the phenyl group substituent was replaced by a thienyl group in order to improve miscibility with thiophene-based polymers [43] . Bis-adduct fullerene has been investigated by Lenes et al. showing promising power conversion efficiency in bulk heterojunction solar cells owing to enhanced open circuit voltage.[44]

For application in photovoltaic cells, the electronic properties of the acceptor are of crucial parameters notably the position of LUMO energy levels. Firstly, the LUMO energy levels of the acceptor have to be positioned higher to the LUMO energy levels of the donor. And secondly the difference between the LUMO energy level of the fullerene acceptors and the HOMO energy level of the donors can determined the open circuit voltage of the photovoltaic device[45]. However in the literature, the values of the LUMO energy levels vary from -4.3 eV to -3.7 eV[37],[41],[46]. Therefore to have adequate correlation with our measured donor material values, we decided to confirm the energy level position of the different fullerenes our laboratory characterization techniques.

We have performed electrochemical characterization measured by cyclic voltammetry (CV) and differential pulse voltammetry (DPV) of the fullerenes derivatives to allow determination of their energy levels. The analyses were performed using a solvent mixture of orthodichlorobenzene: acetonitrile 4:1 with tetrabutylammonium hexafluorophosphate as supporting electrolyte at 0.1 M concentration. Utilisation of orthodichlorobenzene is necessary to allowed complete dissolution of the fullerenes derivatives.

Here we only present the reduction measurements of the fullerenes derivatives for determination of LUMO energy levels. Furthermore, the oxidation potentials of fullerenes derivatives could hardly be determined as fullerenes are generally irreversible in many solvents[47] as well as our solvent mixture. We performed cyclic voltamperometry analysis as well as differential pulse voltammetry for PCBMC60, PCBMC70, ThCBM and bisPCBMC60. The differential pulse voltammetry DPV afford higher current sensitivity and better resolution than cyclic voltammetry CV[48].

CV and DPV voltammograms are presented in Figure 201.

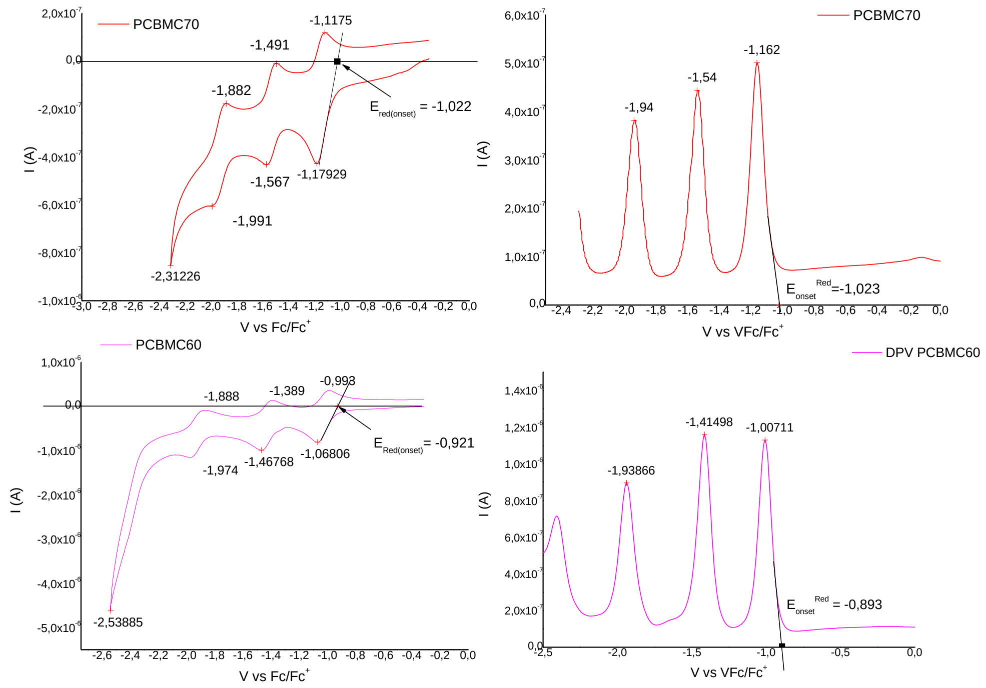


**Figure 201: Up:Cyclic voltammogram (left) and differential pulse voltammogram ( right) of PCBMC60 Bottom: Cyclic voltammogram (left) and differential pulse voltammogram ( right) of PCBMC70**

PCBMC60 gives three reversible reduction potentials at -1.066 V, -1.467 V and -1.974 V in cyclic voltammetry. The cathodic potentials observed by differential pulse voltammetry are slightly lower with -1.007 V, -1.414 and -1.938 V. The onset reduction potential values are found to be -0.92 V (LUMO: -3.88 eV) from CV measurement and -0.89 V (LUMO:-3.91 eV) from DPV measurement. The average LUMO value at -3.895 eV obtained are closed to the value of -3.90 eV[31] and -3.91 eV[49] obtained from CV measurement.

PCBMC70 also shows three reduction potentials but with much lower potentials at -1.179 V, -1.567 V and -1.991 V. The onset reduction potential is found at -1.02 V equals to a LUMO energy level at -3.76 eV from CV and DPV measurement. The LUMO level of PCBMC70 is found to be ca. 100 mV lower than the value of PCBMC60.[50]

An analog of PCBMC60, the thienyl fullerene derivatives ThCBM differ from PCBMC60 only by the change of substituent group from benzene ring to a thienyl group. The ThCBMC60 shows interestingly four reduction peaks. In terms of reduction potential, they afford similar onset reduction potential to PCBMC60 value at -0.93 V giving a LUMO energy level at -3.87 eV (CV) and -3,89 (DPV). The LUMO energy levels of ThCBM has reported to be similar to the value of PCBMC60 by other groups[51],[52] confirming the values obtained in our experiment.

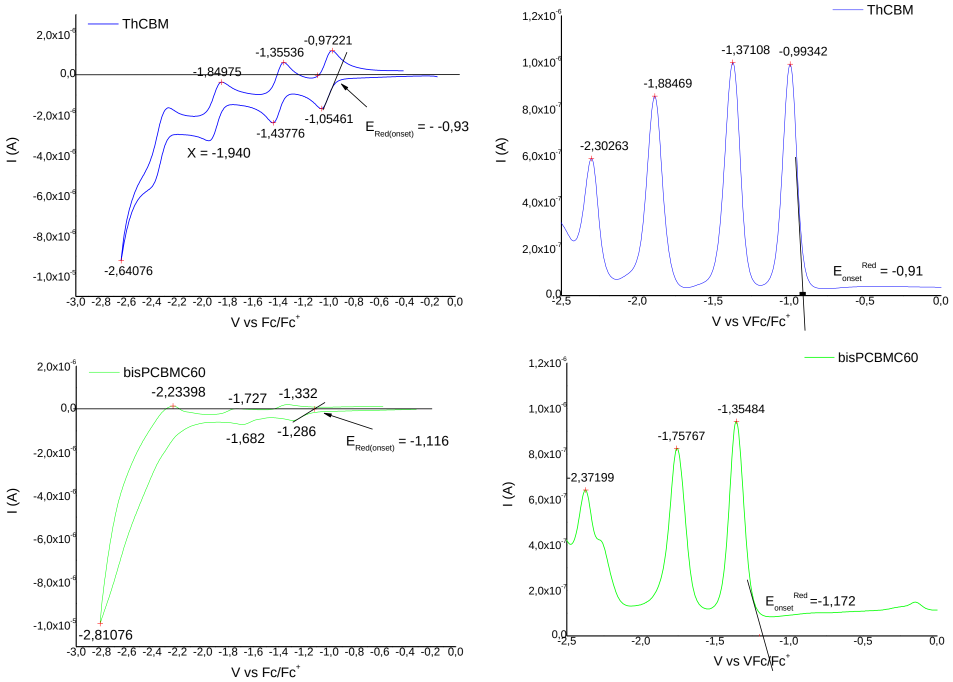


**Figure 202: Cyclic voltammogram and differential pulse voltammogram of ThCBMC60 and bisPCBMC60**

The bisadduct bisPCBMC60 is another type of fullerene functionalized with two phenyl butyric acid methyl ester. The additional functional group on the fullerene C60 has indeed lower the reduction potential as compared to monoadduct PCBMC60 with an onset reduction potential value at -1.12 V equals to a LUMO energy level of -3.68 eV from CV and -1,17 V from DPV (-3,63 eV). Our experimental LUMO energy level value found is closed to the reported value of -3,7 eV by the group Hummelen et al.[35] . This gives a lower position of 200 mV as compared to PCBMC60.

By comparing the results obtained from experimental data and the values from literatures, the values of LUMO energy levels for each fullerenes throughout our study are -3,9 eV (PCBMC60) , -3,8 eV (PCBMC70), -3,9 eV (ThCBM) and -3,7 eV (bisPCBM). In Table 60 is presented all the different values for the four different fullerenes derivatives.

| | Cyclic voltammetry | | | | Differentiel pulse voltammetry | | | | LUMO | | |
|---|---|---|---|---|---|---|---|---|---|---|---|
| Compound | $E_{on}^{red}$ | $E_{red1}$ (V) | $E_{red2}$ (V) | $E_{red3}$ (V) | $E_{on}^{Red}$ | $E_{red1}$ (V) | $E_{red2}$ (V) | $E_{red3}$ (V) | CV (eV) | DPV (eV) | Exp (eV) |
| PCBMC60 | -0.92 | -1.07 | -1.47 | -1.97 | -0.89 | -1.01 | -1.41 | -1.94 | -3.88 | -3.91 | -3.9 |
| PCBMC70 | -1.02 | -1.18 | -1.57 | -1.99 | -1.02 | -1.16 | -1.54 | -1.94 | -3.76 | -3.76 | -3.8 |
| ThCBM | -0.93 | -1.05 | -1.43 | -1.94 | -0.91 | -0.99 | -1.37 | -1.88 | 3.87 | -3.89 | -3.9 |
| bisPCBM | -1.12 | -1.31 | -1.68 | | -1.17 | -1.35 | -1.57 | -2.37 | -3.68 | -3.63 | -3.7 |

**Table 60: Reduction potentials of fullerenes derivatives and LUMO energy levels of PCBMC60, PCBMC70, ThCBM and bisPCBMC60. LUMO Exp values will be the values used throughout our study.**

### II.2.2. CdSe nanorods

Following the work in our laboratory on solar cells based on blends of polymer 3-hexylthiophene P3HT and Cadmium Selenide CdSe nanorods,[53] , we have decided to make use CdSe nanorods as acceptor material in combination with our donor materials for fabrication of hybrid organic solar cells. Cadmium selenide CdSe nanorods were synthesized by Angela Fiore from our laboratory. The CdSe nanorods are of 5 mm in diameter and 60 nm of length, confirmed by transmission electronic miscroscopy TEM as shown in Figure 203. In order to perform solar cell test with TVF2, ligand exchange is required using pyridine as surfactant around the nanocrystals' surfaces. The ligand exchange was carried out by adding the excess of new ligand (pyridine) to a chloroform solution of coated nanocrystals. After sonication, the solvent mixture is concentrated and precipitated in hexane. The nanorods of CdSe were then dispersed in orthodichlorobenzene (ODCB): pyridine (90 %: 10% volume:volume). The final concentration of the solution was 60 mg/ml as estimated by gravimetric measurements. HOMO and LUMO energy levels determined by electrochemistry were found at -5.59 eV and -3.62 eV respectively.

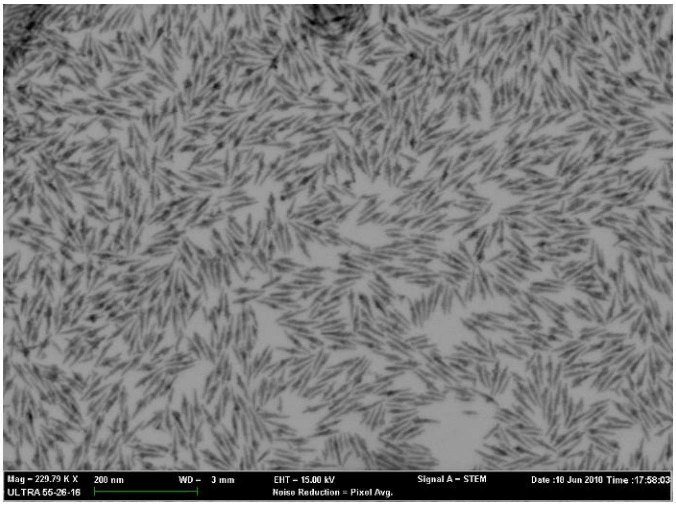


**Figure 203 : TEM images of CdSe nanorods**

# III. Reference


1 Bernd Trathnigg in Encyclopedia of Analytical Chemistry, R.A. Meyers (Ed.),pp. 8008–8034, John Wiley & Sons Ltd, Chichester, 2000. http://www.uni-graz.at/~trathnig/2032- a.pdf

2 http://www.aquafineuv.com/UVTechnology/UVScience.aspx

3 André Moliton, Electronique et optoélectronique organiques, edition Springer 2001.

4 a) Forster, R. 'Organic Charge-Transfer complexes; Academic Press: London. 1969.
b)Miken, R. S.; Person, W. B. "Molealar complexes; Wiley-Intersience: New York. 1969.
c) Nagakwa, S.; Tanaka, J. J. Chem. phys. 1054, 22, 236.
d)R. O. Loutfy, C. K. Hsiao, B. S. Ong, B. Keoshkerian, Can. J., Electrochemistry and Spectroscopy of Intramolecular Charge Transfer Complexes, Chem. 1984, 62, 1877–1885.

5 N. S. Sariciftci, L. Smilowitz, A. J. Heeger, and F. Wudl, Photoinduced Electron Transfer from a Conducting Polymer to Buckminsterfullerene, Science 27 November 1992: Vol. 258 no. 5087 pp. 1474-1476

6 A Pron , P Gawrys , M Zagorska , D Djurado and R Demadrille, Electroactive materials for organic electronics: preparation strategies, structural aspects and characterization techniques, Chem. Soc. Rev., 2010,39, 2577-2632

7 Polec, I., Henckens, A., Goris, L., Nicolas, M., Loi, M. A., Adriaensens, P. J., Lutsen, L., Manca, J. V., Vanderzande, D. and Sariciftci, N. S. (2003), Convenient synthesis and polymerization of 5,6-disubstituted dithiophthalides toward soluble poly(isothianaphthene): An initial spectroscopic characterization of the resulting low-band-gap polymers. J. Polym. Sci. A Polym. Chem., 41: 1034–1045.

8 Pommerehne, J., Vestweber, H., Guss, W., Mahrt, R. F., Bässler, H., Porsch, M. and Daub, J. (1995), Efficient two layer leds on a polymer blend basis. Adv. Mater., 7: 551–554.

9 N. S. Sariciftci, L. Smilowitz, A. J. Heeger, and F. Wudl, Photoinduced Electron Transfer from a Conducting Polymer to Buckminsterfullerene, Science 27 November 1992: Vol. 258 no. 5087 pp. 1474-1476

10 A. Carrington and McLaclan A.D., In introduction to magnetic Resonance with applications to Chemistry and Chemical physics. New York: Harper and Row, 1967.

11 V. I. Krinichnyi, LEPR spectroscopy of charge carriers photoinduced in polymer/fullerene composites, 2009th ed. Hauppauge, New York,: In Encyclopedia of Polymer Composites, pp. 417–446.

12 R. S. Alger, "Electron Paramagnetic Resonance, Techniques and Applications," American Journal of Physics, vol. 37, no. 8, p. 847, 1968.

13 J. P. C.P., Electron Spin Resonance: A comprehensive Treatrise on Experimental Techniques, 2 nd ed. New York: John Wiley and Sons, 1983.

14 J. A. Weil, J. R. Bolton, and J. E. Wertz, Electron Paramagnetic Resonance: Elementary Theory and Practical Applications. New York: John Wiley and Sons, 1994.

15 B. Pepin-Donat. et Al., "EPR tracing method," E.S.T. under considerations, 2012

16 G. Horowitz, Organic Field-Effect Transistors, Adv. Mater. 1998, 10, No. 5

17 H. Klauk, Organic thin-film transistors, Chem. Soc. Rev., 2010,39, 2643-2666

18 T. B. Singh and N. S. Sariciftci, Progress in plastic electronics devices, Annu. Rev. Mater. Res. 2006. 36:199–230

19 Demadrille, R., Firon, M., Leroy, J., Rannou, P. and Pron, A. (2005), Plastic Solar Cells Based on Fluorenone-Containing Oligomers and Regioregular Alternate Copolymers. Adv. Funct. Mater., 15: 1547–1552.

20 Groenendaal, L., Jonas, F., Freitag, D., Pielartzik, H. and Reynolds, J. R. (2000), Poly(3,4-ethylenedioxythiophene) and Its Derivatives: Past, Present, and Future. Adv. Mater., 12: 481–494.

21 http://rredc.nrel.gov/solar/spectra/am1.5/

22 Binnig, G., Atomic Force Microscope and Method for Imaging Surfaces with Atomic Resolution, US Patent 4,724,318, (1986)

23 R. Garcia and R. Pérèz, Dynamic atomic force microscopy methods, Surf. Sci. Reports 47, 197-301, 2002.

24 Ph. Leclère, M. Surin, P. Brocorens, M. Cavallini, F. Biscarini, R. Lazzaroni, Supramolecular assembly of conjugated polymers: From molecular engineering to solid-state properties, Mater. Sci. Eng. Rep. R55, 1-56, 2006

25 R. Garcia, R. Magerle and R. Pérèz, Nanoscale compositional mapping with gentle forces, Nature Mater 6, 405-411, 2007.

26 E. J. Spadafora, M. Linares, W. Z. Nisa Yahya, F. Lincker, R. Demadrille and B. Grevin, Local contact potential difference of molecular self-assemblies investigated by Kelvin probe force microscopy, Appl. Phys. Lett. 99, 233102-1-3 (2011).

27 E. J. Spadafora, R. Demadrille, B. Ratier, and Benjamin Grévin, Imaging the Carrier Photogeneration in Nanoscale Phase Segregated Organic Heterojunctions by Kelvin Probe Force Microscopy, Nano Lett. 10, 3337–3342 (2010)

28 Nanosurf AG, Grammetstrasse 14, CH4410 Liestal, Switzerland

29 Omicron NanoTechnology GmbH, Limburger Strasse 75, D-65232 Taunusstein, Germany

30 Anthony, J. E., Facchetti, A., Heeney, M., Marder, S. R. and Zhan, X. n-Type Organic Semiconductors in Organic Electronics, Adv. Mater., (2010), 22, 3876–3892.

31 Y He and Y Li, Fullerene derivative acceptors for high performance polymer solar cells, Phys. Chem. Chem. Phys., 2011,13, 1970-1983

32 G. Yu, J. Gao, J. C. Hummelen, F. Wudl and A. J. Heeger, Science, 1995, 270, 1789

33 Wienk, M. M., Kroon, J. M., Verhees, W. J. H., Knol, J., Hummelen, J. C., van Hal, P. A. and Janssen, R. A. J. (2003), Efficient Methano[70]fullerene/MDMO-PPV Bulk Heterojunction Photovoltaic Cells. Angew. Chem. Int. Ed., 42: 3371–3375.

34 P. A. Troshin, H. Hoppe, J. Renz, M. Egginger, J. Y. Mayorova, A. E. Goryachev, A. S. Peregudov, R. N. Lyubovskaya, G. Gobsch, N. S. Sariciftci and V. F. Razumov, Material Solubility-Photovoltaic Performance

Relationship in the Design of Novel Fullerene Derivatives for Bulk Heterojunction Solar Cells, Adv. Funct. Mater., 2009, 19, 779

35 M. Lenes, G. J. A. H. Wetzelaer, F. B. Kooist, S. J. Veenstra, J. C. Hummelen and P. W. M. Blom, Fullerene Bisadducts for Enhanced Open-Circuit Voltages and Efficiencies in Polymer Solar Cells, Adv. Mater., 2008, 20, 2116

36 G. Yu, J. Gao, J. C. Hummelen, F. Wudl and A. J. Heeger, Science, 1995, 270, 1789

37 Scharber, M.C., Mühlbacher, D., Koppe, M., Denk, P., Waldauf, C., Heeger, A.J. and Brabec, C.J., Design Rules for Donors in Bulk-Heterojunction Solar Cells—Towards 10% Energy-Conversion Efficiency. Adv. Mater., (2006), 18: 789–794

38 Dang, M. T., Hirsch, L. and Wantz, G. (2011), P3HT:PCBM, Best Seller in Polymer Photovoltaic Research. Adv. Mater., 23: 3597–3602.

39 Wienk, M. M., Kroon, J. M., Verhees, W. J. H., Knol, J., Hummelen, J. C., van Hal, P. A. and Janssen, R. A. J. (2003), Efficient Methano[70]fullerene/MDMO-PPV Bulk Heterojunction Photovoltaic Cells. Angew. Chem. Int. Ed., 42: 3371–3375.

40 Troshin, P. A., Hoppe, H., Peregudov, A. S., Egginger, M., Shokhovets, S., Gobsch, G., Sariciftci, N. S. and Razumov, V. F. (2011), [70]Fullerene-Based Materials for Organic Solar Cells. ChemSusChem, 4: 119–124.

41 S. H. Park, A. Roy, S. Beaupre, S. Cho, N. Coates, J. S. Moon, D. Moses, M. Leclerc, K. Lee and A. J. Heeger, Bulk heterojunction solar cells with internal quantum efficiency approaching 100%, Nat. Photonics, 2009, 3, 297–303

42 L M. Popescu, P van 't Hof, A B. Sieval, H T. Jonkman, and J C. Hummelen, Thienyl analog of 1-(3-methoxycarbonyl)propyl-1-phenyl-[6,6]-methanofullerene for bulk heterojunction photovoltaic devices in combination with polythiophenes, Appl. Phys. Lett. 89, 213507 (2006)

43 P. A. Troshin, H. Hoppe, J. Renz, M. Egginger, J. Y. Mayorova, A. E. Goryachev, A. S. Peregudov, R. N. Lyubovskaya, G. Gobsch, N. S. Sariciftci and V. F. Razumov, Adv. Funct. Mater., 2009, 19, 779

44 Lenes, M., Wetzelaer, G.-J. A. H., Kooistra, F. B., Veenstra, S. C., Hummelen, J. C. and Blom, P. W. M. (2008), Fullerene Bisadducts for Enhanced Open-Circuit Voltages and Efficiencies in Polymer Solar Cells. Adv. Mater., 20: 2116–2119.

45 C. J. Brabec, A. Cravino, D. Meissner, N. S. Sariciftci, T. Fromherz, M. T. Rispens, L. Sanchez and J. C. Hummelen, Adv. Funct. Mater., 2001, 11, 374

46 C-W Chu, V Shrotriya, G Li, and Y Yang, Tuning acceptor energy level for efficient charge collection in copper-phthalocyanine-based organic solar cells, Applied Physics Letters 88, 153504, 2006

47 Dubois, D.; Kadish, K. M.; Flanagan, S.; Wilson, L. J. , Electrochemical Detection of Fulleronium and Highly Reduced Fulleride (C60) Ions in Solution, J. Am. Chem. Soc. 1991, 113, 7773-7774

48 S P. Kounaves, Handbook of Instrumental Techniques for Analytical Chemistry, Upper Saddle River, NJ : Prentice Hall PTR, ©1997.

49 Y He, C Chen, E Richard, LDou, Y Wu, G Li and Y Yang, Novel fullerene acceptors: synthesis and application in low band gap polymer solar cells, J. Mater. Chem, 2012

50 F B. Kooistra, V D. Mihailetchi, L M. Popescu, D Kronholm, P W. M. Blom, and J C. Hummelen, New C84 Derivative and Its Application in a Bulk Heterojunction Solar Cell, *Chem. Mater.* 2006, *18*, 3068-3073

51 L M. Popescu, P V Hof, A B. Sieval, H T. Jonkman, and J C. Hummelen, Thienyl analog of 1-(3-methoxycarbonyl)propyl-1-phenyl-[6,6]-methanofullerene for bulk heterojunction photovoltaic devices in combination with polythiophenes, Appl. Phys. Lett. 89, 213507 (2006)

52 Yamamoto, S., Orimo, A., Ohkita, H., Benten, H. and Ito, S. (2012), Molecular Understanding of the Open-Circuit Voltage of Polymer:Fullerene Solar Cells. Adv. Energy Mater., 2: 229–237.

53 T. G. Jiu, P. Reiss, S. Guillerez, R. de Bettignies, S. Bailly and F. Chandezon, IEEE J. Sel. Top. Quantum Electron., 2010, 16, 1619–1626

# SYNTHESIS PROCEDURES

# I. Materials

All reagents and chemicals were purchased from Aldrich or Acros and used as received, except for THF which was distilled over sodium–benzophenone prior to use. Thin layer chromatography was performed on silica gel-coated aluminium plates with a particle size of 2–25 mm and a pore size of 60 A°. Merck 60 (70–230 mesh) silica was used for flash chromatography.

# II. Synthesis

## II.1. Synthesis of TVF2

**(E)-1,2 -bis(3-octylthiophen-2-yl)ethane (1)**

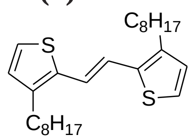


**1**

A suspension of low-valent of Ti was prepared by reducing $TiCl_4$ (2.8 ml, 25.6 mmol) with zinc powder (3.36 g, 53.5 mmol) in 100 ml of distilled THF at 0 °C. 3-octylthiophene-2-carbaldehyde (4.74 g, 22.3 mmol) was then added. The mixture was allowed to warm to room temperature before heating at reflux (70°C) for 2 h. A dark suspension was obtained was poured at room temperature into a solution of HCl 1M. The product was extracted with $CH_2Cl_2$, and the organic phase was washed with water and dried over $Na_2SO_4$. After solvent removal, the crude was purified by column chromatography (silica gel, hexane) to give 2.54 g (6.1 mmol, 55%) of bright yellow solid.

$^1$H NMR ($CDCl_3$): $\delta$ 7.08 (d, 2H, 5.1 Hz); 6.99 (s, 2H); 6.85 (d,2H,5.1 Hz); 2.68 (t, 4H, 7.3 Hz) ; 1.55 (m, 4H); 1.29 (m, 20H); 0.87 (m, 6H)

**(E)-trimethyl(4-octyl-5-(2-(3-octylthiophen-2-yl)vinyl)thiophen-2-yl)stannane (2)**

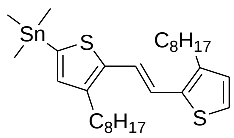


**2**

A solution of (E)-1,2-bis(3-octylthiophen-2-yl)ethylene (800 mg,1.9 mmol) in 15 ml of dry THF was cooled at -78°C and a solution of n-BuLi in hexane (2.8 ml, 0.8 M, 2.24 mmol) was added dropwise. The solution was allowed to warm at -45°C and after 50 min stirring, the

reddish solution was then cooled to -78°C.A solution of $Me_3SnCl$ (382 mg, 1.9 mmol) in 4 ml of dry THF is added. The reactant was then allowed to warm at room temperature. An orange solution was obtained. The solution was quenched with $NH_4Cl$, and extracted by ethyl ether for several times. The organic phase is washed with water and dried over $Na_2SO_4$ and the solvent was removed under vacuum. Dark red oil is obtained and used without further purification. $^1$H NMR analysis indicates a quantitative reaction.
$^1$H NMR ($CDCl_3$): $\delta$ 7.07 (d, 2H, 5.1 Hz); 6.99 (s, 2H); 6.92 (s, 1H); 6.85 (d, 2H, 5.1Hz); 2.69 (t, 4H, 7.3 Hz) ; 1.56 (m, 4H); 1.27 (m, 20H); 0.87 (m, 6H) ;0.37 ( t, 9H)

**2-bromo-7-(5-octylthiophen-2-yl)-9H-fluoren-9-one (3)**

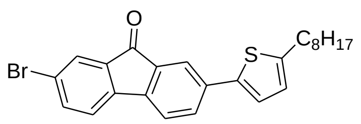


**3**

5,5-dimethyl-2-(5-octylthiophen-2-yl)-1,3,2-dioxaborinane (2 g, 6.48 mmol) and 2,7-dibromo-9H-fluoren-9-one (2.41 g, 7.1 mmol) were dissolved in 30 ml of DMF and heated slowly under argon atmosphere. At 60 °C, $Pd(PPh_3)_4$ ( 224 mg, 0.11 mmol) and potassium phosphate $K_3PO_4$ ( 1.358 g, 6.4 mmol) were then added. The mixture was heated at reflux overnight under vigorous stirring. After a night, the mixture was washed with 50 ml of HCl 1.0M solution and the product was extracted with diethyl ether. The organic phase was separated and concentrated. An orange powder was obtained by recristallisation in chloroform, and washed with acetonitrile to remove impurities. (1.48 g, Yield: 48%);
$^1$H NMR ($CDCl_3$): 7.842 ( s, 1H), 7.763 (d, J= 1.7 Hz, 1H) , 7.670-7.587 ( m, 2H) , 7.477 ( d, J=7.3 Hz, 1H) 7.387 (d, J=7.3 Hz, 1H) 7.202 (d, J=3.6 Hz, 1H), , 6.772 (d, J=3.6 Hz, 1H), 2.859 (t, J=7.5 Hz, 2H), 1.733 (m, 2H) 1.281 (m, 10H), 0.885 (t, 3H).
$^{13}$C NMR (200 MHz, $CDCl_3$, δ): 146.681, 137.046, 131.105, 130.980, 127.383, 125.124, 123.390, 123.158, 122.418, 121.442, 121.032, 120.690, 116.214, 31.641, 31.397, 30.061, 29.115, 29.005, 28.874, 22.452, 13.906

**(E)-2-(4-octyl-5-(2-(3-octylthiophen-2-yl)vinyl)thiophen-2-yl)-7-(5-octylthiophen-2-yl)-9H-fluoren-9-one (4)**

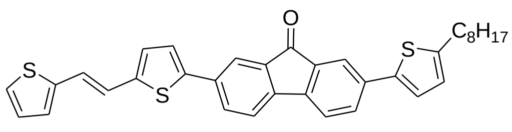


**4**

Following classical Stille coupling reaction procedure, in a 100 ml two neck flask were introduced (E)-trimethyl(4-octyl-5-(2-(3-octylthiophen-2-yl)vinyl)thiophen-2-yl)stannane (2)

(681.7 mg, 1.92 mmol ) , 2-bromo-7-(5-octylthiophen-2-yl)-9H-fluoren-9-one (3) ( 887.9 mg, 1.96 mmol) , and palladium (0) catalyst $Pd(PPh_3)_4$ ( 66 mg, 0.06 mmol, 3 % eq). Potassium phosphate $K_3PO_4$ (400 mg, 1.92 mmol) salts was also added to help improving the reaction. All the reactants were dissolved in 20 ml of DMF and heated at reflux in argon environment overnight. The mixture was treated the next day with 50 ml of HCl 1.0M solution and the product was extracted with diethyl ether. The organic phase was separated and concentrated. The crude product was further purified by column chromatography (silica gel, hexane: ether 98:2) to give 520 mg (0.66 mmol, 34 %) of red viscous oil.

$^1$H NMR (200 MHz, CDCl3) d (ppm): 7.80 (dd, $J_1$=1.6 Hz, $J_2$= 5.0 Hz, 2H), 7.64 (m, 2H), 7.44 (dd, J=7.8 Hz, J=1.6 Hz, 2H), 7.20 (t, J= 3.6, 2), 7.11 (d, J=5.0, 1H), 7.00 ( d, J=4.3Hz, 2H), 1.79 (m, 4H), 1.14 (m, 20H), 0.95 (m, 4H), 0.84 (t, J = 6.8 Hz, 6H), 0.38 (s, J=28.5 Hz, 9H).

$^{13}$C NMR (200 MHz, $CDCl_3$, δ): 146.647, 142.642, 142.307, 142.102, 141.188, 140.271, 139.293, 136.798, 136.141, 135.693, 135.054, 135.018, 131.189, 131.092, 129.918, 129.536, 126.412, 125.274, 123.387, 122.869, 121.087, 121.030, 120.707, 120.641, 119.791, 118.841, 31.899, 31.861, 31.614, 30.980, 30.279, 29.448, 29.395, 29.338, 29.281, 29.103, 22.668

Mass spectrometry $[M^+ Na]^+$ ($C_{51}H_{64}ONaS_3$): Exact Mass: 811.4017 z = 1 m/z Calculated: 811.40115; Found: 811.4011 (0 ppm)

**7,7'-(5,5'-(1E,1'E)-2,2'-(4,4'-dioctyl-2,2'-bithiophene-5,5'-diyl)bis(ethene-2,1-diyl)bis(4-octylthiophene-5,2-diyl))bis(2-(5-octylthiophen-2-yl)-9H-fluoren-9-one) (5) : TVF2**

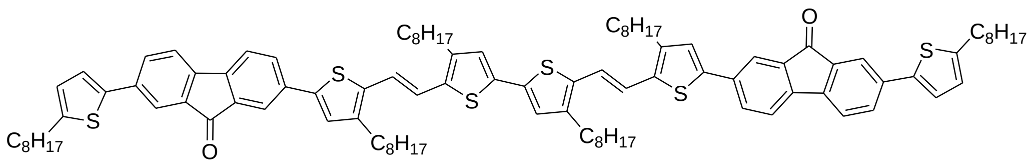


**TVF2**

(E)-2-(4-octyl-5-(2-(3-octylthiophen-2-yl)vinyl)thiophen-2-yl)-7-(5-octylthiophen-2-yl)-9H-fluoren-9-one (500 mg, 0.63 mmol) was dissolved in 15 ml of anhydrous dichloromethane and was cooled to 0° C in argon environment. Iron (III) chloride (123 mg, 0.756 mmol) dissolved in 2 ml of nitromethane was added drop wise. The mixture was allowed to warm to room temperature and stirred overnight. The product was allowed to precipitate by adding drop wise into methanol. Few drops of hydrazine were added to increase precipitation. The powder was filtered and washed by vigorous stir in a mixture of 0.1 M ammoniac solution and 0.02 M of EDTA for 15 hours. The precipitate was filtered and the crude was further purified by column chromatography (silica gel, pentane). Dark metallic violet flakes were obtained. (262 mg, 52%)

[1]H NMR (200 MHz, CDCl3) d (ppm): 7.849 ( br, 4H) , 7.657 (br, 4H), 7.475 (br, 4H) , 7.196 (br, 4H), 6.908 (br, 4H), 6.751 (br, 2H), 2.814 (br, 6H) , 2.631 (br, 6H), 1.658 (br, 12H) , 1.29 (br, 60H), 0.884 (br, 18H).

[13]C NMR (200 MHz, $CDCl_3$, δ): 193.406, 146.398, 142.332, 142.172, 142.111, 141.897, 140.244, 139.307, 136.971, 135.547, 134.905, 134.729, 134.548, 129.553, 120.505, 31.976, 31.886, 29.553, 29.366, 29.327, 29.270, 22.725, 14.168

Mass spectrometry $M^+$ ($C_{102}H_{126}O_2S_6$): Exact Mass: 1574.80822 z = 1 m/z Calculated: 1574.80767; Found: 1574.8073 (0 ppm)

Infrared spectroscopy analysis:

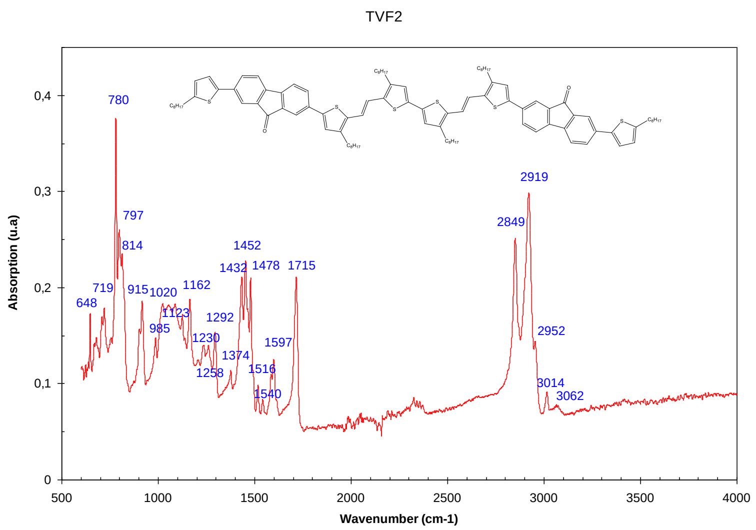


**Figure 204: Infra-red spectrum of TVF2**

| Wavenumber ($cm^{-1}$) | Attribution |
|---|---|
| 780 | C-H bend ( Z) (vinylene) |
| 1162-1020 | C-H deformation in plane (thiophene rings) |
| 1432-1478 | C=C (aromatic) stretch |
| 1452 | $CH_2$ bend |
| 1715 | C=O stretch |
| 2849; 2919;2952 | C-H stretch (alkyl chains) |
| 3014; 3062 | C-H stretch (thiophene rings and phenyl ring) |

**Table 61: Table list of wavenumbers of infrared absorption spectroscopy of the molecule TVF2 with its attribution.**

## II.2. Synthesis of QTF8

### 2-bromo-3-octylthiophene (6)

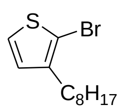


**6**

3-octylthiophene (6 g, 30.55 mmol) was dissolved in 30 ml of anhydrous DMF and placed in a light protected flask. N-bromosuccinimide (5.71 g, 32 mmol) was dissolved in 40 ml of anhydrous DMF then added dropwise. The mixture was well stirred in room temperature overnight under argon atmosphere. After stirring for overnight at room temperature, the resulting mixture was poured into 20 ml of water, and then extracted with diethyl ether. After solvent removal, the crude product was purified by silica gel column chromatography with hexane as eluent to afford 2-bromo-3-octylthiophene as colorless oil. (7.92 g, 94 %) $^{1}$H NMR (200 MHz, $CDCl_3$, δ): 7.195 (d, J= 5.6 Hz, 1H); 6.806 (d, J= 5.6 Hz, 1H), 2.593 (t, J= 7.3 Hz, 2 Hz), 1.267 (m, 12H), 0.881 (m, 3H)

**(3-octylthiophen-2-yl) magnesium bromide (7)**

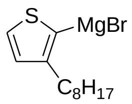


**7**

1.3 g of magnesium (5.4 mmol) was highly heated to remove the oxides for activation. After cooling, 10 ml of dry diethyl ether was added and heated at 50°C. 2-bromo-3-octylthiophene (5.53 g, 2.2 mmol) diluted in 20 ml of dry diethyl ether was added drop wise and the solution became troubled. It is necessary to maintain the activation of the magnesium by controlling the flux of addition. At the end of the addition, the mixture was stirred vigorously for 3h at 50°C.

**5,5'-dibromo-2,2'-bithiophene (8)**

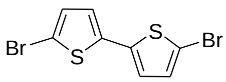


**8**

2,2-dithiophène (166 g/mol; 60,7 mmol) was dissolved in 30 ml of DMF in a light protected two-neck flask and cooled to 0°C in an inert environment. N-bromosuccinimide (22 g, 123 mmol) was dissolved in a solvent mixture ( DMF: Methanol 90 ml: 60 ml) , and was added drop wise to the flask. White precipitates were formed and after 1 hour, the ice bath was removed and the reaction was left to stir at room temperature for 12 h. The precipitates were washed with water then extracted with dichloromethane. The organic phase was separated and concentrated. The crude was purified by recristallisation in hexane. (17.62 g, white flakes, 90 %).

$^{1}$H NMR (200 MHz, CDCl3) d (ppm): 7,13 (d, 2H) 7,06 (d, 2H)

**3,3'''-dioctyl-[2,2'; 5,2'';5",2'''] quaterthiophen-5-yl (9)**

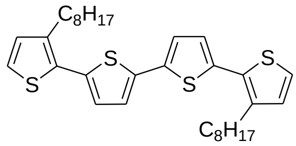

**9**

5,5'-dibromo-2,2'-bithiophene (3.56 g, 11 mmol) and NiCl$_2$dppp were dissolved in 60 ml of dry diethyl ether and 10 ml of freshly distilled THF. The Grignard reactant (3-octylthiophen-2-yl) magnesium bromide was then added drop wise via a canula. After complete addition, the mixture was stirred vigorously at reflux for 12 h. An orange solution with formation of precipitates was obtained. The solution was washed with HCl 1N and extracted with diethyl ether. After solvent removal, the crude product was further purified by silica gel column chromatography in hexane. (3 g, 49%, yellow viscous gel)

$^1$H NMR (200 MHz, CDCl3) d (ppm): 7.194 (d, J= 5.2 Hz, 2H), 7.136 (d, J= 3.8 Hz, 2H), 7.029 (d, J= 3.8 Hz, 2H), 6.954 (d, J= 5.2 Hz, 2H), 2.818 (t, J= 7.6 Hz, 4H), 1.265 (m, 24H), 0.874 (t, 3H)

**Trimethyl (3,3'''-dioctyl-[2,2'; 5,2'';5",2'''] quaterthiophen-5-yl )stannane (10)**

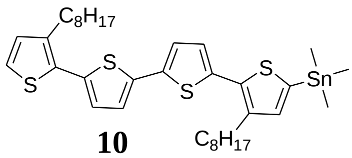

**10**

3,3'''-dioctyl-[2,2'; 5,2'';5",2'''] quaterthiophen-5-yl ( 2 g, 3.6 mmol) was dissolved in 40 ml of freshly distilled THF and cooled at -78 °C. A solution of 2.5 M n-BuLi in hexane (1.92 ml, 4.8 mmol) was added drop wise. The mixture was stirred for 1 h at -40°C. The mixture was cooled again to -78°C before addition of a solution of Me$_3$SnCl in 7 ml of anhydrous THF. The mixture was then stirred for another 2 hours at room temperature. The mixture was washed with NH$_4$Cl then extracted with diethyl ether. The organic phase was dried by Na$_2$SO$_4$ and concentrated. The conversion rate to stannic product was quantified by RMN to be 100%.

$^1$H NMR (200 MHz, CDCl3) d (ppm): 7.188 - 7.162 (d, J= 5.2 Hz, 1H) ,7.132 - 7.106 (dd, J= 3.7, J= 1.2, 2H) , 7.027 - 7.003 (m, 2H) , 6.950 (d, J= 5.2 Hz, 2H), 2.777 (t, J=7.2 Hz, 4H), 1.266 (m, 24 H) , 0.871 (m, 6H), 0.381 (t, 9H)

**2,7-bis-(3,3'''-dioctyl-[2,2'; 5,2'';5",2'''] quaterthiophen-5-yl)-fluoren-9-one (QTF8) (10) :**

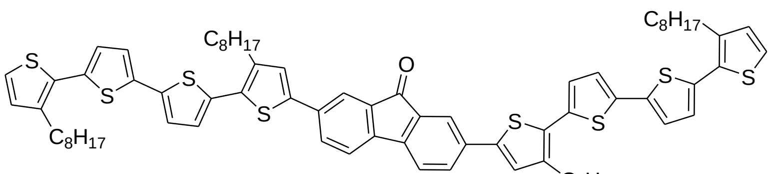

**QTF8**

Trimethyl (3,3'''-dioctyl-[2,2'; 5,2'';5'',2'''] quaterthiophen-5-yl )stannane was introduced in the flask from previous reaction without further purification and dissolved in 50 ml of DMF with 2,7-dibromo-9H-fluoren-9-one (536 mg, 1.59 mmol). The mixture was purged with argon before addition of freshly prepared catalyst $Pd(OAc)_2$ (17.85 mg, 0.08 mmol) and triphenylphosphine $P(Ph)_3$ (85 mg, 0.4 mmol) in 2 ml of distilled THF. The mixture was stirred vigorously in argon atmosphere at 100°C for 12 h. The product was treated following the previous procedure in Stille coupling (HCl, extraction) and further purified by silica gel column chromatography with hexane as eluent. (560 mg, 30%)

$^1$H NMR (200 MHz, CDCl3) d (ppm): 7,84 (d, 2H), 7,64 (dd, 2H), 7,44 (d, 2H), 7,21 (s, 2H), 7,18 (d, 2H), 7,12 (d, 4H), 7,05 (d, 2H), 7,02 (d, 2H), 6,94 (d, 2H), 2,28 (t, 8H), 1,66 (m, 8H), 1,29 (m, 40H), 0,88 (t, 12H).

$^{13}$C NMR (200 MHz, $CDCl_3$, δ): 193.3, 142.7, 140.7, 140.3, 139.9, 136.9, 136.7, 135.5, 135.1, 135.0, 134.81, 138.8, 131.1, 130.8, 130.4, 130.2, 126.8, 126.5, 126.4, 124.0, 123.9, 120.9, 120.8, 32.03, 32.0, 30.7, 30.5, 29.81, 29.77, 29.7, 29.6, 29.5, 29.4, 29.4, 22.8, 22.8, 14.3. Elemental analysis for $C_{77}H_{88}OS_8$ (calculated) : C 73.95; H: 8.01 . Elemental analysis for Found : C, 73.38; H, 8.02

## II.3. Preparation of monomers BTB

**4,7-bis(4-octylthiophen-2-yl)benzo[c][1,2,5]thiadiazole (11)**

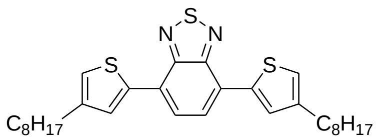

**11**

A mixture of 4,7-dibromobenzo[c][1,2,5]thiadiazole ( 478 mg, 1.6 mmol), 5,5-dimethyl-2-(4-octylthiophen-2-yl)-1,3,2-dioxaborinane (1) (1.5 g, 4.8 mmol), and $Pd(PPh_3)_4$ (55.5 mg, 3% molar) in 2.0 M $K_2CO_3$ aqueous solution (4 ml) and THF (20 ml) was refluxed overnight. The mixture was then allowed to cool to room temperature before addition of 1 M HCl and extracted with diethyl ether. The organic layer was dried over $Na_2SO_4$ and the solvent was evaporated. The crude product was purified by silica gel column chromatography with hexane/chloroform (4:1 v/v) as eluent to afford 4,7-bis(4-octylthiophen-2-yl)benzo[c][1,2,5]thiadiazole (11) as a brown viscous oil. (233 mg, yield: 28%)**.**

$^1$H NMR (200 MHz, $CDCl_3$, δ): 8.08 (s, 1H; Ar H), 8.07 (s, 1H; Ar H), 7.93 (s, 2H; Ar H), 7.15 (s, 1H; Ar H), 2.79 (t, $J$ = 7.2 Hz, 4H; $CH_2$), 1.88-1.73 (m, 4H; $CH_2$), 1.53-1.34 (m, 20H, $CH_2$), 0.98 (t, $J$ = 6.6 Hz ,6H; $CH_3$)

**4,7-bis(5-bromo-4-octylthiophen-2-yl)benzo[c][1,2,5]thiadiazole (12)**

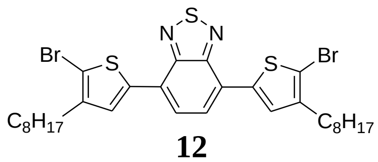


**12**

4,7-bis(4-octylthiophen-2-yl)benzo[c][1,2,5]thiadiazole (11) (417 mg, 0.79 mmol) was dissolved in 10 ml of chloroform and placed in a light protected two-neck round bootom flask. N-bromosuccinimide (297 mg, 1.67 mmol) dissolved in 10 ml of chloroform was placed in a dropping funnel, and then added drop wise to the flask at room temperature. After stirring for overnight at room temperature, the resulting mixture was poured into 20 ml of water, and then extracted with dichloromethane. After solvent removal, the crude product was purified by silica gel column chromatography with hexane/chloroform (9:1 v/v) as eluent to afford 4,7-bis(5-bromo-4-octylthiophen-2-yl)benzo[c][1,2,5]thiadiazole (12) as reddish flakes. (240 mg, 44 %)

$^1$H NMR (200 MHz, $CDCl_3$, δ): 7.77 (s, 2H; Ar H), 7.75 (2H, s; Ar H), 2.64 (t, $J$ = 7.2 Hz, 4H; $CH_2$), 1.73-1.59 (m, 4H; $CH_2$), 1.43-1.26 (m, 20H; $CH_2$), 0.88 (t, $J$ = 6.5 Hz, 6H; $CH_3$)

**4,7-bis(3-octyl-2,2'-bithiophen-5-yl)benzo[c][1,2,5]thiadiazole (BTB)**

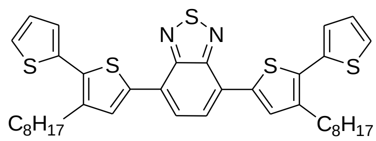


**BTB**

A mixture of 4,7-bis(5-bromo-4-octylthiophen-2-yl)benzo[c][1,2,5]thiadiazole (12) ( 217 mg, 0.32 mmol) , 5,5-dimethyl-2-(thiophen-2-yl)-1,3,2-dioxaborinane (149 g, 0.76 mmol), and $Pd(PPh_3)_4$ (15 mg, 4% molar), $K_3PO_4$ ( 155 mg, 0.76 mmol) dissolved in 30 ml of DMF was refluxed overnight. The mixture was then allowed to cool to room temperature before addition of 1M HCl and extracted with diethyl ether. The organic layer was dried over $Na_2SO_4$ and the solvent was evaporated. The crude product was purified by silica gel column chromatography with hexane/chloroform (4:1 v/v) as eluent to afford 4,7-bis(3-octyl-2,2'-bithiophen-5-yl)benzo[c][1,2,5]thiadiazole (BTB) as reddish powder. (50 mg, 23 %)

$^1$H NMR (200 MHz, $CDCl_3$, δ): 7.99 (s, 2H; Ar H), 7.83 (s, 2H; Ar H), 7.36 (dd, $J_1$ = 5 Hz, $J_2$ = 1.2 Hz, 2H; Ar H), 7.25 (dd, $J_1$ = 3.6 Hz, $J_2$ = 1.2 Hz, 2H; Ar H), 7.13 (dd, $J_1$ =5.2 Hz, $J_2$ = 3.6 Hz, 2H; Ar H), 2.85 (t, $J$= 7.2 Hz, 4H; $CH_2$), 1.83-1.55 (m, 4H; $CH_2$), 1.47-1.21 (m, 20H; $CH_2$), 0.88 (t, 6H, $J$ = 6.6 Hz; $CH_3$) ;

$^{13}$C NMR (200 MHz, $CDCl_3$, δ): 152.49, 140.48, 136.86, 136.01, 132.31, 130.54, 127.48, 126.01, 125.54, 125.39, 31.88, 30.66, 29.62, 29.44, 29.29, 22.68, 14.14

Elemental analysis for $C_{38}H_{44}N_2S_5$ (calculated): C, 66.23; H, 6.44 ; N, 4.07 ; S, 23.27 ; found: C, 65.53 ; H, 6.64 ; N, 3.88 ; S, 22.12

**4,7-bis(5'-bromo-3-octyl-2,2'-bithiophen-5-yl)benzo[c][1,2,5]thiadiazole (BTB-Br2)**

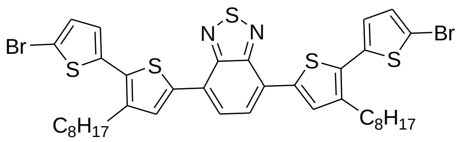

**BTB-Br2**

4,7-bis(3-octyl-2,2'-bithiophen-5-yl)benzo[c][1,2,5]thiadiazole (**3**) (267 mg, 0.39 mmol) was dissolved in 10 ml of chloroform. N-bromosuccinimide (145 mg, 0.81 mmol) dissolved in 10 ml of chloroform was then added dropwise at room temperature. After stirring for overnight at room temperature, the resulting mixture was poured into 20 ml of water,then extracted with dichloromethane. After solvent removal, the crude product was purified by silica gel column chromatography with cyclohexaneas eluent to afford 4,7-bis(5'-bromo-3-octyl-2,2'-bithiophen-5-yl)benzo[c][1,2,5]thiadiazole (**4**) as violet powder. (312 mg, 95 %)

$^1$H NMR (200 MHz, $CDCl_3$, δ): 7.95 (s, 2H; Ar H), 7.81 (s, 2H; Ar H), , 7.05 (d, $J$ = 3.8 Hz, 2H; Ar H), 6.97 (d, $J$ =3.8 Hz, 2H; Ar H), 2.79 (t, $J$= 7.8 Hz, 4H; $CH_2$), 1.78-1.64 (m, 4H; $CH_2$), 1.21 (m, 20H; $CH_2$), 0.89 (t, 6H, $J$ = 6.6 Hz; $CH_3$) ;

Elemental analysis for $C_{38}H_{42}Br_2N_2S_5$ (calculated): C, 53.89 ; H, 5.00 ; N, 3.31 ; S, 18.93 ; found: C, 53.67 ; H, 5.08 ; N, 3.29 ; S, 18.92

## II.4. Preparation of monomers BTF

**2,7-bis(4-octylthiophen-2-yl)-9H-fluoren-9-one (13)**

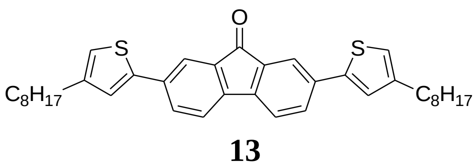

**13**

1.3 g of 2,7 dibromo-9H-fluoren-9-one (3.89 mmol) and 3.0 g of 5,5-dimethyl-2 (4-octylthiophen-2-yl)-1,3,2-dioxaborinane (9.7 mmol, 2.5 eq) were dissolved in 40 ml of anhydrous DMF and the mixture was stirred under argon at 60 °C. 2.1 g of $K_3PO_4$ (9.7 mmol, 2.5 eq) and 255 mg of $Pd(PPh_3)_4$ ( 5% eq) were then added and the mixture was heated with constant stirring at 100°C for 15 h, then allowed to cool at 25 °C. 15 ml of diethyl ether was added then allowed to cool at 4 °C to allow precipitation of the product. 15 ml of HCl 2N was added to increase precipitation. The precipitates were then filtered, washed subsequently with ether, pentane and acetone, and dried to afford fluorescence orange powder was obtained (1g, 45 %).

$^{1}$H NMR (200 MHz, CDCl3) d (ppm): 7.88 (2H, s), 7.70 (2H dd, J=7.75 Hz, J=1.82 Hz), 7.48 (2H, d, J=7.74 Hz), 7.25 (2H, s), 6.90 (2H, s), 2.61 (4H , t, J=15.13 Hz), 1.64 (4H, m), 1.28 (20H, m), 0.88 (6H, t, $^{3}$J=12.36)

**2,7-bis(5-iodo-4-octylthiophen-2-yl)-9H-fluoren-9-one (14)**

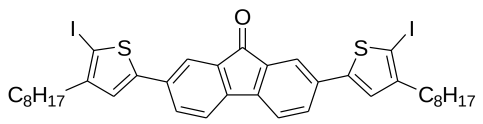

**14**

In a light protected flask, N-iodosuccinimide (0.87 g, 3.87 mmol) was dissolved in 15 ml of chloroform and 15 ml of acetic acid at room temperature. 2,7-bis(4-octylthiophen-2-yl)-9H-fluoren-9-one (1 g, 1.758 mmol ) dissolved in 10 ml of chloroform was then added drop wise to the NIS solution. After complete addition, a red precipitate was obtained and the mixture was stirred for an additional period of 12 h at room temperature. The reaction was then poured into water and extracted with chloroform. After solvent removal, a minimum volume of chloroform was added to dissolve the product and methanol was then added to allow precipitation and cooled in the refrigerator. Bright orange powder were then filtered and dried (1.34 g, yield: 93 %).

$^{1}$H NMR (200 MHz, CDCl3) d (ppm): 7.78 (2H,d,J=1.6 Hz), 7.58 (2H, dd, J= 7.8 and 1.8 Hz), 7.46 (2H, d, J= 7.8 Hz), 7.07 (2H,s), 2.56 (4H, t, J= 8.05 Hz), 1.65-1.56 (4H, m), 1.20-1.70 (20H, m), 0.89 (6H, m)

**2,7-bis(5-bromo-4-octylthiophen-2-yl)-9H-fluoren-9-one (14)**

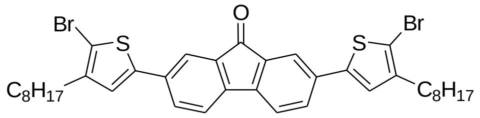

**14**

In a light protected flask, N-bromosuccinimide (0.782 g, 4.38 mmol) was dissolved in 10 ml of chloroform at room temperature. 2,7-bis(4-octylthiophen-2-yl)-9H-fluoren-9-one (1 g, 1.758 mmol ) dissolved in 20 ml of chloroform was then added drop wise to the NBS solution. After complete addition, a red precipitate was obtained and the mixture was stirred for an additional period of 12 h at room temperature. The reaction was then poured into water and extracted with diethyl ether. After solvent removal, a minimum volume of chloroform was added to dissolve the product and methanol was then added to allow precipitation and cooled in the refrigerator. Bright orange powder were then filtered and dried (0.92 g, yield: 72 %).

[1]H NMR (200 MHz, CDCl3) d (ppm): 7.78 (2H,d,J=1.6 Hz), 7.58 (2H, dd, J= 7.8 and 1.8 Hz), 7.46 (2H, d, J= 7.8 Hz), 7.07 (2H,s), 2.56 (4H, t, J= 8.05 Hz), 1.65-1.56 (4H, m), 1.20-1.70 (20H, m), 0.89 (6H, m)

**2,7-Bis(4-octyl-5,29-bithien-2-yl)-fluoren-9-one (1st synthesis)**

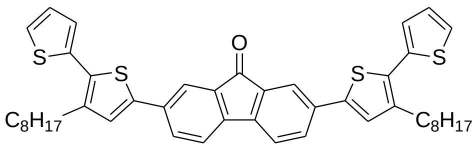

**BTF**

1 g of 2,7-bis(5-iodo-4-octylthien-2-yl)-fluoren-9-one (2) (1.22 mmol) and 0.53 g of 5,5-dimethyl-2-(thien-2 yl)[1,3,2]dioxoborinane (2.68 mmol, 2.2 eq.) were placed in 50 mL of anhydrous DMF and the mixture was stirred under argon for 10 min at 60°C and then 569 mg of $K_3PO_4$ (2.7 mmol, 2.2 eq.) and 73 mg of $Pd(PPh_3)_4$ (0.06 mmol) were added. The mixture was kept for an additional period of 15 h at 100 °C with constant stirring and then allowed to cool to 25 °C. The reaction was treated with hydrochloric acid (2.0 M) and the product was extracted with dichloromethane. The crude was then purified by column chromatography (silica gel, hexane/chloroform, 1: 1) to afford a deep red waxy product. (530 mg, yield = 60 %).

[1]H NMR (200 MHz, $CDCl_3$) d (ppm): : 7.85 (2H, d, J = 1.3 Hz), 7.63 (2H, dd, J = 7.9 and 1.3 Hz), 7.44 (2H, d, J = 7.6 Hz), 7.32 (2H, dd, J = 5.1 and 1.3 Hz), 7.21 (2H, s), 7.15 (2H, dd, J = 3.5 and 1.3 Hz), 7.07 (2H, dd, J = 5.1 and 3.5 Hz), 2.75 (4H, t, J = 7.3 Hz), 1.65 (4H, quint, J = 7.6 Hz), 1.40–1.20 (m, 20H), 0.9–0.8 (m, 6H).

[13]C NMR (200 MHz, $CDCl_3$) d (ppm): 193.31, 142.64, 140.66, 140.29, 135.92, 135.03, 134.96, 131.19, 130.88, 127.45, 126.58, 125.90, 125.44, 120.98, 120.74, 31.89, 30.57, 29.59, 29.43, 29.26, 22.68, 14.13.

Elemental analysis for $C_{45}H_{48}OS_4$ (calculated): C, 73.72 %; H, 6.60 %; Elemental analysis (found): C, 73.42%; H, 6.50%.

**2,7-Bis(4-octyl-5,29-bithien-2-yl)-fluoren-9-one (BTF) (2nd synthesis)**

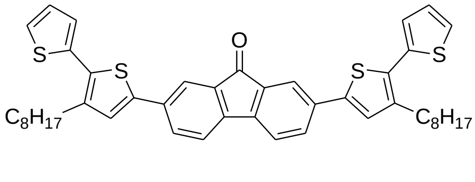

**BTF**

0.9 g of 2,7-bis(5-bromo-4-octylthien-2-yl)-fluoren-9-one (2) (1.26 mmol) and 0.62 mg of 5,5-dimethyl-2-(thien-2 yl)[1,3,2]dioxoborinane (3.15 mmol, 2.5 eq.) were placed in 50 mL of anhydrous DMF and the mixture was stirred under argon for 10 min at 60°C and then 800 mg of $K_3PO_4$ (3.7 mmol, 3 eq.) and 73 mg of $Pd(PPh_3)_4$ (0.06 mmol) were added. The mixture was kept at reflux for 16h with constant stirring and then allowed to cool to 25 °C. The reaction was treated with hydrochloric acid (2.0 M) and the product was extracted with diethyl ether. The crude was concentrated and dissolved in a minimum of chloroform and the addition of methanol allows precipitation of pure product. We obtained deep red precipitates. (930 mg, yield= 88 %).

$^1$H NMR (200 MHz, $CDCl_3$) d (ppm): : 7.85 (2H, d, J = 1.3 Hz), 7.63 (2H, dd, J = 7.9 and 1.3 Hz), 7.44 (2H, d, J = 7.6 Hz), 7.32 (2H, dd, J = 5.1 and 1.3 Hz), 7.21 (2H, s), 7.15 (2H, dd, J = 3.5 and 1.3 Hz), 7.07 (2H, dd, J = 5.1 and 3.5 Hz), 2.75 (4H, t, J = 7.3 Hz), 1.65 (4H, quint, J = 7.6 Hz), 1.40–1.20 (m, 20H), 0.9–0.8 (m, 6H).

$^{13}$C NMR (200 MHz, $CDCl_3$) d (ppm): 193.31, 142.64, 140.66, 140.29, 135.92, 135.03, 134.96, 131.19, 130.88, 127.45, 126.58, 125.90, 125.44, 120.98, 120.74, 31.89, 30.57, 29.59, 29.43, 29.26, 22.68, 14.13.

Elemental analysis for $C_{45}H_{48}OS_4$ (calculated): C, 73.72 %; H, 6.60 %; Elemental analysis (found): C, 73.42%; H, 6.50%.

**2,7-bis(5'-bromo-3-octyl-2,2'-bithiophen-5-yl)-9H-fluoren-9-one (BTF-Br2)**

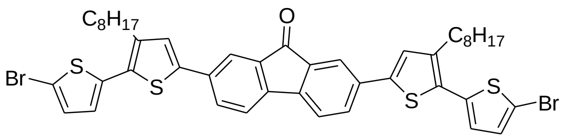


**BTF-Br2**

500 mg of 2,7-Bis(4-octyl-5,29-bithien-2-yl)-fluoren-9-one (0.68 mmol) (17) were dissolved in 15 ml of chloroform in a flask at room temperature. 267 mg of NBS dissolved in 15 ml of chloroform was added drop wise to the flask and leave to stir overnight at room temperature. After overnight, the mixture was washed with water then extracted by dichloromethane, and further purify by column chromatography (silica gel, hexane/dichloromethane, 7: 3). (386 mg, yield = 64%)

$^1$H NMR (200 MHz, $CDCl_3$, δ): 7.86 (s, 2H; Ar H), 7.68 (d, *J*=7.8 Hz , 2H; Ar H), 7.50 (d, *J* = 7.8 Hz, 2H; Ar H), 7.21 (s, 2H; Ar H), 7.04 (d, *J* = 3.8 Hz, 2H; Ar H), 6.90 (d, *J* =3.8 Hz, 2H; Ar H), 2.74 (t, *J*= 7.6 Hz, 4H; $CH_2$), 1.62 (t, J= 7.6 Hz 4H; $CH_2$), 1.28 (m, 20H; $CH_2$), 0.89 (t, 6H, *J* = 6.6 Hz; $CH_3$) ;

Elemental analysis for $C_{45}H_{46}Br_2OS_4$ (calculated): C, 60.67; H, 5.20; S, 14.40 ; found: C, 61.94; H, 5.41; S, 14.59

## II.5. Synthesis of polymers PQTB, PQTF,

**Poly[(5,5--dioctyl-[2,29;59,20;50,2-]quaterthiophene)-alt-(benzo[c][1,2,5]thiadiazole)] (PQTB)**

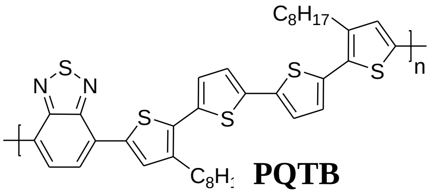

**PQTB**

4,7-bis(3-octyl-2,2'-bithiophen-5-yl)benzo[c][1,2,5]thiadiazole (13) (600 mg, 0.87 mmol) was dissolved in 25 ml of anhydrous chloroform and was cooled to 0° C in argon environment. Iron (III) chloride (565 mg, 3.48 mmol) dissolved in 8 ml of nitromethane was added drop wise. The mixture was allowed to warm to room temperature and stirred overnight. The product was allowed to precipitate by adding drop wise into methanol. Few drops of hydrazine were added to increase precipitation. The powder was filtered and washed by vigorous stir in a mixture of 0.1 M ammoniac solution and 0.02 M of EDTA for 15 hours. The precipitate was filtered and the crude was further purified by column chromatography (silica gel, pentane). Dark metallic flakes were obtained. The crude polymer was then purified by sequential fractionation with different solvent by soxhlet extraction (Batch: 600 mg, 100%; acetone: 95 mg, 16 %; $CH_2Cl_2$: 80 mg, 13 % ; $CHCl_3$: 65 mg, 11 %; Toluene: 45 mg, 7.5 %; chlorobenzene: 120 mg, 20 %)

$^1$H NMR (200 MHz, CDCl3) d (ppm): 7.98 (br, 2H) , 7.82 (br, 2H), 7.34 (br, 1H), 7.24 (br, 1H), 7.18-7.10 (br, 2H), 2.85 (br, 4H), 1.75 (br, 4H), 1.293 (br, 22H), 0.885 (br, 6H)

**Poly[(5,5--dioctyl-[2,29;59,20;50,2-]quaterthiophene)-alt- 9H-fluoren-9-one)] PQTF**

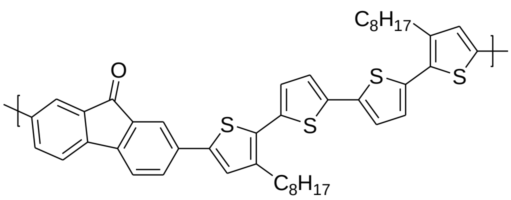

**PQTF**

2,7-bis(3-octyl-2,2'-bithiophen-5-yl)-9H-fluoren-9-one (17) (850 mg, 1.16 mmol) was dissolved in 25 ml of anhydrous chloroform and was cooled to 0° C in argon environment. Iron (III) chloride (752 mg, 4.63 mmol) dissolved in 8 ml of nitromethane was added drop wise. The mixture was then allowed to warm to room temperature and stirred overnight. The product was allowed to precipitate by adding drop wise into methanol. Few drops of hydrazine were added to increase precipitation. The powder was filtered and washed by vigorous stir in a mixture of 0.1 M ammoniac solution and 0.02 M of EDTA for 15 hours. The precipitate was filtered and the crude was further purified by column chromatography (silica gel, pentane). Dark metallic flakes were obtained. The crude polymer was then purified by sequential fractionation with different solvent by soxhlet extraction

$^{1}$H NMR (200 MHz, $C_2D_2Cl_4$) d (ppm): d: 7.78 (s), 7.60 (d, J = 7.30 Hz), 7.41 (d, J = 7.60 Hz), 7.25 (d, J = 5.08 Hz), 7.16 (s), 7.08 (br s), 7.01 (d, J = 3.49 Hz), 2.60–2.78 (m), 1.74–1.07 (m), 0.95–0.75 (m).

Elemental analysis: Calcd for monomer unit: C, 73.72%; H, 6.60%; S, 17.50%. Found: C, 73.59%; H, 6.49%; S, 15.70%.

**Poly [4-(5'-(9,9-dihexyl-7-(3'-octyl-2,2'-bithiophen-5-yl)-9H-fluoren-2-yl)-3-octyl-2,2'-bithiophen-5-yl)benzo[c][1,2,5]thiadiazole] (6) (PTFB)**

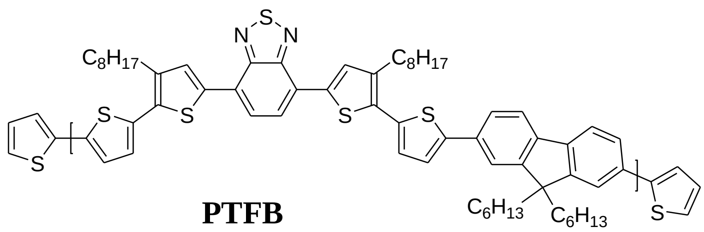


**PTFB**

4,7-bis(5'-bromo-3-octyl-2,2'-bithiophen-5-yl)benzo[c][1,2,5] thiadiazole (14) (400 mg, 0.47 mmol), and 2,2'-(9,9-dihexyl-9H-fluorene-2,7-diyl)bis(5,5-dimethyl-1,3,2-dioxaborinane) (238 mg, 0.47 mmol) were charged in a 25 ml flask and purged under $N_2$. After adding toluene (6 ml) the mixture was degassed by following the addition of $Na_2CO_3$ solution (2 ml, 2.0 M) , and the catalysts $Pd_2(dba)_3$ (8.6 mg, 9 $10^{-3}$ mmol) and $P(o\text{-tolyl})_3$ (17 mg, 5.4 x $10^{-2}$ mmol). The mixture was then heated at 120 °C for 72 h. For end-capping, 2-thiophene boronic ester (185 mg, 0.94 mmol) and 2-bromothiophene (154 mg, 0.94 mmol) were added and the mixture was heated for another 2 h. After cooling to room temperature, the mixture was poured into methanol. The precipitate was collected and washed with methanol vigorously then extracted by soxhlet extraction with acetone and chloroform. The chloroform fraction was concentrated and used for further use. (375 mg, 67 %) Mn : 5.64 kDa (eq PS) ; Mw: 8.61 kDa (eq PS); PDI : 1.56;

$^{1}$H NMR (200 MHz, $CDCl_3$, δ): 7.95 (s, 2H; Ar H), 7.81 (s, 2H; Ar H), , 7.05 (d, *J* = 3.8 Hz, 2H; Ar H), 6.97 (d, *J* =3.8 Hz, 2H; Ar H), 2.79 (t, *J*= 7.8 Hz, 4H; $CH_2$), 1.78-1.64 (m, 4H; $CH_2$), 1.21 (m, 20H; $CH_2$), 0.89 (t, 6H, *J* = 6.6 Hz; $CH_3$) ;

$^{13}$C NMR (200 MHz, $CDCl_3$, δ): 152.97, 152.22, 145.46, 145.33, 140.93, 137.25, 135.75, 133.38, 133.10, 131.16, 127.29, 125.80, 125.59, 120.17, 78.10, 77.46, 76.83, 55.79, 40.90, 32.39, 30.16, 29.96, 29.82, 23.17, 23.06, 14.62, 14.50

Elemental Analysis for $C_{126}H_{149}BrN_4S_{10}$: C, 71.38; H, 7.08; Br, 3.77; N, 2.64; S, 15.12; Found: C, 71.54; H, 7.01; N: 2.51; S, 14.34

**Poly[2-(5'-(9,9-dihexyl-7-(3'-octyl-2,2'-bithiophen-5-yl)-9H-fluoren-2-yl)-3-octyl-2,2'-bithiophen-5-yl)-9H-fluoren-9-one] (PTFF)**

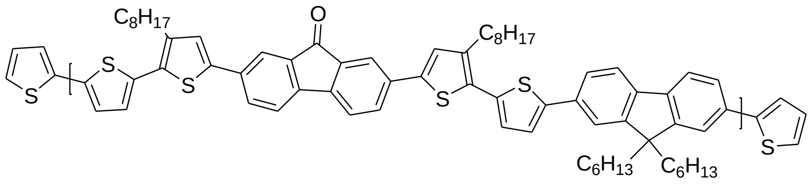


**PTFF**

2,7-bis(5'-bromo-3-octyl-2,2'-bithiophen-5-yl)-9H-fluoren-9-one (18) (200 mg, 0.22 mmol), and 2,2'-(9,9-dihexyl-9H-fluorene-2,7-diyl)bis(5,5-dimethyl-1,3,2-dioxaborinane) (113 mg, 0.22 mmol) were charged in a 25 ml flask and purged under $N_2$. After adding toluene (6 ml), the mixture was degassed by following the addition of $Na_2CO_3$ solution (2 ml, 2.0 M) , and the catalysts $Pd_2(dba)_3$ (4 mg, 4,4 $10^{-3}$ mmol) and $P(o\text{-tolyl})_3$ (8 mg, 2.6 x $10^{-2}$ mmol). The mixture was then heated at 120 °C for 72 h. For end-capping, of 2-thiophene boronic ester (94 mg, 0.44 mmol) and 2-bromothiophene (73 mg, 0.44 mmol) were added and the mixture was heated for another 2 h. After cooling to room temperature, the mixture was poured into methanol. The precipitates were collected and washed with methanol vigorously then extracted by soxhlet extraction with acetone and chloroform. The chloroform fraction was concentrated and used for further use. ( 92 mg, 33 % ) ; Mn : 3.24 kDa (eq PS)**;** Mw : 4.96 kDa (eq PS)**;** I : 1.53

$^1$H NMR (200 MHz, $CDCl_3$, δ): 7.83-6.86 (m, 16H), 2.80 (br, 4H), 2.01 (br, 4H), 1.68-1.07 (br, 40H), 0.89 (br, 6H), 0.76 (br,6H) ;

$^{13}$C NMR (200 MHz, $CDCl_3$, δ): 151.14, 150.45, 146.66, 142.42, 140.47, 137.99, 134.60, 134.55, 134.35, 130.71, 129.83, 129.15, 126.33, 126.25, 124.16, 120.61, 120.41, 120.371, 119.300, 119.240, 89.450, 77.234, 76.599, 75.964, 40.020, 31.528, 31.495, 31.085, 30.137, 29.299, 29.257, 23.332, 22.300, 22.178, 13.756

Elemental Analysis (Calculated for $C_{115}H_{124}Br_2O_2S_8$: C, 70.67; H, 6.39; Br, 8.18; O, 1.64; S, 13.12

Elemental analysis found: C, 69.27; H, 6.37; S, 11.70

**Poly [4-(5'-(9,9-dihexyl-7-(3'-octyl-2,2'-bithiophen-5-yl)-9H-fluoren-2-yl)-3-octyl-2,2'-bithiophen-5-yl)benzo[c][1,2,5]thiadiazole]-alt-[2-(5'-(9,9-dihexyl-7-(3'-octyl-2,2'-bithiophen-5-yl)-9H-fluoren-2-yl)-3-octyl-2,2'-bithiophen-5-yl)-9H-fluoren-9-one] (PTFBF)**

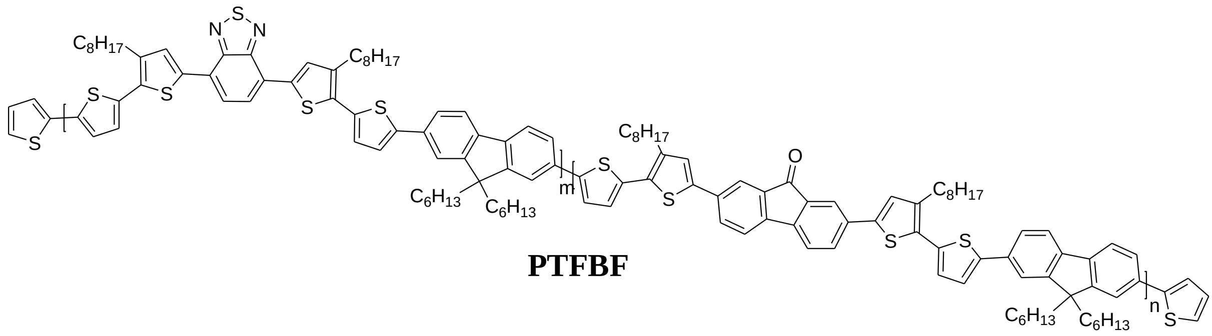

**PTFBF**

4,7-bis(5'-bromo-3-octyl-2,2'-bithiophen-5-yl)benzo[c][1,2,5] thiadiazole (14) (169.4 mg, 0.2 mmol), 2,7-bis(5'-bromo-3-octyl-2,2'-bithiophen-5-yl)-9H-fluoren-9-one (178.2 mg, 0.2 mmol), and 2,2'-(9,9-dihexyl-9H-fluorene-2,7-diyl)bis(5,5-dimethyl-1,3,2-dioxaborinane) (201.5 mg, 0.4 mmol) were charged in a 25 ml flask and purged under $N_2$. After adding toluene (12 ml) the mixture was degassed by following the addition of $Na_2CO_3$ solution (2 ml, 2.0 M) , and the catalysts $Pd_2(dba)_3$ (7.3 mg, 7.6 $10^{-3}$ mmol) and $P(o\text{-tolyl})_3$ (15 mg, 4.8 x $10^{-2}$ mmol). The mixture was then heated at 120 °C for 72 h. For end-capping, 2-thiophene boronic ester (185 mg, 0.94 mmol) and 2-bromothiophene (154 mg, 0.94 mmol) were added and the mixture was heated for another 2 h. After cooling to room temperature, the mixture was poured into methanol. The precipitate was collected and washed with methanol vigorously then extracted by soxhlet extraction with acetone and chloroform. The chloroform fraction was concentrated and used for further use.

(300 mg, 68 %) Mn : 2.48 kDa (eq PS) ; Mw: 4.87 kDa (eq PS); PDI : 1.96;

$^1$H NMR (200 MHz, $CDCl_3$, δ): 8.028 (br, 2H), 7.878 (br, 4H), 7.701 -7.611 (br, 14H), 7.40-7.06 (br, 14H), 2.881 (br, 8H), 2.029 (br,8H) , 1.745 (br,8H), 1.30 (br, 40H), 1.067 (br, 24H), 0.86 -0.74 (br, 32H)

$^{13}$C NMR (200 MHz, $CDCl_3$, δ):151.180, 150.482, 140.163, 136.381, 134.590, 132.385, 130.735, 130.325, 130.294, 129.173, 126.433, 126.402, 124.192, 122.471, 119.334, 108.275, 106.047, 105.234, 104.592, 104.378, 76.623, 54.781, 40.050, 31.553, 31.110, 29.328, 22.336, 22.207, 13.778, 13.639

Proposed polymer structure:

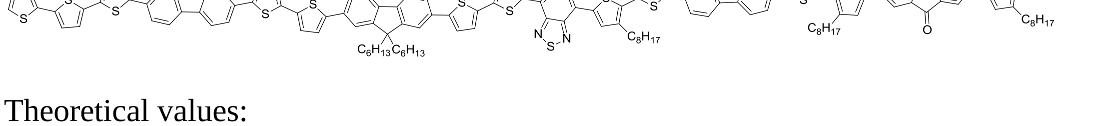

Theoretical values:

Chemical Formula: $C_{186}H_{204}N_2O_2S_{15}$

Exact Mass: 2977,17

Molecular Weight: 2980,60

Elemental Analysis: C, 74.95; H, 6.90; N, 0.94; O, 1.07; S, 16.14

Elemental analysis:Found: C, 74.85; H, 7.26; N, 1.25; S, 12.46

SEC Mpeak= 2.9913 kDa

## II.6. Synthesis of polymers indacenodithiophenes PIDTB, PIDTF and PIDTBF

**Diethyl 2,5-di(thiophen-2-yl)terephthalate (16)**

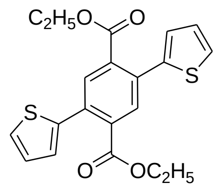


**(16)**

Diethtyl 2,5-dibromoterephtalate (4.27 g, 11.24 mmol) and 2-thienylzinc bromide (0.5 M in THF, 50 ml, 25 mmol) was introduced in a bicol flask. $Pd(PPh_3)_4$ palladium (0) catalyst was then introduced into the mixture flask. The mixture was heated at reflux (70°C) for 3 h. After cooled to room temperature, the reaction mixture was poured into saturated $NH_4Cl$ solution. The product was extracted with ethyl acetate (3 x 100 ml). The extracts were combined and washed with water then dried over $Na_2SO_4$. After filtration, the solvent was removed under reduced pressure. The crude product was purified by column chromatography (silica gel, hexane/dichloromethane, 10:1 v/v)) to afford white solid. (3.5 g, 80 %);

$^1$H NMR (200 MHz, $CDCl_3$, δ): 7.82 (s, 2H), 7.40 (dd, J=4.4 and 1.9 Hz, 2H), 7.09-7.05 (m, 4H), 4.24 (q, J=7.2 Hz), 1.15 (t, J= 7,2 Hz)

**Monomer indacenodithiophene (IDT)**

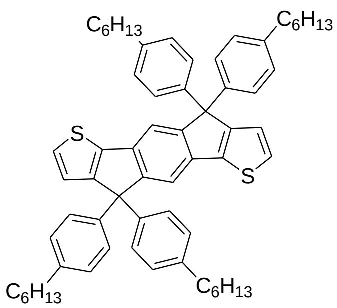


1- bromo-4 hexylbenzene (3 g, 12.5 m **(16)** as dissolved in 15 ml of freshly distilled THF and cooled to -78 °C in argon atmosphere before drop wise addition of a solution of n-BuLi

(1.6 M in hexane, 8 ml, 12.5 mmol). The mixture was vigorously stirred for 1h at -50 °C before the addition of diethyl 2,5-di(thiophen-2-yl)terephthalate (19) (1 g, 2.6 mmol) dissolved in 10 ml of distilled THF. After complete addition, it was allowed to warm to room temperature then stirred vigorously for overnight. The reaction was quenched with 100 ml of water then extracted with ethyl acetate (3 X 50 ml) and dried over $Na_2SO_4$. After solvent removal, brown solids were obtained. The crude product was placed in a 250 ml bicol and dissolved in 50 ml of acetic acid.1 ml of concentrated $H_2SO_4$ was added to the solution and we observed rapid changes of colour from yellow to violet then green. The mixture was heated in reflux for 2h. After 2h the colour turned to yellow and the solution was poured into water. The product was extracted by ethyl acetate. After evaporation of the solvent, the crude was further purified by column chromatography (silica gel, hexane/dichloromethane, 10:1 v/v). Brown solid was obtained (2.08 g, 74 %).

$^1$H NMR (200 MHz, $CDCl_3$, δ): 7.42 (2H, s), 7.24 (2H, d, J=4.2 Hz), 7.174 (2H, d, J=8.2 Hz), 7.064 (2H, d, J=8.2 Hz), 7.006 (2H, d, J=4.2 Hz), 2.586 (4H, t, J= 7.3 Hz), 1.543 (8H,m), 1.281 (32H, m), 0.871 (t, 12H)

$^{13}$C NMR (200 MHz, $CDCl_3$, δ): 156.05, 153.60, 142.28, 141.57, 141.40, 135.29, 128.48, 128.10, 127.60, 123.33, 117.69, 62.86, 35.79, 31.96, 31.58, 29.38, 22.84, 14.34

Elemental Analysis calculated for $C_{64}H_{74}S_2$: C, 84.71; H, 8.22; S, 7.07

Found: C, 81.40; H, 7.88; S, 6.51

**Monomer indacenothiophene distannic ($Me_3$Sn-IDT-Sn$Me_3$)**

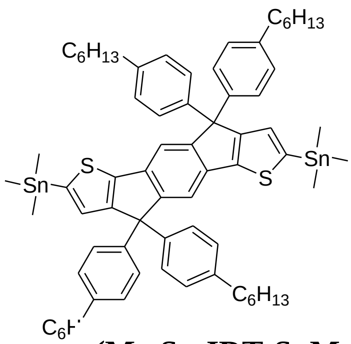


**($Me_3$Sn-IDT-Sn$Me_3$)**

To a solution of IDT (20) (500 mg, 0.55 mmol) in THF (30 ml) kept at -78 °C , a solution of n-BuLi (1.6 M in hexane, 0.8 ml, 1.27 mmol) was added dropwise. The obtained mixture was vigorously stirred for 1h at -50 °C before the addition of trimethyl tin chloride (255 mg, 1.78 mmol) dissolved in 3 ml of THF at -78 °C. The mixture was then allowed to reach room temperature and to react for overnight. The resulting solution was then quenched with water and the product was extracted with hexane. The organic phase was dried over $Na_2SO_4$ and the solvent was evaporated. A brown solid was obtained with no further purification. (678 mg, 77 %).

$^{1}H$ NMR (200 MHz, $CDCl_3$, δ) : 7.379 (2H,s) , 7.169-7.055(16H, m), 7.014 (2H, s), 2.584 ((8H, t, J= 7.5 Hz) 1.556 (8H,m) , 1.295 (24H,m) , 0.869 (12H,m), 0.332 (18H, t)

**Polymer (indacenothiophene-alt-benzothiadiazole) PIDTB**

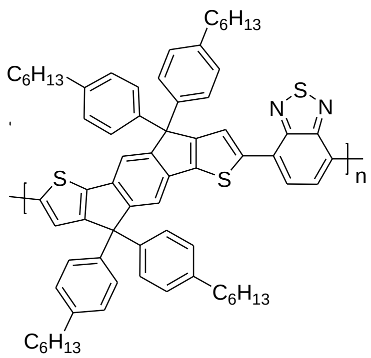

**PIDTB**

300 mg (0.24 mmol) of (Sn-IDT-Sn), 70.5 mg (0.24 mmol) of 4,7-dibromobenzo[c][1,2,5]thiadiazole were placed in a three-bottom neck flask in a mixture of solvent (Toluene/DMF 10:1). The mixture was well degassed and stirred in argon environment for 5 min before the addition of tris(dibenzylideneacetone)dipalladim (0) (4.6 mg, 0.005 mmol) and tri(o-tolylphosphine) (12.1 mg , 0.04 mmol). The resulting mixture were then refluxed with vigorous stirring for 48 h. After cooling to room temperature, the mixture was poured into methanol to allow precipitation. The crude polymer was filtered then purified by soxhlet sequentiel extraction with acetone then chloroform. Yield : Crude: 334 mg, polymer-acetone fraction: 99 mg, (40%), polymer-chloroform fraction: 106 mg (42 %)
$^{1}H$ NMR (200 MHz, $CDCl_3$, δ): 8.041 (1H, broad), 7.812 (1H, broad), 7.532 (2H, br), 7.128 (8H,br) , 7.089 (8H,br), 2.573 (8H,br), 2.571 (8H,br) , 1.598 (24H,br), 0.869 (12H,br).
$^{13}C$ NMR (200 MHz, $CDCl_3$, δ):153.469, 152.062, 141.541, 141.292, 128.154, 127.707, 62.860, 35.343, 31.474, 31.108, 28.922, 22.352, 13.862

Proposed polymer structure:

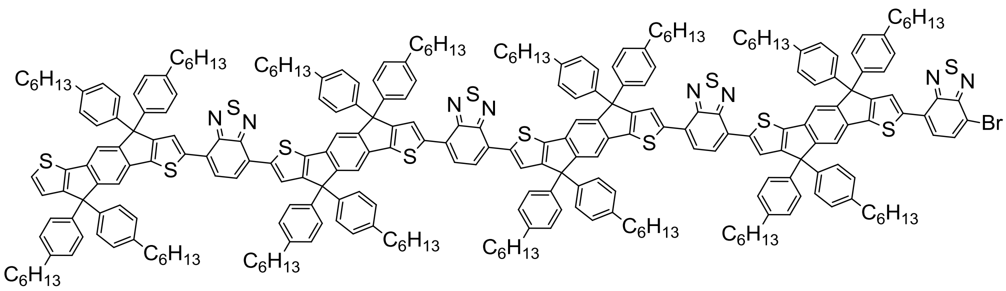

Theoretical values:
Chemical Formula: $C_{280}H_{297}BrN_8S_{12}$
Exact Mass: 4233,93 kg/mol
Molecular Weight: 4239,09 . Elemental Analysis: C, 79.33; H, 7.06; Br, 1.88; N, 2.64; S, 9.08

SEC (found) : 4711.8 kDa equivalent PS.
Elemental analysis (found): C: 78.91; H: 7.07; N: 2.68 ; S: 9.01

**Polymer (indacenothiophene-alt-fluorenone) PIDTF**

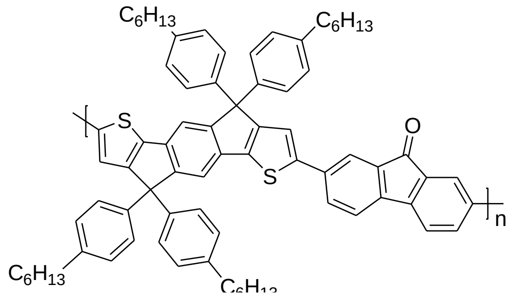

**PIDTF**

The polymerisation of PIDTF was carried out following the same procedure of PIDTB with 300 mg (0.24 mmol) of (Sn-IDT-Sn) , 80.88 mg (0.24 mmol) of 2,7-dibromo-9H-fluoren-9-one, and the same amount for the catalyst. Yield : Crude: 342 mg, polymer-acetone fraction: 121 mg, (46%), polymer-chloroform fraction: 159 mg (61 %)
$^{1}$H NMR (200 MHz, $CDCl_3$, δ): 7.944-7.395 (10H, br) , 7.324 - 7.151 (16H,br), 2.643 (8H,br) 1.671(8H,br), 1.369 (24H,br) 0.941 (12H,br) ;
$^{13}$C NMR (200 MHz, $CDCl_3$, δ): 157.861, 156.974, 153.371, 151.118, 149.011, 145.559, 141.617, 135.925, 135.292, 135.055, 131.057, 128.426, 127.851, 121.067, 121.007, 120.797, 119.918, 117.464, 63.083, 35.582, 31.721, 31.352, 29.150, 22.600, 14.111
Propsoed structure:

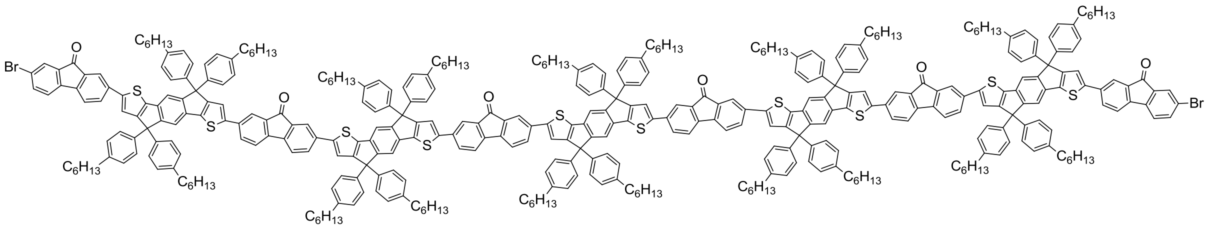

Chemical Formula: $C_{398}H_{396}Br_2O_6S_{10}$

Exact Mass: 5748,63

Molecular Weight: 5755,86 :

Elemental Analysis: C, 83.05; H, 6.93; Br, 2.78; O, 1.67; S, 5.57

SEC (found) : 5426.2 kDaequivalent PS.

Elemental Analysis (found) : C, 83.04; H, 7.14; S, 5.66

**Polymer (indacenothiophene-alt-benzothiadiazole-indacenothiophene-alt-fluorenone) PIDTBF**

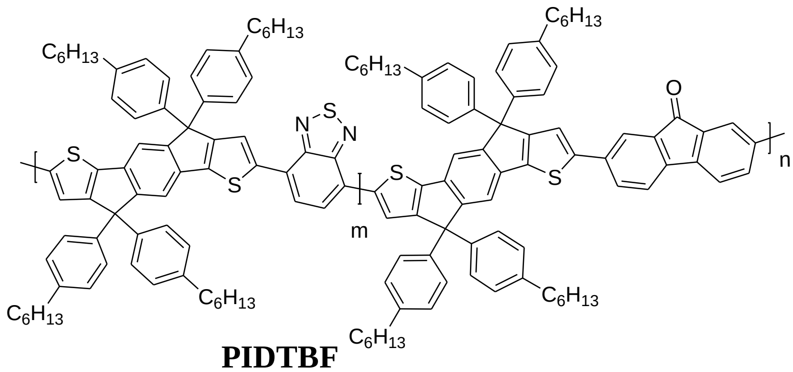

**PIDTBF**

The polymerisation of PIDTF was carried out following the same procedure of PIDTB with 300 mg (0.24 mmol) of (Sn-IDT-Sn) , 70.5 mg (0.24 mmol) of 4,7-dibromobenzo[c][1,2,5]thiadiazole, 80.88 mg (0.24 mmol) of 2,7-dibromo-9H-fluoren-9-one, and the same amount of catalyst. Yield: Crude: 259 mg, polymer-acetone fraction: 53 mg, (20%), polymer-chloroform fraction: 154 mg (60 %)

$^{1}$H NMR (200 MHz, $CDCl_3$, δ): 8.01 (br,2H) , 7.864-7.765 (br, 4H), 7.696 - 7.587 (br, 4H), 7.522 - 7.443 (br, 4H), 7.395 - 7.322 (br, 4H), 7.241-7.145 (br,14H) , 7.113-7.079 (br,16H), 2.563 (br,16H), 1.572 (m, 32H), 1.291 (m,32 H) , 0.867 (m, 24H)

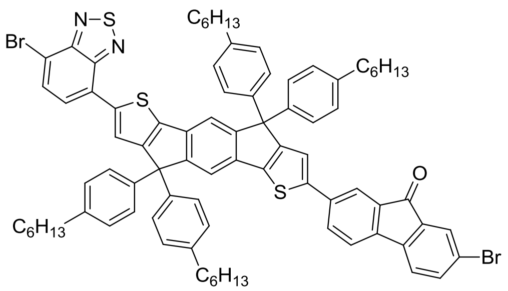

Chemical Formula: $C_{83}H_{80}Br_2N_2OS_3$

Exact Mass: 1374,38

Molecular Weight: 1377,54 . SEC (found): 1528.7 kDaeq. PS (Mw up to 17.5 kg/mol)

Elemental Analysis: C, 72.37; H, 5.85; Br, 11.60; N, 2.03; O, 1.16; S, 6.98

# ABBREVIATIONS

| | |
|---|---|
| A | acceptor |
| AFM | atomic force microscopy |
| AM1.5 | air mass 1.5 |
| $C_{60}$ | Buckminsterfullerene-60 |
| $C_{70}$ | Buckminsterfullerene-70 |
| $CHCl_3$ | chloroform |
| CV | cyclic voltammetry |
| D | donor |
| DMF | dimethylformamide |
| DPV | differential pulse voltammetry |
| EPR | electron paramagnetic resonance spectroscopy |
| HOMO | highest occupied molecular orbital |
| IPCE | incident photon to current efficiency |
| IR | infra-red |
| ITO | Indium Tin Oxide |
| J-V | current density-voltage |
| LUMO | lowest unoccupied molecular orbital |
| NBS | N-bromo-succinimide |
| $Ni(dppp)Cl_2$ | [1,3-bis(diphenylphosphino)-propane]dichloronickel(II) |
| NMR | nuclear magnetic resonance spectroscopy |
| MDMO-PPV | poly(2-methoxy-5-(3’,7’-dimethyloctyloxy)-1,4-phenylene-vinylene) |
| MEH-PPV | poly(2-methoxy-5-(2’-hexyloxy)-1,4-phenylenevinylene) |
| Mn | Average number molecular weight in kDa |
| Mw | Average weight molecular weight in kDa |
| OPV | organic photovoltaic |
| P3AT | poly(3-alkylthiophene) |
| P3HT | poly(3-hexylthiophene) |
| PCBM | [6,6]-phenyl-$C_{61}$-butyric acid methylester |
| PEDOT:PSS | poly(3,4-ethylenedioxythiophene) doped with poly(styrenesulfonate) |
| PET | polyethylene |
| PIDTB | poly(indacenodithiophene-benzothiadiazole) |
| PIDTF | poly(indacenodithiophene-fluorenone) |
| PIDTBF | poly([indacenodithiophene-benzothiadiazole]-[indacenodithiophene-fluorenone]) |
| PQTB | poly(quaterthiophene-benzothiadiazole) |
| PQTF | poly(quaterthiophene-fluorenone) |
| PTFB | poly(bithiophene fluorene-benzothiadiazole) |
| PTFF | poly(bithiophene fluorene-fluorenone) |
| QTF | bis(dialkylquaterthiophene)-fluorenone |
| THF | tetrahydrofuran |
| TVF | thienylene vinylene fluorenone |
| TVF2 | dimer thienylene vinylene fluorenone |
| PPV | poly(phenylene-vinylene) |
| PV | photovoltaic |
| SEC | size exclusion chromatography |
| TMS | trimethylsilane |
| UV-vis | ultraviolet visible |